

Petrogenesis of the Bissett Creek flake graphite deposit: Implications for regional graphite mineralization models in the Grenville Province, Ontario

by

Cameron Reid Drever

A thesis
presented to the University of Waterloo
in fulfillment of the
thesis requirement for the degree of
Master of Science
in
Earth Sciences

Waterloo, Ontario, Canada, 2018

© Cameron Reid Drever 2018

Author's Declaration

This thesis consists of material all of which I authored or co-authored: see Statement of Contributions included in the thesis. This is a true copy of the thesis, including any required final revisions, as accepted by my examiners.

I understand that my thesis may be made electronically available to the public.

Statement of Contributions

The work for the project entitled “Petrogenesis of the Bissett Creek flake graphite deposit: Implications for regional graphite mineralization models in the Grenville Province, Ontario” was completed in the following manner. The project was conceived by my supervisor, Dr. Yakymchuk and I. I was responsible for project planning, data collection, processing and interpretation. Dr. Yakymchuk assisted me with proofreading, editing and interpretation discussion.

Some of the preliminary results of this project were published in 2017 as part of the paper entitled “Origin of graphite in the Southwestern Grenville Province” in the Canadian Mineralogist on which I was a co-author. As a co-author I was responsible for documenting the petrography of the Bissett Creek flake graphite deposit, independent modelling of carbon isotope fractionation to confirm results, proofreading, and minor editing. Dr. Taner completed the preliminary draft of the article. Dr. Yakymchuk completed revisions of the initial article, carbon isotope modelling and drafted the figures. Dr. Longstaffe analyzed the carbon isotopes values of graphite separates.

Abstract

Graphite is a critical component of green and renewable energy technologies. In Ontario, graphite deposits are scattered throughout the pre-Grenvillian Laurentian Margin and the Composite Arc Belt of the Grenville Province. The Bissett Creek deposit in central Ontario is one of the most advanced graphite exploration properties in the region with a large proportion (~70%) of high purity >180 μm graphite. Large flake graphite size, as seen in the Bissett Creek deposit, is one of the key factors affecting the economic viability of graphite concentrates for manufacturing applications. However, the geological processes responsible for the formation of this deposit and similar deposits, in the region and internationally, are unclear. To facilitate successful exploration and production of flake graphite deposits, an understanding of the processes controlling mineralization and the timing of mineralization must be determined. At Bissett Creek, graphite is hosted in quartzofeldspathic, aluminous and calc-silicate gneisses. These units are stratabound by barren quartzofeldspathic gneisses. All units have undergone polyphase folding and have foliations with shallow to moderate dips predominantly to the east and north. Graphite mineralization is characterized by homogeneously distributed and disseminated graphite flakes, about 1 to 6mm in size, that compose 2–10 vol.% of the mineralized gneisses. Graphite flakes are interleaved with metamorphic minerals, most notably biotite and garnet. Geothermobarometry using the metamorphic minerals interleaved with the graphite yields conditions of 620°C to 790°C at 0.8 GPa to 1.5 GPa, which is consistent with regional upper amphibolite- to granulite-facies metamorphism. Whole-rock samples have carbon isotope values ($\delta^{13}\text{C}_{\text{VPDB}}$) ranging from -28.3‰ to -14.0‰, which suggests that graphite formed from organic materials. Carbon isotope modelling indicates that this range of the values could be generated through either single or multicomponent (CH_4 and CO_2) fractionation of a fluid from an isotopically homogeneous source, although a single component (CO_2) fractionation is more likely. Whole-rock sulfur isotopes ($\delta^{34}\text{S}_{\text{CDT}}$) have values ranging from 9.7‰ to 15.0‰ and are compatible with an organic source and a sedimentary origin. Therefore, the Bissett Creek flake graphite deposit was likely formed from metamorphism of *in situ* organic material, but interactions with carbon bearing metamorphic fluids generated during high-temperature metamorphism and partial melting could have played a role in the formation of the extra-large graphite flakes found in the deposit. The conclusions of this study have also been used to formulate exploration guidelines to help assist in the discovery and development of additional flake graphite deposits in the pre-Grenvillian Laurentian Margin.

Acknowledgements

There are a multitude of people, without whom, I would not have been able to complete this thesis. I am eternally thankful for all of their support. I would like to begin by acknowledging the plethora of people from a variety of universities and labs who assisted me with the acquisition of my data. To Alysha McNeil and Marc Beauchamp of the Earth and Planetary Materials Analysis Lab at the University of Western Ontario, thank you for your assistance in analyzing many mineral compositions and your support for all of my inquiries. To Evelyne Leduc at the Queen's Facility for Isotope Research, thank you for your persistence in acquiring the carbon isotope values. To Rick Heemskerk and William Mark of the University of Waterloo Environmental Isotope Lab, thank you for your hard work and diligence in sulfur isotope acquisition. To the staff at SGS – Lakefield, thank you for the tour of your facilities and the wealth of knowledge I obtained in processing graphite bearing samples for geochemical purposes. Finally, thank you to the staff at Actlabs for their help in determining major and trace element geochemistry.

Next, I would like to thank all the project staff. Thank you to Gregory Bowes and Peter Bruzas of Northern Graphite. Thanks to Greg for obtaining financial support and approvals. Peter was a phenomenal support in the field. His knowledge of the property, navigational skill and assistance in clearing paths made our mapping progress much greater and contributed to an overall better understanding of the deposit. Thank you to Mehmet Taner for his detailed core logging notes, prior petrographic understanding of the property and general geology orientation. Additional thanks to Nickie Patrizio, Yolanda Zhang and Ivan Edgeworth for their field support and Anthony Zamperoni for lab support.

Additionally, it is important to recognize my committee members, who have spent countless hours helping me on my path to becoming a better scientist. I sincerely appreciate all of the time and effort that you have invested. Chris, Jean and Brian, I only hope I can make you proud as I proceed further in my career as a scientist and a professional. Chris deserves particular recognition for his patience, wisdom, and guidance. I would also like to recognize my fellow graduate students. Thanks to Alex, Dylan, Jesse, Josee, Katia, Stacey, and Tyler for all the fun times on and off campus and impromptu rock talks. Thanks to the Hardrock Café crew for broadening my horizons every time I attended and helping me to develop as a critical thinker.

Thanks to Dylan Klazinga for eight wonderful years of friendship throughout our degrees at Waterloo. I will miss your incredible sense of humour. We had a bat screeching good time.

Finally, thank you to my friends and family. Your patience and continual support were greatly appreciated and did not go unnoticed. I owe you more than I could ever give back. I would also like to thank the Jennings family for their assistance with accommodations, which made field work more affordable and the pursuit of other techniques attainable.

My thesis has shown me that it takes a dedicated community to do science well, and that is a lesson I will carry forward through my entire career. Hopefully, I will be able to impart this key lesson to my students and mentees in the future.

For my Aunt Kathy

Who always took me to the beach and encouraged me to keep digging.

Table of Contents

Author's Declaration.....	ii
Statement of Contributions	iii
Abstract	iv
Acknowledgements.....	v
Dedication	vi
List of Figures	xii
List of Tables	xiii
1.0 Introduction.....	1
1.1 Economics and Applications of Graphite.....	2
1.2 Graphite Mineralization Models	6
1.3 Hypothesis and Research Objectives	10
2.0 Geology and Tectonic Setting.....	12
2.1 Introduction	12
2.2 Grenville Province in Ontario	12
2.2.1 Frontenac-Adirondack Belt	12
2.2.2 Composite Arc Belt	14
2.2.3 Pre-Grenvillian Laurentian Margin	14
2.2.4 Graphite in the Grenville Province.....	15
2.3 Summary of Previous Work.....	16
3.0 Geology of the Bissett Creek flake graphite deposit	18
3.1 Graphitic Gneisses.....	18
3.1.1 Biotite-Graphite-Quartzofeldspathic Gneiss	20
3.1.2 Clinopyroxene-Amphibole-Biotite-Graphite Gneiss.....	22
3.1.3 Garnet-Amphibole-Biotite-Graphite-Gneiss	23
3.1.4 Garnet-Biotite-Sillimanite-Graphite Gneiss	25
3.2 Barren Gneisses.....	27
3.2.1 Biotite-Quartzofeldspathic Gneiss.....	29
3.2.2 Amphibole-Biotite-Quartzofeldspathic Gneiss	29
3.2.3 Garnet-Sillimanite-Biotite Gneiss	31

3.3 Intrusive Units	32
3.3.1 Granitic Pegmatite	32
3.3.2 Metagabbro Intrusive.....	34
3.4 Structural Geology	34
4.0 Major and Trace Element Lithogeochemistry	39
4.1 Sample Collection and Preparation	39
4.2 Analytical Methods	40
4.3 Quality Assurance/Quality Control.....	41
4.4 Results	47
4.4.1 Biotite-Graphite-Quartzofeldspathic Gneiss	47
4.4.2 Clinopyroxene-Amphibole-Biotite-Graphite Gneiss.....	53
4.4.3 Garnet-Amphibole-Biotite-Graphite Gneiss.....	53
4.4.4 Garnet-Biotite-Sillimanite-Graphite Gneiss	54
4.4.5 Biotite-Quartzofeldspathic Gneiss.....	54
4.4.6 Amphibole-Biotite-Quartzofeldspathic Gneiss	55
4.4.7 Garnet-Biotite-Sillimanite Gneiss	56
4.4.8 Granitic Pegmatite	56
4.4.9 Metagabbro Intrusive.....	56
5.0 Stable Isotope Geochemistry	57
5.1 Carbon Isotopes.....	57
5.1.2 Methodology.....	59
5.2.2 Results	61
5.2 Sulfur Isotopes.....	65
5.2.1 Methodology.....	66
5.2.2 Results	67
6.0 Carbon Isotope Fractionation Modelling	72
6.1 Methodology	72
6.2 Results	75
7.0 Mineral Compositions and Geothermobarometry	77
7.1 Analytical Methods	77

7.2 Mineral Composition Results.....	78
7.2.1 Biotite-Graphite-Quartzofeldspathic Gneiss	78
7.2.2 Garnet-Amphibole-Biotite-Graphite Gneiss.....	79
7.2.3 Garnet-Sillimanite-Biotite-Graphite Gneiss	84
7.2.4 Amphibole-Biotite-Quartzofeldspathic Gneiss	88
7.2.5 Garnet-Amphibole-Biotite-Muscovite Schist.....	90
7.3 Thermobarometry	92
7.3.1 Thermobarometry Methods	92
7.3.2 Thermobarometry Results	94
8.0 Comparison with other Flake Graphite Deposits.....	98
8.1 Comparison with Flake Graphite Deposits in the pre-Grenvillian Laurentian Margin.....	98
8.2 Comparison with International Flake Graphite Deposits	99
9.0 Discussion	105
9.1 Rock Units and Potential Protoliths	105
9.2 Structural Controls on Mineralization.....	109
9.3 Pressure, Temperature and Fluid Conditions of Mineralization	109
9.4 Metamorphic History and Relative Timing of Mineralization.....	112
9.5 Carbon Source Responsible for Mineralization	113
9.6 Mineralization Process	117
10.0 Conclusions.....	120
11.0 Recommendations for Future Study	122
12.0 Recommendations for Graphite Exploration and Mining.....	123
References	124
Appendix A: Bissett Creek property structural measurements.....	139
Appendix B: Regional structural measurements.....	144
Appendix C: Sample information	147
Appendix D: Quality assurance and quality control data	150
Appendix E: Lithogeochemistry data	179
Appendix F: Microprobe calibration values and settings	192

Appendix G: Microprobe data – Part 1 – Plagioclase.....	197
Appendix G: Microprobe data – Part 2 – Potassium Feldspar.....	206
Appendix G: Microprobe data – Part 3 – Garnet.....	211
Appendix G: Microprobe data – Part 4 – Biotite.....	251
Appendix G: Microprobe data – Part 5 – Amphibole.....	276
Appendix G: Microprobe data – Part 6 – Sulfides.....	283

List of Figures

Fig. 1.1. Critical raw materials in the European Union as of 2017.....	5
Fig. 1.2. 2017 worldwide graphite production by country	6
Fig. 1.3. Graphitization process	8
Fig. 1.4. Graphite precipitation from crustal fluids	9
Fig. 2.1. Location of the Bissett Creek flake graphite deposit and simplified geology of the southwestern Grenville Province	13
Fig. 3.1. Geology classification for Bissett Creek	19
Fig. 3.2. Photos of the biotite-graphite-quartzofeldspathic gneiss.....	21
Fig. 3.3. Photos of the clinopyroxene-amphibole-biotite-graphite gneiss.....	24
Fig. 3.4. Photos of the garnet-amphibole-biotite-graphite gneiss	26
Fig. 3.5. Photos of the garnet-sillimanite-biotite-graphite gneiss.....	28
Fig. 3.6. Photos of the biotite-quartzofeldspathic gneiss	30
Fig. 3.7. Photos of the amphibole-biotite-quartzofeldspathic gneiss	31
Fig. 3.8. Photos of the garnet-sillimanite-biotite gneiss	32
Fig. 3.9. Photos of the granitic pegmatite	33
Fig. 3.10. Photos of the metagabbro intrusive	34
Fig. 3.11. Bissett Creek property geology map	36
Fig. 3.12. Equal area stereonet showing all structural measurements	37
Fig. 3.13. Photos of graphitic and barren gneiss contacts.....	38
Fig. 3.14. Photos of potential partial melting indicators.....	38
Fig. 4.1. Harker variance diagrams	50
Fig. 4.2. Carbonaceous chondrite normalized rare earth element plots.....	52
Fig. 4.3. Total alkali silica (TAS) diagram for igneous plutonic rock classification.....	55
Fig. 5.1. Total carbon (C_{Tot}) versus graphitic carbon (C_g) content	60
Fig. 5.2. Carbon isotope values for whole rock powders and potential reservoirs	63
Fig. 5.3. Carbon isotope value ranges for the graphitic gneisses.....	64
Fig. 5.4. Carbon isotope values ($\delta^{13}\text{C}_{\text{VPDB}}$) versus graphitic carbon (C_g)	65
Fig. 5.5. Sulfur isotope values for whole rock powders and potential reservoirs	69
Fig. 5.6. Sulfur isotope value ranges for the graphitic gneisses	70
Fig. 5.7. Sulfur isotope values ($\delta^{34}\text{S}_{\text{CDT}}$) versus total sulfur (S_{Tot})	71

Fig. 6.1. Distribution of carbon isotope values at the Bissett Creek deposit	73
Fig. 6.2. Graphite crystallized versus carbon isotope signature	73
Fig. 6.3. Carbon isotope modelling results	76
Fig. 7.2.1. Garnet cross sections for the biotite-graphite-quartzofeldspathic gneiss	79
Fig. 7.2.2. Feldspar classification for the biotite-graphite-quartzofeldspathic gneiss	80
Fig. 7.2.3. Garnet cross sections for the garnet-amphibole-biotite-graphite gneiss	82
Fig. 7.2.4. Feldspar classification for the garnet-amphibole-biotite-graphite gneiss.....	83
Fig. 7.2.5. Classification of calcic amphiboles	84
Fig. 7.2.6. Garnet cross sections for the garnet-sillimanite-biotite-graphite gneiss	85
Fig. 7.2.7. Feldspar classification for the garnet-sillimanite-biotite-graphite gneiss.....	87
Fig. 7.2.8. Garnet cross sections for the amphibole-biotite-quartzofeldspathic gneiss	89
Fig. 7.2.9. Feldspar classification for the amphibole-biotite-quartzofeldspathic gneiss	90
Fig. 7.2.10. Garnet cross sections for the garnet-amphibole-biotite-muscovite schist	91
Fig 7.2.11. Feldspar classification for the garnet-amphibole-biotite-muscovite schist	92
Fig. 7.3.1. Graphical representation of <i>P-T</i> estimate by type	97
Fig. 9.1. Trace metals (V, Mo, U) versus graphitic carbon (C_g) and total sulfur (S_{Tot}).....	107
Fig. 9.2. ACF classification of the graphitic gneisses showing potential protoliths.....	108
Fig. 9.3. Proposed process of graphite formation at the Bissett Creek flake graphite deposit ...	119

List of Tables

Table 1.1. Flake graphite size, purity and pricing.....	2
Table 1.2. Graphite uses by physical property.....	3
Table 1.3. Thesis structure	11
Table 2.1. Summary of previous work.....	17
Table 4.1. Quality assurance and quality control information for major elements.....	43
Table 4.2. Quality assurance and quality control information for minor and trace elements.....	44
Table 4.3. Summary of geochemical results	48
Table 5.1. Carbon isotope values and abundances	62
Table 5.2. Sulfur isotope values.....	68
Table 7.3.1. Conventional thermobarometry results.....	95
Table 7.3.2. Thermobarometry results from THERMOCALC.....	96
Table 8.1. Summary of selected flake graphite occurrences in the pre-Grenvillian Laurentian Margin.....	100
Table 8.2. Summary of international flake graphite occurrences	104

“Always remember, never accept the world as it appears to be.

Dare to see it for what it could be.”

- Dr. Harold Winston

1.0 Introduction

One of the most important aspects of successful exploration and production of mineral resources, independent of the commodity, is understanding of the timing and mechanisms of mineralization ([Jebrak and Marcoux, 2014](#)). Frequently, this geologic knowledge is expressed in the form of genetic mineralization models detailing the source, transport mechanisms and traps of minerals of economic interest ([Jebrak and Marcoux, 2014](#)). Accurate genetic models, in turn, can be used to expand resources, increase extraction efficiency and prioritize exploration targets. One of the best ways to develop regional models is through the investigation of mineral deposits at active exploration and mining sites where the preliminary extent and nature of mineralization are known. Exploration and mining sites can provide a spatial, geochemical and geochronological context for mineralization because of the established infrastructure and availability of geological data. The role of this study is to establish a genetic model by constraining the conditions of formation for the Bissett Creek flake graphite deposit.

The prominence of graphite is increasing because it is incorporated into many new technologies, particularly those in the green energy sector. Flake graphite is desirable because of its high purity, which is important for high-end applications such as lithium-ion batteries, and large size which reduces processing costs when compared to fine-grained amorphous deposits ([Scogings, 2015](#)).

The Bissett Creek flake graphite deposit is one of the best natural laboratories available for the evaluation of flake graphite mineralization in the pre-Grenvillian Laurentian Margin (formerly known as the Central Gneiss Belt ([Carr et al., 2000](#))) of Ontario because a key factor affecting the economic viability of graphite deposits is flake size (Table 1.1). The Bissett Creek deposit was selected for this study because of the large size of the flake graphite. Nearly 70% of the graphite at the Bissett Creek deposit can be classified as large or extra-large flake graphite ([Rosseau and Duplessis, 2010](#)). Large flake graphite is graphite that is 180 to 300 μm in diameter, while extra large flake graphite is any graphite that is >300 μm in diameter ([Scogings, 2015](#)). Flake graphite is more highly sought after than finer grained or amorphous graphite since larger flake graphite produces a higher purity concentrate (90–97% C) ([Scogings, 2015](#)). Higher purity concentrates are of greater value to high-tech and green electronic applications ([Scogings, 2015](#); Table 1.1). Furthermore, as higher purity graphite end-products become available through

**Table 1.1. Flake graphite size, purity and pricing
(modified from Scogings, 2015)**

Graphite Classification	Flake Size (μm)	Purity of End Product (%C)	Approximate Price/Tonne (\$US)
Extra Large Flake Graphite	>300	90 - 97	2,000
Large Flake Graphite	180 - 300	91 - 97	1,300
Medium Flake Graphite	150 - 180	92 - 97	1,100
Small Flake Graphite	75 - 150	93 - 97	750
Amorphous Graphite	<75	80 - 85	450

new processes such as thermal and acid leaching techniques, it is likely that the number of applications for graphite will continue to increase (Olson, 2014).

Bissett Creek was also selected because of easy access to the deposit, pre-existing infrastructure on the property, and good regional outcrop exposure. These features facilitated easier access to rock exposures which were helpful when determining the source of carbon that formed the graphite in the deposit, potential transport pathways for carbon-bearing fluids, and the physiochemical mechanisms responsible for graphite mineralization. Assessing these three factors will provide a better understanding of both the Bissett Creek deposit, other deposits in the pre-Grenvillian Laurentian Margin, and international graphite deposits.

1.1 Economics and Applications of Graphite

Graphite is an important material for manufacturing a variety of products because of its unique physical properties (Table 1.2). Graphite's physical properties include high thermal conductivity, high electrical conductivity, low coefficient of friction, chemical inertness, low absorption of neutrons and X-rays, and resistance to high temperatures (Beyssac and Rumble, 2014). It is involved in the production of electric motors, batteries, pencils, lubricants, rubber, sporting equipment and is critical in several industries such as steelmaking, laboratory analyses, solar and nuclear energy (Spence, 1920; Hewitt, 1965; Garland, 1987; Mackinnon and Lebaron, 1992; Kelly *et al.*, 2005). Graphite is of interest to the steelmaking and laboratory analyses industries because of its use in refractories (Olson, 2012). Worldwide consumption of graphite has been continuously increasing since 2012 because of the introduction of graphite into many

Table 1.2. Graphite uses by physical property
(modified from Beyssac and Rumble, 2014)

Products containing or manufactured with graphite	Physical Property					
	High Electrical Conductivity	High Thermal Conductivity	Low Coefficient of Friction	Chemical Inertness	Resistance to thermal shock, low expansion coefficient	High Temperature Resistance
Batteries	✓			✓		
Carbon Brushes			✓			
Electrodes in electrical ovens	✓			✓	✓	
Refractories		✓		✓	✓	✓
Manufacturing of brakes & clutch linings		✓			✓	✓
Crucibles		✓		✓	✓	✓
Foundry Additives			✓			✓
Foundry Moulds		✓	✓			✓
Steel, Alloys					✓	✓
Pencils			✓			
Lubricants	✓	✓	✓			
Nuclear Industry				✓		✓

new applications such as electric vehicles, high-end electronics, fuel cells and a variety of other green technologies ([Olson, 2016](#)). As a result, both the United States (U.S.) and the European Union (EU) have designated natural graphite as a strategic and/or critical mineral (Fig. 1.1) ([European Commission, 2017](#); [Krauss *et al.*, 1988](#)).

A critical mineral is a mineral that meets two criteria ([European Commission, 2017](#); [National Research Council, 2008](#)). First, there must be a risk to supply. For the EU, the risk to supply is determined by an assessment of the political stability of the region hosting the commodity, the ability to substitute the mineral for another mineral or material, and the ability to recycle the mineral ([Graedel *et al.*, 2014](#)). The second criterion is that the mineral must be a material of high economic importance ([European Commission, 2017](#)). In the EU, the economic importance is determined in two steps ([European Commission, 2017](#)). The first step measures the proportion of the material consumed by major industries (e.g. steel manufacturing), which is then

combined with the gross value that the commodity contributes to the EU Gross Domestic Product (GDP). The second step is to scale the value against the total EU GDP. In the U.S., another criterion used is the impact of supply disruption to the economy (Graedel *et al.*, 2014). The strategic mineral classification modifies the second criterion such that instead of having a high economic importance, it has a high military or strategic importance (National Research Council, 2008).

The world graphite supply has recently become a subject of concern due to the large proportion of graphite produced by China. China has been a dominant supplier of graphite since the 1990s when the country extensively developed their graphite deposits and flooded the market, making other graphite mining and production operations unprofitable (Fauvet, 2000; Mining Markets, 2012; Green, 2013). China produced nearly 67% of the world's natural graphite in 2017 (Fig. 1.2) (Olson, 2016). China's willingness to halt the supply of mineral exports to countries over political disputes, such as the recent cut-off of rare earth elements to Japan (e.g. Humphries, 2013), has left many in the global market searching for alternative sources of natural graphite. Thus, to diversify the mineral supply chain and decrease the supply risk for graphite, it is important for Canada to develop its own supply. Thus, regional scale genetic models of graphite mineralization that can be used to prioritize exploration and promote graphite mining are needed.

In 2015, the United States required 65,900 tons of graphite for a variety of end uses (Olson, 2016). Tesla Motors had further stipulated that the production of new electric vehicles will require an additional 93,000 to 126,000 tons of flake graphite per year for use as anode materials which is to be sourced from North America (Moores, 2014; Olson, 2016). Increased demand for natural graphite, the lack of domestic graphite production in the United States, the high number of undeveloped graphite resources in the southwestern Grenville Province, and the fact that Canada already supplies 2.5% of current U.S. demand means that Canada, specifically Ontario and Quebec, are well poised to enter the world graphite market.

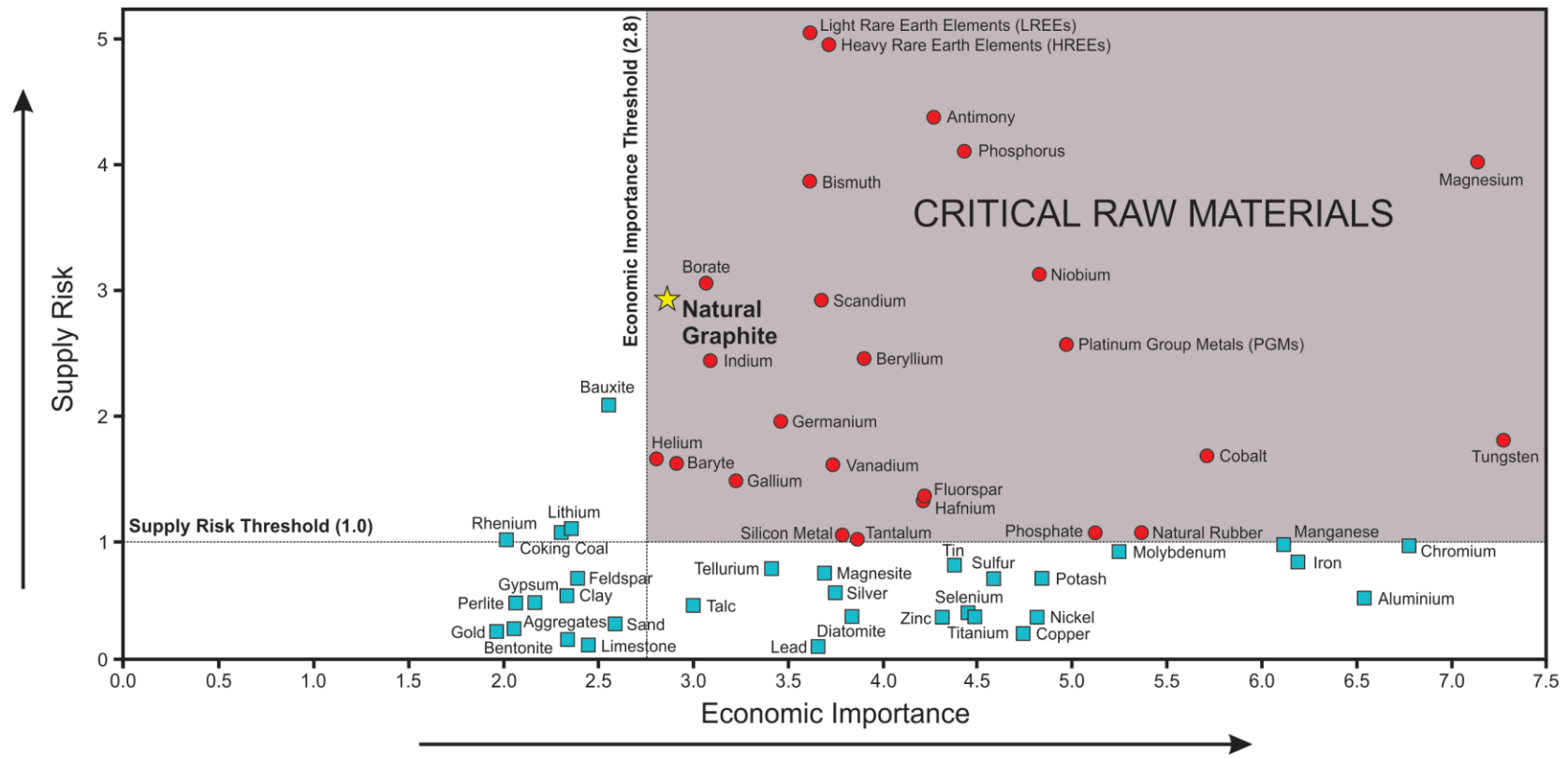


Fig. 1.1. Critical raw materials in the European Union as of 2017 (modified from [European Commission \(2017\)](#)). Due to the high importance of natural graphite in several applications, and the dominance of the market by certain countries, predominantly China, natural graphite (denoted by the star) plots within the critical domain indicated by the dark-grey shaded area.

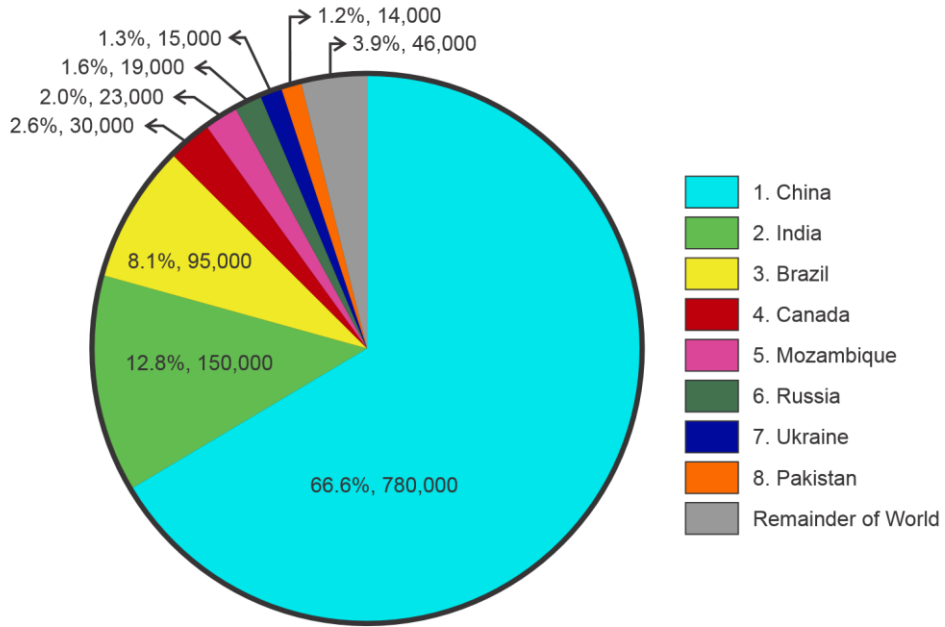


Fig. 1.2. 2017 Worldwide graphite production by country. Data from [Olson \(2018\)](#). The first number is the percentage of the world's total graphite production that a specific country accounts for, while the second number is the amount of graphite produced in metric tons. Countries are ranked in order of production from first to eighth. The remaining production has been lumped into the remainder of world category.

1.2 Graphite Mineralization Models

There are currently two main genetic models that describe flake graphite mineralization ([Beyssac and Rumble, 2014](#); [Luque et al., 2012](#)). These two end-member models include the generation of graphite through metamorphic processes, also known as graphitization, and the deposition of graphite by hydrothermal fluids ([Beyssac and Rumble, 2014](#); [Luque et al., 2012](#)). Because these two processes are end members, some graphite deposits are postulated to be formed through both metamorphism and hydrothermal deposition ([e.g. Papineau et al., 2010](#); [Luque et al., 2012](#)).

Graphitization begins with sedimentary rocks that are host to organic compounds. To generate graphite from organic materials, there are two main steps ([Buseck and Beyssac, 2014](#)). The first step is carbonization, which is the formation of kerogen as a direct result of the burial of sediments and diagenesis ([Buseck and Beyssac, 2014](#)). During diagenesis, the carbonaceous

material is heated causing the kerogen to crack and undergo a series of decomposition reactions, producing oil and gas as well as a carbon-rich residue (Vandenbroucke and Largeau, 2007). At this point, the hydrocarbons can leave the source rock or can be trapped. The carbon-rich residue is composed of a complex set of organic compounds made of carbon, hydrogen, oxygen, nitrogen, and sulfur (Buseck and Beyssac, 2014). This residue is the carbon source for further graphitization (Buseck and Beyssac, 2014). The second step of graphitization involves an increase in temperature, which results in the conversion of the disordered carbonaceous material into crystalline graphite (Fig. 1.3).

The precipitation of graphite from carbon-rich hydrothermal fluids is a second mechanism that can generate graphite deposits (Luque *et al.*, 2012; Rumble, 2014). There are four processes that generate carbon-rich fluids, including: (1) the exsolution of volatiles from magmas during crystallization or ascent, (2) the release of fluids from metamorphic rocks due to changes in pressure and temperature, (3) interaction of H₂O-rich hydrothermal fluids with carbonate-rich sediments, and (4) the release of methane from heated organic debris (Rumble, 2014). Although graphitic carbon is generally insoluble in pure H₂O, the pressure and temperature conditions associated with crustal burial can allow carbon to be transported as a variety of molecular species such as CO₂, CH₄, HCO₃⁻, and CO₃²⁻ (Rumble, 2014).

Three main physiochemical processes can precipitate graphite from a CO₂ and/or CH₄ enriched fluid: (1) an increase in pressure, (2) a decrease in temperature, or (3) fluid mixing (Ferry and Baumgartner, 1987; Spear, 1995). These processes are summarized on a carbon-oxygen-hydrogen (C-O-H) ternary diagram in Fig. 1.4. Graphite precipitation can occur during an increase in pressure (Fig. 1.4A), a decrease in temperature (Fig. 1.4B), or during the mixing of a relatively hydrogen-rich fluid with that of a relatively oxygen-rich fluid (Fig. 1.4C).

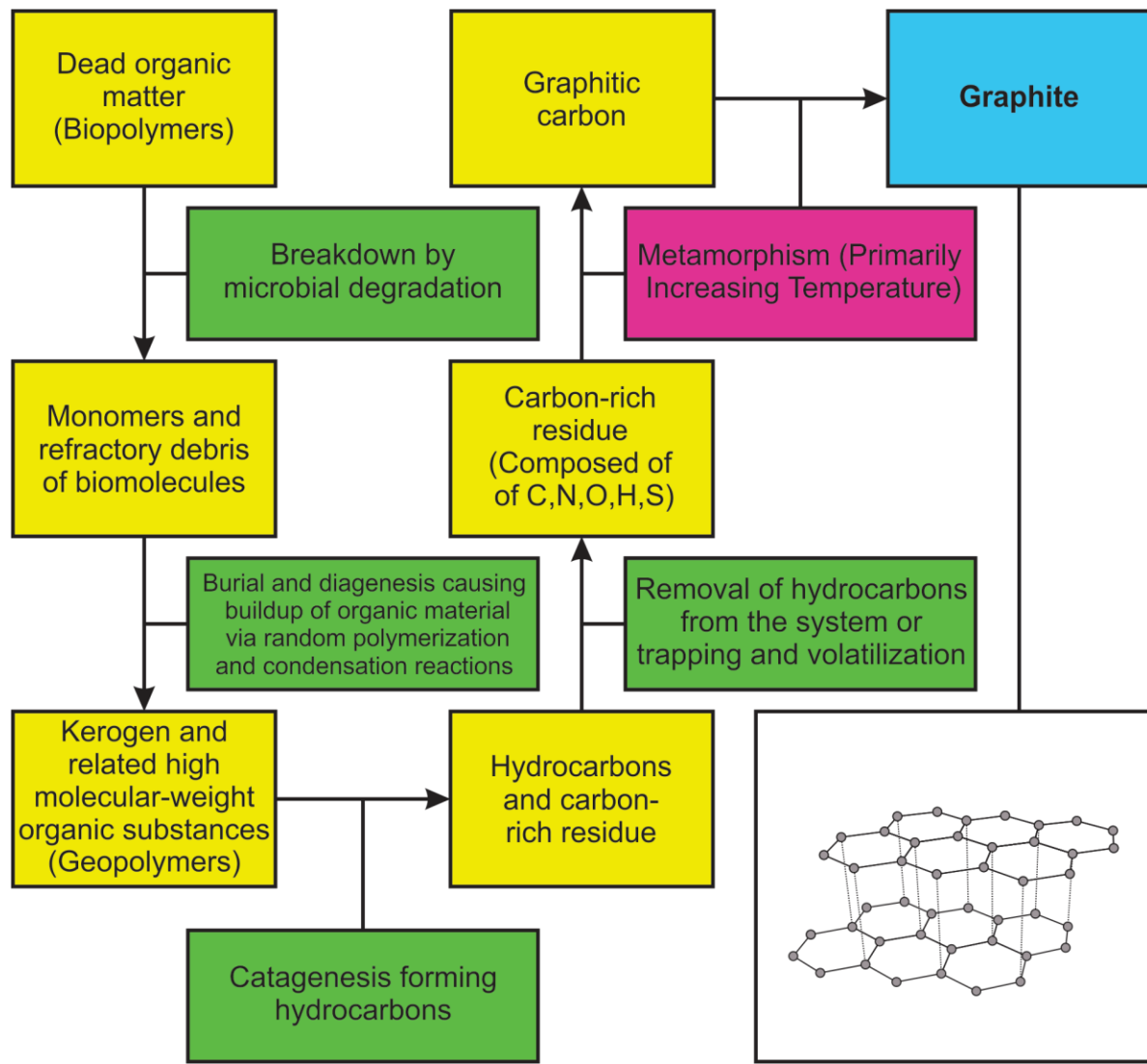


Fig. 1.3. Graphitization process compiled from Schidlowski (2001), Vanderbroucke and Largeau (2007) and Buseck and Beyssac (2014). Temperatures of metamorphism greater than 200°C are required to transform organic carbon into graphitic carbon, while temperatures greater than 650°C are required to generate fully ordered graphite (Beyssac *et al.*, 2002; Buseck and Beyssac, 2014).

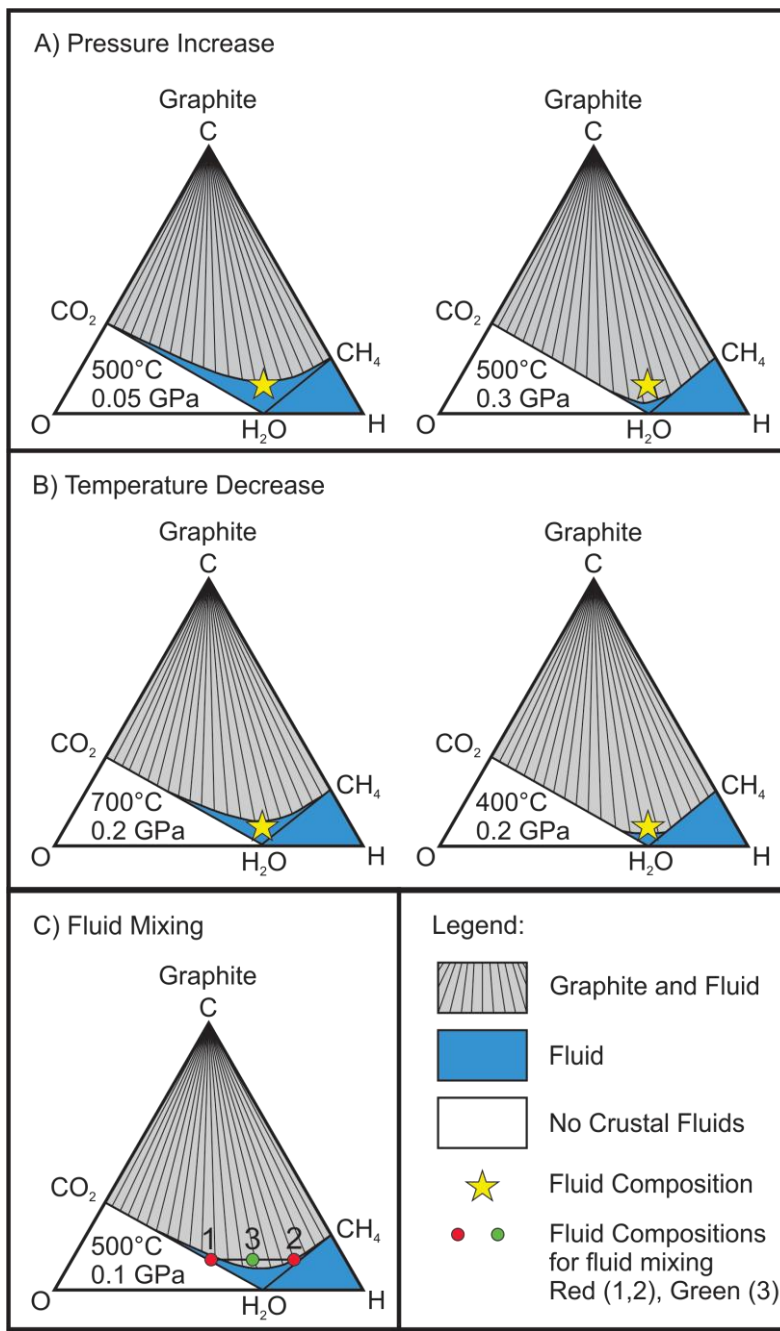


Fig. 1.4. Graphite precipitation from crustal fluids. C-O-H phase diagrams modified from Spear (1995), Ferry and Baumgartner (1987) and Rumble (2014). The yellow stars in A and B represent a constant arbitrary fluid composition. (A) The increase in pressure in from 0.05 to 0.3 GPa expands the graphite stability field (grey) allowing for graphite to precipitate. (B) Decreasing temperature from 700°C to 400°C expands the graphite stability field and allows graphite to precipitate. (C) Graphite precipitation from fluid mixing. Fluid 1 (red circle left) is composed of CO₂ and H₂O, while fluid 2 (red circle right) is composed of CH₄ and H₂O. While neither fluid individually plots within the graphite stability field, a mixture of the two fluids (fluid 3 - green center circle) can.

1.3 Hypothesis and Research Objectives

[Garland \(1987\)](#) suggested a metamorphic origin (carbonization and graphitization) for the flake graphite found at the Bissett Creek deposit based upon petrographic observations and a single measured carbon isotope value. This thesis evaluates whether a solely metamorphic origin for this deposit is adequate, or if additional mechanisms were responsible for mineralization.

I investigate the petrogenesis of the Bissett Creek flake graphite deposit through the following objectives:

1. Determine the protoliths and differentiate each of the rock units found on the Bissett Creek property and nearby road outcrops.
2. Determine the source of the carbon that formed graphite in the Bissett Creek deposit and the surrounding area.
3. Elucidate if and how geologic structure-controlled mineralization.
4. Reconstruct the temperature, pressure and, if required, fluid conditions at the time of graphite deposition.
5. Develop a metamorphic history for the local site and regional outcrops and determine when and how graphite mineralization fits into this history.
6. Evaluate if the graphite was generated through *in situ* metamorphic processes, through the introduction of hydrothermal fluids, or through some combination of both.
7. Compare and contrast the results of this study with other graphite deposits in the pre-Grenvillian Laurentian Margin to develop a regional genetic model.

Some of the preliminary results of this thesis were published in [Taner et al. \(2017\)](#) on which I was a co-author. This thesis expands on these results with more detailed petrographic observations, structural observations, mapping, a larger carbon isotope dataset, a sulfur isotope dataset, more refined stable isotope modelling, thermobarometry and comparison with other flake graphite deposits in Ontario and around the world. To address these objectives, the thesis will be structured as seen in Table 1.3.

Table 1.3. Thesis structure

Chapter #:	Chapter Title	Research Objectives Addressed
1.0	Introduction	None
2.0	Regional Geology and Tectonic Setting	3, 5
3.0	Geology of the Bissett Creek flake graphite deposit	1, 2, 5
4.0	Major and Trace Element Lithogeochemistry	1
5.0	Stable Isotope Geochemistry	1, 2, 6
6.0	Carbon Isotope Fractionation Modelling	2, 6
7.0	Mineral Compositions and Thermobarometry	4, 6
8.0	Comparison with other Flake Graphite Deposits	7
9.0	Discussion	1 - 7
10.0	Conclusions	1 - 7
11.0	Recommendations for Further Study	6
12.0	Recommendations for Graphite Exploration and Mining	None

2.0 Geology and Tectonic Setting

2.1 Introduction

The Bissett Creek graphite deposit is located approximately 300 km NNE of Toronto, Ontario and lies just south of the Ontario–Quebec border along the Ottawa River in the Algonquin Terrane of the pre-Grenvillian Laurentian Margin of the Grenville Province (Fig. 2.1). The Algonquin Terrane formed due to the accretion of 1800–1690 Ma arc-related rocks to the margin of the Archean Laurentian craton (Carr *et al.*, 2000). After accretion, the pre-Grenvillian Laurentian Margin underwent several episodes of deformation and metamorphism, including: (1) >1600 Ma events from pre-Grenvillian periods of metamorphism and deformation, (2) 1450–1420 Ma events associated with the intrusion of volumetrically significant plutons and other magmatic activity, and (3) 1120–980 Ma compressional and extensional tectonism related to the formation of the Grenville Orogen as a result of the collision of Laurentia with Amazonia (Carr *et al.*, 2000; Li *et al.*, 2008; Rivers *et al.*, 2012).

2.2 Grenville Province in Ontario

The Grenville Province in Ontario is made up of three lithotectonic domains, each with a distinct tectonic history (Fig. 2.1). From east to west, these are the Frontenac–Adirondack Belt, the Composite Arc Belt and pre-Grenvillian Laurentia and its margin (Carr *et al.*, 2000).

2.2.1 Frontenac-Adirondack Belt

The Frontenac-Adirondack Belt is composed of three distinct lithotectonic domains that share a common magmatic and metamorphic history (Carr *et al.*, 2000). The domains, from east to west, are the Adirondack Highlands, the Adirondack Lowlands, and the Frontenac Terrane. The Frontenac-Adirondack Belt is bounded in the West by the Maberly Shear Zone and in the East by overlying Paleozoic rocks (Fig. 2.1). The Adirondack Highlands are predominantly composed of the 1150–1125 Ma Marcy Anorthosite and anorthosite-mangerite-charnockite-granite granitoid rocks and corresponding orthogneisses (McLelland *et al.*, 1996; McLelland *et al.*, 2010). However, some minor occurrences of marble and quartzofeldspathic gneiss have also been noted within this domain. Compared to the Adirondack Highlands, the Adirondack Lowlands and Frontenac Terrane are composed of supracrustal rocks such as quartzofeldspathic gneisses, quartzites, and marbles (McLelland *et al.*, 1996; McLelland *et al.*, 2010).

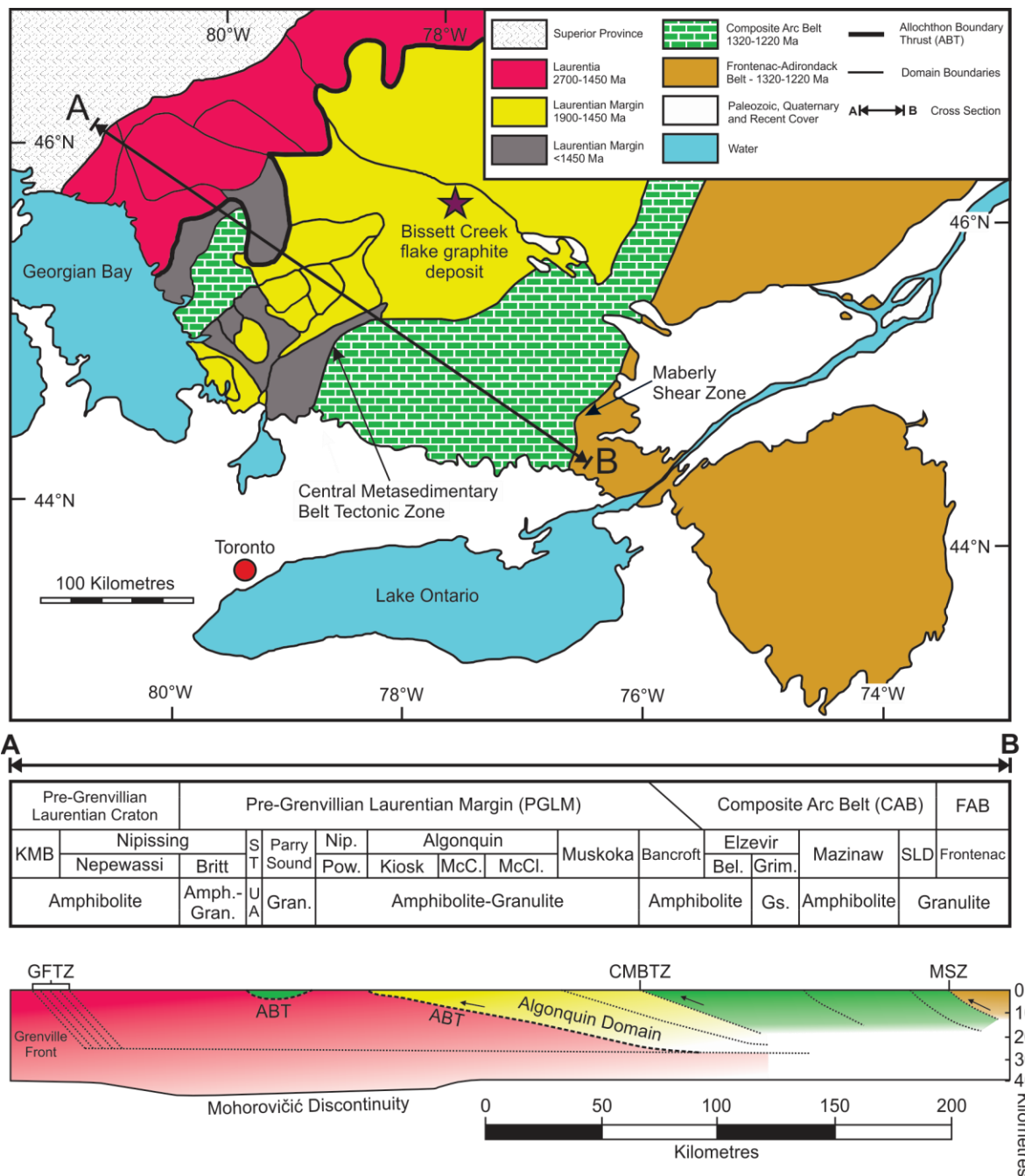


Fig. 2.1. Location of the Bissett Creek flake graphite deposit and simplified geology of the southwestern Grenville Province (modified from Carr *et al.*, 2000). A simplified cross section showing the traverse from A to B shows the key structural domains of the Grenville Province (Modified from Carr et al., 2000). Fig. 2.1 Terms: GFTZ – Grenville Front Tectonic Zone, ABT – Allochthon Boundary Thrust, CMBTZ – Central Metasedimentary Belt Tectonic Zone, MSZ – Maberly Shear Zone, FAB – Frontenac-Adirondack Belt, ST – Shawanaga Domain, Nip. – Nipissing, Pow. – Powassan, McC. – McCraney, McCl. – McClintock, Bel. – Belmont, Grim. – Grimsthorpe, SLD – Sharbot Lake Domain, Amph – Amphibolite, Gran. – Granulite, Gs. – Greenschist, UA – Upper Amphibolite.

All the domains underwent amphibolite- to granulite-facies metamorphism at around 1160 Ma. However, the Frontenac Terrane and Lowlands underwent lower grade metamorphism (~650°C, 0.6 GPa) whereas, the Highlands underwent high-grade metamorphism (~800°C, 0.8 GPa) (McLelland *et al.*, 2010). Further high-pressure granulite-facies metamorphism of the Adirondack Highlands also took place from approximately 1070 to 1040 Ma (Carr *et al.*, 2000).

2.2.2 Composite Arc Belt

The Composite Arc Belt (previously known as the Central Metasedimentary Belt (Carr *et al.*, 2000)) is composed of greenschist- to amphibolite-facies marbles, paragneisses, and orthogneisses (Van der Pluijm and Carlson, 1989; Carr *et al.*, 2000). It is bounded to the west by the Central Metasedimentary Belt Tectonic Zone (CMBTZ) and to the east by the Maberly Shear Zone (Fig. 2.1). The CMBTZ is a major shear zone that contains the highly deformed equivalents of rocks found in the Composite Arc Belt (Hamner *et al.*, 1985). Thus, the Composite Arc Belt can be distinguished from the underlying rocks of the pre-Grenvillian Laurentian Margin by the decrease in metamorphic grade from upper amphibolite-granulite to greenschist-amphibolite and the presence of a major structural boundary (Rivers *et al.*, 2012, and references therein).

2.2.3 Pre-Grenvillian Laurentian Margin

Pre-Grenvillian Laurentia and its margin (previously known as the Central Gneiss Belt (Carr *et al.*, 2000)) are bounded to the west by the Grenville Front Tectonic Zone (GFTZ) and to the east by the Central Metasedimentary Belt boundary thrust zone (Fig. 2.1). Both boundaries are major shear zones that were active during Grenville orogenesis (Davidson *et al.*, 1985). In Ontario, Pre-Grenvillian Laurentia is made up of gently dipping, upper-amphibolite to granulite facies orthogneiss interleaved with a minor supracrustal rock component (Ketchum and Davidson, 2000). It has been subdivided into several thrust sheets that represent different structural levels with distinct tectonometamorphic histories; individual sheets are bounded by high strain zones (Davidson and Morgan 1981; Culshaw *et al.*, 1983; Davidson 1984; Davidson *et al.*, 1985; Rivers *et al.*, 1989).

The Algonquin Terrane represents the lowest structural level of Laurentian Margin rocks (Fig. 2.1) and it is underlain by rocks of the pre-Grenvillian Laurentian Craton and overlain by migmatitic gneisses of the Muskoka Domain (Carr *et al.*, 2000). The Algonquin Terrane also

forms the structurally lowest allochthonous unit in the series of thrust sheets (Fig. 2.1; [Ketchum and Davidson, 2000](#)). The western margin of the lower thrust sheet is known as the allochthon boundary thrust (ABT) ([Ketchum and Davidson, 2000](#)). Both [Carr et al. \(2000\)](#) and [Ketchum and Davidson \(2000\)](#), identify two major periods of pre-Grenvillian magmatism in the region spanning from 1.8 Ga to 1.6 Ga and 1.5 Ga to 1.4 Ga. Plutons that intruded during the Grenville Orogeny only represent a small portion of exposed crust ([Ketchum and Davidson, 2000](#)). The main metamorphic episode recorded in the Algonquin Terrane comes from the Ottawan phase of the Grenville Orogeny between 1080 and 1020 Ma ([Rivers et al., 2012](#)). Peak metamorphic conditions in the allochthonous medium pressure belt, which the Algonquin Terrane is a part of, mostly range from 800-900°C and $1.0 \pm 0.2\text{GPa}$ ([Rivers et al., 2012](#), and references therein).

2.2.4 Graphite in the Grenville Province

Historically, graphite has been mined from graphite-bearing marbles in the Composite Arc Belt of the Grenville Province ([Garland, 1987](#)). However, the larger tonnage deposits with lower graphite content which are of economic interest due to the prospect of open-pit mining, are more commonly found in the pre-Grenvillian Laurentian Margin ([Garland, 1987](#)). Graphite-bearing units of the pre-Grenvillian Laurentian Margin are quartz-biotite schists, quartz-feldspar-biotite gneisses as well as semi-pelitic and pelitic schists and gneisses that are part of larger paragneiss sequences ([Davidson, 1982; Garland, 1987](#)). The carbon present in the paragneiss sequence is thought to be of biogenic origin based on $\delta^{13}\text{C}$ analysis on graphite (e.g. [Garland, 1987; Taner et al., 2017](#)), and graphite is thought to have been generated during metamorphism of carbonaceous shales, siltstone or greywackes ([Davidson, 1982; Garland, 1987](#)). Deposition of these sedimentary rocks predated the Ottawan phase of Grenvillian metamorphism from approximately 1080 to 1020 Ma and postdated formation of the Laurentian basement ~1450 Ma ([Carr et al., 2000; Rivers et al., 2012](#)). Graphite occurrences appear to be limited to the lowest allochthonous thrust sheet of the pre-Grenvillian Laurentian Margin in paragneisses of upper amphibolite to granulite grade ([Gignac et al., 2012](#)).

Graphite-bearing units in the pre-Grenvillian Laurentian Margin extend from hundreds of meters to kilometers along strike and have highly variable widths of meters to kilometers ([Garland, 1987](#)). These layers are frequently sulfide bearing and so weather to a rusty colour on the surface ([Davidson, 1982](#)). The weathering of the surficial graphite-bearing paragneisses to a

rusty gossan has been used as an exploration tool when locating graphite deposits in the pre-Grenvillian Laurentian Margin ([Garland, 1987](#)).

2.3 Summary of Previous Work

Exploration for graphite throughout the Grenville Province of Ontario has been conducted since the 1800s ([Storey and Vos, 1981](#)). However, very little of the early work was recorded. Historical graphite production in Ontario arose from disseminated flake graphite and high graphite content lenses associated with marbles, sometimes with accompanying interbedded gneisses, in the Composite Arc Belt ([Garland, 1987](#)). The most noteworthy of these deposits was the Black Donald graphite deposit, which was in sporadic operation from 1896 until 1954 ([Garland, 1987](#)). However, larger tonnage deposits hosted in siliceous metasediments with lower graphite contents, such as Bissett Creek, became more favourable as it became apparent that they could be mined through open pit methods ([Garland, 1987](#)).

The Bissett Creek flake graphite deposit has had numerous owners, companies, contractors, and members of government agencies complete work on the site (Table 2.1). Two publications discuss the potential origins of the deposit. [Garland \(1987\)](#) postulated that the flake graphite in the deposit formed because of the *in situ* metamorphism of organic materials based on 1) the disseminated nature of the graphite, 2) the restriction of the graphite to a quartz-rich metasedimentary horizon, 3) the light carbon isotope value of the graphite and 4) REE concentrations that are consistent with greywackes.

[Taner et al., \(2017\)](#) re-examined this hypothesis and provided reconnaissance-scale datasets for the petrography of the host rocks, carbon isotopes of graphite, and an isotope fractionation model. [Taner et al., \(2017\)](#) also favoured a metamorphic origin for the deposit but instead suggested that the flake graphite formed due to precipitation from fluids formed because of the breakdown of organic materials during metamorphism. This model of graphite mineralization at the Bissett Creek deposit is thought to be supported by 1) the disseminated nature of the flake graphite, 2) the graphite size distribution consistency with other metamorphic deposits, 3) the graphite intergrowth with metamorphic minerals, and 4) the wide range of carbon isotope values from the site, consistent with fractionation from a carbonic fluid.

Table 2.1. Summary of previous work
(Gignac et al., 2012; Wilson, 2013)

Company/Contributor Name(s):	Year(s)	Work Completed
S. Lumbers	1976	Regional Geological Map
Ontario Department of Mines		
Tagliamonte and Associates	1980	Staked Property
Donegal Resources Corp.	1980	Magnometer Survey, Trenching
Hartford Resources Inc.	1981 - 1984	Very Low Frequency Electromagnetic Survey, Trenching
D.G. Innes Consulting Geologist	1982	Preliminary Report
Princeton Resources Corp.	1984 - 1986	Stripping, Trenching, Mapping Sampling, Drilling, Bulk Sample (~3300 tonnes)
U. Schmidt Consulting Geologist	1985	Summary Report
Consolidated North Coast Industries	1986 - 1991	Stripping, Trenching, Mapping, Bulk Sampling (60 tonnes), Drilling, Metallurgical Testing, Reserve Calculation, Preliminary Feasibility Study
M. Garland Ontario Geological Survey Mines and Minerals Division	1987	Sampling, Petrography, Carbon Isotope, Rare Earth Element Geochemistry
Industrial Minerals Canada Inc.	2002 - 2007	Beneficiation Studies, Bulk Sampling (63.5 tonnes), Prospecting, Trenching, Drilling
Northern Graphite Corp.	2009 - Present	Drilling, Bulk Sampling, Metallurgical Testing, Pilot Plant Testing, Graphene Production Testing
M. Taner Consulting Geologist	2010-2012	Drilling Reports Petrography and Mineralogy Report
G Mining Services Inc.	2012	Preliminary Feasibility Study
M. Taner C. Drever C. Yakymchuk F. Longstaffe	2017	Research Paper Petrography Carbon Isotopes & Modelling

3.0 Geology of the Bissett Creek flake graphite deposit

This chapter provides the field relationships, structural geology, and petrography of units at the Bissett Creek deposit. [Taner \(2011\)](#) provided the first in-depth petrological study of the various geological units at the Bissett Creek flake graphite deposit. A feasibility study completed in 2012 and updated in 2014 estimated 40.5 Mt of potentially economically extractable resources with a graphitic carbon content of 1.83% (Gignac et al., 2012; Northern Graphite, 2014). The project is currently in the process of raising funds to cover its capital expenditures so that it can commence operations. I completed additional fieldwork and mapping of the deposit in June 2016, October 2016 and June 2017 to provide further insight into the property's geology. Three main lithological groups were identified, including graphitic gneisses, barren gneisses, and intrusive rocks. These three groups were further subdivided into nine distinct geological units based on the mineralogy, textures, and structures (Fig. 3.1). Where possible, mineral end-members have been identified from electron microprobe data, which will be discussed further in Chapter 7.0. The structural and petrographic evidence presented in this chapter will be used to address Research Objectives 1, 2, and 5.

3.1 Graphitic Gneisses

Graphitic gneisses are located within the Bissett Creek flake graphite deposit and along the regional transect defined by the trajectory of Highway 17. These gneisses can be subdivided into four geological units based on distinct metamorphic mineral assemblages. These four units are the biotite-graphite-quartzofeldspathic gneiss, the clinopyroxene-amphibole-biotite-graphite gneiss, the garnet-amphibole-biotite-graphite gneiss and the garnet-sillimanite-biotite-graphite gneiss. The different graphitic gneiss units have gradational contacts that range in scale from decimeters to meters. The graphitic gneiss units are most easily differentiated from the barren gneisses by the rusty orange-brown colour of the weathered surface and the presence of graphite flakes. Weathering can permeate to a depth of greater than 1 m. Due to the friability of the rock as a result of intense weathering, the graphitic gneiss unit is recessive relative to the surrounding barren gneisses. In extreme cases, outcrops of this unit are covered by graphite-rich orange sand. From drill core, it has been noted that sections with high graphitic carbon (C_g) contents of 3–4 wt. % commonly coincide with fault zones.

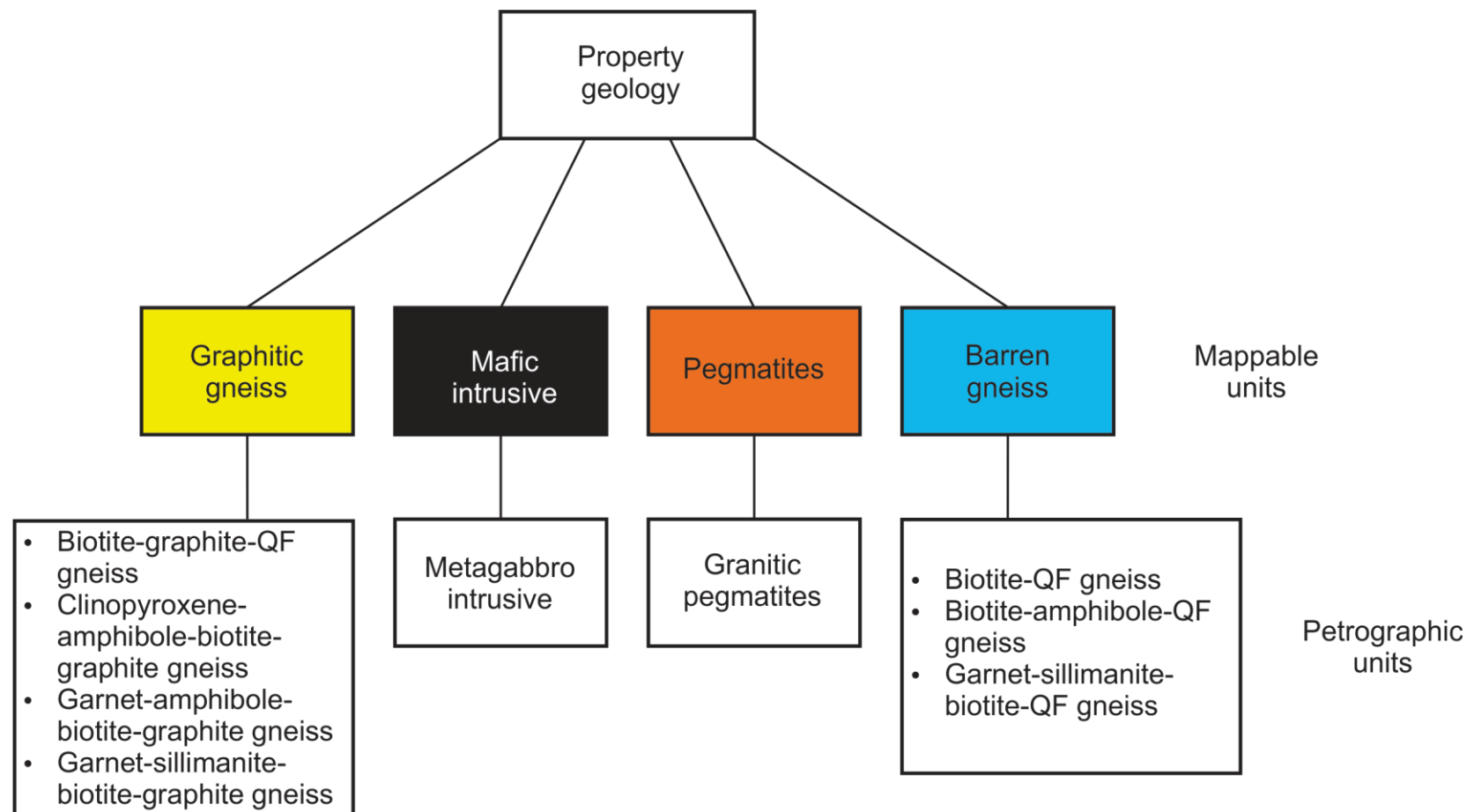


Fig. 3.1. Classification of various geological units at the Bissett Creek flake graphite deposit. QF – Quartzofeldspathic.

3.1.1 Biotite-Graphite-Quartzofeldspathic Gneiss

In outcrop, the biotite-graphite-quartzofeldspathic gneiss typically presents as a weathered rusty orange-brown colour (Fig 3.2A). Outcrops with relatively high proportions of sulfide minerals can also show a slight yellow colouration. Fresh surfaces are light- to medium-grey in colour (Fig 3.2B). Grain size usually ranges from medium (0.3 mm) to coarse-grained (>1.0mm). The foliation is defined by the parallel alignment of biotite and graphite, which are homogeneously distributed throughout the rock.

In order of decreasing abundance, the biotite-graphite quartzofeldspathic unit is composed of quartz, plagioclase feldspar (andesine), potassium feldspar, biotite, graphite, pyrrhotite and pyrite with or without garnet and minor amphibole (edenite). Accessory minerals include titanite, allanite, chalcopyrite, and sphalerite. In thin section, alignment of biotite and graphite define the dominant foliation (Fig. 3.2C). In some cases, a gneissosity is present that is defined by biotite-rich domains and quartz-rich domains.

Quartz and feldspar grains are xenoblastic and some show undulose extinction. Biotite forms irregularly shaped lathes that are smaller in size than the surrounding quartz and feldspar grains. The abundance of biotite in this unit is highly variable ranging from approximately 5 vol.% to approximately 25 vol.%. Biotite can also occur as inclusions in graphite grains (Fig. 3.2D). Samples with less biotite tend to have larger proportions of pyrite and pyrrhotite (up to 8 vol.%). Garnet is poikiloblastic with inclusions of quartz, feldspar, biotite, and occasionally graphite and amphibole (Fig 3.2E). Inclusions within the garnet are not aligned. Where present, amphibole has irregular boundaries and is elongate. Amphibole is spatially associated with biotite-rich domains or garnet.

Graphite, found exclusively as the flake variant, is homogenously disseminated throughout the unit and makes up 5 to 10 vol.% of the unit. Graphite flakes range in length from 0.1 mm to 6.5 mm and range in width from 0.05 mm to 0.3 mm. The graphite is commonly interleaved with biotite and spatially associated with pyrrhotite and pyrite (Fig 3.2F). Graphite also appears as inclusions within garnet. In areas where the graphite is interleaved with metamorphic minerals, the graphite is aligned with the foliation.

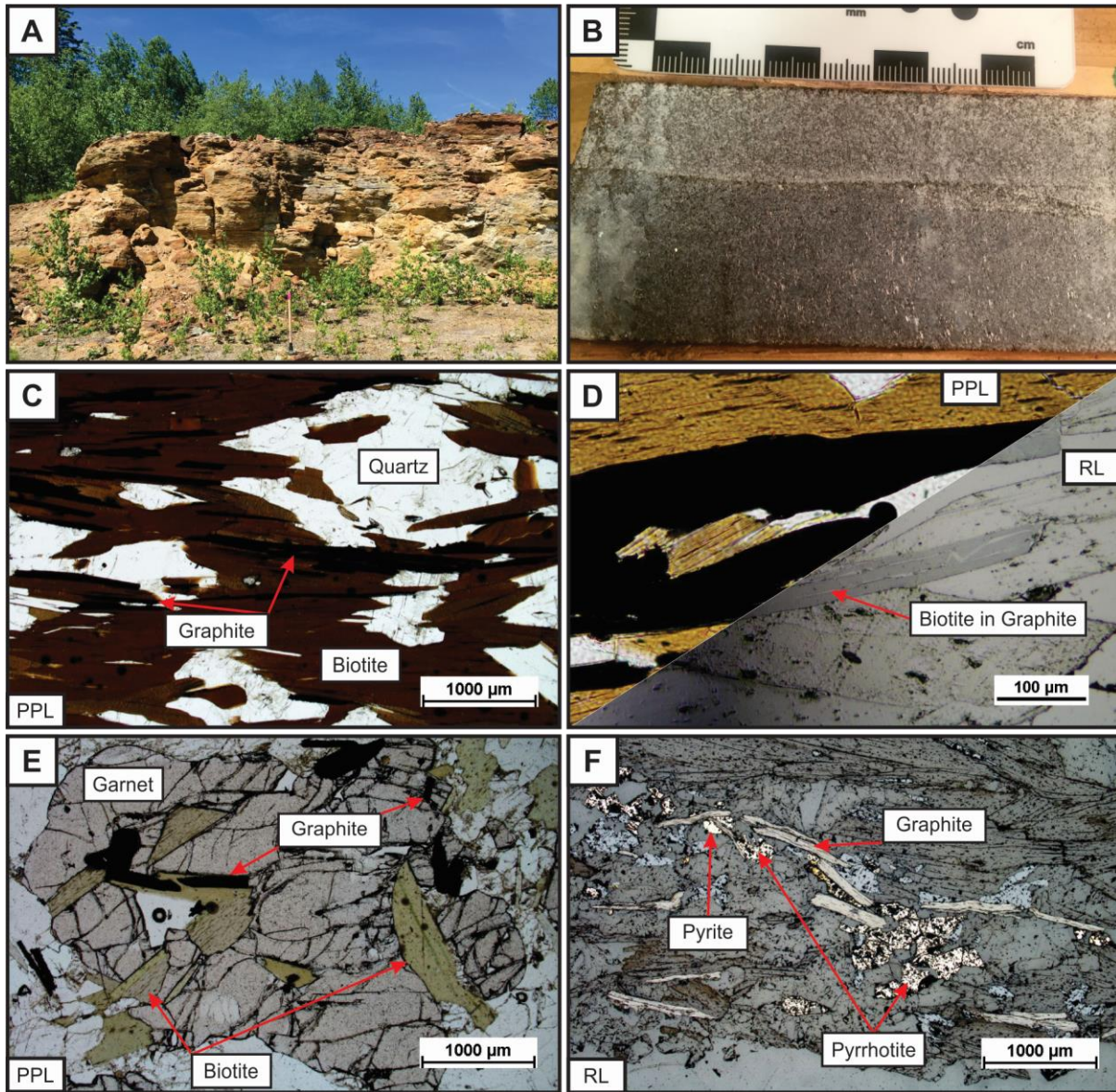


Fig. 3.2. Photos of the biotite-graphite-quartzofeldspathic gneiss. **A.** Weathered surface of the biotite-graphite-quartzofeldspathic gneiss unit, hammer for scale (handle wrapped in pink flagging tape – 90.5 cm in height). **B.** Fresh light grey coloured biotite-graphite-quartzofeldspathic gneiss as seen in core. **C.** Foliation is defined by the parallel alignment of disseminated graphite and biotite in a quartz and feldspar matrix. **D.** Biotite inclusions in graphite flakes. **E.** Poikiloblastic garnet with inclusions of biotite and graphite. **F.** Graphite interleaved with biotite and spatially associated with pyrite and pyrrhotite. PPL – Plane-polarized light, RL – Reflected light.

3.1.2 Clinopyroxene-Amphibole-Biotite-Graphite Gneiss

In outcrop, the clinopyroxene-amphibole-biotite-graphite gneiss unit weathers to a rusty brown-orange colour (Fig 3.3A). The fresh surface of the clinopyroxene-amphibole-biotite-graphite gneiss ranges from medium to dark grey (Fig 3.3B). Grains range in size from medium to coarse-grained (0.3 mm to >1.0 mm). The foliation is defined by a combination of aligned graphite and biotite grains as well as centimeter-to-decimeter scale compositional layering into leucocratic and melanocratic domains (Fig 3.3 A, B). Leucocratic domains show larger proportions of quartz and feldspar (60–70 vol.%) whereas melanocratic layers have greater proportions of biotite (15–25 vol.%). The unit is distinguished from the biotite-graphite quartzofeldspathic gneiss by the presence of clinopyroxene and a more pronounced gneissosity.

The clinopyroxene-amphibole-biotite-graphite gneiss unit is composed of quartz, plagioclase feldspar (andesine), potassium feldspar, biotite, amphibole (actinolite, tremolite), clinopyroxene (diopside), graphite, pyrrhotite, and pyrite. This unit may also contain garnet, titanite, minor calcite and trace sulfide minerals. Microscopically, rocks from this unit only show a single foliation, which is defined by a combination of the alignment of graphite, biotite, and amphibole as well as compositional layering (Fig 3.3C). The compositional layering is defined by leucocratic domains with quartz, feldspar, tremolite, and diopside that contrast with darker melanocratic biotite-rich domains. Graphite, pyrite, pyrrhotite and other trace sulfide minerals are disseminated throughout the unit. No discernable increased concentration of graphite was found along microscopic fold hinges in the clinopyroxene-amphibole-biotite-graphite gneiss. However, the graphite is aligned with the enveloping surface of these folds.

Quartz is xenoblastic, shows subgrain rotation and grain boundary migration textures, and has undulose extinction. Feldspars are hypidioblastic, with sharp planar and curviplanar boundaries. Biotite grains are less common in the leucocratic domains in this unit, which contrasts with the more disseminated nature of biotite throughout the biotite-quartzofeldspathic gneiss. Biotite is hypidioblastic, forms elongate lathes with sharp planar boundaries. Tremolite is xenoblastic, elongate and comprises up to 5 vol.%. Diopside presents as xenoblastic grains with sharp boundaries. Calcite is xenoblastic. Minor calcite can be found in contact with graphite grains (Fig. 3.3D). Actinolite is hypidioblastic with sharp boundaries. The actinolite is also

poikiloblastic with inclusions of quartz and feldspar. The inclusions within the actinolite are not aligned with the matrix foliation (Fig 3.3E).

Similar to the biotite-graphite-quartzofeldspathic unit, graphite within the clinopyroxene-amphibole-biotite-graphite gneiss is found only in flake form. Graphite accounts for 3 to 5 vol.% of the unit. Graphite flakes range from 0.3 mm to 3.2 mm in length and 0.05 mm to 0.12 mm in width. Graphite is commonly interleaved with biotite and spatially associated with metamorphic minerals such as biotite, diopside, tremolite, and actinolite (Fig 3.3F) as well as pyrrhotite and pyrite. However, sulfide minerals are not as prominent in this unit as in the biotite-graphite-quartzofeldspathic gneiss.

3.1.3 Garnet-Amphibole-Biotite-Graphite-Gneiss

In outcrop, the garnet-amphibole-biotite-graphite gneiss weathers to a rusty brown-orange colour (Fig. 3.4A). The fresh surface of the garnet-amphibole-biotite-graphite gneiss ranges in colour from dark-grey to black (Fig 3.4.B). Grain size in outcrop ranges from medium to coarse-grained (0.3 mm to >1.0 mm). The foliation is defined by a combination of aligned biotite, amphibole and graphite grains as well as centimeter- to decimeter-scale compositional layering defined by melanocratic and leucocratic domains. Melanocratic domains are composed of garnet, amphibole, biotite, and graphite, while the leucocratic domains are dominantly composed of quartz and feldspar. This unit is distinguished from the clinopyroxene-amphibole-biotite-graphite gneiss and the biotite-quartzofeldspathic gneiss by the presence of darker amphiboles (hornblende group) in melanocratic domains, and the presence of garnet.

In order of decreasing abundance, the garnet-amphibole-biotite-graphite gneiss is composed of quartz, potassium feldspar (K-feldspar), plagioclase feldspar (mostly andesine), biotite, amphibole (ferropargasite, ferroedenite, edenite), garnet, graphite, pyrrhotite, pyrite, and titanite. Microscopically, only a single foliation is apparent and is defined by a combination of compositional layering and the alignment of platy minerals such as biotite, amphibole, and graphite (Fig 3.4C). The compositional layering is defined by leucocratic quartz–feldspar-rich domains contrasting with melanocratic biotite–amphibole–garnet–graphite-rich domains. Graphite is disseminated throughout the unit and is commonly found in close association with pyrrhotite and pyrite (Fig. 3.4D).

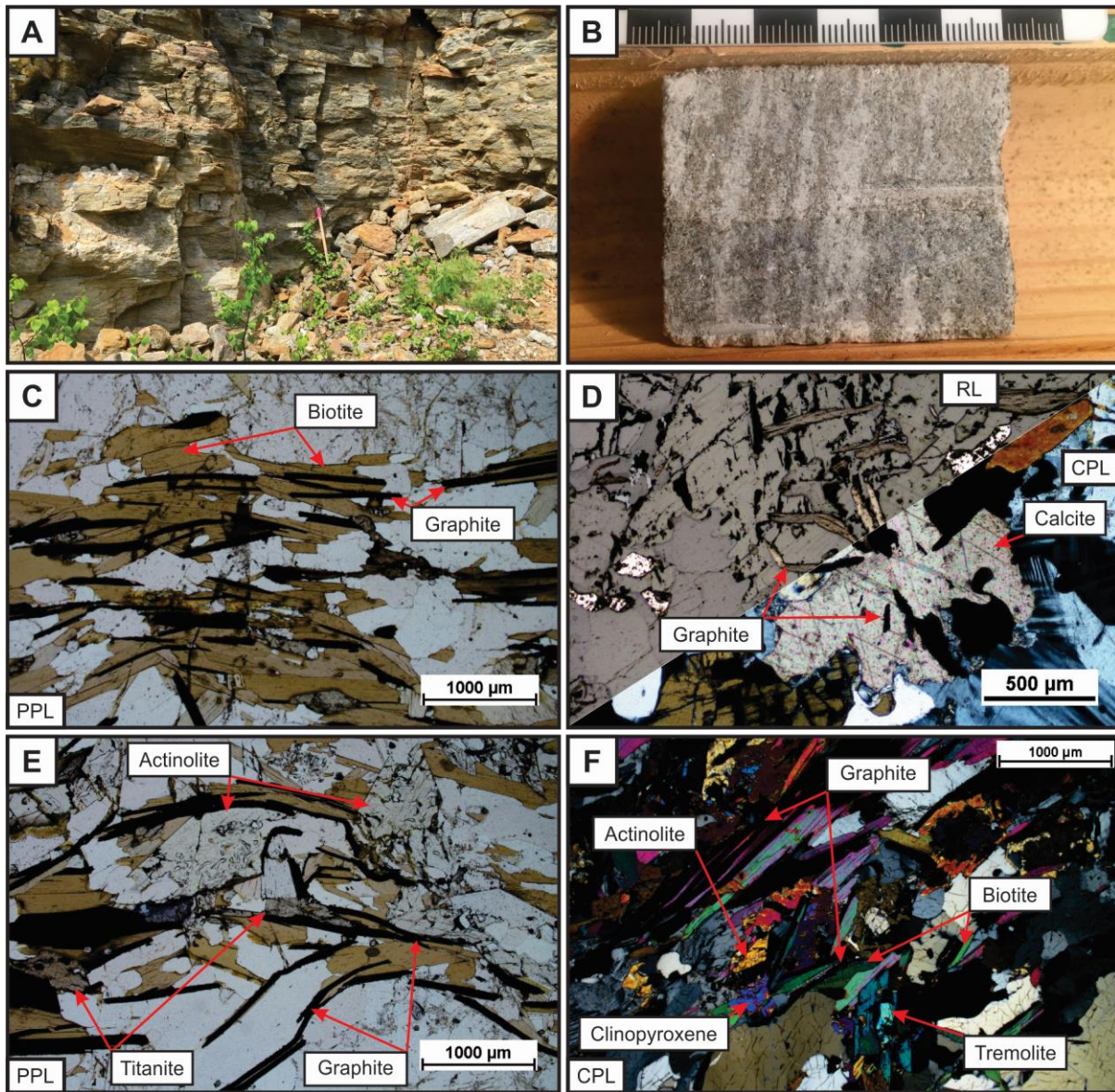


Fig. 3.3. Photos of the clinopyroxene-amphibole-biotite-graphite gneiss. **A.** Field photo showing the weathered surface of the clinopyroxene-amphibole-biotite-graphite gneiss, hammer for scale (handle wrapped in pink flagging tape - 90.5 cm in height). **B.** Fresh surface of the clinopyroxene-amphibole-biotite-graphite gneiss as seen in core, scale on scale card is in centimeters. **C.** Foliation shown by alignment of elongate and platy minerals as well as compositional layering. **D.** Calcite in contact with graphite grains. **E.** Poikiloblastic actinolite with inclusions of quartz and feldspar in close association with graphite. **F.** Flake graphite interleaved with biotite and in close association with biotite, diopside, tremolite, and actinolite. PPL – Plane-polarized light, CPL – Cross-polarized light, RL – Reflected light.

Quartz is xenoblastic and has undulose extinction. Feldspars are hypidioblastic with sharp planar to curviplanar boundaries. Biotite grains are less common in the leucocratic domains in this unit, which contrasts with the more disseminated nature of biotite throughout the biotite-quartzofeldspathic gneiss and is more consistent with the clinopyroxene-amphibole-biotite-graphite gneiss. Biotite is hypidioblastic, forming elongate lathes with planar and curviplanar boundaries. Garnet shows a poikiloblastic texture with inclusions of quartz, feldspar, biotite, amphibole, and graphite (Fig 3.4E, F). The inclusions are not aligned into an internal fabric. Amphibole grains are xenoblastic, with curved to curviplanar boundaries. In some cases, amphibole pseudomorphs biotite, which suggests that amphibole has replaced biotite (Fig 3.4F).

Graphite within the garnet-amphibole-biotite-graphite gneiss is found only in flake form. Visually, graphite accounts for 2 to 3 vol.% of the unit. Graphite flakes range from 0.3 mm to 2.2 mm in length and 0.05 mm to 0.15 mm in width. Graphite is commonly interleaved with biotite and spatially associated with metamorphic minerals such as biotite, amphibole, and garnet as well as pyrrhotite and pyrite.

3.1.4 Garnet-Biotite-Sillimanite-Graphite Gneiss

The garnet-sillimanite-biotite-graphite gneiss is not well exposed at surface and is only found in core. The fresh surface of the garnet-sillimanite-biotite-graphite gneiss is medium-grey to dark-brown. Grain sizes range from 0.3 mm to >1.0 mm. This unit is distinguished from the other graphitic gneiss units by the presence of garnet and sillimanite, a decrease in graphite content (1–3 vol.% visible graphite) and a strong foliation defined by alternating light to medium grey leucocratic zones and dark brown melanocratic zones (Fig 3.5A). The foliation is also defined by the alignment of platy and elongate minerals such as biotite, sillimanite, and graphite.

The minerals that compose this unit, in order of decreasing abundance, are quartz, potassium feldspar (K-feldspar), biotite, garnet, sillimanite, graphite, and rare plagioclase (albite). The foliation in this rock is defined by both the alignment of elongate and platy minerals, such as biotite, graphite, and sillimanite as well as compositional layering (Fig. 3.5B). Garnets can also show an elongate shape in the direction of the foliation (Fig 3.5C). Melanocratic zones are composed of biotite, garnet, sillimanite, and kaolinite. Kaolinite is interpreted to have formed as a weathering product of sillimanite and is not a part of the peak metamorphic assemblage because of the close spatial relationship between altered sillimanite and

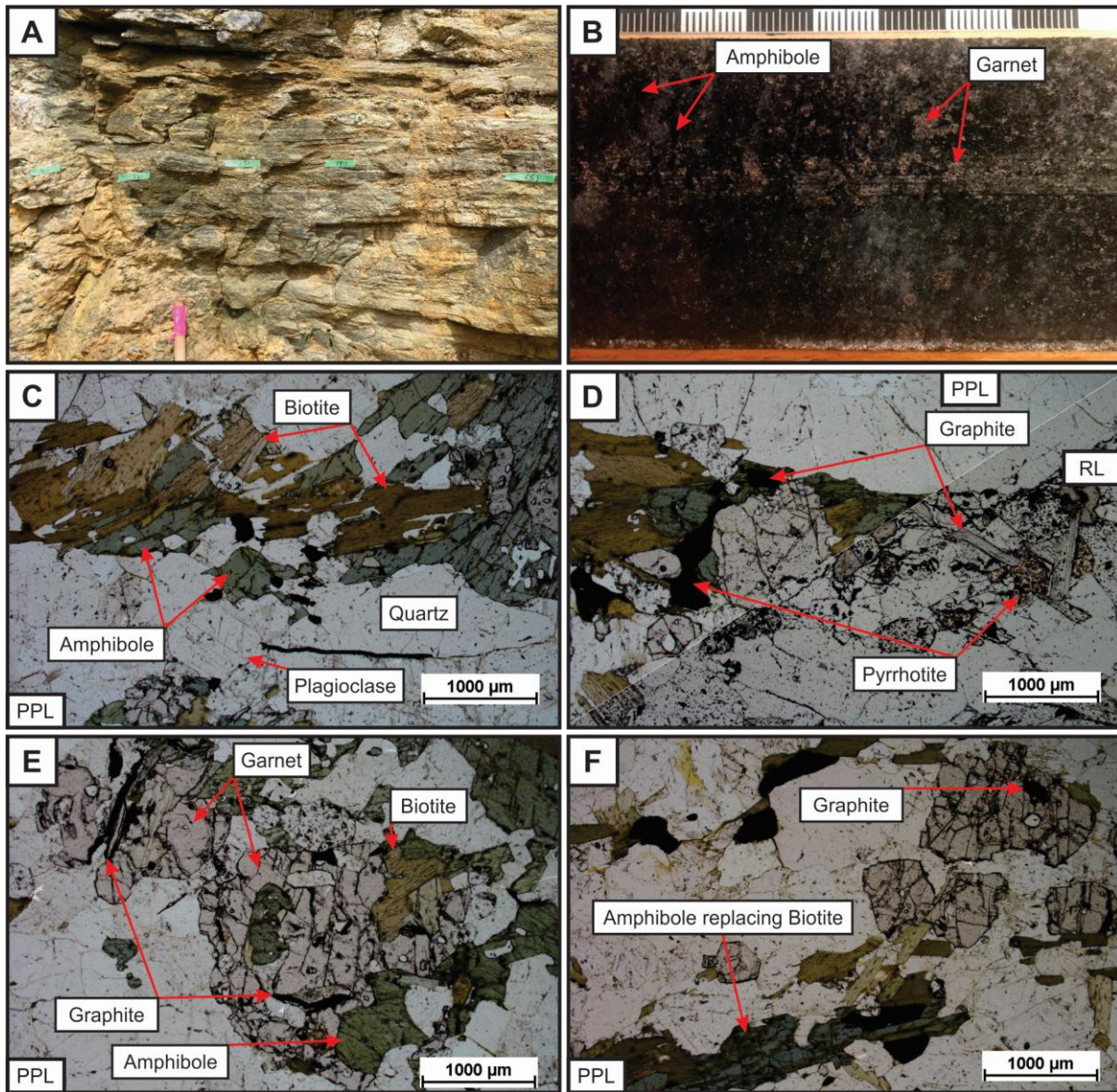


Fig. 3.4. Photos of the garnet-amphibole-biotite-graphite gneiss. **A.** Field photo showing the weathered surface of the garnet-amphibole-biotite-graphite gneiss located above the pegmatite vein, hammer handle for scale (wrapped in pink flagging tape - ~4 cm width). **B.** Fresh surface (wet) of the garnet-amphibole-biotite-graphite gneiss in core. The surface was wetted for easier identification of garnets and amphiboles. The scale on the scale card at the top is in centimeters. **C.** Foliation defined by the alignment of elongate biotite and amphibole as well as compositional zoning. **D.** Graphite in close spatial association with pyrrhotite. **E.** Quartz, feldspar, biotite, amphibole and graphite inclusions in garnet. **F.** Amphibole replacing biotite and a graphite inclusion in garnet. PPL – Plane-polarized light, RL – Reflected light.

kaolinite. Additionally, the alteration of the sillimanite to kaolinite does not appear to have affected any of the more weathering resistant minerals (e.g. quartz, feldspar, and garnet) in close proximity. Leucocratic zones are composed of predominantly quartz and feldspar. Melanocratic zones have a higher modal abundance of graphite and most graphite is interleaved with biotite.

Quartz is xenoblastic, shows grain boundary migration textures and has undulose extinction. Feldspar is hypidioblastic with sharp planar to curviplanar edges. Biotite is xenoblastic, has planar to curviplanar boundaries and common pleochroic haloes. Garnets are xenoblastic and are elongate in the direction of the foliation. Garnet is poikiloblastic with inclusions of quartz and feldspars, and these are not aligned as inclusion trails. Sillimanite shows a bimodal grain size distribution and is found as both small needles and larger elongate lathes and is frequently surrounded by kaolinite, except when found as inclusions in garnet. Plagioclase grains are rare and are only found along grain boundaries between potassium feldspar and garnet. Plagioclase grain boundaries are very irregular and vary from planar where in contact with garnet to curved where in contact with potassium feldspar.

Graphite within the garnet-biotite-sillimanite-graphite gneiss is found as flakes interleaved with biotite and as small veinlets (Fig. 3.5D) but graphite is less abundant than in other graphitic gneiss units. Graphite accounts for 1 to 3 vol.% of the garnet-sillimanite-biotite-graphite gneiss unit. Graphite flakes vary in length from 0.2 mm to 1.4 mm and are 0.05 mm to 0.1 mm in width; this is smaller than grains in the other graphite bearing units. These flakes can also have inclusions of biotite and quartz (Fig 3.5E). Graphite veinlets can be seen along grain boundaries and are frequently associated with pyrrhotite and pyrite (Fig 3.5F).

3.2 Barren Gneisses

The barren gneisses surrounding the Bissett Creek flake graphite deposit can be subdivided into three distinct geological units based upon their metamorphic mineral assemblages. These units include biotite-quartzofeldspathic gneiss, amphibole-biotite-quartzofeldspathic gneiss, and garnet-sillimanite-biotite gneiss. In outcrop, the barren gneisses are differentiated from the graphitic gneisses by their weathered surfaces, which are bleached to a light grey to light pink colour. The barren gneisses are also commonly covered in lichen and moss, while the graphitic gneisses are not. The fresh surface varies from light and medium grey to light pink. Weathering of the barren gneisses rarely penetrates more than a few centimeters.

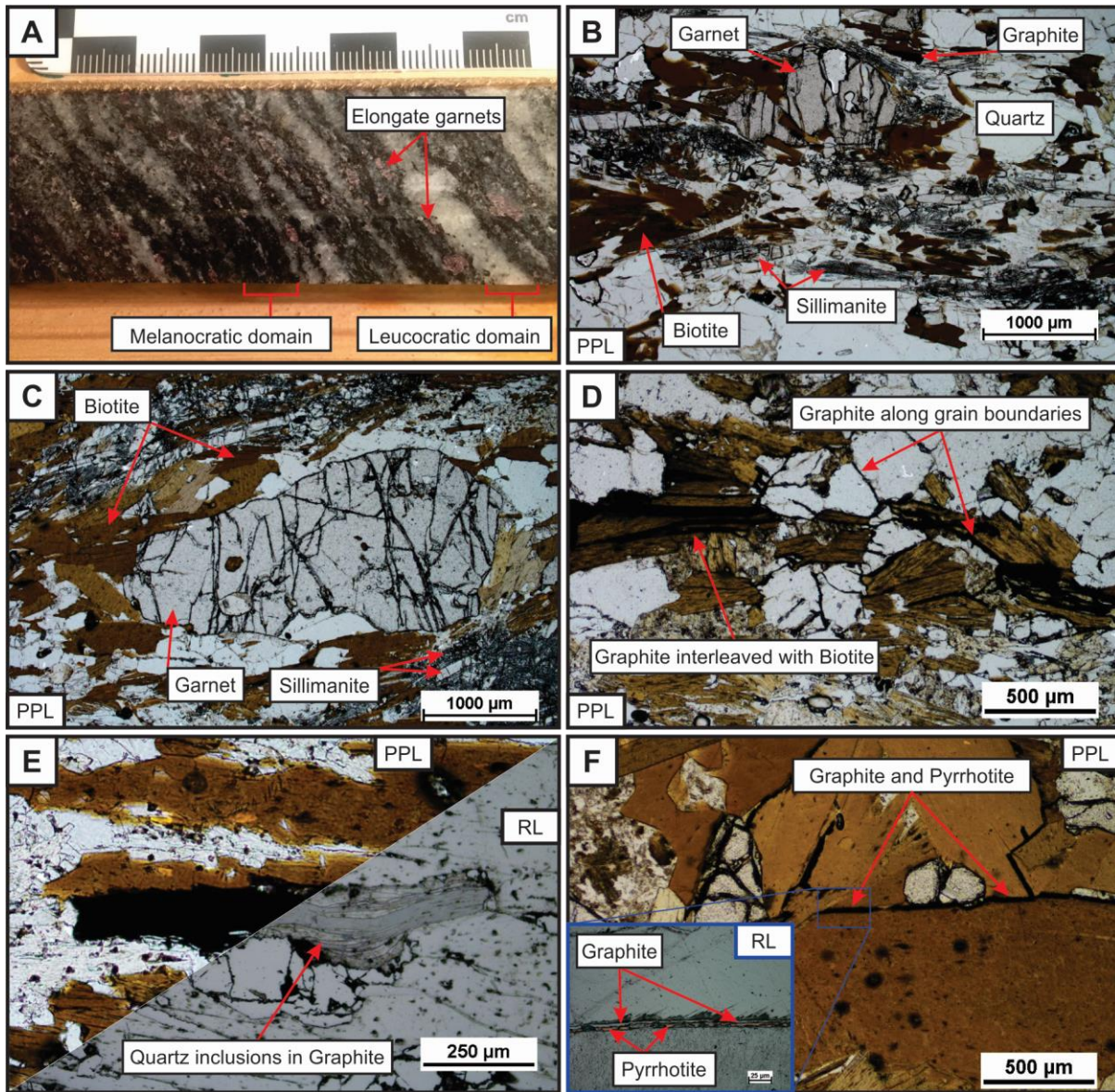


Fig. 3.5. Photos of the garnet-sillimanite-biotite-graphite gneiss. **A.** Fresh surface (wet) of the garnet-sillimanite-biotite-graphite gneiss as observed in core. The foliation is defined by leucocratic domains, composed of quartz and potassium feldspar, and melanocratic domains that are composed of biotite, sillimanite, garnet, and graphite. **B.** Foliation defined by aligned biotite, sillimanite, and graphite. **C.** Garnets elongated in the direction of the foliation. **D.** Graphite flakes interleaved with biotite and graphite veinlets with inclusions of quartz and biotite. **E.** Graphite with quartz inclusions. **F.** Graphite and pyrrhotite form a small veinlet along grain boundaries between biotite. PPL – Plane-polarized light, RL – Reflected light.

The barren gneisses form both the underlying and overlying units for the graphitic gneisses and have sharp contacts with the graphitic gneiss.

3.2.1 Biotite-Quartzofeldspathic Gneiss

Biotite-quartzofeldspathic gneiss commonly forms topographic highs surrounding the Bissett Creek deposit (Fig 3.6A). Fresh surfaces, as seen in core, are light-to-medium grey-to-pink (Fig 3.6B). The grain size varies from medium to coarse-grained (0.5 mm to 3.0 mm). A foliation is defined by the parallel alignment of biotite as well as compositional banding formed by centimeter-scale leucocratic (quartz and feldspar-rich) and melanocratic (biotite-rich) domains (Fig 3.6C).

This biotite-quartzofeldspathic gneiss unit contains a mineral assemblage of granoblastic quartz, biotite, potassium feldspar, and plagioclase. Minor amounts of garnet, titanite, and amphibole can also be present. Quartz shows grain boundary migration textures. Biotite is hypidioblastic and occasionally poikiloblastic with inclusions of quartz and feldspar (Fig 3.6D). Garnet grains are sometimes in contact with minor amounts of biotite and chlorite.

3.2.2 Amphibole-Biotite-Quartzofeldspathic Gneiss

The amphibole-biotite-quartzofeldspathic gneiss unit is very similar to the biotite quartzofeldspathic gneiss unit. In outcrop, the amphibole-biotite-quartzofeldspathic gneiss unit shows the same weathering and vegetation coverage characteristics. The fresh surface of the amphibole-biotite-quartzofeldspathic gneiss is light-to-dark grey in colour (Fig 3.7A). The grain size ranges from medium-to-coarse grained (0.4 mm to 2.7 mm). The chief distinguishing feature of this unit is the increase in amphibole content (>15%) and the decrease in biotite content (<10%). The foliation is defined by both the alignment of biotite and amphibole grains, as well as centimeter- to decimeter-scale compositional layering (Fig 3.7B). Leucocratic domains are composed of quartz and feldspar whereas melanocratic domains are composed of amphibole and biotite.

This unit is made up of a granoblastic mineral assemblage of quartz, feldspars, amphibole, and biotite. Garnet can also be found within this unit in small amounts. Quartz is xenoblastic, with curved to curviplanar boundaries, and shows grain boundary migration textures. Feldspars are also xenoblastic with planar to curviplanar boundaries. Biotites are

irregularly shaped with sharp boundaries that are commonly in contact with amphibole. Amphiboles are elongate, irregularly shaped, and hypidioblastic. Locally, amphibole pseudomorphs biotite and contains inclusions of quartz and feldspars (Fig 3.7C). Garnet is rare and can be poikiloblastic with inclusions of quartz and feldspars, and occasionally biotite altering to chlorite (Figure 3.7D).

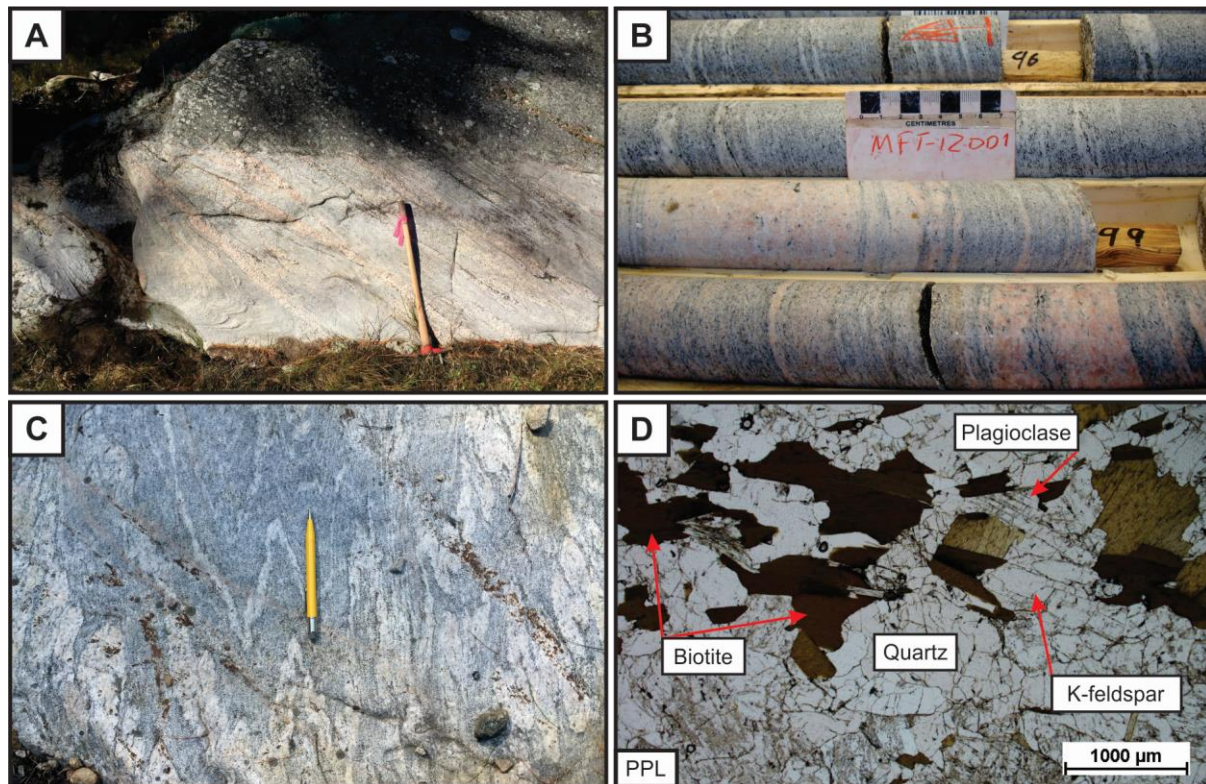


Fig. 3.6. Photos of the biotite-quartzofeldspathic gneiss. **A.** Weathered surface of the biotite-quartzofeldspathic gneiss with moss and lichen (top) and a fresh surface (bottom). Pick with pink flagging tape on the handle for scale – 90 cm in height. **B.** Fresh surface of the biotite-quartzofeldspathic gneiss as seen in core (Photo from Mehmet Taner). **C.** Foliation as seen in outcrop, pencil for scale - ~14.5 cm in height. **D.** Disseminated, aligned biotite and compositional layering forming the foliation. PPL – Plane polarized light.

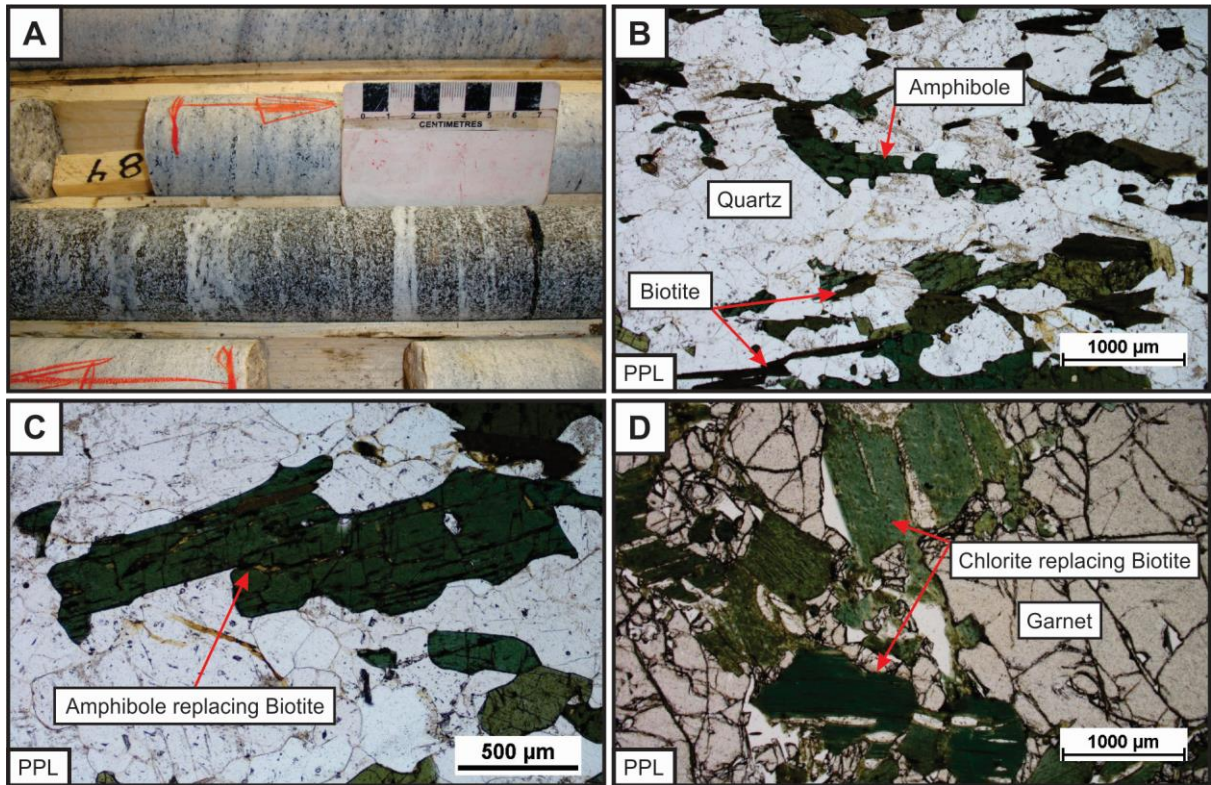


Fig. 3.7. Photos from the amphibole-biotite-quartzofeldspathic gneiss unit. **A.** Fresh surface of the amphibole-biotite-quartzofeldspathic gneiss showing compositional layering defining the foliation as seen in core (Photo from Mehmet Taner). **B.** Foliation defined by the alignment of platy biotite and elongate amphibole grains as well as compositional layering. **C.** Amphibole replacing biotite. **D.** Poikoblastic garnet with inclusions of quartz and feldspar and chlorite, which is altered from biotite. PPL – Plane-polarized light.

3.2.3 Garnet-Sillimanite-Biotite Gneiss

In outcrop, the garnet-sillimanite-biotite gneiss is light grey and commonly covered with greenish-grey moss and lichen. The fresh surface of the garnet-sillimanite-biotite gneiss is light-to-dark grey in colour. The grain size ranges from medium-to-coarse grained (0.3 mm to >1.0 mm). The foliation is defined by both the alignment of biotite and sillimanite, as well as centimeter to decimeter-scale compositional layering (Fig. 3.8A). Leucocratic domains are composed of quartz and feldspar whereas melanocratic domains are composed of garnet, biotite, and sillimanite.

In thin section, this unit is made up of a granoblastic mineral assemblage of quartz, feldspars, biotite, sillimanite, and garnet. Quartz is sub-angular to sub-rounded, xenoblastic and shows grain boundary migration textures. Feldspars are also xenoblastic and sub-rounded to sub-angular. Biotite forms angular, irregularly shaped lathes that are commonly in contact with sillimanite. Sillimanite is elongate and hypidiomorphic forming long lathes. Garnet can be poikiloblastic with inclusions of quartz and feldspar (Fig. 3.8A). One key difference between the barren garnet-sillimanite-biotite gneiss and the garnet-sillimanite-biotite-graphite is that the barren gneiss contains both potassium feldspar and plagioclase, whereas its mineralized equivalent does not (Fig. 3.8B). The significance of this will be discussed in Chapter 9.3.

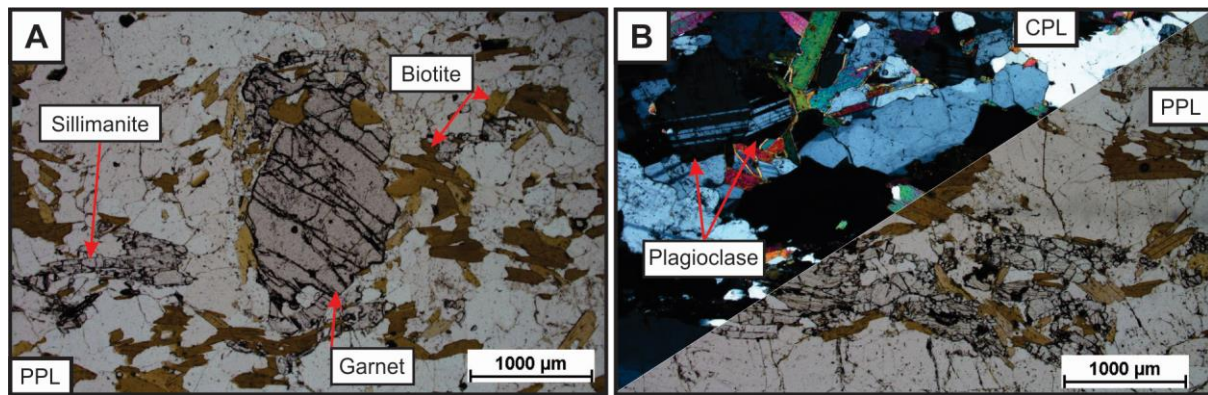


Fig. 3.8. Photos from the garnet-biotite-sillimanite gneiss. **A.** Foliation shown by alignment of biotite, sillimanite, and garnet. **B.** Presence of plagioclase in the garnet-sillimanite-biotite gneiss. PPL – Plane-polarized light, CPL – Cross-polarized light.

3.3 Intrusive Units

There are two intrusive units present at the Bissett Creek flake graphite deposit. These units are the granitic pegmatites and the metagabbro intrusives.

3.3.1 Granitic Pegmatite

In outcrop, the granitic pegmatites vary from light pink (buff) to light grey (Fig 3.9A, B). The weathered and fresh surfaces are nearly identical, but sometimes the weathered surface is stained orange-brown or yellow by the surrounding graphitic gneiss units. Granitic pegmatites are medium-grained to very coarse-grained (0.3mm to >10mm). The minerals that compose the pegmatite units are quartz, potassium feldspar, biotite, and muscovite with rare graphite,

pyrrhotite, and allanite. Quartz and feldspars are large (>1.0 mm), equant, and euhedral to subhedral. The contact between the pegmatites and the graphitic gneiss is sharp, with a small alteration halo surrounding the intrusion, and there is a lack of graphite in the zone directly adjacent to the pegmatite intrusions (Fig. 3.9A). The pegmatites do not appear to have undergone any significant alteration.

Graphite occurs either as infrequent flake inclusions in or at the edge of, larger biotite grains or as small spherulitic radiating grains in quartz and feldspar (Fig 3.9C, D). The size of the graphite flakes ranges from 0.3 mm to 0.7 mm in length and 0.05 mm to 0.15 mm in width. Graphite spherules are approximately 1.5 mm in diameter. No graphite xenocrysts were noted in pegmatites that crosscut the barren gneisses.

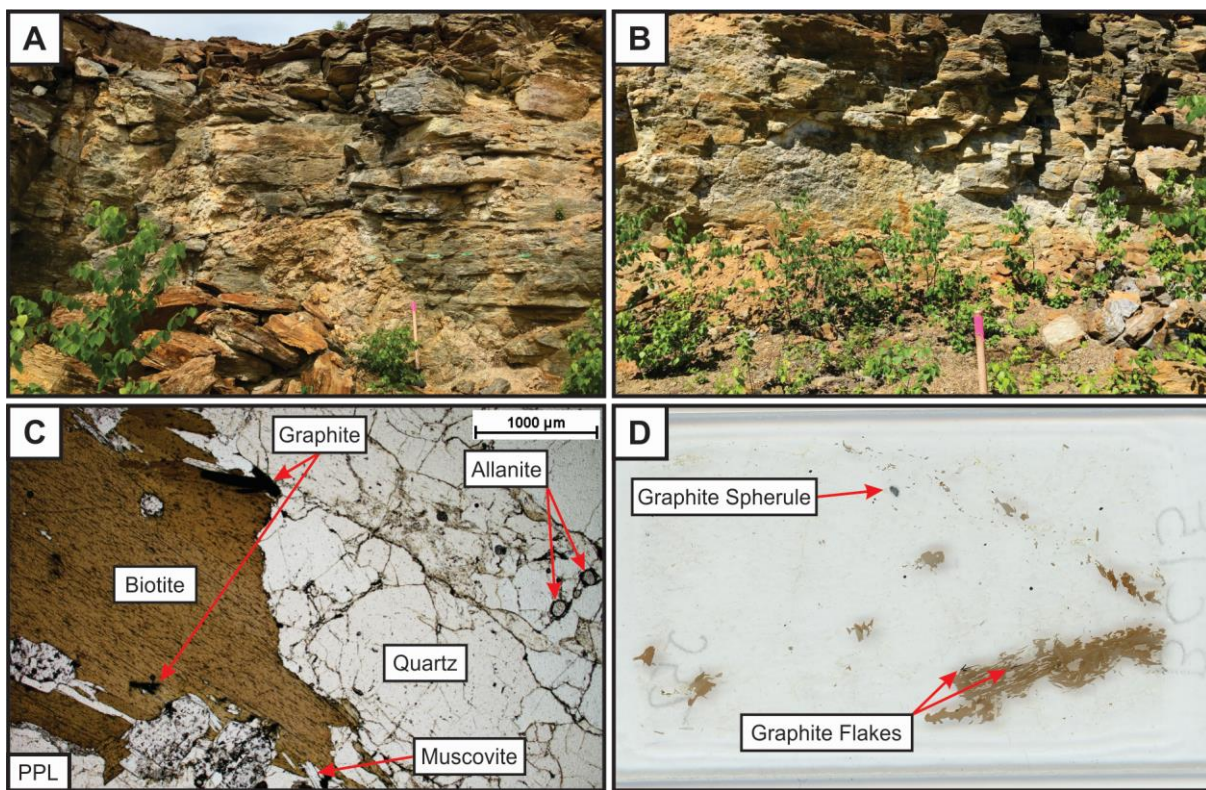


Fig. 3.9. Photos of the granitic pegmatite unit. **A.** Buff pegmatite crosscutting graphitic gneiss. Hammer for scale (handle wrapped in pink flagging – 90 cm in height). **B.** Grey pegmatite in graphitic gneiss, hammer handle for scale (~ 4cm width). **C.** Flake graphite grains interleaved with biotite. **D.** Graphite spherules and flakes in thin section. Thin section dimensions are 27mm by 46mm. PPL – Plane-polarized light.

3.3.2 Metagabbro Intrusive

Several instances of metagabbro intrusives are noted in drill core and only a single outcrop exposure was found at the Bissett Creek flake graphite deposit (Fig 3.10A). In this case, the weathered surface is rusty brown, while the fresh surface is greenish black to black. The grain size of the metagabbro intrusive ranges from fine to coarse-grained (<0.3 mm to 1.8 mm). The mineralogy of the metagabbro, in order of decreasing abundance, is amphibole, biotite, quartz, plagioclase feldspar, and orthopyroxene. A foliation is defined by the alignment of elongate grains of amphibole and orthopyroxene as well as biotite lathes (Fig. 3.10B).

Where the metagabbro intrusive cuts through the graphitic gneiss, there is a small alteration halo of ~0.3 m, which is devoid of graphite mineralization (Fig 3.10A). The contact between the graphitic and barren gneisses and the metagabbro intrusive is sharp.

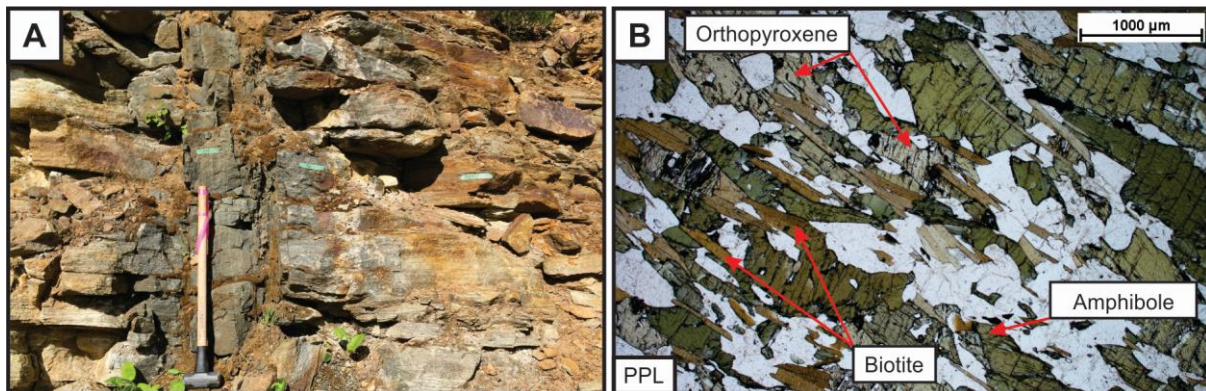


Fig. 3.10. Photos of the metagabbro intrusive. **A.** Metagabbro intrusion into graphitic gneiss showing the alteration halo surrounding the intrusion, hammer for scale – 90.5 cm in height. **B.** Foliation defined by the alignment of elongate and/or platy minerals such as biotite, amphibole, and orthopyroxene. PPL – Plane-polarized light.

3.4 Structural Geology

The geology of the Bissett Creek flake graphite deposit is summarized in Figure 3.11. The mappable units are graphitic gneisses, barren gneisses and intrusive rocks (Fig 3.1). Due to lack of clean surficial exposure because of heavy weathering, vegetation and overburden cover, it was not possible to further differentiate the graphitic and barren gneisses into their individual petrographic units in the field. The extents of the intrusive units were too small to be plotted on

the map. Contacts between the graphitic gneisses are gradational over a scale of centimeters to decimeters.

The foliations in the barren and graphitic gneisses generally strike southeast to northwest with gentle to moderate dips to the east (Fig 3.12A). These orientations are consistent with regional structures and likely represent a single population (Figure 3.12B, C). Structural measurements were taken at 118 stations across the Bissett Creek property, with one to three structural measurements being taken at each station. Regionally, structural measurements were taken at 34 stations, with one orientation measurement taken at each station. The full set of the structural measurement data is available in Appendix A and Appendix B.

The graphitic gneisses are underlain and overlain (i.e. stratabound) by barren gneisses. The contact between the graphitic gneisses and the barren gneisses is sharp and undulating where apparent on the surface and in drill core (Fig 3.13A, B). The graphitic gneisses commonly show a flaggy texture (Fig 3.13A, B), which is absent in the barren gneisses. Flaggy texture is a term used to describe rocks which split into thicknesses suitable for used as flagstones, typically on the order of 10 to 100 cm. Similarly, the contacts between the gneisses and the intrusive units are also sharp (Fig 3.9A, B; Fig 3.10A).

Some partial melting textures were noted in the barren gneiss units while field mapping (Fig 3.14A, B). These indicators consist of irregularly shaped leucosome material that cross-cuts the dominant fabric and does not appear to have a preferred orientation. Figure 3.14A shows branches originating from leucocratic compositional layers within the barren gneiss. The borders of the leucosome material are diffuse and consist of biotite and garnet melanosome (Fig 3.14B).

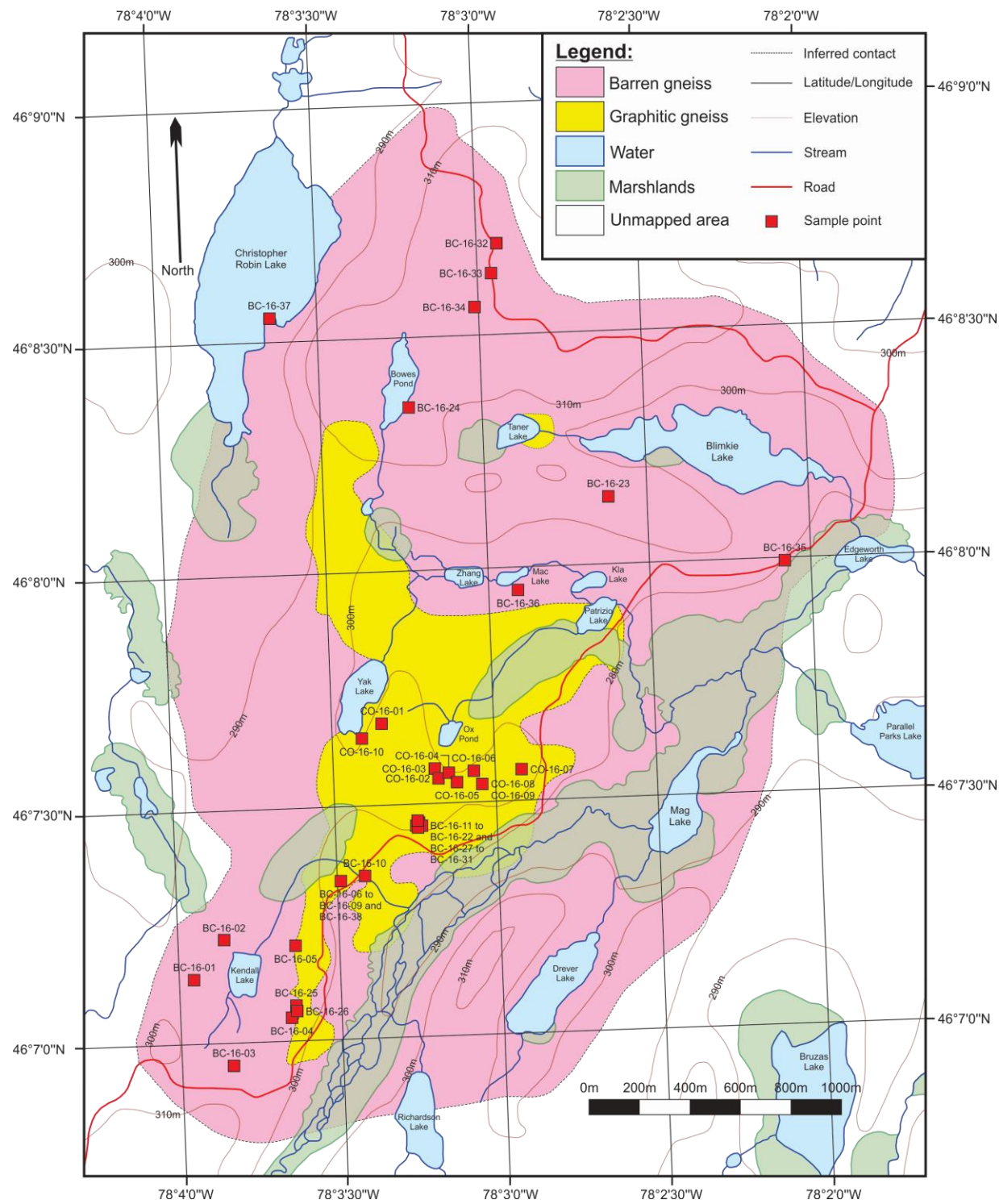


Fig. 3.11. Bissett Creek property geology map. Topographic lines, marsh areas, and waterways were sourced from the World Topographic Map database compiled and maintained by Esri and which was most recently updated on June 27th, 2018.

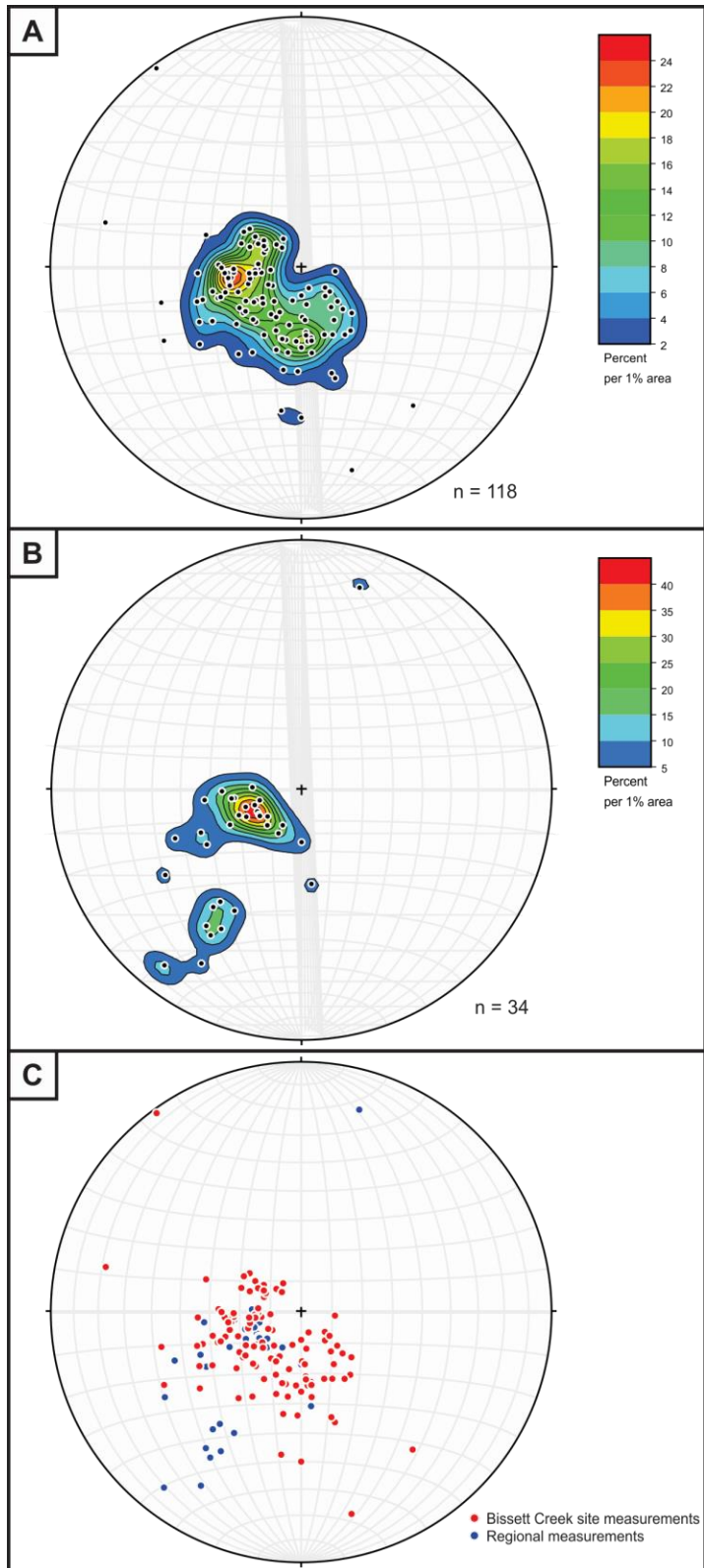


Fig. 3.12. Equal-area stereonet showing the poles to the planes measured at: (A) the Bissett Creek flake graphite deposit, (B) regionally, (C) both for comparison.

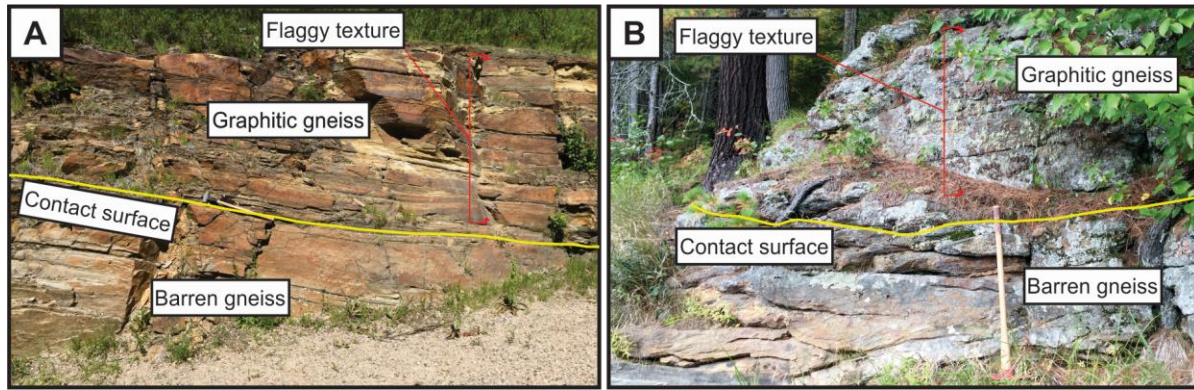


Fig. 3.13. Photos showing sharp undulating contacts between the graphitic and barren gneisses in the field. The contact surface is shown as a yellow line, while the flaggy textures are highlighted using red parentheses.

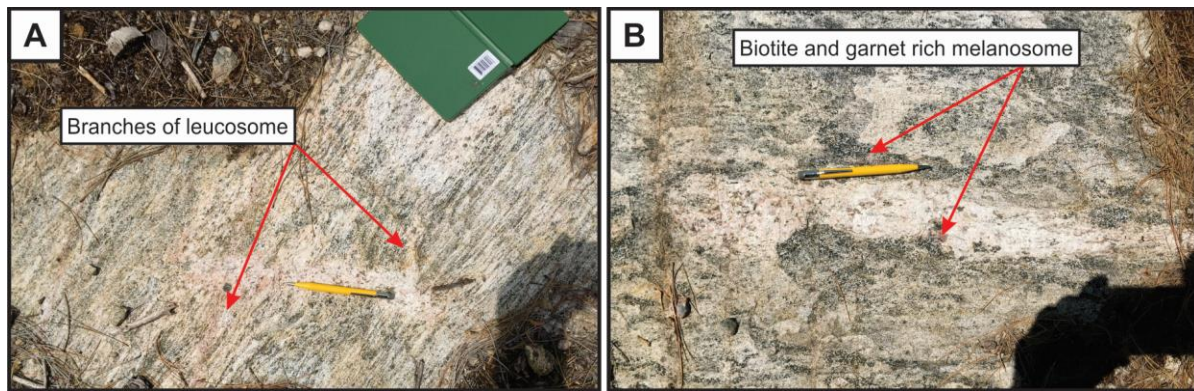


Fig. 3.14. Photos of potential partial melting indicators from the barren gneisses on the Bissett Creek flake graphite deposit property.

4.0 Major and Trace Element Lithogeochemistry

Lithogeochemistry was used to address the first research objective by attempting to determine the protoliths for each of the units, thus differentiating them. To address this, values for major elements (62 samples), trace elements (45 samples), total carbon (30 samples), graphitic carbon (30 samples) and total sulfur (30 samples) were analyzed. A full list of the details associated with each sample is in Appendix C. The analyses were carried out at Activation Laboratories Ltd. (Actlabs) in Ancaster, Ontario using their standard procedures, which are detailed further below and available on their website (<http://www.actlabs.com>).

4.1 Sample Collection and Preparation

To ensure representative sampling of each of the different units, samples were taken from a variety of locations across the site and the region (Fig 3.11. and Appendix C). Samples were collected if the samples showed minimal surficial weathering and were representative of one of the geological units based on the mineral assemblage. Samples obtained ranged in weight from ~1.5 kg to >10 kg depending on lithology, structural features, and grain size. If adequate surficial exposure of a unit could not be found, a representative sample was taken from drill core. Sample spatial resolution was determined by the availability of outcrop and the extent of weathering. Representative barren gneiss samples were obtained on both a North-South and an East-West traverse. Graphitic gneiss samples were limited to pit exposures and core samples as a result of the extent of surficial weathering.

Samples were cut with a rock saw to remove weathering. Clean samples were cut into thin (5-8 mm) slabs and crushed to ~2 mm using a stainless-steel mortar and pestle. Samples were then screened to < 2mm (No. 10 Mesh) using a plastic sieve container with metal mesh at the bottom. Material not passing the 2mm screen was placed back into the mortar and pestle assembly for additional crushing until 100% passed. Between each sample the mortar and pestle were decontaminated by rinsing the assembly in water, washing with a microfiber cloth, rinsing again with water, wiping with ethanol and finally drying with high-pressure air. A Kimwipe was then used to evaluate if the mortar and pestle were clean by wiping the inside. If particulate matter was present on the Kimwipe, then the process was repeated until no material was found. The same decontamination procedure mentioned above for the mortar and pestle was also used for the sieve assembly, but ethanol was only used on the metal mesh portion.

Agate jars were used for milling and are commonly used by industry in studies of graphite deposits ([R. McCarley, pers. comm., 2016](#)). Dry ball milling was completed using a planetary ball mill (Retsch PM-200-CM). Before each sample was processed, the jars and charge were cleaned using beach sand and pre-contaminated using some of the sample material. The cleaning and pre-contamination cycles were each run for 5 minutes at 550 rotations per minute (rpm). The sample processing cycle ran for 45 minutes at 550 rpm.

After this cycle, a portion of the sample material was screened at 75-micron (200 Mesh) using a metal screen, if all of the material passed, then the end product was packaged for further analysis by Actlabs. If the material did not pass, then it was subjected to an additional 10-15 minutes of grinding at 550 rpm. This step was repeated as needed. The final product (~20 to 30g) was packaged in 20 mL plastic scintillation vials and shipped to Actlabs.

4.2 Analytical Methods

Major, minor and trace elements were analyzed as part of the Actlabs 4 Lithoresearch package. Major element concentrations were determined by Inductively Coupled Plasma Optical Emission Spectrometer (ICP-OES), while trace element concentrations were determined by Inductively Coupled Plasma Mass Spectrometer (ICP-MS). To prepare the samples for analysis, approximately 1g of material was melted in an induction furnace using lithium metaborate and lithium tetraborate as fluxes. The molten material was then poured directly into a solution of 5% nitric acid, which was stirred until the molten material was completely dissolved. The final solution was then analyzed by ICP-OES and ICP-MS.

Total carbon and sulfur concentrations were measured using Actlabs package 4F and used an infrared (IR) detector. To start the procedure, an accelerator material was combined with 0.2 g of sample material. The combined material was then placed in an induction furnace and heated until the carbon and sulfur combust. The combustion took place in a pure oxygen environment, causing the formation of CO, CO₂, and SO₂. The CO was converted into CO₂ in a catalytic heater assembly. These gases then flowed into the IR cell where the gases absorbed specific wavelengths of the infrared spectrum. The absorption of the wavelengths reduced the amount of energy that reached the IR detectors, which was used to determine the total amount of CO₂ or SO₂ gas passed and correspondingly, the total amounts of carbon and sulfur.

Graphitic carbon was measured in a very similar manner to total carbon and sulfur (part of package 4F), but there are two main differences. The first difference was that 0.5 g of sample material is used per analysis. The second was that the sample undergoes a multistage furnace treatment to remove the carbonate component of the total carbon prior to analysis, leaving only carbon in the form of graphitic carbon behind. Afterward, the sample was subjected to the same process outlined above for combustion and detection.

Ferrous (Fe^{2+}) iron concentrations were determined as part of Actlabs package 4F. Values of FeO were determined through titration. In this method, the sample material was prepared using a cold acid digestion (ammonium metavanadate and hydrochloric acid) in an apparatus that maintained an open system. After digestion, ferrous ammonium sulfate was added. From this point, potassium dichromate was used as a titrating agent, and the end point of the titration was determined by the final solution colour.

4.3 Quality Assurance/Quality Control

All samples were submitted to Activation Laboratories (Actlabs) in Ancaster, Ontario for analysis. Actlabs is accredited by the International Organization for Standardization/International Electrotechnical Commission and has obtained the designation of ISO/IEC 17025. Actlabs also has the CAN-P-1579 accreditation for mineral analysis and geological tests provided by the Standards Council of Canada (SCC). All samples were run using commercially available services.

To help ensure the precision and accuracy of the results of the major and trace element geochemistry, I sent additional samples for quality control and quality assurance purposes. These included 2 blanks (both beach sand), 1 international reference material which was run twice (both SY-4 Diorite Gneiss) and 2 duplicates (BC-20 and CO-04). This forms a ratio of 28:1 samples to full method blanks, standards and duplicates for major and minor element geochemistry, and 19.5:1 for trace element geochemistry. These ratios further improve to 12:1 for total carbon, graphitic carbon, and total sulfur, although I could not provide a certified reference material for these samples. These ratios exclude certified reference materials run by Actlabs.

The certified reference material SY-4 (Diorite Gneiss) was selected based on the availability of standard materials, and the potential for matching with barren gneiss samples on the property. The barren gneisses on the property contained higher concentrations of SiO₂ and MgO than SY-4. The barren gneisses also had lower concentrations of Al₂O₃, CaO, Na₂O, and K₂O than SY-4. Finally, Fe₂O₃, MnO, TiO₂ and P₂O₅ were comparable (<1 wt. % variation) with the values obtained from SY-4. Actlabs ran additional certified reference materials for all elements measured, including carbon and sulfur, as part of their commercial analyses packages. These certified reference materials included NIST 694 (Phosphate rock), DNC-1 (Dolerite), GBW 07113 (Rhyolite), LKSD-3 (Lake sediment composite), TBD-1, W-2a (Diabase), SY-4 (Diorite gneiss), CTA-AC-1 (Apatite concentrate), BIR-1a (Icelandic basalt), NCS DC86312 (Rare earth ore), JGb-2 (Gabbro), NCS DC70009 (Tungsten ore), SGR-1b (Green River formation shale), OREAS 100a (Mt. Gee uranium prospect), OREAS 101a (Mt. Gee uranium prospect), OREAS 101b (Mt. Gee uranium prospect), JR-1 (Rhyolite), GS311-4 (Carbon and sulfur reference material), GS900-5 (Carbon and sulfur reference material), Graphite 4A (Internal graphite reference material), and Graphite 14 (Internal graphite reference material). Overall, this selection of reference materials is a poor matrix match for the Bissett Creek gneisses as only one gneiss CRM (SY-4) was run by Actlabs.

A summary of the analytes, method of analysis, limit of detection (LOD = 3.3*standard deviation of the blank), limit of quantification (LOQ = 10*standard deviation of the blank), accuracy and number of certified reference materials used to quantify the accuracy are summarized below in Table 4.1 and Table 4.2 ([Currie, 1968](#)). Accuracy was calculated using the formula of [Skoog and West \(1963\)](#):

$$\sum_{i=1}^n \left[\frac{(O_i - A) * 100}{A} \right] / n \quad (1)$$

where O_i is the *i*th value obtained from a measurement on a certified reference material, A is the actual value for that certified reference material, and n is the number of runs. Precision of the data, supplied by Actlabs, is as follows: ±100% at the detection limit, ±20% at 10 times the detection limit and ± 5% at 100 times the detection limit and was based on their control measurements during the analytical runs, which was not supplied ([A. Yung, pers. comm., 2018](#)). A full set of the Quality Assurance/Quality Control results are presented in Appendix D.

Table 4.1. Quality assurance and quality control information for major elements

Analyte	Method of Analysis	Limit of Detection (LOD) (wt. %)	Limit of Quantification (LOQ) (wt. %)	Accuracy lower bound (%)	Accuracy upper bound (%)	Average accuracy (%)	# of measurements on CRM's
SiO ₂	FUS-ICP-OES	0.01	0.03	-2.3	1.5	0.3	11
Al ₂ O ₃	FUS-ICP-OES	0.01	0.03	-1.3	8.9	1.9	11
Fe ₂ O _{3(T)}	FUS-ICP-OES	0.01	0.03	-5.1	2.9	0.1	11
MnO	FUS-ICP-OES	0.001	0.00	-13.8	7.1	0.4	11
MgO	FUS-ICP-OES	0.01	0.03	-1.5	6.1	1.2	11
CaO	FUS-ICP-OES	0.01	0.03	-2.1	3.4	0.5	11
Na ₂ O	FUS-ICP-OES	0.01	0.03	-4.3	7.3	1.3	11
K ₂ O	FUS-ICP-OES	0.01	0.03	-66.7	5.9	-5.4	11
TiO ₂	FUS-ICP-OES	0.001	0.00	-6.7	9.1	1.7	11
P ₂ O ₅	FUS-ICP-OES	0.01	0.03	-3.0	42.9	2.8	11
FeO	Titration	0.1	0.30	-5.7	3.2	-2.0	6
C _{graphitic}	IR	0.05	0.15	-4.1	1.0	-2.2	9
C _{Total}	IR	0.01	0.03	-4.6	0.4	-1.6	12
S _{Total}	IR	0.01	0.03	-3.5	2.0	-0.2	15

Table 4.2. Quality assurance and quality control information for minor and trace elements

Analyte	Method of Analysis	Limit of Detection (LOD) (ppm)	Limit of Quantification (LOQ) (ppm)	Accuracy lower bound (%)	Accuracy upper bound (%)	Average accuracy (%)	# of measurements on CRM's
Ba	FUS-ICP-OES	2	6	-11.0	1.5	-3.3	5
Sr	FUS-ICP-OES	2	6	-4.7	7.9	1.3	5
Y	FUS-ICP-OES	1	3	-25.0	3.0	-8.4	5
Sc	FUS-ICP-OES	1	3	-2.3	9.1	2.8	9
Zr	FUS-ICP-OES	2	6	-5.3	3.3	-1.8	5
Be	FUS-ICP-OES	1	3	0.0	15.4	7.7	6
V	FUS-ICP-OES	5	15	-7.6	4.7	0.2	5
V	FUS-ICP-OES	5	15	-11.1	4.8	7.0	9
Cr	FUS-ICP-MS	20	60	-4.4	8.7	20.5 ^a	5
Co	FUS-ICP-MS	1	3	-6.1	64.3	8.0	11
Ni	FUS-ICP-MS	20	60	-13.0	6.4	0.1	6
Cu	FUS-ICP-MS	10	30	-14.3	11.1	1.6	11
Zn	FUS-ICP-MS	30	90	-2.0	14.3	4.1	12
Ga	FUS-ICP-MS	1	3	-7.7	17.1	1.3	9
Ge	FUS-ICP-MS	0.5	1.5	-6.3	30.0	8.7	9
As	FUS-ICP-MS	5	15	-9.9	4.3	-3.1	3
Rb	FUS-ICP-MS	1	3	-8.7	1.8	-2.2	10
Sr	FUS-ICP-OES	2	6	-4.7	7.9	0.8	9
Y	FUS-ICP-MS	0.5	1.5	-12.3	5.1	-1.8	16
Zr	FUS-ICP-OES	1	3	-22.2	16.7	-0.2	9

Table 4.2. (Continued) Quality assurance and quality control information for minor and trace elements

Analyte	Method of Analysis	Limit of Detection (LOD) (ppm)	Limit of Quantification (LOQ) (ppm)	Accuracy lower bound (%)	Accuracy upper bound (%)	Average accuracy (%)	# of measurements on CRM's
Nb	FUS-ICP-MS	0.2	0.6	-15.4	9.1	-2.8	6
Mo	FUS-ICP-MS	2	6	-7.7	3.7	-3.1	7
Ag	FUS-ICP-MS	0.5	1.5	-25.9	200.0	65.7 ^b	3
In	FUS-ICP-MS	0.1	0.3	-23.1	-	-23.1 ^c	1
Sn	FUS-ICP-MS	1	3	-33.3	-	-33.3 ^d	1
Sb	FUS-ICP-MS	0.2	0.6	-6.3	9.7	1.7	2
Cs	FUS-ICP-MS	0.1	0.3	-9.1	4.3	-0.8	7
Ba	FUS-ICP-OES	2	6	-11.0	16.7	0.7	9
La	FUS-ICP-MS	0.05	0.15	-6.0	11.1	3.9	13
Ce	FUS-ICP-MS	0.05	0.15	-6.8	8.7	2.7	13
Pr	FUS-ICP-MS	0.01	0.03	-4.2	3.3	0.6	8
Nd	FUS-ICP-MS	0.05	0.15	-6.3	9.6	1.6	15
Sm	FUS-ICP-MS	0.01	0.03	-7.5	6.8	1.9	12
Eu	FUS-ICP-MS	0.005	0.015	-3.6	4.8	2.4	13
Gd	FUS-ICP-MS	0.01	0.03	-5.9	8.8	2.2	9
Tb	FUS-ICP-MS	0.01	0.03	-9.5	10.8	-0.9	10
Dy	FUS-ICP-MS	0.01	0.03	-3.0	14.3	4.1	11
Ho	FUS-ICP-MS	0.01	0.03	-4.4	4.8	0.6	10

Table 4.2. (Continued) Quality assurance and quality control information for minor and trace elements

Analyte	Method of Analysis	Limit of Detection (LOD) (ppm)	Limit of Quantification (LOQ) (ppm)	Accuracy lower bound (%)	Accuracy upper bound (%)	Average accuracy (%)	# of measurements on CRM's
Er	FUS-ICP-MS	0.01	0.03	-8.0	7.4	1.1	10
Tm	FUS-ICP-MS	0.005	0.015	-9.9	11.0	1.5	9
Yb	FUS-ICP-MS	0.01	0.03	-4.4	7.4	1.2	15
Lu	FUS-ICP-MS	0.002	0.006	-23.3	8.6	0.4	13
Hf	FUS-ICP-MS	0.1	0.3	-12.5	3.8	-4.3	6
Ta	FUS-ICP-MS	0.01	0.03	-7.5	21.1	5.2	7
W	FUS-ICP-MS	0.5	1.5	-33.3	800.0	253.1 ^e	3
Tl	FUS-ICP-MS	0.05	0.15	-4.5	15.0	5.4	3
Pb	FUS-ICP-MS	5	15	0.0	11.1	4.6	5
Bi	FUS-ICP-MS	0.1	0.3	-	-	-	0
Th	FUS-ICP-MS	0.05	0.15	-6.1	11.4	1.2	12
U	FUS-ICP-MS	0.01	0.03	-4.5	8.7	1.6	10

^a – One of the CRM concentrations analyzed was less than the LOQ.

^b – CRM concentrations analyzed for Ag were between the LOD and LOQ (0.5-1.5 ppm).

^c – The value analyzed for In was very close to the LOQ (~1.3 ppm).

^d – The values analyzed for Sn were between the LOD and LOQ (1-3ppm).

^e – One of the values measured very close to the limit of detection (~1 ppm)

4.4 Results

Geochemical data are presented in Appendix E. A summary of the major element geochemistry is found in Table 4.3 and Fig 4.1. All REE plots (Fig 4.2) were normalized using the carbonaceous chondrite values from [Anders and Grevesse \(1989\)](#). While initially several different REE profiles were plotted for comparison, the Post-Archean Average Australian Shale was selected for plotting because of the visual similarity between the profile and the profiles found through analysis and normalization of the gneisses. Where field relationships suggest a potential igneous origin for the rocks (e.g. the biotite-quartzofeldspathic gneiss and the amphibole-biotite-quartzofeldspathic gneiss), the rocks have been plotted on a Total Alkali Silica (TAS) diagram to provide some potential inference as to their potential igneous origins.

4.4.1 Biotite-Graphite-Quartzofeldspathic Gneiss

The biotite-graphite-quartzofeldspathic gneiss has concentrations of SiO_2 that range from 66.0 % to 79.6 wt.%. With increasing SiO_2 , values of Al_2O_3 , $\text{Fe}_2\text{O}_{3(\text{T})}$, MgO , CaO , Na_2O , TiO_2 and P_2O_5 decrease. Concentrations of K_2O and MnO do not covary with variations in SiO_2 (Fig 4.1). A carbonaceous chondrite-normalized REE plot shows gently to moderately sloping lines with $\text{La}_{\text{N}}/\text{Yb}_{\text{N}}$ ratios that vary from 1.6 to 11.4 (Fig 4.2A). All samples in this unit show a negative Eu anomaly. The Eu/Eu^* ratio is used to help quantify Eu anomalies and may be expressed in the following form as shown by [Condie \(1993\)](#):

$$\text{Eu}/\text{Eu}^* = \text{Eu}_{\text{N}}/(\text{Sm}_{\text{N}}^* \text{Gd}_{\text{N}})^{0.5} \quad (2)$$

Eu/Eu^* values range from 0.48 to 0.81, with a median of 0.68. The REE patterns of most biotite-graphite-quartzofeldspathic gneiss are similar to the values from the Post-Archean Average Australian Shale (PAAS). Notable exceptions are samples BC-11, CO-02, CO-04, CO-06 and CO-07. Sample BC-11 shows an irregular signature that does not agree well with other samples in this set and may have been generated due to the relatively high proportion of graphite in the sample when compared to others in the set and the fact that the 4Lithoresearch package is primarily meant for unmineralized materials.

Table 4.3. Summary of geochemical results

Analyte wt. %	Biotite-graphite-quartzofeldspathic gneiss			Clinopyroxene-amphibole-biotite-graphite gneiss			Garnet-amphibole-biotite-graphite gneiss		
	n = 8			n = 9			n = 4		
	Max.	Min.	Average	Max.	Min.	Average	Max.	Min.	Average
SiO ₂	79.55	66.00	70.96	79.71	65.96	71.61	68.27	50.40	57.59
Al ₂ O ₃	13.51	6.78	9.95	11.68	4.92	8.84	18.28	13.31	16.07
Fe ₂ O _{3(T)}	6.56	0.45	4.55	5.85	1.85	3.56	12.78	5.31	9.31
MnO	0.24	0.02	0.10	2.15	0.03	0.30	0.56	0.20	0.31
MgO	3.60	1.76	2.57	5.54	0.72	3.30	6.14	2.24	3.78
CaO	4.81	1.48	3.35	8.27	1.97	4.60	6.76	4.11	5.57
Na ₂ O	2.21	1.00	1.75	2.26	0.79	1.58	2.66	0.62	2.05
K ₂ O	3.38	1.32	2.08	3.92	0.61	2.32	3.56	1.83	2.64
TiO ₂	0.41	0.28	0.35	0.51	0.16	0.36	1.35	0.09	0.54
P ₂ O ₅	0.35	0.09	0.23	0.33	0.12	0.20	0.73	0.18	0.43

Analyte wt. %	Garnet-sillimanite-biotite-graphite gneiss			Amphibole-biotite-quartzofeldspathic gneiss			Biotite-quartzofeldspathic gneiss		
	n = 4			n = 2			n = 7		
	Max.	Min.	Average	Max.	Min.	Average	Max.	Min.	Average
SiO ₂	74.41	65.01	69.23	65.02	47.62	56.32	72.81	69.18	70.47
Al ₂ O ₃	15.65	9.75	12.96	22.14	15.37	18.76	15.88	11.59	14.24
Fe ₂ O _{3(T)}	6.07	3.77	4.98	11.91	4.84	8.38	5.61	2.49	3.48
MnO	0.96	0.06	0.29	0.33	0.08	0.20	0.12	0.06	0.08
MgO	4.17	2.26	2.82	3.38	2.29	2.84	1.45	0.15	0.90
CaO	6.21	0.39	2.23	3.84	1.68	2.76	1.64	0.68	1.38
Na ₂ O	1.76	0.79	1.23	3.29	3.16	3.23	4.59	1.55	3.46
K ₂ O	5.89	2.09	3.78	6.20	3.94	5.07	5.27	4.09	4.71
TiO ₂	0.63	0.42	0.53	0.82	0.54	0.68	0.57	0.39	0.46
P ₂ O ₅	0.16	0.04	0.09	0.19	0.16	0.18	0.12	0.03	0.08

Table 4.3. (Continued) Summary of geochemical results

Analyte wt. %	Garnet-sillimanite-biotite gneiss			Granitic pegmatites			Metagabbro intrusives		
	n = 1			n = 4			n = 1		
		Max.	Min.	Average	Max.	Min.	Average		
SiO ₂	82.49	73.29	69.34	71.82			45.96		
Al ₂ O ₃	8.17	15.97	14.10	14.79			16.27		
Fe ₂ O _{3(T)}	2.80	1.43	0.30	0.70			13.04		
MnO	0.03	0.01	0.00	0.01			0.164		
MgO	1.14	0.20	0.06	0.15			6.68		
CaO	0.19	1.26	0.16	0.45			8.65		
Na ₂ O	0.29	2.43	1.39	1.77			3.44		
K ₂ O	3.04	11.41	6.75	9.32			1.82		
TiO ₂	0.43	0.08	0.05	0.06			1.525		
P ₂ O ₅	0.07	0.03	0.01	0.02			0.29		

Analyte wt. %	RO - Biotite-graphite-quartzofeldspathic gneiss			RO - Amphibole-biotite-quartzofeldspathic gneiss			RO - Biotite-quartzofeldspathic gneiss		
	n = 5			n = 3			n = 5		
	Max.	Min.	Average	Max.	Min.	Average	Max.	Min.	Average
SiO ₂	75.10	60.92	69.71	70.49	51.28	64.03	73.44	62.14	68.54
Al ₂ O ₃	16.06	9.25	12.85	16.03	13.14	14.47	16.54	13.22	14.96
Fe ₂ O _{3(T)}	8.76	1.62	4.26	8.91	3.58	5.64	7.54	1.65	4.01
MnO	0.14	0.03	0.07	0.12	0.07	0.09	0.10	0.03	0.06
MgO	3.23	0.73	1.43	2.60	0.55	1.74	2.66	0.37	1.31
CaO	3.42	1.48	2.26	13.52	1.75	6.68	3.04	1.35	2.11
Na ₂ O	2.90	1.35	2.04	3.48	2.46	2.95	4.49	2.93	3.55
K ₂ O	4.72	2.16	3.67	5.00	0.75	2.19	4.61	3.10	3.77
TiO ₂	0.97	0.19	0.54	1.51	0.31	0.77	1.04	0.20	0.58
P ₂ O ₅	0.34	0.07	0.20	0.24	0.08	0.16	0.23	0.06	0.14

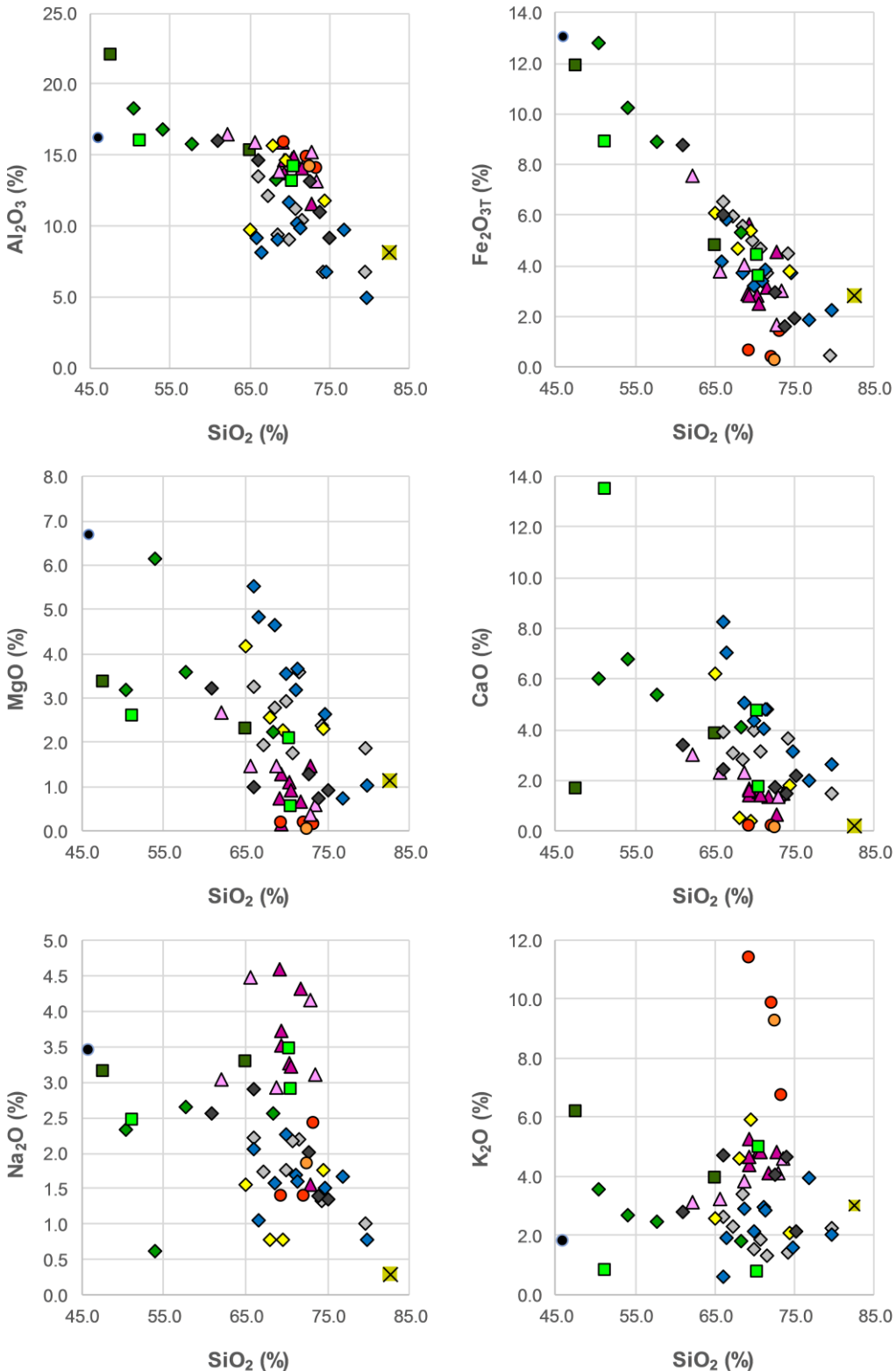


Fig. 4.1. Harker variance diagrams showing major element (Al_2O_3 , $\text{Fe}_2\text{O}_3(\text{T})$, MgO , CaO , Na_2O , K_2O , MnO , TiO_2 , P_2O_5) variation as it relates to SiO_2 . All data are presented as weight %.

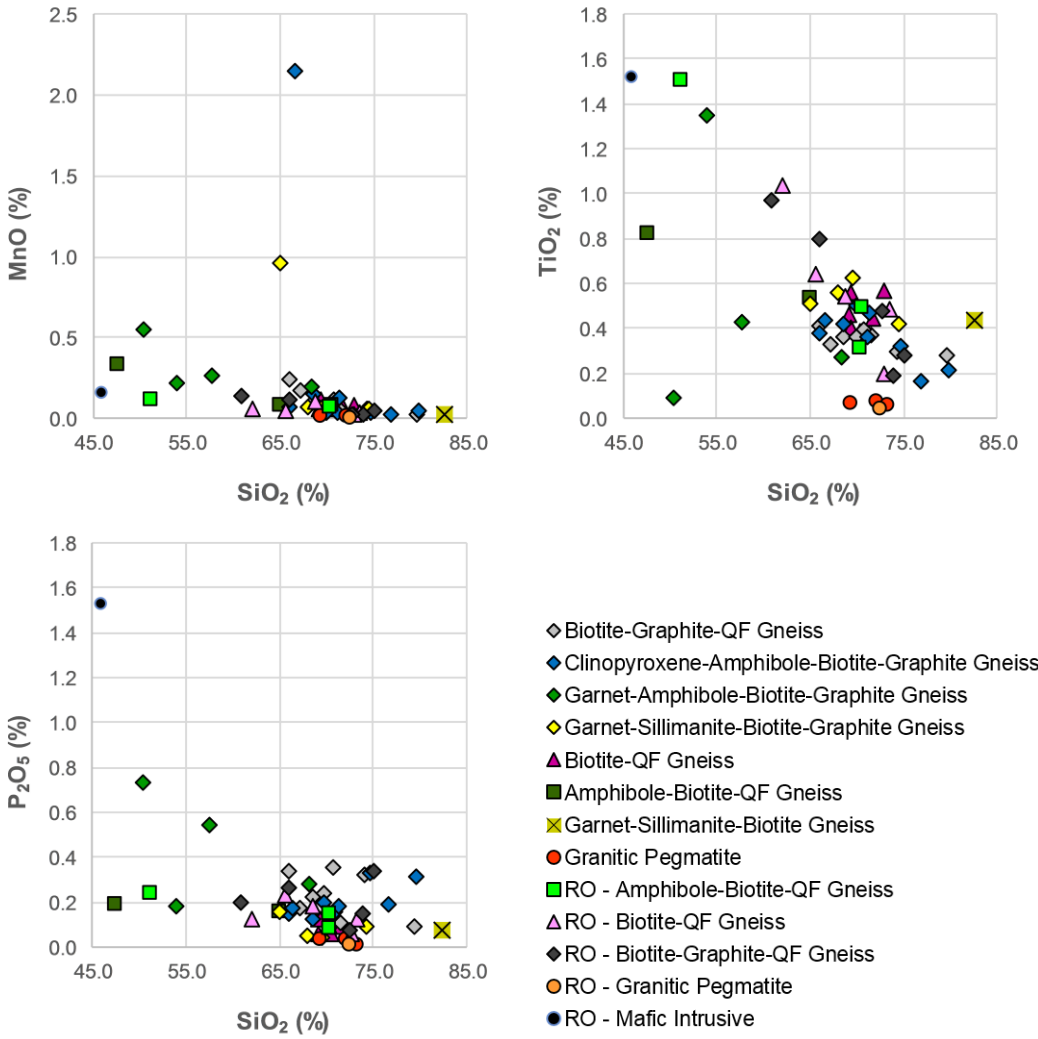


Fig. 4.1. (Continued) Harker variance diagrams showing major element (Al_2O_3 , $\text{Fe}_2\text{O}_3(\text{T})$, MgO , CaO , Na_2O , K_2O , MnO , TiO_2 , P_2O_5) variation as it relates to SiO_2 . All data are presented as weight %. QF – Quartzofeldspathic. RO – Road outcrop series of regional samples.

Sample CO-02 shows enrichment in heavy rare earth elements (HREEs, defined as the group from Tb to Lu) relative to other samples in the unit. CO-04 and CO-07 show slight depletion in HREE. CO-06 shows lower concentrations of La. There is good agreement between the Bissett Creek site samples and the road outcrop samples. Of the samples obtained, the amount of graphitic carbon (C_g) in the biotite-graphite-quartzofeldspathic gneiss unit varies from 0.54 to 4.12 wt. % with a median of 2.61 wt. % ($n = 11$). Total sulfur (S_{Tot}) concentrations ranged from 0.59 to 2.41 wt. % with a median of 1.17 wt. % ($n = 11$).

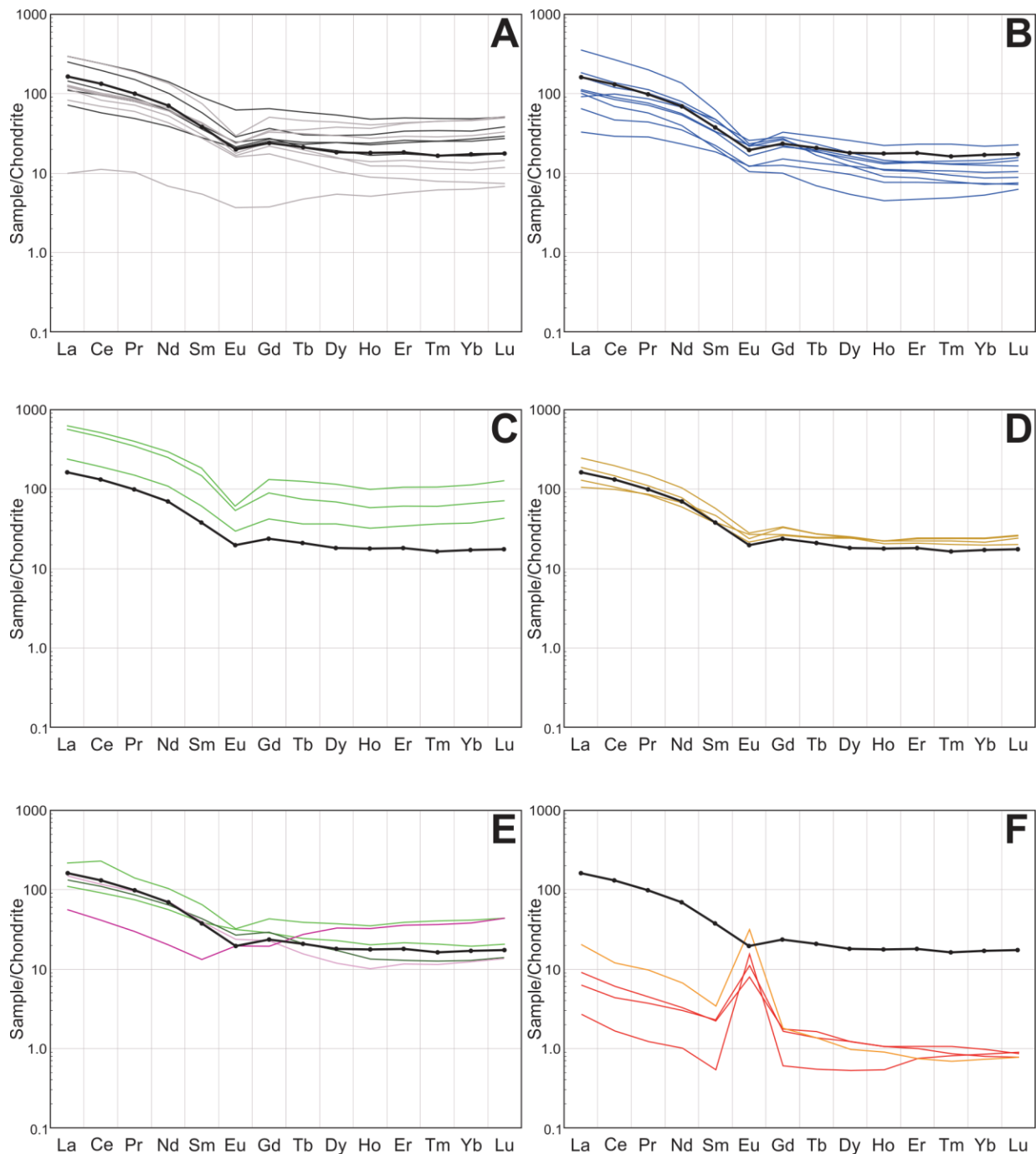


Fig. 4.2. Carbonaceous chondrite-normalized REE plots for (A) the biotite-graphite-quartzofeldspathic gneiss (light grey – Bissett site, dark grey – road outcrops), (B) the clinopyroxene-amphibole-biotite-graphite gneiss (C) the garnet-amphibole-biotite-graphite gneiss (D) the garnet-sillimanite-biotite graphite gneiss, (E) the biotite-quartzofeldspathic gneiss (dark pink – Bissett site, light pink -road outcrops) and the garnet-amphibole-biotite quartzofeldspathic gneiss (dark green – Bissett site, light green – road outcrops) and (F) the granitic pegmatites (red – Bissett site, buff – road outcrops. All values were normalized to the carbonaceous chondrite of [Anders and Grevesse \(1989\)](#). The thick black line represents REE values from the PAAS ([Taylor and McLennan, 1985](#)).

4.4.2 Clinopyroxene-Amphibole-Biotite-Graphite Gneiss

The clinopyroxene-amphibole-biotite-graphite gneiss has concentrations of SiO_2 that range from 65.9 to 79.7 wt.%. With increasing SiO_2 , concentrations of Al_2O_3 , $\text{Fe}_2\text{O}_{3(\text{T})}$, MgO , CaO , Na_2O , and TiO_2 decrease (Fig 4.1). MgO and CaO show particularly strong negative correlations with SiO_2 . Values of K_2O , MnO , and P_2O_5 do not covary with SiO_2 . Carbonaceous chondrite-normalized REE patterns have gentle to steep slopes with $\text{La}_{\text{N}}/\text{Yb}_{\text{N}}$ ratios that vary from 4.2 to 49.2 (Fig 4.2B). All samples show a slight negative Eu anomaly and depleted HREEs relative to PAAS. Eu/Eu^* values ranged from 0.55 to 0.81 with a median of 0.64. Sample BC-13 shows enrichment in the light rare earth elements (LREEs, defined as the group from La to Gd) relative to other samples in this unit. BC-08 has a depleted and flat chondrite-normalized REE profile relative to other samples. BC-22 has a steeper profile than BC-08 but is also depleted relative to other samples in this unit. BC-22 also appears to have a higher concentration of La. The amount of graphitic carbon in these samples range from 0.52 to 3.67 wt. % with a median of 1.08 wt. % ($n = 9$). Total sulfur (S_{Tot}) concentrations in this unit ranges from 0.72 to 1.96 wt. % with a median of 0.91 wt. % ($n = 8$).

4.4.3 Garnet-Amphibole-Biotite-Graphite Gneiss

The garnet-amphibole-biotite-graphite gneiss has values of SiO_2 that range from 50.4 to 68.3 wt. %. As the amount of SiO_2 increases the values of Al_2O_3 , $\text{Fe}_2\text{O}_{3(\text{T})}$, CaO , K_2O , MnO and P_2O_5 decrease (Fig. 4.1). MgO , Na_2O , and TiO_2 do not covary with SiO_2 . Carbonaceous chondrite-normalized REE signatures have gentle to moderate slopes with $\text{La}_{\text{N}}/\text{Yb}_{\text{N}}$ ratios that range from 4.8 to 8.6 (Fig 4.2C). All samples show a negative Eu anomaly, as Eu/Eu^* values range from 0.39 to 0.96 with a median value of 0.53. All samples from this unit have higher concentrations of the REE relative to the PAAS. The garnet-amphibole-biotite-graphite gneiss is enriched in REE compared to other graphitic gneiss units at the Bissett Creek flake graphite deposit. Two samples have graphitic carbon concentrations of 0.47 wt. % and 0.70 wt. %. Total sulfur (S_{Tot}) was measured for one sample in this unit and a value of 0.71 wt. % was returned.

4.4.4 Garnet-Biotite-Sillimanite-Graphite Gneiss

The garnet-biotite-sillimanite-graphite gneiss has SiO_2 concentrations that range from 65.0 to 74.4 wt.%. As the values of SiO_2 increase, Al_2O_3 , $\text{Fe}_2\text{O}_{3(\text{T})}$, MgO , TiO_2 and P_2O_5 decrease (Fig. 4.1). Concentrations of Na_2O and K_2O show a positive correlation with increasing SiO_2 . CaO and MnO do not vary systematically with SiO_2 . Carbonaceous chondrite-normalized REE patterns show gentle to moderate slopes with $\text{La}_{\text{N}}/\text{Yb}_{\text{N}}$ ratios that vary from 5.4 to 11.4 (Fig 4.2D). Concentrations of REEs in this unit are similar to PAAS. All samples show negative Eu anomalies and enrichment in HREEs relative to PAAS. Eu/Eu^* values range from 0.60 to 0.83, with a median value of 0.66. Sample CO-05 contains a less significant Eu anomaly than other samples in this set. The values of graphitic carbon are 0.11, 0.28 and 1.02 wt. %. The 0.11 wt. % value is lower than the limit of quantification of 0.15 wt. %. Two total sulfur concentrations were measured for this unit, which was 1.34 and 1.96 wt. %.

4.4.5 Biotite-Quartzofeldspathic Gneiss

The biotite-quartzofeldspathic gneiss has SiO_2 concentrations that vary from 69.2 to 72.8 wt.%. As the concentrations of SiO_2 increase, the values of Al_2O_3 , $\text{Fe}_2\text{O}_{3(\text{T})}$, MgO , CaO , TiO_2 , and P_2O_5 decrease. K_2O shows a small increase as the amount of SiO_2 increases. Na_2O and MnO do not systematically covary with SiO_2 (Fig 4.1). One sample from the Bissett Creek property and one regional sample were analyzed for REEs in this unit. Carbonaceous chondrite-normalized REE values from two samples show gentle to moderate sloping lines with a $\text{La}_{\text{N}}/\text{Yb}_{\text{N}}$ ratios of 1.5 and 12.0 (Fig 4.2E). BC-26 is depleted in LREEs and enriched in HREEs, with the exception of Eu, when compared to PAAS. Eu/Eu^* values are 1.21 for BC-26 and 0.79 for RO-03. Plotting of these samples on a TAS diagram for plutonic rocks ([Middlemost, 1994](#)) yields a tight cluster near the triple junction point between granite, granodiorite and a quartz monzonite, with most samples plotting in the granite field (Fig 4.3).

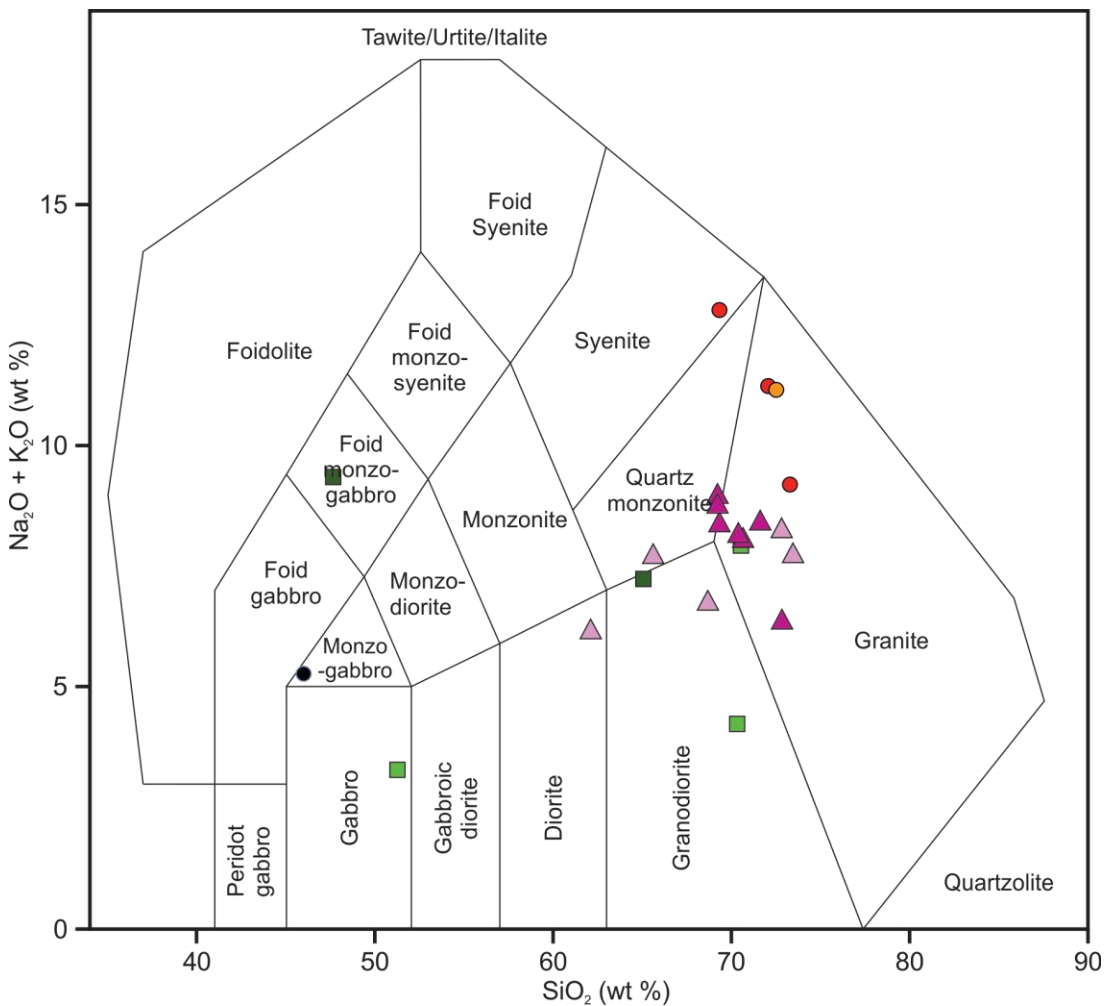


Fig. 4.3. Total Alkali Silica (TAS) diagram for igneous plutonic rock classification from Middlemost (1994). Symbols are the same as in Figure 4.1.

4.4.6 Amphibole-Biotite-Quartzofeldspathic Gneiss

The amphibole-biotite-quartzofeldspathic gneiss has SiO_2 concentrations that vary from 47.6 to 65.0 wt.%. As the concentrations of SiO_2 increase, the values of Al_2O_3 , $\text{Fe}_2\text{O}_{3(\text{T})}$, MgO , CaO , TiO_2 , and P_2O_5 decrease. Na_2O shows a positive correlation with SiO_2 . K_2O and MnO do not covary with SiO_2 . One sample from the Bissett Creek property and two regional samples were analyzed for REEs in this unit. Carbonaceous chondrite-normalized REE values show moderate slopes with La_N/Yb_N ratios of 10.1, 5.2 and 5.6, respectively (Fig 4.2E). All samples show negative Eu anomalies with Eu/Eu^* values of 0.76, 0.96 and 0.62, respectively. The signature of sample BC-24 is broadly consistent with the average continental crust (Wedepohl,

1995). Plotting of these samples on a TAS diagram for plutonic rocks (Middlemost, 1994) yields a wide array of potential compositions for the amphibole-biotite-quartzofeldspathic protoliths such as gabbro, foid monzogabbro, granodiorite and granite (Fig 4.3).

4.4.7 Garnet-Biotite-Sillimanite Gneiss

As only one sample was obtained from this unit, the opportunities for comparison are limited. However, comparison with the garnet-sillimanite-graphite gneiss can be completed. The garnet-biotite-sillimanite barren gneiss has a much higher proportion of SiO₂ and is depleted in Al₂O₃, Fe₂O_{3(T)}, MgO, CaO and Na₂O relative to its mineralized counterpart. Concentrations of K₂O, MnO, TiO₂, and P₂O₅ are similar in the two units.

4.4.8 Granitic Pegmatite

The granitic pegmatites have concentrations of SiO₂ that range from 69.3% to 73.3%. As the concentrations of SiO₂ increase, the values of Al₂O₃, K₂O and P₂O₅ decrease. Fe₂O_{3(T)}, MgO, CaO, MnO, and TiO₂ do not have clear trends with SiO₂. Na₂O is positively correlated with SiO₂. Carbonaceous chondrite-normalized REE slopes are gentle to steep with a range of La_N/Yb_N ratios from 3.2 to 27.9. All samples have strong positive Eu anomalies, with Eu/Eu* values that range from 4.0 to 26.5 with a median of 9.1 (Fig 4.2F). Plotting of these samples on a TAS diagram for plutonic rocks (Middlemost, 1994) yields a trend of classifications ranging from syenite to granite, with three out of four samples plotting in the granite field (Fig 4.3).

4.4.9 Metagabbro Intrusive

Plotting of the sample RO-16-13 on the TAS geochemical classification for plutonic rocks of Middlemost (1994) identifies the potential protolith as a monzogabbro. A thin section of sample BC-16-21 revealed significant weathering/alteration and was therefore not analyzed for geochemistry.

5.0 Stable Isotope Geochemistry

Stable carbon isotopes are commonly used to study the origins of carbon in graphite deposits (Luque *et al.*, 2012; Volkert *et al.*, 2000). In this thesis, carbon isotopes and sulfur isotopes are used to help determine the source of the carbon that formed the flake graphite in the Bissett Creek deposit and surrounding area, as well as evaluate if the graphite was generated through *in situ* metamorphic processes, by the introduction of hydrothermal fluids, or by some combination of both. These two goals coincide with Research Objectives 2 and 6, respectively. Depending on the sources, stable isotopes could also be helpful in constraining the protoliths of the deposit as well, helping to address Research Objective 1.

5.1 Carbon Isotopes

Isotopically stable carbon occurs in two main states: isotopically light carbon (^{12}C) which accounts for 98.9% of carbon abundance and isotopically heavy carbon (^{13}C) which accounts for 1.1% of carbon abundance (Schidlowski, 2001). Carbon isotopes are usually reported as $\delta^{13}\text{C}$ measured in relation to the VPDB standard (Vienna Pee Dee Cretaceous belemnite standard replacement for the now exhausted Pee Dee belemnite from South Carolina) (Gonfiantini, 1984; Coplen, 1994). This notation is expressed in the following form (Coplen, 1994):

$$\delta^{13}\text{C} \text{ (units of ‰)} = \{[(^{13}\text{C}/^{12}\text{C}_{\text{sample}})/(^{13}\text{C}/^{12}\text{C}_{\text{standard}})] - 1\} \times 1000 \quad (3)$$

Carbon isotope ratios can be used to discern the source of carbon for graphite deposits because these ratios can vary between different geological reservoirs. There are three main sources of carbon that form graphite: (1) carbon from organic materials, (2) carbon from carbonates and (3) igneous carbon from mantle sources (Luque *et al.*, 2012). Organic materials commonly have negative (isotopically light) carbon isotope signatures because of biological processes (Schidlowski, 1988; Schidlowski, 2001). Carbon with isotopically lighter signatures can also be generated from 1) high-temperature disproportionation of siderite, 2) low-temperature Fischer-Tropsch synthesis and 3) inclusion of meteoritic carbonaceous matter (Perry and Ahmad, 1977; Schidlowski *et al.*, 1979; van Zuilen *et al.*, 2003; Horita, 2005; Tashiro *et al.*, 2017). The carbon isotope signature of carbonates is restricted to around 0 (± 3) ‰ (Schidlowski, 1988; Schidlowski, 2001). Carbon sourced from the mantle has a range of isotope ratios between -8 and -3 ‰ (Javoy *et al.* 1986; Deines *et al.*, 1991; Viljoen, 1995). Carbon from organic sources

has signatures that vary from -85 ‰ to 6 ‰ depending on the source of the organic material, but most sources fall in the range between -40 ‰ and 6 ‰ (Schidlowski 1988; Schidlowski 2001; Luque *et al.*, 2012).

Carbon isotope data for Proterozoic black shales are relatively scarce. However, three Mesoproterozoic black shales have carbon isotope ratios that fall within a consistent range from -35.6 ‰ to -29.0 ‰ (Ho *et al.*, 1990; Blumberg *et al.*, 2012). The first is the Tourist Formation black shale (~1.1 Ga) located in Mauritania, whose biomarkers ranges in composition from -35.6 ‰ to -30 ‰ (n = 83) (Blumberg *et al.*, 2012). The second is the Nonesuch Formation (~1.1 Ga) located in Michigan, USA with carbon isotope compositions that range from -33.6 ‰ to -31.3 ‰ (n = 6) (Ho *et al.*, 1990). The third is the black shales of the Roper Group in Australia, which includes the McMinn Formation and Velkerri Formation (~1.36 Ga), with carbon isotope values that range from -34.6‰ to -32.1 ‰ (n = 32) (Johnston *et al.*, 2008).

A complication of using carbon isotope ratios to determine the source of carbon in graphite deposits is that metamorphism can affect the ratios. High-grade metamorphic rocks contain isotopically heavier carbon than their lower grade equivalents (Hoefs and Frey, 1976; Wada *et al.*, 1994). Thus, the signature can fluctuate based on peak metamorphic grade, mostly as it relates to temperature. Determining the source of fluids using carbon isotopes can be even more challenging as the isotopic signature is similar to that of the fluid source or materials that buffer with the fluid (Luque *et al.*, 1998; Rosing-Schow *et al.*, 2016).

Graphite derived from metamorphic processes that have a predecessor of a biogenic carbon source is isotopically light, with $\delta^{13}\text{C}$ signatures values that range from -49‰ to -18‰, averaging around -25‰ (Schidlowski, 2001, Luque *et al.*, 2012). The isotopic ratio formed under these conditions can be homogeneous if graphite is formed from the same precursor material under a similar metamorphic grade (Luque *et al.*, 2012). The stable carbon isotope ratios of hydrothermally deposited graphite are more enigmatic because isotopic ratios are affected by the fluid source and the processes associated with precipitation (Luque *et al.*, 1998). Thus, the carbon isotope values for fluid deposited graphite can range through all potentially known compositions of the source materials whether they be carbonates, mantle-derived fluids or biogenic materials. Additionally, fluid deposited graphite can form through multi-stage

precipitation from fluids (e.g. Binu-Lal *et al.*, 2003; Satish-Kumar *et al.*, 2011) which can result in different isotopic signatures within a single grain.

5.1.2 Methodology

Samples were measured from the whole-rock powders used for geochemistry (section 4.1). The use of whole rock powders for carbon isotopes was appropriate because graphitic carbon made up most of the total carbon content of the samples (Fig 5.1). However, it should be noted that even samples with small amounts (>5% of carbon content in the rock) of non-graphitic carbon could have some shift in their values because of isotopic exchange between carbon species. Samples for carbon isotope analysis were sent to the Queen's Facility for Isotope Research (QFIR) at Queen's University and samples were processed in compliance with their standard carbon isotope analysis procedures. Samples with weights ranging from 0.09 to 12.37 milligrams were placed into tin capsules. The tin capsules were then placed into the instrument. Initial combustion to CO₂ was followed by analysis in a Costech ECS 4010 Elemental Analyzer coupled to a Thermo-Finnigan DeltaPlus XP Continuous-Flow Isotope Ratio Mass Spectrometer (CF-IRMS).

The δ¹³C values obtained from the measurement are reported using delta (δ) notation with units of per mil (‰) relative to VPDB international standard. The precision of the VPDB standard was 0.2‰ (E. Leduc, pers. comm., 2017). The quality assurance and control program at QFIR includes the analysis of (1) Certified Reference Materials and secondary standards, (2) random duplication of unknown samples and (3) blanks (E. Leduc, pers. comm., 2017). These materials constitute a minimum of 10% of the total analyses (E. Leduc, pers. comm., 2017). The primary reference material was the VPDB, while the secondary reference material was NBS-21 (graphite) (E. Leduc, pers. comm., 2018).

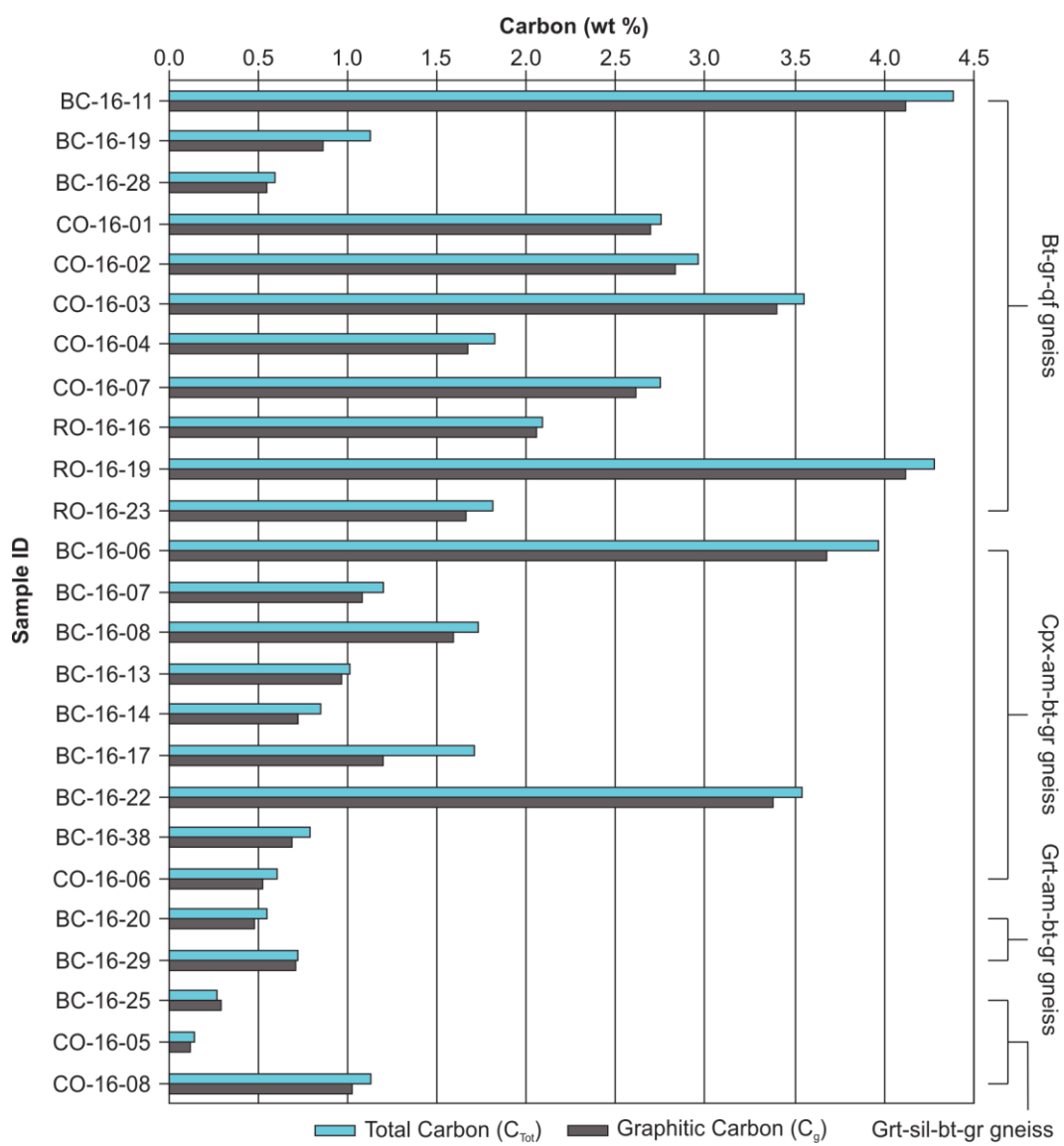


Fig. 5.1. Total carbon content (C_{Tot}) versus graphitic carbon (C_g) content of samples analyzed for carbon isotopes. Bt-gr-qf gneiss: Biotite-graphite-quartzofeldspathic gneiss, Cpx-am-bt-gr gneiss: Clinopyroxene-amphibole-biotite-graphite gneiss, Grt-am-bt-gr: Garnet-amphibole-biotite-graphite gneiss, Grt-sil-bt-gr gneiss: Garnet-sillimanite-biotite-graphite gneiss. Sample BC-16-25 likely shows a greater amount C_g than C_{Tot} because of the precision related to determining the C_g value at low concentrations. Given the potential for up to 20 % variation in the data at 10 times the graphitic carbon detection limit (0.50 wt %), this value falls within the range of analytical uncertainty of measurements at low concentrations.

5.2.2 Results

The $\delta^{13}\text{C}$ signatures for each of the samples analyzed from the Bissett Creek flake graphite deposit and surrounding regional outcrops are summarized below in Table 5.1 and Fig. 5.2. A summary of carbon isotope values by the unit is provided in Fig. 5.3. The carbon isotope values obtained from the Bissett Creek deposit ranged from $-28.3\text{\textperthousand}$ to $-14.0\text{\textperthousand}$, with an average of $-21.8\text{\textperthousand}$ ($n = 30$; Fig 5.1). Carbon isotope ratios from the biotite-graphite-quartzofeldspathic gneiss ranged from $-28.3\text{\textperthousand}$ to $-17.9\text{\textperthousand}$ with an average of $-24.2\text{\textperthousand}$ ($n=8$). Carbon isotope values from the clinopyroxene-amphibole-biotite-graphite gneiss ranged from $-27.2\text{\textperthousand}$ to $-14.1\text{\textperthousand}$ with an average of $-21.3\text{\textperthousand}$ ($n=9$). Carbon isotope values from the garnet-amphibole-biotite-graphite gneiss fluctuated from $-24.6\text{\textperthousand}$ to $-16.6\text{\textperthousand}$, with an average of $-21.5\text{\textperthousand}$ ($n=3$). Finally, carbon isotope ratios in the garnet-sillimanite-biotite-graphite gneiss ranged from $-24.4\text{\textperthousand}$ to $-15.5\text{\textperthousand}$ with an average of $-20.6\text{\textperthousand}$ ($n=4$). The regional samples, which were found in a biotite-graphite-quartzofeldspathic gneiss, ranged from $-31.7\text{\textperthousand}$ to $-19.3\text{\textperthousand}$ with an average of $-27.4\text{\textperthousand}$ ($n=3$). A plot of the carbon isotopes against the graphite content of the rocks analyzed yielded a loose linear relationship between the two variables (Fig 5.4). As the graphitic carbon content increases, the isotope signature becomes lighter (more negative).

Table 5.1. Carbon isotope values and abundances

Sample ID:	Lithology:	$\delta^{13}\text{C}$ ‰ vs VPDB:	C_{Tot} (wt %)	$C_{\text{graphitic}}$ (wt %)	$\Delta C = C_{\text{tot}} - C_g$	% $C_{\text{non-graphitic}}$
BC-16-11	Biotite-graphite-quartzofeldspathic gneiss	-24.4	4.38	4.11	0.27	6.2
BC-16-19	Biotite-graphite-quartzofeldspathic gneiss	-17.9	1.12	0.85	0.27	24.1
BC-16-28	Biotite-graphite-quartzofeldspathic gneiss	-23.3	0.59	0.54	0.05	8.5
CO-16-01	Biotite-graphite-quartzofeldspathic gneiss	-28.3	2.74	2.69	0.05	1.8
CO-16-02	Biotite-graphite-quartzofeldspathic gneiss	-26.7	2.95	2.83	0.12	4.1
CO-16-03	Biotite-graphite-quartzofeldspathic gneiss	-27.4	3.55	3.4	0.15	4.2
CO-16-04	Biotite-graphite-quartzofeldspathic gneiss	-20.1	1.82	1.67	0.15	8.2
CO-16-07	Biotite-graphite-quartzofeldspathic gneiss	-25.5	2.74	2.61	0.13	4.7
RO-16-16	Biotite-graphite-quartzofeldspathic gneiss	-31.3	2.08	2.05	0.03	1.4
RO-16-19	Biotite-graphite-quartzofeldspathic gneiss	-31.7	4.28	4.12	0.16	3.7
RO-16-23	Biotite-graphite-quartzofeldspathic gneiss	-19.3	1.80	1.66	0.14	7.8
BC-16-06	Clinopyroxene-amphibole-biotite-graphite gneiss	-27.2	3.96	3.67	0.29	7.3
BC-16-07	Clinopyroxene-amphibole-biotite-graphite gneiss	-19.4	1.19	1.08	0.11	9.2
BC-16-08	Clinopyroxene-amphibole-biotite-graphite gneiss	-23.7	1.72	1.59	0.13	7.6
BC-16-13	Clinopyroxene-amphibole-biotite-graphite gneiss	-24.5	1.01	0.96	0.05	5.0
BC-16-14	Clinopyroxene-amphibole-biotite-graphite gneiss	-17.1	0.84	0.72	0.12	14.3
BC-16-17	Clinopyroxene-amphibole-biotite-graphite gneiss	-17.3	1.7	1.19	0.51	30.0
BC-16-22	Clinopyroxene-amphibole-biotite-graphite gneiss	-25.9	3.54	3.37	0.17	4.8
BC-16-38	Clinopyroxene-amphibole-biotite-graphite gneiss	-22.6	0.78	0.68	0.1	12.8
CO-16-06	Clinopyroxene-amphibole-biotite-graphite gneiss	-14.0	0.6	0.52	0.08	13.3
BC-16-20	Garnet-amphibole-biotite-graphite gneiss	-16.6	0.54	0.47	0.07	13.0
BC-16-29	Garnet-amphibole-biotite-graphite gneiss	-24.6	0.72	0.7	0.02	2.8
CO-16-09	Garnet-amphibole-biotite-graphite gneiss	-23.3	-	-	-	-
BC-16-25	Garnet-sillimanite-biotite-graphite gneiss	-22.9	0.26	0.28*	-0.02	-7.7
CO-16-05	Garnet-sillimanite-biotite-graphite gneiss	-19.5	0.14	0.11	0.03	21.4
CO-16-08	Garnet-sillimanite-biotite-graphite gneiss	-15.5	1.12	1.02	0.1	8.9
CO-16-10	Garnet-sillimanite-biotite-graphite gneiss	-24.4	-	-	-	-

The bolded value is below the limit of quantification (LOQ). LOQ \approx 3*LOD (Currie, 1968). *- value suspect as C_g cannot be greater than C_{Tot}

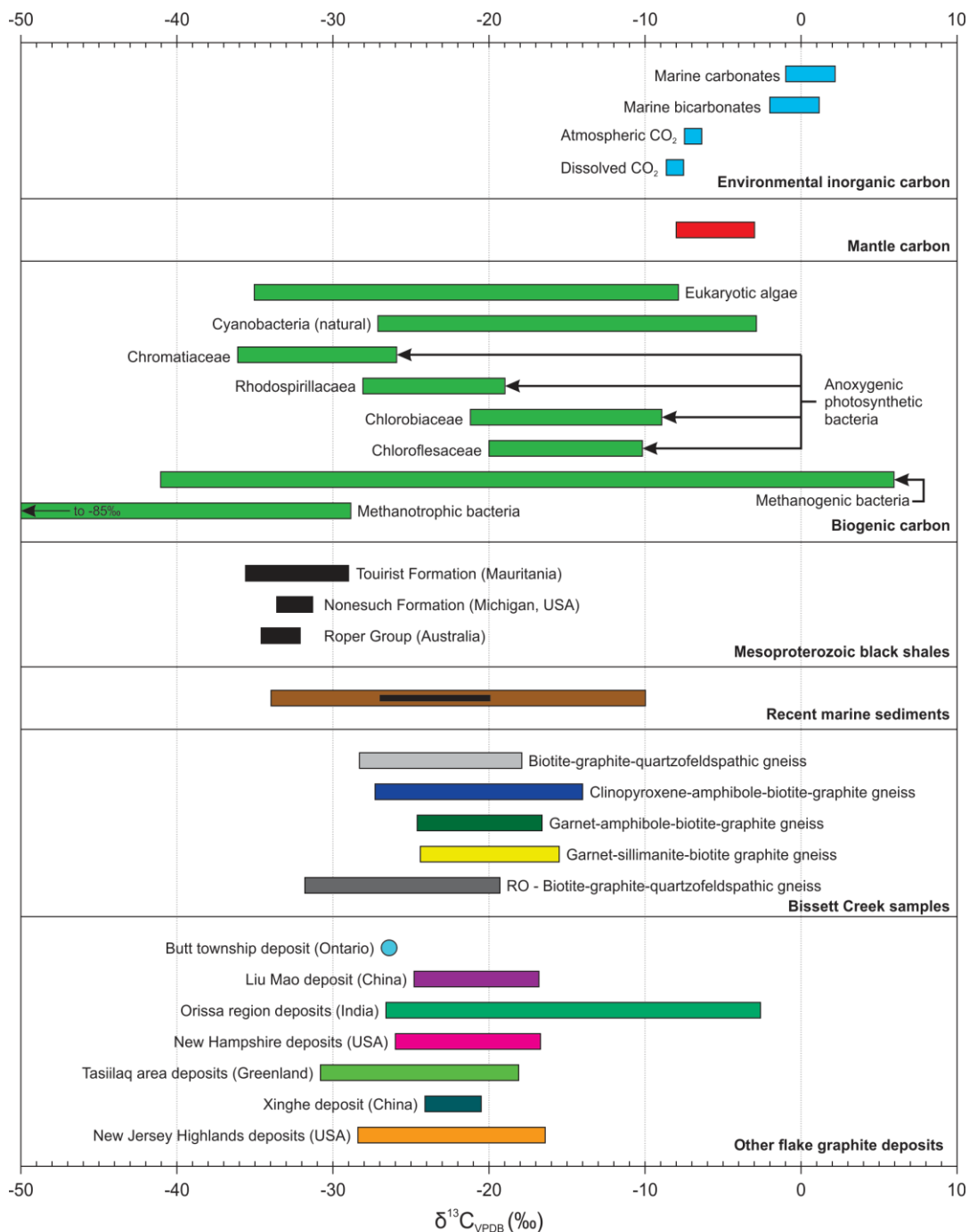


Fig. 5.2. Carbon isotope values for whole rock powders at the Bissett Creek property and surrounding area compared with the carbon isotope values from different potential reservoirs and similar units from other flake graphite deposits. Organic and marine carbon isotope values are supplied from Schidlowski (1988) and Schidlowski (2001). Mantle carbonate values are from a variety of sources (Javoy *et al.* 1986; Deines *et al.*, 1991; Viljoen, 1995). Mesoproterozoic black shales are from Ho *et al.*, (1990), Johnston *et al.*, (2008), and Blumenburg *et al.*, (2012). Carbon isotopes from deposits are from a variety of sources (Duke and Rumble, 1986; Garland, 1987; Wilde *et al.*, 1999; Volkert *et al.*, 2000; Sanyal *et al.*, 2009; Yang *et al.*, 2014; Rosing-Schow *et al.*, 2016). RO - Samples from road outcrops in the region surrounding the Bissett Creek deposit.

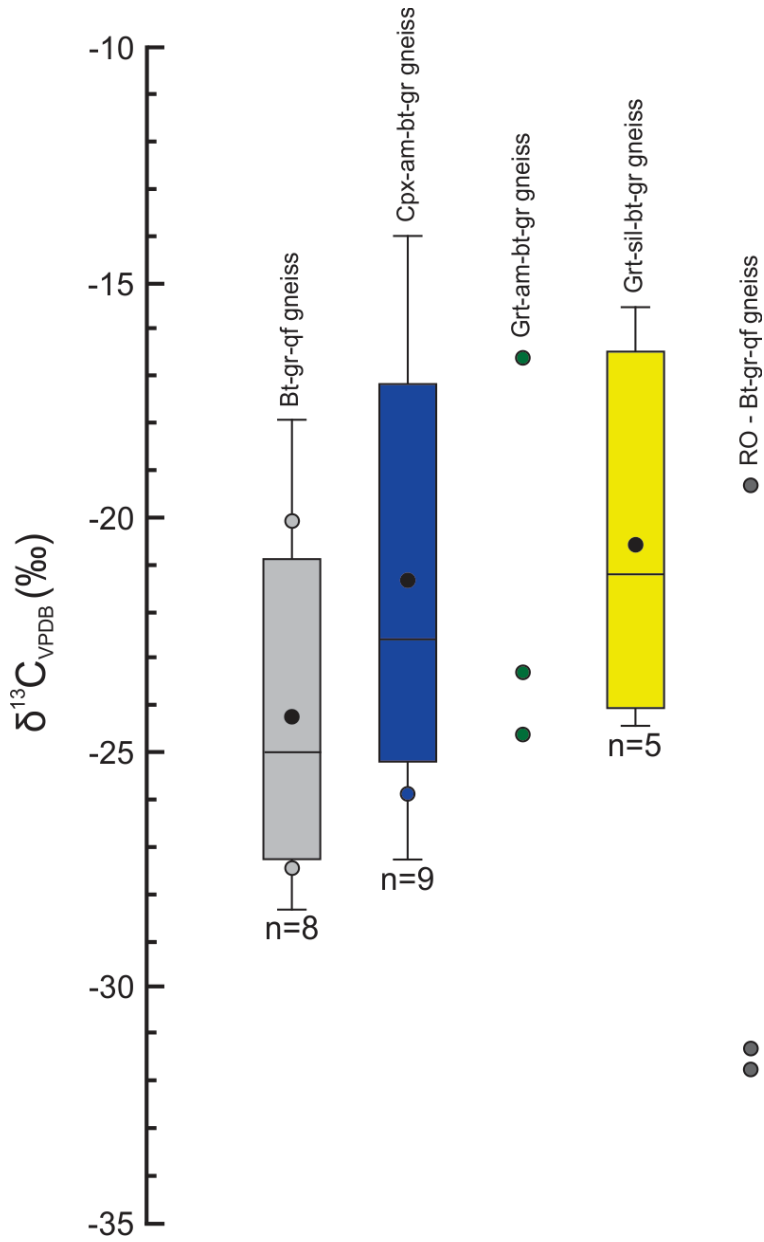


Fig. 5.3. Box plot of carbon isotope values for the graphitic gneisses found at Bissett Creek. Whiskers extend to the full range of values reported. The horizontal black line in the box represents the median. The black circle represents the mean. The box extends to the upper and lower quartiles of the ranges. Where values extended outside of the quartiles, they were plotted as individual circles. In the case where there were not enough values ($n=<5$) to generate a box and whisker plot, individual values were plotted. RO - Samples from road outcrops in the region surrounding the Bissett Creek deposit.

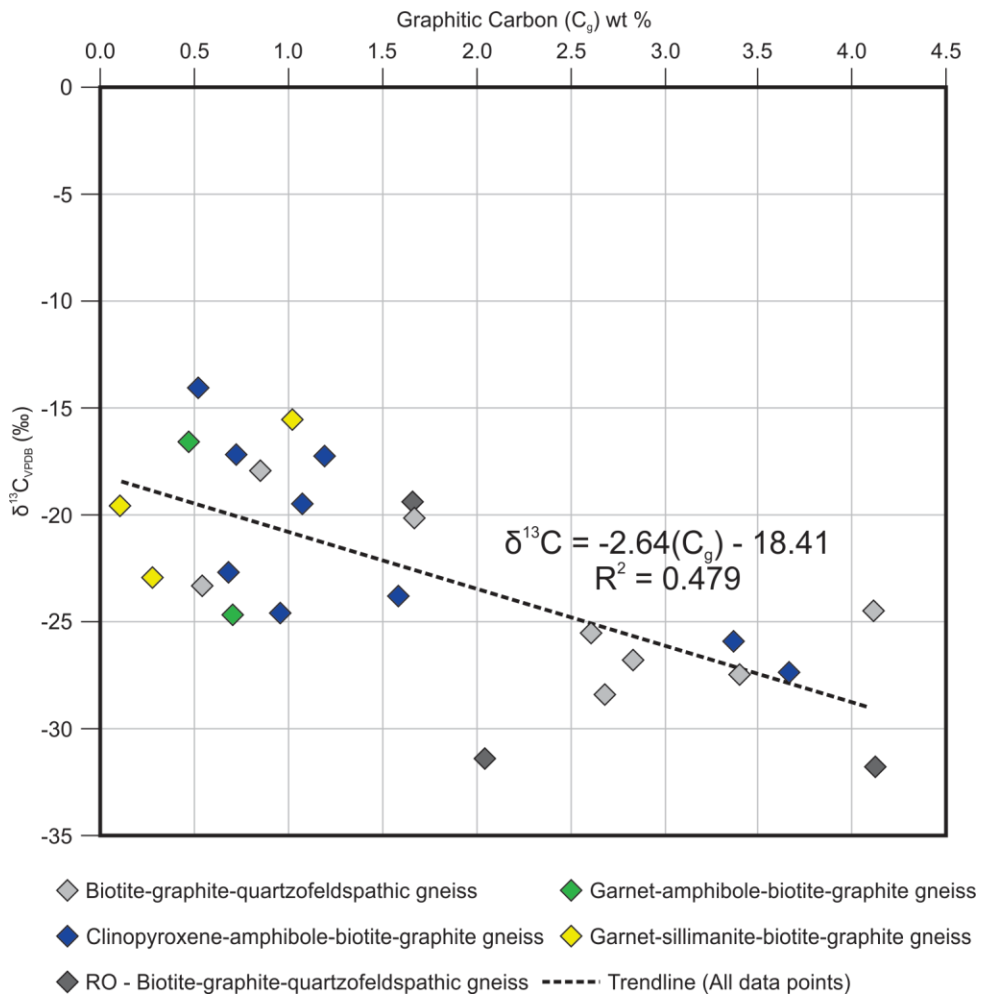


Fig. 5.4. Carbon isotope signatures ($\delta^{13}\text{C}_{\text{VPDB}}$) versus graphitic carbon (C_g).

5.2 Sulfur Isotopes

Sulfur has four stable isotopes, including ^{32}S , ^{33}S , ^{34}S , and ^{36}S . The relative abundance of each of these sulfur isotopes in nature are approximately: 95.02%, 0.75%, 4.21% and 0.02%, respectively, as determined from meteorites thought to be representative of the primordial earth (Macnamara and Thode, 1950). Sulfur isotopes are presented in the $\delta^{34}\text{S}$ measured in relation to the VCDT standard (Vienna Canyon Diablo Troilite standard replacement for the now exhausted Canyon Diablo troilite) (Krouse and Coplen, 1997). This notation is expressed as (Krouse and Coplen, 1997):

$$\delta^{34}\text{S} \text{ (units of ‰)} = \{[(^{34}\text{S}/^{32}\text{S}_{\text{sample}})/(^{34}\text{S}/^{32}\text{S}_{\text{standard}})] - 1\} \times 1000 \quad (4)$$

Previous studies of graphite deposits have mostly focused on carbon isotopes to evaluate the source of carbon responsible for graphite precipitation and the protoliths of graphite-bearing rocks (e.g. [Luque et al., 2012](#)). This is the second study to also use sulfur isotopes to help distinguish the protolith from which the deposit originated. The isotopic signature of sulfur varies in different geological reservoirs (Fig 5.5). Sulfur from seawater and ancient marine evaporites have positive $\delta^{34}\text{S}$ values that range from 9 to 41‰ ([Nielsen, 1979; Seal et al., 2000](#)). Igneous rocks and petroleum and coal deposits have values that vary from slightly negative (~ -10‰) to moderately positive (~20‰) ([Nielsen, 1979; Seal et al., 2000](#)). Modern and ancient sedimentary pyrite has a very wide range of possible values and ranges from < -50‰ to ~20‰ ([Nielsen, 1979; Seal et al., 2000](#)).

Mesoproterozoic black shales show a wide range of potential sulfide (predominantly pyrite) compositions. The Mesoproterozoic black shales of the Roper Group in Australia have sulfur isotope compositions that range from -23.4‰ to 24.7‰ with a median value of 11.9‰ (n = 32) ([Johnston et al., 2008](#)). The sulfur isotope signature of the Nonesuch Formation ranges from -0.9‰ to 13.1‰ with a median of 6.2‰ (n = 14) ([Imbus et al., 1992](#)). While the overall values have a wide range, most values are positive (i.e. isotopically heavy).

Unlike carbon isotopes, sulfur isotopes do not show significant fractionation in response to metamorphism. Metamorphism in a closed system metamorphism is thought to homogenize the sulfur isotope signature. Homogenization causes the range of isotope values to narrow, but the range will still retain the isotope signature from the reservoir associated with deposition ([Zheng, 1990; Cook and Hoefs, 1997](#)). In an open system, where components may be removed, or new components added by an influx of fluids, a wider range of sulfur isotope values would be expected.

5.2.1 Methodology

Sample material for sulfur isotope analysis was taken from the whole rock powders used for geochemistry (Section 4.1). The primary sulfur-bearing mineral species in these samples were pyrrhotite and pyrite. Samples were sent to the Environmental Isotope Laboratory (UW-EIL) at the University of Waterloo. Samples ranging from 1.3 mg to 3.1 mg (depending on the concentration of sulfur) were loaded into 3.5 mm x 5mm tin capsules. Loaded tin capsules were dropped into the Costech ECS 4010 Elemental Analyzer. The isotopic composition of the sample

was determined through combustion conversion (1000°C reactor, 90°C column, 115ml/min. He) of the solid sulfur-bearing materials into SO₂ gas. The gas was then run through an Isochrom Continuous Flow Isotope Ratio Mass Spectrometer which was connected to the Costech ECS 4010 Elemental Analyzer. The δ³⁴S values were reported using the delta (δ) notation with units of per mil (‰) relative to the VCDT international standard with a standard deviation ranging from 0.30 to 0.31‰ during the two analytical runs. The UW-EIL quality assurance and quality control program consisted of two aspects. Firstly, during the analytical runs, at least 20% of all materials analyzed were either in-house references or international reference materials. For the sulfur isotopes measured, the international reference materials used were: IAEA-S1, IAEA-S2, IAEA-S3 (AgS). Secondly, to ensure repeatability, 1 in 10 analyses was duplicated.

5.2.2 Results

Twenty-two samples were analyzed for sulfur isotope signatures and the results are summarized in Table 5.2 and Fig 5.5. A summary of the sulfur isotope values by the unit is shown in Fig. 5.6. Nineteen samples are from the Bissett Creek deposit and three samples are from regional outcrops. At the Bissett Creek deposit, δ³⁴S values range from 9.7‰ to 15.0‰, with an average of 12.4‰ (Fig 5.4). Values of δ³⁴S in the biotite-graphite-quartzofeldspathic gneiss ranged from 10.0‰ to 13.6‰, with an average of 11.6‰ (n = 8). Clinopyroxene-amphibole-biotite-graphite gneiss yielded values ranging from 9.7‰ to 15.0‰, with an average of 12.9‰ (n = 8). One sample from the garnet-amphibole-biotite-graphite gneiss produced a value of 11.3‰. Two samples from the garnet-sillimanite-graphite-biotite unit yielded values of 14.2‰ and 14.3‰. The regional samples were found in a biotite-graphite-quartzofeldspathic gneiss and the sulfur isotope values ranged from 10.1‰ to 12.8‰ with an average of 11.2‰ (n=3). Sulfur isotope values do not systematically vary with sulfur concentrations (Fig 5.7).

Table 5.2. Sulfur isotope values

Sample ID:	Lithology:	$\delta^{34}\text{S}$ ‰ vs VCDT:	S _{Tot} (wt. %):
BC-16-11	Biotite-graphite-quartzofeldspathic gneiss	13.6	0.59
BC-16-19	Biotite-graphite-quartzofeldspathic gneiss	12.7	0.69
BC-16-28	Biotite-graphite-quartzofeldspathic gneiss	10.0	0.63
CO-16-01	Biotite-graphite-quartzofeldspathic gneiss	12.7	1.17
CO-16-02	Biotite-graphite-quartzofeldspathic gneiss	10.7	1.42
CO-16-03	Biotite-graphite-quartzofeldspathic gneiss	10.8	1.88
CO-16-04	Biotite-graphite-quartzofeldspathic gneiss	11.0	2.34
CO-16-07	Biotite-graphite-quartzofeldspathic gneiss	11.0	1.62
RO-16-16	Biotite-graphite-quartzofeldspathic gneiss	10.1	0.73
RO-16-19	Biotite-graphite-quartzofeldspathic gneiss	12.8	0.77
RO-16-23	Biotite-graphite-quartzofeldspathic gneiss	10.8	2.41
BC-16-06	Clinopyroxene-amphibole-biotite-graphite gneiss	9.7	0.99
BC-16-07	Clinopyroxene-amphibole-biotite-graphite gneiss	15.0	1.02
BC-16-08	Clinopyroxene-amphibole-biotite-graphite gneiss	12.2	0.77
BC-16-13	Clinopyroxene-amphibole-biotite-graphite gneiss	12.5	0.74
BC-16-14	Clinopyroxene-amphibole-biotite-graphite gneiss	14.0	0.90
BC-16-17	Clinopyroxene-amphibole-biotite-graphite gneiss	12.9	0.91
BC-16-22	Clinopyroxene-amphibole-biotite-graphite gneiss	12.7	1.69
BC-16-38	Clinopyroxene-amphibole-biotite-graphite gneiss	14.0	0.72
BC-16-29	Garnet-amphibole-biotite-graphite gneiss	11.3	0.71
CO-16-06	Garnet-sillimanite-biotite-graphite gneiss	14.2	1.96
CO-16-08	Garnet-sillimanite-biotite-graphite gneiss	14.3	1.34

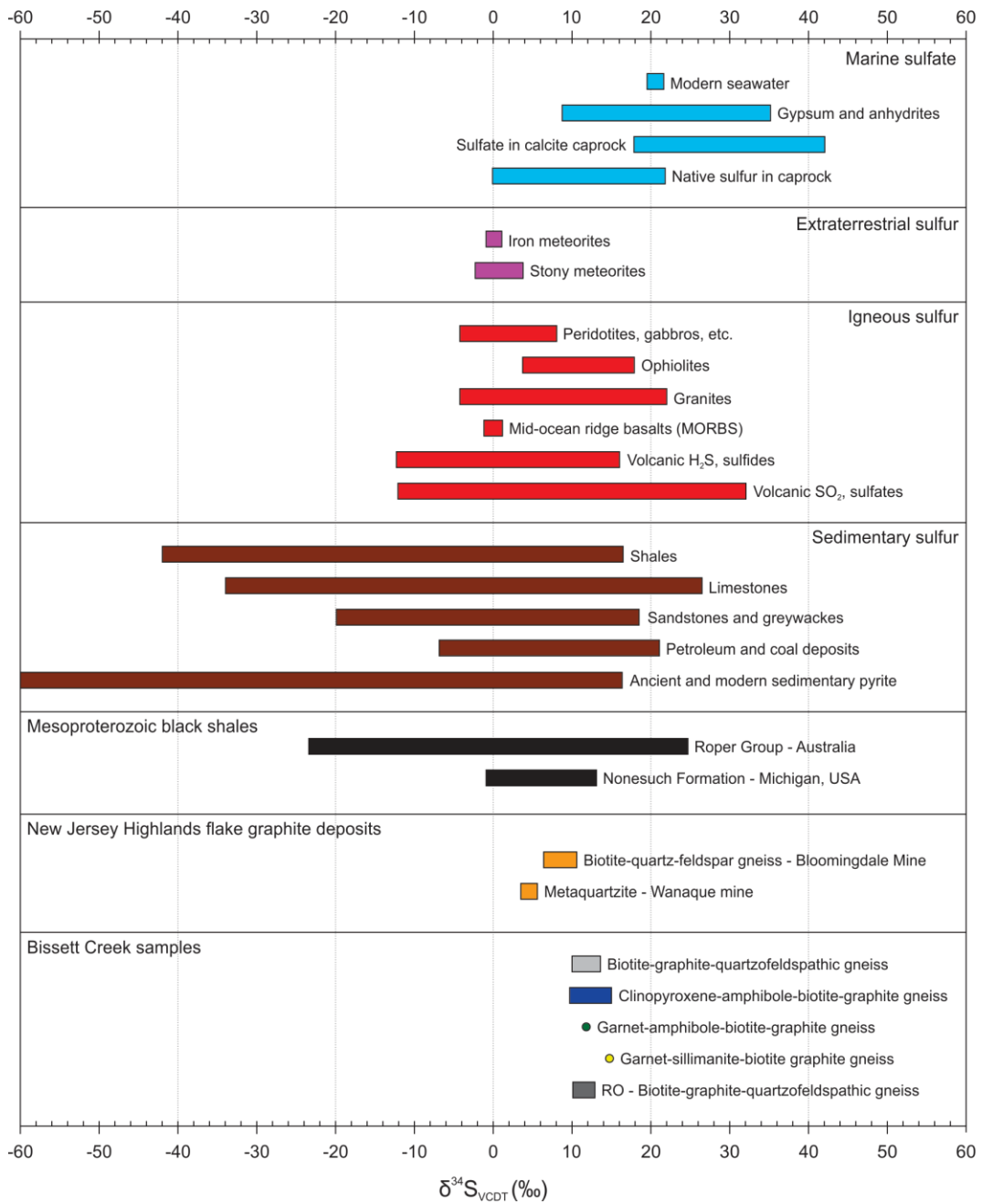


Fig. 5.5. Sulfur isotope values for whole rock powders at the Bissett Creek deposit and surrounding area compared with the sulfur isotope values from different potential reservoirs and the New Jersey Highlands flake graphite deposits (Volkert *et al.*, 2000). Sulfur isotope value ranges are from Nielsen (1979) and Seal *et al.*, (2000). Sulfur isotope values from Mesoproterozoic black shales are from Imbus *et al.*, (1992) and Johnston *et al.*, (2008). RO - Samples from road outcrops in the region surrounding the Bissett Creek deposit.

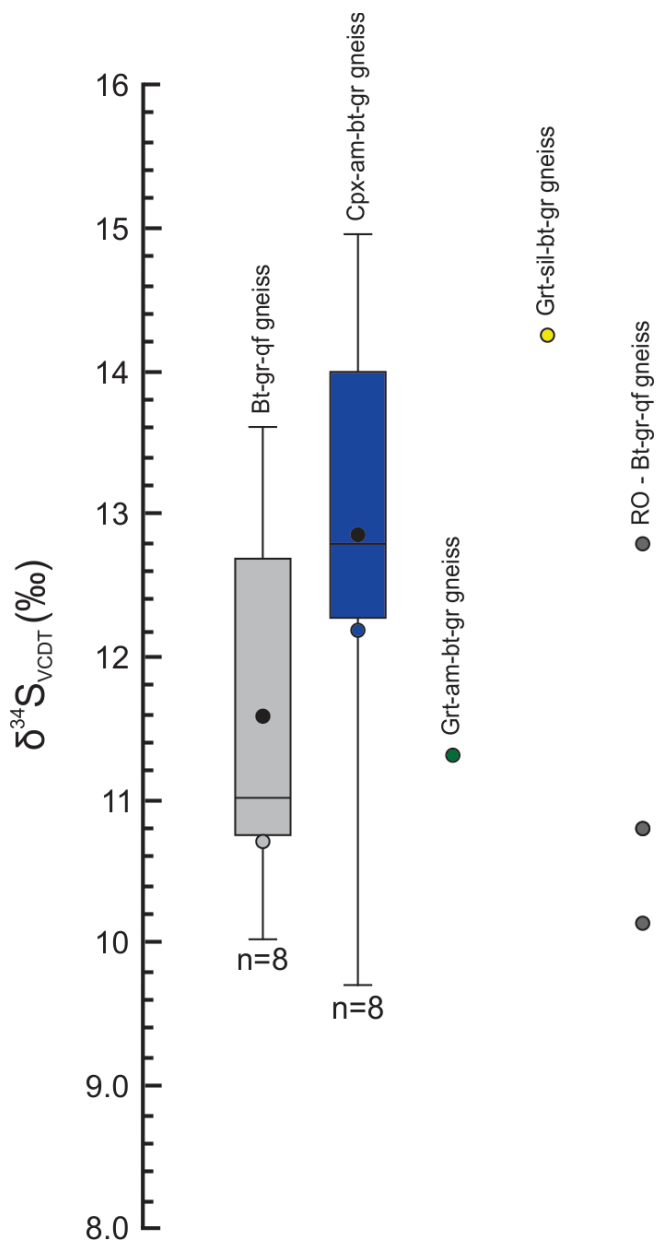


Fig. 5.6. Sulfur isotope values for the graphitic gneisses. Whiskers extend to the full range of values reported. The horizontal black line in the box represents the median. The black circle represents the mean. The box extends to the upper and lower quartiles of the ranges. Where values extended outside of the quartiles, they were plotted as individual circles. In the case where there were not enough values ($n=5$) to generate a box and whisker plot, individual values were plotted. RO - Samples from road outcrops in the region surrounding the Bissett Creek deposit.

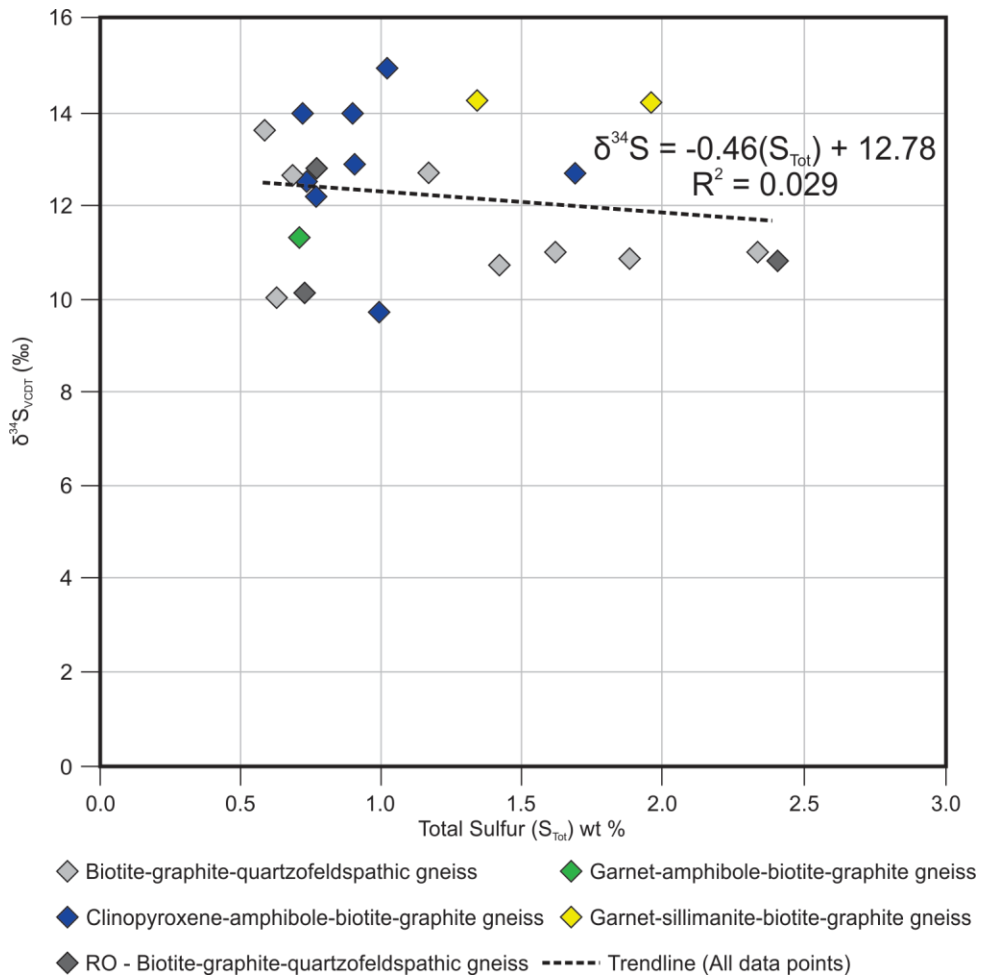


Fig. 5.7. Sulfur isotope values ($\delta^{34}\text{S}_{\text{CDT}}$) versus total sulfur (S_{Tot}).

6.0 Carbon Isotope Fractionation Modelling

Heterogeneity of carbon isotope values in graphite deposits can be attributed to isotope fractionation during precipitation from fluids. This can result from the influx of hydrothermal fluids or fractionation of fluids derived from *in situ* metamorphic processes (Papineau *et al.*, 2010; Luque *et al.*, 2012). Rayleigh fractionation is a process by which the composition of a homogeneous isotopic reservoir changes because one of the phases is consistently removed (Rayleigh, 1896). In terms of graphite deposits, Rayleigh fractionation is used to track the evolution of carbon-bearing fluids in response to carbon being removed from the system through precipitation of graphite (Ray and Ramesh, 2009). To determine if the distribution of isotope values found at the Bissett Creek deposit could have been developed through a Rayleigh fractionation process because of precipitation from a fluid undergoing carbon isotope fractionation, modelling using both a single-component (CO_2) and multi-component (CH_4 and CO_2) process was undertaken using the methods described in Ray (2009) and Ohtomo *et al.* (2014). While CO_2 has been identified as the primary fluid present during high-temperature metamorphism of pelites (Chu and Ague, 2013), CH_4 can also be a factor in the formation of graphite deposits (e.g. Rumble *et al.*, 1986; Barrenchea *et al.*, 1997; Huff and Nabelek, 2007).

6.1 Methodology

The range of carbon isotope values from Bissett Creek are shown in Fig. 6.1. Only samples with clear genetic links to the Bissett Creek flake graphite deposit were used. Thus, the values from the bulk mill samples and road outcrops were not included because their genetic links to the deposit were unclear. To model the isotope fractionation during Rayleigh fractionation, an initial carbon isotope value of the fluid reservoir was required. First, the data in Fig. 6.1 are converted into frequency values (f). Log values of the frequency (expressed as %) against the log value of $1000 + \delta^{13}\text{C}$ are then plotted in Figure 6.2. Linear regression of this log-normalized data (Figure 6.2) is used to determine the initial composition ($\delta^{13}\text{C}_s^i$) of the carbon at a $\log_{10}f$ value of 2 (representing 100% of the fluid). For Bissett Creek, the $\delta^{13}\text{C}_s^i$ value is approximately -26‰.

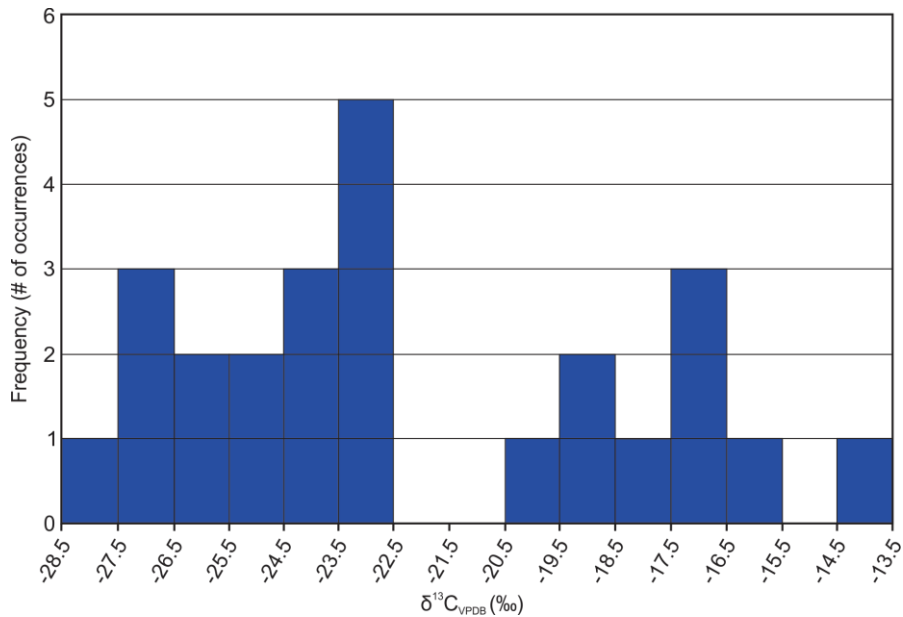


Fig. 6.1. Distribution of carbon isotope values at the Bissett Creek flake graphite deposit. Values were gathered into 1.0‰ increments.

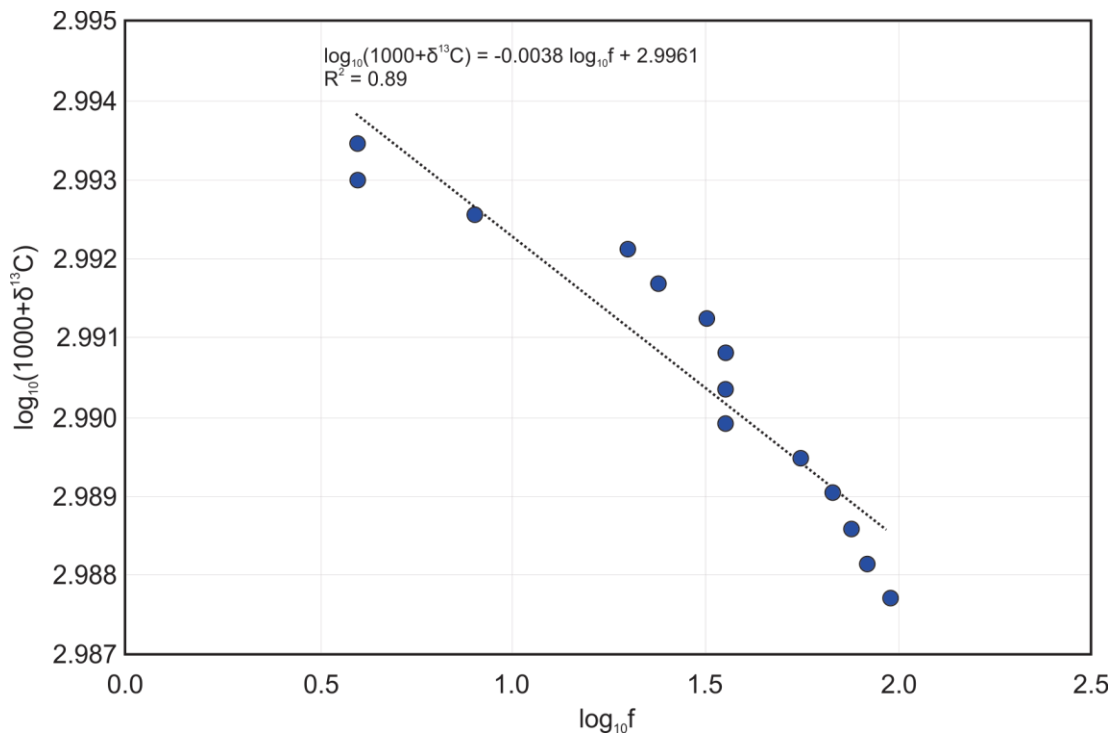


Fig. 6.2. Linear regression of the amount of graphite that has crystallized (in % - $\log_{10}f$) and the change in carbon isotopic composition ($\log_{10}(1000+\delta^{13}\text{C})$) for the Bissett Creek deposit.

Then, the distribution of $\delta^{13}\text{C}$ values through single component (CO_2) fractionation is modelled by the equation (Rayleigh, 1896; Broecker and Oversby, 1971):

$$\delta^{13}\text{C}_g = \alpha (\delta^{13}\text{C}_s^i + 1000) f^{(\alpha-1)} - 1000 \quad (5)$$

where $\delta^{13}\text{C}_g$ is the isotopic signature of the graphite product, α is the fractionation factor between the graphite and the largest source component, which for the single-component model is CO_2 , $\delta^{13}\text{C}_s^i$ is the initial isotopic composition of the reservoir, and f is the fraction of the remaining source reservoir. The distribution of the $\delta^{13}\text{C}$ values through a multi-component (CO_2 and CH_4) fractionation process is modelled by the equation (Ray, 2009):

$$\delta^{13}\text{C}_g = 10^3((\alpha_{g-1}/(a - b/f)) - 1) + (\alpha_{g-1}/(a-b/f)) \delta^{13}\text{C}_s \quad (6)$$

where $\delta^{13}\text{C}_g$ is the isotopic signature of the graphite product, $\delta^{13}\text{C}_s$ is the varying composition of the source material during fractionation, α is the fractionation factor between graphite and the largest source component (CO_2 or CH_4) in the multi-component case, f is the fraction of the remaining source reservoir and a and b are defined by two separate equations (7 and 8).

$$a = (1+\alpha_{\text{CH}_4-\text{CO}_2})/2 \quad (7)$$

$$b = (1-r_{\text{CH}_4-\text{CO}_2})(\alpha_{\text{CH}_4-\text{CO}_2} - 1)/2(1+r_{\text{CH}_4-\text{CO}_2}) \quad (8)$$

where $\alpha_{\text{CH}_4-\text{CO}_2}$ is the fractionation factor between CH_4 and CO_2 , $r_{\text{CH}_4-\text{CO}_2}$ is the molar ratio of CH_4 and CO_2 in the source fluid.

Finally, $\delta^{13}\text{C}_s$, the initial isotopic composition of the source reservoir, may be determined using the following equation from Ray (2009):

$$(\delta^{13}\text{C}_s - \delta^{13}\text{C}_s^i) \approx 10^3 [(\alpha_{g-1}/a) \ln((af-b)/(a-b)) - \ln f] \quad (9)$$

There are three unknown inputs that need to be accounted for to model the Rayleigh isotope fractionation from a multi-component source. These inputs are: (1) the temperature of graphite deposition which controls the fractionation factors $\alpha_{g-\text{CO}_2}$ (Scheele and Hoefs, 1992) and $\alpha_{\text{CH}_4-\text{CO}_2}$ (Horita, 2001), (2) the initial molar ratio of carbon-bearing fluids in the source solution

($r_{CH_4-CO_2}$) and (3) the initial isotopic composition of the source material ($\delta^{13}C_s^i$). For Bissett Creek, thermobarometry constrains the temperatures of metamorphism from approximately 650 to 850°C (Section 7.3). Furthermore, based on linear regression of the log-normalized frequency data from Bissett Creek, the $\delta^{13}C_s^i$ value is approximately -26‰. Finally, it is possible to model for the variety of molar ratios of the carbon bearing source fluids.

6.2 Results

The results of the carbon isotope fractionation modelling are presented in Figure 6.3. The single component model predicts carbon isotope composition from -28‰ to -14‰ (Fig 6.3A). Multi-component modelling using a $r_{CH_4-CO_2}$ value of 0.99 predicts a wider range of carbon isotope compositions ranging from -33‰ to 7‰ (Fig 6.3B). For the multicomponent model, a shift to higher temperatures causes an increase in the amount of ^{13}C causing a shift to heavier carbon isotope signatures for cases where lower molar ratios of CH₄ to CO₂ exist (Fig 6.3C and D). An increase in the $r_{CH_4-CO_2}$ value allows for greater fractionation between the two species increasing the range of potential values from a fluid. Greater $r_{CH_4-CO_2}$ values, with a larger component of CH₄ in the fluid, cause a shift to isotopically heavier signatures compared to more CO₂ dominant fluids.

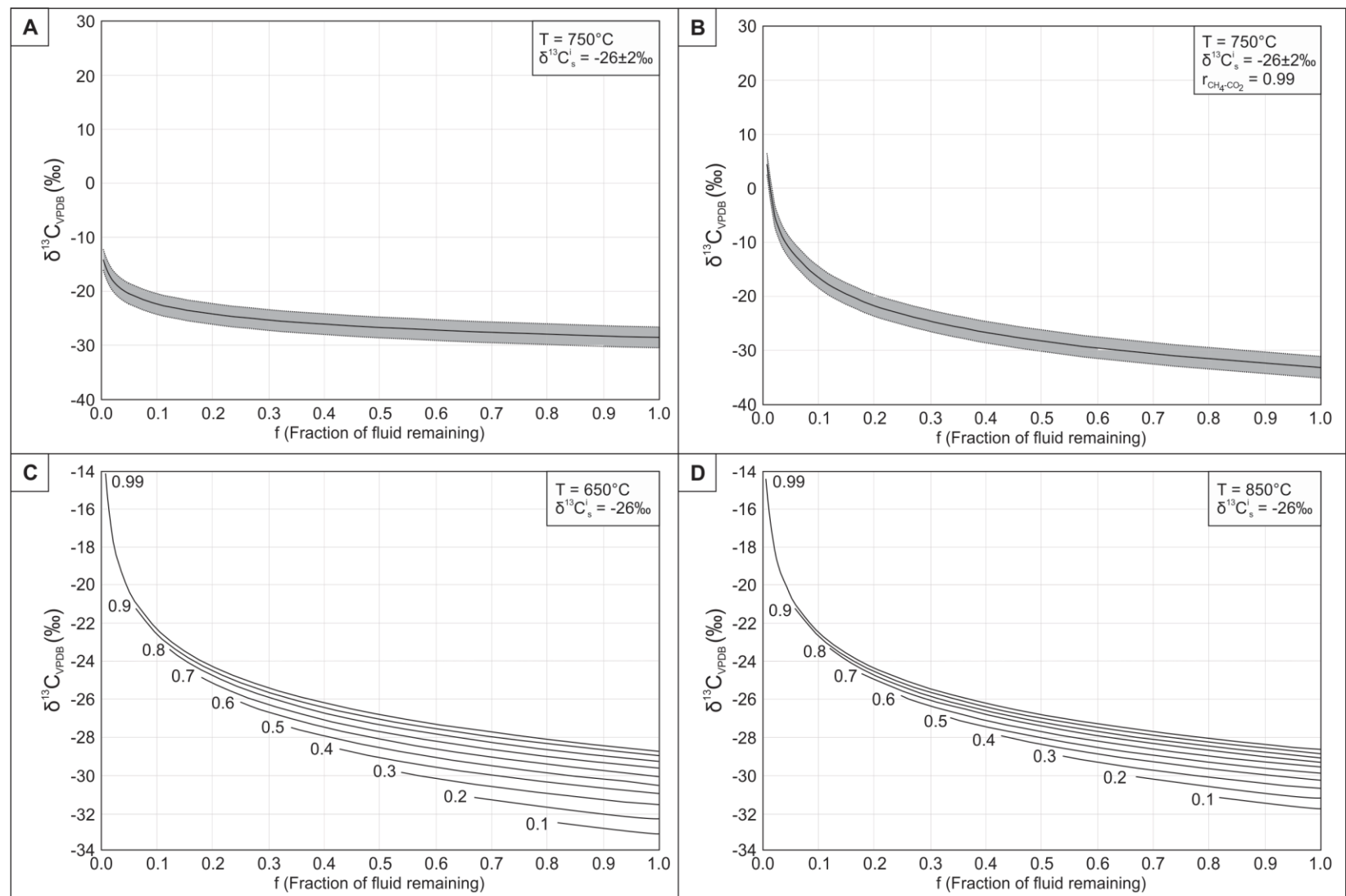


Fig. 6.3. Carbon isotope modelling results. **A.** Single-component fractionation model (CO₂ only). **B.** Multi-component fractionation model (CO₂ and CH₄). **C.** Multi-component model with a range of starting molar ratios of components in fluid ($r_{\text{CH}_4-\text{CO}_2}$) at 650°C. **D.** Multi-component model with a range of starting molar ratios of components in fluid ($r_{\text{CH}_4-\text{CO}_2}$) at 850°C.

7.0 Mineral Compositions and Geothermobarometry

Mineral compositions were analyzed for use in geothermometers and geobarometers.

Geothermometers and geobarometers were used to determine the pressure, temperature and fluid composition conditions at the time of graphite deposition (Research Objective 4) and elucidate the processes responsible for graphite deposition in the deposit (Research Objective 6). From previous research on graphite formation, it is known that natural graphite formed as a result of metamorphism of *in situ* organic materials requires temperatures >700°C, which correspond to high grade (upper amphibolite to granulite-facies) metamorphic conditions, while hydrothermal precipitation of graphite can take place at a variety of temperatures and pressures ([Holloway, 1984](#); [Rumble and Hoering, 1986](#); [Buseck and Beyssac, 2014](#); [Rosing-Schow *et al.*, 2016](#)).

Samples from the biotite-graphite-quartzofeldspathic gneiss (n=1), garnet-amphibole-biotite-graphite gneiss (n=3), garnet-sillimanite-biotite-graphite gneiss (n=5), garnet-amphibole-biotite-quartzofeldspathic gneiss (n=2) and garnet-amphibole-biotite-muscovite schist (n=1) were selected for analysis by electron microprobe based on the presence of useful metamorphic mineral assemblages for thermometry and barometry.

7.1 Analytical Methods

Mineral compositions were determined quantitatively for garnet, biotite, amphibole, plagioclase, potassium feldspar and sulfides using a JEOL JXA-8530F field-emission electron microprobe at the Earth and Planetary Materials Analysis (EPMA) Lab at Western University in London, Ontario. All the samples were analyzed as 27 mm by 46 mm polished thin sections made by Vancouver Petrographics. These thin sections were carbon coated prior to analysis. Copper tape was applied from the corners of the thin section to the mount to assist with conductivity. A total of twelve thin sections were analyzed in two analytical sessions.

Garnets were analyzed using 10-25 1µm spots in the line function to assess compositional variation across the grain. The accelerating voltage used for these analyses was 15 kV with a current of 20 nA ([M. Beauchamp, pers. comm., 2017](#)). Biotite, amphibole, plagioclase, potassium feldspar and sulfides were analyzed using two 5µm spots on each grain near the core and rim to assess for compositional variation within individual grains. The accelerating voltage used for these analyses was 15 kV with a current of 20 nA ([M. Beauchamp, pers. comm., 2017](#)). Analyses of biotite, amphibole, plagioclase, and potassium feldspar were selected based on

proximity to garnet porphyroblasts and other metamorphic minerals, with some grains analyzed that are in contact with garnet. Total time per analysis was ~3 minutes. Calibration of the instrument was undertaken prior to the start of analyses using a combination of natural and synthetic materials. The materials, corresponding counts and the detectors used for each element are found in Appendix F. The data were reduced using the default ZAF corrections in the JEOL software ([M. Beauchamp, pers. comm., 2017](#)).

7.2 Mineral Composition Results

Mineral composition data is presented in Appendix G. Mineral compositions are further broken down based on unit and mineral in the following sections.

7.2.1 Biotite-Graphite-Quartzofeldspathic Gneiss

Sample BC-16-28 was analyzed from the biotite-graphite-quartzofeldspathic unit because of the presence of garnet, biotite, and plagioclase. This allowed for the compositions to be used with the garnet-biotite thermometers as well as the garnet-biotite-plagioclase-quartz barometer.

Garnets in this sample shows minor zoning. The concentrations of the four main end-members of garnet from highest to lowest are Fe, Ca, Mg, and Mn. The molar proportions of Fe and Ca as well as Mg and Mn appear to be coupled (Fig 7.2.1). As the concentration of one end-member fluctuates, the concentration of the second parameter does the inverse. For instance, Fe zoning shows enrichment in the cores relative to the rims. The opposite is true of Ca, where the rims are enriched relative to the cores of the crystals. The changes in the magnitude of the proportion of the two mole fractions change in unison across the grain. This is also observed for Mg and Mn, with Mg being depleted in the rims relative to the cores, and Mn being enriched in the rims relative to the cores. The profiles of all mole fractions are relatively flat within the garnets.

Biotite has X_{Fe} ($X_{\text{Fe}} = \text{Fe}_{(\text{Tot})}/(\text{Fe}_{(\text{Tot})} + \text{Mg})$) values that range from 0.263 to 0.439, with a median of 0.412. Biotite with lower Fe values (e.g. 0.263 and 0.267) came from the matrix of the sample and was near pyrrhotite grains. Biotite with lower X_{Fe} values was not used for thermobarometry because of their deviation from the normal range and the lack of contact with garnet, which may have prevented cation exchange. Molar Ti values range from 0.034 to 0.118 with a median value of 0.043. High Ti values (e.g. 0.111 and 0.118) were from the cores of

biotites in the matrix of the thin section. Similar observations were not found in biotites near garnet.

Plagioclase composition varies from An₃₆₋₄₀ ($An\# = (\text{molar Ca}/(\text{Ca+Na+K})) \times 100$), classifying it as andesine (Fig 7.2.2). No significant core-rim compositional variations were noted in plagioclase from this sample. Potassium feldspar compositions ranged from Or₉₀₋₉₆ ($Or\# = (\text{molar K}/(\text{Ca+Na+K})) \times 100$). Potassium feldspars also showed minor enrichment in Ba with concentrations varying from 1.04 to 1.89 wt %.

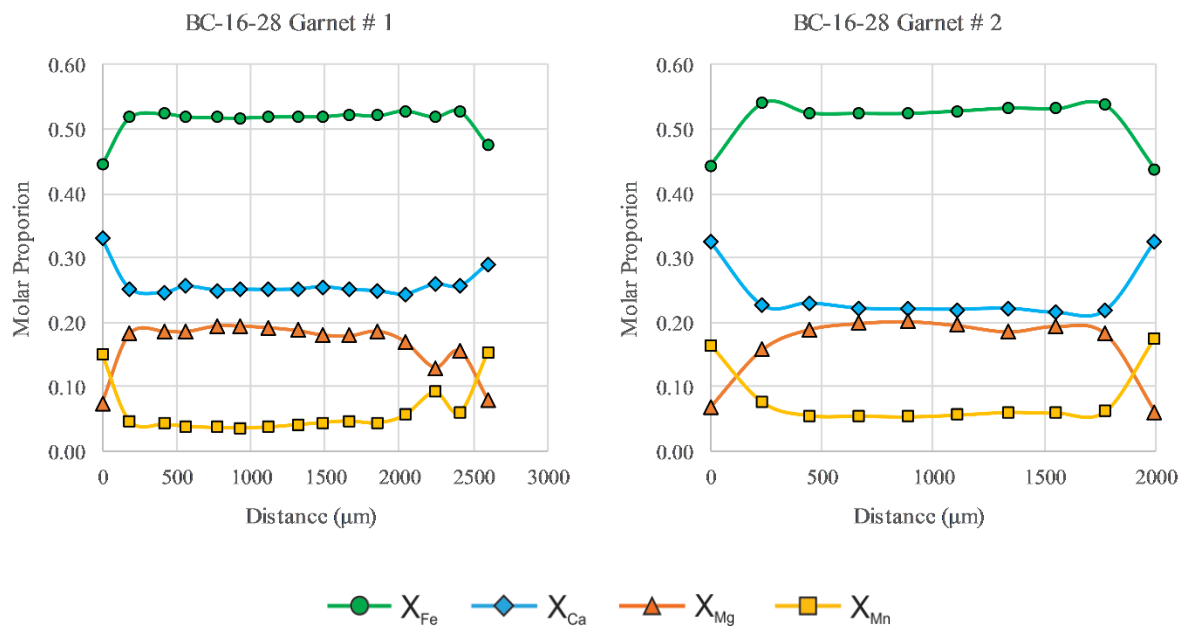


Fig. 7.2.1. Compositional cross sections of garnet from the biotite-graphite-quartzofeldspathic gneiss unit. The vertical axis on the left-hand side of the graph represents the modal proportion of garnet variants.

7.2.2 Garnet-Amphibole-Biotite-Graphite Gneiss

Three samples, BC-16-18B, BC-16-20B and BC-16-29B, were analyzed from the garnet-amphibole-biotite-graphite gneiss. The mineral assemblage of this unit allows for the use of the garnet-biotite and garnet-hornblende thermometers, which were then coupled with the garnet-biotite-plagioclase-quartz barometer.

Garnets in the samples from the garnet-amphibole-biotite-graphite gneiss show minor zoning (Fig 7.2.3). In the garnets from sample BC-16-18B the rims are enriched in Ca and Mn and depleted in Fe and Mg relative to the cores. Variation in the composition of the garnets

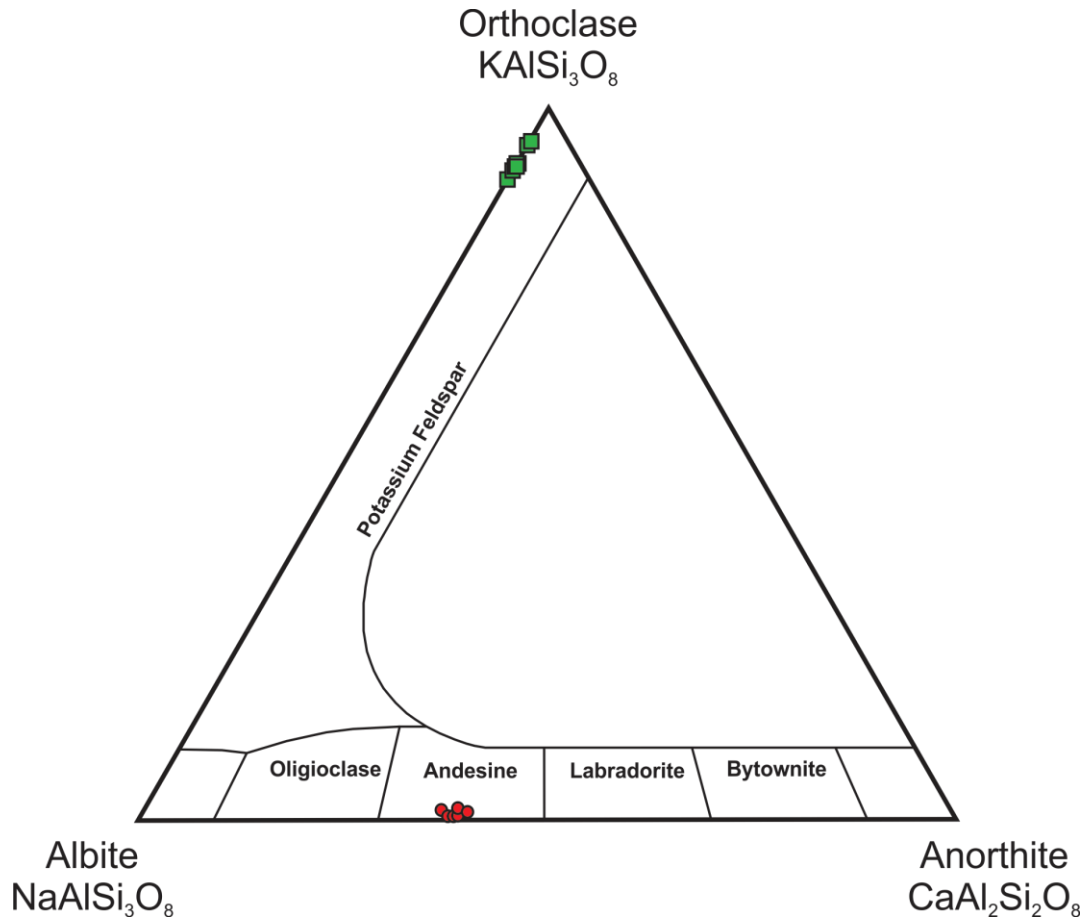


Fig. 7.2.2. Feldspar classification in the biotite-graphite-quartzofeldspathic gneiss. Ternary classification diagram for feldspars modified from [Greenwood and Earnshaw \(1998\)](#). Green squares represent alkali feldspars and red circles represent plagioclase feldspars.

affects all mole fractions simultaneously. Garnets in samples BC-16-20B and BC-16-29B show the same pattern as garnets in sample BC-16-28. Concentrations of Fe and Ca appear coupled and vary inversely, as do the concentrations of Mg and Mn. Rims are enriched in Ca and Mn and depleted in Fe and Mg relative to the cores. Internal profiles of the garnets show very little variation, except for BC-16-20B garnet # 1 and garnet # 2.

Biotite has X_{Fe} values that range from 0.332 to 0.537, with a median of 0.475. Ti values range from 0.010 to 0.116, with a median of 0.035. Biotite with the lowest X_{Fe} values is from

inclusions within garnets. These biotites were not used during thermobarometry as they likely represent prograde biotite and not biotite that equilibrated with the matrix assemblage at peak T . Biotite with elevated Ti values were found near pyrrhotite in the matrix and were far from garnets. No significant core-rim compositional variations in biotite were observed.

The composition of plagioclase ranges from An₃₆₋₄₂, falling in the range for andesine (Fig.7.2.4). One grain has a composition of An₁₉, but it was an inclusion in garnet # 2 of sample BC-16-20B. No significant core-rim compositional variations were noted in plagioclase from this sample. Alkali feldspar compositions varied from Or₇₅₋₉₉ with the bulk of compositions in the Or₈₅₋₉₅ range. Alkali feldspars also show minor enrichment in Ba with concentrations varying from 0 to 1.23 wt %.

Amphiboles have X_{Fe} values that range from 0.450 to 0.588, with a median value of 0.505. According to the [Leake et al. \(1997\)](#) classification of amphiboles, since Ca_B>1.50 moles, (Na+K)_A≥0.50 moles and Ti<0.50 moles the amphiboles are part of the calcic amphibole classification. This classification is further broken down into six fields dependent on X_{Mg} ratio (X_{Mg} = Mg/(Mg+Fe²⁺)) and Si (moles) (Fig. 7.2.5). The amphiboles have a diverse range of classifications, but plot near the junction of the edenite, ferroedenite and ferropargasite fields.

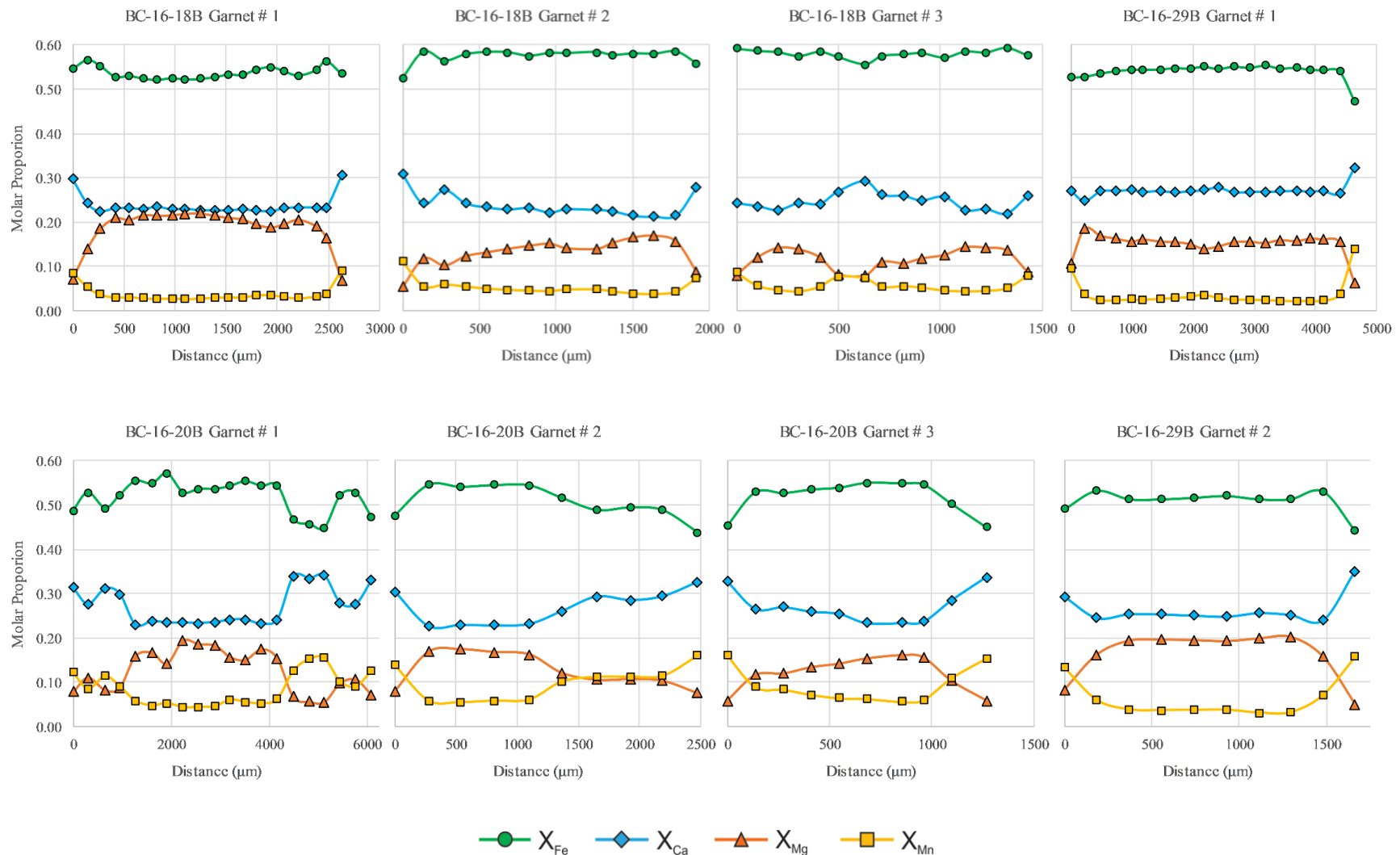


Fig. 7.2.3. Compositional cross sections of garnet from the garnet-amphibole-biotite-graphite gneiss. The vertical axis on the left-hand side of the graph represents the modal proportion of garnet variants.

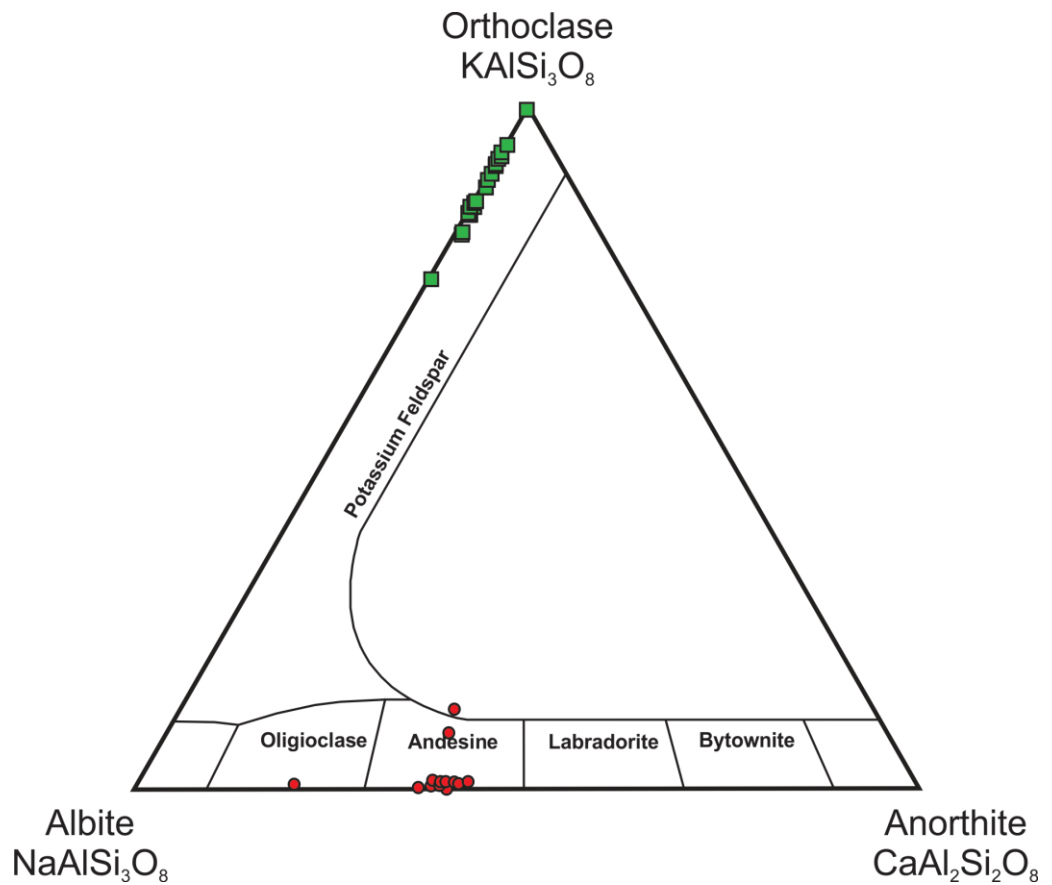


Fig. 7.2.4. Felspar classification for the garnet-amphibole-biotite-graphite gneiss. Ternary classification diagram for feldspars modified from [Greenwood and Earnshaw \(1998\)](#). Green squares represent alkali feldspars and red circles represent plagioclase feldspars.

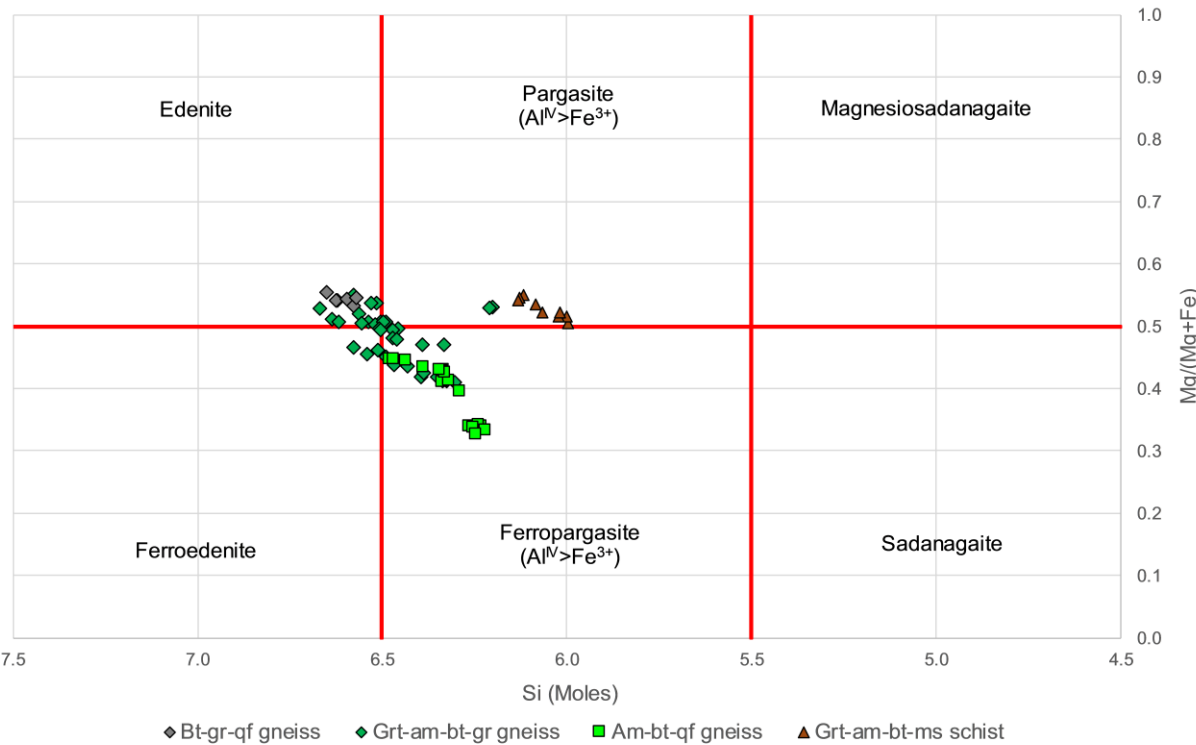


Fig. 7.2.5. Classification of calcic amphiboles according to [Leake et al. \(1997\)](#). Bt – biotite, gr – graphite, qf – quartzofeldspathic, grt – garnet, am – amphibole, ms – muscovite. This figure assumes $\text{Fe}^{2+} = \text{Fe}_{\text{Tot}}$ (i.e. all ferrous iron).

7.2.3 Garnet-Sillimanite-Biotite-Graphite Gneiss

Five samples, BC-10-06, CO-16-05A, CO-16-05B, CO-16-08 and CO-16-10, were analyzed from the garnet-sillimanite-biotite-graphite gneiss. This unit was selected for analysis because of the presence of garnet, biotite and sillimanite. The presence of sillimanite added the potential to use an additional barometer based on the presence of Al_2SiO_5 polymorphs.

Garnets in this unit show some zonation across grains (Fig 7.2.6). Garnet is enriched in Fe relative to the garnet in other units. Iron and Ca are enriched in the rims of garnets relative to the cores. Fluctuations in the values of molar fractions of Fe and Mg appear to be inversely coupled. The rims are also depleted in Mg relative to the cores. In most cases the proportion of Mn is low and does not vary from core to rim, except in garnet # 1 of CO-16-10 where Mn appears inversely coupled with Ca. Garnet # 1 from CO-16-08 appear anomalous because of the high concentration of Mn and Ca and lower values of Mg and Fe. Additionally, the concentrations of Mg and Fe are not coupled.

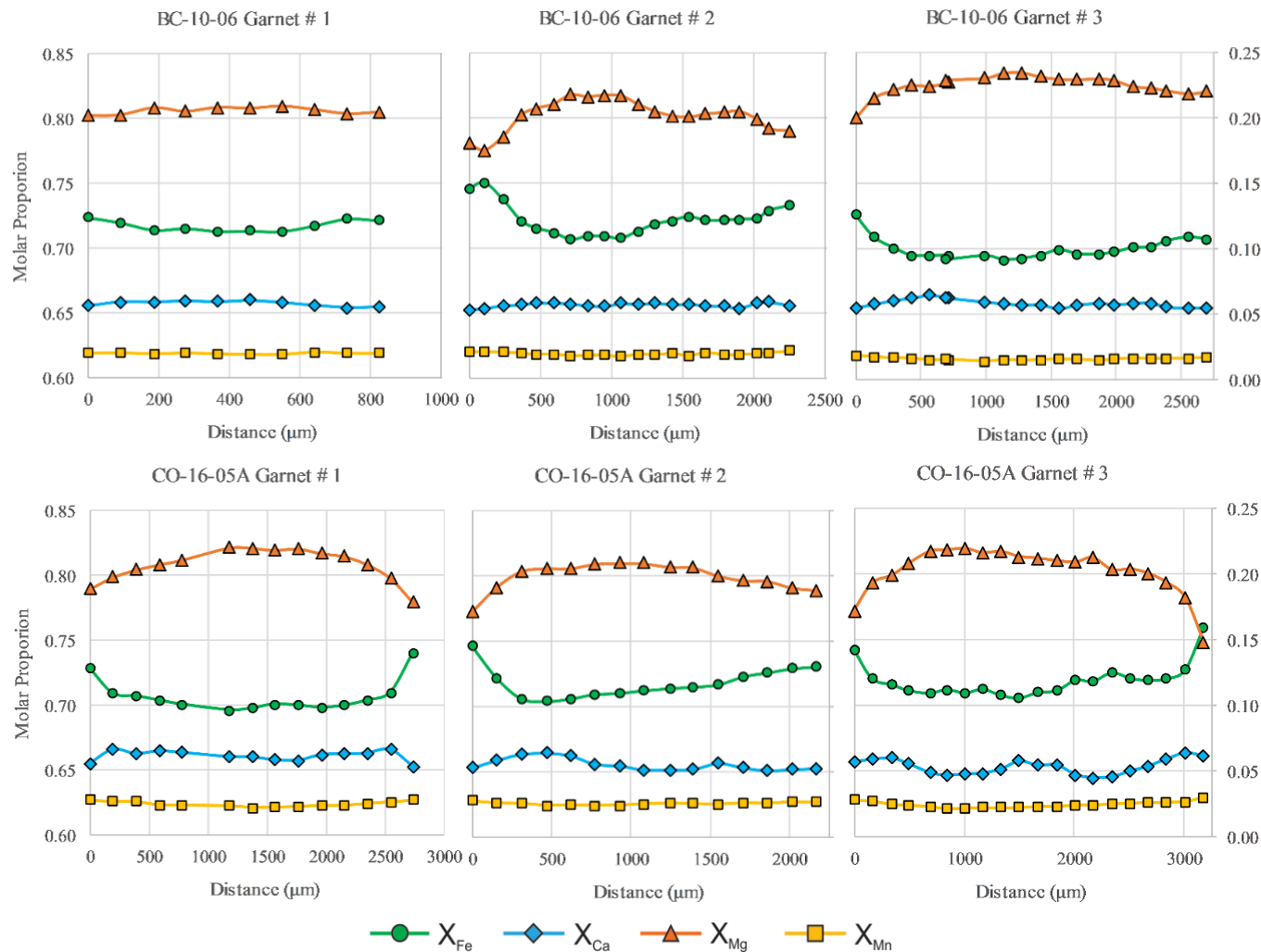


Fig. 7.2.6. Compositional cross sections of garnet from the garnet-sillimanite-biotite-graphite gneiss unit. The vertical axis on the left side represents the molar values of Fe (almandine), while the right represents the values of Ca (grossular), Mg (pyrope) and Mn (spessartine).

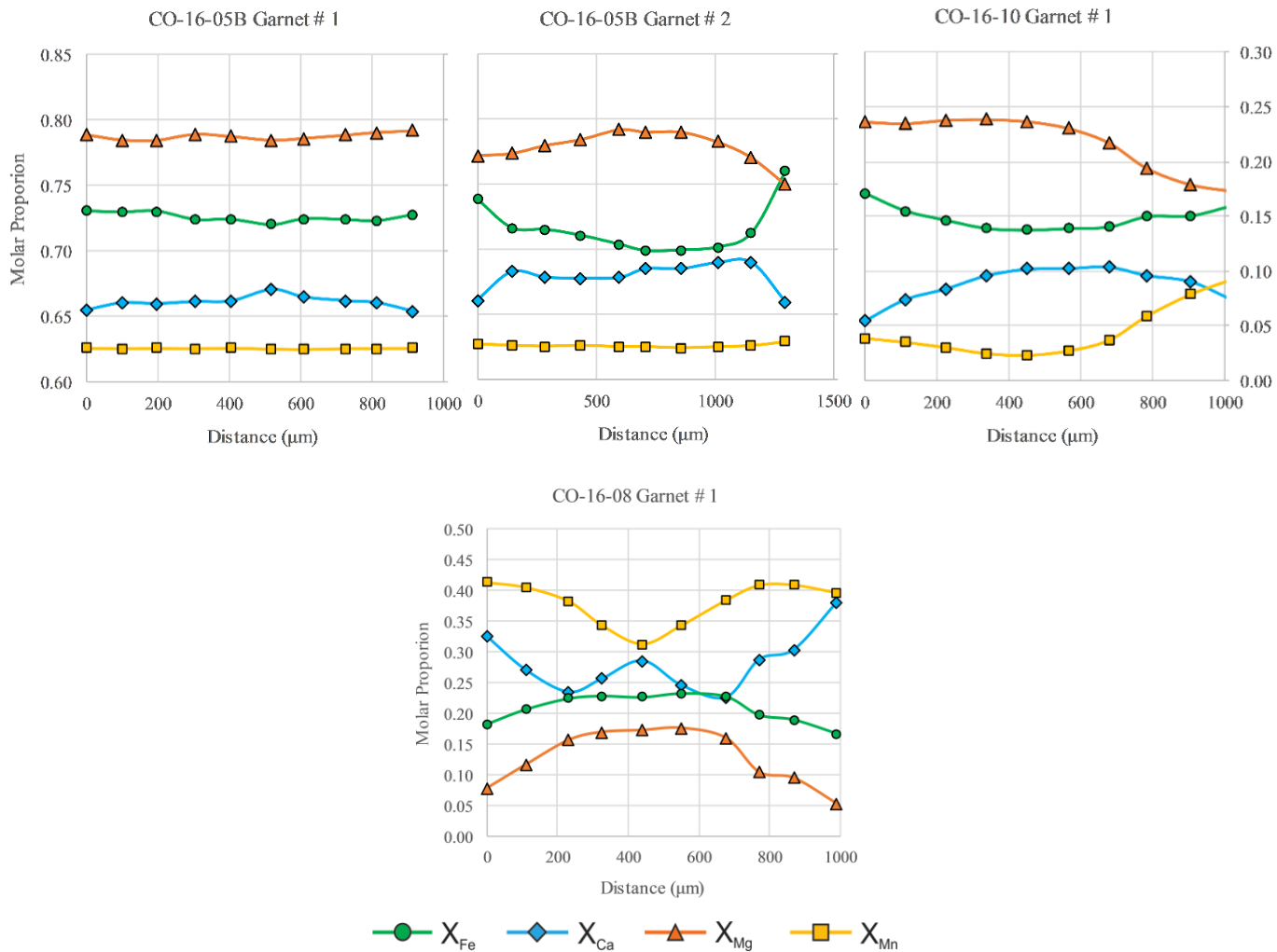


Fig. 7.2.6. (Continued) Compositional cross sections of garnet from the garnet-sillimanite-biotite-graphite gneiss unit. The vertical axis on the left side represents the molar values of Fe (almandine), while the right represents the values of Ca (grossular), Mg(pyrope) and Mn (spessartine).

X_{Fe} values in biotite range from 0.174 to 0.440, with a median of 0.402. Moles of Ti range from 0.018 to 0.232, with a median of 0.195. Most low Ti values are from CO-16-10. Biotite within this unit has noticeably lower X_{Fe} values and higher number of moles of Ti relative to other units. Biotite with these values are disseminated throughout the sample and do not show a preferential spatial association with any particular mineral. No significant core-rim variations in composition were seen in the biotite from this unit.

Three compositionally distinct feldspars are present in the garnet-sillimanite-biotite-graphite gneiss (Fig 7.2.7). The first set of compositions ranges from Or_{30-39} , while the second is Or_{83-91} . A single plagioclase grain was analyzed from CO-16-05B with a composition of $\sim An_2$ (i.e. albite). Minor plagioclase was noted along the edges of other potassium feldspar grains, but otherwise appears to be depleted within this sample. The absence of plagioclase eliminated the potential to use the garnet-aluminosilicate-silica-plagioclase barometer.

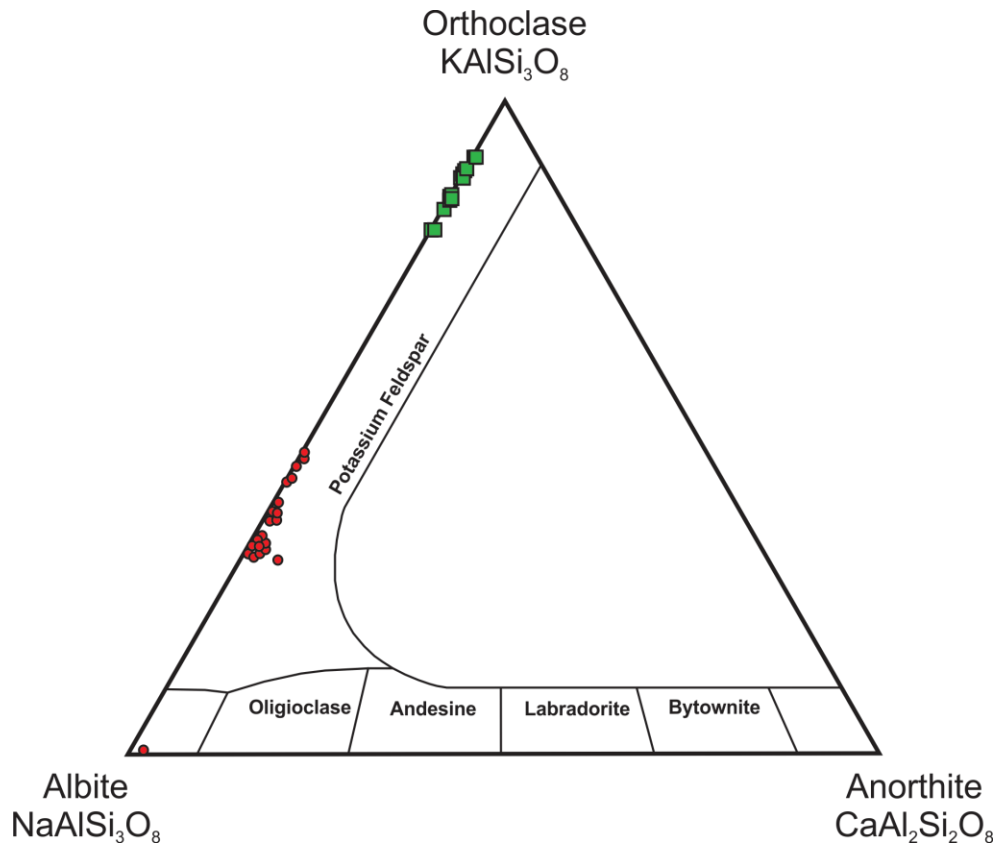


Fig. 7.2.7. Feldspar classification for the garnet-biotite-sillimanite-graphite gneiss. Ternary classification diagram for feldspars modified from [Greenwood and Earnshaw \(1998\)](#). Green squares represent more potassium-rich feldspars and red circles represent more sodium-rich feldspars.

7.2.4 Amphibole-Biotite-Quartzofeldspathic Gneiss

Two samples, RO-16-08A and RO-16-09B, were analyzed from this unit. Both samples are from the road outcrop set and will be used to compare regional *P-T* conditions to conditions at the Bissett Creek flake graphite deposit. These samples were selected because of the assemblage containing garnet-amphibole-biotite and plagioclase, which makes the unit a good candidate for the garnet-biotite and garnet hornblende thermometer as well as the garnet-biotite-plagioclase-quartz barometer.

Garnet in RO-16-08A contains many inclusions and as a result did not provide a very useful profile, as clear trends could not be easily defined. However, the three garnets in sample RO-16-09B shows clear zonation trends (Fig 7.2.8). Rims of the garnet grains are depleted in Mg and enriched in Fe, Ca and Mn relative to the cores. Garnet # 2 has a strong positive Ca accompanied by a strong negative Fe spike near the rim on one side. Similar to previous units, Fe and Ca as well as Mg and Mn appear coupled, whereby changes in one mole fraction are linked to the inverse proportional change in the second mole fraction. Similar to the garnet-sillimanite-biotite-graphite gneiss, this unit has garnet with high concentrations of Fe.

Biotite has a wide range of X_{Fe} values spanning from 0.454 to 0.683, with a median value of 0.545. The moles of Ti also showed a large variation from 0.004 to 0.210, with a median of 0.173. No intragrain compositional zonation was noted in the biotite analyzed.

Plagioclase varied in composition from An₂₋₃₉, with the majority of compositions falling within the An₃₅₋₃₉ range (Fig 7.2.9). The albite-rich compositions ($n=2$) came from a plagioclase grain inside of the garnet # 1 from sample RO-16-08A. K-feldspar compositions varied from Or₉₄₋₉₉.

Amphibole from this unit had X_{Fe} values ranging from 0.552 to 0.672, with a median of 0.587. All grains analyzed have $Ca_B > 1.50$ moles, $(Na+K)_A \geq 0.50$ moles and $Ti < 0.50$ moles, meaning that they once again fall under the calcic amphibole classification scheme (Leake et al., 1997). The amphibole grains from this unit plot within the ferropargasite field (Fig. 7.2.5).

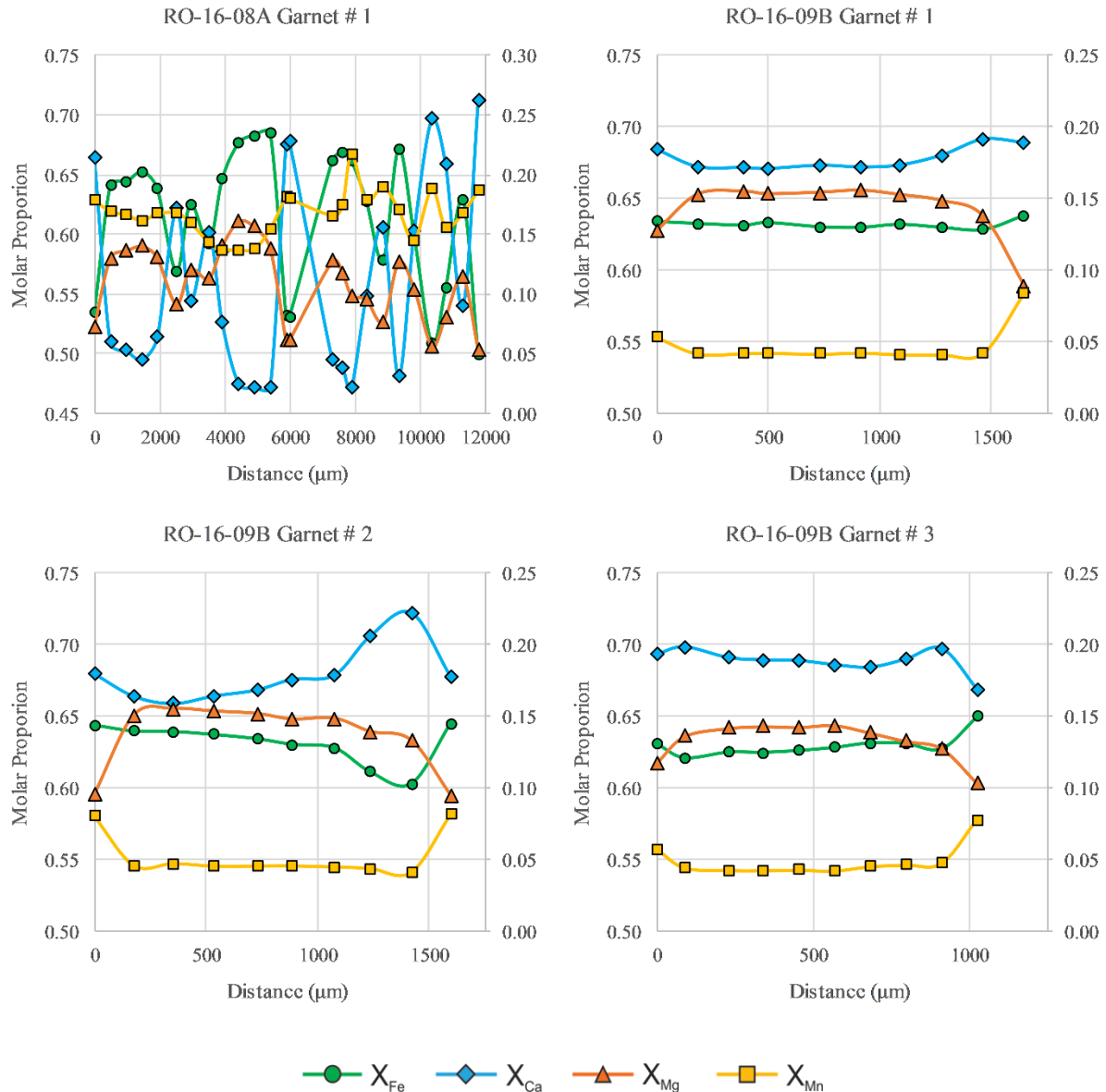


Fig. 7.2.8. Compositional cross sections of garnet from the amphibole-biotite-quartzofeldspathic gneiss. The vertical axis on the left-hand side of the graph represents the modal proportion of iron (almandine), while the right vertical axis represents the modal proportions of calcium (grossular), magnesium (pyrope) and manganese (spessartine). The distance along the traverse of the garnet grains is expressed on the horizontal axis in micrometers.

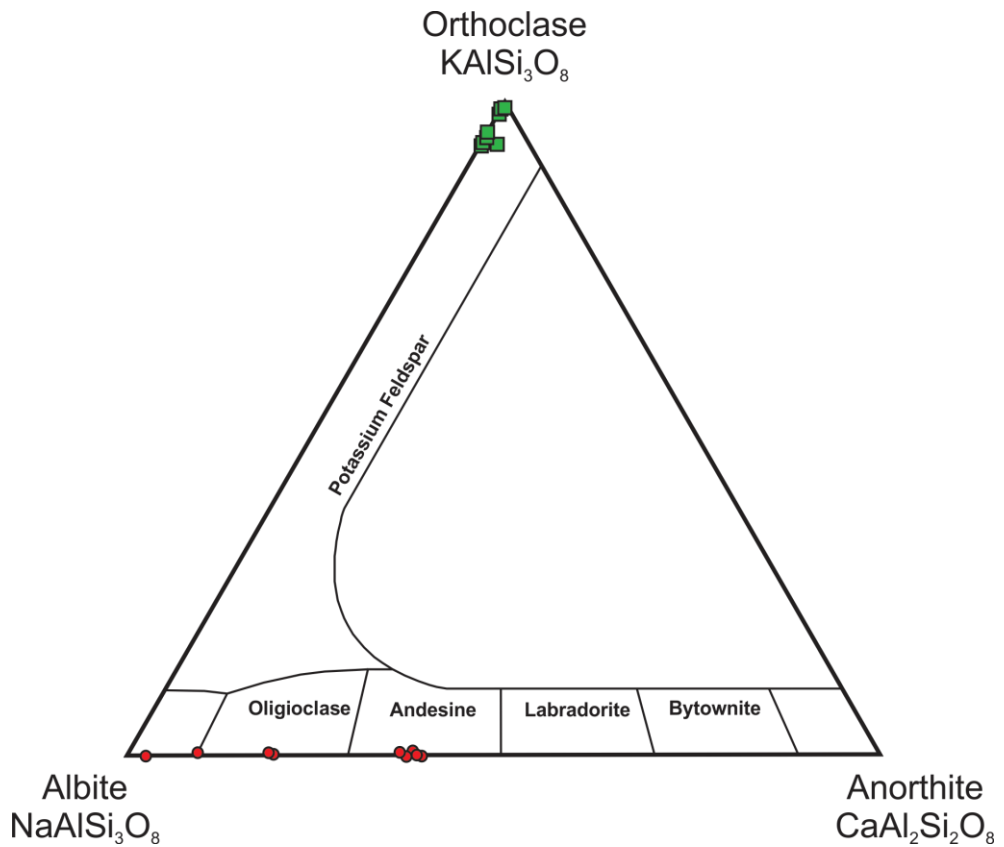


Fig. 7.2.9. Feldspar classification for the amphibole-biotite-quartzofeldspathic gneiss. Ternary classification diagram for feldspars modified from [Greenwood and Earnshaw \(1998\)](#). Green squares represent potassium feldspars and red circles represent plagioclase feldspars.

7.2.5 Garnet-Amphibole-Biotite-Muscovite Schist

One sample, RO-16-04 was analyzed from this unit. The purpose of analyzing this sample was to compare regional *P-T* conditions to conditions at the Bissett Creek flake graphite deposit on the local site, by examining a lithology that is not found on the Bissett Creek site. The sample also contains garnet-amphibole-biotite and plagioclase, which makes the unit a good candidate for the garnet-biotite and garnet hornblende thermometer as well as the garnet-biotite-plagioclase-quartz barometer.

Garnets in these samples show minor zoning (Fig 7.2.10). The concentrations of the four main end-members of garnet from highest to lowest are Fe, Ca, Mg, and Mn. The molar proportions of Fe, Ca and Mn is greatest at the rims of the garnets and decrease toward the core. The exception to this is Mn, which shows slight increases in molar fraction toward the core in

both garnets. The molar proportions of Mg and Mn appear to be inversely coupled. The profiles of Fe and Ca are flatter lying and do not show clear relationships to one another.

Biotite has a narrower range of X_{Fe} values than other units, spanning from 0.286 to 0.353, with a median value of 0.343. The moles of Ti also showed a narrow variation from 0.034 to 0.072, with a median of 0.057. Biotite with the lowest X_{Fe} and Ti values was in direct contact with the garnet grains. No intragrain compositional zonation was noted in the biotite analyzed.

Plagioclase varied in composition from An₅₅₋₇₅ (Fig 7.2.11). More sodic plagioclase feldspars An₅₅₋₅₉ were located in close proximity to garnet, while more calcic plagioclase was disseminated in the matrix of the schist. Potassium feldspar compositions were very consistent with a uniform composition of ~Or₉₉.

Amphibole from this unit had a range of X_{Fe} values from 0.449 to 0.494, with a median of 0.477. All grains analyzed have $Ca_B > 1.50$ moles, $(Na+K)_A \geq 0.50$ moles and $Ti < 0.50$ moles, meaning that they once again fall under the calcic amphibole classification scheme ([Leake et al., 1997](#)). The amphibole grains from this unit plot within the pargasite field (Fig. 7.2.5).

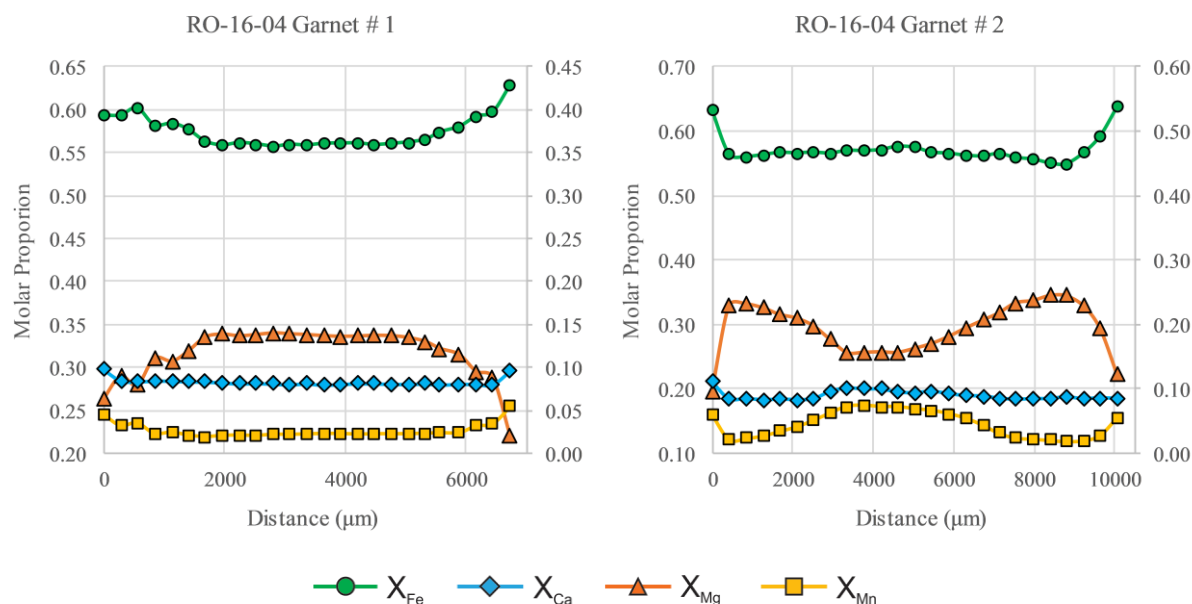


Fig. 7.2.10. Compositional cross sections of garnet from the garnet-amphibole-biotite-muscovite schist unit. The vertical axis on the left-hand side of the graph represents the modal proportion of iron (almandine) and magnesium (pyrope), while the right vertical axis represents the modal proportions of calcium (grossular) and manganese (spessartine). The distance along the traverse of the garnet grains is expressed on the horizontal axis in micrometers.

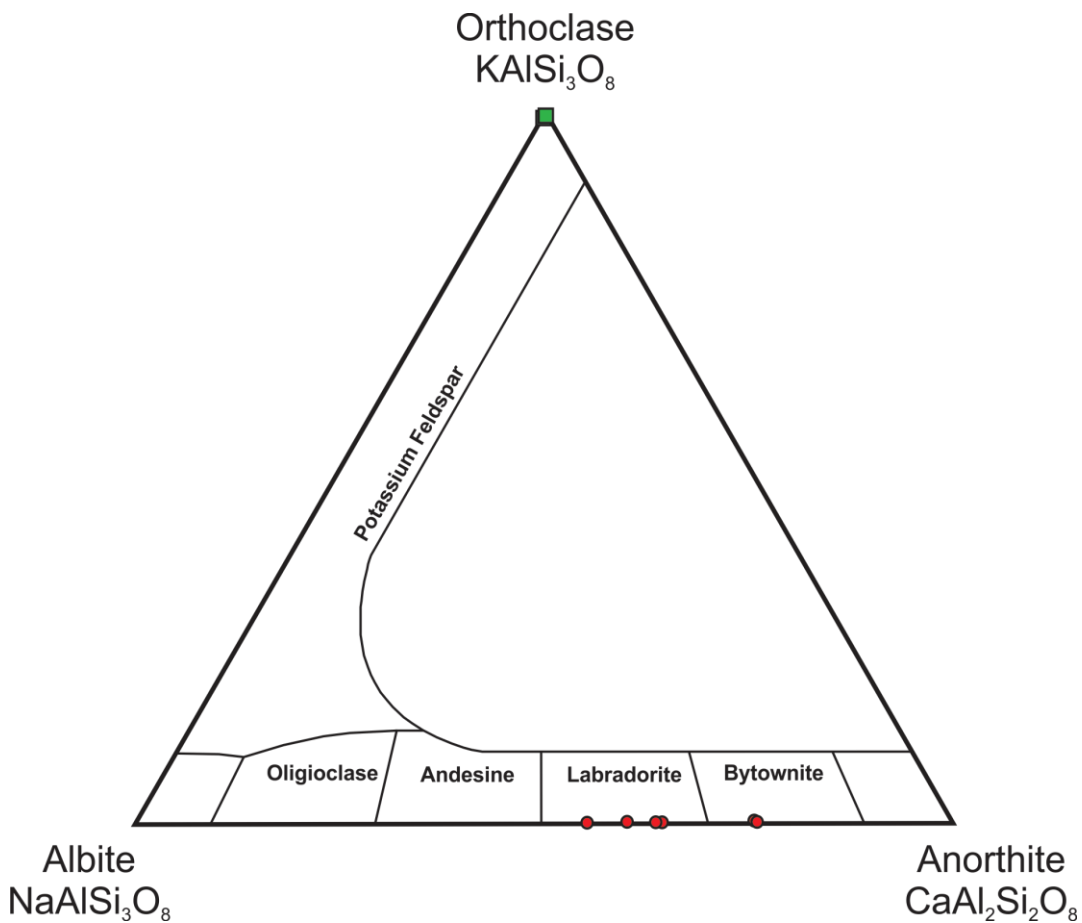


Fig. 7.2.11. Feldspar classification for the garnet-amphibole-biotite-muscovite schist. Ternary classification diagram for feldspars modified from [Greenwood and Earnshaw \(1998\)](#). Green squares represent potassium feldspars and red circles represent plagioclase feldspars.

7.3 Thermobarometry

To establish the pressure, temperature and fluid conditions responsible for the generation of the Bissett Creek flake graphite deposits, as outlined in objective 3, a thermobarometry study was undertaken using two methods. The first method uses conventional geothermometers and geobarometers, while the second employed multi-equilibrium thermobarometry using an internally consistent thermodynamic database.

7.3.1 Thermobarometry Methods

Conventional thermobarometry was conducted with the garnet-biotite ([Holdaway, 2000](#)) and garnet-hornblende ([Graham and Powell, 1984](#)) thermometers to constrain temperature and

the garnet-biotite-plagioclase-quartz barometer (Wu *et al.*, 2004) to constrain pressure. All values calculated from these datasets were reported (Table 7.3.1). Multi-equilibrium thermobarometry was conducted with THERMOCALC (v. 3.33, June 2009 update) in average P - T mode (Powell and Holland, 1988, 1994, 2008; Holland and Powell, 1998) to calculate pressures and temperatures in conjunction with AX2 software (Holland, 2014) that calculates component activities from measured mineral compositions and the internally consistent thermodynamic database (ds55) of Holland and Powell (1998). THERMOCALC has an additional functionality in that it can be used to evaluate the effect of fluid composition on estimates of P and T . Because graphite is a main mineral in most of the studied samples, this will have an important effect on the composition of equilibrated fluid so that the fluid is not expected to be pure H₂O, but a binary combination of H₂O and CO₂ (e.g. Ohmoto and Kerrick, 1977). The mole fraction of H₂O in a binary H₂O–CO₂ fluid is expressed here as $X_{\text{H}_2\text{O}}$.

Component activities are sensitive to P and T . Therefore, the P - T conditions estimated by the Holdaway (2000) calibration of the garnet-biotite thermometer and Wu *et al.* (2004) calibration of the garnet-biotite-plagioclase-quartz barometer were used as preliminary inputs into the AX2 software, which is used to calculate component activities from mineral compositions at a specific P - T condition. Calculated component activities were then inputted into THERMOCALC, which calculated new P - T conditions based on multiple thermobarometers that use an internally-consistent thermodynamic database. These refined estimates were then inputted into AX2 and this process was repeated iteratively until the pressure and temperature conditions output by AX and THERMOCALC converged to +/- 5°C and +/- 0.01 GPa. After this, the fluid composition ($X_{\text{H}_2\text{O}}$) was varied in 0.10 increments starting at 0.15 up to 0.95 and at 1.00 (pure H₂O). All calculations took place in a temperature window of 500–1000°C and pressure window of 0.7–1.5 GPa with the exception of sample BC-16-20B garnet # 2 where the temperature window was changed to 300–1200°C. P - T estimates from THERMOCALC are reported at $X_{\text{H}_2\text{O}} = 1$ and the value of $X_{\text{H}_2\text{O}}$ that yields the closest match to the temperature estimate provided by the Holdaway (2000) calibration of the garnet-biotite thermometer in Table 7.3.2 (e.g. Yakymchuk and Godin, 2012).

Retrograde metamorphic reactions can have a significant influence on mineral compositions through exchange reactions for rocks that have undergone medium- to high-grade

metamorphism (Kohn and Spear, 2000). To best approximate the peak metamorphic composition of garnet, points along garnet transects (Section 7.2) with the lowest X_{Fe} and X_{Mn} concentrations were paired with biotite, plagioclase and amphibole surrounding or in contact with the garnet grains (Yakymchuk and Godin, 2012). Compositional variations in biotite, plagioclase, and amphibole in the matrix are minimal. Mineral inclusions within the garnet show more variation but are excluded from thermobarometry calculations as they relate to the prograde evolution and not the peak metamorphic conditions.

7.3.2 Thermobarometry Results

The pressure and temperature estimates using conventional thermobarometry are summarized in Table 7.3.1. Results from THERMOCALC are summarized in Table 7.3.2. Results from both data sets are plotted on Figure 7.3.1. $P-T$ estimates using conventional thermobarometry range from 621–786°C at 0.9 GPa to 1.5 GPa. $P-T$ values using multi-equilibrium thermobarometry and $X_{H2O}=1$ vary from 709–881°C at 0.9 GPa to 1.4 GPa. Using the refined X_{H2O} values, $P-T$ estimates vary from 670–750°C at 0.8 GPa to 1.3 GPa. Note that most of the estimates plot in the stability field of kyanite (Fig. 7.3.1). This is important because sillimanite is the only aluminosilicate found within the rocks at Bissett Creek. There are several potential reasons for this which will be covered further in the discussion.

Variation between the temperature values provided by THERMOCALC for the $X_{H2O} = 1$ and the X_{H2O} which matched the temperature of the garnet-biotite thermometer varied from 12 °C and 196°C. Variation between the pressure values provided by THERMOCALC for the $X_{H2O} = 1$ and the X_{H2O} which matched the temperature of the garnet-biotite thermometer varied from 0.02 GPa and 0.24 GPa. Differences in $P-T$ estimates were most significant when the difference in the X_{H2O} values for the two data sets was high (e.g. X_{H2O} of the garnet-biotite match = 0.15, 0.25, 0.35). The datasets for the garnet-biotite and garnet-hornblende thermometry with pressures calculated from the garnet-biotite-plagioclase-quartz barometer overlap with those calculated from THERMOCALC where the fluid condition was estimated based on the matching temperature, only with slightly lower pressures, while those with the fluid condition $X_{H2O} = 1$ calculated from THERMOCALC have much high peak temperatures coupled with lower pressures (Fig 7.3.1).

Table 7.3.1. Conventional thermobarometry results

Sample	Mineral Assemblage	Garnet Location Used	Grt-Bt Thermometer (°C) Holdaway, 2000	Grt-Hb Thermometer (°C) Graham and Powell, 1984	Grt-Bt-Pl-Qtz Barometer (GPa) for Grt-Bt, Wu <i>et al.</i> , 2004	Grt-Bt-Pl-Qtz Barometer (GPa) for Grt-Hb, Wu <i>et al.</i> , 2004
BC-16-18B Garnet #1	Grt-Bt-Am-Pl-Qtz-Gr	Core	786	-	1.47	-
BC-16-18B Garnet # 2	Grt-Bt-Am-Pl-Qtz-Gr	Core	714	783	1.21	1.41
BC-16-18B Garnet # 3	Grt-Bt-Am-Pl-Qtz-Gr	Core	735	735	1.10	1.30
BC-16-20B Garnet # 1	Grt-Bt-Am-Pl-Qtz-Gr	Core	703	738	1.26	1.37
BC-16-20B Garnet # 2	Grt-Bt-Am-Pl-Qtz-Gr	Core	686	703	1.16	1.22
BC-16-20B Garnet # 3	Grt-Bt-Am-Pl-Qtz-Gr	Core	701	725	1.21	1.29
BC-16-28 Garnet # 1	Grt-Bt-Am-Pl-Qtz-Gr	Core	699	761	1.29	1.50
BC-16-28 Garnet # 2	Grt-Bt-Am-Pl-Qtz-Gr	Core	714	-	1.28	-
BC-16-29B Garnet # 1	Grt-Bt-Am-Pl-Qtz-Gr	Core	665	773	1.18	1.54
BC-16-29B Garnet # 2	Grt-Bt-Am-Pl-Qtz-Gr	Core	738	-	1.40	-
RO-16-04 Garnet # 1	Grt-Am-Bt-Ms-Pl-Qtz	Core	688	-	1.97	-
RO-16-04 Garnet # 2	Grt-Am-Bt-Ms-Pl-Qtz	Core	693	-	0.86	-
RO-16-08A Garnet # 1	Grt-Bt-Am-Pl-Qtz	Core	721	-	0.89	-
RO-16-09B Garnet # 1	Grt-Bt-Am-Pl-Qtz	Core	687	-	1.21	-
RO-16-09B Garnet # 2	Grt-Bt-Am-Pl-Qtz	Core	688	703	1.08	1.14
RO-16-09B Garnet # 3	Grt-Bt-Am-Pl-Qtz	Core	673	718	1.09	1.21
BC-10-06 Garnet # 1	Grt-Bt-Sil-K-Gr	Core	638	-	-	-
CO-16-05A Garnet # 1	Grt-Bt-Sil-K-Gr	Core	639	-	-	-
CO-16-05A Garnet # 2	Grt-Bt-Sil-K-Gr	Core	636	-	-	-
CO-16-05A Garnet # 3	Grt-Bt-Sil-K-Gr	Core	643	-	-	-
CO-16-05B Garnet # 1	Grt-Bt-Sil-K-Gr	Core	621	-	-	-
CO-16-05B Garnet # 2	Grt-Bt-Sil-K-Gr	Core	638	-	-	-
CO-16-08 Garnet # 1	Grt-Bt-Sil-K-Gr	Core	722	-	-	-
CO-16-10 Garnet # 1	Grt-Bt-Sil-K-Gr	Core	648	-	-	-

'-' represent sections where values could not be calculated due to limitations of mineral assemblage or data set. grt – garnet, bt – biotite, am – amphibole, pl – plagioclase, qtz – quartz, gr – graphite, ms – muscovite, sil – sillimanite, k – potassium feldspar.

Table 7.3.2. Thermobarometry results from THERMOCALC

Mineral Assemblage	Garnet Location Used	Grt-Bt (Hold) (°C)	Grt-Hb (G & P) (°C)	Fluid (X _{H2O})	T (°C)	1σ	P (GPa)	1σ	Corr.	σ _{fit}	n	Excluded End Members
Grt-Bt-Am-Pl-Qtz	Core	714	783	1.00 0.25	808 718	206 182	1.07 0.94	0.34 0.32	0.662 0.599	2.40 2.64	6	Spss
Grt-Bt-Am-Pl-Qtz	Core	735	735	1.00 0.85	747 735	182 178	1.05 1.03	0.30 0.29	0.688 0.679	2.27 2.30	6	Spss
Grt-Bt-Am-Pl-Qtz	Core	703	738	1.00 0.15	881 738	212 174	1.20 0.99	0.34 0.31	0.669 0.582	2.28 2.61	6	Spss
Grt-Bt-Am-Pl-Qtz	Core	686	703	1.00 0.45	717 687	195 182	1.07 1.02	0.31 0.29	0.676 0.640	2.47 2.52	8	Spss
Grt-Bt-Am-Pl-Qtz	Core	701	725	1.00 0.25	842 715	165 122	1.15 0.96	0.32 0.29	0.411 0.318	2.79 2.88	8	Spss
Grt-Bt-Am-Pl-Qtz	Core	699	761	1.00 0.35	785 710	50 59	1.34 1.21	0.11 0.15	0.327 0.359	0.95 1.48	3*	Spss
Grt-Bt-Am-Pl-Qtz	Core	714	-	1.00 0.35	789 716	50 40	1.38 1.26	0.12 0.11	0.347 0.288	0.69 0.18	3*	Spss
Grt-Bt-Am-Pl-Qtz	Core	665	773	1.00 0.15	820 699	217 171	1.22 1.02	0.35 0.29	0.718 0.631	2.44 2.57	6	Spss
Grt-Bt-Am-Pl-Qtz	Core	693	-	1.00 0.15	946 750	97 63	1.04 0.80	0.25 0.23	0.108 0.107	1.71 1.79	7	Spss
Grt-Bt-Am-Pl-Qtz	Core	688	703	1.00 0.35	744 689	161 147	0.96 0.88	0.25 0.24	0.658 0.607	1.93 2.04	6	Spss
Grt-Bt-Am-Pl-Qtz	Core	673	718	1.00 0.45	709 670	132 126	0.91 0.85	0.22 0.22	0.622 0.587	1.72 1.84	6	Spss

"-" represent sections where values could not be calculated due to limitations of mineral assemblage or data set.

* - represents an incomplete set of reactions.

(Hold) – represents the grt-bt geothermometer calibration of Holdaway (2000).

(G & P) – represents the grt-hb geothermometer calibration of Graham and Powell (1984). See table 7.3.1 for mineral abbreviations.

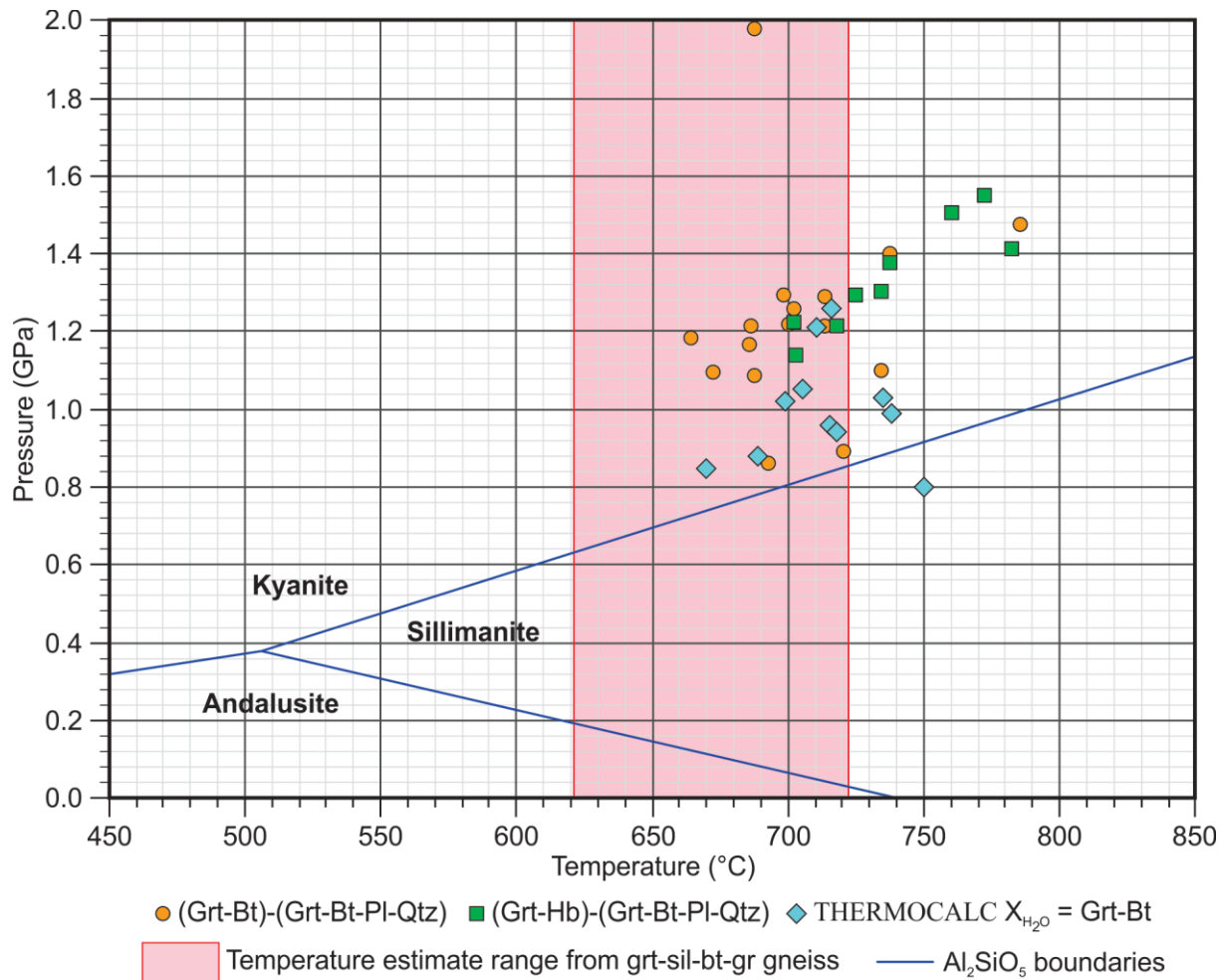


Fig. 7.3.1. Graphical representation of P - T estimates by type. Al_2SiO_5 polymorph boundaries obtained from Wei *et al.* (2004). Grt-Bt: garnet-biotite thermometer of Holdaway (2000). Grt-Hb: garnet-hornblende thermometer of Graham and Powell (1984). Grt-Bt-Pl-Qtz: garnet-biotite-plagioclase-quartz barometer of Wu *et al.* (2004). Grt-sil-bt-gr gneiss: garnet-sillimanite-biotite-graphite gneiss.

8.0 Comparison with other Flake Graphite Deposits

There are a number of regional and international flake graphite occurrences and deposits that share similar characteristics to the Bissett Creek flake graphite deposit. Summaries of the main characteristics of graphite mineralization are summarized in Table 8.1 (regional) and Table 8.2 (international).

8.1 Comparison with Flake Graphite Deposits in the pre-Grenvillian Laurentian Margin

[Garland \(1987\)](#) documented numerous graphite occurrences within semipelitic and pelitic gneiss units delineated during previous work by [Davidson et al., \(1982\)](#) in the Algonquin region of the Grenville Province. Four of these occurrences located in Butt Township (Kearney flake graphite deposit – Ontario Graphite Ltd.), Laurier Township, Ryerson Township and Maria Township (Bissett Creek flake graphite deposit – Northern Graphite Corporation), were further examined by [Garland \(1987\)](#). Table 8.1 summarizes the results of the study by [Garland \(1987\)](#), as well as new data from this study relevant to the Bissett Creek Deposit. A comparison of the characteristics from these four different localities across the Southwestern Grenville Province of Ontario allows for five key observations to be made. First, all of the occurrences have disseminated flake graphite as the dominant form of mineralization. Second, graphite mineralization is consistently found in biotite-quartzofeldspathic schist and gneiss units with only minor changes in the mineral assemblages. These changes could be due to compositional differences of the protoliths or subtle differences in the grade of metamorphism at each location (Table 8.1). Third, the whole-rock carbon content and flake size are consistent between the deposits in the pre-Grenvillian Laurentian margin. Fourth, a single carbon isotope value (-25.9‰; [Garland, 1987](#)) for the Butt Township deposit falls within the range of the carbon isotope signature of the Bissett Creek flake graphite deposit (Fig 5.2). Finally, interlayered graphite and biotite are documented at each of these deposits ([Garland, 1987](#)).

The combination of these five observations suggests that the protoliths could have originated from a similar depositional environment and that the conditions that resulted in graphite formation were generally similar at all localities. [Garland \(1987\)](#) concluded that these graphite occurrences are found in metasedimentary rocks that were likely part of the same shallow water depositional environment and that changes in metamorphic mineral assemblages were the result of changes in the type of sediment being deposited and differences in *P-T*

conditions. Mineral assemblages with more aluminous metamorphic minerals (e.g. garnet, sillimanite, biotite) may reflect more pelitic protoliths. [Davidson and Grant \(1986\)](#) proposed that the graphite occurrence in Maria Township may be part of the same band of pelitic gneisses as those of the Ryerson and Butt townships.

Graphite-bearing pelitic metasediments (easily identified in the field by their rusty gossan texture) could become important marker beds for reconstruction of tectonic histories for the region as they represent lithological units from a similar depositional environment with similar metamorphic histories, as shown by the formation of graphite. However, it would be important to separate deposits that are from primary metamorphism and deposits that may have undergone a secondary upgrading in response to hydrothermal activity from fluid influxes, such as those associated with igneous intrusions (e.g. Orissa Deposit in India) which may be the case for the vein style mineralization at the Laurier Township occurrence ([Garland, 1987](#)).

8.2 Comparison with International Flake Graphite Deposits

Flake graphite deposits are found in many metamorphic terranes around the world. The following section discusses the main characteristics of each deposit including the host rock lithology, carbon isotope signature, metamorphic grade, style of mineralization and the relative ages of the protoliths and metamorphic events, where available. The results of this review are summarized in Table 8.2.

The Lui Mao deposit in China contains flake graphite in a number of different metasedimentary units distributed throughout the Jiamusi Massif. The protoliths within the deposit are as old as 1300 Ma, and regional granulite facies metamorphism took place around 500 Ma ([Wilde et al., 1997](#)). Many of the units described by [Wilde et al. \(1999\)](#) have similar mineral assemblages to units found at the Bissett Creek deposit. The carbon isotope signature for this deposit ranges from -24.8 to -16.8 ‰ relative to the VPDB and is therefore interpreted to be derived from organic source materials ([Wilde et al., 1999](#)). Here, the formation of graphite has been attributed to the metamorphism of U- and V-rich black shales under upper amphibolite to granulite-facies $P-T$ conditions ([Wilde et al., 1999](#)).

Table 8.1. Summary of selected flake graphite occurrences in the pre-Grenvillian Laurentian Margin

Occurrence Location:	Ore style:	Crystalline habit:	Units hosting mineralization:	Mineralogy:	Average C (% weight):	Flake size (mm):	Carbon Isotopes $\delta^{13}\text{C}_{(\text{VPDB})}$ (‰):	References:
Maria Township (Bissett Creek)	Disseminated flake graphite	Flake	Biotite-Graphite-Quartzofeldspathic Gneiss, Clinopyroxene-Amphibole-Biotite-Graphite Gneiss, Garnet-Amphibole-Biotite-Graphite Gneiss, Garnet-Sillimanite-Biotite-Graphite Gneiss	See Chapter 3.0 for detailed mineralogy and petrology of each of the units.	2.7	0.04 to 6.5	-31.7 to -14.0 (n = 30)	Garland (1987)
Butt Township (Kearney)	Disseminated flake graphite	Flake	Biotite-Quartzofeldspathic Schist, Garnet-Hornblende Quartzofeldspathic Gneiss	Quartz-Plagioclase-Microcline-Graphite-Biotite-Diopside-Sillimanite-Titanite-Pyrite-Pyrrhotite-Scapolite, Quartz-Plagioclase-Biotite-Hornblende-Diopside-Garnet-Graphite	2.4	0.05 to 3.0	-25.9 (n=1)	Constable and Dunks (1986), Garland (1987), Garland (1991)
Laurier Township	Disseminated flake graphite, flake graphite in vein structure	Flake	Biotite-Quartzofeldspathic Schist	Quartz-Plagioclase-Biotite-Muscovite-Graphite-Hornblende-Clinopyroxene-Chlorite-Sillimanite-Pyrrhotite-Pyrite-Garnet	2.0 ^a 25 ^b	0.05 to 1.5	-	Garland (1987)
Ryerson Township	Disseminated flake graphite	Flake	Biotite-Quartzofeldspathic Schist	Quartz-Microcline-Plagioclase-Biotite-Graphite-Tremolite-Sillimanite-Garnet-Pyrite-Chalcopyrite-Sphene	2.0 ^c 2.5 ^d	0.07 to 1.4	-	Garland (1987)

^a – Average C weight % from the disseminated style of mineralization.

^b – Average C weight % from the vein style of mineralization.

^c – Average C weight % from the northern section of the occurrence.

^d – Average C weight % from the southern section of the occurrence.

The Orissa region in the Eastern Ghats Mobile Belt of India has multiple graphite morphologies related to a complex mineralization history. The primary mineralizing event, responsible for the formation of flake graphite, is interpreted to have occurred as a result of metamorphism of *in situ* organic material during one of three metamorphic events which occurred from 1600 Ma to 500 Ma (Sanyal *et al.*, 2009). The carbon isotope values for the flake graphite in the deposit range from -26.6 to -2.4 ‰ relative to the VPDB (Sanyal *et al.*, 2009). The variation in carbon isotope signature is attributed to carbon isotope exchange with calcite and carbon-bearing fluids during further metamorphism as well as mantle-derived carbon from several igneous intrusions (Sanyal *et al.*, 2009). The igneous intrusions caused remobilization of the graphite, resulting in vein-type mineralization on the margins of the intrusive rocks and within shear zones related to the intrusions (Sanyal *et al.*, 2009).

The flake graphite of the Spaulding Suite located in the New Hampshire Plutonic series appears to have a similar formation process to the Orissa Region deposits of India. The disseminated flake graphite is found in both the surrounding metasedimentary wall-rocks as well as the igneous plutons. Disseminated flake graphite in the plutons is thought to represent xenocrystic material that was assimilated into the igneous rocks during intrusion (Duke and Rumble, 1986). The assimilation of this material also allowed for the formation of graphite veinlets and spherules as a result of graphite remobilization as a carbon bearing fluid during intrusion (Duke and Rumble, 1986). However, primary flake graphite formation is thought to have occurred as a result of the metamorphism of *in situ* organic material from Early Silurian through to Early Devonian pelitic and calcareous basin facies sedimentary rocks (Duke and Rumble, 1986). Flake graphite from within the metasedimentary rocks of the Spaulding Suite have carbon isotope values that range from -26.0 to -16.7 ‰ relative to VPDB (Duke and Rumble, 1986). The igneous plutonic rocks have an overlapping signature that ranges from -26.5 to -13.8 ‰, which further supports the assimilation interpretation (Duke and Rumble, 1986).

The flake graphite found in the Mesoproterozoic rocks of the New Jersey Highlands is interpreted to have formed as a result of graphitization during *in situ* metamorphism of organic material in sedimentary rocks, predominantly sandstones and mudstones (Volkert *et al.*, 2000). The supracrustal sequence that hosts the graphite mineralization was laid down prior to 1.1 Ga (Volkert *et al.*, 2000). Volkert *et al.* (2000) further link the host rocks to those in southern New

York and Canada as part of the Grenville Province, meaning that the main metamorphic event responsible for graphite formation was associated with the Grenvillian Orogeny. The carbon isotopes for the flake graphite found in the graphitic metaquartzite and biotite-quartz-feldspar-graphite gneiss range from -28.4 to -16.4 ‰ (n=16) relative to the VPDB, which supports a biogenic source for the graphite (Volkert *et al.*, 2000). The spread in carbon isotope values may have come from carbonic fluids generated during metamorphism (Volkert *et al.*, 2000). Furthermore, the flake graphite mineralization is limited to the proposed metasedimentary sequence formed by the graphitic metaquartzite and the biotite-quartz-feldspar-graphite gneiss (i.e. stratabound) (Volkert *et al.*, 2000).

Volkert *et al.*, (2000) also performed sulfur isotope analyses on the sulfides found within the graphite-bearing units, which yielded values ranging from 6.4 to 10.6 ‰ (n=11) relative to the VCDT for the biotite-quartz-feldspar-graphite gneiss and 3.6 to 5.5 ‰ (n=10) relative to VCDT for the metaquartzite. A single value from another deposit in the region, from the biotite-quartz-feldspar gneiss, yielded a value of -0.6‰ (Volkert *et al.*, 2000). The narrow range of sulfur isotope values was interpreted to have been generated by the formation of pyrrhotite from sedimentary pyrite during metamorphism and was likely to reflect the signature of primary pyrite deposition through bacterial sulfate reduction (Volkert *et al.*, 2000). Combining all of this information, Volkert *et al.*, (2000) interpreted that the supracrustal rocks that hosted the graphite mineralization were part of a shallow water sedimentary sequence which facilitated the rapid burial of organic matter under anoxic conditions, which then underwent granulite facies metamorphism and potentially partial melting.

The flake graphite of the Tasiilaq Area in the Kuummiut Terrane of Greenland was likely formed as a result of graphitization, followed by remobilization during metamorphism and deposition from hydrothermal fluids (Rosing-Schow *et al.*, 2016). The main metamorphic episode, thought to be responsible for primary graphite formation took place around 1870-1820 Ma (Rosing-Schow *et al.*, 2016). The disseminated flake graphite cross-cuts a number of lithological boundaries and is not stratabound like other flake graphite deposits (e.g. Liu Mao Deposit). The $\delta^{13}\text{C}_{\text{VPDB}}$ values in this area range from -30.8 to -18.1 ‰, meaning that the fluid that formed the graphite must have come from an organic source material (Rosing-Schow *et al.*, 2016).

Finally, the graphite of the Xinghe Deposit is stratabound in Paleoproterozoic granulite facies garnet and sillimanite bearing gneisses and occurs as either disseminated flakes and massive fine-grained concentrations (Yang *et al.*, 2014). The disseminated flake graphite is interpreted to have been formed by the graphitization process as a result of metamorphism of *in situ* organic materials in pelitic sediments. The $\delta^{13}\text{C}_{\text{VPDB}}$ values in this area range from -24.1 to -20.5 ‰ and represent carbon derived from an organic source (Yang *et al.*, 2014). Graphite veins are interpreted to be derived from fluids formed from high-grade metamorphism (Yang *et al.*, 2014).

Based on the review of international flake graphite deposits, there are four key common observations that can serve as defining characteristics for these deposit types. First, the protoliths of each of the deposits are inferred to be sedimentary in origin, and vary from sandstones to greywackes to mudstones, with or without a carbonate component. The deposits are commonly stratabound to this sedimentary sequence (e.g. Bissett Creek, Liu Mao, New Jersey and Xinghe). This does not hold true when the graphite mineralization is thought to have been generated through infiltration of an externally derived fluid or later fluids have remobilized the graphite to form new morphologies (e.g. Tasiilaq and Orissa region deposits). Second, flake graphite deposits with a metasedimentary origin frequently have accompanying sulfide mineralization in the form of pyrite and pyrrhotite. Third, the deposits of this type commonly possess carbon isotope signatures consistent with organic materials. Fourth, the metamorphic grades most commonly associated with graphite deposits are upper amphibolite to granulite facies with and without anatexis. However, anatexis may play a role in graphite remobilization (e.g. Bissett Creek, Liu Mao, and New Jersey).

Table 8.2. Summary of international flake graphite occurrences

Occurrence Location:	Ore style:	Crystalline habit:	Grade and Tonnage:	Units hosting mineralization:	Temperature of formation (°C)	Flake size (mm):	Carbon Isotopes $\delta^{13}\text{C}_{(\text{VPDB})}$ (‰):	References:
Bissett Creek Deposit, pre-Grenvillian Laurentian Margin, Ontario, Canada	Disseminated flake graphite	Flake	1,83 % 40.5 Mt	Biotite-Graphite-Quartzofeldspathic Gneiss, Clinopyroxene-Amphibole-Biotite-Graphite Gneiss, Garnet-Amphibole-Biotite-Graphite Gneiss, Garnet-Sillimanite-Biotite-Graphite Gneiss	620 to 780	0.04 to 6.5	-31.7 to -14.0 (n = 30)	Garland (1987), Taner <i>et al.</i> , (2017)
Liu Mao Deposit, Jiamusi Massif, Jilin-Heilongjiang Fold Belt, China	Disseminated flake graphite	Flake	360 Mt	Graphite Schists, Diopside-Graphite Schist/Gneiss, Garnet-Biotite-Plagioclase-Graphite Gneiss, Sillimanite-Quartz-Graphite Schist, Graphite-Plagioclase Gneiss, Garnet-Cordierite-Graphite Gneiss	500 to 850	-	-24.8 to -16.8 (n = 22)	Wilde <i>et al.</i> , (1999)
Orissa Region Deposits, Eastern Ghats Mobile Belt, India	Disseminated flake graphite, vein graphite	Flake, Vein	Not available	Calc-Silicate Granulite, Khondalite, Khondalite Migmatite, Graphite Schist, Calcareous Graphite Schist	620 to 945	-	^a -26.6 to -2.4 (n = 14) ^b -24.4 to -8.8 (n = 16)	Sanyal <i>et al.</i> , (2009)
Spaulding Suite, New Hampshire Plutonic Series, USA	Disseminated flake graphite, vein graphite, spherulitic graphite	^c Flake, Vein, Spherules	Not available	Plutonic Rocks, Pelitic (Staurolite to Cordierite-Sillimanite-K-Spar) and Calcareous Metasedimentary Rocks	600 to >750	^c 0.1 to 1.0	^d -26.0 to -16.7 (n=39) ^e -26.5 to -13.8 (n=55)	Duke and Rumble (1986)
New Jersey Highlands (USA)	Disseminated flake graphite	Flake	Not available	Graphitic Metaquartzite, Biotite-Quartz-Feldspar-Graphite Gneiss, Pegmatites	680 to 760	1.0 to 2.0	-28.4 to -16.4 (n=16)	Volkert <i>et al.</i> , (2000)
Tasiilaq Area, Kuummiut Terrane, Greenland	Disseminated flake graphite	Flake	Not available	Biotite Schist, Amphibolite, Orthogneiss, Garnet-Quartz Veins	600	0.1 to 5.0	-30.8 to -18.1 (n = 24)	Rosing-Schow <i>et al.</i> , (2016)
Xinghe Graphite Deposit, Huai'an Terrain, North China Craton, China	Disseminated flake graphite, vein graphite	Flake, Vein	Not available	Garnet-Sillimanite-Biotite-Plagioclase Gneiss, Graphite-Quartz Veins	>900	0.2 to 3.0	-24.1 to -20.5	Wang (1989), Yang <i>et al.</i> , 2014, Zhang <i>et al.</i> , (2014)

^a – Carbon isotope values from flake style mineralization.

^b – Carbon isotope values from vein style mineralization.

^c – All remaining data for this deposit refers exclusively to the flake graphite variant.

^d – Carbon isotope values from metasedimentary rocks.

^e – Carbon isotope values from plutonic rocks.

9.0 Discussion

9.1 Rock Units and Potential Protoliths

Nine units were identified at the Bissett Creek property based on field mapping (Chapter 3.0), petrography (Chapter 3.0), and geochemistry (Chapter 4.0). The units are: (1) biotite-graphite-quartzofeldspathic gneiss, (2) clinopyroxene-amphibole-biotite-graphite gneiss, (3) garnet-amphibole-biotite-graphite-quartzofeldspathic gneiss, (4) garnet-sillimanite-biotite-graphite gneiss, (5) biotite-quartzofeldspathic gneiss, (6) amphibole-biotite-quartzofeldspathic gneiss, (7) garnet-sillimanite-biotite gneiss, (8) granitic pegmatites and (9) metagabbro intrusives. Granitic pegmatites and the metagabbro intrusives are clearly younger and igneous in origin based on their sharp cross-cutting relationship with the host gneisses (Fig. 3.8A, 3.8B and 3.9A). However, no primary features of the protoliths of the seven gneiss units remain due to pervasive ductile deformation (Chapter 3.0), reworking during high-temperature metamorphism (Chapter 7.0) and partial melting (Fig. 3.12).

The graphitic gneisses (units 1 to 4) are thought to have originated from a sedimentary sequence. The graphitic gneisses have gradational contacts that span from centimeters to meters; these contacts are inferred to represent the compositional variation arising from deposition. Additionally, flake graphite and sulfide minerals are present in all the graphitic gneiss units.

The carbon isotope signature of the local graphitic gneisses ranges from -28.3‰ to -14.0‰, which is consistent with an organic origin for the carbonaceous materials that formed the graphite (Section 5.1) ([Schidlowski 1988, 2001; Luque *et al.*, 2012](#)). The sulfur isotope values of the sulfides range from 9.7‰ to 14.2‰, which is consistent with multiple reservoir types including those of a sedimentary origin. Sediments containing organic material also commonly contain pyrite as a result of bacterial sulfate reduction, which could have provided the sulfur for sulfide mineralization at Bissett Creek ([Berner, 1984; Volkert *et al.*, 2000](#)).

Additionally, the REE plots show a similar pattern between the graphitic gneiss units and Post Archean Average Shale (Fig 4.1 to 4.4), which indicates that the REE compositions of the graphitic gneiss are compatible with pelitic protoliths. Another geochemical indicator consistent with the deposition of organic-rich pelagic sediments is elevated concentrations of Zn, Cd, Cu, Ni, V, Mo, and U when compared to upper continental crust values and values for an average

shale (Wedepohl, 1971; 1995). Elevated values of these redox-sensitive elements are commonly associated with organic carbon in black shales, which is documented in other international flake graphite deposits (e.g. Lui Mao, China) (Vine and Tourtelot, 1970; Brumsack 1986; Wedepohl, 1971; Mitchell, 1993; Wilde *et al.*, 1999).

Another key element which supports the black shale origin is the correlation between C_{graphitic} (%), which is thought to represent organic carbon from the black shales, and S (%), which is thought to represent pyrite formation in the black shales, with the concentrations of V, Mo and U as shown by Brumsack (1986) (Fig 9.1). The relationship between C (%) and S (%) with V, Mo, and U is thought to represent relationships formed during the primary deposition of black shales (Brumsack, 1986). While the correlations of carbon with V and Mo is strong and weaker with U, the correlations with sulfur are very weak to negligible, which supports the hypothesis that sulfur could have been remobilized during metamorphism and the formation of pyrrhotite (e.g. Zheng, 1990). Remobilization of sulfur during metamorphism would also explain the homogenization of the sulfur isotope signature and the sulfides infrequently seen intercalated with graphite (e.g. Zheng, 1990). The preserved relationships between carbon and selected trace metals (V, Mo, U) could have implications for the mobility of these elements during metamorphism. However, the sulfur isotope signature would not have shifted very far, and likely represents the sulfur isotope signature of the protolith recorded during deposition because the fractionation between sulfide minerals and H₂S at high metamorphic temperatures, which lead to pyrrhotite formation are relatively small (Ohtomo and Rye, 1979; Zheng, 1990; Volkert *et al.*, 2000). Due to the lack of cross-cutting relationships with the surrounding lithological units, as seen in other hydrothermal flake graphite deposits (e.g. the Tasiilaq region deposits) the graphite and sulfides are interpreted to have formed as part of a closed system.

Both the carbon and sulfur isotope signatures support a potential sedimentary origin for the protoliths because of the biogenic signature associated with the carbon (e.g. Schidlowski 1988, 2001) and the overlap of the range for the sulfides with those of Proterozoic sulfates (e.g. Strauss, 1993; Canfield, 1998). The overlap with Proterozoic sulfates is significant because the sulfates from evaporites are interpreted to represent paleo-seawater compositions from which pyrite and subsequently pyrrhotite would have developed (Strauss, 1993).

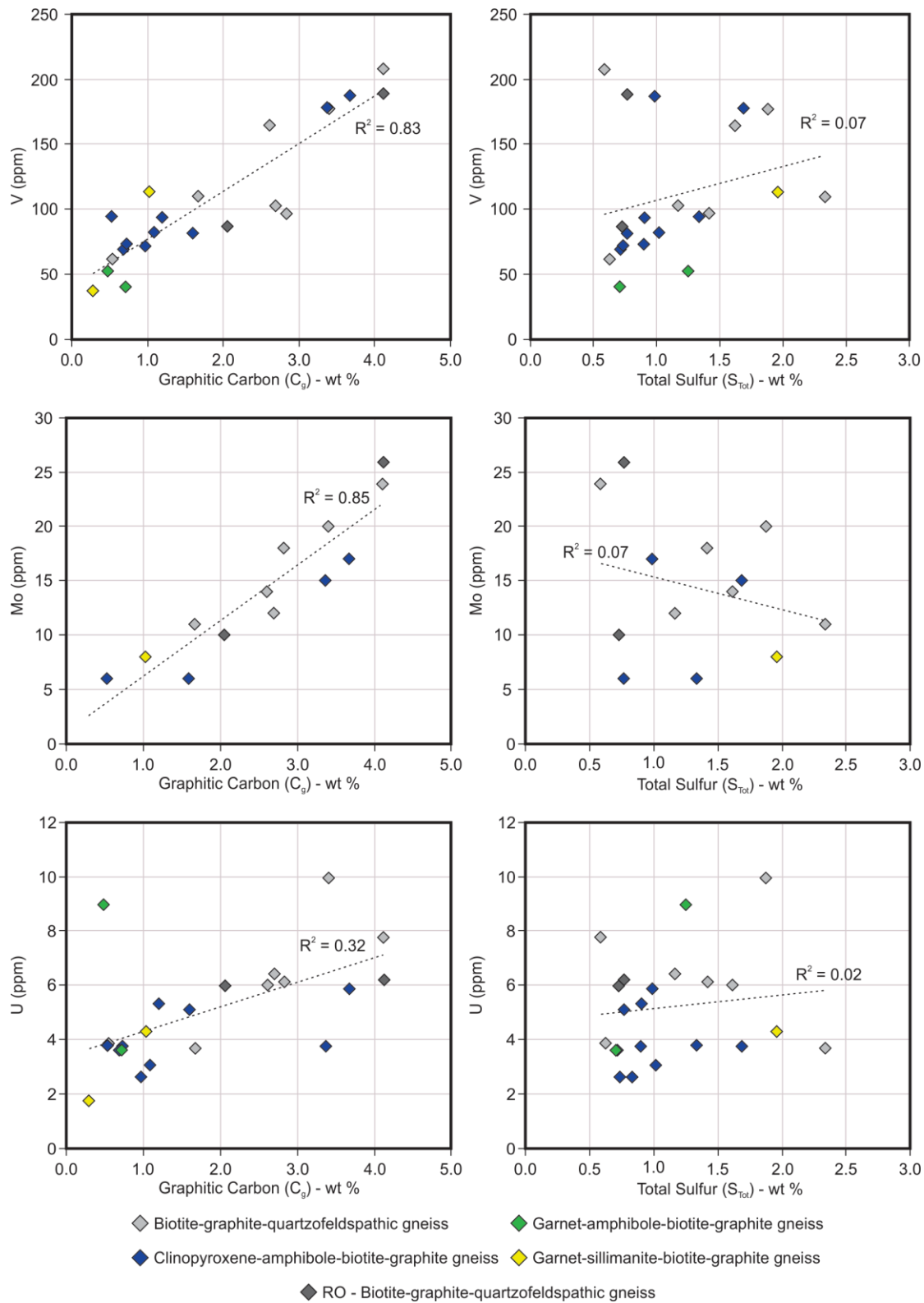


Fig. 9.1. Trace metals (V, Mo, U) versus graphitic carbon (C_g) and total sulfur (S_{tot}) after Brumsack (1986). All values below the LOQ were removed before generating the linear relationships.

The clinopyroxene-amphibole-biotite-graphite gneiss unit has relatively higher concentrations of CaO than the other graphitic gneisses. This unit may have a more calcareous metasedimentary protolith. Finally, plotting the compositions of the samples analyzed for FeO on the ACF diagram of [Vernon and Clarke \(2008\)](#) shows compositions consistent with feldspathic sandstones to psammopelites (Fig. 9.2). Thus, the Bissett Creek graphitic gneiss units are thought to represent an organic-rich sedimentary sequence, with various pelitic, psammitic and more calcareous layers.

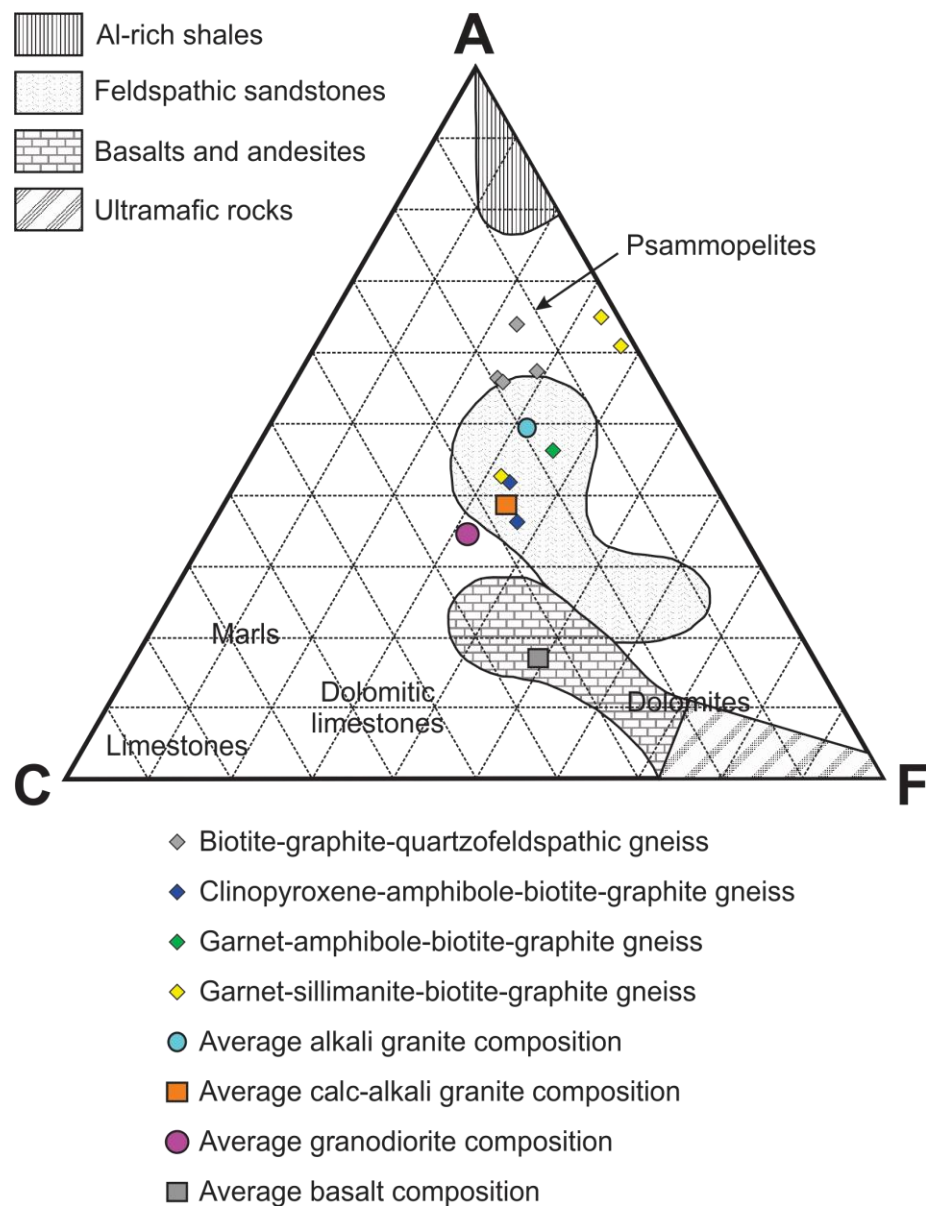


Fig. 9.2. ACF classification of the graphitic gneisses showing potential protoliths (modified from [Vernon and Clarke \(2008\)](#)).

The origins of the barren gneisses (units 5 to 7) are more enigmatic. The barren gneisses have sharp contacts with the graphitic gneisses (Fig 3.13), which is consistent with an intrusive relationship. The barren gneisses plot in a tight cluster in the “granite” field on a TAS classification plot (Section 4.3 & 4.4). This classification, along with the tight clustering, could suggest that the barren gneisses either started as a felsic igneous rock or were the immature sedimentary derivatives of one. Finally, granitoids are the dominant rock type in the region and commonly contain enclaves and rafts of inferred metasedimentary material (e.g. Davidson, 1982; Davidson, 1984; Carr *et al.*, 2000). On balance, an intrusive origin for the barren gneisses is most likely, however, the possibility that these are relatively immature metasedimentary rocks that have been pervasively deformed and recrystallized cannot be dismissed on the basis of the limited evidence available.

9.2 Structural Controls on Mineralization

The Bissett Creek flake graphite deposit is composed of pervasively folded shallowly to moderately dipping (6° to 38°) gneiss units with a strong metamorphic fabric dominantly trending from the northwest to the southeast (Chapter 3.0). The graphitic gneiss layers are stratabound by sharp contacts with barren gneisses (Fig 3.13). Since graphite mineralization is limited to the inferred metasedimentary package and does not permeate into the surrounding gneisses, the barren gneisses could represent an impermeable barrier that trapped carbonic fluids generated in the carbon-rich metasedimentary rocks during metamorphism. Additionally, flake graphite is homogeneously distributed throughout the graphitic gneisses, which further supports a relatively closed (i.e. stratabound) system.

9.3 Pressure, Temperature and Fluid Conditions of Mineralization

Estimated peak metamorphic temperatures at the Bissett Creek flake graphite deposit range from 621°C to 786°C , with a median value of 688°C (Chapter 7.0). Pressures at peak temperatures vary from 0.86 GPa to 1.47 GPa, with a median value of 1.21 GPa (Chapter 7.0). These values are consistent with upper-amphibolite to granulite-facies metamorphism equivalent to what has been documented in neighbouring regions in the pre-Grenvillian Laurentian Margin in the southwestern Grenville Orogen (Indares and Dunning, 1997; Carr *et al.*, 2000; Rivers *et al.*, 2012). However, calculated peak P - T conditions plot in the kyanite stability field, which is inconsistent with the observed sillimanite-bearing assemblages (Fig. 7.3.1). There are several

possible reasons for this, including retrograde diffusive exchange, difficulty in determining fluid composition, disequilibrium, and anatexis.

Exchange thermometers (e.g. garnet–biotite) are sensitive to retrograde diffusive exchange in high-temperature metamorphic rocks ([e.g. Dempster, 1985; Fitzsimons and Harley, 1994](#)) and thus the calculated peak temperatures can be significantly less than true peak temperatures. Barometers are less sensitive to retrograde diffusion because these are related to net transfer reactions and not cation exchange reactions. It is also possible that Fe-Mg exchange between biotite and garnet continued to occur during retrograde metamorphism after the peak conditions were reached, thus yielding an estimate lower than peak conditions.

At 0.9–1.5 GPa, the temperature of the kyanite-to-sillimanite transition is expected to range from ~780 to >900°C, which is higher than most of the calculated temperatures (Fig. 7.3.1). Peak metamorphic conditions associated with Ottawan and Rigolet metamorphism in the allochthonous high pressure belt, where the Bissett Creek flake graphite deposit is situated, were estimated to range from 700–850°C and 0.9 to 1.4 GPa in previous work ([Anovitz and Essene, 1990; Timmerman *et al.*, 2002; Kendrick and Jamieson, 2016](#)). Considering the results of previous work and the relatively low temperatures calculated from the garnet–biotite exchange thermometer compared with *P*–*T* estimates based on the visible assemblage, it is likely that the true peak metamorphic temperatures at Bissett Creek were >780°C.

Another challenge in determining the peak *P*–*T* conditions at Bissett Creek is the fluid composition during metamorphism, which could not be accounted for using conventional thermobarometry. In graphite-bearing metamorphic systems, fluid compositions are buffered to values of $X_{\text{H}_2\text{O}} < 0.9$ and $a_{\text{H}_2\text{O}} < 1$ ([Ohmoto and Kerrick, 1977; Chu and Ague, 2013](#)). In Chapter 7.3, the molar proportion ($X_{\text{H}_2\text{O}}$) for a $\text{H}_2\text{O}-\text{CO}_2$ fluid was varied until the temperature conditions output by THERMOCALC in AVGPT (Mode 2) agreed with the temperature conditions generated by the conventional garnet-biotite thermometer and garnet-biotite-plagioclase-quartz barometer (e.g. [Yakymchuk and Godin, 2012](#)). The molar proportions of H_2O that corresponded with the temperature values produced by the conventional thermobarometers ranged from 0.15 to 0.85, with a median of 0.35. This indicates that H_2O was not the dominant component in the fluid during metamorphism in some cases and that CO_2 (or possibly CH_4) would have made up a larger proportion. [Chu and Ague \(2013\)](#) showed that fluids in graphite-bearing metapelitic

systems become more enriched in CO₂ as pressure and temperature increase. Thus, the fluid present during graphite formation at Bissett Creek was likely CO₂-rich. However, the specific role of CO₂-rich fluids on high-temperature metamorphic assemblages is still not well understood (i.e. Chu and Ague, 2013).

Another issue with the results of the thermobarometric estimates in Chapter 7.0 is the relatively large errors propagated by THERMOCALC for individual *P*–*T* estimates (>100°C, >0.1 GPa). The inability to reconcile a precise pressure and temperature conditions could indicate that the samples evaluated from the site and surrounding area were not in chemical equilibrium. Although most *P*–*T* sensitive minerals (i.e. garnet, biotite, plagioclase) have sharp boundaries with each other—indicating textural equilibrium—they may be chemically out of equilibrium possibly due to retrograde exchange reactions as discussed earlier. An alternative method for calculating peak *P*–*T* conditions is phase equilibria modelling using pseudosections that are less sensitive to chemical disequilibrium (e.g. Powell and Holland, 2008). However, pseudosection models appropriate for graphite-bearing systems are still in their infancy (e.g. Chu and Ague, 2013).

A final issue to consider is the generation of melt due to anatexis of the amphibolite- to granulite-facies metapelitic assemblage. Partial melting at the Bissett Creek site is supported by field partial melting indicators (Fig 3.12), the high-temperature mineral assemblage of the garnet-sillimanite-biotite(+/-graphite) gneiss, thermobarometry results from the garnet-biotite-sillimanite(+/-graphite) gneiss and regional *P*–*T* estimates of >800°C (e.g. Rivers *et al.*, 2012) that are well above the temperatures of wet solidus (~650°C) for metapelites (e.g. White *et al.*, 2007). For graphite-rich metapelites where CO₂ and CH₄ can be dissolved in the melt, the minimum temperature of melting may be slightly lower than the wet solidus (Ohmoto and Kerrick, 1977; Chu and Ague, 2013). However, the role of carbonic fluids in anatexic systems is not well understood due to uncertainties of the solubility of CO₂ and CH₄ in the melt (e.g. Connolly and Cesare, 1993). Nonetheless, the estimated temperatures of metamorphism are likely much greater than the minimum melting temperature for metapelites (~650°C).

9.4 Metamorphic History and Relative Timing of Mineralization

Graphite mineralization is found as flakes and veinlets along grain boundaries within the Bissett Creek deposit. Disseminated flake mineralization is found in all the graphitic gneiss units, while veinlets are found almost exclusively in the garnet-sillimanite-graphite gneiss and so could be a product of carbon remobilization in response to partial melting. For the disseminated flake variant of graphite, it is commonly interleaved with biotite (Fig. 3.2C, 3.2D, 3.3C, 3.4D, 3.5B, 3.5D) and other metamorphic minerals (Fig. 3.3E, 3.3F, 3.4D), it can be found with intergrowths of quartz and garnet (Fig. 3.2E, 3.4E, 3.4F, 3.5E), and it shows close spatial association with sulphides (Fig. 3.2F, 3.5F). The prominence of the disseminated flake graphite style of mineralization within the graphitic gneiss units is important because flake graphite is the only crystal habit associated with metamorphic deposits ([Luque et al., 2012](#)). Conversely, hydrothermal deposits commonly contain multiple crystal habits such as flake, spherules, colloform, cryptocrystalline, rings, cones and tubes ([Mitchell, 1993](#); [Jaszczak et al., 2003](#); [Doroshkevich et al., 2007](#); [Barrenchea et al., 2009](#); [Luque et al., 2012](#)).

Due to the prominence of the disseminated flake graphite mineralization style at the Bissett Creek deposit, the interleaving and intergrowth of graphite with metamorphic minerals, the fact that the graphite orientation is consistent with the dominant foliation, the restriction of graphite to units that have mineral assemblages consistent with inferred pelitic and semipelitic protoliths, the lack of graphite concentration in fold hinges, and the restriction of graphite veinlets to the garnet-sillimanite-biotite-graphite gneiss, it is likely that primary graphite mineralization was developed *in situ* in response to metamorphism and not from precipitation from an externally derived carbon-rich fluid. The presence of graphite in veinlets with sulfides (Fig 3.5D, 3.5F) in the garnet-sillimanite-biotite-graphite gneiss could be due to graphite remobilization as a result of partial melting ([Chu and Ague, 2013](#)). Therefore, graphite mineralization and remobilization are likely contemporaneous with prograde metamorphism. The transformation from graphitic carbon to crystalline graphite takes place at ~700°C ([e.g. Buseck and Beyssac, 2014](#)), and peak temperatures recorded at Bissett were expected to be higher than this value (Chapter 9.3).

9.5 Carbon Source Responsible for Mineralization

Carbon isotope values of graphite are commonly used to infer the source of carbon responsible for graphite crystallization (e.g. Wada *et al.*, 1994; Luque *et al.*, 1998; Wilde *et al.*, 1999; Luque *et al.*, 2012; Rosing-Schow *et al.*, 2016). Since the carbon present at Bissett Creek is predominantly graphitic (Table 5.1, Fig 5.1), the isotope values generated from the whole rock powders in this study are thought to represent the composition of the graphite. The carbon isotope values of whole-rock samples from this study range from -28.3‰ to -14.0‰ with a median of -23.3‰ at the Bissett Creek flake graphite deposit ($n = 27$). Regionally, the values were -31.7‰, -31.3‰, and -19.7‰. Taner *et al.* (2017) reported carbon isotope values of graphite separates from Bissett Creek that ranges from -29.1‰ to -17.4‰, with a median of -21.8‰ ($n = 8$). Garland (1987) reported a single carbon isotope value for the Bissett Creek flake graphite deposit of -15.6‰. Thus, there is generally good agreement between the data from this study and previous carbon isotope work completed at the deposit. Based upon this range, it is likely that the carbon source responsible for mineralization was organic in origin.

Biogenic carbonaceous materials generally have lighter isotopic compositions (-43‰ to -3‰) than carbon from the mantle (-8‰ to -3‰) or from carbonates precipitated from seawater (~0‰) (Javoy *et al.* 1986; Deines *et al.*, 1991; Deines, 1992; Viljoen, 1995; Schidlowski, 1988; Schidlowski 2001). Schidlowski (2001) summarized the carbon isotope signatures over the extent of modern autotrophic organisms and those preserved in the geologic record. Most modern autotrophic organisms fall within the range of -43‰ to -3‰, except for methanogenic bacteria, whose carbon isotope ratios extend from -41.5‰ to 6‰ and methanotrophic bacteria, which ranges from -85.0‰ to -29‰ (Fig 9.1) (Schidlowski, 2001).

The isotopic signature of carbon in the geologic record also varies with respect to time. For instance, at the start of the Proterozoic (2.5 Ga), the range for organic carbon was from approximately -40‰ to -10‰ (Schidlowski, 2001). By the end of the Proterozoic (0.54 Ga), the extents of the signature had changed, ranging from approximately -33‰ to -10‰ (Schidlowski, 2001).

At the beginning of Grenvillian orogenesis (~1.25 Ga) the range of isotopic compositions for organic carbon preserved in the rock record ranged from approximately -35.5‰ to -12.5‰, with an approximate mean of -22‰ (Schidlowski, 2001). By the end of Grenvillian orogenesis

(~0.98 Ga), the range had narrowed slightly with values from -34.5‰ to -13‰, with an approximate mean of -22‰ (Schidlowski, 2001). The range for recent marine sediments, which encompasses the range of most of the important modern autotrophic organisms, extends from -34‰ to -10‰ based on 1600 data points (Deines, 1980). However, 90% of the data within that range falls within the smaller subset from -29‰ to -18‰ (Deines 1980, Schidlowski, 1988; Schidlowski 2001).

As previously mentioned carbon with isotopically lighter signatures may also be generated from 1) high temperature disproportionation of siderite, 2) low-temperature Fischer-Tropsch synthesis and 3) inclusion of meteoritic carbonaceous matter (Perry and Ahmad, 1977; Schidlowski *et al.*, 1979; van Zuiden *et al.*, 2003; Horita, 2005; Tashiro *et al.*, 2017). It is unlikely that the graphite formed from the disproportionation of siderite ($6\text{FeCO}_3 \rightarrow 2\text{Fe}_3\text{O}_4 + 5\text{CO}_2 + \text{C}$), due to the lack of both siderite and magnetite within the rocks (Tashiro *et al.*, 2017). Secondly, Fischer-Tropsch synthesis takes place at low temperatures (200-350°C), requires a Ni-Fe metal catalyst and a source of H₂ and CO₂ (Tashiro *et al.*, 2017). Given the high metamorphic temperatures estimated for metamorphism at Bissett Creek along with the absence of a suitable catalyst, it is unlikely that the graphite was formed through this process. Finally, the sulfur isotope signature rules out the possibility of a meteoritic carbon contribution as the $\delta^{34}\text{S}_{\text{CDT}}$ value for meteoric carbon is ~0‰, versus a signature from Bissett ranging from 9.7‰ to 15.0‰.

Graphite deposits that are generated exclusively from metamorphic processes usually have a narrow range (±2‰) of carbon isotope values because the precursor material is similar across the area of mineralization and then undergoes the same metamorphic conditions (e.g. Xinghe Graphite Deposit, China) (Luque *et al.*, 2012). The range of values at Bissett is ~14‰. Thus, the continuum of isotopic compositions seen at the Bissett Creek deposit could have been developed as a result of three factors. The variations of the isotopic signature of the carbon at the Bissett Creek flake graphite deposit could be in response to (1) metamorphism, (2) exchange with isotopically heavier minerals (i.e. carbonates), (3) isotope fractionation during graphite deposition.

Hoefs and Frey (1976) and Wada *et al.* (1994) demonstrated that high-grade metamorphism can cause a shift in the isotopic signature of carbon in graphite, causing the isotopic composition to become heavier as the metamorphic grade increases, mostly with respect

to temperature. [Barker and Friedman \(1969\)](#) and [Wada et al., \(1994\)](#) quantified the shift in the $\delta^{13}\text{C}$ signature as ~5‰ isotopically heavier as the metamorphic grade increased from amphibolite to granulite facies. The reason for this shift is thought to originate through the release of isotopically light methane in response to metamorphism ([Morikiyo, 1986](#); [Luque et al., 2012](#)). Even considering this shift to heavier values, the measured $\delta^{13}\text{C}$ values at Bissett Creek are still within the range of biogenic carbon.

Another mechanism that can shift the $\delta^{13}\text{C}$ signature of graphite from that of the original carbon source is isotope exchange between graphite and carbonates during metamorphism ([Hahn-Weinheimer and Hirner, 1981](#); [Dunn and Valley, 1992](#)). [Dunn and Valley \(1992\)](#) demonstrated that the fractionation between graphite and carbonates, specifically calcite, is strongly temperature dependent, so much so that it may be used as a thermometer. Using the model of [Dunn and Valley \(1992\)](#), peak metamorphic temperatures of ~750–800°C at Bissett Creek (Chapter 7.0) could fractionate carbon isotopes by 2 to 3‰. However, calcite-graphite isotope exchange is more efficient at lower temperatures, such as during slow cooling during retrograde metamorphism. This cooling could facilitate further exchange and cause larger ranges of carbon isotope composition in the calcite and graphite ([Dunn and Valley, 1992](#)). The clinopyroxene-amphibole-biotite-graphite gneisses may have formed from the decarbonation of carbonate minerals because clinopyroxene (e.g. diopside) and amphibole (e.g. tremolite) are minerals that are commonly found in high-temperature calc-silicate rocks ([e.g. Valley and Essene, 1980](#)). Carbonate and calc-silicate rocks are also found in the neighbouring Composite Arc Belt and the Frontenac Adirondack Terrane ([Hanmer et al., 1985](#); [Valley and Essene, 1980](#)).

Minor calcite has been found in association with the clinopyroxene-amphibole-biotite-graphite gneiss (Fig 3.3D) and the garnet-amphibole-biotite-graphite gneiss. Isotopic exchange between isotopically light graphite and carbonate minerals could have shifted the carbon isotope signature, causing the values in the graphite to become isotopically heavier. Decarbonation reactions during metamorphism could have generated carbon-bearing fluid species which could have interacted with graphite during formation, accounting for some of the spread in the carbon isotope values at Bissett Creek.

Mesoproterozoic black shales have carbon and sulfur isotope ranges signatures that partially overlap with those of Bissett Creek and the surrounding region, as the carbon isotopes

range in composition from -35.6 ‰ to -29.0 ‰ (Fig. 5.2), and the sulfur isotopes range in composition from -23.4 ‰ to 24.7 ‰ (Fig. 5.5) (Ho *et al.*, 1990; Imbus *et al.*, 1992; Johnston *et al.*, 2008; Blumenburg *et al.*, 2012). In general, carbon isotope values from Bissett Creek are isotopically heavier than those from Mesoproterozoic black shales. This could indicate modification during metamorphism (up to 5 ‰ shift heavier), exchange with isotopically heavy carbonate minerals (2 to 3 ‰ shift heavier) or may suggest that the precursor shales to the paragneisses were isotopically heavier than the others. The available Mesoproterozoic black shale sulfur isotope compositions share signatures similar to Bissett Creek. With the transitions in isotope composition that can take place in response to metamorphism and exchange with carbonates, Mesoproterozoic black shales represent a plausible source rock for the formation of the Bissett Creek flake graphite deposit.

Finally, many graphite deposits of hydrothermal origins have $\delta^{13}\text{C}$ signatures that range from -33.7 ‰ to -1.6 ‰ because of fluid–rock interactions and carbon isotope fractionation during graphite formation (Luque *et al.*, 2012). Single or multi-component Rayleigh fractionation between CO_2 and CH_4 fluid from a single homogenous isotopic source (e.g. -26.2‰ in Chapter 6) can produce a spread of values from -33‰ to -10‰ (Chapter 6.0). However, to explain this range in the multi-component system, a starting fluid composition of dominantly CH_4 (not CO_2) must be present. Considering that CH_4 is a very minor fraction of carbonic fluids at the high pressures and temperatures (e.g. Chu and Ague, 2013), it is unlikely that a multi-component system was responsible for fractionation. The single component (i.e. CO_2 is the only carbonic fluid) fractionation model (Fig. 6.3A) corresponds well with the distribution of carbon isotopes in the Bissett Creek flake graphite deposit and is supported by the relationship between carbon content and isotopic signature (Fig 5.4). Although carbonate–fluid interaction and metamorphic fractionation could have had a minor impact on the C isotope ratios of graphite at Bissett Creek, the dominant cause of the large spread of values is expected to result from single-component fractionation of a carbonic fluid mobilized during metamorphism. However, a contribution from carbonic fluids derived from carbonates cannot be ruled out and may have attributed to some of the spread in values seen at Bissett Creek.

9.6 Mineralization Process

A hybrid metamorphic–hydrothermal genetic model for flake graphite at Bissett Creek is most consistent with the observed textures and measured carbon isotope signatures (Fig. 9.3). Hydrothermal fluids were likely generated *in situ* in response to metamorphism from dehydration reactions, decarbonation reactions, and partial melting. The development of fluids *in situ* is likely because of the sharp boundary between the mineralized graphitic gneisses (Fig 3.12) and the unmineralized barren gneisses. In other deposits, such as in the Tasiilaq area of Greenland, where hydrothermal fluids are interpreted to be externally derived, mineralization cross-cuts all units regardless of protolith (Rosing-Schow *et al.*, 2016). Organic material represents the main source of carbon at Bissett Creek and was likely from bacteria based organic matter deposited into a sedimentary sequence containing psammitic and pelagic rocks, with some calcareous layers (represented now by the calc-silicate unit), consistent with either a shallow marine or closed basin (Volkert *et al.*, 2000; Brumsack, 2006). The deposition of organic carbon in conjunction with sedimentation processes is supported by the positive correlations between graphitic carbon and other redox-sensitive metals such as V, Mo, and U as seen in black shales, the ACF classification of graphitic gneisses, the sulfur isotope values, and the carbon isotope values (Nielsen, 1979; Brumsack, 1986; Schidlowski, 1988; Schidlowski, 2001; Vernon and Clarke, 2008;).

Burial of organic-rich sediments can prompt the formation of kerogen and could have been associated with the generation (and possibly extraction) of hydrocarbons (Vandenbroucke and Largeau, 2007). Carbon-rich residues of complex organic compounds can become gradually dehydrated during diagenesis and metamorphism (e.g. Buseck and Beyssac, 2014), typically in response to basin formation followed by metamorphism associated with the Grenvillian Orogen (Ketchum and Davidson, 2000; Rivers *et al.*, 2012). At Bissett Creek, such prograde metamorphism could have caused the formation of graphitic carbon, and later graphite. Primary formation of graphite through the graphitization process at Bissett Creek is supported by the disseminated nature of the graphite mineralization, the interleaving and intergrowth of graphite with metamorphic minerals, and the fact that flake graphite is the sole crystal habit in most units.

At Bissett Creek, continuing increases in temperature could have caused partial melting prompting remobilization of graphite by H₂O-rich melt associated with partial melting given the reaction: 2C solid + 2H₂O fluid → CO₂ fluid + CH₄ fluid ([Chu and Ague, 2013](#)). Graphite remobilization seems limited to the garnet-sillimanite-graphite gneiss unit. While the range of carbon and sulfur isotopes overlap with other units at Bissett Creek, the signatures from the garnet-sillimanite-biotite-graphite gneiss are consistently on the isotopically heavy side of the ranges. Graphite deposition along grain boundaries could have occurred during cooling and/or decompression (Chapter 1.2 – Fig. 1.3). Partial melting of these rocks is supported by the results of thermobarometry in this study (~620°C to 790 °C and 0.9 GPa to 1.5 GPa), supporting thermobarometry from studies in the surrounding areas of the Grenville ([e.g. Anovitz and Essene, 1999; Timmerman et al., 2002; Kendrick and Jamieson, 2016](#)), and field partial melting indicators (Fig 3.13). Evidence of remobilization of the graphite includes small graphite veinlets seen in Fig 3.4 (D, F) and the agreement between carbon isotope values at Bissett Creek and a single component isotope fractionation model (Chapter 6.2).

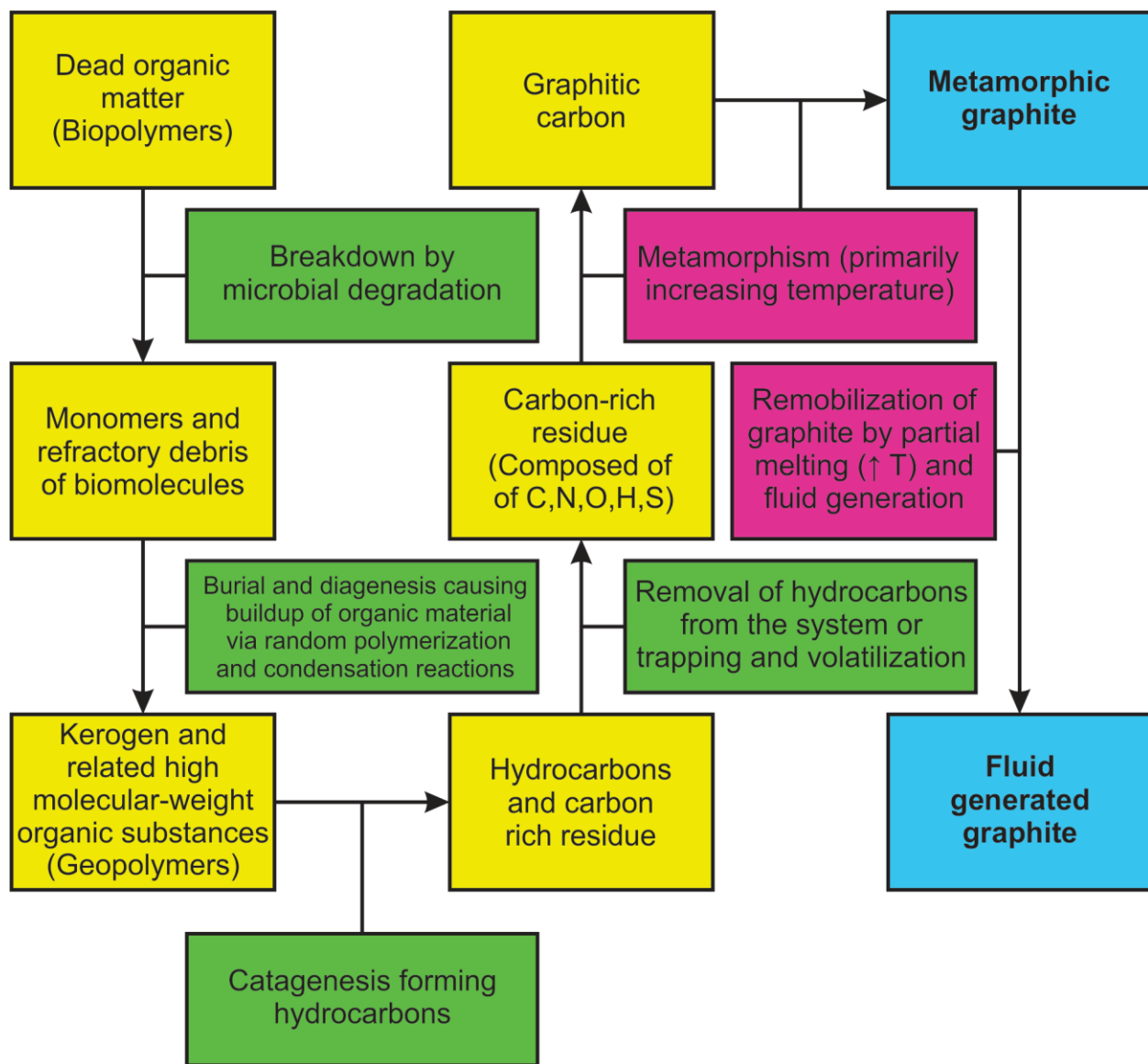


Fig. 9.3. Proposed process of graphite formation for the Bissett Creek flake graphite deposit.

10.0 Conclusions

The conclusions of this study are:

1. The graphitic gneisses were derived from an organic-rich sedimentary protolith as shown by the organic source for the carbon, the metamorphic mineral assemblages consistent with pelitic and semi-pelitic rocks, major and trace element geochemistry of the graphitic gneisses, the geochemical similarities with black shales, the gradational contacts between the graphitic gneisses, and the disseminated style of graphite mineralization.
2. The barren gneisses were likely igneous in origin as shown by the sharp boundary with the graphitic gneisses which suggests an intrusive relationship, a consistent composition for the barren gneisses, the lack of graphite mineralization, and the fact that granitic plutons make up a volumetrically significant proportion of the pre-Grenvillian Laurentian Margin. However, the formation of these gneisses from a relatively immature sediment cannot be ruled out on the basis of the aforementioned evidence.
3. The source of carbon that formed the flake graphite at the Bissett Creek deposit is most likely biogenic material that was deposited during sedimentation. A biogenic source for the carbon is supported by the carbon isotopes ranging from -28.3 ‰ to -14.0 ‰, the relationship between graphitic carbon and trace elements suggesting formation from primary deposition, the sulfur isotopes being consistent with Mesoproterozoic black shales, and the disseminated nature of the graphite mineralization. However, a minor contribution from the breakdown of carbonate minerals in response to metamorphism could have also been a factor. This may explain why carbon isotope values from Bissett Creek are isotopically heavier than those reported from Mesoproterozoic black shales.
4. Graphite mineralization at the Bissett Creek deposit is stratabound and pervasively folded. Minor graphite enrichment around fault structures has been noted in core logs. However, there does not appear to be any correlation between graphite concentration and fold structures. The barren gneisses may have acted as an impermeable barrier to metamorphically derived fluids as shown by the stratabound nature of the mineralization.
5. Primary flake graphite mineralization was contemporaneous with prograde metamorphism at temperatures and pressures consistent with amphibolite to granulite facies (620 to 790°C at 0.9 to 1.5 GPa). Secondary remobilization of graphite along grain boundaries in one lithology could have been associated with high-temperature

metamorphism and partial melting. Secondary remobilization of some of the graphite materials is supported by the presence of small graphite veinlets within the garnet-sillimanite-biotite-graphite gneiss. The occurrence of partial melting at the Bissett Creek deposit is supported by the results of the thermobarometry, potential field partial melting indicators and the notation of partial melting in other parts of the pre-Grenvillian Laurentian Margin surrounding the Bissett Creek deposit.

6. The Bissett Creek deposit formed under amphibolite to granulite-facies $P-T$ conditions associated with the Grenville Orogen. This is supported by the consistent regional fabric as defined by the foliations documented petrographically and measured structurally at the Bissett Creek property and across the region, as well as the consistency between the P-T conditions experienced at Bissett Creek and the surrounding region.
7. Primary flake graphite mineralization at the Bissett Creek deposit formed because of *in situ* metamorphic processes that included graphitization of organic material and deposition from metamorphic fluids. This model of mineralization is supported by the disseminated nature of the graphite, the orientation of the graphite with the dominant tectonic fabric, the predominantly flake crystalline habit of the graphite, the intergrowth with metamorphic minerals, the stratabound nature of the deposit, the likely sedimentary origin of the protoliths that host graphite mineralization, the biogenic source for the carbon that formed the deposit, the consistency of the carbon isotope signature with a single-component carbon isotope fractionation modelling for the deposit, and the $P-T$ conditions of deposit formation.
8. This model of mineralization is consistent with other flake graphite deposits within the pre-Grenvillian Laurentian margin including the occurrences in Butt Township and Ryerson Townships. Internationally, the Bissett Creek deposit is very similar to the Liu Mao and Xinghe flake graphite deposits in Northern China.

11.0 Recommendations for Future Study

Based on the conclusions in Chapter 10.0, the following are recommendations for further study:

- *In situ* analysis of the $\delta^{13}\text{C}$ values for individual graphite grains to determine if the isotopic signature is relatively homogeneous across the graphite grains (metamorphic), or if there is a large change (fluid derived or fluid overprint).
- *In situ* analysis of the $\delta^{13}\text{C}$ values for graphite grains in contact with carbonates to quantify the extent of isotopic exchange between the two. This could then be used as an independent geothermometer ([Dunn and Valley, 1992](#)).
- X-ray Diffraction or Raman Spectroscopy of the graphite to determine crystallinity (how well ordered the graphite is), which will further evaluate if graphite is metamorphic or hydrothermal in origin ([i.e. Buseck and Beyssac, 2014](#)). Metamorphic graphite has a range of potential crystallinity values and increases with metamorphic grade, while fluid deposited graphite shows universally high crystallinity values (Luque *et al.*, 2012 and references therein). Raman spectroscopy of graphitic carbon may also be used as a geothermometer ([Beyssac *et al.*, 2002](#)). Although this method is ineffective at temperatures $>650^\circ\text{C}$, it could be used to confirm the high-temperature formation of metamorphic graphite and better constrain the formation of graphite along grain boundaries.
- Further fieldwork in the region surrounding the Bissett Creek deposit to find less ambiguous field evidence of the protoliths of the gneisses. Future researchers should look for any gneisses, or other rocks, with lower amounts of deformation and recrystallization that may have preserved some of the primary textures related to their formation.
- Generation of $P-T$ pseudosections to better constrain pressure and temperature conditions at the Bissett Creek flake graphite deposit.
- U–Pb geochronology to constrain the timing of metamorphism within the context of the Ottawan and Rigolet phases of metamorphism of the Grenville Orogeny.

12.0 Recommendations for Graphite Exploration and Mining

Based upon the results of this thesis, the following are some recommendations for future flake graphite deposit exploration in the Grenville Province:

- From a large-scale perspective, these types of deposits are limited to stratabound metasedimentary sequences in high grade (amphibolite to granulite) grade metamorphic terranes.
- Airborne electromagnetic surveys are a good way to delineate additional targets within a specified area, as the high conductivity of the graphite produces easily detectable responses and targets for further examination.
- Zones of intense weathering (dark brown to orange colour) and association with sulfides (predominantly pyrrhotite and pyrite) are common in areas with graphite mineralization. These zones may have turned to a rusty orange sand depending on the extent of the weathering. Rusty soil and graphite flakes could also be transported via glaciation and compose part of the overburden material forming a footprint for the flake graphite deposit.
- Graphitic gneiss exposures commonly show a decrease in vegetation cover when compared to their barren gneiss counterparts. Graphitic gneisses outcrops will also more commonly have coniferous trees growing over them than deciduous. This could be attributed to soil acidity as a result of the break down of pyrite and pyrrhotite.
- Deposits of this type tend to be elongate along strike, with variable widths and can be elongate in the down-dip direction ([Garland, 1987](#)).
- The carbon associated with the graphite in these deposits appears to be biologically derived, and therefore association with carbonates as seen in other terranes (e.g. the Composite Arc Belt) is not required.

References

- Anders, E., and Grevesse, N. 1989. Abundances of the elements: Meteoritic and solar. *Geochimica et Cosmochimica Acta* **53**(1): 197-214. doi: [https://doi.org/10.1016/0016-7037\(89\)90286-X](https://doi.org/10.1016/0016-7037(89)90286-X).
- Anovitz, L.M., and Essene, E.J. 1990. Thermobarometry and Pressure-Temperature Paths in the Grenville Province of Ontario. *Journal of Petrology* **31**(1): 197-241. doi: <https://doi.org/10.1093/petrology/31.1.197>.
- Barker, F., and Friedman, I. 1969. Carbon Isotopes in Pelites of the Precambrian Uncompahgre Formation, Needle Mountains, Colorado. *GSA Bulletin* **80**(7): 1403-1408. doi: [https://doi.org/10.1130/0016-7606\(1969\)80\[1403:CIIPOT\]2.0.CO;2](https://doi.org/10.1130/0016-7606(1969)80[1403:CIIPOT]2.0.CO;2).
- Barrenechea, J.F., Luque, J., Rodas, M., and Pasteris, J.D. 1997. Vein-type graphite mineralization in the Jurassic volcanic rocks of the external zone of the Betic Cordillera, Southern Spain. *The Canadian Mineralogist* **35**(6): 1379-1390.
- Beauchamp, M. 2017. Questions regarding microprobe work. *Received by C. Drever*.
- Berner, R.A. 1984. Sedimentary pyrite formation: An update. *Geochimica et Cosmochimica Acta* **48**(4): 605-615. doi: [https://doi.org/10.1016/0016-7037\(84\)90089-9](https://doi.org/10.1016/0016-7037(84)90089-9).
- Beyssac, O., Goffe, B., Chopin, C., and Rouzaud, J.N. 2002. Raman spectra of carbonaceous material in metasediments: a new geothermometer. *Journal of Metamorphic Geology* **20**(9): 859-871. doi: <https://doi.org/10.1046/j.1525-1314.2002.00408.x>.
- Beyssac, O., and Rumble, D. 2014. Graphitic carbon; A ubiquitous, diverse and useful geomaterial. *Elements* **10**: 415-420.
- Binu-Lal, S.S., Kehelpannala, K.V.W., Kumar, M.S., and Wada, H. 2003. Multistage graphite precipitation through protracted fluid flow in sheared metagranitoid, Digana, Sri Lanka: evidence from stable isotopes. *Chemical Geology* **197**(1-4): 253-270. doi: [https://doi.org/10.1016/S0009-2541\(02\)00400-X](https://doi.org/10.1016/S0009-2541(02)00400-X).
- Broecker, W.S., and Oversby, V.M. 1971. Chemical equilibria in the earth. McGraw-Hill, New York.
- Brumsack, H.J. 1986. The inorganic geochemistry of Cretaceous black shales (DSDP Leg 41) in comparison to modern upwelling sediments from the Gulf of California. In *North Atlantic Palaeoceanography*. Edited by C.P. Summerhayes and N.J. Shackleton. Geological Society, London. pp. 447-462.

- Brumsack, H.J. 2006. The trace metal content of recent organic carbon-rich sediments: Implications for Cretaceous black shale formation. *Palaeogeography, Palaeoclimatology, Palaeoecology* **232**(2-4): 344-361. doi: <https://doi.org/10.1016/j.palaeo.2005.05.011>.
- Buseck, P.R., and Beyssac, O. 2014. From organic matter to graphite: Graphitization. *Elements* **10**(6): 421-426. doi: <https://doi.org/10.2113/gselements.10.6.421>.
- Canfield, D.E. 1998. A new model for Proterozoic ocean chemistry. *Nature* **396**: 450-453. doi: <https://doi.org/10.1038/24839>.
- Carr, S.D., Easton, R.M., Jamieson, R.A., and Culshaw, N.G. 2000. Geologic transect across the Grenville orogen of Ontario and New York. *Canadian Journal of Earth Sciences* **37**: 193-216.
- Blumenberg, M., Thiel, V., Riegel, W., Kah, L.C., and Reitner, J. 2012. Biomarkers of black shales formed by microbial mats, Late Mesoproterozoic (1.1 Ga) Taoudeni Basin, Mauritania. *Precambrian Research* **196-197**: 113-127. doi: <https://doi.org/10.1016/j.precamres.2011.11.010>.
- Chu, X., and Ague, J.J. 2013. Phase equilibria for graphitic metapelite including solution of CO₂ in melt and cordierite: implications for dehydration, partial melting and graphite precipitation. *Journal of Metamorphic Geology* **31**(8): 843-862. doi: <https://doi.org/10.1111/jmg.12047>.
- Condie, K.C. 1993. Chemical composition and evolution of the upper continental crust: Contrasting results from surface samples and shales. *Chemical Geology* **104**(1-4): 1-37. doi: [https://doi.org/10.1016/0009-2541\(93\)90140-E](https://doi.org/10.1016/0009-2541(93)90140-E).
- Connolly, J.A.D., and Cesare, B. 1993. C-O-H-S fluid composition and oxygen fugacity in graphitic metapelites. *Journal of Metamorphic Geology* **11**(3): 379-388. doi: <https://doi.org/10.1111/j.1525-1314.1993.tb00155.x>.
- Constable, D.W., and Dunks, L.T. 1986. Feasibility report for Cal Graphite Corporation Butt Township Graphite Property.
- Cook, N.J., and Hoefs, J. 1997. Sulphur isotope characteristics of metamorphosed Cu-(Zn) volcanogenic massive sulphide deposits in the Norwegian Caledonides. *Chemical Geology* **135**(3-4): 307-324. doi: [https://doi.org/10.1016/S0009-2541\(96\)00119-2](https://doi.org/10.1016/S0009-2541(96)00119-2).
- Coplen, T.B. 1994. Reporting on stable hydrogen, carbon and oxygen isotopic abundances. *Pure and Applied Chemistry* **66**(2): 273-276.

- Culshaw, N.G., Davidson, A., and Nadeau, L. 1983. Structural subdivisions of the Grenville province in the Parry Sound-Algonquin Geological Survey of Canada. Current Research Part A. Report 83-1B. pp. 243-252.
- Currie, L.A. 1968. Limits for qualitative detection and quantitative detection: Application to radiochemistry. Analytical Chemistry **40**(3): 586-593. doi: <https://doi.org/10.1021/ac60259a007>.
- Davidson, A. 1982. Graphite occurrences in the Algonquin Region, Grenville Province, Ontario. Geological Survey of Canada Open File Report 870.
- Davidson, A. 1984. Tectonic boundaries within the Grenville Province of the Canadian Shield. Journal of Geodynamics **1**(3-5): 433-444. doi: [https://doi.org/10.1016/0264-3707\(84\)90018-8](https://doi.org/10.1016/0264-3707(84)90018-8).
- Davidson, A., and Grant, S.M. 1986. Reconnaissance geology of western and central Algonguin Park and detailed study of coronitic olivine metagabbro, Central Gneiss Belt, Grenville Province of Ontario. Geological Survey of Canada. Current Research Part B. Report 86-1B. pp. 837-848.
- Davidson, A., and Morgan, W.C. 1981. Preliminary notes on the geology east of Georgian Bay, Grenville Structural Province, Ontario. Geological Survey of Canada. Current Research Part A. Report 81-1A. pp. 291-298.
- Davidson, A., Culshaw, N.G., and Nadeau, L. 1983. A tectono-metamorphic framework for part of the Grenville Province, Ontario. Geological Survey of Canada. Current Research Part A. Report 82-1A. pp. 175-190.
- Davidson, A., Nadeau, L., Grant, S.M., and Pryer, L.L. 1985. Studies in the Grenville Province of Ontario. Geological Survey of Canada. Current Research Part A. Report 85-1A. pp. 463-483.
- Deines, P. 1980. The isotopic composition of reduced organic carbon. In *Handbook of environmental isotope geochemistry*. Edited by P. Fritz and J.C. Fontes. Elsevier Scientific Publishing Company, New York. pp. 329-406.
- Deines, P. 1992. Mantle Carbon: Concentration, Mode of Occurrence, and Isotopic Composition. In *Early Organic Evolution*. Edited by M. Schidlowski and S. Golubic and M.M. Kimberley and D.M. McKirdy and P.A. Trudinger. Springer- Verlag Berlin Heidelberg. pp. 133-146.

- Deines, P., Harris, J.W., Robinson, D.N., Gurney, J.J., and Shee, S.R. 1991. Carbon and oxygen isotope variations in diamond and graphite eclogites from Orapa, Botswana, and the nitrogen content of their diamonds. *Geochimica et Cosmochimica Acta* **55**(2): 515-524. doi: [https://doi.org/10.1016/0016-7037\(91\)90009-T](https://doi.org/10.1016/0016-7037(91)90009-T).
- Dempster, T.J. 1985. Garnet zoning and metamorphism of the Barrovian Type Area, Scotland. *Contributions to Mineralogy and Petrology* **89**(1): 30-38. doi: <https://doi.org/10.1007/BF01177588>.
- Doroshkevich, A.G., Wall, F., and Ripp, G.S. 2007. Magmatic graphite in dolomite carbonatite at Pogranichnoe, North Transbaikalia, Russia. *Contributions to Mineralogy and Petrology* **153**(3): 339353. doi: <https://doi.org/10.1007/s00410-006-0150-z>.
- Duke, E.F., and Rumble, D. 1986. Textural and isotopic variations in graphite from plutonic rocks, South-Central New Hampshire. *Contributions to Mineralogy and Petrology* **93**(4): 409-419. doi: <https://doi.org/10.1007/BF00371711>.
- Dunn, S.R., and Valley, J.W. 1992. Calcite-graphite isotope thermometry: a test for polymetamorphism in marble, Tudor gabbro aureole, Ontario, Canada. *Journal of Metamorphic Geology* **10**(4): 487-501. doi: <https://doi.org/10.1111/j.1525-1314.1992.tb00100.x>.
- European Commission, Deloitte Sustainability, British Geological Survey, Bureau de Recherches Géologiques et Minières, and Netherlands Organization for Applied Scientific Research. 2017. Study on the review of the list of Critical Raw Materials.
- Fauvet, P. 2000. Mozambique: growth with poverty. *Africa Recovery*(October): 12-19.
- Ferry, J.M., and Baumgartner, L. 1987. Thermodynamic models of molecular fluids at the elevated pressures and temperatures of crustal metamorphism. *Reviews in Mineralogy and Geochemistry* **17**(1): 323-365.
- Fitzsimons, I.C.W., and Harley, S.L. 1994. The Influence of Retrograde Cation Exchange on Granulite P-T Estimates and a Convergence Technique for the Recovery of Peak Metamorphic Conditions. *Journal of Petrology* **35**(2): 543-576. doi: <https://doi.org/10.1093/petrology/35.2.543>.
- Garland, M.I. 1987. Graphite in the Central Gneiss Belt of the Grenville Province of Ontario. Open File Report 5649.

- Garland, M.I. 1991. The geology of the Cal Graphite flake graphite deposit. Ministry of Northern Development and Mines. Open File Report 5816.
- Gignac, L., Marchand, R., Menard, R., Phillips, A., Aiken, S., Bouajila, A., Menard, N., Houde, D., Thibert, F., Rousseau, G., and Champagne, A. 2012. Feasibility study: Bissett Creek graphite project Ontario, Canada. G Mining Services Inc.
- Gonfiantini, R. 1984. I.A.E.A. advisory group meeting on stable isotope reference samples for geochemical and hydrological investigations. *Isotope Geoscience* **2**: 85.
- Graedel, T.E., Gunn, G., and Espinoza, L.T. 2014. Metal resources, use and criticality. In Critical metals handbook. John Wiley and Sons, Ltd.. pp. 1-19.
- Graham, C.M., and Powell, R. 1984. A garnet-hornblende geothermometer : calibration, testing, and application to the Pelona Schist, Southern California. *Journal of Metamorphic Geology* **2**(1): 13-31. doi: <https://doi.org/10.1111/j.1525-1314.1984.tb00282.x>.
- Green, J. 2013. Kearney mine gets the go-ahead to reopen. In Toronto Star. Toronto Star Newspapers Limited, Toronto, ON. Available from https://www.thestar.com/business/economy/2013/05/13/kearney_mine_gets_the_goahead_to_reopen.html
- Greenwood, N., and Earnshaw, A. 1998. Silicon. In Chemistry of Elements. Elsevier Butterworth-Heinemann, Oxford. pp. 328-366.
- Hanmer, S., Thivierge, R.H., and Henderson, J.R. 1985. Anatomy of a ductile thrust zone: part of the northwest boundary of the Central Metasedimentary Belt, Grenville Province, Ontario.
- Han-Weinheimer, P., and Hirner, A. 1981. Isotopic evidence for the origin of graphite. *Geochemical Journal* **15**: 9-15. doi: <https://doi.org/10.2343/geochemj.15.9>.
- Hewitt, D.F. 1965. Graphite in Ontario. Ontario Department of Mines, Industrial Mineral Report No. 20. pp. 1-66.
- Hoefs, J., and Frey, M. 1976. The isotopic composition of carbonaceous matter in a metamorphic profile from the Swiss Alps. *Geochimica et Cosmochimica Acta* **40**(8): 945-951. doi: [https://doi.org/10.1016/0016-7037\(76\)90143-5](https://doi.org/10.1016/0016-7037(76)90143-5).
- Holdaway, M.J. 2000. Application of new experimental and garnet Margules data to the garnet-biotite geothermometer. *American Mineralogist* **85**(7-8): 881-892. doi: <https://doi.org/10.2138/am-2000-0701>.
- Holland, T.J.B. 2014. AX2.

- Holland, T.J.B., and Powell, R. 1998. An internally consistent thermodynamic data set for phases of petrological interest. *Journal of Metamorphic Geology* **16**(3): 309-343. doi: <https://doi.org/10.1111/j.1525-1314.1998.00140.x>.
- Holloway, J.R. 1984. Graphite-CH₄-H₂O-CO₂ equilibria at low-grade metamorphic conditions. *Geology* **12**(8): 455-458. doi: [https://doi.org/10.1130/0091-7613\(1984\)12<455:GEALMC>2.0.CO;2](https://doi.org/10.1130/0091-7613(1984)12<455:GEALMC>2.0.CO;2).
- Ho, E.S., Meyers, P.A., and Mauk, J.L. 1990. Organic geochemical study of mineralization in the Keweenawan Nonesuch Formation at White Pine, Michigan. *Advances in Organic Chemistry* **16**(1-3): 229-234. doi: [https://doi.org/10.1016/0146-6380\(90\)90043-Y](https://doi.org/10.1016/0146-6380(90)90043-Y).
- Horita, J. 2001. Carbon isotope exchange in the system CO₂-CH₄ at elevated temperatures. *Geochimica et Cosmochimica Acta* **65**(12): 1907-1919.
- Horita, J. 2005. Some perspectives on isotope biosignatures for early life. *Chemical Geology* **218**(1-2): 171-186. doi: <https://doi.org/10.1016/j.chemgeo.2005.01.017>.
- Huff, T.A., and Nabelek, P.I. 2007. Production of carbonic fluids during metamorphism of graphitic pelites in a collisional orogen—An assessment from fluid inclusions. *Geochimica et Cosmochimica Acta* **71**(20): 4997-5015. doi: <https://doi.org/10.1016/j.gca.2007.08.001>.
- Humphries, M. 2013. Rare earth elements: The global supply chain. Congressional research report.
- Imbus, S.W., Macko, S.A., Elmore, R.D., and Engel, M.H. 1992. Stable isotope (C, S, N) and molecular studies on the Precambrian Nonesuch Shale (Wisconsin-Michigan, U.S.A.): Evidence for differential preservation rates, depositional environment and hydrothermal influence *Chemical Geology* **101**(3-4): 255-281. doi: [https://doi.org/10.1016/0009-2541\(92\)90007-R](https://doi.org/10.1016/0009-2541(92)90007-R).
- Indares, A., and Dunning, G. 1997. Coronitic metagabbro and eclogite from the Grenville Province of western Quebec: interpretation of U - Pb geochronology and metamorphism. *Canadian Journal of Earth Sciences* **34**(7): 891-901. doi: <https://doi.org/10.1139/e17-074>.
- Jaszczak, J.A., Robinson, G.W., Dimovski, S., and Gogotsi, Y. 2003. Naturally occurring graphite cones. *Carbon* **41**(11): 2085-2092. doi: [https://doi.org/10.1016/S0008-6223\(03\)00214-8](https://doi.org/10.1016/S0008-6223(03)00214-8).

- Javoy, M., Pineau, F., and Delorme, H. 1986. Carbon and nitrogen isotopes in the mantle. *Chemical Geology* **57**(1-2): 41-62. doi: [https://doi.org/10.1016/0009-2541\(86\)90093-8](https://doi.org/10.1016/0009-2541(86)90093-8).
- Jebrak, M., and Marcoux, E. 2014. Geology of mineral resources. Geological Association of Canada.
- Johnston, D.T., Farquhar, J., Summons, R.E., Shen, Y., Kaufman, A.J., Masterson, A.J., and Canfield, D.E. 2008. Sulfur isotope biogeochemistry of the Proterozoic McArthur Basin. *Geochimica et Cosmochimica Acta* **72**(17): 4278-4290. doi: <https://doi.org/10.1016/j.gca.2008.06.004>.
- Kelly, T.D., Matos, G.R., and Olson, D.W. 2005. Natural graphite: Historical statistics for mineral and material commodities in the United States. U.S. Geological Survey, Online.
- Kendrick, J.L., and Jamieson, R.A. 2016. The fate of olivine in the lower crust: Pseudomorphs after olivine in coronitic metagabbro from the Grenville Orogen, Ontario. *Lithos* **260**: 356-370. doi: <http://dx.doi.org/10.1016/j.lithos.2016.06.002>.
- Ketchum, J.W.F., and Davidson, A. 2000. Crustal architecture and tectonic assembly of the Central Gneiss Belt, southwestern Grenville Province, Canada: a new interpretation. *Canadian Journal of Earth Sciences* **37**(2-3): 217-2314. doi: <https://doi.org/10.1139/e98-099>.
- Kohn, M.J., and Spear, F. 2000. Retrograde net transfer reaction insurance for pressure-temperature estimates. *Geology* **28**(12): 1127-1130. doi: [https://doi.org/10.1130/0091-7613\(2000\)28<1127:RNTRIF>2.0.CO;2](https://doi.org/10.1130/0091-7613(2000)28<1127:RNTRIF>2.0.CO;2).
- Krauss, U.H., Schmidt, H.W., Jr., H.A.T., and Sutphin, D.M. 1988. International strategic minerals inventory summary report - natural graphite, U.S. Geological Survey circular 930-H.
- Krouse, H.R., and Coplen, T.B. 1997. Reporting of relative sulfur isotope-ratio data. *Pure and Applied Chemistry* **69**(2): 293-295.
- Leake, B.E., Woolley, A.R., Arps, C.E.S., Birch, W.D., Gilbert, M.C., Grice, J.D., Hawthorne, F.C., Kato, A., Kisich, H.J., Krivovichev, V.G., Linthout, K., Laird, J., Mandarino, J.A., Maresch, W.V., Nickel, E.H., Rock, N.M.S., Schumacher, J.C., Smith, D.C., Stephenson, N.C.N., Ungaretti, L., Whittaker, E.J.W., and Youzhi, G. 1997. Nomenclature of amphiboles: Report of the subcommittee on amphiboles of the International Mineralogical Association commission on new minerals and mineral names. *Canadian Mineralogist* **35**(1): 219-246.

- Leduc, E. 2017. Sample submission questions. *Received by C. Drever*.
- Leduc, E. 2018. Sample submission questions. *Received by C. Drever*.
- Li, Z.X., Bogdanova, S.V., Collins, A.S., Davidson, A., Waele, B.D., Ernst, R.E., Fitzsimons, I.C.W., Fuck, R.A., Gladkochub, D.P., Jacobs, J., Karlstrom, K.E., Lu, S., Natapov, L.M., Pease, V., Pisarevsky, S.A., Thane, K., and Vernikovsky, V. 2008. Assembly, configuration, and break-up history of Rodinia: A synthesis. *Precambrian Research* **160**(1-2): 179-210. doi: <https://doi.org/10.1016/j.precamres.2007.04.021>.
- Luque, F.J., Crespo-Feo, E., Barrenchea, J.F., and Ortega, L. 2012. Carbon isotopes of graphite: Implications on fluid history. *Geoscience Frontiers* **3**(2): 197-207. doi: <https://doi.org/10.1016/j.gsf.2011.11.006>.
- Luque, F.J., Pasteris, J.D., Wopenka, B., Rodas, M., and Barrenchea, J.F. 1998. Natural fluid-deposited graphite; mineralogical characteristics and mechanisms of formation. *American Journal of Science* **298**(6): 471-498. doi: <https://doi.org/10.2475/ajs.298.6.471>.
- Mackinnon, A., and LeBaron, P.S. 1990. Major graphite occurrences within the Frontenac Axis, southeastern Ontario. Open File Report 5729.
- Macnamara, J., and Thode, H.G. 1950. Comparison of the isotopic constitution of terrestrial and meteoritic sulfur. *Physical Review* **78**(3). doi: <https://doi.org/10.1103/PhysRev.78.307>.
- McCarley, R. 2016. Processing of graphite ore materials for geochemistry. *Received by C. Drever*. p. 4.
- McLlland, J., Daly, J.S., and McLlland, J.M. 1996. The Grenville Orogenic Cycle (ca. 1350-1000 Ma): an Adirondack perspective. *Tectonophysics* **265**(1-2): 1-28. doi: [https://doi.org/10.1016/S0040-1951\(96\)00144-8](https://doi.org/10.1016/S0040-1951(96)00144-8).
- McLlland, J.M., Selleck, B.W., and Bickford, M.E. 2010. Review of the Proterozoic evolution of the Grenville Province, its Adirondack outlier, and the Mesoproterozoic inliers of the Appalachians. In *From Rodinia to Pangea: the lithotectonic record of the Appalachian Region*. Edited by R.P. Tollo and M.J. Bartholomew and J.P. Hibbard and P.M. Karabinos. Geological Society of America. pp. 1-29.
- Middlemost, E.A.K. 1994. Naming materials in the magma/igneous rock system. *Earth Science Reviews* **37**(3-4): 215-224. doi: [https://doi.org/10.1016/0012-8252\(94\)90029-9](https://doi.org/10.1016/0012-8252(94)90029-9).

- Mining Markets. 2012. Rewriting the book on graphite. *In* Mining Markets. The Northern Miner Group. Available from <http://www.miningmarkets.ca/news/rewriting-the-book-on-graphite/>
- Mitchell, C.J. 1993. Industrial Minerals Laboratory Manual - Flake Graphite. British Geological Survey.
- Moores, S. 2014. Tesla's gigafactory: Needs 6 new graphite mines, but where will cobalt be sourced? Available from <http://www.mining.com/web/tesla-motors-gigafactory-to-revolutionise-critical-mineral-demand/>.
- Morikiyo, T. 1986. Hydrogen and carbon isotope studies on the graphite-bearing metapelites in the northern Kiso district of central Japan. Contributions to Mineralogy and Petrology **94**(2): 165-177. doi: <https://doi.org/10.1007/BF00592933>.
- National Research Council. 2008. Minerals, Critical Minerals, and the U.S. Economy. The National Academies Press, Washington DC. pp. 262.
- Nielsen, H. 1979. Sulfur isotopes. *In* Lectures in Isotope Geology. Edited by E. Jager and J.C. Hunziker. Springer-Verlag Berlin Heidelberg. pp. 283-312.
- Northern Graphite. 2014. Northern Graphite Announces Update of Expansion Case PEA: Project shows robust economics despite low graphite price environment. Northern Graphite, SEDAR. pp. 1-5.
- Ohmoto, H., and Kerrick, D. 1977. Devolatilization equilibria in graphitic systems. American Journal of Science **277**(8): 1013-1044. doi: <https://doi.org/10.2475/ajs.277.8.1013>.
- Ohmoto, H., and Rye, R.O. 1979. Isotopes of sulfur and carbon. *In* Geochemistry of hydrothermal ore deposits. Edited by H.L. Barnes. Wiley, New York. pp. 509-567.
- Ohtomo, Y., Kakegawa, T., Ishida, A., Nagese, T., and Rosing, M.T. 2014. Evidence for biogenic graphite in early Archaean Isua metasedimentary rocks. Nature Geoscience **7**: 25-28. doi: <https://doi.org/10.1038/ngeo2025>.
- Olson, D.W. 2012. Graphite (Natural). *In* Mineral Commodity Summaries 2012. U.S. Geological Survey, U.S. Department of the Interior, Reston, Virginia. pp. 68-69.
- Olson, D.W. 2014. Graphite (Natural). *In* Mineral Commodity Summaries 2014. U.S. Geological Survey, U.S. Department of the Interior, Reston, Virginia. pp. 68-69.
- Olson, D.W. 2016. Graphite (Natural). *In* Mineral Commodity Summaries 2016. U.S. Geological Survey, U.S. Department of the Interior, Reston, Virginia. pp. 74-75.

- Olson, D.W. 2018. Graphite (Natural). In *Mineral Commodity Summaries 2018*. U.S. Geological Survey, U.S. Department of the Interior, Reston, Virginia. pp. 72-73.
- Papineau, D., Gregorio, B.T.D., Cody, G.D., Fries, M.D., Mojzsis, S.J., Steele, A., Stroud, R.M., and Fogel, M.L. 2010. Ancient graphite in the Eoarchean quartz–pyroxene rocks from Akilia in southern West Greenland I: Petrographic and spectroscopic characterization. *Geochimica et Cosmochimica Acta* **74**(20): 5862-5883. doi: <https://doi.org/10.1016/j.gca.2010.05.025>.
- Perry, E.C., and Ahmad, S.N. 1977. Carbon isotope composition of graphite and carbonate minerals from 3.8-AE metamorphosed sediments, Isukasia, Greenland. *Earth and Planetary Science Letters* **36**(2): 280-284. doi: [https://doi.org/10.1016/0012-821X\(77\)90210-2](https://doi.org/10.1016/0012-821X(77)90210-2).
- Powell, R., and Holland, T.J.B. 1988. An internally consistent dataset with uncertainties and correlations: 3. Applications to geobarometry, worked examples and a computer program. *Journal of Metamorphic Geology* **6**(2): 173-204. doi: <https://doi.org/10.1111/j.1525-1314.1988.tb00415.x>.
- Powell, R., and Holland, T.J.B. 1994. Optimal geothermometry and geobarometry. *American Mineralogist* **79**(1): 120-133.
- Powell, R., and Holland, T.J.B. 2008. On thermobarometry. *Journal of Metamorphic Geology* **26**(2): 155-179. doi: <https://doi.org/10.1111/j.1525-1314.2007.00756.x>.
- Ray, J.S. 2009. Carbon isotopic variations in fluid-deposited graphite: evidence for multicomponent Rayleigh isotopic fractionation. *International Geology Review* **51**(1): 45-57. doi: <https://doi.org/10.1080/00206810802625057>.
- Ray, J.S., and Ramesh, R. 2000. Rayleigh fractionation of stable isotopes from a multicomponent source. *Geochimica et Cosmochimica Acta* **64**(2): 299-306. doi: [https://doi.org/10.1016/S0016-7037\(99\)00181-7](https://doi.org/10.1016/S0016-7037(99)00181-7).
- Rayleigh, J.W.S. 1896. Theoretical considerations respecting the separation of gases by diffusion and similar processes. *Philosophical Magazine* **42**: 493-593.
- Rivers, T., Culshaw, N., Hynes, A., Indares, A., Jamieson, R., and Martignole, J. 2012. The Grenville orogen - a post Lithoprobe perspective. In *Tectonic styles in Canada: The Lithoprobe perspective*. Edited by J.A. Percival and F.A. Cook and R.M. Clowes. Geological Association of Canada. pp. 97-236.

- Rivers, T., Martignole, J., Gower, C.F., and Davidson, A. 1989. New tectonic divisions of the Grenville Province, southeast Canadian Shield. *Tectonics* **8**(1): 63-84. doi: <https://doi.org/10.1029/TC008i001p00063>.
- Rosing-Schow, N., Bagas, L., Kolb, J., Balic-Zunic, T., Korte, C., and Fiorentini, M.L. 2016. Hydrothermal flake graphite mineralisation in Paleoproterozoic rocks of south-east Greenland. *Mineralium Deposita* **52**(5): 769-789. doi: <https://doi.org/10.1007/s00126-016-0701-9>.
- Rosseau, G., and Duplessis, C. 2010. Preliminary Assessment on the Bissett Creek Graphite Property of Northern Graphite Corporation. SGS Canada Inc.
- Rumble, D. 2014. Hydrothermal graphitic carbon. *Elements* **10**(6): 427-433. doi: <https://doi.org/10.2113/gselements.10.6.427>.
- Rumble, D., Duke, E.F., and Hoering, T.L. 1986. Hydrothermal graphite in New Hampshire: Evidence of carbon mobility during regional metamorphism. *Geology* **14**(6): 452-455. doi: [https://doi.org/10.1130/0091-7613\(1986\)14<452:GINHE>2.0.CO;2](https://doi.org/10.1130/0091-7613(1986)14<452:GINHE>2.0.CO;2).
- Rumble, D., and Hoering, T.C. 1986. Carbon isotope geochemistry of graphite vein deposits from New Hampshire, U.S.A. *Geochimica et Cosmochimica Acta* **50**(6): 1239-1247. doi: [https://doi.org/10.1016/0016-7037\(86\)90407-2](https://doi.org/10.1016/0016-7037(86)90407-2).
- Sanyal, P., Acharya, B.C., Bhattacharya, S.K., Sarkar, A., Agrawal, S., and Bera, M.K. 2009. Origin of graphite, and temperature of metamorphism in Precambrian Eastern Ghats Mobile Belt, Orissa, India: A carbon isotope approach. *Journal of Asian Earth Sciences* **36**(2-3): 252-260. doi: <https://doi.org/10.1016/j.jseaes.2009.06.008>.
- Satish-Kumar, M., Yurimoto, H., Itoh, S., and Cesare, B. 2011. Carbon isotope anatomy of a single graphite crystal in a metapelitic migmatite revealed by high-spatial resolution SIMS analysis. *Contributions to Mineralogy and Petrology* **162**: 821-834. doi: <https://doi.org/10.1007/s00410-011-0626-3>.
- Scheele, N., and Hoefs, J. 1992. Carbon isotope fractionation between calcite, graphite and CO₂: an experimental study. *Contributions to Mineralogy and Petrology* **112**(1): 35-45. doi: <https://doi.org/10.1007/BF00310954>.
- Schidlowski, M. 1988. A 3,800-million-year isotopic record of life from carbon in sedimentary rocks. *Nature* **333**: 313-318. doi: <https://doi.org/10.1038/333313a0>.

- Schidlowski, M. 2001. Carbon isotopes as biogeochemical recorders of life over 3.8Ga of Earth history: evolution of a concept. *Precambrian Research* **106**(1-2): 117-134. doi: [https://doi.org/10.1016/S0301-9268\(00\)00128-5](https://doi.org/10.1016/S0301-9268(00)00128-5).
- Schidlowski, M., Appel, P.W.U., Eichmann, R., and Junge, C.E. 1979. Carbon isotope geochemistry of the 3.7×10^9 -yr-old Isua sediments, West Greenland; implications for the Archaean carbon and oxygen cycles. *Geochimica et Cosmochimica Acta* **43**(2): 189-199. doi: [https://doi.org/10.1016/0016-7037\(79\)90238-2](https://doi.org/10.1016/0016-7037(79)90238-2).
- Scogings, A. 2015. Graphite: Where size matters. In Australia's Paydirt. pp. 78-79.
- Seal II, R.R., Alpers, C.N., and Rye, R.O. 2000. Stable isotope systematics of sulfate minerals. *Reviews in Mineralogy and Geochemistry* **40**(1): 541-602. doi: <https://doi.org/10.2138/rmg.2000.40.12>.
- Skoog, D.A., and West, D.M. 1963. Fundamentals of analytical chemistry. Holt, Rinehart and Winston, New York.
- Spear, F.S. 1995. The determination of fluid composition from mineral-fluid equilibria and fluid inclusions. In *Metamorphic phase equilibria and pressure-temperature-time paths*. Mineralogical Society of America, Washington D.C. pp. 647-670.
- Spence, H.S. 1920. Graphite. Publication No. 511, Department of Mines, Canada.
- Storey, C.C., and Vos, M.A. 1981. Industrial minerals of the Pembroke-Renfrew area. Part 2. Ontario Geological Survey Mineral Deposits Circular 22. pp. 214.
- Strauss, H. 1993. The sulfur isotopic record of Precambrian sulfates: new data and a critical evaluation of the existing record. *Precambrian Research* **63**(4-5): 225-246. doi: [https://doi.org/10.1016/0301-9268\(93\)90035-Z](https://doi.org/10.1016/0301-9268(93)90035-Z).
- Taner, M.F. 2011. Report on the petrographic and mineralogical study of selected samples from the Bissett Creek Graphite Deposit, Maria Township, Ontario.
- Taner, M.F., Drever, C., Yakymchuk, C., and Longstaffe, F.J. 2017. Origin of graphite in the southwestern Grenville Province. *Canadian Mineralogist* **55**(6): 1041-1055. doi: <http://dx.doi.org/10.3749/canmin.1700029>.
- Taylor, S.R., and McClenan, S.M. 1985. The continental crust: Its composition and evolution. Blackwell Scientific Publications, Oxford.
- Timmerman, H., Jamieson, R.A., Parrish, R.R., and Culshaw, N.G. 2002. Coeval migmatites and granulites, Muskoka domain, southwestern Grenville Province, Ontario. *Canadian*

- Journal of Earth Sciences **39**(2): 239-258. doi: <https://doi.org/10.1139/e01-076>.
- Tashiro, T., Ishida, A., Hori, M., Igisu, M., Koike, M., Mejean, P., Takahata, N., Sano, Y., and Komiya, T. 2017. Early trace of life from 3.95 Ga sedimentary rocks in Labrador, Canada. *Nature* **549**: 516-518. doi: <https://doi.org/10.1038/nature24019>.
- Valley, J.W., and Essene, J. 1980. Calc-silicate reactions in Adirondack marbles: The role of fluids and solid solutions: Summary. *GSA Bulletin* **91**(2): 114-117. doi: [https://doi.org/10.1130/0016-7606\(1980\)91<114:CRIAMT>2.0.CO;2](https://doi.org/10.1130/0016-7606(1980)91<114:CRIAMT>2.0.CO;2).
- Vandenbroucke, M., and Largeau, C. 2007. Kerogen origin, evolution and structure. *Organic Geochemistry* **38**(5): 719-833. doi: <https://doi.org/10.1016/j.orggeochem.2007.01.001>.
- Van der Pluijm, B., and Carlson, K.A. 1989. Extension in the Central Metasedimentary Belt of the Ontario Grenville: Timing and tectonic significance. *Geology* **17**(2): 161-164. doi: [https://doi.org/10.1130/0091-7613\(1989\)017<0161:EITCMB>2.3.CO;2](https://doi.org/10.1130/0091-7613(1989)017<0161:EITCMB>2.3.CO;2).
- van Zuilen, M.A., Lepland, A., Teranes, J., Finarelli, J., Wahlen, M., and Arrhenius, G. 2003. Graphite and carbonates in the 3.8 Ga old Isua Supracrustal Belt, southern West Greenland. *Precambrian Research* **126**(3-4): 331-348. doi: [https://doi.org/10.1016/S0301-9268\(03\)00103-7](https://doi.org/10.1016/S0301-9268(03)00103-7).
- Vernon, R.H., and Clarke, G.L. 2008. Parent Rocks. In *Principles of Metamorphic Petrology*. Cambridge University Press, New York. pp. 306-350.
- Viljoen, K.S. 1995. Graphite- and diamond-bearing eclogite xenoliths from the Bellsbank kimberlites, Northern Cape, South Africa. *Contributions to Mineralogy and Petrology* **121**(4): 414-423. doi: <https://doi.org/10.1007/s004100050106>.
- Vine, J.D., and Tourtelot, E.B. 1970. Geochemistry of black shale deposits - A summary report. *Economic Geology* **65**(3): 253-272. doi: <https://doi.org/10.2113/gsecongeo.65.3.253>.
- Volkert, R.A., Johnson, C.A., and Tamashausky, A.V. 2000. Mesoproterozoic graphite deposits, New Jersey Highlands: geologic and stable isotopic evidence for possible algal origins. *Canadian Journal of Earth Sciences* **37**(12): 1665-1675. doi: <https://doi.org/10.1139/e00-050>.
- Wada, H., Tomita, T., Matsuura, K., Tuchi, K., Ito, M., and Morikiyo, T. 1994. Graphitization of carbonaceous matter during metamorphism with references to carbonate and pelitic rocks of contact and regional metamorphisms, Japan. *Contributions to Mineralogy and Petrology* **118**(3): 217-228. doi: <https://doi.org/10.1007/BF00306643>.

- Wang, S. 1989. Characteristics of ore-bearing formation and genesis of the Xinghe graphite deposit in Inner Mongolia. *Mineral Deposit* **8**(1): 85-96.
- Wedepohl, K.H. 1971. Environmental influences on the chemical composition of shales and clays. *Physics and Chemistry of the Earth* **8**: 307-333. doi: [https://doi.org/10.1016/0079-1946\(71\)90020-6](https://doi.org/10.1016/0079-1946(71)90020-6).
- Wedepohl, K.H. 1995. The composition of the continental crust. *Geochimica et Cosmochimica Acta* **59**(7): 1217-1232.
- Wei, C.J., Powell, R., and Clarke, G.L. 2004. Calculated phase equilibria for low- and medium-pressure metapelites in the KFMASH and KMnFMASH systems. *Journal of Metamorphic Geology* **22**(5): 495-508. doi: <https://doi.org/10.1111/j.1525-1314.2004.00530.x>.
- White, R.W., Powell, R., and Holland, T.J.B. 2007. Progress relating to calculation of partial melting equilibria for metapelites. *Journal of Metamorphic Geology* **25**(5): 511-527. doi: <https://doi.org/10.1111/j.1525-1314.2007.00711.x>.
- Wilde, S.A., Dorsett-Bain, H.L., and Lennon, R.G. 1999. Geological setting and controls on the development of graphite, sillimanite and phosphate mineralization within the Jiamusi Massif: An exotic fragment of Gondwanaland located in North-Eastern China? *Gondwana Research* **2**(1): 21-46. doi: [https://doi.org/10.1016/S1342-937X\(05\)70125-8](https://doi.org/10.1016/S1342-937X(05)70125-8).
- Wilson, A. 2013. Mineral Deposit Inventory for Ontario - Deposit MDI31L01SE00002. Available from <http://www.geologyontario.mndm.gov.on.ca/mndmfiles/MDI/data/records/MDI31L01SE00002.html>.
- Wu, C.-M., Zhang, J., and Ren, L.-D. 2004. Empirical garnet–biotite–plagioclase–quartz (GPBQ) geobarometry in medium- to high-grade metapelites. *Journal of Petrology* **45**(9): 1907-1921. doi: <https://doi.org/10.1093/petrology/egh038>.
- Yakymchuk, C., and Godin, L. 2012. Coupled role of deformation and metamorphism in the construction of inverted metamorphic sequences: an example from far-northwest Nepal. *Journal of Metamorphic Geology* **30**(5): 513-535. doi: <https://doi.org/10.1111/j.1525-1314.2012.00979.x>.
- Yang, Q.-Y., Santosh, M., and Wada, H. 2014. Graphite mineralization in Paleoproterozoic khondalites of the North China Craton: A carbon isotope study. *Precambrian Research* **255**(2): 641-652. doi: <https://doi.org/10.1016/j.precamres.2014.04.005>.

- Yung, A. 2018. Questions regarding WO#A16-13954. *Received by C. Drever.*
- Zhang, H.-F., Zhai, M.-G., Santosh, M., Wang, H.-Z., Zhao, L., and Ni, Z.-Y. 2014. Paleoproterozoic granulites from the Xinghe graphite mine, North China Craton: Geology, zircon U–Pb geochronology and implications for the timing of deformation, mineralization and metamorphism. *Ore Geology Reviews* **63**: 478-497. doi: <https://doi.org/10.1016/j.oregeorev.2014.03.014>.
- Zheng, Y.-F. 1990. Sulfur isotopes in metamorphic rocks. *Neues Jahrbuch für Mineralogie - Abhandlungen* **161**(3): 303-325.

Appendix A:
Bissett Creek property structural measurements

Point name:	Zone:	Easting (m):	Northing (m):	Surface elevation (masl):	Mapping classification:	Feature:	Number of measurements at location	Strike (°):	Dip (°):
0012	17T	726693	5111454	303	Barren gneiss	Foliation	1	233	16
0016	17T	727188	5111288	288	Graphitic gneiss	Foliation	1	310	23
0017	17T	727103	5111339	305	Barren gneiss	Foliation	1	324	18
0018	17T	727105	5111350	296	Graphitic gneiss	Foliation	1	357	22
0021	17T	727111	5111409	297	Graphitic gneiss	Foliation	1	19	33
0022	17T	727095	5111444	302	Barren gneiss	Foliation	1	351	24
0023	17T	727120	5111486	297	Graphitic gneiss	Foliation	1	357	24
0024	17T	727184	5111546	293	Graphitic gneiss	Foliation	1	43	11
0027	17T	726827	5111552	303	Barren gneiss	Foliation	1	232	26
0032	17T	726854	5111114	306	Barren gneiss	Foliation	1	342	34
0043	17T	727085	5111305	306	Barren gneiss	Foliation	1	352	23
0044	17T	727069	5111317	295	Barren gneiss	Foliation	1	2	27
0045	17T	727125	5111328	294	Graphitic gneiss	Foliation	1	282	24
0065	17T	727114	5111586	295	Graphitic gneiss	Foliation	1	328	11
0068	17T	727146	5111728	300	Graphitic gneiss	Foliation	1	292	22
0069	17T	727212	5111749	292	Graphitic gneiss	Foliation	1	322	16
0070	17T	727277	5111844	287	Graphitic gneiss	Foliation	3	31	15
0082	17T	727309	5111831	285	Graphitic gneiss	Foliation	1	34	18
0088	17T	727340	5111923	290	Graphitic gneiss	Foliation	3	33	14
0090	17T	727347	5111988	291	Graphitic gneiss	Foliation	2	22	13
0100	17T	727343	5112164	291	Graphitic gneiss	Foliation	1	356	10
0101	17T	727334	5112197	295	Graphitic gneiss	Foliation	2	353	13
0106	17T	727392	5112544	289	Graphitic gneiss	Foliation	1	264	24
0109	17T	727436	5112566	292	Graphitic gneiss	Foliation	1	265	24
0118	17T	727581	5112077	289	Graphitic gneiss	Foliation	1	230	12
0121	17T	727595	5112072	298	Pegmatite	Orientation	1	13	69
0122	17T	727595	5112072	-	Mafic intrusive	Orientation	1	54	88
0123	17T	727595	5112072	-	Graphitic gneiss	Foliation	1	359	14
0124	17T	727609	5112059	288	Graphitic gneiss	Foliation	1	357	15
0134	17T	728347	5113380	299	Barren gneiss	Foliation	1	256	72
0143	17T	728209	5112690	280	Graphitic gneiss	Foliation	1	266	21
0144	17T	728173	5112610	280	Graphitic gneiss	Foliation	1	303	18
0151	17T	727391	5113038	292	Graphitic gneiss	Foliation	1	296	16

Point name:	Zone:	Easting (m):	Northing (m):	Surface elevation (masl):	Mapping classification:	Feature:	Number of measurements at location	Strike (°):	Dip (°):
0161	17T	727466	5114006	326	Barren gneiss	Foliation	1	322	24
0162	17T	727487	5113827	316	Barren gneiss	Foliation	1	340	29
0166	17T	727470	5113687	310	Barren gneiss	Foliation	1	37	21
0183	17T	727640	5114840	295	Barren gneiss	Foliation	1	279	28
0184	17T	727602	5114715	304	Barren gneiss	Foliation	1	280	34
0188	17T	727897	5114387	323	Barren gneiss	Foliation	1	250	7
0189	17T	727876	5114272	329	Barren gneiss	Foliation	1	270	50
0190	17T	727876	5114147	333	Barren gneiss	Foliation	1	270	9
0192	17T	727661	5114155	338	Barren gneiss	Foliation	1	327	24
0193	17T	727721	5114154	332	Barren gneiss	Foliation	1	339	22
0199	17T	728152	5113989	326	Barren gneiss	Foliation	1	287	28
0201	17T	728067	5113683	296	Graphitic gneiss	Foliation	1	272	34
0203	17T	728075	5113619	300	Graphitic gneiss	Foliation	1	237	26
0214	17T	729047	5113132	289	Barren gneiss	Foliation	1	345	30
0218	17T	727761	5112491	281	Graphitic gneiss	Foliation	1	186	11
0219	17T	727040	5112988	292	Barren gneiss	Foliation	1	329	34
0220	17T	727042	5113008	290	Barren gneiss	Foliation	1	332	38
0221	17T	727082	5112999	292	Barren gneiss	Foliation	1	346	48
0222	17T	727128	5113041	284	Barren gneiss	Foliation	2	348	24
0223	17T	727175	5113060	294	Barren gneiss	Foliation	1	286	24
0224	17T	727228	5113087	291	Barren gneiss	Foliation	1	313	23
0225	17T	727232	5113097	293	Graphitic gneiss	Foliation	1	342	26
0227	17T	727237	5113177	294	Graphitic gneiss	Foliation	3	324	19
0228	17T	727234	5113211	306	Graphitic gneiss	Foliation	1	269	16
0229	17T	727186	5113212	302	Graphitic gneiss	Foliation	2	343	18
0230	17T	727222	5113232	312	Graphitic gneiss	Foliation	2	317	17
0235	17T	728141	5113301	303	Barren gneiss	Foliation	2	306	35
0236	17T	727985	5113003	288	Barren gneiss	Foliation	1	253	38
0237	17T	727975	5113009	289	Barren gneiss	Foliation	1	254	36
0238	17T	728034	5113027	290	Barren gneiss	Foliation	2	231	60
0239	17T	728365	5112935	286	Graphitic gneiss	Foliation	1	263	28
0240	17T	728348	5112917	286	Graphitic gneiss	Foliation	1	274	24
0241	17T	728319	5112874	286	Graphitic gneiss	Foliation	1	262	23

Point name:	Zone:	Easting (m):	Northing (m):	Surface elevation (masl):	Mapping classification:	Feature:	Number of measurements at location	Strike (°):	Dip (°):
0242	17T	728364	5112689	288	Barren gneiss	Foliation	1	285	11
0243	17T	728328	5112692	290	Barren gneiss	Foliation	1	251	23
0245	17T	727386	5114096	313	Barren gneiss	Foliation	2	278	48
0246	17T	727340	5114069	315	Barren gneiss	Foliation	1	332	52
0247	17T	727352	5114046	312	Barren gneiss	Foliation	1	323	42
0248	17T	727338	5114077	313	Barren gneiss	Foliation	2	342	36
0252	17T	727137	5114091	299	Barren gneiss	Foliation	2	282	19
0253	17T	727023	5114089	281	Barren gneiss	Foliation	1	348	17
0254	17T	726992	5114089	279	Barren gneiss	Foliation	1	356	22
0255	17T	726984	5113999	277	Barren gneiss	Foliation	1	353	15
0256	17T	726886	5113915	281	Barren gneiss	Foliation	1	333	12
0259	17T	727113	5113871	306	Barren gneiss	Foliation	1	270	26
0260	17T	727126	5113875	316	Barren gneiss	Foliation	1	245	24
0261	17T	727451	5113661	313	Barren gneiss	Foliation	1	359	22
0262	17T	727550	5113759	312	Barren gneiss	Foliation	1	319	28
0264	17T	726910	5112945	294	Barren gneiss	Foliation	1	346	24
0265	17T	727030	5112955	294	Barren gneiss	Foliation	1	356	24
0266	17T	727164	5113008	305	Barren gneiss	Foliation	2	262	24
0267	17T	727174	5112970	302	Barren gneiss	Foliation	2	297	18
0268	17T	727184	5112954	299	Graphitic gneiss	Foliation	2	322	23
0269	17T	727186	5112936	300	Graphitic gneiss	Foliation	1	356	25
0270	17T	727203	5112922	303	Graphitic Gneiss	Foliation	1	266	22
0274	17T	727123	5112348	296	Barren gneiss	Foliation	1	58	11
0276	17T	727074	5112319	295	Barren gneiss	Foliation	1	46	9
0277	17T	727893	5112982	292	Barren gneiss	Foliation	1	329	21
0278	17T	727010	5112277	299	Barren gneiss	Foliation	2	28	13
0279	17T	727817	5112965	294	Barren gneiss	Foliation	1	299	25
0281	17T	727669	5113040	298	Barren gneiss	Foliation	2	266	17
0286	17T	727658	5112404	294	Graphitic gneiss	Foliation	1	220	10
0287	17T	727719	5112391	291	Graphitic gneiss	Foliation	1	220	12
0288	17T	727796	5112540	288	Graphitic gneiss	Foliation	2	225	19
0289	17T	727985	5112495	301	Graphitic Gneiss	Foliation	1	222	22
0299	17T	728221	5112530	297	Barren gneiss	Foliation	1	223	16

Point name:	Zone:	Easting (m):	Northing (m):	Surface elevation (masl):	Mapping classification:	Feature:	Number of measurements at location	Strike (°):	Dip (°):
0301	17T	728155	5112499	302	Barren gneiss	Foliation	1	340	28
0303	17T	728124	5112450	296	Barren gneiss	Foliation	2	238	20
0305	17T	728073	5112452	293	Barren gneiss	Foliation	1	309	14
0308	17T	728130	5112547	281	Barren gneiss	Foliation	1	262	12
0311	17T	727126	5113106	287	Barren gneiss	Foliation	1	285	24
0314	17T	727133	5113416	285	Barren gneiss	Foliation	1	300	32
0320	17T	727364	5111912	-	Graphitic gneiss	Foliation	1	36	15
0321	17T	727347	5111871	-	Graphitic gneiss	Foliation	1	22	18
0323	17T	727536	5113504	-	Graphitic gneiss	Foliation	1	29	16
0324	17T	727463	5113530	-	Barren gneiss	Foliation	1	329	34
0325	17T	727449	5113539	-	Barren gneiss	Foliation	1	352	24
0326	17T	727423	5113544	-	Graphitic gneiss	Foliation	1	357	34
0329	17T	727189	5113569	-	Barren gneiss	Foliation	1	30	14
0332	17T	727672	5111349	-	Barren gneiss	Foliation	1	354	17
0333	17T	727639	5111350	-	Barren gneiss	Foliation	1	22	21
0335	17T	727667	5111437	-	Barren gneiss	Foliation	1	5	14
0336	17T	727731	5111544	-	Barren gneiss	Foliation	1	32	22
0337	17T	727852	5111667	-	Barren gneiss	Foliation	1	0	26
0341	17T	728452	5111691	-	Barren gneiss	Foliation	1	359	22

Notes:

- All elevation values supplied are from a handheld GPS and should be used as approximate values.

Any suspect values have been removed.

- In areas where multiple measurements were taken, structural measurements were determined by averaging the readings and rounding to the nearest whole degree.

- Only foliation measurements were used in the stereonet structural analysis.

- Magnetic declination of 12°W was applied to all structural measurements.

Appendix B:
Regional structural measurements

Point name:	Zone:	Easting (m):	Northing (m):	Surface elevation (masl):	Mapping classification:	Feature:	Number of measurements at location	Strike (°):	Dip (°):
0504	18T	294824	5117361	155	Barren gneiss	Foliation	1	264	31
0506	18T	295159	5117294	152	Barren gneiss	Foliation	1	328	54
0507	18T	294665	5117385	166	Barren gneiss	Foliation	1	270	17
0508	18T	287430	5118083	185	Garnet-biotite-muscovite-amphibole schist	Foliation	1	337	36
0509	18T	287441	5118082	184	Barren gneiss	Foliation	1	354	32
0510	18T	287533	5118110	188	Barren gneiss	Foliation	1	298	16
0511	18T	287549	5118114	188	Barren gneiss	Foliation	1	314	16
0512	18T	287574	5118112	191	Barren gneiss (potential migmatite)	Foliation	1	359	26
0513	18T	287627	5118116	189	Barren gneiss	Foliation	1	334	26
0515	17T	728377	5122305	209	Pegmatite	Orientation	1	106	73
0516	17T	728364	5122309	209	Barren gneiss	Foliation	1	338	22
0517	17T	728327	5122321	211	Mafic intrusive	Orientation	1	334	16
0518	17T	728331	5122316	210	Barren gneiss	Foliation	1	346	14
0519	17T	728360	5122314	210	Barren gneiss	Foliation	1	298	13
0520	17T	728302	5122326	211	Barren gneiss	Foliation	1	334	20
0521	17T	728277	5122337	213	Graphitic gneiss	Foliation	1	330	16
0522	17T	728244	5122352	216	Barren gneiss	Foliation	1	3	16
0522	17T	728244	5122352	216	Graphitic gneiss	Foliation	1	328	16
0522	17T	728244	5122352	216	Contact between graphitic and barren gneisses	Contact	1	353	22
0523	17T	728229	5122355	215	Barren gneiss	Foliation	1	353	23
0523	17T	728229	5122355	215	Graphitic gneiss	Foliation	1	342	16
0523	17T	728229	5122355	215	Contact between graphitic and barren gneisses	Contact	1	343	19
0524	17T	728205	5122362	211	Graphitic gneiss	Foliation	1	322	14
0528	17T	722383	5125108	302	Graphitic gneiss	Foliation	1	308	78
0529	17T	722389	5125111	302	Graphitic gneiss	Foliation	1	308	78
0531	17T	722407	5125109	301	Graphitic gneiss	Foliation	1	339	45
0532	17T	722436	5125155	302	Graphitic gneiss	Foliation	1	300	69
0535	17T	722616	5125143	301	Graphitic gneiss	Foliation	1	330	36
0536	17T	722639	5125148	300	Graphitic gneiss	Foliation	1	302	58
0537	17T	722646	5125154	301	Graphitic gneiss	Foliation	1	306	46
0537	17T	722646	5125154	301	Barren gneiss	Foliation	1	299	46

Point name:	Zone:	Easting (m):	Northing (m):	Surface elevation (masl):	Mapping classification:	Feature:	Number of measurements at location	Strike (°):	Dip (°):
0537	17T	722646	5125154	301	Contact between graphitic and barren gneisses	Contact	1	307	49
0538	17T	722724	5125170	302	Barren gneiss	Foliation	1	305	56
0539	17T	722669	5125155	301	Barren gneiss	Foliation	1	300	54

Notes:

- All elevation values supplied are from a handheld GPS and should be used as approximate values.

Any suspect values have been removed.

- In areas where multiple measurements were taken, structural measurements were determined by averaging the readings and rounding to the nearest whole degree.

- Only foliation measurements were used in the stereonet structural analysis.

- Magnetic declination of 12°W was applied to all structural measurements.

Appendix C:
Sample information

Point ID:	Sample ID:	Lithology:	Sample Type:	Obtained from:	Zone:	Easting (m):	Northing (m):	Surface Elevation (m):	Date collected (DD-Month-YYYY):	Methods of Analysis:
N/A	BC-10-06	Garnet-sillimanite-biotite-graphite gneiss	Primary	BC-10-26 at 41m (Mehmet's samples)	17T	727697	5112226	288.7	Unknown	TS, EM
0012	BC-16-01	Biotite-quartzofeldspathic gneiss	Primary	Outcrop	17T	726693	5111454	303	02-June-2016	TS, ME
0028	BC-16-02	Biotite-quartzofeldspathic gneiss	Primary	Outcrop	17T	726816	5111613	305	03-June-2016	TS, ME
0032	BC-16-03	Biotite-amphibole-quartzofeldspathic gneiss	Primary	Outcrop	17T	726854	5111114	306	03-June-2016	TS, ME
0043	BC-16-04	Biotite-quartzofeldspathic gneiss	Primary	Outcrop	17T	727085	5111305	306	04-June-2016	TS, ME
0064	BC-16-05	Biotite-quartzofeldspathic gneiss	Primary	Outcrop	17T	727097	5111591	293	06-June-2016	TS, ME
0070	BC-16-06	Clinopyroxene-amphibole-biotite-graphite gneiss	Primary	Southern bulk sample pit	17T	727277	5111844	287	06-June-2016	TS, ME, TE, CA, ST, CI, SI
0070	BC-16-07	Clinopyroxene-amphibole-biotite-graphite gneiss	Primary	Southern bulk sample pit	17T	727277	5111844	287	06-June-2016	TS, ME, TE, CA, ST, CI, SI
0070	BC-16-08	Clinopyroxene-amphibole-biotite-graphite gneiss	Primary	Southern bulk sample pit	17T	727277	5111844	287	06-June-2016	TS, ME, TE, CA, ST, CI, SI
0070	BC-16-09	Clinopyroxene-amphibole-biotite-graphite gneiss	Primary	Southern bulk sample pit	17T	727277	5111844	287	06-June-2016	TS
0084	BC-16-10	Garnet-sillimanite-biotite gneiss	Primary	Outcrop	17T	727370	5111867	278	08-June-2016	TS, ME
0116	BC-16-11	Biotite-graphite-quartzofeldspathic gneiss	Primary	Northern bulk sample pit	17T	727584	5112065	287	10-June-2016	TS, ME, TE, CA, ST, CI, SI
0117	BC-16-12	Granitic pegmatite	Primary	Northern bulk sample pit	17T	727583	5112073	289	10-June-2016	TS, ME, TE
0119	BC-16-13	Clinopyroxene-amphibole-biotite-graphite gneiss	Primary	Northern bulk sample pit	17T	727587	5112081	296	10-June-2016	TS, ME, TE, CA, ST, CI, SI
0120	BC-16-14	Clinopyroxene-amphibole-biotite-graphite gneiss	Primary	Northern bulk sample pit	17T	727595	5112072	296	10-June-2016	TS, ME, TE, CA, ST, CI, SI
0121	BC-16-15	Granitic pegmatite	Primary	Northern bulk sample pit	17T	727595	5112072	298	10-June-2016	TS, ME, TE
0121	BC-16-16	Pegmatite-graphitic gneiss boundary	Primary	Northern bulk sample pit	17T	727595	5112072	298	10-June-2016	TS
0121	BC-16-17	Clinopyroxene-amphibole-biotite-graphite gneiss	Primary	Northern bulk sample pit	17T	727595	5112072	298	10-June-2016	TS, ME, TE, CA, ST, CI, SI
0121	BC-16-18	Garnet-amphibole-biotite-graphite gneiss	Primary	Northern bulk sample pit	17T	727595	5112072	298	10-June-2016	TS, ME, TE, EM
0121	BC-16-19	Biotite-graphite-quartzofeldspathic gneiss	Primary	Northern bulk sample pit	17T	727595	5112072	298	10-June-2016	TS, ME, CA, ST, CI, SI
0121	BC-16-20	Garnet-amphibole-biotite-graphite gneiss	Primary	Northern bulk sample pit	17T	727595	5112072	298	10-June-2016	TS, ME, TE, CA, ST, CI, EM
0122	BC-16-21	Metagabbro intrusive	Primary	Northern bulk sample pit	17T	727595	5112072	-	10-June-2016	TS, ME
0122	BC-16-22	Clinopyroxene-amphibole-biotite-graphite gneiss	Primary	Northern bulk sample pit	17T	727595	5112072	-	10-June-2016	TS, ME, TE, CA, ST, CI, SI
0134	BC-16-23	Biotite-quartzofeldspathic gneiss	Primary	Outcrop	17T	728347	5113380	299	12-June-2016	TS, ME
0169	BC-16-24	Biotite-amphibole-quartzofeldspathic gneiss	Primary	Outcrop	17T	727545	5113740	313	13-June-2016	TS, ME, TE
0018	BC-16-25	Garnet-sillimanite-biotite-graphite gneiss	Primary	Outcrop	17T	727105	5111350	297	16-June-2016	TS, ME, TE, CA, ST, CI
0017	BC-16-26	Biotite-quartzofeldspathic gneiss	Primary	Outcrop	17T	727103	5111339	305	16-June-2016	TS, ME, TE
0121	BC-16-27	Granitic pegmatite	Primary	Northern bulk sample pit	17T	727595	5112072	298	16-June-2016	TS, ME, TE
0121	BC-16-28	Biotite-graphite-quartzofeldspathic gneiss	Primary	Northern bulk sample pit	17T	727595	5112072	298	16-June-2016	TS, ME, TE, CA, ST, CI, SI, EM
0121	BC-16-29	Garnet-amphibole-biotite-graphite gneiss	Primary	Northern bulk sample pit	17T	727595	5112072	298	16-June-2016	TS, ME, TE, CA, ST, CI, SI, EM
0121	BC-16-30	Clinopyroxene-amphibole-biotite-graphite gneiss	Primary	Northern bulk sample pit	17T	727595	5112072	298	16-June-2016	TS
0121	BC-16-31	Clinopyroxene-amphibole-biotite-graphite gneiss	Primary	Northern bulk sample pit	17T	727595	5112072	298	16-June-2016	TS
0188	BC-16-32	Biotite-amphibole-quartzofeldspathic gneiss	Primary	Outcrop	17T	727897	5114387	323	04-October-2016	-
0189	BC-16-33	Biotite-quartzofeldspathic gneiss	Primary	Outcrop	17T	727876	5114272	329	04-October-2016	TS, ME, TE
0194	BC-16-34	Garnet amphibolite	Primary	Float near outcrop	17T	727812	5114130	334	05-October-2016	TS, ME, TE
0214	BC-16-35	Biotite-quartzofeldspathic gneiss	Primary	Outcrop	17T	729047	5113132	289	07-October-2016	TS
0236	BC-16-36	Biotite-quartzofeldspathic gneiss	Primary	Outcrop	17T	727985	5113003	288	11-October-2016	-
0254	BC-16-37	Biotite-quartzofeldspathic gneiss	Primary	Outcrop	17T	726992	5114089	279	13-October-2016	-
0070	BC-16-38	Clinopyroxene-amphibole-biotite-graphite gneiss	Primary	Float from southern bulk sample pit	17T	727277	5111844	287	18-October-2016	TS, ME, TE, CA, ST, CI, SI
N/A	BC-16-39	Duplicate of BC-16-20	Duplicate	Northern bulk sample pit	17T	727595	5112072	298	10-June-2016	TS, ME, TE, CA, ST, CI
N/A	BC-16-40	Beach Sand	Blank	-	-	-	-	-	-	ME, TE, CA, ST
N/A	BC-16-41	Diorite Gneiss (SY-4)	Standard	-	-	-	-	-	-	ME, TE
N/A	BC-16-50	Graphite separates from Bin # 1 in Mine Garage	Primary	-	-	-	-	-	18-October-2016	CI
N/A	BC-16-51	Graphite separates from Bin # 1 in Mine Garage	Primary	-	-	-	-	-	18-October-2016	CI
0504	RO-16-01	Biotite-quartzofeldspathic gneiss	Primary	Outcrop	18T	294824	5117361	155	15-June-2016	TS, ME
0506	RO-16-02	Biotite-quartzofeldspathic gneiss	Primary	Outcrop	18T	295159	5117294	152	15-June-2016	TS, ME
0507	RO-16-03	Biotite-quartzofeldspathic gneiss	Primary	Outcrop	18T	294655	5117385	166	15-June-2016	TS, ME, TE
0508	RO-16-04	Garnet-biotite-muscovite-amphibole schist	Primary	Outcrop	18T	287430	5118083	185	15-June-2016	TS, ME, TE, EM
0509	RO-16-05	Biotite-amphibole-quartzofeldspathic gneiss	Primary	Outcrop	18T	287441	5118082	185	15-June-2016	TS, ME
0510	RO-16-06	Biotite-amphibole-quartzofeldspathic gneiss	Primary	Outcrop	18T	287533	5118110	188	15-June-2016	TS, ME, TE
0511	RO-16-07	Weathering too severe for analysis - possible graphitic gneiss?	Primary	Outcrop	18T	287549	5118114	188	15-June-2016	-
0512	RO-16-08	Biotite-amphibole-quartzofeldspathic gneiss	Primary	Outcrop	18T	287574	5118112	191	15-June-2016	TS, EM
0513	RO-16-09	Biotite-quartzofeldspathic gneiss	Primary	Outcrop	18T	287627	5118116	189	15-June-2016	TS, ME, TE, EM
0514	RO-16-10	Carbonate from gneiss surface	Primary	Outcrop	18T	287630	5118120	187	15-June-2016	-
0515	RO-16-11	Granitic pegmatite	Primary	Outcrop	17T	728377	5122305	209	16-June-2016	TS, ME, TE, CA, ST
0516	RO-16-12	Biotite-quartzofeldspathic gneiss	Primary	Outcrop	17T	728364	5122309	209	16-June-2016	TS, ME

Point ID:	Sample ID:	Lithology:	Sample Type:	Obtained from:	Zone:	Easting (m):	Northing (m):	Surface Elevation (m):	Date collected (DD-Month-YYYY):	Methods of Analysis:
0517	RO-16-13	Metagabbro intrusive	Primary	Outcrop	17T	728327	5122321	211	16-June-2016	TS, ME
0518	RO-16-14	Biotite-amphibole-quartzofeldspathic gneiss	Primary	Outcrop	17T	728331	5122316	210	16-June-2016	TS, ME, TE
0520	RO-16-15	Biotite-quartzofeldspathic gneiss	Primary	Outcrop	17T	728302	5122326	211	16-June-2016	TS
0521	RO-16-16	Biotite-graphite-quartzofeldspathic gneiss	Primary	Outcrop	17T	728277	5122337	213	16-June-2016	TS, ME, TE, CA, ST, CI
0522	RO-16-17	Biotite-quartzofeldspathic gneiss	Primary	Outcrop	17T	728244	5122352	216	16-June-2016	TS, ME
0524	RO-16-18	Biotite-graphite-quartzofeldspathic gneiss	Primary	Outcrop	17T	728205	5122362	211	16-June-2016	TS
0525	RO-16-19	Biotite-graphite-quartzofeldspathic gneiss	Primary	Outcrop	17T	722429	5125084	301	19-October-2016	TS, ME, TE, CA, ST, CI
0528	RO-16-20	Biotite-graphite-quartzofeldspathic gneiss	Primary	Outcrop	17T	722383	5125108	302	19-October-2016	-
0536	RO-16-21	Biotite-graphite-quartzofeldspathic gneiss	Primary	Outcrop	17T	722639	5125148	300	19-October-2016	TS, ME, TE
0538	RO-16-22	Biotite-graphite-quartzofeldspathic gneiss	Primary	Outcrop	17T	722724	5125170	302	19-October-2016	TS, ME, TE
N/A	RO-16-23	Duplicate of CO-16-04	Duplicate	BC-12-203, Box 4, 18.45m to 18.90m	17T	727707	5112276	290.1	18-October-2016	ME, TE, CA, ST, CI
N/A	RO-16-24	Beach Sand	Blank	-	-	-	-	-	-	ME, TE, CA, ST
N/A	RO-16-25	Diorite Gneiss (SY-4)	Standard	-	-	-	-	-	-	ME, TE
N/A	CO-16-01	Biotite-graphite-quartzofeldspathic gneiss	Primary	BC-12-108, Box 4, 19.07m to 19.46m	17T	727441	5112474	-	18-October-2016*	TS, ME, TE, CA, ST, CI, SI
N/A	CO-16-02	Biotite-graphite-quartzofeldspathic gneiss	Primary	BC-12-201, Box 13, 53.62m to 54.00m	17T	727669	5112255	290.7	18-October-2016*	TS, ME, TE, CA, ST, CI, SI
N/A	CO-16-03	Biotite-graphite-quartzofeldspathic gneiss	Primary	BC-12-202, Box 4, 24.67m to 24.94m	17T	727654	5112295	287.7	18-October-2016*	TS, ME, TE, CA, ST, CI, SI
N/A	CO-16-04	Biotite-graphite-quartzofeldspathic gneiss	Primary	BC-12-203, Box 4, 18.45m to 18.90m	17T	727707	5112276	290.1	18-October-2016*	TS, ME, TE, CA, ST, CI, SI
N/A	CO-16-05	Garnet-sillimanite-biotite-graphite gneiss	Primary	BC-12-204, Box 13, 52.07m to 53.00m	17T	727740	5112245	289.9	18-October-2016*	TS, ME, TE, CA, ST, CI, EM
N/A	CO-16-06	Clinopyroxene-amphibole-biotite-graphite gneiss	Primary	BC-12-205, Box 15, 21.96m to 22.22m and 22.97m to 23.09m	17T	727810	5112283	289.3	18-October-2016*	TS, ME, TE, CA, ST, CI, SI
N/A	CO-16-07	Biotite-graphite-quartzofeldspathic gneiss	Primary	BC-12-208, Box 6, 26.77m to 27.00m	17T	727998	5112297	290.3	18-October-2016*	TS, ME, TE, CA, ST, CI, SI
N/A	CO-16-08	Garnet-sillimanite-biotite-graphite gneiss	Primary	BC-12-210, Box 4, 17.77m to 17.92m	17T	727841	5112236	286.6	18-October-2016*	TS, ME, TE, CA, ST, CI, SI, EM
N/A	CO-16-09	Garnet-amphibole-biotite-graphite gneiss	Primary	BC-12-210, Box 8, 30.78m to 30.90m and 32.59m to 32.75m	17T	727841	5112236	286.6	18-October-2016*	TS, ME, TE, CI
N/A	CO-16-10	Garnet-sillimanite-biotite-graphite gneiss	Primary	BC-12-107, Box 3, 13.05m to 13.20m	17T	727361	5112413	289.5	18-October-2016*	TS, ME, TE, CI, EM

Notes:

* - All core sampled was originally drilled in the period from 02-October-2012 to 18-October-2012. Core was then logged and stored indoors in the on-site core shacks.

All elevation values supplied in italics are from a handheld GPS and should be used as approximate values. Any suspect values have been removed.

Thin section billets were submitted to Vancouver Petrographics for processing on 17-August-2016 and 04-January-2017.

All samples were submitted to Actlabs for major and trace element geochemistry on 27-December-2016, and were confirmed received by the lab

All samples were submitted to QFIR for carbon isotopes on 06-January-2017 and were confirmed as received by the lab on 16-January-2017.

Samples were submitted to the UW-EIL for sulfur isotope analyses on 06-January-2017 and 08-January-2017 and were confirmed on the same dates as submission.

Methods for analysis are as follows: TS - Thin Section, ME - Major Element Geochemistry, TE - Trace Element Geochemistry, CA - carbon Analyses (Total and Graphitic), ST - Total Sulfur,

CI - Carbon Isotopes, SI - Sulfur Isotopes, EM - Electron Microprobe.

Appendix D:

Quality assurance and quality control data

List of Abbreviations – See analytical methods for further description.

- FUS-ICP – Value determined by fusion, dissolution and analysis in an ICP-OES.
- FUS-MS – Value determined by fusion, dissolution and analysis in an ICP-MS.
- TITR – Value determined by titration.
- IR – Value determined by infrared using the graphitic carbon procedure.
- CS – Value determined by infrared using the total C and S procedure.
- % - % weight.
- ppm – parts per million.
- < - Less than the detection limit.
- ‘-’ – No value analyzed for this parameter.

Note: All certified reference materials, blanks, and duplicates in this section were selected and analyzed by Activation Laboratories (Actlabs).

Analyte Symbol	SiO ₂	Al ₂ O ₃	Fe ₂ O _{3(T)}	MnO	MgO	CaO	Na ₂ O	K ₂ O	TiO ₂	P ₂ O ₅	LOI
Unit Symbol	(%)	(%)	(%)	(%)	(%)	(%)	(%)	(%)	(%)	(%)	(%)
Detection Limit	0.01	0.01	0.01	0.001	0.01	0.01	0.01	0.01	0.001	0.01	-
Analysis Method	FUS-ICP	FUS-ICP	FUS-ICP	FUS-ICP	FUS-ICP	FUS-ICP	FUS-ICP	FUS-ICP	FUS-ICP	FUS-ICP	FUS-ICP
NIST 694 Meas	-	-	-	-	-	-	-	-	-	-	-
NIST 694 Cert	-	-	-	-	-	-	-	-	-	-	-
NIST 694 Meas	-	-	-	-	-	-	-	-	-	-	-
NIST 694 Cert	-	-	-	-	-	-	-	-	-	-	-
NIST 694 Meas	11.31	1.96	0.75	0.01	0.35	42.69	0.87	0.54	0.12	30.15	-
NIST 694 Cert	11.2	1.8	0.79	0.0116	0.33	43.6	0.86	0.51	0.11	30.2	-
DNC-1 Meas	-	-	-	-	-	-	-	-	-	-	-
DNC-1 Cert	-	-	-	-	-	-	-	-	-	-	-
DNC-1 Meas	-	-	-	-	-	-	-	-	-	-	-
DNC-1 Cert	-	-	-	-	-	-	-	-	-	-	-
DNC-1 Meas	47.21	18.71	9.75	0.15	10.07	11.49	1.91	0.22	0.48	0.08	-
DNC-1 Cert	47.15	18.34	9.97	0.15	10.13	11.49	1.89	0.234	0.48	0.07	-
GBW 07113 Meas	-	-	-	-	-	-	-	-	-	-	-
GBW 07113 Cert	-	-	-	-	-	-	-	-	-	-	-
GBW 07113 Meas	-	-	-	-	-	-	-	-	-	-	-
GBW 07113 Cert	-	-	-	-	-	-	-	-	-	-	-
GBW 07113 Meas	71.13	12.83	3.24	0.15	0.15	0.61	2.46	5.39	0.28	0.04	-
GBW 07113 Cert	72.8	13	3.21	0.14	0.16	0.59	2.57	5.43	0.3	0.05	-
LKSD-3 Meas	-	-	-	-	-	-	-	-	-	-	-
LKSD-3 Cert	-	-	-	-	-	-	-	-	-	-	-
TDB-1 Meas	-	-	-	-	-	-	-	-	-	-	-
TDB-1 Cert	-	-	-	-	-	-	-	-	-	-	-
BaSO ₄ Meas	-	-	-	-	-	-	-	-	-	-	-
BaSO ₄ Cert	-	-	-	-	-	-	-	-	-	-	-
BaSO ₄ Meas	-	-	-	-	-	-	-	-	-	-	-
BaSO ₄ Cert	-	-	-	-	-	-	-	-	-	-	-
BaSO ₄ Meas	-	-	-	-	-	-	-	-	-	-	-
BaSO ₄ Cert	-	-	-	-	-	-	-	-	-	-	-
W-2a Meas	-	-	-	-	-	-	-	-	-	-	-
W-2a Cert	-	-	-	-	-	-	-	-	-	-	-
W-2a Meas	-	-	-	-	-	-	-	-	-	-	-
W-2a Cert	-	-	-	-	-	-	-	-	-	-	-

Analyte Symbol	SiO ₂	Al ₂ O ₃	Fe ₂ O _{3(T)}	MnO	MgO	CaO	Na ₂ O	K ₂ O	TiO ₂	P ₂ O ₅	LOI
Unit Symbol	(%)	(%)	(%)	(%)	(%)	(%)	(%)	(%)	(%)	(%)	(%)
Detection Limit	0.01	0.01	0.01	0.001	0.01	0.01	0.01	0.01	0.001	0.01	-
Analysis Method	FUS-ICP	FUS-ICP	FUS-ICP	FUS-ICP	FUS-ICP	FUS-ICP	FUS-ICP	FUS-ICP	FUS-ICP	FUS-ICP	FUS-ICP
W-2a Meas	52.72	15.64	10.81	0.17	6.36	11.09	2.23	0.62	1.07	0.15	-
W-2a Cert	52.4	15.4	10.7	0.163	6.37	10.9	2.14	0.626	1.06	0.13	-
SY-4 Meas	-	-	-	-	-	-	-	-	-	-	-
SY-4 Cert	-	-	-	-	-	-	-	-	-	-	-
SY-4 Meas	-	-	-	-	-	-	-	-	-	-	-
SY-4 Cert	-	-	-	-	-	-	-	-	-	-	-
SY-4 Meas	50.19	20.07	6.15	0.11	0.52	8.11	6.9	1.66	0.28	0.13	-
SY-4 Cert	49.9	20.69	6.21	0.108	0.54	8.05	7.1	1.66	0.287	0.131	-
CTA-AC-1 Meas	-	-	-	-	-	-	-	-	-	-	-
CTA-AC-1 Cert	-	-	-	-	-	-	-	-	-	-	-
BIR-1a Meas	-	-	-	-	-	-	-	-	-	-	-
BIR-1a Cert	-	-	-	-	-	-	-	-	-	-	-
BIR-1a Meas	-	-	-	-	-	-	-	-	-	-	-
BIR-1a Cert	-	-	-	-	-	-	-	-	-	-	-
BIR-1a Meas	47.77	15.54	11.18	0.17	9.55	13.47	1.79	0.01	0.96	0.03	-
BIR-1a Cert	47.96	15.5	11.3	0.175	9.7	13.3	1.82	0.03	0.96	0.021	-
NCS DC86312 Meas	-	-	-	-	-	-	-	-	-	-	-
NCS DC86312 Cert	-	-	-	-	-	-	-	-	-	-	-
JGb-2 Meas	-	-	-	-	-	-	-	-	-	-	-
JGb-2 Cert	-	-	-	-	-	-	-	-	-	-	-
JGb-2 Meas	-	-	-	-	-	-	-	-	-	-	-
JGb-2 Cert	-	-	-	-	-	-	-	-	-	-	-
JGb-2 Meas	-	-	-	-	-	-	-	-	-	-	-
JGb-2 Cert	-	-	-	-	-	-	-	-	-	-	-
NCS DC70009 (GBW07241) Meas	-	-	-	-	-	-	-	-	-	-	-
NCS DC70009 (GBW07241) Cert	-	-	-	-	-	-	-	-	-	-	-
SGR-1b Meas	-	-	-	-	-	-	-	-	-	-	-
SGR-1b Cert	-	-	-	-	-	-	-	-	-	-	-
SGR-1b Meas	-	-	-	-	-	-	-	-	-	-	-
SGR-1b Cert	-	-	-	-	-	-	-	-	-	-	-
SGR-1b Meas	-	-	-	-	-	-	-	-	-	-	-
SGR-1b Cert	-	-	-	-	-	-	-	-	-	-	-

Analyte Symbol	SiO ₂	Al ₂ O ₃	Fe ₂ O _{3(T)}	MnO	MgO	CaO	Na ₂ O	K ₂ O	TiO ₂	P ₂ O ₅	LOI
Unit Symbol	(%)	(%)	(%)	(%)	(%)	(%)	(%)	(%)	(%)	(%)	(%)
Detection Limit	0.01	0.01	0.01	0.001	0.01	0.01	0.01	0.01	0.001	0.01	-
Analysis Method	FUS-ICP	FUS-ICP	FUS-ICP	FUS-ICP	FUS-ICP	FUS-ICP	FUS-ICP	FUS-ICP	FUS-ICP	FUS-ICP	FUS-ICP
OREAS 100a (Fusion) Meas	-	-	-	-	-	-	-	-	-	-	-
OREAS 100a (Fusion) Cert	-	-	-	-	-	-	-	-	-	-	-
OREAS 101a (Fusion) Meas	-	-	-	-	-	-	-	-	-	-	-
OREAS 101a (Fusion) Cert	-	-	-	-	-	-	-	-	-	-	-
OREAS 101b (Fusion) Meas	-	-	-	-	-	-	-	-	-	-	-
OREAS 101b (Fusion) Cert	-	-	-	-	-	-	-	-	-	-	-
JR-1 Meas	-	-	-	-	-	-	-	-	-	-	-
JR-1 Cert	-	-	-	-	-	-	-	-	-	-	-
GS311-4 Meas	-	-	-	-	-	-	-	-	-	-	-
GS311-4 Cert	-	-	-	-	-	-	-	-	-	-	-
GS311-4 Meas	-	-	-	-	-	-	-	-	-	-	-
GS311-4 Cert	-	-	-	-	-	-	-	-	-	-	-
GS311-4 Meas	-	-	-	-	-	-	-	-	-	-	-
GS311-4 Cert	-	-	-	-	-	-	-	-	-	-	-
GS900-5 Meas	-	-	-	-	-	-	-	-	-	-	-
GS900-5 Cert	-	-	-	-	-	-	-	-	-	-	-
GS900-5 Meas	-	-	-	-	-	-	-	-	-	-	-
GS900-5 Cert	-	-	-	-	-	-	-	-	-	-	-
Graphite 4A Meas	-	-	-	-	-	-	-	-	-	-	-
Graphite 4A Cert	-	-	-	-	-	-	-	-	-	-	-
Graphite 4A Meas	-	-	-	-	-	-	-	-	-	-	-
Graphite 4A Cert	-	-	-	-	-	-	-	-	-	-	-
Graphite 4A Meas	-	-	-	-	-	-	-	-	-	-	-
Graphite 4A Cert	-	-	-	-	-	-	-	-	-	-	-
Graphite 14 Meas	-	-	-	-	-	-	-	-	-	-	-
Graphite 14 Cert	-	-	-	-	-	-	-	-	-	-	-
Graphite 14 Meas	-	-	-	-	-	-	-	-	-	-	-
Graphite 14 Cert	-	-	-	-	-	-	-	-	-	-	-
Graphite 14 Meas	-	-	-	-	-	-	-	-	-	-	-
Graphite 14 Cert	-	-	-	-	-	-	-	-	-	-	-

Analyte Symbol	SiO ₂	Al ₂ O ₃	Fe ₂ O _{3(T)}	MnO	MgO	CaO	Na ₂ O	K ₂ O	TiO ₂	P ₂ O ₅	LOI
Unit Symbol	(%)	(%)	(%)	(%)	(%)	(%)	(%)	(%)	(%)	(%)	(%)
Detection Limit	0.01	0.01	0.01	0.001	0.01	0.01	0.01	0.01	0.001	0.01	-
Analysis Method	FUS-ICP	FUS-ICP	FUS-ICP	FUS-ICP	FUS-ICP	FUS-ICP	FUS-ICP	FUS-ICP	FUS-ICP	FUS-ICP	FUS-ICP
BC21 Orig	31.32	7.1	12.81	0.196	14.04	13.72	0.68	1.65	2.934	1.23	13.33
BC21 Dup	31.29	7	12.82	0.196	13.88	13.71	0.68	1.64	2.909	1.26	13.33
BC-22 Orig	-	-	-	-	-	-	-	-	-	-	-
BC-22 Dup	-	-	-	-	-	-	-	-	-	-	-
RO-23 Orig	-	-	-	-	-	-	-	-	-	-	-
RO-23 Dup	-	-	-	-	-	-	-	-	-	-	-
CO-03 Orig	73.71	6.84	4.5	0.058	2.39	3.63	1.32	1.41	0.302	0.32	4.77
CO-03 Dup	74.74	6.87	4.52	0.058	2.4	3.66	1.33	1.41	0.299	0.33	4.77
CO-03 Orig	-	-	-	-	-	-	-	-	-	-	-
CO-03 Dup	-	-	-	-	-	-	-	-	-	-	-
CO-08 Orig	-	-	-	-	-	-	-	-	-	-	-
CO-08 Dup	-	-	-	-	-	-	-	-	-	-	-
CO-10 Orig	-	-	-	-	-	-	-	-	-	-	-
CO-10 Dup	-	-	-	-	-	-	-	-	-	-	-
BC-15 Orig	69.86	15.9	0.64	0.008	0.17	0.18	1.42	11.48	0.071	0.03	0.37
BC-15 Dup	68.82	16.03	0.63	0.008	0.17	0.18	1.39	11.35	0.068	0.04	0.37
Method Blank	-	-	-	-	-	-	-	-	-	-	-
Method Blank	-	-	-	-	-	-	-	-	-	-	-
Method Blank	-	-	-	-	-	-	-	-	-	-	-
Method Blank	-	-	-	-	-	-	-	-	-	-	-
Method Blank	-	-	-	-	-	-	-	-	-	-	-
Method Blank	-	-	-	-	-	-	-	-	-	-	-
Method Blank	-	-	-	-	-	-	-	-	-	-	-
Method Blank	-	-	-	-	-	-	-	-	-	-	-
Method Blank	-	-	-	-	-	-	-	-	-	-	-
Method Blank	-	-	-	-	-	-	-	-	-	-	-

Analyte Symbol	Total (%)	Ba (ppm)	Sr (ppm)	Y (ppm)	Sc (ppm)	Zr (ppm)	Be (ppm)	V (ppm)	C-Graphitic (%)	C-Total (%)	Total S (%)
Unit Symbol	0.01	2	2	1	1	2	1	5	0.05	0.01	0.01
Detection Limit		FUS-ICP	FUS-ICP	FUS-ICP	FUS-ICP	FUS-ICP	FUS-ICP	FUS-ICP	IR	CS	CS
Analysis Method											
NIST 694 Meas	-	-	-	-	-	-	-	1607	-	-	-
NIST 694 Cert	-	-	-	-	-	-	-	1740	-	-	-
NIST 694 Meas	-	-	-	-	-	-	-	-	-	-	-
NIST 694 Cert	-	-	-	-	-	-	-	-	-	-	-
NIST 694 Meas	-	-	-	-	-	-	-	-	-	-	-
NIST 694 Cert	-	-	-	-	-	-	-	-	-	-	-
DNC-1 Meas	-	105	147	15	-	36	-	155	-	-	-
DNC-1 Cert	-	118	144	18	-	38	-	148	-	-	-
DNC-1 Meas	-	-	-	-	-	-	-	-	-	-	-
DNC-1 Cert	-	-	-	-	-	-	-	-	-	-	-
DNC-1 Meas	-	-	-	-	31	-	-	-	-	-	-
DNC-1 Cert	-	-	-	-	31	-	-	-	-	-	-
GBW 07113 Meas	-	492	41	43	-	391	-	5	-	-	-
GBW 07113 Cert	-	506	43	43	-	403	-	5	-	-	-
GBW 07113 Meas	-	-	-	-	-	-	-	-	-	-	-
GBW 07113 Cert	-	-	-	-	-	-	-	-	-	-	-
GBW 07113 Meas	-	-	-	-	5	-	4	-	-	-	-
GBW 07113 Cert	-	-	-	-	5	-	4	-	-	-	-
LKSD-3 Meas	-	-	-	-	-	-	-	-	-	-	-
LKSD-3 Cert	-	-	-	-	-	-	-	-	-	-	-
TDB-1 Meas	-	-	-	-	-	-	-	-	-	-	-
TDB-1 Cert	-	-	-	-	-	-	-	-	-	-	-
BaSO4 Meas	-	-	-	-	-	-	-	-	-	-	14.2
BaSO4 Cert	-	-	-	-	-	-	-	-	-	-	14
BaSO4 Meas	-	-	-	-	-	-	-	-	-	-	13.7
BaSO4 Cert	-	-	-	-	-	-	-	-	-	-	14
BaSO4 Meas	-	-	-	-	-	-	-	-	-	-	13.8
BaSO4 Cert	-	-	-	-	-	-	-	-	-	-	14
W-2a Meas	-	174	205	18	-	90	-	270	-	-	-
W-2a Cert	-	182	190	24	-	94	-	262	-	-	-
W-2a Meas	-	-	-	-	-	-	-	-	-	-	-
W-2a Cert	-	-	-	-	-	-	-	-	-	-	-

Analyte Symbol	Total (%)	Ba (ppm)	Sr (ppm)	Y (ppm)	Sc (ppm)	Zr (ppm)	Be (ppm)	V (ppm)	C-Graphitic (%)	C-Total (%)	Total S (%)
Unit Symbol	0.01	2	2	1	1	2	1	5	0.05	0.01	0.01
Detection Limit											
Analysis Method	FUS-ICP	FUS-ICP	FUS-ICP	FUS-ICP	FUS-ICP	FUS-ICP	FUS-ICP	FUS-ICP	IR	CS	CS
W-2a Meas	-	-	-	-	36	-	< 1	-	-	-	-
W-2a Cert	-	-	-	-	36	-	1.3	-	-	-	-
SY-4 Meas	-	345	1190	115	-	534	-	8	-	-	-
SY-4 Cert	-	340	1191	119	-	517	-	8	-	-	-
SY-4 Meas	-	-	-	-	-	-	-	-	-	-	-
SY-4 Cert	-	-	-	-	-	-	-	-	-	-	-
SY-4 Meas	-	-	-	-	1	-	3	-	-	-	-
SY-4 Cert	-	-	-	-	1.1	-	2.6	-	-	-	-
CTA-AC-1 Meas	-	-	-	-	-	-	-	-	-	-	-
CTA-AC-1 Cert	-	-	-	-	-	-	-	-	-	-	-
BIR-1a Meas	-	7	109	13	-	14	-	325	-	-	-
BIR-1a Cert	-	6	110	16	-	18	-	310	-	-	-
BIR-1a Meas	-	-	-	-	-	-	-	-	-	-	-
BIR-1a Cert	-	-	-	-	-	-	-	-	-	-	-
BIR-1a Meas	-	-	-	-	43	-	< 1	-	-	-	-
BIR-1a Cert	-	-	-	-	44	-	0.58	-	-	-	-
NCS DC86312 Meas	-	-	-	-	-	-	-	-	-	-	-
NCS DC86312 Cert	-	-	-	-	-	-	-	-	-	-	-
JGb-2 Meas	-	-	-	-	-	-	-	-	-	-	-
JGb-2 Cert	-	-	-	-	-	-	-	-	-	-	-
JGb-2 Meas	-	-	-	-	-	-	-	-	-	-	-
JGb-2 Cert	-	-	-	-	-	-	-	-	-	-	-
JGb-2 Meas	-	-	-	-	-	-	-	-	-	-	-
JGb-2 Cert	-	-	-	-	-	-	-	-	-	-	-
NCS DC70009 (GBW07241) Meas	-	-	-	-	-	-	-	-	-	-	-
NCS DC70009 (GBW07241) Cert	-	-	-	-	-	-	-	-	-	-	-
SGR-1b Meas	-	-	-	-	-	-	-	-	-	27.7	1.52
SGR-1b Cert	-	-	-	-	-	-	-	-	-	28	1.53
SGR-1b Meas	-	-	-	-	-	-	-	-	-	28.1	1.56
SGR-1b Cert	-	-	-	-	-	-	-	-	-	28	1.53
SGR-1b Meas	-	-	-	-	-	-	-	-	-	27.4	1.55
SGR-1b Cert	-	-	-	-	-	-	-	-	-	28	1.53

Analyte Symbol	Total (%)	Ba (ppm)	Sr (ppm)	Y (ppm)	Sc (ppm)	Zr (ppm)	Be (ppm)	V (ppm)	C-Graphitic (%)	C-Total (%)	Total S (%)
Unit Symbol	0.01	2	2	1	1	2	1	5	0.05	0.01	0.01
Detection Limit		FUS-ICP	FUS-ICP	FUS-ICP	FUS-ICP	FUS-ICP	FUS-ICP	FUS-ICP	IR	CS	CS
Analysis Method											
OREAS 100a (Fusion) Meas	-	-	-	-	-	-	-	-	-	-	-
OREAS 100a (Fusion) Cert	-	-	-	-	-	-	-	-	-	-	-
OREAS 101a (Fusion) Meas	-	-	-	-	-	-	-	-	-	-	-
OREAS 101a (Fusion) Cert	-	-	-	-	-	-	-	-	-	-	-
OREAS 101b (Fusion) Meas	-	-	-	-	-	-	-	-	-	-	-
OREAS 101b (Fusion) Cert	-	-	-	-	-	-	-	-	-	-	-
JR-1 Meas	-	-	-	-	-	-	-	-	-	-	-
JR-1 Cert	-	-	-	-	-	-	-	-	-	-	-
GS311-4 Meas	-	-	-	-	-	-	-	-	-	1.11	0.55
GS311-4 Cert	-	-	-	-	-	-	-	-	-	1.11	0.54
GS311-4 Meas	-	-	-	-	-	-	-	-	-	1.1	0.55
GS311-4 Cert	-	-	-	-	-	-	-	-	-	1.11	0.54
GS311-4 Meas	-	-	-	-	-	-	-	-	-	1.1	0.54
GS311-4 Cert	-	-	-	-	-	-	-	-	-	1.11	0.54
GS900-5 Meas	-	-	-	-	-	-	-	-	-	0.62	0.33
GS900-5 Cert	-	-	-	-	-	-	-	-	-	0.65	0.34
GS900-5 Meas	-	-	-	-	-	-	-	-	-	0.64	0.34
GS900-5 Cert	-	-	-	-	-	-	-	-	-	0.65	0.34
Graphite 4A Meas	-	-	-	-	-	-	-	-	4.01	-	-
Graphite 4A Cert	-	-	-	-	-	-	-	-	4.18	-	-
Graphite 4A Meas	-	-	-	-	-	-	-	-	3.96	-	-
Graphite 4A Cert	-	-	-	-	-	-	-	-	4.18	-	-
Graphite 4A Meas	-	-	-	-	-	-	-	-	4.01	-	-
Graphite 4A Cert	-	-	-	-	-	-	-	-	4.18	-	-
Graphite 14 Meas	-	-	-	-	-	-	-	-	14.2	-	-
Graphite 14 Cert	-	-	-	-	-	-	-	-	14.55	-	-
Graphite 14 Meas	-	-	-	-	-	-	-	-	14.2	-	-
Graphite 14 Cert	-	-	-	-	-	-	-	-	14.55	-	-
Graphite 14 Meas	-	-	-	-	-	-	-	-	14.4	-	-
Graphite 14 Cert	-	-	-	-	-	-	-	-	14.55	-	-

Analyte Symbol	Total (%)	Ba (ppm)	Sr (ppm)	Y (ppm)	Sc (ppm)	Zr (ppm)	Be (ppm)	V (ppm)	C-Graphitic (%)	C-Total (%)	Total S (%)
Unit Symbol											
Detection Limit	0.01	2	2	1	1	2	1	5	0.05	0.01	0.01
Analysis Method	FUS-ICP	FUS-ICP	FUS-ICP	FUS-ICP	FUS-ICP	FUS-ICP	FUS-ICP	FUS-ICP	IR	CS	CS
BC21 Orig	99.01	1070	685	35	23	356	3	274	-	-	-
BC21 Dup	98.72	1069	675	34	23	356	3	272	-	-	-
BC-22 Orig	-	-	-	-	-	-	-	-	3.38	3.51	1.66
BC-22 Dup	-	-	-	-	-	-	-	-	3.36	3.57	1.72
RO-23 Orig	-	-	-	-	-	-	-	-	1.64	1.79	2.41
RO-23 Dup	-	-	-	-	-	-	-	-	1.67	1.82	2.41
CO-03 Orig	99.24	-	-	-	8	-	1	-	-	-	-
CO-03 Dup	100.4	-	-	-	8	-	1	-	-	-	-
CO-03 Orig	-	-	-	-	-	-	-	-	-	-	-
CO-03 Dup	-	-	-	-	-	-	-	-	-	-	-
CO-08 Orig	-	-	-	-	-	-	-	-	1.03	1.12	1.95
CO-08 Dup	-	-	-	-	-	-	-	-	1.02	1.12	1.97
CO-10 Orig	-	-	-	-	-	-	-	-	-	-	-
CO-10 Dup	-	-	-	-	-	-	-	-	-	-	-
BC-15 Orig	100.1	-	-	-	< 1	-	< 1	-	-	-	-
BC-15 Dup	99.04	-	-	-	< 1	-	< 1	-	-	-	-
Method Blank	-	-	-	-	-	-	-	-	-	-	-
Method Blank	-	-	-	-	-	-	-	-	-	-	-
Method Blank	-	-	-	-	-	-	-	-	-	-	-
Method Blank	-	-	-	-	-	-	-	-	-	-	-
Method Blank	-	-	-	-	-	-	-	-	< 0.05	-	-
Method Blank	-	-	-	-	-	-	-	-	< 0.05	-	-
Method Blank	-	-	-	-	-	-	-	-	-	-	-
Method Blank	-	-	-	-	-	-	-	-	< 0.05	-	-

Analyte Symbol	FeO	V	Cr	Co	Ni	Cu	Zn	Ga	Ge	As	Rb
Unit Symbol	(%)	(ppm)	(ppm)	(ppm)	(ppm)	(ppm)	(ppm)	(ppm)	(ppm)	(ppm)	(ppm)
Detection Limit	0.1	5	20	1	20	10	30	1	0.5	5	1
Analysis Method	TITR	FUS-ICP	FUS-MS								
NIST 694 Meas	-	-	-	-	-	-	-	-	-	-	-
NIST 694 Cert	-	-	-	-	-	-	-	-	-	-	-
NIST 694 Meas	-	1607	-	-	-	-	-	-	-	-	-
NIST 694 Cert	-	1740	-	-	-	-	-	-	-	-	-
NIST 694 Meas	-	-	-	-	-	-	-	-	-	-	-
NIST 694 Cert	-	-	-	-	-	-	-	-	-	-	-
DNC-1 Meas	-	-	-	-	-	-	-	-	-	-	-
DNC-1 Cert	-	-	-	-	-	-	-	-	-	-	-
DNC-1 Meas	-	155	280	58	250	100	70	15	-	-	-
DNC-1 Cert	-	148	270	57	247	100	70	15	-	-	-
DNC-1 Meas	-	-	-	-	-	-	-	-	-	-	-
DNC-1 Cert	-	-	-	-	-	-	-	-	-	-	-
GBW 07113 Meas	1.8	-	-	-	-	-	-	-	-	-	-
GBW 07113 Cert	1.86	-	-	-	-	-	-	-	-	-	-
GBW 07113 Meas	-	5	-	-	-	-	-	-	-	-	-
GBW 07113 Cert	-	5	-	-	-	-	-	-	-	-	-
GBW 07113 Meas	-	-	-	-	-	-	-	-	-	-	-
GBW 07113 Cert	-	-	-	-	-	-	-	-	-	-	-
LKSD-3 Meas	-	-	90	31	50	30	150	-	-	26	75
LKSD-3 Cert	-	-	87	30	47	35	152	-	-	27	78
TDB-1 Meas	-	-	240	-	80	340	160	-	-	-	21
TDB-1 Cert	-	-	251	-	92	323	155	-	-	-	23
BaSO4 Meas	-	-	-	-	-	-	-	-	-	-	-
BaSO4 Cert	-	-	-	-	-	-	-	-	-	-	-
BaSO4 Meas	-	-	-	-	-	-	-	-	-	-	-
BaSO4 Cert	-	-	-	-	-	-	-	-	-	-	-
BaSO4 Meas	-	-	-	-	-	-	-	-	-	-	-
BaSO4 Cert	-	-	-	-	-	-	-	-	-	-	-
W-2a Meas	-	-	-	-	-	-	-	-	-	-	-
W-2a Cert	-	-	-	-	-	-	-	-	-	-	-
W-2a Meas	-	270	100	43	70	110	80	18	1.3	-	20
W-2a Cert	-	262	92	43	70	110	80	17	1	-	21

Analyte Symbol	FeO	V	Cr	Co	Ni	Cu	Zn	Ga	Ge	As	Rb
Unit Symbol	(%)	(ppm)	(ppm)	(ppm)	(ppm)	(ppm)	(ppm)	(ppm)	(ppm)	(ppm)	(ppm)
Detection Limit	0.1	5	20	1	20	10	30	1	0.5	5	1
Analysis Method	TITR	FUS-ICP	FUS-MS								
W-2a Meas	-	-	-	-	-	-	-	-	-	-	-
W-2a Cert	-	-	-	-	-	-	-	-	-	-	-
SY-4 Meas	2.9	-	-	-	-	-	-	-	-	-	-
SY-4 Cert	2.86	-	-	-	-	-	-	-	-	-	-
SY-4 Meas	-	8	-	-	-	-	-	-	-	-	-
SY-4 Cert	-	8	-	-	-	-	-	-	-	-	-
SY-4 Meas	-	-	-	-	-	-	-	-	-	-	-
SY-4 Cert	-	-	-	-	-	-	-	-	-	-	-
CTA-AC-1 Meas	-	-	-	-	-	60	40	-	-	-	-
CTA-AC-1 Cert	-	-	-	-	-	54	38	-	-	-	-
BIR-1a Meas	8.4	-	-	-	-	-	-	-	-	-	-
BIR-1a Cert	8.34	-	-	-	-	-	-	-	-	-	-
BIR-1a Meas	-	325	380	53	180	130	80	16	-	-	-
BIR-1a Cert	-	310	370	52	170	125	70	16	-	-	-
BIR-1a Meas	-	-	-	-	-	-	-	-	-	-	-
BIR-1a Cert	-	-	-	-	-	-	-	-	-	-	-
NCS DC86312 Meas	-	-	-	-	-	-	-	-	-	-	-
NCS DC86312 Cert	-	-	-	-	-	-	-	-	-	-	-
JGb-2 Meas	5.1	-	-	-	-	-	-	-	-	-	-
JGb-2 Cert	5.41	-	-	-	-	-	-	-	-	-	-
JGb-2 Meas	5.2	-	-	-	-	-	-	-	-	-	-
JGb-2 Cert	5.41	-	-	-	-	-	-	-	-	-	-
JGb-2 Meas	5.2	-	-	-	-	-	-	-	-	-	-
JGb-2 Cert	5.41	-	-	-	-	-	-	-	-	-	-
NCS DC70009 (GBW07241) Meas	-	-	-	-	-	990	100	17	10.5	63	502
NCS DC70009 (GBW07241) Cert	-	-	-	-	-	960	100	16.5	11.2	69.9	500
SGR-1b Meas	-	-	-	-	-	-	-	-	-	-	-
SGR-1b Cert	-	-	-	-	-	-	-	-	-	-	-
SGR-1b Meas	-	-	-	-	-	-	-	-	-	-	-
SGR-1b Cert	-	-	-	-	-	-	-	-	-	-	-
SGR-1b Meas	-	-	-	-	-	-	-	-	-	-	-
SGR-1b Cert	-	-	-	-	-	-	-	-	-	-	-

Analyte Symbol	FeO	V	Cr	Co	Ni	Cu	Zn	Ga	Ge	As	Rb
Unit Symbol	(%)	(ppm)	(ppm)	(ppm)	(ppm)	(ppm)	(ppm)	(ppm)	(ppm)	(ppm)	(ppm)
Detection Limit	0.1	5	20	1	20	10	30	1	0.5	5	1
Analysis Method	TITR	FUS-ICP	FUS-MS								
OREAS 100a (Fusion) Meas	-	-	-	17	-	180	-	-	-	-	-
OREAS 100a (Fusion) Cert	-	-	-	18.1	-	169	-	-	-	-	-
OREAS 101a (Fusion) Meas	-	-	-	48	-	440	-	-	-	-	-
OREAS 101a (Fusion) Cert	-	-	-	48.8	-	434	-	-	-	-	-
OREAS 101b (Fusion) Meas	-	-	-	45	-	420	-	-	-	-	-
OREAS 101b (Fusion) Cert	-	-	-	47	-	416	-	-	-	-	-
JR-1 Meas	-	-	-	-	< 20	-	30	17	2	17	253
JR-1 Cert	-	-	-	-	1.67	-	30.6	16.1	1.88	16.3	257
GS311-4 Meas	-	-	-	-	-	-	-	-	-	-	-
GS311-4 Cert	-	-	-	-	-	-	-	-	-	-	-
GS311-4 Meas	-	-	-	-	-	-	-	-	-	-	-
GS311-4 Cert	-	-	-	-	-	-	-	-	-	-	-
GS311-4 Meas	-	-	-	-	-	-	-	-	-	-	-
GS311-4 Cert	-	-	-	-	-	-	-	-	-	-	-
GS900-5 Meas	-	-	-	-	-	-	-	-	-	-	-
GS900-5 Cert	-	-	-	-	-	-	-	-	-	-	-
GS900-5 Meas	-	-	-	-	-	-	-	-	-	-	-
GS900-5 Cert	-	-	-	-	-	-	-	-	-	-	-
Graphite 4A Meas	-	-	-	-	-	-	-	-	-	-	-
Graphite 4A Cert	-	-	-	-	-	-	-	-	-	-	-
Graphite 4A Meas	-	-	-	-	-	-	-	-	-	-	-
Graphite 4A Cert	-	-	-	-	-	-	-	-	-	-	-
Graphite 4A Meas	-	-	-	-	-	-	-	-	-	-	-
Graphite 4A Cert	-	-	-	-	-	-	-	-	-	-	-
Graphite 14 Meas	-	-	-	-	-	-	-	-	-	-	-
Graphite 14 Cert	-	-	-	-	-	-	-	-	-	-	-
Graphite 14 Meas	-	-	-	-	-	-	-	-	-	-	-
Graphite 14 Cert	-	-	-	-	-	-	-	-	-	-	-
Graphite 14 Meas	-	-	-	-	-	-	-	-	-	-	-
Graphite 14 Cert	-	-	-	-	-	-	-	-	-	-	-

Analyte Symbol	FeO	V	Cr	Co	Ni	Cu	Zn	Ga	Ge	As	Rb
Unit Symbol	(%)	(ppm)	(ppm)	(ppm)	(ppm)	(ppm)	(ppm)	(ppm)	(ppm)	(ppm)	(ppm)
Detection Limit	0.1	5	20	1	20	10	30	1	0.5	5	1
Analysis Method	TITR	FUS-ICP	FUS-MS								
BC21 Orig	-	-	-	-	-	-	-	-	-	-	-
BC21 Dup	-	-	-	-	-	-	-	-	-	-	-
BC-22 Orig	-	-	-	-	-	-	-	-	-	-	-
BC-22 Dup	-	-	-	-	-	-	-	-	-	-	-
RO-23 Orig	-	-	-	-	-	-	-	-	-	-	-
RO-23 Dup	-	-	-	-	-	-	-	-	-	-	-
CO-03 Orig	-	176	190	9	70	50	130	7	1	< 5	63
CO-03 Dup	-	178	190	9	70	50	120	8	0.9	< 5	64
CO-03 Orig	-	-	180	10	70	50	130	10	0.5	< 5	62
CO-03 Dup	-	-	180	9	60	50	120	9	0.6	< 5	60
CO-08 Orig	-	-	-	-	-	-	-	-	-	-	-
CO-08 Dup	-	-	-	-	-	-	-	-	-	-	-
CO-10 Orig	3.2	-	-	-	-	-	-	-	-	-	-
CO-10 Dup	3.1	-	-	-	-	-	-	-	-	-	-
BC-15 Orig	-	8	20	1	< 20	< 10	240	12	0.7	< 5	168
BC-15 Dup	-	9	20	1	< 20	< 10	230	13	0.7	< 5	170
Method Blank	< 0.1	-	-	-	-	-	-	-	-	-	-
Method Blank	< 0.1	-	-	-	-	-	-	-	-	-	-
Method Blank	< 0.1	-	-	-	-	-	-	-	-	-	-
Method Blank	< 0.1	-	-	-	-	-	-	-	-	-	-
Method Blank	-	-	< 20	< 1	< 20	< 10	< 30	< 1	< 0.5	< 5	< 1
Method Blank	-	-	-	-	-	-	-	-	-	-	-
Method Blank	-	-	-	-	-	-	-	-	-	-	-
Method Blank	< 0.1	-	-	-	-	-	-	-	-	-	-
Method Blank	-	-	-	-	-	-	-	-	-	-	-

Analyte Symbol	Sr (ppm)	Y (ppm)	Zr (ppm)	Nb (ppm)	Mo (ppm)	Ag (ppm)	In (ppm)	Sn (ppm)	Sb (ppm)	Cs (ppm)	Ba (ppm)
Unit Symbol	2	0.5	1	0.2	2	0.5	0.1	1	0.2	0.1	2
Detection Limit	FUS-ICP	FUS-MS	FUS-ICP	FUS-MS	FUS-ICP						
Analysis Method											
NIST 694 Meas	-	-	-	-	-	-	-	-	-	-	-
NIST 694 Cert	-	-	-	-	-	-	-	-	-	-	-
NIST 694 Meas	-	-	-	-	-	-	-	-	-	-	-
NIST 694 Cert	-	-	-	-	-	-	-	-	-	-	-
NIST 694 Meas	-	-	-	-	-	-	-	-	-	-	-
NIST 694 Cert	-	-	-	-	-	-	-	-	-	-	-
DNC-1 Meas	-	-	-	-	-	-	-	-	-	-	-
DNC-1 Cert	-	-	-	-	-	-	-	-	-	-	-
DNC-1 Meas	147	16.8	36	-	-	-	-	-	0.9	-	105
DNC-1 Cert	144	18	38	-	-	-	-	-	0.96	-	118
DNC-1 Meas	-	-	-	-	-	-	-	-	-	-	-
DNC-1 Cert	-	-	-	-	-	-	-	-	-	-	-
GBW 07113 Meas	-	-	-	-	-	-	-	-	-	-	-
GBW 07113 Cert	-	-	-	-	-	-	-	-	-	-	-
GBW 07113 Meas	41	-	391	-	-	-	-	-	-	-	492
GBW 07113 Cert	43	-	403	-	-	-	-	-	-	-	506
GBW 07113 Meas	-	-	-	-	-	-	-	-	-	-	-
GBW 07113 Cert	-	-	-	-	-	-	-	-	-	-	-
LKSD-3 Meas	-	28	-	-	< 2	2	-	2	-	2.4	-
LKSD-3 Cert	-	30	-	-	2	2.7	-	3	-	2.3	-
TDB-1 Meas	-	36.4	-	-	-	-	-	-	-	-	-
TDB-1 Cert	-	36	-	-	-	-	-	-	-	-	-
BaSO4 Meas	-	-	-	-	-	-	-	-	-	-	-
BaSO4 Cert	-	-	-	-	-	-	-	-	-	-	-
BaSO4 Meas	-	-	-	-	-	-	-	-	-	-	-
BaSO4 Cert	-	-	-	-	-	-	-	-	-	-	-
BaSO4 Meas	-	-	-	-	-	-	-	-	-	-	-
BaSO4 Cert	-	-	-	-	-	-	-	-	-	-	-
W-2a Meas	-	-	-	-	-	-	-	-	-	-	-
W-2a Cert	-	-	-	-	-	-	-	-	-	-	-
W-2a Meas	205	21.1	90	7.2	< 2	-	-	-	-	0.9	174
W-2a Cert	190	24	94	7.9	0.6	-	-	-	-	0.99	182

Analyte Symbol	Sr (ppm)	Y (ppm)	Zr (ppm)	Nb (ppm)	Mo (ppm)	Ag (ppm)	In (ppm)	Sn (ppm)	Sb (ppm)	Cs (ppm)	Ba (ppm)
Unit Symbol	2	0.5	1	0.2	2	0.5	0.1	1	0.2	0.1	2
Detection Limit	FUS-ICP	FUS-MS	FUS-ICP	FUS-MS	FUS-ICP						
Analysis Method											
W-2a Meas	-	-	-	-	-	-	-	-	-	-	-
W-2a Cert	-	-	-	-	-	-	-	-	-	-	-
SY-4 Meas	-	-	-	-	-	-	-	-	-	-	-
SY-4 Cert	-	-	-	-	-	-	-	-	-	-	-
SY-4 Meas	1190	-	534	-	-	-	-	-	-	-	345
SY-4 Cert	1191	-	517	-	-	-	-	-	-	-	340
SY-4 Meas	-	-	-	-	-	-	-	-	-	-	-
SY-4 Cert	-	-	-	-	-	-	-	-	-	-	-
CTA-AC-1 Meas	-	280	-	-	-	-	-	-	-	-	-
CTA-AC-1 Cert	-	272	-	-	-	-	-	-	-	-	-
BIR-1a Meas	-	-	-	-	-	-	-	-	-	-	-
BIR-1a Cert	-	-	-	-	-	-	-	-	-	-	-
BIR-1a Meas	109	15.3	14	-	-	-	-	-	-	-	7
BIR-1a Cert	110	16	18	-	-	-	-	-	-	-	6
BIR-1a Meas	-	-	-	-	-	-	-	-	-	-	-
BIR-1a Cert	-	-	-	-	-	-	-	-	-	-	-
NCS DC86312 Meas	-	988	-	-	-	-	-	-	-	-	-
NCS DC86312 Cert	-	976	-	-	-	-	-	-	-	-	-
JGb-2 Meas	-	-	-	-	-	-	-	-	-	-	-
JGb-2 Cert	-	-	-	-	-	-	-	-	-	-	-
JGb-2 Meas	-	-	-	-	-	-	-	-	-	-	-
JGb-2 Cert	-	-	-	-	-	-	-	-	-	-	-
JGb-2 Meas	-	-	-	-	-	-	-	-	-	-	-
JGb-2 Cert	-	-	-	-	-	-	-	-	-	-	-
NCS DC70009 (GBW07241) Meas	-	139	-	-	-	1.6	1	> 1000	3.4	42	-
NCS DC70009 (GBW07241) Cert	-	128	-	-	-	1.8	1.3	1701	3.1	41	-
SGR-1b Meas	-	-	-	-	-	-	-	-	-	-	-
SGR-1b Cert	-	-	-	-	-	-	-	-	-	-	-
SGR-1b Meas	-	-	-	-	-	-	-	-	-	-	-
SGR-1b Cert	-	-	-	-	-	-	-	-	-	-	-
SGR-1b Meas	-	-	-	-	-	-	-	-	-	-	-
SGR-1b Cert	-	-	-	-	-	-	-	-	-	-	-

Analyte Symbol	Sr (ppm)	Y (ppm)	Zr (ppm)	Nb (ppm)	Mo (ppm)	Ag (ppm)	In (ppm)	Sn (ppm)	Sb (ppm)	Cs (ppm)	Ba (ppm)
Unit Symbol	2	0.5	1	0.2	2	0.5	0.1	1	0.2	0.1	2
Detection Limit	FUS-ICP	FUS-MS	FUS-ICP	FUS-MS	FUS-ICP						
Analysis Method											
OREAS 100a (Fusion) Meas	-	138	-	-	25	-	-	-	-	-	-
OREAS 100a (Fusion) Cert	-	142	-	-	24.1	-	-	-	-	-	-
OREAS 101a (Fusion) Meas	-	177	-	-	21	-	-	-	-	-	-
OREAS 101a (Fusion) Cert	-	183	-	-	21.9	-	-	-	-	-	-
OREAS 101b (Fusion) Meas	-	176	-	-	20	-	-	-	-	-	-
OREAS 101b (Fusion) Cert	-	178	-	-	20.9	-	-	-	-	-	-
JR-1 Meas	-	44.3	-	14.4	3	-	< 0.1	3	-	20.8	-
JR-1 Cert	-	45.1	-	15.2	3.25	-	0.028	2.86	-	20.8	-
GS311-4 Meas	-	-	-	-	-	-	-	-	-	-	-
GS311-4 Cert	-	-	-	-	-	-	-	-	-	-	-
GS311-4 Meas	-	-	-	-	-	-	-	-	-	-	-
GS311-4 Cert	-	-	-	-	-	-	-	-	-	-	-
GS311-4 Meas	-	-	-	-	-	-	-	-	-	-	-
GS311-4 Cert	-	-	-	-	-	-	-	-	-	-	-
GS900-5 Meas	-	-	-	-	-	-	-	-	-	-	-
GS900-5 Cert	-	-	-	-	-	-	-	-	-	-	-
GS900-5 Meas	-	-	-	-	-	-	-	-	-	-	-
GS900-5 Cert	-	-	-	-	-	-	-	-	-	-	-
Graphite 4A Meas	-	-	-	-	-	-	-	-	-	-	-
Graphite 4A Cert	-	-	-	-	-	-	-	-	-	-	-
Graphite 4A Meas	-	-	-	-	-	-	-	-	-	-	-
Graphite 4A Cert	-	-	-	-	-	-	-	-	-	-	-
Graphite 14 Meas	-	-	-	-	-	-	-	-	-	-	-
Graphite 14 Cert	-	-	-	-	-	-	-	-	-	-	-
Graphite 14 Meas	-	-	-	-	-	-	-	-	-	-	-
Graphite 14 Cert	-	-	-	-	-	-	-	-	-	-	-
Graphite 14 Meas	-	-	-	-	-	-	-	-	-	-	-
Graphite 14 Cert	-	-	-	-	-	-	-	-	-	-	-

Analyte Symbol	Sr (ppm)	Y (ppm)	Zr (ppm)	Nb (ppm)	Mo (ppm)	Ag (ppm)	In (ppm)	Sn (ppm)	Sb (ppm)	Cs (ppm)	Ba (ppm)
Unit Symbol	2	0.5	1	0.2	2	0.5	0.1	1	0.2	0.1	2
Detection Limit	FUS-ICP	FUS-MS	FUS-ICP	FUS-MS	FUS-ICP						
Analysis Method											
BC21 Orig	-	-	-	-	-	-	-	-	-	-	-
BC21 Dup	-	-	-	-	-	-	-	-	-	-	-
BC-22 Orig	-	-	-	-	-	-	-	-	-	-	-
BC-22 Dup	-	-	-	-	-	-	-	-	-	-	-
RO-23 Orig	-	-	-	-	-	-	-	-	-	-	-
RO-23 Dup	-	-	-	-	-	-	-	-	-	-	-
CO-03 Orig	84	24	95	3.3	19	< 0.5	< 0.1	< 1	< 0.2	3.1	166
CO-03 Dup	85	24.2	101	3.9	20	< 0.5	< 0.1	< 1	< 0.2	3.2	164
CO-03 Orig	-	23.8	-	3.5	19	< 0.5	< 0.1	< 1	< 0.2	3	-
CO-03 Dup	-	23.6	-	3.4	18	< 0.5	< 0.1	< 1	< 0.2	3	-
CO-08 Orig	-	-	-	-	-	-	-	-	-	-	-
CO-08 Dup	-	-	-	-	-	-	-	-	-	-	-
CO-10 Orig	-	-	-	-	-	-	-	-	-	-	-
CO-10 Dup	-	-	-	-	-	-	-	-	-	-	-
BC-15 Orig	615	1.6	7	1.2	33	< 0.5	< 0.1	< 1	< 0.2	1	5565
BC-15 Dup	604	1.8	6	1.1	33	< 0.5	< 0.1	< 1	< 0.2	1	5519
Method Blank	-	-	-	-	-	-	-	-	-	-	-
Method Blank	-	-	-	-	-	-	-	-	-	-	-
Method Blank	-	-	-	-	-	-	-	-	-	-	-
Method Blank	-	-	-	-	-	-	-	-	-	-	-
Method Blank	-	< 0.5	-	< 0.2	< 2	< 0.5	< 0.1	< 1	< 0.2	< 0.1	-
Method Blank	-	-	-	-	-	-	-	-	-	-	-
Method Blank	-	-	-	-	-	-	-	-	-	-	-
Method Blank	-	-	-	-	-	-	-	-	-	-	-
Method Blank	-	-	-	-	-	-	-	-	-	-	-

Analyte Symbol	La (ppm)	Ce (ppm)	Pr (ppm)	Nd (ppm)	Sm (ppm)	Eu (ppm)	Gd (ppm)	Tb (ppm)	Dy (ppm)	Ho (ppm)	Er (ppm)
Unit Symbol	0.05	0.05	0.01	0.05	0.01	0.005	0.01	0.01	0.01	0.01	0.01
Detection Limit	FUS-MS										
Analysis Method											
NIST 694 Meas	-	-	-	-	-	-	-	-	-	-	-
NIST 694 Cert	-	-	-	-	-	-	-	-	-	-	-
NIST 694 Meas	-	-	-	-	-	-	-	-	-	-	-
NIST 694 Cert	-	-	-	-	-	-	-	-	-	-	-
NIST 694 Meas	-	-	-	-	-	-	-	-	-	-	-
NIST 694 Cert	-	-	-	-	-	-	-	-	-	-	-
DNC-1 Meas	-	-	-	-	-	-	-	-	-	-	-
DNC-1 Cert	-	-	-	-	-	-	-	-	-	-	-
DNC-1 Meas	3.9	-	-	4.9	-	0.6	-	-	-	-	-
DNC-1 Cert	3.6	-	-	5.2	-	0.59	-	-	-	-	-
DNC-1 Meas	-	-	-	-	-	-	-	-	-	-	-
DNC-1 Cert	-	-	-	-	-	-	-	-	-	-	-
GBW 07113 Meas	-	-	-	-	-	-	-	-	-	-	-
GBW 07113 Cert	-	-	-	-	-	-	-	-	-	-	-
GBW 07113 Meas	-	-	-	-	-	-	-	-	-	-	-
GBW 07113 Cert	-	-	-	-	-	-	-	-	-	-	-
GBW 07113 Meas	-	-	-	-	-	-	-	-	-	-	-
GBW 07113 Cert	-	-	-	-	-	-	-	-	-	-	-
LKSD-3 Meas	48.9	94.2	-	44.6	8	1.5	-	-	5	-	-
LKSD-3 Cert	52	90	-	44	8	1.5	-	-	4.9	-	-
TDB-1 Meas	18.1	41.3	-	25.2	-	2.2	-	-	-	-	-
TDB-1 Cert	17	41	-	23	-	2.1	-	-	-	-	-
BaSO4 Meas	-	-	-	-	-	-	-	-	-	-	-
BaSO4 Cert	-	-	-	-	-	-	-	-	-	-	-
BaSO4 Meas	-	-	-	-	-	-	-	-	-	-	-
BaSO4 Cert	-	-	-	-	-	-	-	-	-	-	-
BaSO4 Meas	-	-	-	-	-	-	-	-	-	-	-
BaSO4 Cert	-	-	-	-	-	-	-	-	-	-	-
W-2a Meas	-	-	-	-	-	-	-	-	-	-	-
W-2a Cert	-	-	-	-	-	-	-	-	-	-	-
W-2a Meas	10.6	25	-	13.6	3.4	1.1	-	0.63	3.9	0.79	2.3
W-2a Cert	10	23	-	13	3.3	1	-	0.63	3.6	0.76	2.5

Analyte Symbol	La (ppm)	Ce (ppm)	Pr (ppm)	Nd (ppm)	Sm (ppm)	Eu (ppm)	Gd (ppm)	Tb (ppm)	Dy (ppm)	Ho (ppm)	Er (ppm)
Unit Symbol	0.05	0.05	0.01	0.05	0.01	0.005	0.01	0.01	0.01	0.01	0.01
Detection Limit											
Analysis Method	FUS-MS										
W-2a Meas	-	-	-	-	-	-	-	-	-	-	-
W-2a Cert	-	-	-	-	-	-	-	-	-	-	-
SY-4 Meas	-	-	-	-	-	-	-	-	-	-	-
SY-4 Cert	-	-	-	-	-	-	-	-	-	-	-
SY-4 Meas	-	-	-	-	-	-	-	-	-	-	-
SY-4 Cert	-	-	-	-	-	-	-	-	-	-	-
SY-4 Meas	-	-	-	-	-	-	-	-	-	-	-
SY-4 Cert	-	-	-	-	-	-	-	-	-	-	-
CTA-AC-1 Meas	> 2000	> 3000	-	1170	166	46.9	133	14.6	-	-	-
CTA-AC-1 Cert	2176	3326	-	1087	162	46.7	124	13.9	-	-	-
BIR-1a Meas	-	-	-	-	-	-	-	-	-	-	-
BIR-1a Cert	-	-	-	-	-	-	-	-	-	-	-
BIR-1a Meas	0.7	2	-	2.6	1.1	0.53	1.9	-	-	-	-
BIR-1a Cert	0.63	1.9	-	2.5	1.1	0.55	2.0	-	-	-	-
BIR-1a Meas	-	-	-	-	-	-	-	-	-	-	-
BIR-1a Cert	-	-	-	-	-	-	-	-	-	-	-
NCS DC86312 Meas	> 2000	177	-	1600	-	-	240	31.3	185	35.1	101
NCS DC86312 Cert	2360	190	-	1600	-	-	225.0	34.6	183	36	96.2
JGb-2 Meas	-	-	-	-	-	-	-	-	-	-	-
JGb-2 Cert	-	-	-	-	-	-	-	-	-	-	-
JGb-2 Meas	-	-	-	-	-	-	-	-	-	-	-
JGb-2 Cert	-	-	-	-	-	-	-	-	-	-	-
JGb-2 Meas	-	-	-	-	-	-	-	-	-	-	-
JGb-2 Cert	-	-	-	-	-	-	-	-	-	-	-
NCS DC70009 (GBW07241) Meas	23.9	61.1	8	32.4	12.7	-	16.1	3.1	22	4.3	14.3
NCS DC70009 (GBW07241) Cert	23.7	60.3	7.9	32.9	12.5	-	14.8	3.3	20.7	4.5	13.4
SGR-1b Meas	-	-	-	-	-	-	-	-	-	-	-
SGR-1b Cert	-	-	-	-	-	-	-	-	-	-	-
SGR-1b Meas	-	-	-	-	-	-	-	-	-	-	-
SGR-1b Cert	-	-	-	-	-	-	-	-	-	-	-
SGR-1b Meas	-	-	-	-	-	-	-	-	-	-	-
SGR-1b Cert	-	-	-	-	-	-	-	-	-	-	-

Analyte Symbol	La (ppm)	Ce (ppm)	Pr (ppm)	Nd (ppm)	Sm (ppm)	Eu (ppm)	Gd (ppm)	Tb (ppm)	Dy (ppm)	Ho (ppm)	Er (ppm)
Unit Symbol	0.05	0.05	0.01	0.05	0.01	0.005	0.01	0.01	0.01	0.01	0.01
Detection Limit											
Analysis Method	FUS-MS										
OREAS 100a (Fusion) Meas	271	495	48.3	159	25.2	3.82	22.4	3.66	24.2	5.04	16
OREAS 100a (Fusion) Cert	260	463	47.1	152	23.6	3.71	23.6	3.80	23.2	4.81	14.9
OREAS 101a (Fusion) Meas	815	1380	130	402	49.6	8.37	-	-	32.3	6.53	20.1
OREAS 101a (Fusion) Cert	816	1396	134	403	48.8	8.06	-	-	33.3	6.46	19.5
OREAS 101b (Fusion) Meas	811	1370	129	389	50	8.12	-	5.23	31.7	6.34	19.2
OREAS 101b (Fusion) Cert	789	1331	127	378	48	7.77	-	5.37	32.1	6.34	18.7
JR-1 Meas	19.9	48.1	5.9	23.8	5.65	0.31	-	0.96	6.22	-	-
JR-1 Cert	19.7	47.2	5.58	23.3	6.03	0.30	-	1.01	5.69	-	-
GS311-4 Meas	-	-	-	-	-	-	-	-	-	-	-
GS311-4 Cert	-	-	-	-	-	-	-	-	-	-	-
GS311-4 Meas	-	-	-	-	-	-	-	-	-	-	-
GS311-4 Cert	-	-	-	-	-	-	-	-	-	-	-
GS311-4 Meas	-	-	-	-	-	-	-	-	-	-	-
GS311-4 Cert	-	-	-	-	-	-	-	-	-	-	-
GS900-5 Meas	-	-	-	-	-	-	-	-	-	-	-
GS900-5 Cert	-	-	-	-	-	-	-	-	-	-	-
GS900-5 Meas	-	-	-	-	-	-	-	-	-	-	-
GS900-5 Cert	-	-	-	-	-	-	-	-	-	-	-
Graphite 4A Meas	-	-	-	-	-	-	-	-	-	-	-
Graphite 4A Cert	-	-	-	-	-	-	-	-	-	-	-
Graphite 4A Meas	-	-	-	-	-	-	-	-	-	-	-
Graphite 4A Cert	-	-	-	-	-	-	-	-	-	-	-
Graphite 4A Meas	-	-	-	-	-	-	-	-	-	-	-
Graphite 4A Cert	-	-	-	-	-	-	-	-	-	-	-
Graphite 14 Meas	-	-	-	-	-	-	-	-	-	-	-
Graphite 14 Cert	-	-	-	-	-	-	-	-	-	-	-
Graphite 14 Meas	-	-	-	-	-	-	-	-	-	-	-
Graphite 14 Cert	-	-	-	-	-	-	-	-	-	-	-
Graphite 14 Meas	-	-	-	-	-	-	-	-	-	-	-
Graphite 14 Cert	-	-	-	-	-	-	-	-	-	-	-

Analyte Symbol	La (ppm)	Ce (ppm)	Pr (ppm)	Nd (ppm)	Sm (ppm)	Eu (ppm)	Gd (ppm)	Tb (ppm)	Dy (ppm)	Ho (ppm)	Er (ppm)
Unit Symbol	0.05	0.05	0.01	0.05	0.01	0.005	0.01	0.01	0.01	0.01	0.01
Detection Limit	FUS-MS										
Analysis Method											
BC21 Orig	-	-	-	-	-	-	-	-	-	-	-
BC21 Dup	-	-	-	-	-	-	-	-	-	-	-
BC-22 Orig	-	-	-	-	-	-	-	-	-	-	-
BC-22 Dup	-	-	-	-	-	-	-	-	-	-	-
RO-23 Orig	-	-	-	-	-	-	-	-	-	-	-
RO-23 Dup	-	-	-	-	-	-	-	-	-	-	-
CO-03 Orig	26.9	49	6.17	23	4.21	0.938	4.22	0.62	3.68	0.76	2.22
CO-03 Dup	26.5	49	6.44	23.7	4.55	0.927	4.22	0.66	3.7	0.77	2.3
CO-03 Orig	25.5	47.7	6.05	23.1	4.57	0.905	4.11	0.65	3.59	0.71	2.17
CO-03 Dup	25.6	48	6.03	22.9	4.52	0.924	4.27	0.65	3.66	0.73	2.2
CO-08 Orig	-	-	-	-	-	-	-	-	-	-	-
CO-08 Dup	-	-	-	-	-	-	-	-	-	-	-
CO-10 Orig	-	-	-	-	-	-	-	-	-	-	-
CO-10 Dup	-	-	-	-	-	-	-	-	-	-	-
BC-15 Orig	1.53	2.64	0.33	1.33	0.34	0.632	0.32	0.05	0.32	0.06	0.15
BC-15 Dup	1.5	2.61	0.33	1.42	0.33	0.622	0.34	0.05	0.28	0.06	0.16
Method Blank	-	-	-	-	-	-	-	-	-	-	-
Method Blank	-	-	-	-	-	-	-	-	-	-	-
Method Blank	-	-	-	-	-	-	-	-	-	-	-
Method Blank	-	-	-	-	-	-	-	-	-	-	-
Method Blank	< 0.05	< 0.05	< 0.01	< 0.05	< 0.01	< 0.005	< 0.01	< 0.01	< 0.01	< 0.01	< 0.01
Method Blank	-	-	-	-	-	-	-	-	-	-	-
Method Blank	-	-	-	-	-	-	-	-	-	-	-
Method Blank	-	-	-	-	-	-	-	-	-	-	-
Method Blank	-	-	-	-	-	-	-	-	-	-	-

Analyte Symbol	Tm (ppm)	Yb (ppm)	Lu (ppm)	Hf (ppm)	Ta (ppm)	W (ppm)	Tl (ppm)	Pb (ppm)	Bi (ppm)	Th (ppm)	U (ppm)
Unit Symbol	0.005	0.01	0.002	0.1	0.01	0.5	0.05	5	0.1	0.05	0.01
Detection Limit	FUS-MS	FUS-MS	FUS-MS	FUS-MS	FUS-MS	FUS-MS	FUS-MS	FUS-MS	FUS-MS	FUS-MS	FUS-MS
Analysis Method											
NIST 694 Meas	-	-	-	-	-	-	-	-	-	-	-
NIST 694 Cert	-	-	-	-	-	-	-	-	-	-	-
NIST 694 Meas	-	-	-	-	-	-	-	-	-	-	-
NIST 694 Cert	-	-	-	-	-	-	-	-	-	-	-
NIST 694 Meas	-	-	-	-	-	-	-	-	-	-	-
NIST 694 Cert	-	-	-	-	-	-	-	-	-	-	-
DNC-1 Meas	-	-	-	-	-	-	-	-	-	-	-
DNC-1 Cert	-	-	-	-	-	-	-	-	-	-	-
DNC-1 Meas	-	2	-	-	-	-	-	7	-	-	-
DNC-1 Cert	-	2	-	-	-	-	-	6.3	-	-	-
DNC-1 Meas	-	-	-	-	-	-	-	-	-	-	-
DNC-1 Cert	-	-	-	-	-	-	-	-	-	-	-
GBW 07113 Meas	-	-	-	-	-	-	-	-	-	-	-
GBW 07113 Cert	-	-	-	-	-	-	-	-	-	-	-
GBW 07113 Meas	-	-	-	-	-	-	-	-	-	-	-
GBW 07113 Cert	-	-	-	-	-	-	-	-	-	-	-
GBW 07113 Meas	-	-	-	-	-	-	-	-	-	-	-
GBW 07113 Cert	-	-	-	-	-	-	-	-	-	-	-
LKSD-3 Meas	-	2.9	0.43	4.5	0.71	< 0.5	-	-	-	10.7	4.6
LKSD-3 Cert	-	2.7	0.4	4.8	0.7	2	-	-	-	11.4	4.6
TDB-1 Meas	-	3.4	-	-	-	-	-	-	-	-	-
TDB-1 Cert	-	3.4	-	-	-	-	-	-	-	-	-
BaSO4 Meas	-	-	-	-	-	-	-	-	-	-	-
BaSO4 Cert	-	-	-	-	-	-	-	-	-	-	-
BaSO4 Meas	-	-	-	-	-	-	-	-	-	-	-
BaSO4 Cert	-	-	-	-	-	-	-	-	-	-	-
BaSO4 Meas	-	-	-	-	-	-	-	-	-	-	-
BaSO4 Cert	-	-	-	-	-	-	-	-	-	-	-
W-2a Meas	-	-	-	-	-	-	-	-	-	-	-
W-2a Cert	-	-	-	-	-	-	-	-	-	-	-
W-2a Meas	-	2.1	0.33	2.3	0.49	< 0.5	< 0.05	-	< 0.1	2.3	0.53
W-2a Cert	-	2.1	0.33	2.6	0.5	0.3	0.2	-	0.03	2.4	0.53

Analyte Symbol	Tm (ppm)	Yb (ppm)	Lu (ppm)	Hf (ppm)	Ta (ppm)	W (ppm)	Tl (ppm)	Pb (ppm)	Bi (ppm)	Th (ppm)	U (ppm)
Unit Symbol	0.005	0.01	0.002	0.1	0.01	0.5	0.05	5	0.1	0.05	0.01
Detection Limit	FUS-MS	FUS-MS	FUS-MS	FUS-MS	FUS-MS	FUS-MS	FUS-MS	FUS-MS	FUS-MS	FUS-MS	FUS-MS
Analysis Method											
W-2a Meas	-	-	-	-	-	-	-	-	-	-	-
W-2a Cert	-	-	-	-	-	-	-	-	-	-	-
SY-4 Meas	-	-	-	-	-	-	-	-	-	-	-
SY-4 Cert	-	-	-	-	-	-	-	-	-	-	-
SY-4 Meas	-	-	-	-	-	-	-	-	-	-	-
SY-4 Cert	-	-	-	-	-	-	-	-	-	-	-
SY-4 Meas	-	-	-	-	-	-	-	-	-	-	-
SY-4 Cert	-	-	-	-	-	-	-	-	-	-	-
CTA-AC-1 Meas	-	10.9	1.13	-	2.45	-	-	-	-	23.3	4.2
CTA-AC-1 Cert	-	11.4	1.08	-	2.65	-	-	-	-	21.8	4.4
BIR-1a Meas	-	-	-	-	-	-	-	-	-	-	-
BIR-1a Cert	-	-	-	-	-	-	-	-	-	-	-
BIR-1a Meas	-	1.6	0.23	0.6	-	-	-	-	-	-	-
BIR-1a Cert	-	1.7	0.3	0.60	-	-	-	-	-	-	-
BIR-1a Meas	-	-	-	-	-	-	-	-	-	-	-
BIR-1a Cert	-	-	-	-	-	-	-	-	-	-	-
NCS DC86312 Meas	13.6	84.9	12.3	-	-	-	-	-	-	24.6	-
NCS DC86312 Cert	15.1	87.79	11.96	-	-	-	-	-	-	23.6	-
JGb-2 Meas	-	-	-	-	-	-	-	-	-	-	-
JGb-2 Cert	-	-	-	-	-	-	-	-	-	-	-
JGb-2 Meas	-	-	-	-	-	-	-	-	-	-	-
JGb-2 Cert	-	-	-	-	-	-	-	-	-	-	-
JGb-2 Meas	-	-	-	-	-	-	-	-	-	-	-
JGb-2 Cert	-	-	-	-	-	-	-	-	-	-	-
NCS DC70009 (GBW07241) Meas	2.3	16	2.42	-	-	2040	2	-	-	28.8	-
NCS DC70009 (GBW07241) Cert	2.2	14.9	2.4	-	-	2200	1.8	-	-	28.3	-
SGR-1b Meas	-	-	-	-	-	-	-	-	-	-	-
SGR-1b Cert	-	-	-	-	-	-	-	-	-	-	-
SGR-1b Meas	-	-	-	-	-	-	-	-	-	-	-
SGR-1b Cert	-	-	-	-	-	-	-	-	-	-	-
SGR-1b Meas	-	-	-	-	-	-	-	-	-	-	-
SGR-1b Cert	-	-	-	-	-	-	-	-	-	-	-

Analyte Symbol	Tm (ppm)	Yb (ppm)	Lu (ppm)	Hf (ppm)	Ta (ppm)	W (ppm)	Tl (ppm)	Pb (ppm)	Bi (ppm)	Th (ppm)	U (ppm)
Unit Symbol	0.005	0.01	0.002	0.1	0.01	0.5	0.05	5	0.1	0.05	0.01
Detection Limit	FUS-MS	FUS-MS	FUS-MS	FUS-MS	FUS-MS	FUS-MS	FUS-MS	FUS-MS	FUS-MS	FUS-MS	FUS-MS
Analysis Method											
OREAS 100a (Fusion) Meas	2.42	15.9	2.37	-	-	-	-	-	-	53	143
OREAS 100a (Fusion) Cert	2.31	14.9	2.26	-	-	-	-	-	-	51.6	135
OREAS 101a (Fusion) Meas	2.9	18.1	2.55	-	-	-	-	-	-	35.4	424
OREAS 101a (Fusion) Cert	2.90	17.5	2.66	-	-	-	-	-	-	36.6	422
OREAS 101b (Fusion) Meas	2.8	18.1	2.7	-	-	-	-	-	-	37.3	400
OREAS 101b (Fusion) Cert	2.66	17.6	2.58	-	-	-	-	-	-	37.1	396
JR-1 Meas	0.67	4.75	0.71	4.1	1.84	1.6	1.49	19	0.6	25.9	9.2
JR-1 Cert	0.67	4.55	0.71	4.51	1.86	1.59	1.56	19.3	0.56	26.7	8.88
GS311-4 Meas	-	-	-	-	-	-	-	-	-	-	-
GS311-4 Cert	-	-	-	-	-	-	-	-	-	-	-
GS311-4 Meas	-	-	-	-	-	-	-	-	-	-	-
GS311-4 Cert	-	-	-	-	-	-	-	-	-	-	-
GS311-4 Meas	-	-	-	-	-	-	-	-	-	-	-
GS311-4 Cert	-	-	-	-	-	-	-	-	-	-	-
GS900-5 Meas	-	-	-	-	-	-	-	-	-	-	-
GS900-5 Cert	-	-	-	-	-	-	-	-	-	-	-
GS900-5 Meas	-	-	-	-	-	-	-	-	-	-	-
GS900-5 Cert	-	-	-	-	-	-	-	-	-	-	-
Graphite 4A Meas	-	-	-	-	-	-	-	-	-	-	-
Graphite 4A Cert	-	-	-	-	-	-	-	-	-	-	-
Graphite 4A Meas	-	-	-	-	-	-	-	-	-	-	-
Graphite 4A Cert	-	-	-	-	-	-	-	-	-	-	-
Graphite 4A Meas	-	-	-	-	-	-	-	-	-	-	-
Graphite 4A Cert	-	-	-	-	-	-	-	-	-	-	-
Graphite 14 Meas	-	-	-	-	-	-	-	-	-	-	-
Graphite 14 Cert	-	-	-	-	-	-	-	-	-	-	-
Graphite 14 Meas	-	-	-	-	-	-	-	-	-	-	-
Graphite 14 Cert	-	-	-	-	-	-	-	-	-	-	-
Graphite 14 Meas	-	-	-	-	-	-	-	-	-	-	-
Graphite 14 Cert	-	-	-	-	-	-	-	-	-	-	-

Analyte Symbol	Tm (ppm)	Yb (ppm)	Lu (ppm)	Hf (ppm)	Ta (ppm)	W (ppm)	Tl (ppm)	Pb (ppm)	Bi (ppm)	Th (ppm)	U (ppm)
Unit Symbol	0.005	0.01	0.002	0.1	0.01	0.5	0.05	5	0.1	0.05	0.01
Detection Limit	FUS-MS	FUS-MS	FUS-MS	FUS-MS	FUS-MS	FUS-MS	FUS-MS	FUS-MS	FUS-MS	FUS-MS	FUS-MS
Analysis Method											
BC21 Orig	-	-	-	-	-	-	-	-	-	-	-
BC21 Dup	-	-	-	-	-	-	-	-	-	-	-
BC-22 Orig	-	-	-	-	-	-	-	-	-	-	-
BC-22 Dup	-	-	-	-	-	-	-	-	-	-	-
RO-23 Orig	-	-	-	-	-	-	-	-	-	-	-
RO-23 Dup	-	-	-	-	-	-	-	-	-	-	-
CO-03 Orig	0.319	2.15	0.341	2.1	0.42	1	0.42	13	< 0.1	6.65	9.76
CO-03 Dup	0.343	2.17	0.353	2.4	0.45	1.5	0.44	13	< 0.1	6.69	10.2
CO-03 Orig	0.313	2.16	0.349	2.4	0.44	1.4	0.53	7	< 0.1	6.64	9.64
CO-03 Dup	0.336	2.27	0.34	2	0.45	< 0.5	0.52	8	< 0.1	6.83	10.8
CO-08 Orig	-	-	-	-	-	-	-	-	-	-	-
CO-08 Dup	-	-	-	-	-	-	-	-	-	-	-
CO-10 Orig	-	-	-	-	-	-	-	-	-	-	-
CO-10 Dup	-	-	-	-	-	-	-	-	-	-	-
BC-15 Orig	0.02	0.13	0.019	< 0.1	0.1	< 0.5	0.81	49	< 0.1	1.2	0.25
BC-15 Dup	0.021	0.13	0.02	< 0.1	0.09	< 0.5	0.81	48	< 0.1	1.2	0.23
Method Blank	-	-	-	-	-	-	-	-	-	-	-
Method Blank	-	-	-	-	-	-	-	-	-	-	-
Method Blank	-	-	-	-	-	-	-	-	-	-	-
Method Blank	-	-	-	-	-	-	-	-	-	-	-
Method Blank	< 0.005	< 0.01	< 0.002	< 0.1	< 0.01	< 0.5	< 0.05	< 5	< 0.1	< 0.05	< 0.01
Method Blank	-	-	-	-	-	-	-	-	-	-	-
Method Blank	-	-	-	-	-	-	-	-	-	-	-
Method Blank	-	-	-	-	-	-	-	-	-	-	-
Method Blank	-	-	-	-	-	-	-	-	-	-	-

Analyte Symbol	Fe ₂ O ₃ (%)	LOI 2 (%)	Total 2 (%)
Unit Symbol	0.01	-	0.01
Detection Limit	FUS-ICP	FUS-ICP	FUS-ICP
Analysis Method			
NIST 694 Meas	-	-	-
NIST 694 Cert	-	-	-
NIST 694 Meas	-	-	-
NIST 694 Cert	-	-	-
NIST 694 Meas	-	-	-
NIST 694 Cert	-	-	-
DNC-1 Meas	-	-	-
DNC-1 Cert	-	-	-
DNC-1 Meas	-	-	-
DNC-1 Cert	-	-	-
DNC-1 Meas	-	-	-
DNC-1 Cert	-	-	-
GBW 07113 Meas	-	-	-
GBW 07113 Cert	-	-	-
GBW 07113 Meas	-	-	-
GBW 07113 Cert	-	-	-
GBW 07113 Meas	-	-	-
GBW 07113 Cert	-	-	-
LKSD-3 Meas	-	-	-
LKSD-3 Cert	-	-	-
TDB-1 Meas	-	-	-
TDB-1 Cert	-	-	-
BaSO ₄ Meas	-	-	-
BaSO ₄ Cert	-	-	-
BaSO ₄ Meas	-	-	-
BaSO ₄ Cert	-	-	-
BaSO ₄ Meas	-	-	-
BaSO ₄ Cert	-	-	-
W-2a Meas	-	-	-
W-2a Cert	-	-	-
W-2a Meas	-	-	-
W-2a Cert	-	-	-

Analyte Symbol	Fe ₂ O ₃ (%)	LOI 2 (%)	Total 2 (%)
Unit Symbol	0.01	-	0.01
Detection Limit			
Analysis Method	FUS-ICP	FUS-ICP	FUS-ICP
W-2a Meas	-	-	-
W-2a Cert	-	-	-
SY-4 Meas	-	-	-
SY-4 Cert	-	-	-
SY-4 Meas	-	-	-
SY-4 Cert	-	-	-
SY-4 Meas	-	-	-
SY-4 Cert	-	-	-
CTA-AC-1 Meas	-	-	-
CTA-AC-1 Cert	-	-	-
BIR-1a Meas	-	-	-
BIR-1a Cert	-	-	-
BIR-1a Meas	-	-	-
BIR-1a Cert	-	-	-
BIR-1a Meas	-	-	-
BIR-1a Cert	-	-	-
NCS DC86312 Meas	-	-	-
NCS DC86312 Cert	-	-	-
JGb-2 Meas	-	-	-
JGb-2 Cert	-	-	-
JGb-2 Meas	-	-	-
JGb-2 Cert	-	-	-
JGb-2 Meas	-	-	-
JGb-2 Cert	-	-	-
NCS DC70009 (GBW07241) Meas	-	-	-
NCS DC70009 (GBW07241) Cert	-	-	-
SGR-1b Meas	-	-	-
SGR-1b Cert	-	-	-
SGR-1b Meas	-	-	-
SGR-1b Cert	-	-	-
SGR-1b Meas	-	-	-
SGR-1b Cert	-	-	-

Analyte Symbol	Fe ₂ O ₃ (%)	LOI 2 (%)	Total 2 (%)
Unit Symbol	0.01	-	0.01
Detection Limit		FUS-ICP	
Analysis Method		FUS-ICP	FUS-ICP
OREAS 100a (Fusion) Meas	-	-	-
OREAS 100a (Fusion) Cert	-	-	-
OREAS 101a (Fusion) Meas	-	-	-
OREAS 101a (Fusion) Cert	-	-	-
OREAS 101b (Fusion) Meas	-	-	-
OREAS 101b (Fusion) Cert	-	-	-
JR-1 Meas	-	-	-
JR-1 Cert	-	-	-
GS311-4 Meas	-	-	-
GS311-4 Cert	-	-	-
GS311-4 Meas	-	-	-
GS311-4 Cert	-	-	-
GS311-4 Meas	-	-	-
GS311-4 Cert	-	-	-
GS900-5 Meas	-	-	-
GS900-5 Cert	-	-	-
GS900-5 Meas	-	-	-
GS900-5 Cert	-	-	-
Graphite 4A Meas	-	-	-
Graphite 4A Cert	-	-	-
Graphite 4A Meas	-	-	-
Graphite 4A Cert	-	-	-
Graphite 4A Meas	-	-	-
Graphite 4A Cert	-	-	-
Graphite 14 Meas	-	-	-
Graphite 14 Cert	-	-	-
Graphite 14 Meas	-	-	-
Graphite 14 Cert	-	-	-
Graphite 14 Meas	-	-	-
Graphite 14 Cert	-	-	-

Analyte Symbol	Fe ₂ O ₃ (%)	LOI 2 (%)	Total 2 (%)
Unit Symbol	0.01	-	0.01
Detection Limit		FUS-ICP	
Analysis Method		FUS-ICP	FUS-ICP
BC21 Orig	-	-	-
BC21 Dup	-	-	-
BC-22 Orig	-	-	-
BC-22 Dup	-	-	-
RO-23 Orig	-	-	-
RO-23 Dup	-	-	-
CO-03 Orig	3.5	4.87	99.34
CO-03 Dup	3.52	4.87	100.5
CO-03 Orig	-	-	-
CO-03 Dup	-	-	-
CO-08 Orig	-	-	-
CO-08 Dup	-	-	-
CO-10 Orig	-	-	-
CO-10 Dup	-	-	-
BC-15 Orig	-	-	-
BC-15 Dup	-	-	-
Method Blank	-	-	-
Method Blank	-	-	-
Method Blank	-	-	-
Method Blank	-	-	-
Method Blank	-	-	-
Method Blank	-	-	-
Method Blank	-	-	-
Method Blank	-	-	-
Method Blank	-	-	-

Appendix E:

Lithogeochemistry data

List of Abbreviations – See analytical methods for further description.

- FUS-ICP – Value determined by fusion, dissolution and analysis in an ICP-OES.
- FUS-MS – Value determined by fusion, dissolution and analysis in an ICP-MS.
- TITR – Value determined by titration.
- IR – Value determined by infrared using the graphitic carbon procedure.
- CS – Value determined by infrared using the total C and S procedure.
- % - % weight.
- ppm – parts per million.
- < - Less than the detection limit.
- ‘-’ – No value analyzed for this parameter.

Analyte Symbol	SiO ₂	Al ₂ O ₃	Fe ₂ O _{3(T)}	MnO	MgO	CaO	Na ₂ O	K ₂ O	TiO ₂	P ₂ O ₅	LOI	Total	Ba
Unit Symbol	(%)	(%)	(%)	(%)	(%)	(%)	(%)	(%)	(%)	(%)	(%)	(%)	(ppm)
Detection Limit	0.01	0.01	0.01	0.001	0.01	0.01	0.01	0.01	0.001	0.01	-	0.01	2
Analysis Method	FUS-ICP	FUS-ICP	FUS-ICP	FUS-ICP	FUS-ICP	FUS-ICP	FUS-ICP	FUS-ICP	FUS-ICP	FUS-ICP	FUS-ICP	FUS-ICP	FUS-ICP
BC-16-01	71.63	14.06	3.14	0.08	0.66	1.34	4.33	4.09	0.44	0.09	0.40	100.30	674
BC-16-02	69.18	15.88	2.90	0.06	0.75	1.42	4.59	4.38	0.46	0.12	0.40	100.10	938
BC-16-03	65.02	15.37	4.84	0.08	2.29	3.84	3.29	3.94	0.54	0.16	0.84	100.20	983
BC-16-04	70.42	14.78	2.85	0.06	1.10	1.52	3.27	4.89	0.39	0.09	0.65	100.00	1300
BC-16-05	70.61	14.95	2.49	0.08	0.93	1.42	3.23	4.84	0.39	0.06	0.67	99.67	1312
BC-16-06	79.71	4.92	2.26	0.05	1.02	2.66	0.79	2.00	0.22	0.31	4.88	98.80	-
BC-16-07	68.60	9.08	3.71	0.15	4.63	5.08	1.59	2.93	0.42	0.12	2.63	98.94	-
BC-16-08	76.77	9.80	1.85	0.03	0.72	1.97	1.66	3.92	0.16	0.19	2.61	99.68	-
BC-16-10	82.49	8.17	2.80	0.03	1.14	0.19	0.29	3.04	0.43	0.07	0.66	99.32	409
BC-16-11	79.55	6.78	0.45	0.02	1.87	1.48	1.00	2.27	0.28	0.09	5.64	99.43	-
BC-16-12	73.29	14.10	1.43	0.01	0.16	1.26	2.43	6.75	0.06	< 0.01	0.60	100.10	-
BC-16-13	69.87	11.68	3.18	0.04	3.55	4.37	2.26	2.14	0.51	0.20	2.07	99.88	-
BC-16-14	71.04	10.19	3.43	0.04	3.19	4.01	1.69	2.94	0.37	0.16	1.90	98.95	-
BC-16-15	69.34	15.97	0.63	0.01	0.17	0.18	1.40	11.41	0.07	0.03	0.37	99.58	-
BC-16-17	65.96	9.17	4.20	0.07	5.54	8.27	2.06	0.61	0.38	0.15	2.95	99.37	-
BC-16-18	50.40	18.28	12.78	0.56	3.17	6.00	2.34	3.56	0.09	0.73	1.10	98.99	-
BC-16-19	71.58	10.47	3.72	0.05	3.60	4.81	2.20	1.32	0.37	0.11	2.36	100.60	163
BC-16-20	57.67	15.82	8.87	0.27	3.57	5.40	2.66	2.46	0.43	0.54	1.85	99.53	-
BC-16-21	31.31	7.05	12.81	0.20	13.96	13.72	0.68	1.65	2.92	1.24	13.33	98.87	1070
BC-16-22	74.69	6.77	3.71	0.04	2.62	3.12	1.52	1.60	0.32	0.33	5.76	100.50	-
BC-16-23	69.37	14.68	2.82	0.06	1.27	1.64	3.72	4.67	0.41	0.12	0.52	99.27	1335
BC-16-24	47.62	22.14	11.91	0.33	3.38	1.68	3.16	6.20	0.82	0.19	1.42	98.84	-
BC-16-25	74.41	11.77	3.77	0.06	2.31	1.77	1.76	2.09	0.42	0.09	1.32	99.77	-
BC-16-26	72.81	11.59	4.54	0.08	1.45	0.68	1.55	4.81	0.57	0.03	1.00	99.11	-
BC-16-27	72.10	14.86	0.42	0.01	0.20	0.20	1.39	9.84	0.08	0.03	0.51	99.64	-
BC-16-28	66.00	13.51	6.56	0.24	3.27	3.89	2.21	2.64	0.41	0.34	1.65	100.70	-
BC-16-29	68.27	13.31	5.31	0.20	2.24	4.11	2.56	1.83	0.27	0.28	1.73	100.10	-
BC-16-33	69.27	13.75	5.61	0.12	0.15	1.63	3.52	5.27	0.56	0.06	0.23	100.20	2452
BC-16-34	44.98	15.72	17.58	0.25	7.24	11.02	0.79	0.39	1.95	0.28	-0.06	100.10	-
BC-16-38	71.36	9.83	3.86	0.12	3.65	4.83	1.61	2.87	0.47	0.18	0.00	98.77	-
BC-16-39	57.36	15.61	9.18	0.27	3.44	5.34	2.64	2.39	0.44	0.53	2.15	99.35	-
BC-16-40	98.66	0.30	0.24	0.01	0.02	0.02	0.01	0.07	0.31	0.03	0.22	99.89	-

Analyte Symbol	SiO ₂	Al ₂ O ₃	Fe ₂ O _{3(T)}	MnO	MgO	CaO	Na ₂ O	K ₂ O	TiO ₂	P ₂ O ₅	LOI	Total	Ba
Unit Symbol	(%)	(%)	(%)	(%)	(%)	(%)	(%)	(%)	(%)	(%)	(%)	(%)	(ppm)
Detection Limit	0.01	0.01	0.01	0.001	0.01	0.01	0.01	0.01	0.001	0.01	-	0.01	2
Analysis Method	FUS-ICP	FUS-ICP	FUS-ICP	FUS-ICP	FUS-ICP	FUS-ICP	FUS-ICP	FUS-ICP	FUS-ICP	FUS-ICP	FUS-ICP	FUS-ICP	FUS-ICP
BC-16-41	50.62	20.45	6.03	0.10	0.51	8.07	6.58	1.58	0.28	0.14	4.45	98.83	-
RO-16-01	72.83	15.20	1.65	0.03	0.37	1.35	4.17	4.10	0.20	0.06	0.50	100.50	1107
RO-16-02	65.62	15.90	3.79	0.05	1.46	2.34	4.49	3.23	0.64	0.23	0.84	98.59	1374
RO-16-03	62.14	16.54	7.54	0.06	2.66	3.04	3.05	3.10	1.04	0.12	0.97	100.30	-
RO-16-04	39.29	19.77	14.22	0.17	11.11	4.33	0.98	4.58	0.52	0.05	3.59	98.60	-
RO-16-05	70.33	13.14	4.44	0.07	2.07	4.77	3.48	0.75	0.31	0.08	0.60	100.00	211
RO-16-06	51.28	16.03	8.91	0.12	2.60	13.52	2.46	0.82	1.51	0.24	1.79	99.29	-
RO-16-09	60.92	16.06	8.76	0.14	3.23	3.42	2.55	2.80	0.97	0.20	0.00	99.05	-
RO-16-11	72.56	14.24	0.30	0.00	0.06	0.16	1.86	9.28	0.05	< 0.01	0.30	98.81	-
RO-16-12	73.44	13.22	3.00	0.04	0.59	1.50	3.10	4.61	0.49	0.12	0.51	100.60	1618
RO-16-13	45.96	16.27	13.04	0.16	6.68	8.65	3.44	1.82	1.53	0.29	0.78	98.62	273
RO-16-14	70.49	14.25	3.58	0.08	0.55	1.75	2.91	5.00	0.49	0.15	0.00	99.24	-
RO-16-16	73.86	11.08	1.62	0.03	0.73	1.48	1.39	4.65	0.19	0.15	3.41	98.58	-
RO-16-17	68.68	13.92	4.05	0.10	1.47	2.34	2.93	3.83	0.54	0.18	0.84	98.88	1476
RO-16-19	75.10	9.25	1.95	0.04	0.91	2.19	1.35	2.16	0.28	0.34	5.68	99.26	-
RO-16-21	72.62	13.17	2.93	0.03	1.28	1.76	2.02	4.03	0.48	0.07	0.69	99.07	-
RO-16-22	66.07	14.70	6.02	0.11	1.00	2.44	2.90	4.72	0.80	0.26	0.00	99.03	-
RO-16-23	67.84	10.12	5.71	0.11	2.77	2.89	1.69	3.52	0.38	0.22	3.93	99.18	-
RO-16-24	98.35	0.32	0.26	0.01	0.02	0.02	0.01	0.07	0.34	< 0.01	0.20	99.60	-
RO-16-25	51.10	19.70	6.03	0.10	0.51	8.13	6.95	1.62	0.28	0.13	4.50	99.05	-
CO-16-01	70.73	11.21	4.66	0.12	1.76	3.15	2.18	1.84	0.39	0.35	3.86	100.30	-
CO-16-02	67.22	12.20	5.93	0.17	1.94	3.07	1.74	2.29	0.33	0.17	5.00	100.10	-
CO-16-03	74.22	6.85	4.51	0.06	2.39	3.64	1.32	1.41	0.30	0.32	4.77	99.80	-
CO-16-04	68.55	9.42	5.57	0.11	2.79	2.80	1.59	3.38	0.36	0.22	4.06	98.84	-
CO-16-05	69.53	14.65	5.39	0.07	2.26	0.39	0.79	5.89	0.63	0.04	0.00	99.64	-
CO-16-06	66.49	8.15	5.85	2.15	4.82	7.07	1.05	1.90	0.44	0.17	1.90	100.00	-
CO-16-07	69.84	9.14	5.03	0.06	2.92	3.95	1.76	1.52	0.36	0.24	4.30	99.13	-
CO-16-08	65.01	9.75	6.07	0.96	4.17	6.21	1.56	2.55	0.51	0.16	2.59	99.55	-
CO-16-09	54.02	16.86	10.26	0.21	6.14	6.76	0.62	2.70	1.35	0.18	0.00	99.11	-
CO-16-10	67.98	15.65	4.70	0.07	2.55	0.53	0.79	4.58	0.56	0.05	2.61	100.10	-

Analyte Symbol	Sr	Y	Sc	Zr	Be	V	C-Graphitic	C-Total	Total S	FeO	V	Cr	Co
Unit Symbol	(ppm)	(ppm)	(ppm)	(ppm)	(ppm)	(ppm)	(%)	(%)	(%)	(%)	(ppm)	(ppm)	(ppm)
Detection Limit	2	1	1	2	1	5	0.05	0.01	0.01	0.1	5	20	1
Analysis Method	FUS-ICP	FUS-ICP	FUS-ICP	FUS-ICP	FUS-ICP	FUS-ICP	IR	CS	CS	TITR	FUS-ICP	FUS-MS	FUS-MS
BC-16-01	258	31	6	330	< 1	42	-	-	-	-	-	-	-
BC-16-02	321	25	6	267	1	36	-	-	-	-	-	-	-
BC-16-03	569	21	11	253	2	94	-	-	-	-	-	-	-
BC-16-04	248	25	7	178	2	40	-	-	-	-	-	-	-
BC-16-05	276	22	5	210	2	42	-	-	-	-	-	-	-
BC-16-06	-	-	7	-	< 1	-	3.67	3.96	0.99	-	187	30	7
BC-16-07	-	-	8	-	1	-	1.08	1.19	1.02	-	82	100	11
BC-16-08	-	-	2	-	2	-	1.59	1.72	0.77	-	81	30	4
BC-16-10	48	24	8	293	< 1	31	-	-	-	-	-	-	-
BC-16-11	-	-	7	-	< 1	-	4.11	4.38	0.59	-	207	50	< 1
BC-16-12	-	-	< 1	-	1	-	-	-	-	-	11	30	4
BC-16-13	-	-	7	-	4	-	0.96	1.01	0.74	-	71	60	7
BC-16-14	-	-	8	-	5	-	0.72	0.84	0.9	-	73	80	10
BC-16-15	-	-	< 1	-	< 1	-	-	-	-	-	8	20	1
BC-16-17	-	-	8	-	6	-	1.19	1.7	0.91	-	93	50	8
BC-16-18	-	-	25	-	1	-	-	-	-	-	30	90	10
BC-16-19	218	10	6	197	6	74	0.85	1.12	0.69	-	-	-	-
BC-16-20	-	-	16	-	3	-	0.47	0.54	1.25	-	52	50	12
BC-16-21	680	34	23	356	3	273	-	-	-	-	-	-	-
BC-16-22	-	-	8	-	1	-	3.37	3.54	1.69	-	178	80	10
BC-16-23	146	22	7	241	4	40	-	-	-	-	-	-	-
BC-16-24	-	-	31	-	1	-	-	-	-	-	203	30	22
BC-16-25	-	-	10	-	4	-	0.28	0.26	0.03	-	37	120	3
BC-16-26	-	-	13	-	< 1	-	-	-	-	-	47	120	6
BC-16-27	-	-	< 1	-	< 1	-	-	-	-	-	10	20	< 1
BC-16-28	-	-	12	-	3	-	0.54	0.59	0.63	-	61	80	9
BC-16-29	-	-	9	-	3	-	0.7	0.72	0.71	-	40	60	8
BC-16-33	145	56	10	796	3	8	-	-	-	-	-	-	-
BC-16-34	-	-	51	-	< 1	-	-	-	-	-	412	150	57
BC-16-38	-	-	7	-	1	-	0.68	0.78	0.72	1.9	69	100	8
BC-16-39	-	-	16	-	3	-	0.48	0.53	1.29	-	52	100	12
BC-16-40	-	-	< 1	-	< 1	-	< 0.05	< 0.01	< 0.01	-	7	< 20	< 1

Analyte Symbol	Sr (ppm)	Y (ppm)	Sc (ppm)	Zr (ppm)	Be (ppm)	V (ppm)	C-Graphitic (%)	C-Total (%)	Total S (%)	FeO (%)	V (ppm)	Cr (ppm)	Co (ppm)
Unit Symbol	2	1	1	2	1	5	0.05	0.01	0.01	0.1	5	20	1
Detection Limit	FUS-ICP	FUS-ICP	FUS-ICP	FUS-ICP	FUS-ICP	FUS-ICP	IR	CS	CS	TITR	FUS-ICP	FUS-MS	FUS-MS
BC-16-41	-	-	1	-	3	-	-	-	-	-	7	< 20	1
RO-16-01	405	4	2	100	2	20	-	-	-	-	-	-	-
RO-16-02	655	12	5	259	2	63	-	-	-	-	-	-	-
RO-16-03	-	-	13	-	1	-	-	-	-	-	130	130	16
RO-16-04	-	-	26	-	2	-	-	-	-	-	151	50	26
RO-16-05	314	15	14	76	< 1	77	-	-	-	-	-	-	-
RO-16-06	-	-	29	-	2	-	-	-	-	-	210	210	33
RO-16-09	-	-	20	-	2	-	-	-	-	-	148	70	24
RO-16-11	-	-	< 1	-	< 1	-	< 0.05	< 0.01	< 0.01	-	< 5	20	< 1
RO-16-12	303	16	5	361	1	33	-	-	-	-	-	-	-
RO-16-13	413	35	26	88	2	239	-	-	-	-	-	-	-
RO-16-14	-	-	10	-	3	-	-	-	-	-	30	30	4
RO-16-16	-	-	4	-	2	-	2.05	2.08	0.73	-	86	30	4
RO-16-17	334	31	11	265	3	69	-	-	-	-	-	-	-
RO-16-19	-	-	6	-	2	-	4.12	4.28	0.77	-	188	170	3
RO-16-21	-	-	22	-	2	-	< 0.05	0.08	0.22	-	67	110	6
RO-16-22	-	-	15	-	3	-	-	-	-	-	42	60	6
RO-16-23	-	-	5	-	2	-	1.66	1.8	2.41	-	103	150	20
RO-16-24	-	-	< 1	-	< 1	-	< 0.05	< 0.01	< 0.01	-	10	< 20	< 1
RO-16-25	-	-	1	-	3	-	-	-	-	-	12	30	2
CO-16-01	-	-	11	-	2	-	2.69	2.74	1.17	1.7	102	160	8
CO-16-02	-	-	13	-	2	-	2.83	2.95	1.42	3.2	96	180	9
CO-16-03	-	-	8	-	1	-	3.4	3.55	1.88	0.9	177	190	9
CO-16-04	-	-	4	-	2	-	1.67	1.82	2.34	1.4	109	160	22
CO-16-05	-	-	14	-	< 1	-	0.11	0.14	0.08	3.5	68	150	10
CO-16-06	-	-	10	-	2	-	0.52	0.6	1.34	2	94	160	26
CO-16-07	-	-	11	-	2	-	2.61	2.74	1.62	1.3	164	200	10
CO-16-08	-	-	12	-	2	-	1.02	1.12	1.96	2	113	190	26
CO-16-09	-	-	23	-	3	-	-	-	-	6.6	186	230	34
CO-16-10	-	-	14	-	1	-	-	-	-	3.2	63	140	9

Analyte Symbol	Ni (ppm)	Cu (ppm)	Zn (ppm)	Ga (ppm)	Ge (ppm)	As (ppm)	Rb (ppm)	Sr (ppm)	Y (ppm)	Zr (ppm)	Nb (ppm)	Mo (ppm)	Ag (ppm)
Unit Symbol	20	10	30	1	0.5	5	1	2	0.5	1	0.2	2	0.5
Detection Limit	-	-	-	-	-	-	-	-	-	-	-	-	-
Analysis Method	FUS-MS	FUS-ICP	FUS-MS	FUS-ICP	FUS-MS	FUS-MS	FUS-MS						
BC-16-01	-	-	-	-	-	-	-	-	-	-	-	-	-
BC-16-02	-	-	-	-	-	-	-	-	-	-	-	-	-
BC-16-03	-	-	-	-	-	-	-	-	-	-	-	-	-
BC-16-04	-	-	-	-	-	-	-	-	-	-	-	-	-
BC-16-05	-	-	-	-	-	-	-	-	-	-	-	-	-
BC-16-06	70	50	210	6	1.1	< 5	65	58	20.6	59	2.2	17	< 0.5
BC-16-07	30	20	70	12	1.1	< 5	81	103	24.2	329	6.5	2	< 0.5
BC-16-08	30	20	40	12	1.2	< 5	132	144	13.2	39	4.6	6	< 0.5
BC-16-10	-	-	-	-	-	-	-	-	-	-	-	-	-
BC-16-11	< 20	< 10	50	9	1.4	< 5	98	79	7.4	82	3.2	24	< 0.5
BC-16-12	< 20	< 10	< 30	15	0.8	< 5	105	447	1.2	49	1.7	3	< 0.5
BC-16-13	30	20	80	18	1.3	< 5	97	177	14.9	317	8.4	3	< 0.5
BC-16-14	30	20	70	14	1.3	< 5	94	184	18.1	282	6.1	3	< 0.5
BC-16-15	< 20	< 10	240	13	0.7	< 5	169	610	1.7	6	1.2	33	< 0.5
BC-16-17	40	50	90	14	1.3	< 5	26	219	24.6	250	7.5	5	< 0.5
BC-16-18	30	20	70	17	3	< 5	101	261	163	803	4.8	6	1.7
BC-16-19	-	-	-	-	-	-	-	-	-	-	-	-	-
BC-16-20	30	30	110	19	2.2	< 5	114	258	93.2	933	11.3	4	2.1
BC-16-21	-	-	-	-	-	-	-	-	-	-	-	-	-
BC-16-22	80	60	260	8	1.3	< 5	60	90	7.4	132	5.2	15	< 0.5
BC-16-23	-	-	-	-	-	-	-	-	-	-	-	-	-
BC-16-24	< 20	40	160	27	1.6	< 5	273	178	21.4	113	20.1	< 2	< 0.5
BC-16-25	< 20	30	70	14	1.6	< 5	93	84	36.5	154	7.4	5	< 0.5
BC-16-26	< 20	< 10	130	10	1.9	< 5	139	206	55.3	323	26.4	3	0.6
BC-16-27	< 20	< 10	100	11	0.8	< 5	164	533	1.8	7	1.2	40	< 0.5
BC-16-28	40	20	100	16	1.8	< 5	109	218	64.1	611	8	3	1.4
BC-16-29	30	20	80	15	1.5	< 5	73	247	52.3	485	4.9	4	1.1
BC-16-33	-	-	-	-	-	-	-	-	-	-	-	-	-
BC-16-34	40	70	90	20	1.9	< 5	7	76	38.7	105	2.1	3	< 0.5
BC-16-38	30	10	70	11	1.1	< 5	87	189	21.9	315	8.1	2	< 0.5
BC-16-39	30	30	110	19	2.2	< 5	108	265	91.7	1032	11.1	7	2.3
BC-16-40	< 20	< 10	< 30	< 1	0.9	< 5	2	7	2.2	274	3.6	< 2	< 0.5

Analyte Symbol	Ni (ppm)	Cu (ppm)	Zn (ppm)	Ga (ppm)	Ge (ppm)	As (ppm)	Rb (ppm)	Sr (ppm)	Y (ppm)	Zr (ppm)	Nb (ppm)	Mo (ppm)	Ag (ppm)
Unit Symbol	20	10	30	1	0.5	5	1	2	0.5	1	0.2	2	0.5
Detection Limit													
Analysis Method	FUS-MS	FUS-ICP	FUS-MS	FUS-ICP	FUS-MS	FUS-MS	FUS-MS						
BC-16-41	< 20	< 10	100	35	1.2	< 5	55	1185	123	548	13.4	< 2	1.2
RO-16-01	-	-	-	-	-	-	-	-	-	-	-	-	-
RO-16-02	-	-	-	-	-	-	-	-	-	-	-	-	-
RO-16-03	30	30	250	25	1.3	< 5	99	235	17.3	232	8.9	3	< 0.5
RO-16-04	20	< 10	330	26	1.9	< 5	151	96	44	197	6.6	> 100	< 0.5
RO-16-05	-	-	-	-	-	-	-	-	-	-	-	-	-
RO-16-06	70	20	120	16	1	< 5	15	247	33	216	16	5	0.6
RO-16-09	40	90	130	20	1.6	< 5	85	209	35	220	8.2	< 2	< 0.5
RO-16-11	< 20	< 10	< 30	12	0.6	< 5	150	614	1.3	9	0.5	< 2	< 0.5
RO-16-12	-	-	-	-	-	-	-	-	-	-	-	-	-
RO-16-13	-	-	-	-	-	-	-	-	-	-	-	-	-
RO-16-14	< 20	< 10	60	18	1.3	< 5	166	194	57.7	331	15.2	< 2	0.6
RO-16-16	30	10	90	12	1.1	< 5	112	212	31.8	114	5	10	< 0.5
RO-16-17	-	-	-	-	-	-	-	-	-	-	-	-	-
RO-16-19	30	30	140	12	0.9	< 5	50	217	48.8	115	3.6	26	< 0.5
RO-16-21	20	10	90	16	1.2	< 5	102	229	48.7	276	9.3	3	0.6
RO-16-22	< 20	< 10	80	21	1.6	< 5	144	220	72.2	527	21.6	2	1
RO-16-23	50	40	80	12	0.8	< 5	104	160	13.3	216	4.7	9	< 0.5
RO-16-24	< 20	< 10	< 30	< 1	0.9	< 5	2	7	2.7	297	4	< 2	0.6
RO-16-25	< 20	< 10	100	29	1	< 5	56	1172	125	586	12.9	< 2	1.8
CO-16-01	50	60	210	12	1.1	< 5	70	114	45.1	153	7.2	12	< 0.5
CO-16-02	50	30	90	12	1.3	< 5	79	125	60.5	222	6.1	18	0.5
CO-16-03	70	50	130	8	0.9	< 5	64	85	24.1	98	3.6	20	< 0.5
CO-16-04	60	40	80	10	0.7	< 5	107	149	13.4	214	6.1	11	0.5
CO-16-05	30	10	70	16	1.9	< 5	164	336	37.2	286	14.9	3	< 0.5
CO-16-06	40	20	100	9	1.5	< 5	54	91	38.6	304	8.9	6	0.7
CO-16-07	70	50	140	11	1.1	< 5	65	127	21.9	191	5.3	14	< 0.5
CO-16-08	50	40	90	10	1.4	< 5	76	158	33.6	245	8.5	8	0.7
CO-16-09	90	< 10	170	20	1.8	< 5	120	82	25.6	108	8.7	3	< 0.5
CO-16-10	30	30	90	16	1.6	< 5	160	227	34.5	258	10.8	4	0.7

Analyte Symbol	In	Sn	Sb	Cs	Ba	La	Ce	Pr	Nd	Sm	Eu	Gd	Tb
Unit Symbol	(ppm)	(ppm)	(ppm)	(ppm)	(ppm)	(ppm)	(ppm)	(ppm)	(ppm)	(ppm)	(ppm)	(ppm)	(ppm)
Detection Limit	0.1	1	0.2	0.1	2	0.05	0.05	0.01	0.05	0.01	0.005	0.01	0.01
Analysis Method	FUS-MS	FUS-MS	FUS-MS	FUS-MS	FUS-ICP	FUS-MS							
BC-16-01	-	-	-	-	-	-	-	-	-	-	-	-	-
BC-16-02	-	-	-	-	-	-	-	-	-	-	-	-	-
BC-16-03	-	-	-	-	-	-	-	-	-	-	-	-	-
BC-16-04	-	-	-	-	-	-	-	-	-	-	-	-	-
BC-16-05	-	-	-	-	-	-	-	-	-	-	-	-	-
BC-16-06	< 0.1	< 1	< 0.2	0.9	251	15.1	28	3.92	15.7	3.28	0.669	2.96	0.48
BC-16-07	< 0.1	< 1	< 0.2	1.8	531	25.2	51.3	6.4	24.3	4.8	0.92	4.23	0.71
BC-16-08	< 0.1	< 1	< 0.2	2.7	514	7.73	17.5	2.53	10.5	2.73	0.681	2.48	0.4
BC-16-10	-	-	-	-	-	-	-	-	-	-	-	-	-
BC-16-11	< 0.1	< 1	< 0.2	6.3	311	2.33	6.63	0.9	3.01	0.79	0.202	0.73	0.17
BC-16-12	< 0.1	< 1	< 0.2	1.4	2135	0.64	1.01	0.11	0.46	0.08	0.855	0.12	0.02
BC-16-13	< 0.1	< 1	< 0.2	2.6	314	83.1	161	17.7	60.6	9.06	1.29	5.35	0.61
BC-16-14	< 0.1	< 1	< 0.2	1.8	778	43	83.3	9.94	35.6	6.93	1.22	5.19	0.69
BC-16-15	< 0.1	< 1	< 0.2	1	5542	1.51	2.63	0.33	1.38	0.34	0.627	0.33	0.05
BC-16-17	< 0.1	< 1	< 0.2	0.6	197	37.3	71.9	9.04	32.8	6.5	1.45	5.61	0.85
BC-16-18	0.1	< 1	< 0.2	2.2	870	148	311	36	134	27.2	3.4	26.1	4.51
BC-16-19	-	-	-	-	-	-	-	-	-	-	-	-	-
BC-16-20	< 0.1	< 1	< 0.2	3.5	356	133	274	31.2	114	21.4	3	17.7	2.69
BC-16-21	-	-	-	-	-	-	-	-	-	-	-	-	-
BC-16-22	< 0.1	< 1	< 0.2	3.1	228	23.8	41.5	5.12	18	2.99	0.582	1.96	0.25
BC-16-23	-	-	-	-	-	-	-	-	-	-	-	-	-
BC-16-24	0.2	4	< 0.2	5.5	1119	31.2	67.6	7.83	29.8	6.34	1.52	5.85	0.78
BC-16-25	< 0.1	< 1	0.2	3.3	197	30.7	64.1	7.45	27.2	5.5	1.2	5.18	0.88
BC-16-26	< 0.1	2	< 0.2	2.9	1369	13.2	25.3	2.69	9.25	1.94	1.09	3.88	1
BC-16-27	< 0.1	< 1	< 0.2	1.2	6291	2.18	3.71	0.4	1.5	0.33	0.448	0.35	0.06
BC-16-28	< 0.1	< 1	< 0.2	3	589	69.2	142	16.6	60	10.8	1.64	9.84	1.65
BC-16-29	< 0.1	< 1	< 0.2	2	411	56.1	115	13.4	49.1	9.01	1.66	8.22	1.33
BC-16-33	-	-	-	-	-	-	-	-	-	-	-	-	-
BC-16-34	< 0.1	1	< 0.2	0.2	67	12	30.6	4.57	21.2	5.69	2.18	6.75	1.11
BC-16-38	< 0.1	< 1	< 0.2	3.1	621	26.5	53.7	6.72	25.2	4.95	1.24	4.39	0.67
BC-16-39	< 0.1	1	< 0.2	3.3	347	127	264	30.5	109	20.4	2.98	17.3	2.69
BC-16-40	< 0.1	< 1	< 0.2	< 0.1	46	3.26	5.93	0.7	2.63	0.49	0.078	0.35	0.06

Analyte Symbol	In	Sn	Sb	Cs	Ba	La	Ce	Pr	Nd	Sm	Eu	Gd	Tb
Unit Symbol	(ppm)	(ppm)	(ppm)	(ppm)	(ppm)	(ppm)	(ppm)	(ppm)	(ppm)	(ppm)	(ppm)	(ppm)	(ppm)
Detection Limit	0.1	1	0.2	0.1	2	0.05	0.05	0.01	0.05	0.01	0.005	0.01	0.01
Analysis Method	FUS-MS	FUS-MS	FUS-MS	FUS-MS	FUS-ICP	FUS-MS							
BC-16-41	< 0.1	8	< 0.2	1.5	332	61.9	130	15.5	59.6	13.1	2.06	15.1	2.69
RO-16-01	-	-	-	-	-	-	-	-	-	-	-	-	-
RO-16-02	-	-	-	-	-	-	-	-	-	-	-	-	-
RO-16-03	< 0.1	3	< 0.2	1	560	35.3	70.9	8.61	32.6	5.96	1.36	4.55	0.57
RO-16-04	0.2	3	< 0.2	4.8	478	35.9	75.2	9.57	38.3	8.54	2.12	8.33	1.27
RO-16-05	-	-	-	-	-	-	-	-	-	-	-	-	-
RO-16-06	< 0.1	2	< 0.2	0.3	113	26	55.8	6.77	25.9	5.75	1.8	5.68	0.9
RO-16-09	< 0.1	2	< 0.2	2.9	465	25.6	56.8	6.93	27	5.17	1.19	5.2	0.87
RO-16-11	< 0.1	< 1	< 0.2	0.7	7990	4.84	7.26	0.88	3.06	0.51	1.76	0.36	0.05
RO-16-12	-	-	-	-	-	-	-	-	-	-	-	-	-
RO-16-13	-	-	-	-	-	-	-	-	-	-	-	-	-
RO-16-14	< 0.1	2	< 0.2	1.5	1322	51.5	139	12.8	47.1	9.58	1.85	8.52	1.44
RO-16-16	< 0.1	< 1	< 0.2	2	737	33.3	66.7	7.7	27.8	5.74	1.37	5.3	0.77
RO-16-17	-	-	-	-	-	-	-	-	-	-	-	-	-
RO-16-19	< 0.1	< 1	< 0.2	2	394	16.8	34.3	4.26	17.5	4.09	1.14	4.87	0.84
RO-16-21	< 0.1	< 1	1.5	1.7	864	58.3	117	13.3	45.4	8.28	1.59	7.12	1.08
RO-16-22	< 0.1	3	< 0.2	1.6	1832	68.5	143	16.8	63.4	13.1	3.41	12.7	2.11
RO-16-23	< 0.1	< 1	< 0.2	2.5	516	19	40.8	5.06	19.8	4.01	0.87	3.26	0.45
RO-16-24	< 0.1	< 1	< 0.2	< 0.1	42	4.43	8.38	0.95	3.36	0.62	0.078	0.4	0.07
RO-16-25	< 0.1	7	< 0.2	1.5	347	61.9	128	15.5	57.9	13.2	1.98	14.7	2.88
CO-16-01	< 0.1	< 1	< 0.2	2.7	246	29.3	60.1	7.47	29.5	6.27	1.32	6.38	1.13
CO-16-02	< 0.1	< 1	< 0.2	3.1	625	28.5	56.5	7.02	27.2	6.06	1.31	6.63	1.26
CO-16-03	< 0.1	< 1	< 0.2	3.2	165	26.7	49	6.31	23.4	4.38	0.933	4.22	0.64
CO-16-04	< 0.1	< 1	< 0.2	2.6	601	19.3	41.1	5.2	19.4	3.98	0.897	3.36	0.49
CO-16-05	< 0.1	< 1	< 0.2	3.5	1659	44	87.8	9.78	35.2	5.66	1.49	5.29	0.9
CO-16-06	< 0.1	< 1	< 0.2	0.6	453	21.3	59.6	7.72	30.4	6.95	1.22	6.44	1.05
CO-16-07	< 0.1	< 1	< 0.2	1.9	199	29	57.9	7.24	27.5	5.67	0.977	4.83	0.71
CO-16-08	< 0.1	< 1	< 0.2	1.3	624	25	59.4	7.73	30.7	6.92	1.33	6.49	0.99
CO-16-09	0.1	6	< 0.2	7.6	327	15.4	33.4	4.19	17.4	4.32	1.4	4.55	0.77
CO-16-10	< 0.1	< 1	< 0.2	4.9	856	57.2	117	13.3	46.8	8.36	1.56	6.65	1

Analyte Symbol	Dy	Ho	Er	Tm	Yb	Lu	Hf	Ta	W	Tl	Pb	Bi	Th
Unit Symbol	(ppm)												
Detection Limit	0.01	0.01	0.01	0.005	0.01	0.002	0.1	0.01	0.5	0.05	5	0.1	0.05
Analysis Method	FUS-MS												
BC-16-01	-	-	-	-	-	-	-	-	-	-	-	-	-
BC-16-02	-	-	-	-	-	-	-	-	-	-	-	-	-
BC-16-03	-	-	-	-	-	-	-	-	-	-	-	-	-
BC-16-04	-	-	-	-	-	-	-	-	-	-	-	-	-
BC-16-05	-	-	-	-	-	-	-	-	-	-	-	-	-
BC-16-06	2.97	0.62	1.74	0.257	1.65	0.255	1.4	0.21	< 0.5	0.46	12	< 0.1	2.99
BC-16-07	3.96	0.76	2.21	0.34	2.36	0.385	7.4	0.56	< 0.5	0.37	10	< 0.1	7
BC-16-08	2.33	0.43	1.22	0.18	1.2	0.176	0.8	0.8	< 0.5	1.07	17	< 0.1	2.09
BC-16-10	-	-	-	-	-	-	-	-	-	-	-	-	-
BC-16-11	1.29	0.28	0.89	0.145	1.01	0.164	1.9	0.35	0.9	0.79	20	< 0.1	3.38
BC-16-12	0.13	0.03	0.12	0.02	0.14	0.022	1.4	0.16	< 0.5	0.56	22	< 0.1	0.21
BC-16-13	2.97	0.5	1.37	0.191	1.17	0.181	7.3	0.31	< 0.5	0.46	8	< 0.1	25.1
BC-16-14	3.43	0.6	1.64	0.227	1.4	0.214	6.6	0.36	< 0.5	0.41	12	< 0.1	19.2
BC-16-15	0.3	0.06	0.16	0.021	0.13	0.019	< 0.1	0.09	< 0.5	0.81	49	< 0.1	1.2
BC-16-17	4.43	0.81	2.15	0.312	2.04	0.299	5.9	0.57	0.5	< 0.05	5	< 0.1	9.36
BC-16-18	28	5.56	16.7	2.56	18.4	3.11	16.5	0.24	< 0.5	0.56	16	< 0.1	44.7
BC-16-19	-	-	-	-	-	-	-	-	-	-	-	-	-
BC-16-20	16.6	3.24	9.68	1.46	10.7	1.74	19.5	0.6	< 0.5	0.5	11	< 0.1	33.9
BC-16-21	-	-	-	-	-	-	-	-	-	-	-	-	-
BC-16-22	1.31	0.25	0.75	0.119	0.86	0.152	2.9	0.47	2.1	0.32	14	< 0.1	3.59
BC-16-23	-	-	-	-	-	-	-	-	-	-	-	-	-
BC-16-24	4.19	0.75	2.08	0.311	2.14	0.344	2.7	0.74	0.7	1.02	27	< 0.1	5.56
BC-16-25	5.85	1.25	3.85	0.589	3.9	0.64	3.5	0.57	< 0.5	0.37	11	< 0.1	8.31
BC-16-26	8.02	1.83	5.73	0.891	6.31	1.07	7	3.31	2	0.58	35	< 0.1	3.58
BC-16-27	0.3	0.06	0.17	0.026	0.16	0.021	< 0.1	0.1	< 0.5	0.74	36	< 0.1	< 0.05
BC-16-28	10.6	2.2	6.79	1.06	7.49	1.23	13.5	0.41	< 0.5	0.55	10	< 0.1	18.6
BC-16-29	8.76	1.8	5.48	0.886	6.09	1.05	10.8	0.31	< 0.5	0.35	11	< 0.1	17.5
BC-16-33	-	-	-	-	-	-	-	-	-	-	-	-	-
BC-16-34	7.08	1.44	4.15	0.606	4.01	0.608	3	0.11	< 0.5	< 0.05	< 5	0.4	0.67
BC-16-38	3.71	0.72	2.14	0.313	2.17	0.348	7.4	0.8	1.7	0.45	12	< 0.1	7.27
BC-16-39	16.1	3.14	9.67	1.47	10.5	1.75	21.5	0.6	0.8	0.58	13	< 0.1	32.1
BC-16-40	0.34	0.08	0.25	0.049	0.36	0.059	5.9	0.27	< 0.5	< 0.05	< 5	< 0.1	0.99

Analyte Symbol	Dy	Ho	Er	Tm	Yb	Lu	Hf	Ta	W	Tl	Pb	Bi	Th
Unit Symbol	(ppm)												
Detection Limit	0.01	0.01	0.01	0.005	0.01	0.002	0.1	0.01	0.5	0.05	5	0.1	0.05
Analysis Method	FUS-MS												
BC-16-41	19.2	4.31	14.4	2.3	15.2	2.24	11	0.73	< 0.5	0.17	10	< 0.1	1.38
RO-16-01	-	-	-	-	-	-	-	-	-	-	-	-	-
RO-16-02	-	-	-	-	-	-	-	-	-	-	-	-	-
RO-16-03	2.94	0.57	1.86	0.282	2.03	0.338	5.8	0.29	0.8	0.26	14	< 0.1	7.42
RO-16-04	7.81	1.55	4.59	0.689	4.69	0.773	5.1	0.49	1.6	0.36	5	0.1	6.75
RO-16-05	-	-	-	-	-	-	-	-	-	-	-	-	-
RO-16-06	5.58	1.14	3.42	0.507	3.22	0.503	4.4	0.99	1.1	< 0.05	10	0.2	2.92
RO-16-09	5.82	1.24	3.81	0.599	4.05	0.652	5.6	0.6	< 0.5	0.3	8	< 0.1	5.46
RO-16-11	0.24	0.05	0.12	0.017	0.12	0.019	0.1	0.04	< 0.5	0.59	31	< 0.1	0.3
RO-16-12	-	-	-	-	-	-	-	-	-	-	-	-	-
RO-16-13	-	-	-	-	-	-	-	-	-	-	-	-	-
RO-16-14	9.19	1.97	6.2	0.999	6.84	1.09	7.9	1.25	< 0.5	0.62	27	< 0.1	18.2
RO-16-16	4.66	0.91	2.74	0.399	2.61	0.428	3.1	0.46	< 0.5	0.81	35	< 0.1	10.4
RO-16-17	-	-	-	-	-	-	-	-	-	-	-	-	-
RO-16-19	5.83	1.31	4.06	0.607	4.27	0.698	2.7	0.38	1.2	0.56	152	< 0.1	5.22
RO-16-21	7.16	1.65	5.31	0.815	5.45	0.916	7	0.36	< 0.5	0.57	26	< 0.1	18.9
RO-16-22	12.8	2.61	7.71	1.16	7.77	1.22	12.6	1.36	< 0.5	0.54	22	< 0.1	14.5
RO-16-23	2.53	0.44	1.28	0.182	1.14	0.172	4.8	0.53	< 0.5	0.82	12	< 0.1	3.46
RO-16-24	0.43	0.09	0.31	0.051	0.38	0.069	6.7	0.32	< 0.5	< 0.05	< 5	< 0.1	1.44
RO-16-25	19.7	4.49	14.6	2.33	15.2	2.28	10.5	0.71	1.8	< 0.05	9	< 0.1	1.24
CO-16-01	7.14	1.51	4.6	0.687	4.77	0.798	3.7	0.61	0.8	0.36	23	< 0.1	5.17
CO-16-02	9.07	2	6.67	1.08	7.37	1.2	5.1	0.37	6.9	0.46	12	< 0.1	4.72
CO-16-03	3.69	0.76	2.26	0.331	2.16	0.347	2.3	0.44	1.3	0.43	13	< 0.1	6.67
CO-16-04	2.52	0.49	1.34	0.189	1.23	0.177	5	0.56	8	0.6	11	< 0.1	3.28
CO-16-05	5.98	1.24	3.75	0.574	3.87	0.627	6.9	0.87	< 0.5	0.67	21	< 0.1	10.7
CO-16-06	6.22	1.25	3.66	0.565	3.54	0.553	6.8	0.8	0.6	0.11	7	< 0.1	3.84
CO-16-07	3.79	0.67	1.93	0.269	1.76	0.286	4.3	0.48	1.6	0.29	10	< 0.1	8.33
CO-16-08	5.97	1.14	3.35	0.483	3.18	0.491	5.6	0.74	< 0.5	0.25	9	< 0.1	5.15
CO-16-09	4.64	0.85	2.37	0.342	2.22	0.334	2.8	0.74	1.4	0.99	10	< 0.1	2.94
CO-16-10	6.06	1.24	3.54	0.536	3.49	0.589	6.4	0.47	0.6	0.36	22	< 0.1	13.5

Analyte Symbol	U	Fe ₂ O ₃	LOI 2	Total 2
Unit Symbol	(ppm)	(%)	(%)	(%)
Detection Limit	0.01	0.01	-	0.01
Analysis Method	FUS-MS	FUS-ICP	FUS-ICP	FUS-ICP
BC-16-01	-	-	-	-
BC-16-02	-	-	-	-
BC-16-03	-	-	-	-
BC-16-04	-	-	-	-
BC-16-05	-	-	-	-
BC-16-06	5.88	-	-	-
BC-16-07	3.06	-	-	-
BC-16-08	5.11	-	-	-
BC-16-10	-	-	-	-
BC-16-11	7.76	-	-	-
BC-16-12	0.81	-	-	-
BC-16-13	2.62	-	-	-
BC-16-14	3.73	-	-	-
BC-16-15	0.24	-	-	-
BC-16-17	5.3	-	-	-
BC-16-18	8.2	-	-	-
BC-16-19	-	-	-	-
BC-16-20	8.95	-	-	-
BC-16-21	-	-	-	-
BC-16-22	3.76	-	-	-
BC-16-23	-	-	-	-
BC-16-24	1.84	-	-	-
BC-16-25	1.72	-	-	-
BC-16-26	1.74	-	-	-
BC-16-27	0.16	-	-	-
BC-16-28	3.85	-	-	-
BC-16-29	3.6	-	-	-
BC-16-33	-	-	-	-
BC-16-34	1.71	-	-	-
BC-16-38	3.59	1.75	0.21	98.98
BC-16-39	8.62	-	-	-
BC-16-40	0.44	-	-	-

Analyte Symbol	U	Fe ₂ O ₃	LOI 2	Total 2
Unit Symbol	(ppm)	(%)	(%)	(%)
Detection Limit	0.01	0.01	-	0.01
Analysis Method	FUS-MS	FUS-ICP	FUS-ICP	FUS-ICP
BC-16-41	0.78	-	-	-
RO-16-01	-	-	-	-
RO-16-02	-	-	-	-
RO-16-03	0.63	-	-	-
RO-16-04	2.07	-	-	-
RO-16-05	-	-	-	-
RO-16-06	1.43	-	-	-
RO-16-09	1.4	-	-	-
RO-16-11	0.11	-	-	-
RO-16-12	-	-	-	-
RO-16-13	-	-	-	-
RO-16-14	2.89	-	-	-
RO-16-16	5.96	-	-	-
RO-16-17	-	-	-	-
RO-16-19	6.2	-	-	-
RO-16-21	2.5	-	-	-
RO-16-22	3.45	-	-	-
RO-16-23	3.59	-	-	-
RO-16-24	0.46	-	-	-
RO-16-25	0.85	-	-	-
CO-16-01	6.41	2.77	4.05	100.4
CO-16-02	6.13	2.37	5.36	100.4
CO-16-03	9.97	3.51	4.87	99.9
CO-16-04	3.69	4.02	4.21	98.99
CO-16-05	1.32	1.5	0.39	100
CO-16-06	3.79	3.63	2.13	100.2
CO-16-07	6.01	3.59	4.44	99.27
CO-16-08	4.28	3.85	2.81	99.77
CO-16-09	13.4	2.92	0.74	99.85
CO-16-10	1.98	1.15	2.96	100.4

Appendix F:
Microprobe calibration values and settings

Mineral Phase: Feldspars

Date Analyzed: February 22nd, 2017

Element:	Reference standard:	Spectrometers					L-Value	Counts	Back+/Back-
		1	2	3	4	5			
		TAP/LDE1	TAP/LDE2	PETJ/LIF	PETH/LIFH	PETL/LIFL			
Si	Albite	TAP	-	-	-	-	77.252	12222	3/6.5
Al	Albite	TAP	-	-	-	-	90.501	3681	5.5/6
Fe	Fayalite	-	-	-	LIFH	-	134.582	7510	4/5
Ca	Anorthite	-	-	PETJ	-	-	107.609	2781	2/3
Na	Albite	-	TAP	-	-	-	129.620	1278	3.5/4
K	Orthoclase	-	-	-	-	PETL	119.724	6406	2.5/2.5
Ba	Barite	-	-	-	LIFH	-	193.019	2152	3/4

Mineral Phase: Garnet

Date Analyzed: February 22nd, 2017

Element:	Reference standard:	Spectrometers					L-Value	Counts	Back+/Back-
		1	2	3	4	5			
		TAP/LDE1	TAP/LDE2	PETJ/LIF	PETH/LIFH	PETL/LIFL			
Si	Almandine	TAP	-	-	-	-	77.257	6558	3/6.5
Al	Almandine	TAP	-	-	-	-	90.501	3732	3.5/6
Cr	Chromite	-	-	-	-	LIFL	159.047	4587	3/3
Fe	Almandine	-	-	-	LIFH	-	134.582	2721	4/5
Ti	Rutile	-	-	PETJ	-	-	88.091	11103	3.5/4
Mg	Pyrope	-	TAP	-	-	-	107.448	3483	3.5/5.5
Mn	Spessartine	-	-	-	LIFH	-	146.126	4289	4/4
Ca	Grossular	-	-	PETJ	-	-	107.604	5284	2/3

Mineral Phase: Sulfides

Date Analyzed: February 22nd, 2017

Element:	Reference standard:	Spectrometers					L-Value	Counts	Back+/Back-
		1	2	3	4	5			
		TAP/LDE1	TAP/LDE2	PETJ/LIF	PETH/LIFH	PETL/LIFL			
Fe	Pyrite	-	-	-	LIFH	-	134.572	7310	4/5
S	Pyrite	-	-	PETJ	-	-	172.056	8152	2.5/6
Cu	Chalcopyrite	-	-	-	-	LIFL	106.976	4327	2.5/5.2
Ni	Pentlandite	-	-	-	LIFH	-	115.199	5430	3/4
As	Arsenopyrite	TAP	-	-	-	-	105.030	3942	3/6.2
Zn	Sphalerite	-	-	-	-	LIFL	99.657	7448	2/6

Mineral Phase: Biotite / Muscovite / Amphiboles / Chlorite

Date Analyzed: February 22nd, 2017

Element:	Reference standard:	Spectrometers					L-Value	Counts	Back+/Back-
		1	2	3	4	5			
		TAP/LDE1	TAP/LDE2	PETJ/LIF	PETH/LIFH	PETL/LIFL			
Si	Cr - Augite	TAP	-	-	-	-	77.257	9018	3/6.5
Al	Cr - Augite	TAP	-	-	-	-	90.512	1280	3.5/6
Ti	Rutile	-	-	PETJ	-	-	88.091	11103	3.5/4
Fe	Fayalite	-	-	-	LIFH	-	134.582	7510	4/5
Mn	Rhodonite	-	-	-	LIFH	-	146.117	4412	4/4
Mg	Cr - Augite	-	TAP	-	-	-	107.480	2843	3.5/5.5
Na	Albite	-	TAP	-	-	-	129.620	1278	3.5/4
Ca	Diopside	-	-	PETJ	-	-	107.609	3745	2/3
K	Orthoclase	-	-	-	-	PETL	119.724	6400	2.5/2.5
F	Fluorite	-	TAP	-	-	-	199.613	3811	4.5/4.7
Cl	Sodalite	-	-	-	-	PETL	151.312	2302	2.5/3

Mineral Phase: Pyroxenes

Date Analyzed: February 22nd, 2017

Element:	Reference standard:	Spectrometers					L-Value	Counts	Back+/Back-
		1	2	3	4	5			
		TAP/LDE1	TAP/LDE2	PETJ/LIF	PETH/LIFH	PETL/LIFL			
Si	Cr - Augite	TAP	-	-	-	-	77.257	9018	3/6.5
Al	Cr - Augite	TAP	-	-	-	-	90.512	1280	3.5/6
Ti	Rutile	-	-	PETJ	-	-	88.091	11103	3.5/4
Fe	Fayalite	-	-	-	LIFH	-	134.582	7510	4/5
Mn	Rhodonite	-	-	-	LIFH	-	146.117	4412	4/4
Mg	San Carlos	-	TAP	-	-	-	107.459	8322	3.5/5.5
Na	Albite	-	TAP	-	-	-	129.620	1278	3.5/4
Ca	Diopside	-	-	PETJ	-	-	107.609	3745	2/3
K	Orthoclase	-	-	-	-	PETL	119.724	6406	2.5/2.5

Mineral Phase: Titanite

Date Analyzed: February 22nd, 2017

Element:	Reference standard:	Spectrometers					L-Value	Counts	Back+/Back-
		1	2	3	4	5			
		TAP/LDE1	TAP/LDE2	PETJ/LIF	PETH/LIFH	PETL/LIFL			
Si	Sphene	TAP	-	-	-	-	77.247	5811	3/6.5
Al	Albite	TAP	-	-	-	-	90.501	3681	3.5/6
Fe	Fayalite	-	-	-	LIFH	-	134.582	7510	4/5
Ti	Sphene	-	-	PETJ	-	-	88.101	3856	3.5/4
Mg	San Carlos	-	TAP	-	-	-	107.459	8322	3.5/5.5
Mn	Rhodonite	-	-	-	LIFH	-	146.117	4412	4/4
Na	Albite	-	TAP	-	-	-	129.620	1278	3.5/4
Ca	Sphene	-	-	PETJ	-	-	107.604	4491	2/3

Mineral Phase: Feldspars
 Date Analyzed: June 29th, 2017

Element:	Reference standard:	Spectrometers					L-Value	Counts	Back+/Back-
		1	2	3	4	5			
		TAP/LDE1	TAP/LDE2	PETJ/LIF	PETH/LIFH	PETL/LIFL			
Si	Albite	TAP	-	-	-	-	77.242	12118	3/6.5
Al	Albite	TAP	-	-	-	-	90.491	3639	3.5/6
Fe	Fayalite	-	-	-	LIFH	-	134.568	7514	4/5
Ca	Anorthite	-	-	-	-	PETL	107.507	7820	2/3
Na	Albite	-	TAP	-	-	-	129.620	1268	3.5/4
K	Orthoclase	-	-	-	-	PETL	119.749	6392	2.5/2.5
Ba	Barite	-	-	-	LIFH	-	193.005	2158	3/4

Mineral Phase: Garnet
 Date Analyzed: June 29th, 2017

Element:	Reference standard:	Spectrometers					L-Value	Counts	Back+/Back-
		1	2	3	4	5			
		TAP/LDE1	TAP/LDE2	PETJ/LIF	PETH/LIFH	PETL/LIFL			
Si	Almandine	TAP	-	-	-	-	77.237	6532	3/6.5
Al	Almandine	TAP	-	-	-	-	90.475	3731	3.5/6
Cr	Chromite	-	-	-	-	LIFL	159.062	4544	3/3
Fe	Almandine	-	-	-	LIFH	-	134.572	2709	4/5
Ti	Rutile	-	-	PETJ	-	-	88.096	11099	3.5/4
Mg	Pyrope	-	TAP	-	-	-	107.490	3540	3.5/5.5
Mn	Spessartine	-	-	-	LIFH	-	146.099	4296	4/4
Ca	Grossular	-	-	PETJ	-	-	107.614	5274	2/3

Mineral Phase: Sulfides
 Date Analyzed: June 29th, 2017

Element:	Reference standard:	Spectrometers					L-Value	Counts	Back+/Back-
		1	2	3	4	5			
		TAP/LDE1	TAP/LDE2	PETJ/LIF	PETH/LIFH	PETL/LIFL			
Fe	Pyrite	-	-	-	LIFH	-	134.564	7296	4/5
S	Pyrite	-	-	PETJ	-	-	172.061	8185	2.5/6
Cu	Chalcopyrite	-	-	-	-	LIFL	106.995	4268	2.5/5.2
Ni	Pentlandite	-	-	-	LIFH	-	115.149	5308	3/4
As	Arsenopyrite	TAP	-	-	-	-	105.030	3944	3/6.2
Zn	Sphalerite	-	-	-	-	LIFL	99.656	7460	2/6

Mineral Phase: Biotite / Muscovite / Amphiboles / Chlorite
 Date Analyzed: June 29th, 2017

Element:	Reference standard:	Spectrometers					L-Value	Counts	Back+/Back-
		1	2	3	4	5			
		TAP/LDE1	TAP/LDE2	PETJ/LIF	PETH/LIFH	PETL/LIFL			
Si	Cr - Augite	TAP	-	-	-	-	77.242	8938	3/6.5
Al	Cr - Augite	TAP	-	-	-	-	90.486	1267	3.5/6
Ti	Rutile	-	-	PETJ	-	-	88.096	11099	3.5/4
Fe	Fayalite	-	-	-	LIFH	-	134.568	7514	4/5
Mn	Rhodonite	-	-	-	LIFH	-	146.108	4745	4/4
Mg	Cr - Augite	-	TAP	-	-	-	107.495	2854	3.5/5.5
Na	Albite	-	TAP	-	-	-	129.620	1268	3.5/4
Ca	Diopside	-	-	PETJ	-	-	107.609	3732	2/3
K	Orthoclase	-	-	-	-	PETL	119.749	6392	2.5/2.5
F	Fluorite	-	TAP	-	-	-	199.635	397	4.5/4.7
Cl	Sodalite	-	-	-	-	PETL	151.292	2225	2.5/3

Mineral Phase: Pyroxenes
 Date Analyzed: June 29th, 2017

Element:	Reference standard:	Spectrometers					L-Value	Counts	Back+/Back-
		1	2	3	4	5			
		TAP/LDE1	TAP/LDE2	PETJ/LIF	PETH/LIFH	PETL/LIFL			
Si	Cr - Augite	TAP	-	-	-	-	77.242	8938	3/6.5
Al	Cr - Augite	TAP	-	-	-	-	90.486	1267	3.5/6
Ti	Rutile	-	-	PETJ	-	-	88.096	11099	3.5/4
Fe	Fayalite	-	-	-	LIFH	-	134.586	7514	4/5
Mn	Rhodonite	-	-	-	LIFH	-	146.108	4745	4/4
Mg	San Carlos	-	TAP	-	-	-	107.501	8387	3.5/5.5
Na	Albite	-	TAP	-	-	-	129.620	1268	3.5/4
Ca	Diopside	-	-	PETJ	-	-	107.609	3732	2/3
K	Orthoclase	-	-	-	-	PETL	119.749	6392	2.5/2.5
Cr	Chromite	-	-	-	-	LIFL	159.062	4544	3/3

Mineral Phase: Titanite
 Date Analyzed: June 29th, 2017

Element:	Reference standard:	Spectrometers					L-Value	Counts	Back+/Back-
		1	2	3	4	5			
		TAP/LDE1	TAP/LDE2	PETJ/LIF	PETH/LIFH	PETL/LIFL			
Si	Sphene	TAP	-	-	-	-	77.247	5796	3/6.5
Al	Albite	TAP	-	-	-	-	90.491	3639	3.5/6
Fe	Fayalite	-	-	-	LIFH	-	134.568	7514	4/5
Ti	Sphene	-	-	PETJ	-	-	88.106	3840	3.5/4
Mg	San Carlos	-	TAP	-	-	-	107.501	8387	3.5/5.5
Mn	Rhodonite	-	-	-	LIFH	-	146.108	4745	4/4
Na	Albite	-	TAP	-	-	-	129.620	1268	3.5/4
Ca	Sphene	-	-	PETJ	-	-	107.604	4463	2/3

Mineral Phase: Kyanite / Sillimanite / Kaolinite
 Date Analyzed: June 29th, 2017

Element:	Reference standard:	Spectrometers					L-Value	Counts	Back+/Back-
		1	2	3	4	5			
		TAP/LDE1	TAP/LDE2	PETJ/LIF	PETH/LIFH	PETL/LIFL			
Si	Kyanite	TAP	-	-	-	-	77.257	5835	3/6.5
Al	Kyanite	TAP	-	-	-	-	90.496	12628	3.5/6
K	Orthoclase	-	-	-	-	PETL	119.749	6392	2.5/2.5
Ca	Diopside	-	-	PETJ	-	-	107.609	3732	2/3
Na	Albite	-	TAP	-	-	-	129.620	1268	3.5/4
Fe	Fayalite	-	-	-	LIFH	-	134.568	7514	4/5
Mg	Cr - Augite	-	TAP	-	-	-	107.495	2854	3.5/5.5
Cr	Chromite	-	-	-	-	LIFL	159.062	4544	3/3
Mn	Rhodonite	-	-	-	LIFH	-	146.108	4745	4/4
Ti	Rutile	-	-	PETJ	-	-	88.096	11099	3.5/4

Appendix G:
Microprobe data
Part 1 - Plagioclase

	Molar Masses	SiO ₂	Al ₂ O ₃	Na ₂ O	CaO	FeO	BaO	K ₂ O	
Comments		Weight (%)							
Point:	Sample ID:	SiO ₂	Al ₂ O ₃	Na ₂ O	CaO	FeO	BaO	K ₂ O	Total
25	BC18B_Plag1_01	58.034	26.720	6.731	8.151	0.026	0.000	0.154	99.816
26	BC18B_Plag1_02	58.168	26.356	7.039	7.861	0.110	0.003	0.132	99.669
27	BC18B_Plag1_03	58.453	26.273	6.956	7.739	0.006	0.025	0.099	99.551
28	BC18B_Plag1_04	58.300	26.315	7.034	7.820	0.114	<LOD	0.106	99.663
29	BC18B_Plag2_01	57.942	26.833	6.879	8.133	0.114	<LOD	0.040	99.924
30	BC18B_Plag2_02	57.794	26.622	6.824	8.073	0.363	<LOD	0.037	99.677
31	BC18B_Plag3_01	58.363	26.435	6.869	7.851	0.021	<LOD	0.235	99.742
32	BC18B_Plag3_02	58.569	26.326	7.096	7.747	0.185	0.016	0.135	100.074
33	BC18B_Plag4_01	58.354	26.307	6.827	7.919	0.019	0.018	0.184	99.628
34	BC18B_Plag4_02	58.265	26.419	6.842	7.873	0.141	0.019	0.160	99.719
35	BC18B_Plag5_01	57.794	26.811	6.597	8.331	0.029	0.036	0.149	99.747
36	BC18B_Plag5_02	58.126	26.252	7.011	7.624	0.248	<LOD	0.094	99.347
37	BC18B_Plag6_01	58.122	26.625	6.828	8.076	0.021	0.055	0.125	99.852
38	BC18B_Plag6_02	59.007	25.908	7.233	7.293	0.211	<LOD	0.081	99.691
18	BC06_Plag1_01	67.748	19.905	11.531	0.356	0.125	0.018	0.111	99.794
1	BC20B_Plag1_01	57.866	26.695	6.722	8.304	0.010	0.021	0.122	99.740
2	BC20B_Plag1_02	57.264	26.940	6.416	8.469	0.317	<LOD	0.215	99.580
3	BC20B_Plag2_01	62.979	23.109	9.150	4.145	0.135	0.046	0.156	99.720
4	BC20B_Plag2_02	62.962	22.995	9.132	4.118	0.211	<LOD	0.152	99.533
5	BC20B_Plag3_01	57.836	26.743	6.668	8.254	0.021	0.016	0.159	99.697
6	BC20B_Plag3_02	57.862	26.920	6.761	8.244	0.067	<LOD	0.115	99.945
7	BC20B_Plag4_01	57.822	26.726	6.707	8.183	<LOD	0.035	0.133	99.594
8	BC20B_Plag4_02	57.898	26.668	6.717	8.197	0.204	0.024	0.120	99.828
9	BC20B_Plag5_01	58.597	25.865	6.246	7.178	0.005	<LOD	1.427	99.314
10	BC20B_Plag5_02	58.706	26.170	6.870	7.557	0.011	<LOD	0.285	99.549
11	BC20B_Plag5_03	58.142	26.601	6.812	8.141	0.015	0.046	0.149	99.906
24	BC28_Plag1_01	58.255	26.496	6.852	7.770	0.002	<LOD	0.122	99.477
25	BC28_Plag1_02	58.519	26.742	6.861	7.860	0.164	<LOD	0.096	100.235
26	BC28_Plag2_01	58.469	26.698	6.844	7.940	0.021	0.030	0.178	100.180
27	BC28_Plag2_02	58.789	26.366	6.992	7.617	0.156	0.055	0.132	100.107

Comments		Weight (%)							
Point:	Sample ID:	SiO ₂	Al ₂ O ₃	Na ₂ O	CaO	FeO	BaO	K ₂ O	Total
28	BC28_Plug3_01	58.365	26.484	6.854	7.785	0.023	<LOD	0.162	99.664
29	BC28_Plug3_02	58.470	26.470	6.946	7.640	0.209	0.021	0.100	99.856
30	BC28_Plug4_01	58.132	26.306	6.698	7.912	0.012	0.019	0.231	99.310
31	BC28_Plug4_02	58.139	26.463	6.684	7.609	0.098	0.030	0.312	99.335
52	BC28_Plug5_01	58.159	26.318	6.824	7.806	0.004	<LOD	0.160	99.249
53	BC28_Plug6_01	59.099	26.174	7.051	7.401	0.011	0.043	0.267	100.046
56	BC28_Plug7_01	57.785	26.596	6.642	8.035	0.010	0.009	0.231	99.308
39	BC29B_Plug1_01	58.213	26.523	6.765	7.756	0.036	0.060	0.230	99.583
40	BC29B_Plug1_02	58.292	26.345	7.062	7.785	0.170	0.015	0.109	99.778
41	BC29B_Plug2_01	58.137	26.726	6.681	8.109	0.040	<LOD	0.176	99.867
42	BC29B_Plug2_02	57.757	26.624	6.893	8.022	0.114	<LOD	0.133	99.505
43	BC29B_Plug3_01	58.637	25.638	5.932	6.961	0.135	0.005	2.011	99.319
44	BC29B_Plug3_02	57.875	26.896	6.635	8.208	0.259	0.005	0.194	100.072
45	BC29B_Plug4_01	58.179	26.652	6.846	8.017	0.020	0.002	0.196	99.912
46	BC29B_Plug4_02	58.204	26.580	6.814	8.009	0.179	0.001	0.142	99.929
47	BC29B_Plug5_01	58.103	26.495	6.771	7.956	0.041	0.044	0.204	99.614
48	BC29B_Plug5_02	58.156	26.347	6.910	7.925	0.162	<LOD	0.095	99.585
13	RO04_Plug1_01	52.814	30.084	4.428	11.969	0.025	<LOD	0.019	99.318
14	RO04_Plug1_02	52.850	30.159	4.454	12.048	0.091	<LOD	0.029	99.592
15	RO04_Plug1_03	53.821	29.296	5.006	11.105	0.047	<LOD	0.021	99.254
20	RO04_Plug2_01	51.852	31.033	3.949	12.827	0.322	0.019	0.010	100.012
21	RO04_Plug2_02	51.892	30.752	4.067	12.853	0.299	<LOD	0.024	99.883
22	RO04_Plug3_01	48.611	32.981	2.642	15.098	0.059	<LOD	0.016	99.369
23	RO04_Plug3_02	48.574	32.990	2.657	15.025	0.204	0.004	0.030	99.484
40	RO08A_Plug1_01	67.569	19.958	11.202	0.474	<LOD	<LOD	0.047	99.225
41	RO08A_Plug1_02	65.815	21.040	10.227	1.826	0.211	<LOD	0.148	99.205
42	RO08A_Plug2_01	58.545	25.783	7.097	7.217	0.054	<LOD	0.167	98.849
43	RO08A_Plug2_02	63.019	22.913	9.146	3.910	0.213	<LOD	0.126	99.308
44	RO08A_Plug3_01	63.076	22.615	9.102	3.733	0.029	<LOD	0.135	98.676
45	RO08A_Plug3_02	63.053	22.688	9.126	3.729	0.139	0.021	0.162	98.918
1	RO09B_Plug1_01	58.661	26.304	7.012	7.471	<LOD	<LOD	0.068	99.481
2	RO09B_Plug1_02	57.771	26.324	6.806	7.797	0.233	<LOD	0.050	98.980

Comments		Weight (%)							
Point:	Sample ID:	SiO ₂	Al ₂ O ₃	Na ₂ O	CaO	FeO	BaO	K ₂ O	Total
3	RO09B_Plug2_01	58.140	26.557	6.781	7.854	0.028	0.008	0.053	99.421
4	RO09B_Plug2_02	58.156	26.518	6.868	7.811	0.237	<LOD	0.071	99.650
5	RO09B_Plug3_01	57.972	26.463	6.900	7.826	0.025	<LOD	0.070	99.246
6	RO09B_Plug3_02	58.145	26.442	6.913	7.732	0.326	0.058	0.098	99.714
7	RO09B_Plug4_01	58.653	26.144	7.067	7.491	0.060	0.008	0.067	99.490
8	RO09B_Plug4_02	57.927	26.419	6.909	7.957	0.153	<LOD	0.063	99.392
9	RO09B_Plug5_01	58.494	26.234	7.079	7.577	0.038	0.011	0.073	99.506
10	RO09B_Plug5_02	58.289	26.567	6.930	7.578	0.245	<LOD	0.218	99.812
11	RO09B_Plug6_01	58.326	26.321	6.945	7.903	0.039	<LOD	0.069	99.596
12	RO09B_Plug6_02	58.761	26.282	6.961	7.835	0.271	0.030	0.094	100.234
1	C005A_Plug_01	61.282	24.613	8.074	0.095	0.008	0.126	5.789	99.987
2	C005A_Plug_02	61.209	24.666	8.241	0.366	0.042	0.126	5.809	100.459
3	C005A_Plug_03	60.963	24.671	8.120	0.096	0.052	0.086	6.006	99.994
4	C005A_Plug_04	61.116	24.751	8.157	0.262	<LOD	0.114	5.893	100.262
5	C005A_Plug_05	60.990	24.540	8.120	0.284	0.015	0.136	5.912	99.997
6	C005A_Plug_06	60.708	24.775	8.074	0.354	0.025	0.134	5.902	99.972
7	C005A_Plug_07	61.301	24.663	8.176	0.202	0.016	0.140	5.740	100.238
8	C005A_Plug_08	61.120	24.514	8.276	0.300	0.005	0.124	5.628	99.967
13	C005A_Plug_09	60.815	24.687	8.190	0.429	0.025	0.127	5.960	100.233
14	C005A_Plug_10	60.925	24.753	8.187	0.496	0.004	0.116	5.949	100.430
15	C005A_Plug_11	60.778	24.702	8.192	0.495	<LOD	0.108	6.018	100.286
16	C005A_Plug_12	61.235	24.661	8.117	0.109	<LOD	0.145	5.756	100.004
17	C005A_Plug_13	61.062	24.560	8.083	0.269	0.028	0.165	5.905	100.072
18	C005A_Plug_14	61.325	24.555	8.184	0.146	<LOD	0.105	5.599	99.910
57	C005A_Plug_15	60.720	24.609	8.053	0.254	<LOD	0.128	5.985	99.735
58	C005A_Plug_16	61.079	24.735	7.985	0.165	<LOD	0.109	5.940	99.992
59	C005A_Plug_17	60.919	24.803	8.033	0.167	<LOD	0.171	5.900	99.978
60	C005A_Plug_18	60.821	24.933	7.853	0.091	0.010	0.165	6.112	99.985
61	C005A_Plug_19	61.020	24.537	7.912	0.213	<LOD	0.157	5.876	99.685
62	C005A_Plug_20	61.174	24.634	7.916	0.114	0.002	0.131	5.944	99.915
63	C005A_Plug_21	61.322	24.840	8.145	0.428	<LOD	0.118	5.903	100.733
64	C005A_Plug_22	61.556	24.526	8.192	0.178	0.002	0.131	5.717	100.302

Comments		Weight (%)							
Point:	Sample ID:	SiO ₂	Al ₂ O ₃	Na ₂ O	CaO	FeO	BaO	K ₂ O	Total
21	C005B_Plug_01	61.279	24.777	8.121	0.295	0.031	0.127	5.869	100.499
22	C005B_Plug_02	60.544	24.890	8.070	0.285	0.009	0.129	5.744	99.671
23	C005B_Plug_03	60.718	24.667	7.989	0.257	0.031	0.122	5.894	99.678
24	C005B_Plug_04	60.771	24.487	8.044	0.173	<LOD	0.140	5.858	99.468
25	C005B_Plug_05	60.273	24.774	7.889	0.134	<LOD	0.156	6.099	99.303
26	C005B_Plug_06	60.511	24.497	8.029	0.146	0.011	0.118	5.943	99.255
27	C005B_Plug_07	60.872	24.414	8.026	0.057	<LOD	0.129	5.874	99.370
28	C005B_Plug_08	60.900	24.610	8.046	0.219	<LOD	0.151	5.881	99.790
29	C005B_Plug_09	60.821	24.612	8.082	0.087	0.013	0.142	5.790	99.547
30	C005B_Plug_10	61.058	24.435	7.837	0.134	0.024	0.140	5.775	99.403
31	C005B_Plug_11	61.198	24.471	8.132	0.150	<LOD	0.169	5.765	99.871
36	C005B_Plug_12	61.394	21.242	2.496	0.332	0.022	11.026	1.736	98.248
37	C005B_Plug_13	64.012	18.352	0.062	0.220	0.002	16.914	0.010	99.572
38	C005B_Plug_14	60.825	24.474	8.056	0.099	0.030	0.172	5.784	99.440
39	C005B_Plug_15	60.651	24.684	8.062	0.277	0.064	0.088	5.899	99.725
40	C005B_Plug_16	61.068	24.406	8.116	0.156	<LOD	0.153	5.680	99.563
41	C005B_Plug_17	60.924	24.756	7.936	0.311	0.004	0.126	5.927	99.984
42	C005B_Plug_18	60.971	24.571	7.993	0.105	0.015	0.169	5.861	99.685
43	C005B_Plug_19	60.734	24.770	7.881	0.295	<LOD	0.149	5.982	99.799
44	C005B_Plug_20	60.483	24.530	7.897	0.237	0.020	0.150	5.841	99.158
51	C008_Plug_01	57.960	26.798	6.534	0.068	<LOD	0.142	8.412	99.905
52	C008_Plug_02	57.533	26.711	6.501	0.021	0.015	0.175	8.471	99.427
53	C008_Plug_03	58.141	26.634	6.743	0.058	0.007	0.135	8.130	99.848
54	C008_Plug_04	58.550	26.085	6.945	0.018	<LOD	0.184	7.669	99.442
55	C008_Plug_05	58.658	26.436	7.001	0.051	<LOD	0.073	7.900	100.099
56	C008_Plug_06	58.060	26.562	6.700	0.024	<LOD	0.069	8.178	99.556
45	C010A_Plug_01	60.130	25.340	7.628	0.335	<LOD	0.096	6.697	100.212
46	C010A_Plug_02	60.277	25.384	7.657	0.190	0.034	0.114	6.625	100.281
47	C010A_Plug_03	60.018	25.590	7.515	0.190	<LOD	0.137	6.842	100.285
48	C010A_Plug_04	59.495	25.518	7.294	0.107	0.007	0.151	7.075	99.647
49	C010A_Plug_05	60.120	25.486	7.680	0.190	0.013	0.124	6.708	100.321
50	C010A_Plug_06	59.916	25.692	7.472	0.100	0.001	0.148	6.836	100.165

Comments		Cations (Based on 8 Oxygens)							Sum	Molar Fractions		
Point:	Sample ID:	Si	Al	Na	Ca	Fe	Ba	K	All Cations	X _{Ab}	X _{An}	X _{Kspar}
25	BC18B_Plag1_01	2.598	1.410	0.584	0.391	0.001	0.000	0.009	4.993	59.37	39.73	0.89
26	BC18B_Plag1_02	2.609	1.393	0.612	0.378	0.004	0.000	0.008	5.004	61.37	37.87	0.76
27	BC18B_Plag1_03	2.620	1.388	0.605	0.372	0.000	0.000	0.006	4.991	61.57	37.85	0.58
28	BC18B_Plag1_04	2.613	1.390	0.611	0.376	0.004	<LOD	0.006	5.000	61.57	37.82	0.61
29	BC18B_Plag2_01	2.592	1.415	0.597	0.390	0.004	<LOD	0.002	5.000	60.34	39.43	0.23
30	BC18B_Plag2_02	2.594	1.408	0.594	0.388	0.014	<LOD	0.002	5.000	60.34	39.45	0.22
31	BC18B_Plag3_01	2.613	1.395	0.596	0.377	0.001	<LOD	0.013	4.995	60.46	38.18	1.36
32	BC18B_Plag3_02	2.616	1.386	0.614	0.371	0.007	0.000	0.008	5.002	61.89	37.34	0.77
33	BC18B_Plag4_01	2.616	1.390	0.593	0.380	0.001	0.000	0.011	4.991	60.29	38.64	1.07
34	BC18B_Plag4_02	2.611	1.395	0.594	0.378	0.005	0.000	0.009	4.993	60.56	38.51	0.93
35	BC18B_Plag5_01	2.591	1.417	0.573	0.400	0.001	0.001	0.009	4.992	58.39	40.75	0.87
36	BC18B_Plag5_02	2.614	1.391	0.611	0.367	0.009	<LOD	0.005	4.999	62.12	37.33	0.55
37	BC18B_Plag6_01	2.602	1.405	0.593	0.387	0.001	0.001	0.007	4.996	60.04	39.24	0.72
38	BC18B_Plag6_02	2.639	1.366	0.627	0.349	0.008	<LOD	0.005	4.994	63.92	35.61	0.47
18	BC06_Plag1_01	2.971	1.029	0.980	0.017	0.005	0.000	0.006	5.008	97.71	1.67	0.62
1	BC20B_Plag1_01	2.594	1.411	0.584	0.399	0.000	0.000	0.007	4.996	59.01	40.28	0.70
2	BC20B_Plag1_02	2.576	1.428	0.560	0.408	0.012	<LOD	0.012	4.996	57.09	41.65	1.26
3	BC20B_Plag2_01	2.794	1.208	0.787	0.197	0.005	0.001	0.009	5.000	79.27	19.84	0.89
4	BC20B_Plag2_02	2.797	1.204	0.786	0.196	0.008	<LOD	0.009	4.999	79.36	19.77	0.87
5	BC20B_Plag3_01	2.594	1.413	0.580	0.397	0.001	0.000	0.009	4.994	58.83	40.24	0.92
6	BC20B_Plag3_02	2.589	1.419	0.586	0.395	0.003	<LOD	0.007	4.998	59.35	39.99	0.66
7	BC20B_Plag4_01	2.595	1.414	0.584	0.393	<LOD	0.001	0.008	4.994	59.27	39.96	0.77
8	BC20B_Plag4_02	2.595	1.409	0.584	0.394	0.008	0.000	0.007	4.996	59.31	39.99	0.70
9	BC20B_Plag5_01	2.640	1.373	0.546	0.346	0.000	<LOD	0.082	4.987	56.01	35.57	8.42
10	BC20B_Plag5_02	2.629	1.381	0.597	0.363	0.000	<LOD	0.016	4.986	61.16	37.17	1.67
11	BC20B_Plag5_03	2.602	1.403	0.591	0.390	0.001	0.001	0.009	4.996	59.71	39.43	0.86
24	BC28_Plag1_01	2.612	1.400	0.596	0.373	0.000	<LOD	0.007	4.989	61.04	38.25	0.72
25	BC28_Plag1_02	2.607	1.404	0.593	0.375	0.006	<LOD	0.005	4.990	60.89	38.55	0.56
26	BC28_Plag2_01	2.607	1.403	0.592	0.379	0.001	0.001	0.010	4.992	60.31	38.66	1.03
27	BC28_Plag2_02	2.622	1.386	0.605	0.364	0.006	0.001	0.008	4.991	61.94	37.29	0.77

Comments		Cations (Based on 8 Oxygens)							Sum	Molar Fractions		
Point:	Sample ID:	Si	Al	Na	Ca	Fe	Ba	K	All Cations	X _{Ab}	X _{An}	X _{Kspar}
28	BC28_Plug3_01	2.614	1.398	0.595	0.373	0.001	<LOD	0.009	4.990	60.86	38.20	0.95
29	BC28_Plug3_02	2.615	1.395	0.602	0.366	0.008	0.000	0.006	4.992	61.83	37.58	0.59
30	BC28_Plug4_01	2.614	1.394	0.584	0.381	0.000	0.000	0.013	4.987	59.69	38.96	1.35
31	BC28_Plug4_02	2.613	1.402	0.582	0.366	0.004	0.001	0.018	4.986	60.25	37.90	1.85
52	BC28_Plug5_01	2.615	1.395	0.595	0.376	0.000	<LOD	0.009	4.990	60.70	38.37	0.94
53	BC28_Plug6_01	2.635	1.375	0.609	0.354	0.000	0.001	0.015	4.990	62.31	36.14	1.55
56	BC28_Plug7_01	2.600	1.410	0.579	0.387	0.000	0.000	0.013	4.991	59.12	39.52	1.35
39	BC29B_Plug1_01	2.611	1.402	0.588	0.373	0.001	0.001	0.013	4.989	60.39	38.26	1.35
40	BC29B_Plug1_02	2.612	1.391	0.613	0.374	0.006	0.000	0.006	5.003	61.75	37.62	0.63
41	BC29B_Plug2_01	2.601	1.409	0.579	0.389	0.001	<LOD	0.010	4.989	59.24	39.73	1.03
42	BC29B_Plug2_02	2.595	1.410	0.600	0.386	0.004	<LOD	0.008	5.004	60.39	38.84	0.77
43	BC29B_Plug3_01	2.647	1.364	0.519	0.337	0.005	0.000	0.116	4.988	53.43	34.65	11.92
44	BC29B_Plug3_02	2.589	1.418	0.575	0.393	0.010	0.000	0.011	4.996	58.73	40.15	1.13
45	BC29B_Plug4_01	2.603	1.405	0.594	0.384	0.001	0.000	0.011	4.997	60.03	38.84	1.13
46	BC29B_Plug4_02	2.604	1.401	0.591	0.384	0.007	0.000	0.008	4.995	60.12	39.05	0.82
47	BC29B_Plug5_01	2.607	1.401	0.589	0.382	0.002	0.001	0.012	4.993	59.91	38.90	1.19
48	BC29B_Plug5_02	2.610	1.393	0.601	0.381	0.006	<LOD	0.005	4.997	60.87	38.58	0.55
13	RO04_Plug1_01	2.401	1.612	0.390	0.583	0.001	<LOD	0.001	4.989	40.06	59.83	0.11
14	RO04_Plug1_02	2.398	1.613	0.392	0.586	0.003	<LOD	0.002	4.993	40.01	59.81	0.17
15	RO04_Plug1_03	2.443	1.567	0.441	0.540	0.002	<LOD	0.001	4.994	44.87	55.01	0.12
20	RO04_Plug2_01	2.351	1.658	0.347	0.623	0.012	0.000	0.001	4.993	35.76	64.18	0.06
21	RO04_Plug2_02	2.357	1.646	0.358	0.625	0.011	<LOD	0.001	5.000	36.36	63.50	0.14
22	RO04_Plug3_01	2.231	1.784	0.235	0.742	0.002	<LOD	0.001	4.995	24.03	75.88	0.10
23	RO04_Plug3_02	2.229	1.784	0.236	0.739	0.008	0.000	0.002	4.998	24.20	75.62	0.18
40	RO08A_Plug1_01	2.973	1.035	0.956	0.022	<LOD	<LOD	0.003	4.989	97.45	2.28	0.27
41	RO08A_Plug1_02	2.910	1.096	0.877	0.086	0.008	<LOD	0.008	4.985	90.24	8.90	0.86
42	RO08A_Plug2_01	2.640	1.370	0.620	0.349	0.002	<LOD	0.010	4.990	63.39	35.62	0.98
43	RO08A_Plug2_02	2.803	1.201	0.789	0.186	0.008	<LOD	0.007	4.994	80.30	18.97	0.73
44	RO08A_Plug3_01	2.818	1.191	0.788	0.179	0.001	<LOD	0.008	4.985	80.88	18.33	0.79
45	RO08A_Plug3_02	2.814	1.193	0.789	0.178	0.005	0.000	0.009	4.989	80.81	18.25	0.94
1	RO09B_Plug1_01	2.627	1.388	0.609	0.358	<LOD	<LOD	0.004	4.986	62.69	36.91	0.40
2	RO09B_Plug1_02	2.607	1.400	0.596	0.377	0.009	<LOD	0.003	4.992	61.05	38.65	0.30

Comments		Cations (Based on 8 Oxygens)							Sum	Molar Fractions		
Point:	Sample ID:	Si	Al	Na	Ca	Fe	Ba	K	All Cations	X _{Ab}	X _{An}	X _{Kspar}
3	RO09B_Plug2_01	2.609	1.404	0.590	0.378	0.001	0.000	0.003	4.985	60.78	38.90	0.31
4	RO09B_Plug2_02	2.607	1.401	0.597	0.375	0.009	<LOD	0.004	4.993	61.15	38.43	0.42
5	RO09B_Plug3_01	2.608	1.403	0.602	0.377	0.001	<LOD	0.004	4.994	61.22	38.37	0.41
6	RO09B_Plug3_02	2.608	1.398	0.601	0.372	0.012	0.001	0.006	4.997	61.45	37.98	0.57
7	RO09B_Plug4_01	2.629	1.381	0.614	0.360	0.002	0.000	0.004	4.990	62.81	36.79	0.39
8	RO09B_Plug4_02	2.604	1.400	0.602	0.383	0.006	<LOD	0.004	4.999	60.89	38.75	0.37
9	RO09B_Plug5_01	2.623	1.386	0.615	0.364	0.001	0.000	0.004	4.994	62.57	37.01	0.42
10	RO09B_Plug5_02	2.609	1.401	0.601	0.363	0.009	<LOD	0.012	4.997	61.54	37.19	1.27
11	RO09B_Plug6_01	2.615	1.391	0.604	0.380	0.001	<LOD	0.004	4.994	61.15	38.45	0.40
12	RO09B_Plug6_02	2.620	1.381	0.602	0.374	0.010	0.001	0.005	4.993	61.32	38.14	0.54
1	C005A_Plug_01	2.758	1.305	0.704	0.005	0.000	0.002	0.332	5.108	67.65	0.44	31.91
2	C005A_Plug_02	2.748	1.305	0.717	0.018	0.002	0.002	0.333	5.124	67.19	1.65	31.16
3	C005A_Plug_03	2.749	1.311	0.710	0.005	0.002	0.002	0.345	5.123	66.97	0.44	32.59
4	C005A_Plug_04	2.747	1.311	0.711	0.013	<LOD	0.002	0.338	5.122	66.98	1.19	31.84
5	C005A_Plug_05	2.751	1.304	0.710	0.014	0.001	0.002	0.340	5.122	66.74	1.29	31.97
6	C005A_Plug_06	2.740	1.318	0.706	0.017	0.001	0.002	0.340	5.124	66.44	1.61	31.95
7	C005A_Plug_07	2.754	1.306	0.712	0.010	0.001	0.002	0.329	5.114	67.77	0.93	31.30
8	C005A_Plug_08	2.754	1.302	0.723	0.014	0.000	0.002	0.323	5.119	68.14	1.37	30.49
13	C005A_Plug_09	2.740	1.311	0.715	0.021	0.001	0.002	0.343	5.133	66.32	1.92	31.76
14	C005A_Plug_10	2.739	1.312	0.714	0.024	0.000	0.002	0.341	5.132	66.16	2.21	31.63
15	C005A_Plug_11	2.738	1.312	0.715	0.024	<LOD	0.002	0.346	5.137	65.93	2.20	31.87
16	C005A_Plug_12	2.756	1.308	0.708	0.005	<LOD	0.003	0.330	5.110	67.84	0.50	31.65
17	C005A_Plug_13	2.752	1.304	0.706	0.013	0.001	0.003	0.339	5.119	66.71	1.23	32.06
18	C005A_Plug_14	2.760	1.302	0.714	0.007	<LOD	0.002	0.321	5.107	68.49	0.68	30.83
57	C005A_Plug_15	2.746	1.312	0.706	0.012	<LOD	0.002	0.345	5.124	66.38	1.16	32.46
58	C005A_Plug_16	2.751	1.313	0.697	0.008	<LOD	0.002	0.341	5.112	66.63	0.76	32.61
59	C005A_Plug_17	2.746	1.318	0.702	0.008	<LOD	0.003	0.339	5.116	66.90	0.77	32.33
60	C005A_Plug_18	2.743	1.325	0.687	0.004	0.000	0.003	0.352	5.114	65.85	0.42	33.72
61	C005A_Plug_19	2.756	1.306	0.693	0.010	<LOD	0.003	0.339	5.107	66.51	0.99	32.50
62	C005A_Plug_20	2.757	1.308	0.692	0.006	0.000	0.002	0.342	5.106	66.58	0.53	32.89
63	C005A_Plug_21	2.745	1.310	0.707	0.021	<LOD	0.002	0.337	5.122	66.41	1.93	31.67
64	C005A_Plug_22	2.762	1.297	0.713	0.009	0.000	0.002	0.327	5.110	67.97	0.82	31.21

Comments		Cations (Based on 8 Oxygens)							Sum	Molar Fractions		
Point:	Sample ID:	Si	Al	Na	Ca	Fe	Ba	K	All Cations	X _{Ab}	X _{An}	X _{Kspar}
21	C005B_Plug_01	2.748	1.310	0.706	0.014	0.001	0.002	0.336	5.118	66.86	1.34	31.79
22	C005B_Plug_02	2.737	1.326	0.707	0.014	0.000	0.002	0.331	5.119	67.21	1.31	31.48
23	C005B_Plug_03	2.746	1.315	0.700	0.012	0.001	0.002	0.340	5.117	66.52	1.18	32.29
24	C005B_Plug_04	2.753	1.307	0.706	0.008	<LOD	0.002	0.338	5.116	67.07	0.80	32.14
25	C005B_Plug_05	2.738	1.326	0.695	0.007	<LOD	0.003	0.353	5.123	65.87	0.62	33.51
26	C005B_Plug_06	2.749	1.311	0.707	0.007	0.000	0.002	0.344	5.121	66.80	0.67	32.53
27	C005B_Plug_07	2.758	1.304	0.705	0.003	<LOD	0.002	0.340	5.112	67.32	0.26	32.42
28	C005B_Plug_08	2.750	1.310	0.704	0.011	<LOD	0.003	0.339	5.116	66.85	1.01	32.15
29	C005B_Plug_09	2.752	1.312	0.709	0.004	0.000	0.003	0.334	5.114	67.69	0.40	31.91
30	C005B_Plug_10	2.763	1.303	0.687	0.006	0.001	0.002	0.333	5.096	66.92	0.63	32.45
31	C005B_Plug_11	2.759	1.300	0.711	0.007	<LOD	0.003	0.332	5.112	67.72	0.69	31.59
36	C005B_Plug_12	2.914	1.188	0.230	0.017	0.001	0.205	0.105	4.660	65.31	4.80	29.89
37	C005B_Plug_13	3.059	1.034	0.006	0.011	0.000	0.317	0.001	4.427	32.61	63.93	3.46
38	C005B_Plug_14	2.755	1.306	0.707	0.005	0.001	0.003	0.334	5.112	67.60	0.46	31.94
39	C005B_Plug_15	2.743	1.316	0.707	0.013	0.002	0.002	0.340	5.123	66.65	1.27	32.09
40	C005B_Plug_16	2.760	1.300	0.711	0.008	<LOD	0.003	0.327	5.109	67.98	0.72	31.30
41	C005B_Plug_17	2.746	1.315	0.694	0.015	0.000	0.002	0.341	5.113	66.09	1.43	32.48
42	C005B_Plug_18	2.755	1.308	0.700	0.005	0.001	0.003	0.338	5.110	67.13	0.49	32.39
43	C005B_Plug_19	2.744	1.319	0.690	0.014	<LOD	0.003	0.345	5.114	65.78	1.36	32.85
44	C005B_Plug_20	2.749	1.314	0.696	0.012	0.001	0.003	0.339	5.112	66.52	1.10	32.37
51	C008_Plug_01	2.648	1.443	0.579	0.003	<LOD	0.003	0.490	5.165	53.97	0.31	45.72
52	C008_Plug_02	2.644	1.447	0.579	0.001	0.001	0.003	0.497	5.171	53.79	0.10	46.12
53	C008_Plug_03	2.655	1.433	0.597	0.003	0.000	0.002	0.474	5.164	55.62	0.26	44.12
54	C008_Plug_04	2.678	1.406	0.616	0.001	<LOD	0.003	0.447	5.151	57.87	0.08	42.05
55	C008_Plug_05	2.667	1.416	0.617	0.002	<LOD	0.001	0.458	5.162	57.26	0.23	42.51
56	C008_Plug_06	2.657	1.432	0.594	0.001	<LOD	0.001	0.477	5.163	55.40	0.11	44.49
45	C010A_Plug_01	2.716	1.349	0.668	0.016	<LOD	0.002	0.386	5.137	62.42	1.51	36.06
46	C010A_Plug_02	2.719	1.349	0.670	0.009	0.001	0.002	0.381	5.132	63.17	0.87	35.96
47	C010A_Plug_03	2.710	1.362	0.658	0.009	<LOD	0.002	0.394	5.135	62.00	0.87	37.14
48	C010A_Plug_04	2.706	1.368	0.643	0.005	0.000	0.003	0.411	5.136	60.74	0.49	38.77
49	C010A_Plug_05	2.713	1.355	0.672	0.009	0.000	0.002	0.386	5.138	62.96	0.86	36.18
50	C010A_Plug_06	2.708	1.368	0.655	0.005	0.000	0.003	0.394	5.132	62.14	0.46	37.40

Appendix G:
Microprobe data
Part 2 – Potassium Feldspar

Molar Masses	SiO ₂	Al ₂ O ₃	Na ₂ O	CaO	FeO	BaO	K ₂ O
	60.08	101.96	61.98	56.08	71.85	153.33	94.2

Comments		Mass (%)							
Point:	Sample ID:	SiO ₂	Al ₂ O ₃	Na ₂ O	CaO	FeO	BaO	K ₂ O	Total
51	BC18B_K1_01	63.991	18.957	0.873	0.019	<LOD	1.072	15.335	100.238
52	BC18B_K1_02	63.775	18.978	0.732	0.014	0.026	1.320	15.402	100.247
53	BC18B_K1_03	63.912	18.950	0.797	0.034	0.020	1.021	15.456	100.190
54	BC18B_K1_04	63.569	18.822	0.570	0.017	<LOD	1.375	15.710	100.059
55	BC18B_K1_05	63.992	18.929	0.837	0.018	0.004	1.171	15.441	100.392
56	BC18B_K2_01	63.925	18.922	0.803	0.011	<LOD	1.010	15.413	100.069
57	BC18B_K2_02	63.971	18.830	0.713	0.001	<LOD	1.043	15.616	100.161
58	BC18B_K2_03	64.101	18.737	0.891	0.026	0.001	1.004	15.252	100.012
12	BC20B_K1_01	64.036	18.802	1.240	0.087	0.024	0.365	14.951	99.505
49	BC20B_K1_01	63.569	18.692	0.831	0.023	0.024	1.278	15.359	99.776
13	BC20B_K1_02	64.424	18.846	1.706	0.067	0.336	0.289	14.555	100.223
14	BC20B_K2_01	64.668	18.720	1.573	0.066	0.016	0.303	14.572	99.918
50	BC20B_K2_01	63.999	18.813	0.846	0.004	0.002	1.070	15.452	100.186
15	BC20B_K2_02	64.665	18.555	0.008	<LOD	0.318	<LOD	17.064	100.606
16	BC20B_K3_01	64.563	18.783	1.969	0.165	0.009	0.263	14.019	99.771
17	BC20B_K3_02	65.169	18.825	2.815	0.047	0.164	0.148	13.026	100.194
19	BC20B_K4_01	64.728	18.700	1.525	0.053	0.026	0.301	14.729	100.062
20	BC20B_K4_02	64.542	18.929	1.485	0.040	0.345	0.192	14.784	100.317
21	BC20B_K5_01	64.248	18.732	1.046	0.055	0.030	0.339	15.385	99.835
22	BC20B_K5_02	64.858	18.730	1.119	0.039	0.272	0.313	15.251	100.582
23	BC20B_K6_01	64.433	18.794	1.020	0.052	0.023	0.301	15.353	99.976
24	BC20B_K6_02	64.379	18.723	1.084	0.064	0.199	0.314	15.295	100.058
32	BC28_K1_01	63.925	18.760	0.857	<LOD	0.016	1.405	15.226	100.181
33	BC28_K1_02	63.040	19.055	0.773	0.029	0.235	1.911	14.939	99.982
34	BC28_K2_01	63.628	18.909	0.799	0.009	0.002	1.160	15.305	99.812
35	BC28_K2_02	63.490	18.779	0.459	0.032	0.154	1.358	15.746	100.018
36	BC28_K3_01	63.689	18.901	0.820	0.012	<LOD	1.182	15.267	99.869
37	BC28_K3_02	63.844	18.830	0.849	0.014	0.108	1.237	15.241	100.123
38	BC28_K4_01	63.921	18.820	0.917	<LOD	0.017	1.212	15.084	99.960

Comments		Mass (%)							
Point:	Sample ID:	SiO ₂	Al ₂ O ₃	Na ₂ O	CaO	FeO	BaO	K ₂ O	Total
39	BC28_K4_02	63.042	18.972	0.527	0.011	0.134	2.111	15.333	100.130
54	BC28_K5_01	63.824	18.946	0.808	0.010	0.001	1.267	15.208	100.064
55	BC28_K6_01	63.916	18.898	1.073	<LOD	<LOD	1.267	14.925	100.065
16	RO04_K1_01	65.397	17.828	0.035	0.019	0.106	0.024	16.315	99.724
17	RO04_K1_02	65.296	18.174	0.035	0.006	0.068	0.060	16.465	100.104
18	RO04_K2_01	65.882	17.807	0.013	0.014	0.057	0.046	16.256	100.075
19	RO04_K2_02	65.369	17.976	0.029	<LOD	0.029	0.063	16.503	99.966
46	RO08A_K1_01	64.084	18.685	0.654	0.015	<LOD	0.211	15.867	99.502
47	RO08A_K1_02	64.345	18.586	0.664	0.013	0.133	0.179	15.888	99.808
48	RO08A_K2_01	64.328	18.553	0.618	<LOD	0.014	0.173	15.942	99.624
49	RO08A_K2_02	64.334	18.593	0.671	0.019	0.152	0.213	15.843	99.825
50	RO08A_K3_01	64.719	18.574	0.523	0.000	<LOD	0.278	16.266	100.351
51	RO08A_K3_02	64.848	18.494	0.459	0.002	0.001	0.299	16.400	100.503
57	RO09B_K1_01	64.046	18.851	0.428	0.408	0.060	0.011	15.984	99.788
58	RO09B_K1_02	64.116	18.484	0.117	0.025	0.100	0.099	16.566	99.507
59	RO09B_K2_01	64.613	18.535	0.046	0.008	0.135	0.018	16.856	100.211
9	C005A_Kspar_01	64.305	18.949	1.206	0.011	0.049	1.014	14.755	100.289
10	C005A_Kspar_02	64.079	18.925	1.102	0.015	0.117	0.980	15.005	100.223
11	C005A_Kspar_03	64.606	18.935	1.633	0.028	0.073	0.838	14.350	100.463
12	C005A_Kspar_04	64.415	18.896	1.162	0.030	0.298	0.808	15.014	100.623
19	C005A_Kspar_05	64.762	18.960	2.145	0.041	0.268	0.656	13.517	100.349
20	C005A_Kspar_06	64.447	18.934	1.248	0.044	0.086	0.771	14.805	100.335
65	C005A_Kspar_07	64.718	18.928	1.561	0.030	0.264	0.808	14.434	100.743
66	C005A_Kspar_08	63.966	18.648	0.883	0.043	0.190	0.780	15.318	99.828
67	C005A_Kspar_09	64.512	18.781	1.261	0.037	0.047	0.777	14.831	100.246
32	C005B_Kspar_01	63.931	18.703	1.228	0.027	0.248	0.594	14.936	99.667
33	C005B_Kspar_02	64.164	18.782	1.783	0.042	0.154	0.622	14.049	99.596
34	C005B_Kspar_03	64.252	18.817	1.585	0.027	0.355	0.613	14.322	99.971
35	C005B_Kspar_04	64.436	18.844	1.156	0.010	0.134	0.699	14.999	100.278

Comments		Cations (Based on 8 Oxygens)				Cations (Based on 8 O)			Sum	Molar Fractions		
Point:	Sample ID:	Si	Al	Na	Ca	Fe	Ba	K	All Cations	X _{Ab}	X _{An}	X _{Kspar}
51	BC18B_K1_01	2.967	1.036	0.078	0.001	<LOD	0.019	0.907	5.008	7.96	0.10	91.95
52	BC18B_K1_02	2.963	1.039	0.066	0.001	0.001	0.024	0.913	5.007	6.73	0.07	93.20
53	BC18B_K1_03	2.966	1.036	0.072	0.002	0.001	0.019	0.915	5.009	7.26	0.17	92.57
54	BC18B_K1_04	2.965	1.034	0.052	0.001	<LOD	0.025	0.935	5.011	5.22	0.09	94.69
55	BC18B_K1_05	2.966	1.034	0.075	0.001	0.000	0.021	0.913	5.011	7.60	0.09	92.31
56	BC18B_K2_01	2.968	1.035	0.072	0.001	<LOD	0.018	0.913	5.007	7.33	0.06	92.61
57	BC18B_K2_02	2.970	1.030	0.064	0.000	<LOD	0.019	0.925	5.009	6.49	0.01	93.51
58	BC18B_K2_03	2.976	1.025	0.080	0.001	0.000	0.018	0.903	5.004	8.14	0.13	91.72
12	BC20B_K1_01	2.973	1.029	0.112	0.004	0.001	0.007	0.885	5.011	11.15	0.43	88.42
49	BC20B_K1_01	2.968	1.029	0.075	0.001	0.001	0.023	0.915	5.012	7.59	0.12	92.29
13	BC20B_K1_02	2.969	1.024	0.152	0.003	0.013	0.005	0.856	5.023	15.07	0.33	84.60
14	BC20B_K2_01	2.983	1.018	0.141	0.003	0.001	0.005	0.857	5.008	14.05	0.33	85.63
50	BC20B_K2_01	2.971	1.029	0.076	0.000	0.000	0.019	0.915	5.010	7.68	0.02	92.30
15	BC20B_K2_02	2.985	1.010	0.001	<LOD	0.012	<LOD	1.005	5.013	0.07	<LOD	99.93
16	BC20B_K3_01	2.978	1.021	0.176	0.008	0.000	0.005	0.825	5.012	17.45	0.81	81.74
17	BC20B_K3_02	2.981	1.015	0.250	0.002	0.006	0.003	0.760	5.017	24.67	0.23	75.10
19	BC20B_K4_01	2.983	1.016	0.136	0.003	0.001	0.005	0.866	5.010	13.56	0.26	86.18
20	BC20B_K4_02	2.971	1.027	0.133	0.002	0.013	0.003	0.868	5.016	13.22	0.20	86.58
21	BC20B_K5_01	2.977	1.023	0.094	0.003	0.001	0.006	0.909	5.013	9.34	0.27	90.39
22	BC20B_K5_02	2.981	1.015	0.100	0.002	0.010	0.006	0.894	5.008	10.01	0.19	89.79
23	BC20B_K6_01	2.978	1.024	0.091	0.003	0.001	0.005	0.905	5.008	9.15	0.26	90.59
24	BC20B_K6_02	2.977	1.020	0.097	0.003	0.008	0.006	0.902	5.013	9.69	0.32	89.99
32	BC28_K1_01	2.971	1.028	0.077	<LOD	0.001	0.026	0.903	5.005	7.88	<LOD	92.12
33	BC28_K1_02	2.949	1.050	0.070	0.001	0.009	0.035	0.891	5.007	7.28	0.15	92.57
34	BC28_K2_01	2.965	1.038	0.072	0.000	0.000	0.021	0.910	5.007	7.35	0.05	92.61
35	BC28_K2_02	2.964	1.033	0.042	0.002	0.006	0.025	0.938	5.009	4.24	0.16	95.60
36	BC28_K3_01	2.966	1.037	0.074	0.001	<LOD	0.022	0.907	5.006	7.54	0.06	92.40
37	BC28_K3_02	2.968	1.031	0.077	0.001	0.004	0.023	0.904	5.007	7.80	0.07	92.13
38	BC28_K4_01	2.971	1.031	0.083	<LOD	0.001	0.022	0.894	5.002	8.46	<LOD	91.54

Comments		Cations (Based on 8 Oxygens)				Cations (Based on 8 O)			Sum	Molar Fractions		
Point:	Sample ID:	Si	Al	Na	Ca	Fe	Ba	K	All Cations	X _{Ab}	X _{An}	X _{Kspar}
39	BC28_K4_02	2.952	1.047	0.048	0.001	0.005	0.039	0.916	5.007	4.96	0.06	94.98
54	BC28_K5_01	2.966	1.038	0.073	0.000	0.000	0.023	0.902	5.002	7.47	0.05	92.48
55	BC28_K6_01	2.968	1.034	0.097	<LOD	<LOD	0.023	0.884	5.005	9.85	<LOD	90.15
16	RO04_K1_01	3.026	0.972	0.003	0.001	0.004	0.000	0.963	4.971	0.32	0.10	99.58
17	RO04_K1_02	3.014	0.988	0.003	0.000	0.003	0.001	0.969	4.978	0.32	0.03	99.65
18	RO04_K2_01	3.034	0.967	0.001	0.001	0.002	0.001	0.955	4.961	0.12	0.07	99.81
19	RO04_K2_02	3.021	0.979	0.003	<LOD	0.001	0.001	0.973	4.977	0.27	<LOD	99.73
46	RO08A_K1_01	2.980	1.024	0.059	0.001	<LOD	0.004	0.941	5.008	5.89	0.07	94.03
47	RO08A_K1_02	2.984	1.016	0.060	0.001	0.005	0.003	0.940	5.008	5.97	0.06	93.97
48	RO08A_K2_01	2.987	1.015	0.056	<LOD	0.001	0.003	0.944	5.006	5.56	<LOD	94.44
49	RO08A_K2_02	2.983	1.016	0.060	0.001	0.006	0.004	0.937	5.007	6.04	0.09	93.86
50	RO08A_K3_01	2.988	1.011	0.047	0.000	<LOD	0.005	0.958	5.009	4.66	0.00	95.34
51	RO08A_K3_02	2.992	1.005	0.041	0.000	0.000	0.005	0.965	5.009	4.08	0.01	95.91
57	RO09B_K1_01	2.970	1.030	0.038	0.020	0.002	0.000	0.945	5.007	3.83	2.02	94.15
58	RO09B_K1_02	2.987	1.015	0.011	0.001	0.004	0.002	0.984	5.003	1.06	0.13	98.81
59	RO09B_K2_01	2.989	1.011	0.004	0.000	0.005	0.000	0.995	5.005	0.41	0.04	99.55
9	C005A_Kspar_01	2.971	1.032	0.108	0.001	0.002	0.018	0.870	5.002	11.04	0.06	88.90
10	C005A_Kspar_02	2.967	1.033	0.099	0.001	0.005	0.018	0.886	5.009	10.03	0.08	89.89
11	C005A_Kspar_03	2.973	1.027	0.146	0.001	0.003	0.015	0.842	5.007	14.72	0.14	85.14
12	C005A_Kspar_04	2.970	1.027	0.104	0.001	0.011	0.015	0.883	5.011	10.51	0.15	89.34
19	C005A_Kspar_05	2.973	1.026	0.191	0.002	0.010	0.012	0.792	5.005	19.39	0.20	80.40
20	C005A_Kspar_06	2.973	1.029	0.112	0.002	0.003	0.014	0.871	5.004	11.33	0.22	88.45
65	C005A_Kspar_07	2.972	1.025	0.139	0.001	0.010	0.015	0.846	5.008	14.10	0.15	85.75
66	C005A_Kspar_08	2.975	1.022	0.080	0.002	0.007	0.014	0.909	5.009	8.04	0.22	91.75
67	C005A_Kspar_09	2.978	1.022	0.113	0.002	0.002	0.014	0.873	5.004	11.42	0.19	88.39
32	C005B_Kspar_01	2.972	1.025	0.111	0.001	0.010	0.011	0.886	5.014	11.09	0.13	88.77
33	C005B_Kspar_02	2.973	1.026	0.160	0.002	0.006	0.011	0.830	5.009	16.14	0.21	83.65
34	C005B_Kspar_03	2.971	1.025	0.142	0.001	0.014	0.011	0.845	5.010	14.38	0.14	85.49
35	C005B_Kspar_04	2.975	1.025	0.103	0.000	0.005	0.013	0.883	5.006	10.48	0.05	89.47

Appendix G:
Microprobe data
Part 3 – Garnet

Molar Masses	SiO ₂	Al ₂ O ₃	MgO	CaO	TiO ₂	FeO	MnO	Cr ₂ O ₃
	60.08	101.96	40.30	56.08	79.87	71.85	70.94	152.00

Comments:		Weight (%)								
Point:	Sample ID:	SiO ₂	Al ₂ O ₃	MgO	CaO	TiO ₂	FeO	MnO	Cr ₂ O ₃	Total
91	BC18B_Garnet1_Line 001	37.815	21.557	1.794	10.472	0.026	24.577	3.822	<LOD	100.050
92	BC18B_Garnet1_Line 002	38.295	22.000	3.568	8.665	0.001	25.855	2.420	<LOD	100.802
93	BC18B_Garnet1_Line 003	38.387	21.973	4.752	8.060	0.014	25.377	1.695	0.008	100.266
94	BC18B_Garnet1_Line 004	38.742	22.147	5.420	8.334	0.036	24.358	1.397	<LOD	100.429
95	BC18B_Garnet1_Line 005	38.617	22.048	5.327	8.353	0.019	24.446	1.436	0.027	100.273
96	BC18B_Garnet1_Line 006	38.553	22.072	5.578	8.253	0.014	24.064	1.320	0.000	99.854
97	BC18B_Garnet1_Line 007	38.634	22.155	5.582	8.469	0.061	24.083	1.266	0.004	100.254
98	BC18B_Garnet1_Line 008	38.776	22.268	5.593	8.250	0.036	24.203	1.314	<LOD	100.437
99	BC18B_Garnet1_Line 009	38.653	22.168	5.666	8.284	0.030	24.040	1.251	<LOD	100.091
100	BC18B_Garnet1_Line 010	38.718	22.337	5.687	8.156	0.023	24.072	1.292	0.011	100.296
101	BC18B_Garnet1_Line 011	38.779	22.203	5.588	8.214	0.008	24.398	1.390	<LOD	100.579
102	BC18B_Garnet1_Line 012	38.360	22.109	5.415	8.109	<LOD	24.454	1.391	0.003	99.839
103	BC18B_Garnet1_Line 013	38.522	22.015	5.364	8.271	0.044	24.593	1.414	<LOD	100.199
104	BC18B_Garnet1_Line 014	38.454	22.045	5.062	8.119	0.018	25.048	1.598	<LOD	100.338
105	BC18B_Garnet1_Line 015	38.356	22.134	4.857	8.075	0.000	25.241	1.653	0.011	100.327
106	BC18B_Garnet1_Line 016	38.447	22.142	5.017	8.237	0.019	24.639	1.430	0.012	99.943
107	BC18B_Garnet1_Line 017	38.404	22.163	5.312	8.384	0.035	24.416	1.332	<LOD	100.028
108	BC18B_Garnet1_Line 018	38.714	22.171	4.940	8.356	0.023	24.911	1.491	<LOD	100.592
109	BC18B_Garnet1_Line 019	38.323	21.985	4.241	8.294	0.003	25.744	1.798	0.018	100.406
110	BC18B_Garnet1_Line 020	37.671	21.626	1.766	10.787	0.008	24.171	4.049	0.019	100.097
111	BC18B_Garnet2_Line 001	37.635	21.658	1.380	10.904	0.005	23.778	4.981	0.018	100.359
112	BC18B_Garnet2_Line 002	37.903	21.809	3.009	8.562	<LOD	26.487	2.516	<LOD	100.275
113	BC18B_Garnet2_Line 003	37.884	21.821	2.626	9.674	0.000	25.598	2.678	0.019	100.300
114	BC18B_Garnet2_Line 004	38.011	21.916	3.151	8.631	<LOD	26.273	2.480	0.006	100.450
115	BC18B_Garnet2_Line 005	37.810	21.819	3.387	8.343	0.007	26.629	2.278	0.004	100.277
116	BC18B_Garnet2_Line 006	38.082	21.698	3.579	8.145	0.003	26.518	2.157	0.003	100.185
117	BC18B_Garnet2_Line 007	38.149	21.962	3.753	8.273	0.001	26.196	2.070	0.007	100.411
118	BC18B_Garnet2_Line 008	38.131	21.966	3.880	7.914	0.015	26.474	2.031	<LOD	100.391

Comments:		Weight (%)								
Point:	Sample ID:	SiO ₂	Al ₂ O ₃	MgO	CaO	TiO ₂	FeO	MnO	Cr ₂ O ₃	Total
119	BC18B_Garnet2_Line 009	38.120	21.707	3.611	8.164	<LOD	26.431	2.180	<LOD	100.194
120	BC18B_Garnet2_Line 010	38.164	21.906	3.604	8.148	<LOD	26.670	2.202	<LOD	100.679
121	BC18B_Garnet2_Line 011	38.113	21.938	3.935	8.028	<LOD	26.317	1.996	0.020	100.343
122	BC18B_Garnet2_Line 012	38.215	22.034	4.263	7.669	0.014	26.557	1.789	<LOD	100.536
123	BC18B_Garnet2_Line 013	38.542	22.044	4.351	7.590	<LOD	26.496	1.735	0.008	100.762
124	BC18B_Garnet2_Line 014	38.237	21.997	4.030	7.719	<LOD	26.813	1.995	0.008	100.792
125	BC18B_Garnet2_Line 015	37.802	21.670	2.262	9.912	0.005	25.394	3.349	0.007	100.401
126	BC18B_Garnet3_Line 001	37.715	21.649	2.026	8.538	0.027	26.738	3.851	<LOD	100.538
127	BC18B_Garnet3_Line 002	38.178	21.781	3.092	8.427	0.025	26.858	2.570	0.009	100.940
128	BC18B_Garnet3_Line 003	38.323	21.903	3.669	8.136	0.025	26.798	2.158	<LOD	100.995
129	BC18B_Garnet3_Line 004	38.248	21.958	3.555	8.648	0.010	26.250	1.998	0.000	100.667
130	BC18B_Garnet3_Line 005	38.108	21.837	3.099	8.572	0.003	26.678	2.469	<LOD	100.744
131	BC18B_Garnet3_Line 006	37.692	21.742	2.111	9.520	0.006	26.022	3.441	0.007	100.541
132	BC18B_Garnet3_Line 007	37.952	21.649	2.030	10.410	<LOD	25.391	3.324	0.013	100.753
133	BC18B_Garnet3_Line 008	37.996	21.801	2.824	9.325	<LOD	26.276	2.449	0.010	100.669
134	BC18B_Garnet3_Line 009	37.967	21.885	2.734	9.161	0.015	26.269	2.504	0.006	100.541
135	BC18B_Garnet3_Line 010	37.949	21.814	3.025	8.849	<LOD	26.532	2.372	<LOD	100.533
136	BC18B_Garnet3_Line 011	38.048	22.012	3.228	9.129	0.010	26.030	2.078	0.002	100.537
137	BC18B_Garnet3_Line 012	38.143	21.873	3.690	8.077	0.011	26.713	1.997	0.012	100.516
138	BC18B_Garnet3_Line 013	38.168	21.742	3.671	8.193	0.009	26.726	2.062	<LOD	100.567
139	BC18B_Garnet3_Line 014	37.981	21.769	3.493	7.822	<LOD	27.134	2.315	0.006	100.516
140	BC18B_Garnet3_Line 015	37.704	21.587	2.217	9.147	<LOD	26.103	3.518	<LOD	100.260
1	BC20B_Garnet1_Line 001	37.774	21.626	1.998	11.135	0.015	22.210	5.491	<LOD	100.239
2	BC20B_Garnet1_Line 002	37.858	21.633	2.822	9.803	0.006	24.015	3.849	<LOD	99.984
3	BC20B_Garnet1_Line 003	37.821	21.605	2.134	11.141	0.000	22.619	5.160	<LOD	100.472
4	BC20B_Garnet1_Line 004	37.624	21.664	2.249	10.634	<LOD	23.830	4.087	0.004	100.091
5	BC20B_Garnet1_Line 005	37.860	21.719	4.075	8.204	0.006	25.400	2.644	0.010	99.918
6	BC20B_Garnet1_Line 006	38.105	21.777	4.298	8.524	0.038	25.239	2.172	<LOD	100.148
7	BC20B_Garnet1_Line 007	37.790	21.810	3.633	8.348	0.017	26.108	2.393	<LOD	100.083
8	BC20B_Garnet1_Line 008	38.386	21.911	5.037	8.496	0.050	24.572	2.000	0.004	100.456
9	BC20B_Garnet1_Line 009	38.305	21.834	4.799	8.415	0.043	24.731	2.037	0.000	100.164
10	BC20B_Garnet1_Line 010	38.105	21.855	4.736	8.511	0.034	24.845	2.119	<LOD	100.202

Comments:		Weight (%)								
Point:	Sample ID:	SiO ₂	Al ₂ O ₃	MgO	CaO	TiO ₂	FeO	MnO	Cr ₂ O ₃	Total
11	BC20B_Garnet1_Line 011	37.968	21.839	4.019	8.590	<LOD	24.843	2.737	0.018	100.010
12	BC20B_Garnet1_Line 012	37.906	21.725	3.852	8.578	0.008	25.263	2.512	0.014	99.858
13	BC20B_Garnet1_Line 013	38.198	21.823	4.507	8.332	0.000	25.046	2.373	<LOD	100.276
14	BC20B_Garnet1_Line 014	38.152	21.901	3.943	8.617	0.002	24.936	2.816	<LOD	100.352
15	BC20B_Garnet1_Line 015	37.742	21.716	1.720	12.081	0.022	21.333	5.704	0.015	100.333
16	BC20B_Garnet1_Line 016	37.689	21.601	1.442	11.899	0.012	20.769	6.881	<LOD	100.292
17	BC20B_Garnet1_Line 017	37.922	21.735	1.430	12.099	0.010	20.397	6.944	0.010	100.547
18	BC20B_Garnet1_Line 018	37.415	21.693	2.505	9.916	0.017	23.778	4.605	0.000	99.929
19	BC20B_Garnet1_Line 019	37.975	21.894	2.737	9.891	0.002	24.198	4.127	<LOD	100.814
20	BC20B_Garnet1_Line 020	37.748	21.643	1.840	11.721	0.006	21.443	5.699	<LOD	100.077
21	BC20B_Garnet2_Line 001	37.926	21.572	2.028	10.758	0.006	21.562	6.242	0.020	100.114
22	BC20B_Garnet2_Line 002	38.178	21.852	4.339	8.184	0.000	25.087	2.670	0.005	100.315
23	BC20B_Garnet2_Line 003	38.132	21.822	4.458	8.186	0.001	24.690	2.480	0.001	99.770
24	BC20B_Garnet2_Line 004	38.125	21.772	4.316	8.196	0.009	24.988	2.637	0.004	100.047
25	BC20B_Garnet2_Line 005	38.232	21.774	4.189	8.319	0.011	24.990	2.759	0.003	100.277
26	BC20B_Garnet2_Line 006	38.006	21.839	3.099	9.274	0.007	23.508	4.581	0.013	100.327
27	BC20B_Garnet2_Line 007	38.122	21.840	2.712	10.433	<LOD	22.283	5.069	0.036	100.475
28	BC20B_Garnet2_Line 008	37.980	21.785	2.734	10.121	0.016	22.468	5.068	0.003	100.175
29	BC20B_Garnet2_Line 009	37.833	21.748	2.636	10.405	<LOD	22.145	5.151	<LOD	99.909
30	BC20B_Garnet2_Line 010	37.659	21.627	1.932	11.526	0.000	19.888	7.201	0.009	99.842
31	BC20B_Garnet3_Line 001	37.603	21.526	1.488	11.575	0.011	20.629	7.195	<LOD	100.021
32	BC20B_Garnet3_Line 002	37.911	21.645	2.990	9.512	<LOD	24.230	4.051	0.009	100.339
33	BC20B_Garnet3_Line 003	38.061	21.852	3.063	9.585	<LOD	24.025	3.771	0.023	100.372
34	BC20B_Garnet3_Line 004	38.099	21.763	3.410	9.192	<LOD	24.265	3.236	<LOD	99.961
35	BC20B_Garnet3_Line 005	37.942	21.796	3.641	9.077	0.001	24.629	2.919	0.001	100.006
36	BC20B_Garnet3_Line 006	38.114	21.856	3.957	8.370	0.012	25.200	2.843	<LOD	100.350
37	BC20B_Garnet3_Line 007	38.107	21.916	4.143	8.366	<LOD	25.109	2.557	0.004	100.199
38	BC20B_Garnet3_Line 008	38.088	21.924	3.993	8.465	0.023	24.907	2.741	0.008	100.149
39	BC20B_Garnet3_Line 009	37.959	21.725	2.643	10.143	0.012	22.958	4.933	<LOD	100.357
40	BC20B_Garnet3_Line 010	37.717	21.687	1.477	11.826	0.013	20.267	6.839	0.008	99.834
81	BC28_Garnet1_Line 001	37.938	21.616	1.909	11.830	0.007	20.425	6.860	0.029	100.614
82	BC28_Garnet1_Line 002	38.637	22.104	4.709	9.041	0.038	23.780	2.150	<LOD	100.442

Comments:		Weight (%)								
Point:	Sample ID:	SiO ₂	Al ₂ O ₃	MgO	CaO	TiO ₂	FeO	MnO	Cr ₂ O ₃	Total
83	BC28_Garnet1_Line 003	38.574	22.004	4.834	8.881	0.031	24.151	1.945	0.015	100.435
84	BC28_Garnet1_Line 004	38.593	22.180	4.800	9.197	0.021	23.914	1.801	<LOD	100.480
85	BC28_Garnet1_Line 005	38.525	21.961	4.995	8.900	0.031	23.637	1.679	0.000	99.728
86	BC28_Garnet1_Line 006	38.651	22.206	5.048	9.039	0.033	23.883	1.690	<LOD	100.538
87	BC28_Garnet1_Line 007	38.873	22.117	4.984	9.037	0.023	23.960	1.740	<LOD	100.725
88	BC28_Garnet1_Line 008	38.749	22.222	4.825	8.979	0.026	23.774	1.886	<LOD	100.453
89	BC28_Garnet1_Line 009	38.683	22.246	4.696	9.209	0.020	24.034	2.060	<LOD	100.933
90	BC28_Garnet1_Line 010	38.704	22.093	4.624	9.000	0.044	24.034	2.159	<LOD	100.637
91	BC28_Garnet1_Line 011	38.811	22.093	4.813	8.917	0.003	23.920	2.030	<LOD	100.568
92	BC28_Garnet1_Line 012	38.527	22.039	4.388	8.720	0.047	24.222	2.556	0.015	100.514
93	BC28_Garnet1_Line 013	38.212	21.829	3.326	9.228	0.041	23.686	4.148	<LOD	100.454
94	BC28_Garnet1_Line 014	38.544	21.962	4.009	9.187	0.022	24.203	2.754	<LOD	100.674
95	BC28_Garnet1_Line 015	38.048	21.804	2.063	10.332	0.028	21.693	6.833	0.017	100.818
96	BC28_Garnet2_Line 001	37.889	21.526	1.727	11.502	0.009	20.092	7.402	0.025	100.172
97	BC28_Garnet2_Line 002	38.250	21.990	4.029	8.059	0.001	24.629	3.476	<LOD	100.416
98	BC28_Garnet2_Line 003	38.521	22.119	4.871	8.214	0.025	24.087	2.542	0.004	100.383
99	BC28_Garnet2_Line 004	38.652	22.094	5.131	7.960	0.012	24.131	2.512	0.009	100.501
100	BC28_Garnet2_Line 005	38.599	22.185	5.214	7.918	0.005	24.159	2.464	<LOD	100.540
101	BC28_Garnet2_Line 006	38.543	22.067	5.043	7.889	0.007	24.274	2.576	<LOD	100.397
102	BC28_Garnet2_Line 007	38.586	22.080	4.772	7.908	<LOD	24.392	2.756	0.002	100.481
103	BC28_Garnet2_Line 008	38.631	22.093	5.015	7.719	<LOD	24.471	2.722	<LOD	100.628
104	BC28_Garnet2_Line 009	38.405	22.078	4.692	7.831	<LOD	24.640	2.841	<LOD	100.474
105	BC28_Garnet2_Line 010	37.695	21.680	1.559	11.476	0.018	19.790	7.823	0.014	100.055
141	BC29B_Garnet1_Line 001	37.985	21.777	2.695	9.653	0.010	23.974	4.326	0.027	100.447
142	BC29B_Garnet1_Line 002	39.183	22.420	4.775	8.857	0.028	24.184	1.734	0.009	101.190
143	BC29B_Garnet1_Line 003	38.414	22.000	4.370	9.655	0.052	24.560	1.107	0.001	100.159
144	BC29B_Garnet1_Line 004	38.490	22.092	4.210	9.712	0.047	24.799	1.096	<LOD	100.440
145	BC29B_Garnet1_Line 005	38.331	21.860	4.038	9.758	0.028	24.973	1.191	0.008	100.187
146	BC29B_Garnet1_Line 006	38.329	22.049	4.153	9.620	0.023	24.928	1.147	0.013	100.262
147	BC29B_Garnet1_Line 007	38.342	21.914	4.023	9.660	0.056	24.949	1.265	<LOD	100.192
148	BC29B_Garnet1_Line 008	38.342	21.920	3.967	9.500	0.038	24.939	1.311	0.013	100.030
149	BC29B_Garnet1_Line 009	38.322	21.997	3.864	9.630	0.020	24.978	1.455	0.004	100.270

Comments:		Weight (%)								
Point:	Sample ID:	SiO ₂	Al ₂ O ₃	MgO	CaO	TiO ₂	FeO	MnO	Cr ₂ O ₃	Total
150	BC29B_Garnet1_Line 010	38.257	21.930	3.604	9.728	0.038	25.226	1.658	<LOD	100.430
151	BC29B_Garnet1_Line 011	36.214	23.276	3.644	9.696	0.036	24.344	1.303	0.007	98.520
152	BC29B_Garnet1_Line 012	38.294	21.845	3.986	9.568	0.058	25.269	1.181	0.009	100.210
153	BC29B_Garnet1_Line 013	38.544	21.953	4.021	9.605	0.044	25.130	1.168	0.022	100.487
154	BC29B_Garnet1_Line 014	37.935	21.859	3.929	9.589	0.047	25.298	1.098	<LOD	99.745
155	BC29B_Garnet1_Line 015	38.441	21.928	4.113	9.647	0.075	25.113	1.061	<LOD	100.361
156	BC29B_Garnet1_Line 016	38.375	22.052	4.058	9.702	0.023	25.132	1.028	0.002	100.372
157	BC29B_Garnet1_Line 017	38.745	22.103	4.196	9.637	0.049	24.973	1.055	0.020	100.778
158	BC29B_Garnet1_Line 018	38.381	21.888	4.178	9.741	0.056	25.032	1.100	0.006	100.382
159	BC29B_Garnet1_Line 019	38.245	22.072	3.989	9.455	0.019	24.698	1.779	<LOD	100.255
160	BC29B_Garnet1_Line 020	37.660	21.646	1.621	11.379	<LOD	21.421	6.279	0.012	100.001
161	BC29B_Garnet2_Line 001	37.480	21.735	2.109	10.430	<LOD	22.336	6.014	0.018	100.119
162	BC29B_Garnet2_Line 002	38.344	22.078	4.165	8.803	0.033	24.437	2.722	0.005	100.587
163	BC29B_Garnet2_Line 003	38.697	22.103	5.017	9.155	0.055	23.724	1.752	<LOD	100.500
164	BC29B_Garnet2_Line 004	38.663	22.321	5.090	9.163	0.039	23.774	1.673	0.026	100.749
165	BC29B_Garnet2_Line 005	38.521	22.107	5.050	9.043	0.037	23.862	1.701	<LOD	100.317
166	BC29B_Garnet2_Line 006	38.528	21.993	4.969	8.912	0.068	23.923	1.695	<LOD	100.077
167	BC29B_Garnet2_Line 007	38.470	22.025	5.149	9.245	0.057	23.705	1.405	0.008	100.064
168	BC29B_Garnet2_Line 008	38.236	22.031	5.206	9.035	0.030	23.563	1.438	0.002	99.541
169	BC29B_Garnet2_Line 009	38.201	22.014	4.056	8.578	0.006	24.297	3.188	0.005	100.345
170	BC29B_Garnet2_Line 010	37.962	21.600	1.265	12.355	0.003	19.938	7.048	0.022	100.193
41	BC6_Garnet1_Line 001	37.878	21.912	5.078	1.937	0.001	32.442	0.837	0.000	100.085
42	BC6_Garnet1_Line 002	37.739	21.683	5.103	2.055	0.007	32.327	0.850	<LOD	99.752
43	BC6_Garnet1_Line 003	37.700	21.942	5.291	2.072	0.016	32.330	0.830	0.003	100.184
44	BC6_Garnet1_Line 004	37.756	21.837	5.180	2.092	0.022	32.159	0.847	0.003	99.896
45	BC6_Garnet1_Line 005	37.818	21.887	5.294	2.078	0.035	32.259	0.830	0.003	100.204
46	BC6_Garnet1_Line 006	37.652	21.795	5.225	2.095	0.016	31.945	0.800	0.017	99.545
47	BC6_Garnet1_Line 007	37.754	21.879	5.311	2.050	0.026	32.212	0.811	0.016	100.059
48	BC6_Garnet1_Line 008	37.774	21.910	5.205	1.956	0.019	32.200	0.871	<LOD	99.926
49	BC6_Garnet1_Line 009	37.834	21.841	5.162	1.906	0.028	32.673	0.847	0.011	100.302
50	BC6_Garnet1_Line 010	37.585	21.896	5.130	1.901	0.016	32.204	0.834	0.006	99.572
51	BC6_Garnet2_Line 001	37.381	21.693	4.518	1.842	0.002	33.237	0.899	0.020	99.592

Comments:		Weight (%)								
Point:	Sample ID:	SiO ₂	Al ₂ O ₃	MgO	CaO	TiO ₂	FeO	MnO	Cr ₂ O ₃	Total
52	BC6_Garnet2_Line 002	36.773	21.741	4.395	1.867	<LOD	33.519	0.910	0.016	99.209
53	BC6_Garnet2_Line 003	37.479	21.669	4.668	1.955	0.010	32.980	0.894	0.015	99.670
54	BC6_Garnet2_Line 004	37.648	21.658	5.096	1.984	0.012	32.364	0.859	0.017	99.638
55	BC6_Garnet2_Line 005	37.614	21.753	5.227	2.041	0.017	32.118	0.820	0.004	99.594
56	BC6_Garnet2_Line 006	37.798	21.872	5.316	2.032	0.016	31.980	0.832	0.001	99.847
57	BC6_Garnet2_Line 007	37.764	21.812	5.510	2.019	0.018	31.839	0.785	<LOD	99.744
58	BC6_Garnet2_Line 008	37.824	22.006	5.495	1.970	0.024	32.078	0.793	0.020	100.210
59	BC6_Garnet2_Line 009	37.939	21.840	5.500	1.943	0.020	31.929	0.797	<LOD	99.956
60	BC6_Garnet2_Line 010	37.891	21.830	5.497	2.027	0.019	31.918	0.745	0.023	99.950
61	BC6_Garnet2_Line 011	37.797	21.931	5.289	1.992	0.009	31.919	0.828	0.007	99.772
62	BC6_Garnet2_Line 012	37.994	21.871	5.182	2.032	0.011	32.324	0.805	0.006	100.225
63	BC6_Garnet2_Line 013	37.770	21.871	5.117	2.005	0.033	32.610	0.860	0.015	100.281
64	BC6_Garnet2_Line 014	37.667	21.923	5.065	2.003	0.000	32.552	0.778	0.014	100.002
65	BC6_Garnet2_Line 015	37.625	21.684	5.102	1.955	<LOD	32.306	0.874	0.000	99.537
66	BC6_Garnet2_Line 016	37.738	21.851	5.169	1.946	0.017	32.512	0.814	0.002	100.049
67	BC6_Garnet2_Line 017	37.610	21.670	5.167	1.887	<LOD	32.423	0.815	0.020	99.583
68	BC6_Garnet2_Line 018	37.641	21.767	5.021	2.043	0.019	32.530	0.849	0.012	99.882
69	BC6_Garnet2_Line 019	37.846	21.909	4.828	2.057	0.010	32.684	0.875	0.016	100.225
70	BC6_Garnet2_Line 020	37.654	21.666	4.751	1.948	<LOD	32.648	0.930	0.005	99.589
71	BC6_Garnet3_Line 001	37.766	21.852	5.016	1.922	<LOD	32.451	0.823	0.020	99.848
72	BC6_Garnet3_Line 002	37.833	21.902	5.451	2.029	0.016	31.981	0.778	0.014	100.004
73	BC6_Garnet3_Line 003	37.844	21.961	5.587	2.133	0.017	31.513	0.740	0.004	99.799
74	BC6_Garnet3_Line 004	37.861	21.928	5.703	2.196	0.035	31.378	0.732	0.024	99.857
75	BC6_Garnet3_Line 005	37.780	21.968	5.656	2.263	0.039	31.188	0.673	0.006	99.573
76	BC6_Garnet3_Line 006	38.284	22.075	5.751	2.206	<LOD	31.332	0.687	0.006	100.338
77	BC6_Garnet3_Line 007	38.068	22.051	5.819	2.210	0.020	31.316	0.702	0.014	100.200
78	BC6_Garnet3_Line 008	37.986	22.059	5.868	2.110	0.046	31.490	0.637	<LOD	100.195
79	BC6_Garnet3_Line 009	37.857	21.977	5.899	2.033	0.014	31.017	0.677	0.014	99.488
80	BC6_Garnet3_Line 010	38.038	22.075	5.959	2.023	0.017	31.339	0.659	0.014	100.124
81	BC6_Garnet3_Line 011	38.081	21.962	5.854	2.018	0.002	31.311	0.676	0.031	99.935
82	BC6_Garnet3_Line 012	38.010	22.077	5.848	1.924	0.031	31.702	0.705	0.007	100.304
83	BC6_Garnet3_Line 013	37.833	21.922	5.839	2.028	0.042	31.559	0.698	0.026	99.947

Comments:		Weight (%)								
Point:	Sample ID:	SiO ₂	Al ₂ O ₃	MgO	CaO	TiO ₂	FeO	MnO	Cr ₂ O ₃	Total
84	BC6_Garnet3_Line 014	38.062	21.784	5.826	2.060	0.019	31.408	0.651	0.012	99.822
85	BC6_Garnet3_Line 015	37.982	22.005	5.775	2.020	0.004	31.378	0.711	0.003	99.878
86	BC6_Garnet3_Line 016	37.926	21.872	5.688	2.065	<LOD	31.692	0.738	0.003	99.977
87	BC6_Garnet3_Line 017	37.829	21.817	5.649	2.065	0.015	31.658	0.727	0.001	99.761
88	BC6_Garnet3_Line 018	37.857	22.015	5.569	1.950	0.018	31.697	0.729	0.013	99.848
89	BC6_Garnet3_Line 019	37.778	21.838	5.506	1.928	<LOD	31.805	0.733	0.026	99.612
90	BC6_Garnet3_Line 020	37.957	21.918	5.501	1.913	<LOD	31.480	0.759	0.017	99.533
31	RO04_Garnet1_Line 001	38.531	22.018	6.709	3.485	<LOD	26.936	2.062	<LOD	99.733
32	RO04_Garnet1_Line 002	38.516	22.041	7.438	3.036	0.015	27.114	1.466	<LOD	99.606
33	RO04_Garnet1_Line 003	38.545	22.061	7.163	2.988	<LOD	27.499	1.619	0.003	99.877
34	RO04_Garnet1_Line 004	38.585	22.368	7.988	3.031	<LOD	26.662	1.057	0.001	99.690
35	RO04_Garnet1_Line 005	38.719	22.205	7.928	3.036	0.003	26.832	1.125	0.006	99.854
36	RO04_Garnet1_Line 006	38.683	22.260	8.217	3.005	0.009	26.477	0.967	<LOD	99.604
37	RO04_Garnet1_Line 007	38.921	22.330	8.650	2.999	<LOD	25.883	0.886	<LOD	99.647
38	RO04_Garnet1_Line 008	38.893	22.335	8.777	2.981	<LOD	25.787	0.953	0.006	99.725
39	RO04_Garnet1_Line 009	39.004	22.419	8.702	2.922	0.004	25.838	0.969	0.006	99.864
40	RO04_Garnet1_Line 010	38.974	22.322	8.721	2.936	0.015	25.720	0.948	<LOD	99.624
41	RO04_Garnet1_Line 011	38.786	22.236	8.773	2.910	0.009	25.602	1.011	0.002	99.329
42	RO04_Garnet1_Line 012	38.944	22.382	8.742	2.882	0.010	25.686	1.005	<LOD	99.641
43	RO04_Garnet1_Line 013	39.055	22.366	8.719	2.917	0.000	25.654	1.031	0.004	99.746
44	RO04_Garnet1_Line 014	38.931	22.266	8.737	2.880	0.019	25.893	1.058	0.005	99.789
45	RO04_Garnet1_Line 015	38.911	22.333	8.675	2.900	0.016	25.780	1.051	<LOD	99.653
46	RO04_Garnet1_Line 016	39.064	22.326	8.721	2.940	<LOD	25.895	1.027	0.001	99.945
47	RO04_Garnet1_Line 017	38.905	22.430	8.733	2.934	0.011	25.789	1.041	0.002	99.845
48	RO04_Garnet1_Line 018	38.810	22.323	8.715	2.916	<LOD	25.823	1.043	<LOD	99.615
49	RO04_Garnet1_Line 019	38.904	22.336	8.656	2.906	0.006	25.899	1.045	0.008	99.760
50	RO04_Garnet1_Line 020	38.917	22.361	8.520	2.919	0.028	25.987	1.069	0.004	99.805
51	RO04_Garnet1_Line 021	38.747	22.387	8.349	2.889	0.030	26.499	1.100	0.009	100.010
52	RO04_Garnet1_Line 022	38.556	22.283	8.108	2.898	0.001	26.616	1.100	0.020	99.582
53	RO04_Garnet1_Line 023	38.793	22.186	7.569	2.883	0.022	27.052	1.455	<LOD	99.956
54	RO04_Garnet1_Line 024	38.029	22.288	7.385	2.856	0.010	27.211	1.554	<LOD	99.329
55	RO04_Garnet1_Line 025	37.933	21.885	5.581	3.401	0.008	28.428	2.453	0.018	99.707

Comments:		Weight (%)								
Point:	Sample ID:	SiO ₂	Al ₂ O ₃	MgO	CaO	TiO ₂	FeO	MnO	Cr ₂ O ₃	Total
56	RO04_Garnet2_Line 001	38.031	21.792	5.014	3.962	0.006	28.812	2.683	<LOD	100.292
57	RO04_Garnet2_Line 002	39.108	22.412	8.552	3.063	0.008	26.153	1.029	<LOD	100.317
58	RO04_Garnet2_Line 003	38.964	22.422	8.632	3.068	0.013	25.966	1.088	<LOD	100.140
59	RO04_Garnet2_Line 004	38.980	22.285	8.413	2.982	0.024	25.909	1.265	0.021	99.879
60	RO04_Garnet2_Line 005	39.019	22.274	8.191	3.024	0.017	26.202	1.578	<LOD	100.296
61	RO04_Garnet2_Line 006	38.922	22.264	7.999	2.995	0.017	26.047	1.885	<LOD	100.121
62	RO04_Garnet2_Line 007	38.680	22.125	7.716	3.038	0.007	26.149	2.330	0.002	100.047
63	RO04_Garnet2_Line 008	38.638	21.938	7.136	3.457	0.001	26.012	2.831	<LOD	100.004
64	RO04_Garnet2_Line 009	38.513	22.053	6.590	3.647	0.022	26.124	3.283	0.006	100.238
65	RO04_Garnet2_Line 010	38.621	22.052	6.611	3.598	0.017	26.157	3.356	0.000	100.412
66	RO04_Garnet2_Line 011	38.439	22.106	6.618	3.585	0.017	26.183	3.266	<LOD	100.202
67	RO04_Garnet2_Line 012	38.528	21.934	6.593	3.419	0.008	26.410	3.261	0.018	100.171
68	RO04_Garnet2_Line 013	38.523	22.084	6.775	3.379	0.014	26.423	3.131	0.000	100.329
69	RO04_Garnet2_Line 014	38.569	22.033	6.951	3.462	0.030	26.009	3.012	<LOD	100.054
70	RO04_Garnet2_Line 015	38.807	22.158	7.246	3.337	<LOD	25.997	2.797	0.006	100.329
71	RO04_Garnet2_Line 016	38.704	22.231	7.616	3.235	0.008	25.961	2.498	<LOD	100.250
72	RO04_Garnet2_Line 017	38.855	22.273	7.956	3.209	<LOD	25.931	2.013	0.012	100.238
73	RO04_Garnet2_Line 018	38.990	22.298	8.270	3.097	0.014	26.190	1.463	0.008	100.330
74	RO04_Garnet2_Line 019	39.243	22.370	8.625	3.009	<LOD	25.733	1.120	0.017	100.113
75	RO04_Garnet2_Line 020	38.990	22.421	8.788	3.075	<LOD	25.822	1.055	<LOD	100.132
76	RO04_Garnet2_Line 021	39.114	22.379	9.016	3.085	<LOD	25.627	0.971	0.006	100.192
77	RO04_Garnet2_Line 022	39.314	22.502	8.987	3.170	0.008	25.476	0.888	0.033	100.378
78	RO04_Garnet2_Line 023	39.106	22.415	8.590	3.082	0.012	26.370	0.949	0.014	100.538
79	RO04_Garnet2_Line 024	38.901	22.335	7.543	3.080	0.012	27.169	1.294	<LOD	100.330
80	RO04_Garnet2_Line 025	38.217	21.873	5.679	3.013	<LOD	28.937	2.436	0.011	100.156
106	RO08A_Garnet1_Line 001	37.353	21.266	1.832	7.518	<LOD	23.986	7.912	<LOD	99.851
107	RO08A_Garnet1_Line 002	37.109	21.342	3.254	2.075	0.001	28.558	7.457	0.004	99.800
108	RO08A_Garnet1_Line 003	37.221	21.450	3.398	1.827	0.012	28.593	7.297	0.011	99.809
109	RO08A_Garnet1_Line 004	37.110	21.472	3.497	1.575	0.022	29.028	7.094	0.005	99.803
110	RO08A_Garnet1_Line 005	37.052	21.378	3.254	2.206	0.027	28.349	7.343	<LOD	99.596
111	RO08A_Garnet1_Line 006	37.342	21.567	2.290	5.985	0.016	25.446	7.419	0.007	100.072
112	RO08A_Garnet1_Line 007	37.388	21.121	3.044	3.300	0.005	28.104	7.105	<LOD	100.064

Comments:		Weight (%)								
Point:	Sample ID:	SiO ₂	Al ₂ O ₃	MgO	CaO	TiO ₂	FeO	MnO	Cr ₂ O ₃	Total
113	RO08A_Garnet1_Line 008	37.403	21.392	2.855	5.319	<LOD	26.719	6.372	0.030	100.089
114	RO08A_Garnet1_Line 009	37.102	21.131	3.528	2.653	0.001	28.937	6.064	0.006	99.422
115	RO08A_Garnet1_Line 010	37.053	21.518	4.032	0.879	0.011	30.157	6.042	0.000	99.692
116	RO08A_Garnet1_Line 011	37.170	21.534	3.922	0.779	0.021	30.496	6.065	0.022	100.009
117	RO08A_Garnet1_Line 012	37.017	21.436	3.435	0.782	0.024	30.315	6.766	<LOD	99.761
118	RO08A_Garnet1_Line 013	37.220	21.489	1.533	7.895	0.006	23.805	8.012	<LOD	99.958
119	RO08A_Garnet1_Line 014	37.271	21.356	1.532	7.941	0.007	23.716	7.937	<LOD	99.756
120	RO08A_Garnet1_Line 015	37.212	21.456	3.189	1.550	0.019	29.460	7.284	<LOD	100.142
121	RO08A_Garnet1_Line 016	37.198	21.385	2.931	1.349	<LOD	29.687	7.655	0.000	100.196
122	RO08A_Garnet1_Line 017	36.746	21.237	2.450	0.767	<LOD	29.177	9.478	<LOD	99.841
123	RO08A_Garnet1_Line 018	37.186	21.443	2.377	3.415	<LOD	27.935	7.833	0.013	100.182
124	RO08A_Garnet1_Line 019	37.228	21.428	1.920	5.436	<LOD	25.809	8.366	<LOD	100.137
125	RO08A_Garnet1_Line 020	37.154	21.498	3.157	1.088	<LOD	29.818	7.489	<LOD	100.187
126	RO08A_Garnet1_Line 021	37.543	21.578	2.620	5.330	<LOD	26.774	6.384	<LOD	100.208
127	RO08A_Garnet1_Line 022	37.297	21.510	1.410	8.595	<LOD	22.746	8.293	0.016	99.858
128	RO08A_Garnet1_Line 023	37.411	21.295	2.022	7.279	<LOD	24.793	6.888	<LOD	99.676
129	RO08A_Garnet1_Line 024	37.345	21.425	2.851	3.102	<LOD	27.898	7.363	0.006	99.968
130	RO08A_Garnet1_Line 025	37.203	21.341	1.319	9.098	<LOD	22.181	8.210	<LOD	99.332
1	RO09B_Garnet1_Line 001	37.596	21.406	3.219	6.470	0.029	28.543	2.376	0.033	99.672
2	RO09B_Garnet1_Line 002	37.584	21.632	3.882	6.089	0.016	28.643	1.874	0.012	99.732
3	RO09B_Garnet1_Line 003	37.704	21.523	3.922	6.047	0.018	28.501	1.878	<LOD	99.581
4	RO09B_Garnet1_Line 004	37.610	21.508	3.909	6.072	0.016	28.812	1.906	0.009	99.842
5	RO09B_Garnet1_Line 005	37.483	21.382	3.922	6.130	0.035	28.578	1.869	0.002	99.401
6	RO09B_Garnet1_Line 006	37.663	21.687	3.936	6.053	0.000	28.404	1.896	0.006	99.645
7	RO09B_Garnet1_Line 007	37.698	21.426	3.887	6.145	0.038	28.699	1.853	0.009	99.755
8	RO09B_Garnet1_Line 008	37.836	21.525	3.774	6.383	0.010	28.562	1.842	0.015	99.947
9	RO09B_Garnet1_Line 009	37.610	21.497	3.490	6.745	<LOD	28.422	1.897	0.037	99.693
10	RO09B_Garnet1_Line 010	37.195	21.326	2.231	6.554	<LOD	28.394	3.697	0.002	99.390
11	RO09B_Garnet2_Line 001	37.325	21.208	2.385	6.246	0.038	28.707	3.545	0.007	99.461
12	RO09B_Garnet2_Line 002	37.769	21.439	3.795	5.747	0.007	28.751	2.027	0.013	99.548
13	RO09B_Garnet2_Line 003	37.778	21.595	3.929	5.602	<LOD	28.896	2.103	0.003	99.900
14	RO09B_Garnet2_Line 004	37.676	21.516	3.882	5.785	0.018	28.792	2.019	0.003	99.691

Comments:		Weight (%)								
Point:	Sample ID:	SiO ₂	Al ₂ O ₃	MgO	CaO	TiO ₂	FeO	MnO	Cr ₂ O ₃	Total
15	RO09B_Garnet2_Line 005	37.625	21.523	3.832	5.924	0.018	28.606	2.018	0.019	99.565
16	RO09B_Garnet2_Line 006	37.671	21.422	3.738	6.191	0.016	28.462	2.025	0.036	99.561
17	RO09B_Garnet2_Line 007	37.615	21.463	3.773	6.323	0.012	28.491	1.999	0.026	99.702
18	RO09B_Garnet2_Line 008	38.018	21.624	3.549	7.310	0.007	27.822	1.963	0.026	100.319
19	RO09B_Garnet2_Line 009	37.849	21.381	3.394	7.890	0.041	27.424	1.834	0.030	99.843
20	RO09B_Garnet2_Line 010	37.459	21.342	2.385	6.223	0.013	28.957	3.629	0.025	100.033
21	RO09B_Garnet3_Line 001	37.533	21.266	2.961	6.784	0.029	28.403	2.553	0.036	99.565
22	RO09B_Garnet3_Line 002	37.593	21.268	3.459	7.013	<LOD	28.126	1.991	0.039	99.475
23	RO09B_Garnet3_Line 003	37.826	21.556	3.606	6.752	<LOD	28.329	1.913	0.007	99.988
24	RO09B_Garnet3_Line 004	37.725	21.359	3.653	6.717	0.022	28.428	1.913	0.014	99.831
25	RO09B_Garnet3_Line 005	37.735	21.537	3.615	6.657	<LOD	28.298	1.913	0.011	99.761
26	RO09B_Garnet3_Line 006	37.871	21.555	3.632	6.527	<LOD	28.280	1.886	0.003	99.749
27	RO09B_Garnet3_Line 007	38.041	21.636	3.527	6.516	0.025	28.642	2.028	0.017	100.432
28	RO09B_Garnet3_Line 008	37.770	21.485	3.365	6.692	0.013	28.517	2.074	0.000	99.916
29	RO09B_Garnet3_Line 009	37.452	21.222	3.246	6.980	0.012	28.449	2.134	0.015	99.510
30	RO09B_Garnet3_Line 010	37.773	21.441	2.604	5.911	0.003	29.210	3.447	0.010	100.399
1	C005A_Garnet1 Line 001	37.222	21.704	4.790	1.938	0.019	32.811	1.195	0.001	99.680
2	C005A_Garnet1 Line 002	37.283	21.717	5.019	2.320	0.004	31.937	1.163	0.010	99.453
3	C005A_Garnet1 Line 003	37.426	21.848	5.188	2.217	<LOD	31.992	1.151	0.014	99.835
4	C005A_Garnet1 Line 004	37.499	21.758	5.277	2.284	<LOD	31.752	1.037	0.008	99.603
5	C005A_Garnet1 Line 005	37.477	21.791	5.396	2.252	0.037	31.790	1.030	0.011	99.784
7	C005A_Garnet1 Line 007	37.496	21.803	5.609	2.131	<LOD	31.456	1.001	0.000	99.479
8	C005A_Garnet1 Line 008	37.635	21.869	5.586	2.106	0.005	31.396	0.934	0.012	99.543
9	C005A_Garnet1 Line 009	37.517	21.773	5.580	2.053	<LOD	31.734	0.949	0.033	99.633
10	C005A_Garnet1 Line 010	37.446	21.753	5.583	2.023	<LOD	31.560	0.970	0.019	99.352
11	C005A_Garnet1 Line 011	37.663	21.769	5.478	2.172	0.001	31.398	1.003	0.014	99.498
12	C005A_Garnet1 Line 012	37.273	21.825	5.474	2.213	<LOD	31.779	1.026	0.021	99.600
13	C005A_Garnet1 Line 013	37.488	21.866	5.288	2.226	0.006	31.774	1.084	0.009	99.741
14	C005A_Garnet1 Line 014	37.566	21.777	5.021	2.327	0.017	32.079	1.146	0.005	99.938
15	C005A_Garnet1 Line 015	37.348	21.599	4.499	1.838	<LOD	33.072	1.194	0.030	99.574
16	C005A_Garnet2 Line 001	37.216	21.594	4.314	1.848	<LOD	33.302	1.255	<LOD	99.507
17	C005A_Garnet2 Line 002	37.206	21.841	4.857	2.080	0.023	32.652	1.186	0.013	99.858

Comments:		Weight (%)								
Point:	Sample ID:	SiO ₂	Al ₂ O ₃	MgO	CaO	TiO ₂	FeO	MnO	Cr ₂ O ₃	Total
18	C005A_Garnet2 Line 003	37.324	21.776	5.153	2.240	0.001	31.840	1.159	0.001	99.494
19	C005A_Garnet2 Line 004	37.701	21.708	5.206	2.266	0.018	31.705	1.078	0.017	99.699
20	C005A_Garnet2 Line 005	37.452	21.775	5.219	2.206	0.020	31.879	1.095	<LOD	99.642
6	C005A_Garnet2 Line 006	37.480	21.790	5.476	2.164	0.008	31.655	1.052	<LOD	99.624
21	C005A_Garnet2 Line 006	37.291	21.713	5.314	1.981	0.025	32.094	1.081	0.002	99.501
22	C005A_Garnet2 Line 007	37.394	21.732	5.316	1.928	0.002	32.060	1.089	0.006	99.527
23	C005A_Garnet2 Line 008	37.189	21.623	5.330	1.827	0.001	32.245	1.139	0.012	99.366
24	C005A_Garnet2 Line 009	37.629	21.775	5.278	1.835	0.000	32.444	1.180	0.028	100.169
25	C005A_Garnet2 Line 010	37.364	21.691	5.206	1.829	0.000	32.141	1.141	0.009	99.381
26	C005A_Garnet2 Line 011	37.333	21.573	5.043	1.985	0.025	32.193	1.125	0.004	99.281
27	C005A_Garnet2 Line 012	37.363	21.761	4.959	1.865	<LOD	32.516	1.175	0.018	99.655
28	C005A_Garnet2 Line 013	37.360	21.818	4.953	1.794	<LOD	32.681	1.169	0.018	99.789
29	C005A_Garnet2 Line 014	36.583	21.197	4.814	1.820	0.005	32.759	1.222	0.004	98.404
30	C005A_Garnet2 Line 015	37.127	21.646	4.764	1.850	0.014	32.790	1.200	<LOD	99.388
71	C005A_Garnet3 Line 001	37.352	21.631	4.330	1.999	0.001	33.236	1.237	0.017	99.803
72	C005A_Garnet3 Line 002	37.590	21.763	4.898	2.086	0.014	32.605	1.203	0.009	100.168
73	C005A_Garnet3 Line 003	37.718	21.737	5.029	2.105	0.010	32.203	1.107	0.002	99.911
74	C005A_Garnet3 Line 004	37.587	21.653	5.299	1.966	0.030	32.281	1.078	0.016	99.910
75	C005A_Garnet3 Line 005	37.581	21.607	5.505	1.719	0.029	32.040	1.038	0.025	99.544
76	C005A_Garnet3 Line 006	37.603	21.696	5.542	1.648	0.039	32.212	0.970	0.018	99.728
77	C005A_Garnet3 Line 007	37.672	21.757	5.615	1.703	0.021	32.367	1.002	0.020	100.157
78	C005A_Garnet3 Line 008	37.845	21.731	5.498	1.709	0.022	32.294	0.997	0.021	100.117
79	C005A_Garnet3 Line 009	37.708	21.623	5.508	1.826	0.027	32.012	1.001	0.025	99.730
80	C005A_Garnet3 Line 010	37.362	21.729	5.409	2.034	0.027	31.914	1.004	0.016	99.495
81	C005A_Garnet3 Line 011	37.739	21.883	5.393	1.924	0.015	32.198	1.047	<LOD	100.198
82	C005A_Garnet3 Line 012	37.577	21.650	5.310	1.924	0.021	32.041	1.036	0.009	99.568
83	C005A_Garnet3 Line 013	37.452	21.663	5.302	1.661	0.009	32.522	1.090	<LOD	99.696
84	C005A_Garnet3 Line 014	37.583	21.744	5.381	1.582	<LOD	32.432	1.086	0.010	99.809
85	C005A_Garnet3 Line 015	37.505	21.808	5.129	1.601	0.029	32.591	1.122	0.014	99.799
86	C005A_Garnet3 Line 016	37.592	21.634	5.157	1.760	<LOD	32.518	1.140	0.012	99.806
87	C005A_Garnet3 Line 017	37.441	21.695	5.064	1.888	0.027	32.359	1.160	<LOD	99.632
88	C005A_Garnet3 Line 018	37.278	21.596	4.889	2.093	0.007	32.464	1.169	0.017	99.513

Comments:		Weight (%)								
Point:	Sample ID:	SiO ₂	Al ₂ O ₃	MgO	CaO	TiO ₂	FeO	MnO	Cr ₂ O ₃	Total
89	C005A_Garnet3 Line 019	37.215	21.545	4.610	2.260	<LOD	32.862	1.196	<LOD	99.686
90	C005A_Garnet3 Line 020	37.138	21.453	3.716	2.156	0.014	33.930	1.319	0.008	99.734
31	C005B_Garnet1 Line 001	37.332	21.581	4.739	1.916	<LOD	32.703	1.148	0.013	99.426
32	C005B_Garnet1 Line 002	37.120	21.573	4.636	2.109	<LOD	32.708	1.131	0.020	99.293
33	C005B_Garnet1 Line 003	37.181	21.639	4.659	2.100	0.003	32.943	1.145	0.006	99.676
34	C005B_Garnet1 Line 004	37.121	21.612	4.752	2.141	0.013	32.457	1.129	<LOD	99.218
35	C005B_Garnet1 Line 005	37.173	21.459	4.712	2.162	0.011	32.500	1.158	0.025	99.200
36	C005B_Garnet1 Line 006	37.075	21.625	4.627	2.457	0.000	32.260	1.107	0.007	99.158
37	C005B_Garnet1 Line 007	36.972	21.635	4.652	2.253	0.009	32.357	1.084	0.015	98.977
38	C005B_Garnet1 Line 008	37.354	21.732	4.741	2.164	0.004	32.481	1.132	0.006	99.614
39	C005B_Garnet1 Line 009	37.148	21.580	4.799	2.117	0.004	32.476	1.133	0.011	99.268
40	C005B_Garnet1 Line 010	37.014	21.403	4.801	1.880	0.003	32.445	1.152	0.005	98.703
41	C005B_Garnet2 Line 001	37.272	21.602	4.345	2.133	0.006	33.198	1.224	0.019	99.799
42	C005B_Garnet2 Line 002	37.373	21.599	4.373	2.893	0.008	32.110	1.164	0.007	99.527
43	C005B_Garnet2 Line 003	37.300	21.622	4.545	2.756	0.007	32.170	1.134	0.016	99.550
44	C005B_Garnet2 Line 004	37.180	21.629	4.670	2.738	0.025	32.018	1.166	<LOD	99.421
45	C005B_Garnet2 Line 005	37.529	21.343	4.865	2.753	0.010	31.727	1.120	0.007	99.354
46	C005B_Garnet2 Line 006	37.457	21.498	4.829	3.002	<LOD	31.575	1.123	0.019	99.494
47	C005B_Garnet2 Line 007	37.448	21.527	4.846	3.017	0.027	31.722	1.083	0.009	99.679
48	C005B_Garnet2 Line 008	37.399	21.529	4.619	3.167	0.024	31.628	1.117	0.004	99.487
49	C005B_Garnet2 Line 009	37.259	21.406	4.312	3.164	0.008	32.098	1.159	0.024	99.430
50	C005B_Garnet2 Line 010	36.867	21.402	3.756	2.072	0.031	33.971	1.304	0.024	99.427
61	C008_Garnet1 Line 001	37.558	21.758	1.969	11.445	0.042	8.211	18.399	0.007	99.389
62	C008_Garnet1 Line 002	37.822	21.738	2.952	9.515	0.041	9.322	18.039	0.012	99.441
63	C008_Garnet1 Line 003	37.935	21.724	4.001	8.354	0.083	10.237	17.220	<LOD	99.553
64	C008_Garnet1 Line 004	37.826	21.747	4.328	9.106	0.092	10.417	15.437	0.021	98.974
65	C008_Garnet1 Line 005	38.285	21.826	4.412	10.163	0.115	10.340	14.072	0.011	99.224
66	C008_Garnet1 Line 006	38.109	21.746	4.503	8.758	0.089	10.627	15.439	0.033	99.304
67	C008_Garnet1 Line 007	37.829	21.764	4.044	7.968	0.058	10.287	17.112	0.028	99.090
68	C008_Garnet1 Line 008	37.595	21.574	2.643	10.101	0.019	8.902	18.171	0.061	99.066
69	C008_Garnet1 Line 009	37.516	21.482	2.397	10.700	0.040	8.558	18.232	0.089	99.014
70	C008_Garnet1 Line 010	37.491	21.486	1.347	13.402	0.056	7.538	17.671	0.082	99.073

Comments:		Weight (%)								
Point:	Sample ID:	SiO ₂	Al ₂ O ₃	MgO	CaO	TiO ₂	FeO	MnO	Cr ₂ O ₃	Total
51	C010A_Garnet1 Line 001	37.373	21.729	5.989	1.919	<LOD	30.336	1.736	0.010	99.071
52	C010A_Garnet1 Line 002	37.753	21.833	5.991	2.631	0.023	29.806	1.584	0.031	99.652
53	C010A_Garnet1 Line 003	37.595	21.909	6.075	2.985	0.019	29.460	1.367	0.056	99.466
54	C010A_Garnet1 Line 004	37.646	21.847	6.105	3.421	0.024	29.190	1.121	0.062	99.416
55	C010A_Garnet1 Line 005	37.608	21.890	6.030	3.612	<LOD	28.986	1.046	0.064	99.211
56	C010A_Garnet1 Line 006	37.536	21.963	5.841	3.616	0.000	28.892	1.220	0.040	99.108
57	C010A_Garnet1 Line 007	37.584	21.727	5.540	3.681	0.043	29.133	1.669	0.042	99.419
58	C010A_Garnet1 Line 008	37.378	21.661	4.920	3.392	0.018	29.395	2.653	0.038	99.455
59	C010A_Garnet1 Line 009	37.047	21.552	4.527	3.183	0.022	29.292	3.518	0.018	99.159
60	C010A_Garnet1 Line 010	37.410	21.724	4.370	2.602	<LOD	29.640	4.124	0.033	99.893

Comments:		Cations (Based on 12 Oxygens)								Sum
Point:	Sample ID:	Si	Al	Mg	Ca	Ti	Fe	Mn	Cr	All Cations
91	BC18B_Garnet1_Line 001	2.996	2.013	0.212	0.889	0.002	1.628	0.256	<LOD	7.996
92	BC18B_Garnet1_Line 002	2.989	2.024	0.415	0.725	0.000	1.687	0.160	<LOD	7.999
93	BC18B_Garnet1_Line 003	2.991	2.018	0.552	0.673	0.001	1.653	0.112	0.000	7.999
94	BC18B_Garnet1_Line 004	2.995	2.017	0.625	0.690	0.002	1.574	0.091	<LOD	7.995
95	BC18B_Garnet1_Line 005	2.993	2.014	0.616	0.694	0.001	1.584	0.094	0.002	7.998
96	BC18B_Garnet1_Line 006	2.994	2.020	0.646	0.687	0.001	1.562	0.087	0.000	7.996
97	BC18B_Garnet1_Line 007	2.988	2.020	0.644	0.702	0.004	1.558	0.083	0.000	7.998
98	BC18B_Garnet1_Line 008	2.992	2.025	0.643	0.682	0.002	1.562	0.086	<LOD	7.993
99	BC18B_Garnet1_Line 009	2.992	2.022	0.654	0.687	0.002	1.556	0.082	<LOD	7.995
100	BC18B_Garnet1_Line 010	2.990	2.033	0.655	0.675	0.001	1.554	0.084	0.001	7.992
101	BC18B_Garnet1_Line 011	2.992	2.019	0.643	0.679	0.000	1.574	0.091	<LOD	7.998
102	BC18B_Garnet1_Line 012	2.985	2.028	0.628	0.676	<LOD	1.591	0.092	0.000	8.001
103	BC18B_Garnet1_Line 013	2.989	2.013	0.621	0.688	0.003	1.596	0.093	<LOD	8.002
104	BC18B_Garnet1_Line 014	2.988	2.019	0.586	0.676	0.001	1.627	0.105	<LOD	8.002
105	BC18B_Garnet1_Line 015	2.984	2.029	0.563	0.673	0.000	1.642	0.109	0.001	8.001
106	BC18B_Garnet1_Line 016	2.992	2.031	0.582	0.687	0.001	1.603	0.094	0.001	7.991
107	BC18B_Garnet1_Line 017	2.983	2.029	0.615	0.698	0.002	1.586	0.088	<LOD	8.000
108	BC18B_Garnet1_Line 018	2.996	2.022	0.570	0.693	0.001	1.612	0.098	<LOD	7.992
109	BC18B_Garnet1_Line 019	2.990	2.022	0.493	0.693	0.000	1.680	0.119	0.001	7.998
110	BC18B_Garnet1_Line 020	2.985	2.020	0.209	0.916	0.000	1.602	0.272	0.001	8.004
111	BC18B_Garnet2_Line 001	2.982	2.023	0.163	0.926	0.000	1.576	0.334	0.001	8.005
112	BC18B_Garnet2_Line 002	2.987	2.025	0.353	0.723	<LOD	1.745	0.168	<LOD	8.001
113	BC18B_Garnet2_Line 003	2.985	2.026	0.308	0.817	0.000	1.686	0.179	0.001	8.002
114	BC18B_Garnet2_Line 004	2.985	2.029	0.369	0.726	<LOD	1.725	0.165	0.000	8.000
115	BC18B_Garnet2_Line 005	2.977	2.025	0.398	0.704	0.000	1.753	0.152	0.000	8.010
116	BC18B_Garnet2_Line 006	2.995	2.011	0.420	0.686	0.000	1.744	0.144	0.000	7.999
117	BC18B_Garnet2_Line 007	2.987	2.027	0.438	0.694	0.000	1.715	0.137	0.000	7.999
118	BC18B_Garnet2_Line 008	2.986	2.027	0.453	0.664	0.001	1.734	0.135	<LOD	7.999

Comments:		Cations (Based on 12 Oxygens)								Sum
Point:	Sample ID:	Si	Al	Mg	Ca	Ti	Fe	Mn	Cr	All Cations
119	BC18B_Garnet2_Line 009	2.996	2.010	0.423	0.687	<LOD	1.737	0.145	<LOD	7.999
120	BC18B_Garnet2_Line 010	2.987	2.021	0.421	0.683	<LOD	1.745	0.146	<LOD	8.003
121	BC18B_Garnet2_Line 011	2.985	2.025	0.460	0.674	<LOD	1.724	0.132	0.001	8.001
122	BC18B_Garnet2_Line 012	2.984	2.027	0.496	0.641	0.001	1.734	0.118	<LOD	8.002
123	BC18B_Garnet2_Line 013	2.997	2.020	0.504	0.632	<LOD	1.723	0.114	0.000	7.992
124	BC18B_Garnet2_Line 014	2.984	2.023	0.469	0.645	<LOD	1.750	0.132	0.000	8.004
125	BC18B_Garnet2_Line 015	2.985	2.016	0.266	0.838	0.000	1.677	0.224	0.000	8.007
126	BC18B_Garnet3_Line 001	2.987	2.020	0.239	0.724	0.002	1.771	0.258	<LOD	8.001
127	BC18B_Garnet3_Line 002	2.991	2.011	0.361	0.707	0.001	1.759	0.171	0.001	8.002
128	BC18B_Garnet3_Line 003	2.990	2.014	0.427	0.680	0.001	1.748	0.143	<LOD	8.002
129	BC18B_Garnet3_Line 004	2.989	2.023	0.414	0.724	0.001	1.716	0.132	0.000	7.999
130	BC18B_Garnet3_Line 005	2.988	2.018	0.362	0.720	0.000	1.749	0.164	<LOD	8.002
131	BC18B_Garnet3_Line 006	2.979	2.025	0.249	0.806	0.000	1.719	0.230	0.000	8.009
132	BC18B_Garnet3_Line 007	2.988	2.009	0.238	0.878	<LOD	1.672	0.222	0.001	8.007
133	BC18B_Garnet3_Line 008	2.984	2.018	0.331	0.785	<LOD	1.726	0.163	0.001	8.007
134	BC18B_Garnet3_Line 009	2.985	2.028	0.320	0.772	0.001	1.727	0.167	0.000	8.000
135	BC18B_Garnet3_Line 010	2.983	2.021	0.355	0.745	<LOD	1.744	0.158	<LOD	8.006
136	BC18B_Garnet3_Line 011	2.981	2.033	0.377	0.766	0.001	1.706	0.138	0.000	8.002
137	BC18B_Garnet3_Line 012	2.988	2.020	0.431	0.678	0.001	1.750	0.133	0.001	8.001
138	BC18B_Garnet3_Line 013	2.991	2.008	0.429	0.688	0.001	1.751	0.137	<LOD	8.004
139	BC18B_Garnet3_Line 014	2.985	2.016	0.409	0.659	<LOD	1.783	0.154	0.000	8.007
140	BC18B_Garnet3_Line 015	2.987	2.015	0.262	0.776	<LOD	1.729	0.236	<LOD	8.005
1	BC20B_Garnet1_Line 001	2.984	2.013	0.235	0.942	0.001	1.467	0.367	<LOD	8.009
2	BC20B_Garnet1_Line 002	2.988	2.013	0.332	0.829	0.000	1.585	0.257	<LOD	8.005
3	BC20B_Garnet1_Line 003	2.981	2.007	0.251	0.941	0.000	1.491	0.344	<LOD	8.015
4	BC20B_Garnet1_Line 004	2.977	2.020	0.265	0.901	<LOD	1.576	0.274	0.000	8.013
5	BC20B_Garnet1_Line 005	2.980	2.014	0.478	0.692	0.000	1.672	0.176	0.001	8.013
6	BC20B_Garnet1_Line 006	2.984	2.010	0.502	0.715	0.002	1.653	0.144	<LOD	8.009
7	BC20B_Garnet1_Line 007	2.976	2.024	0.427	0.704	0.001	1.719	0.160	<LOD	8.011
8	BC20B_Garnet1_Line 008	2.983	2.006	0.583	0.707	0.003	1.597	0.132	0.000	8.011
9	BC20B_Garnet1_Line 009	2.988	2.007	0.558	0.703	0.003	1.613	0.135	0.000	8.006
10	BC20B_Garnet1_Line 010	2.976	2.012	0.551	0.712	0.002	1.623	0.140	<LOD	8.016

Comments:		Cations (Based on 12 Oxygens)								Sum
Point:	Sample ID:	Si	Al	Mg	Ca	Ti	Fe	Mn	Cr	All Cations
11	BC20B_Garnet1_Line 011	2.981	2.021	0.470	0.722	<LOD	1.631	0.182	0.001	8.008
12	BC20B_Garnet1_Line 012	2.984	2.016	0.452	0.723	0.000	1.663	0.167	0.001	8.007
13	BC20B_Garnet1_Line 013	2.985	2.010	0.525	0.697	0.000	1.636	0.157	<LOD	8.010
14	BC20B_Garnet1_Line 014	2.985	2.019	0.460	0.722	0.000	1.631	0.187	<LOD	8.005
15	BC20B_Garnet1_Line 015	2.978	2.019	0.202	1.021	0.001	1.407	0.381	0.001	8.011
16	BC20B_Garnet1_Line 016	2.982	2.014	0.170	1.009	0.001	1.374	0.461	<LOD	8.010
17	BC20B_Garnet1_Line 017	2.987	2.018	0.168	1.021	0.001	1.344	0.463	0.001	8.003
18	BC20B_Garnet1_Line 018	2.967	2.027	0.296	0.842	0.001	1.577	0.309	0.000	8.019
19	BC20B_Garnet1_Line 019	2.977	2.023	0.320	0.831	0.000	1.586	0.274	<LOD	8.011
20	BC20B_Garnet1_Line 020	2.984	2.016	0.217	0.993	0.000	1.417	0.381	<LOD	8.008
21	BC20B_Garnet2_Line 001	2.996	2.009	0.239	0.911	0.000	1.424	0.418	0.001	7.998
22	BC20B_Garnet2_Line 002	2.985	2.014	0.506	0.686	0.000	1.640	0.177	0.000	8.008
23	BC20B_Garnet2_Line 003	2.991	2.017	0.521	0.688	0.000	1.619	0.165	0.000	8.001
24	BC20B_Garnet2_Line 004	2.988	2.011	0.504	0.688	0.001	1.638	0.175	0.000	8.006
25	BC20B_Garnet2_Line 005	2.991	2.008	0.489	0.697	0.001	1.635	0.183	0.000	8.004
26	BC20B_Garnet2_Line 006	2.986	2.022	0.363	0.781	0.000	1.544	0.305	0.001	8.002
27	BC20B_Garnet2_Line 007	2.989	2.018	0.317	0.876	<LOD	1.461	0.337	0.002	8.001
28	BC20B_Garnet2_Line 008	2.989	2.020	0.321	0.853	0.001	1.478	0.338	0.000	8.000
29	BC20B_Garnet2_Line 009	2.985	2.023	0.310	0.880	<LOD	1.461	0.344	<LOD	8.003
30	BC20B_Garnet2_Line 010	2.983	2.019	0.228	0.978	0.000	1.317	0.483	0.001	8.008
31	BC20B_Garnet3_Line 001	2.984	2.013	0.176	0.984	0.001	1.369	0.483	<LOD	8.009
32	BC20B_Garnet3_Line 002	2.984	2.008	0.351	0.802	<LOD	1.595	0.270	0.001	8.011
33	BC20B_Garnet3_Line 003	2.987	2.021	0.358	0.806	<LOD	1.577	0.251	0.001	8.001
34	BC20B_Garnet3_Line 004	2.995	2.016	0.400	0.774	<LOD	1.595	0.215	<LOD	7.996
35	BC20B_Garnet3_Line 005	2.983	2.019	0.427	0.765	0.000	1.619	0.194	0.000	8.007
36	BC20B_Garnet3_Line 006	2.985	2.017	0.462	0.702	0.001	1.650	0.189	<LOD	8.006
37	BC20B_Garnet3_Line 007	2.984	2.022	0.484	0.702	<LOD	1.644	0.170	0.000	8.005
38	BC20B_Garnet3_Line 008	2.984	2.025	0.466	0.711	0.001	1.632	0.182	0.000	8.002
39	BC20B_Garnet3_Line 009	2.987	2.014	0.310	0.855	0.001	1.510	0.329	<LOD	8.006
40	BC20B_Garnet3_Line 010	2.989	2.026	0.175	1.004	0.001	1.343	0.459	0.001	7.997
81	BC28_Garnet1_Line 001	2.984	2.004	0.224	0.997	0.000	1.344	0.457	0.002	8.012
82	BC28_Garnet1_Line 002	2.995	2.019	0.544	0.751	0.002	1.541	0.141	<LOD	7.993

Comments:		Cations (Based on 12 Oxygens)								Sum
Point:	Sample ID:	Si	Al	Mg	Ca	Ti	Fe	Mn	Cr	All Cations
83	BC28_Garnet1_Line 003	2.993	2.012	0.559	0.738	0.002	1.567	0.128	0.001	7.999
84	BC28_Garnet1_Line 004	2.989	2.024	0.554	0.763	0.001	1.549	0.118	<LOD	7.998
85	BC28_Garnet1_Line 005	3.000	2.016	0.580	0.743	0.002	1.539	0.111	0.000	7.990
86	BC28_Garnet1_Line 006	2.988	2.023	0.582	0.749	0.002	1.544	0.111	<LOD	7.998
87	BC28_Garnet1_Line 007	3.000	2.011	0.573	0.747	0.001	1.546	0.114	<LOD	7.993
88	BC28_Garnet1_Line 008	2.998	2.026	0.556	0.744	0.002	1.538	0.124	<LOD	7.988
89	BC28_Garnet1_Line 009	2.987	2.024	0.541	0.762	0.001	1.552	0.135	<LOD	8.000
90	BC28_Garnet1_Line 010	2.997	2.016	0.534	0.747	0.003	1.556	0.142	<LOD	7.993
91	BC28_Garnet1_Line 011	3.002	2.014	0.555	0.739	0.000	1.547	0.133	<LOD	7.991
92	BC28_Garnet1_Line 012	2.994	2.019	0.508	0.726	0.003	1.574	0.168	0.001	7.993
93	BC28_Garnet1_Line 013	2.992	2.015	0.388	0.774	0.002	1.551	0.275	<LOD	7.998
94	BC28_Garnet1_Line 014	2.997	2.012	0.465	0.765	0.001	1.574	0.181	<LOD	7.996
95	BC28_Garnet1_Line 015	2.989	2.018	0.242	0.869	0.002	1.425	0.455	0.001	8.000
96	BC28_Garnet2_Line 001	2.994	2.005	0.203	0.974	0.001	1.328	0.495	0.002	8.002
97	BC28_Garnet2_Line 002	2.989	2.025	0.469	0.675	0.000	1.609	0.230	<LOD	7.998
98	BC28_Garnet2_Line 003	2.991	2.024	0.564	0.683	0.001	1.564	0.167	0.000	7.995
99	BC28_Garnet2_Line 004	2.995	2.017	0.593	0.661	0.001	1.563	0.165	0.001	7.995
100	BC28_Garnet2_Line 005	2.989	2.025	0.602	0.657	0.000	1.564	0.162	<LOD	7.998
101	BC28_Garnet2_Line 006	2.993	2.019	0.584	0.656	0.000	1.576	0.169	<LOD	7.997
102	BC28_Garnet2_Line 007	2.997	2.021	0.552	0.658	<LOD	1.584	0.181	0.000	7.993
103	BC28_Garnet2_Line 008	2.994	2.018	0.579	0.641	<LOD	1.586	0.179	<LOD	7.997
104	BC28_Garnet2_Line 009	2.988	2.024	0.544	0.653	<LOD	1.603	0.187	<LOD	8.000
105	BC28_Garnet2_Line 010	2.985	2.023	0.184	0.973	0.001	1.310	0.525	0.001	8.002
141	BC29B_Garnet1_Line 001	2.987	2.018	0.316	0.813	0.001	1.577	0.288	0.002	8.002
142	BC29B_Garnet1_Line 002	3.007	2.028	0.546	0.728	0.002	1.552	0.113	0.001	7.977
143	BC29B_Garnet1_Line 003	2.991	2.019	0.507	0.805	0.003	1.599	0.073	0.000	7.997
144	BC29B_Garnet1_Line 004	2.990	2.023	0.488	0.808	0.003	1.611	0.072	<LOD	7.995
145	BC29B_Garnet1_Line 005	2.992	2.011	0.470	0.816	0.002	1.630	0.079	0.000	8.000
146	BC29B_Garnet1_Line 006	2.987	2.025	0.482	0.803	0.001	1.624	0.076	0.001	7.999
147	BC29B_Garnet1_Line 007	2.992	2.015	0.468	0.808	0.003	1.628	0.084	<LOD	7.997
148	BC29B_Garnet1_Line 008	2.996	2.019	0.462	0.795	0.002	1.630	0.087	0.001	7.992
149	BC29B_Garnet1_Line 009	2.991	2.023	0.450	0.805	0.001	1.630	0.096	0.000	7.996

Comments:		Cations (Based on 12 Oxygens)								Sum
Point:	Sample ID:	Si	Al	Mg	Ca	Ti	Fe	Mn	Cr	All Cations
150	BC29B_Garnet1_Line 010	2.988	2.019	0.420	0.814	0.002	1.648	0.110	<LOD	8.000
151	BC29B_Garnet1_Line 011	2.880	2.181	0.432	0.826	0.002	1.619	0.088	0.000	8.028
152	BC29B_Garnet1_Line 012	2.991	2.011	0.464	0.801	0.003	1.650	0.078	0.001	8.000
153	BC29B_Garnet1_Line 013	2.998	2.012	0.466	0.800	0.003	1.634	0.077	0.001	7.992
154	BC29B_Garnet1_Line 014	2.979	2.023	0.460	0.807	0.003	1.661	0.073	<LOD	8.006
155	BC29B_Garnet1_Line 015	2.993	2.012	0.477	0.805	0.004	1.635	0.070	<LOD	7.997
156	BC29B_Garnet1_Line 016	2.988	2.024	0.471	0.809	0.001	1.636	0.068	0.000	7.998
157	BC29B_Garnet1_Line 017	2.999	2.016	0.484	0.799	0.003	1.617	0.069	0.001	7.989
158	BC29B_Garnet1_Line 018	2.989	2.009	0.485	0.813	0.003	1.630	0.073	0.000	8.003
159	BC29B_Garnet1_Line 019	2.985	2.030	0.464	0.790	0.001	1.612	0.118	<LOD	7.999
160	BC29B_Garnet1_Line 020	2.984	2.021	0.191	0.966	<LOD	1.419	0.421	0.001	8.005
161	BC29B_Garnet2_Line 001	2.969	2.029	0.249	0.885	<LOD	1.479	0.403	0.001	8.016
162	BC29B_Garnet2_Line 002	2.985	2.025	0.483	0.734	0.002	1.591	0.179	0.000	8.000
163	BC29B_Garnet2_Line 003	2.993	2.015	0.578	0.759	0.003	1.534	0.115	<LOD	7.997
164	BC29B_Garnet2_Line 004	2.982	2.029	0.585	0.757	0.002	1.533	0.109	0.002	8.000
165	BC29B_Garnet2_Line 005	2.986	2.020	0.584	0.751	0.002	1.547	0.112	<LOD	8.002
166	BC29B_Garnet2_Line 006	2.994	2.014	0.576	0.742	0.004	1.554	0.112	<LOD	7.995
167	BC29B_Garnet2_Line 007	2.987	2.015	0.596	0.769	0.003	1.539	0.092	0.000	8.002
168	BC29B_Garnet2_Line 008	2.983	2.025	0.605	0.755	0.002	1.537	0.095	0.000	8.003
169	BC29B_Garnet2_Line 009	2.985	2.027	0.472	0.718	0.000	1.587	0.211	0.000	8.001
170	BC29B_Garnet2_Line 010	2.999	2.011	0.149	1.046	0.000	1.317	0.472	0.001	7.995
41	BC6_Garnet1_Line 001	2.991	2.039	0.598	0.164	0.000	2.142	0.056	0.000	7.990
42	BC6_Garnet1_Line 002	2.992	2.026	0.603	0.175	0.000	2.143	0.057	<LOD	7.995
43	BC6_Garnet1_Line 003	2.975	2.041	0.622	0.175	0.001	2.133	0.055	0.000	8.003
44	BC6_Garnet1_Line 004	2.986	2.035	0.611	0.177	0.001	2.127	0.057	0.000	7.995
45	BC6_Garnet1_Line 005	2.982	2.034	0.622	0.176	0.002	2.127	0.055	0.000	7.999
46	BC6_Garnet1_Line 006	2.986	2.037	0.618	0.178	0.001	2.119	0.054	0.001	7.994
47	BC6_Garnet1_Line 007	2.981	2.036	0.625	0.173	0.002	2.127	0.054	0.001	7.999
48	BC6_Garnet1_Line 008	2.986	2.041	0.613	0.166	0.001	2.128	0.058	<LOD	7.993
49	BC6_Garnet1_Line 009	2.985	2.031	0.607	0.161	0.002	2.155	0.057	0.001	7.998
50	BC6_Garnet1_Line 010	2.982	2.048	0.607	0.162	0.001	2.137	0.056	0.000	7.993
51	BC6_Garnet2_Line 001	2.983	2.040	0.537	0.157	0.000	2.217	0.061	0.001	7.997

Comments:		Cations (Based on 12 Oxygens)								Sum
Point:	Sample ID:	Si	Al	Mg	Ca	Ti	Fe	Mn	Cr	All Cations
52	BC6_Garnet2_Line 002	2.955	2.059	0.526	0.161	<LOD	2.252	0.062	0.001	8.015
53	BC6_Garnet2_Line 003	2.985	2.034	0.554	0.167	0.001	2.196	0.060	0.001	7.997
54	BC6_Garnet2_Line 004	2.989	2.027	0.603	0.169	0.001	2.149	0.058	0.001	7.996
55	BC6_Garnet2_Line 005	2.984	2.034	0.618	0.173	0.001	2.131	0.055	0.000	7.997
56	BC6_Garnet2_Line 006	2.987	2.037	0.626	0.172	0.001	2.113	0.056	0.000	7.993
57	BC6_Garnet2_Line 007	2.986	2.032	0.649	0.171	0.001	2.105	0.053	<LOD	7.997
58	BC6_Garnet2_Line 008	2.978	2.042	0.645	0.166	0.001	2.112	0.053	0.001	7.999
59	BC6_Garnet2_Line 009	2.992	2.030	0.647	0.164	0.001	2.105	0.053	<LOD	7.992
60	BC6_Garnet2_Line 010	2.989	2.030	0.646	0.171	0.001	2.105	0.050	0.001	7.994
61	BC6_Garnet2_Line 011	2.988	2.043	0.623	0.169	0.001	2.110	0.055	0.000	7.990
62	BC6_Garnet2_Line 012	2.994	2.031	0.609	0.172	0.001	2.130	0.054	0.000	7.990
63	BC6_Garnet2_Line 013	2.981	2.034	0.602	0.170	0.002	2.152	0.057	0.001	7.999
64	BC6_Garnet2_Line 014	2.980	2.044	0.597	0.170	0.000	2.153	0.052	0.001	7.998
65	BC6_Garnet2_Line 015	2.989	2.030	0.604	0.166	<LOD	2.146	0.059	0.000	7.995
66	BC6_Garnet2_Line 016	2.983	2.036	0.609	0.165	0.001	2.149	0.054	0.000	7.998
67	BC6_Garnet2_Line 017	2.987	2.028	0.612	0.161	<LOD	2.153	0.055	0.001	7.998
68	BC6_Garnet2_Line 018	2.983	2.033	0.593	0.173	0.001	2.156	0.057	0.001	7.998
69	BC6_Garnet2_Line 019	2.989	2.039	0.569	0.174	0.001	2.159	0.059	0.001	7.990
70	BC6_Garnet2_Line 020	2.995	2.031	0.563	0.166	<LOD	2.171	0.063	0.000	7.989
71	BC6_Garnet3_Line 001	2.990	2.039	0.592	0.163	<LOD	2.149	0.055	0.001	7.990
72	BC6_Garnet3_Line 002	2.984	2.036	0.641	0.171	0.001	2.109	0.052	0.001	7.996
73	BC6_Garnet3_Line 003	2.985	2.041	0.657	0.180	0.001	2.079	0.049	0.000	7.993
74	BC6_Garnet3_Line 004	2.984	2.036	0.670	0.185	0.002	2.068	0.049	0.001	7.995
75	BC6_Garnet3_Line 005	2.983	2.044	0.666	0.191	0.002	2.059	0.045	0.000	7.992
76	BC6_Garnet3_Line 006	2.996	2.036	0.671	0.185	<LOD	2.051	0.046	0.000	7.985
77	BC6_Garnet3_Line 007	2.986	2.038	0.680	0.186	0.001	2.054	0.047	0.001	7.993
78	BC6_Garnet3_Line 008	2.981	2.040	0.687	0.177	0.003	2.066	0.042	<LOD	7.996
79	BC6_Garnet3_Line 009	2.987	2.044	0.694	0.172	0.001	2.046	0.045	0.001	7.990
80	BC6_Garnet3_Line 010	2.984	2.041	0.697	0.170	0.001	2.056	0.044	0.001	7.994
81	BC6_Garnet3_Line 011	2.993	2.034	0.686	0.170	0.000	2.058	0.045	0.002	7.988
82	BC6_Garnet3_Line 012	2.981	2.041	0.684	0.162	0.002	2.079	0.047	0.000	7.996
83	BC6_Garnet3_Line 013	2.980	2.035	0.686	0.171	0.002	2.078	0.047	0.002	8.000

Comments:		Cations (Based on 12 Oxygens)								Sum
Point:	Sample ID:	Si	Al	Mg	Ca	Ti	Fe	Mn	Cr	All Cations
84	BC6_Garnet3_Line 014	2.997	2.022	0.684	0.174	0.001	2.068	0.043	0.001	7.990
85	BC6_Garnet3_Line 015	2.989	2.041	0.678	0.170	0.000	2.065	0.047	0.000	7.990
86	BC6_Garnet3_Line 016	2.988	2.030	0.668	0.174	<LOD	2.088	0.049	0.000	7.997
87	BC6_Garnet3_Line 017	2.987	2.030	0.665	0.175	0.001	2.090	0.049	0.000	7.997
88	BC6_Garnet3_Line 018	2.985	2.046	0.655	0.165	0.001	2.090	0.049	0.001	7.991
89	BC6_Garnet3_Line 019	2.989	2.036	0.649	0.163	<LOD	2.104	0.049	0.002	7.992
90	BC6_Garnet3_Line 020	2.999	2.041	0.648	0.162	<LOD	2.080	0.051	0.001	7.980
31	RO04_Garnet1_Line 001	3.003	2.022	0.779	0.291	<LOD	1.755	0.136	<LOD	7.986
32	RO04_Garnet1_Line 002	2.996	2.020	0.863	0.253	0.001	1.764	0.097	<LOD	7.993
33	RO04_Garnet1_Line 003	2.997	2.021	0.830	0.249	<LOD	1.788	0.107	0.000	7.992
34	RO04_Garnet1_Line 004	2.986	2.040	0.922	0.251	<LOD	1.725	0.069	0.000	7.994
35	RO04_Garnet1_Line 005	2.994	2.024	0.914	0.252	0.000	1.735	0.074	0.000	7.993
36	RO04_Garnet1_Line 006	2.992	2.029	0.947	0.249	0.001	1.712	0.063	<LOD	7.993
37	RO04_Garnet1_Line 007	2.997	2.027	0.993	0.247	<LOD	1.667	0.058	<LOD	7.989
38	RO04_Garnet1_Line 008	2.993	2.026	1.007	0.246	<LOD	1.659	0.062	0.000	7.994
39	RO04_Garnet1_Line 009	2.997	2.030	0.997	0.241	0.000	1.660	0.063	0.000	7.988
40	RO04_Garnet1_Line 010	3.000	2.025	1.001	0.242	0.001	1.656	0.062	<LOD	7.986
41	RO04_Garnet1_Line 011	2.996	2.024	1.010	0.241	0.001	1.654	0.066	0.000	7.991
42	RO04_Garnet1_Line 012	2.997	2.030	1.003	0.238	0.001	1.653	0.066	<LOD	7.987
43	RO04_Garnet1_Line 013	3.002	2.026	0.999	0.240	0.000	1.649	0.067	0.000	7.984
44	RO04_Garnet1_Line 014	2.996	2.020	1.002	0.237	0.001	1.666	0.069	0.000	7.993
45	RO04_Garnet1_Line 015	2.997	2.027	0.996	0.239	0.001	1.660	0.069	<LOD	7.989
46	RO04_Garnet1_Line 016	3.000	2.020	0.998	0.242	<LOD	1.663	0.067	0.000	7.990
47	RO04_Garnet1_Line 017	2.991	2.032	1.001	0.242	0.001	1.658	0.068	0.000	7.992
48	RO04_Garnet1_Line 018	2.992	2.028	1.002	0.241	<LOD	1.664	0.068	<LOD	7.994
49	RO04_Garnet1_Line 019	2.995	2.027	0.993	0.240	0.000	1.667	0.068	0.000	7.991
50	RO04_Garnet1_Line 020	2.996	2.029	0.978	0.241	0.002	1.673	0.070	0.000	7.988
51	RO04_Garnet1_Line 021	2.985	2.033	0.959	0.238	0.002	1.707	0.072	0.001	7.996
52	RO04_Garnet1_Line 022	2.987	2.034	0.936	0.241	0.000	1.724	0.072	0.001	7.995
53	RO04_Garnet1_Line 023	3.002	2.023	0.873	0.239	0.001	1.751	0.095	<LOD	7.985
54	RO04_Garnet1_Line 024	2.971	2.052	0.860	0.239	0.001	1.777	0.103	<LOD	8.003
55	RO04_Garnet1_Line 025	2.987	2.031	0.655	0.287	0.000	1.872	0.164	0.001	7.997

Comments:		Cations (Based on 12 Oxygens)								Sum
Point:	Sample ID:	Si	Al	Mg	Ca	Ti	Fe	Mn	Cr	All Cations
56	RO04_Garnet2_Line 001	2.989	2.019	0.588	0.334	0.000	1.894	0.179	<LOD	8.001
57	RO04_Garnet2_Line 002	2.996	2.024	0.977	0.251	0.000	1.676	0.067	<LOD	7.991
58	RO04_Garnet2_Line 003	2.990	2.028	0.988	0.252	0.001	1.666	0.071	<LOD	7.995
59	RO04_Garnet2_Line 004	3.001	2.022	0.965	0.246	0.001	1.668	0.082	0.001	7.987
60	RO04_Garnet2_Line 005	2.999	2.017	0.939	0.249	0.001	1.684	0.103	<LOD	7.991
61	RO04_Garnet2_Line 006	2.999	2.022	0.919	0.247	0.001	1.678	0.123	<LOD	7.989
62	RO04_Garnet2_Line 007	2.993	2.018	0.890	0.252	0.000	1.692	0.153	0.000	7.998
63	RO04_Garnet2_Line 008	3.000	2.007	0.826	0.288	0.000	1.689	0.186	<LOD	7.996
64	RO04_Garnet2_Line 009	2.993	2.020	0.764	0.304	0.001	1.698	0.216	0.000	7.996
65	RO04_Garnet2_Line 010	2.996	2.016	0.765	0.299	0.001	1.697	0.221	0.000	7.995
66	RO04_Garnet2_Line 011	2.988	2.025	0.767	0.299	0.001	1.702	0.215	<LOD	7.998
67	RO04_Garnet2_Line 012	2.998	2.012	0.765	0.285	0.000	1.719	0.215	0.001	7.995
68	RO04_Garnet2_Line 013	2.991	2.020	0.784	0.281	0.001	1.715	0.206	0.000	7.998
69	RO04_Garnet2_Line 014	2.996	2.017	0.805	0.288	0.002	1.689	0.198	<LOD	7.994
70	RO04_Garnet2_Line 015	2.999	2.018	0.835	0.276	<LOD	1.680	0.183	0.000	7.992
71	RO04_Garnet2_Line 016	2.989	2.024	0.877	0.268	0.000	1.677	0.163	<LOD	7.998
72	RO04_Garnet2_Line 017	2.993	2.022	0.914	0.265	<LOD	1.670	0.131	0.001	7.996
73	RO04_Garnet2_Line 018	2.995	2.019	0.947	0.255	0.001	1.682	0.095	0.000	7.994
74	RO04_Garnet2_Line 019	3.007	2.020	0.985	0.247	<LOD	1.649	0.073	0.001	7.982
75	RO04_Garnet2_Line 020	2.990	2.026	1.005	0.253	<LOD	1.656	0.069	<LOD	7.997
76	RO04_Garnet2_Line 021	2.994	2.018	1.029	0.253	<LOD	1.640	0.063	0.000	7.997
77	RO04_Garnet2_Line 022	2.999	2.023	1.022	0.259	0.000	1.625	0.057	0.002	7.988
78	RO04_Garnet2_Line 023	2.992	2.021	0.980	0.253	0.001	1.687	0.061	0.001	7.996
79	RO04_Garnet2_Line 024	2.999	2.029	0.867	0.254	0.001	1.751	0.084	<LOD	7.986
80	RO04_Garnet2_Line 025	2.996	2.021	0.664	0.253	<LOD	1.897	0.162	0.001	7.993
106	RO08A_Garnet1_Line 001	2.991	2.007	0.219	0.645	<LOD	1.606	0.537	<LOD	8.005
107	RO08A_Garnet1_Line 002	2.984	2.023	0.390	0.179	0.000	1.920	0.508	0.000	8.004
108	RO08A_Garnet1_Line 003	2.988	2.029	0.407	0.157	0.001	1.919	0.496	0.001	7.997
109	RO08A_Garnet1_Line 004	2.981	2.033	0.419	0.136	0.001	1.950	0.483	0.000	8.001
110	RO08A_Garnet1_Line 005	2.983	2.028	0.391	0.190	0.002	1.908	0.501	<LOD	8.002
111	RO08A_Garnet1_Line 006	2.983	2.030	0.273	0.512	0.001	1.700	0.502	0.000	8.001
112	RO08A_Garnet1_Line 007	2.997	1.995	0.364	0.283	0.000	1.884	0.482	<LOD	8.005

Comments:		Cations (Based on 12 Oxygens)								Sum
Point:	Sample ID:	Si	Al	Mg	Ca	Ti	Fe	Mn	Cr	All Cations
113	RO08A_Garnet1_Line 008	2.985	2.012	0.340	0.455	<LOD	1.783	0.431	0.002	8.008
114	RO08A_Garnet1_Line 009	2.988	2.006	0.424	0.229	0.000	1.949	0.414	0.000	8.009
115	RO08A_Garnet1_Line 010	2.975	2.036	0.483	0.076	0.001	2.025	0.411	0.000	8.006
116	RO08A_Garnet1_Line 011	2.978	2.033	0.468	0.067	0.001	2.043	0.412	0.001	8.004
117	RO08A_Garnet1_Line 012	2.981	2.035	0.412	0.067	0.001	2.042	0.461	<LOD	8.000
118	RO08A_Garnet1_Line 013	2.980	2.028	0.183	0.677	0.000	1.594	0.543	<LOD	8.006
119	RO08A_Garnet1_Line 014	2.989	2.018	0.183	0.682	0.000	1.590	0.539	<LOD	8.002
120	RO08A_Garnet1_Line 015	2.985	2.028	0.381	0.133	0.001	1.976	0.495	<LOD	8.000
121	RO08A_Garnet1_Line 016	2.989	2.025	0.351	0.116	<LOD	1.995	0.521	0.000	7.998
122	RO08A_Garnet1_Line 017	2.981	2.030	0.296	0.067	<LOD	1.979	0.651	<LOD	8.004
123	RO08A_Garnet1_Line 018	2.985	2.029	0.284	0.294	<LOD	1.875	0.533	0.001	8.000
124	RO08A_Garnet1_Line 019	2.984	2.024	0.229	0.467	<LOD	1.730	0.568	<LOD	8.003
125	RO08A_Garnet1_Line 020	2.983	2.034	0.378	0.094	<LOD	2.002	0.509	<LOD	8.000
126	RO08A_Garnet1_Line 021	2.991	2.026	0.311	0.455	<LOD	1.783	0.431	<LOD	7.996
127	RO08A_Garnet1_Line 022	2.984	2.028	0.168	0.737	<LOD	1.522	0.562	0.001	8.002
128	RO08A_Garnet1_Line 023	2.996	2.010	0.241	0.625	<LOD	1.660	0.467	<LOD	7.999
129	RO08A_Garnet1_Line 024	2.993	2.024	0.341	0.266	<LOD	1.870	0.500	0.000	7.994
130	RO08A_Garnet1_Line 025	2.989	2.021	0.158	0.783	<LOD	1.490	0.559	<LOD	8.000
1	RO09B_Garnet1_Line 001	2.993	2.008	0.382	0.552	0.002	1.900	0.160	0.002	8.000
2	RO09B_Garnet1_Line 002	2.981	2.022	0.459	0.517	0.001	1.900	0.126	0.001	8.007
3	RO09B_Garnet1_Line 003	2.992	2.013	0.464	0.514	0.001	1.891	0.126	<LOD	8.001
4	RO09B_Garnet1_Line 004	2.983	2.010	0.462	0.516	0.001	1.911	0.128	0.001	8.011
5	RO09B_Garnet1_Line 005	2.984	2.006	0.466	0.523	0.002	1.903	0.126	0.000	8.010
6	RO09B_Garnet1_Line 006	2.986	2.026	0.465	0.514	0.000	1.883	0.127	0.000	8.001
7	RO09B_Garnet1_Line 007	2.990	2.003	0.460	0.522	0.002	1.904	0.124	0.001	8.006
8	RO09B_Garnet1_Line 008	2.994	2.007	0.445	0.541	0.001	1.890	0.123	0.001	8.002
9	RO09B_Garnet1_Line 009	2.988	2.012	0.413	0.574	<LOD	1.888	0.128	0.002	8.005
10	RO09B_Garnet1_Line 010	2.989	2.020	0.267	0.564	<LOD	1.908	0.252	0.000	8.001
11	RO09B_Garnet2_Line 001	2.997	2.007	0.285	0.537	0.002	1.927	0.241	0.000	7.997
12	RO09B_Garnet2_Line 002	3.001	2.007	0.450	0.489	0.000	1.910	0.136	0.001	7.995
13	RO09B_Garnet2_Line 003	2.992	2.015	0.464	0.475	<LOD	1.913	0.141	0.000	8.001
14	RO09B_Garnet2_Line 004	2.990	2.013	0.459	0.492	0.001	1.911	0.136	0.000	8.002

Comments:		Cations (Based on 12 Oxygens)								Sum
Point:	Sample ID:	Si	Al	Mg	Ca	Ti	Fe	Mn	Cr	All Cations
15	RO09B_Garnet2_Line 005	2.989	2.015	0.454	0.504	0.001	1.900	0.136	0.001	8.001
16	RO09B_Garnet2_Line 006	2.994	2.006	0.443	0.527	0.001	1.891	0.136	0.002	8.001
17	RO09B_Garnet2_Line 007	2.987	2.008	0.447	0.538	0.001	1.892	0.134	0.002	8.008
18	RO09B_Garnet2_Line 008	2.994	2.007	0.417	0.617	0.000	1.832	0.131	0.002	8.001
19	RO09B_Garnet2_Line 009	2.996	1.995	0.401	0.669	0.002	1.815	0.123	0.002	8.003
20	RO09B_Garnet2_Line 010	2.993	2.009	0.284	0.533	0.001	1.934	0.246	0.002	8.001
21	RO09B_Garnet3_Line 001	2.996	2.000	0.352	0.580	0.002	1.896	0.173	0.002	8.001
22	RO09B_Garnet3_Line 002	2.993	1.996	0.411	0.598	<LOD	1.873	0.134	0.002	8.007
23	RO09B_Garnet3_Line 003	2.992	2.010	0.425	0.572	<LOD	1.874	0.128	0.000	8.002
24	RO09B_Garnet3_Line 004	2.992	1.997	0.432	0.571	0.001	1.885	0.129	0.001	8.008
25	RO09B_Garnet3_Line 005	2.992	2.012	0.427	0.565	<LOD	1.876	0.128	0.001	8.002
26	RO09B_Garnet3_Line 006	3.000	2.012	0.429	0.554	<LOD	1.873	0.127	0.000	7.994
27	RO09B_Garnet3_Line 007	2.997	2.009	0.414	0.550	0.001	1.887	0.135	0.001	7.996
28	RO09B_Garnet3_Line 008	2.995	2.008	0.398	0.569	0.001	1.891	0.139	0.000	8.000
29	RO09B_Garnet3_Line 009	2.989	1.996	0.386	0.597	0.001	1.898	0.144	0.001	8.012
30	RO09B_Garnet3_Line 010	3.001	2.008	0.308	0.503	0.000	1.941	0.232	0.001	7.994
1	C005A_Garnet1 Line 001	2.968	2.039	0.569	0.166	0.001	2.188	0.081	0.000	8.011
2	C005A_Garnet1 Line 002	2.970	2.039	0.596	0.198	0.000	2.127	0.078	0.001	8.010
3	C005A_Garnet1 Line 003	2.968	2.042	0.613	0.188	<LOD	2.121	0.077	0.001	8.011
4	C005A_Garnet1 Line 004	2.976	2.035	0.624	0.194	<LOD	2.107	0.070	0.001	8.006
5	C005A_Garnet1 Line 005	2.969	2.035	0.637	0.191	0.002	2.106	0.069	0.001	8.011
7	C005A_Garnet1 Line 007	2.973	2.038	0.663	0.181	<LOD	2.086	0.067	0.000	8.008
8	C005A_Garnet1 Line 008	2.979	2.040	0.659	0.179	0.000	2.078	0.063	0.001	8.000
9	C005A_Garnet1 Line 009	2.973	2.034	0.659	0.174	<LOD	2.103	0.064	0.002	8.009
10	C005A_Garnet1 Line 010	2.974	2.036	0.661	0.172	<LOD	2.096	0.065	0.001	8.007
11	C005A_Garnet1 Line 011	2.985	2.033	0.647	0.184	0.000	2.081	0.067	0.001	7.998
12	C005A_Garnet1 Line 012	2.960	2.042	0.648	0.188	<LOD	2.110	0.069	0.001	8.019
13	C005A_Garnet1 Line 013	2.971	2.042	0.625	0.189	0.000	2.106	0.073	0.001	8.007
14	C005A_Garnet1 Line 014	2.977	2.034	0.593	0.198	0.001	2.126	0.077	0.000	8.005
15	C005A_Garnet1 Line 015	2.983	2.033	0.536	0.157	<LOD	2.209	0.081	0.002	8.000
16	C005A_Garnet2 Line 001	2.979	2.037	0.515	0.158	<LOD	2.229	0.085	<LOD	8.003
17	C005A_Garnet2 Line 002	2.960	2.048	0.576	0.177	0.001	2.172	0.080	0.001	8.015

Comments:		Cations (Based on 12 Oxygens)								Sum
Point:	Sample ID:	Si	Al	Mg	Ca	Ti	Fe	Mn	Cr	All Cations
18	C005A_Garnet2 Line 003	2.969	2.042	0.611	0.191	0.000	2.118	0.078	0.000	8.010
19	C005A_Garnet2 Line 004	2.987	2.027	0.615	0.192	0.001	2.101	0.072	0.001	7.997
20	C005A_Garnet2 Line 005	2.973	2.037	0.618	0.188	0.001	2.116	0.074	<LOD	8.007
6	C005A_Garnet2 Line 006	2.972	2.036	0.647	0.184	0.000	2.099	0.071	<LOD	8.009
21	C005A_Garnet2 Line 006	2.967	2.036	0.630	0.169	0.001	2.136	0.073	0.000	8.013
22	C005A_Garnet2 Line 007	2.973	2.036	0.630	0.164	0.000	2.131	0.073	0.000	8.009
23	C005A_Garnet2 Line 008	2.966	2.033	0.634	0.156	0.000	2.151	0.077	0.001	8.017
24	C005A_Garnet2 Line 009	2.976	2.029	0.622	0.155	0.000	2.145	0.079	0.002	8.009
25	C005A_Garnet2 Line 010	2.976	2.036	0.618	0.156	0.000	2.141	0.077	0.001	8.005
26	C005A_Garnet2 Line 011	2.979	2.029	0.600	0.170	0.002	2.148	0.076	0.000	8.004
27	C005A_Garnet2 Line 012	2.973	2.041	0.588	0.159	<LOD	2.164	0.079	0.001	8.006
28	C005A_Garnet2 Line 013	2.970	2.044	0.587	0.153	<LOD	2.173	0.079	0.001	8.007
29	C005A_Garnet2 Line 014	2.962	2.023	0.581	0.158	0.000	2.218	0.084	0.000	8.026
30	C005A_Garnet2 Line 015	2.969	2.040	0.568	0.158	0.001	2.193	0.081	<LOD	8.010
71	C005A_Garnet3 Line 001	2.980	2.034	0.515	0.171	0.000	2.217	0.084	0.001	8.002
72	C005A_Garnet3 Line 002	2.977	2.031	0.578	0.177	0.001	2.159	0.081	0.001	8.006
73	C005A_Garnet3 Line 003	2.988	2.029	0.594	0.179	0.001	2.133	0.074	0.000	7.997
74	C005A_Garnet3 Line 004	2.979	2.022	0.626	0.167	0.002	2.139	0.072	0.001	8.008
75	C005A_Garnet3 Line 005	2.984	2.022	0.652	0.146	0.002	2.127	0.070	0.002	8.003
76	C005A_Garnet3 Line 006	2.980	2.026	0.655	0.140	0.002	2.135	0.065	0.001	8.004
77	C005A_Garnet3 Line 007	2.975	2.025	0.661	0.144	0.001	2.137	0.067	0.001	8.011
78	C005A_Garnet3 Line 008	2.987	2.021	0.647	0.145	0.001	2.131	0.067	0.001	8.000
79	C005A_Garnet3 Line 009	2.987	2.019	0.650	0.155	0.002	2.120	0.067	0.002	8.001
80	C005A_Garnet3 Line 010	2.970	2.035	0.641	0.173	0.002	2.121	0.068	0.001	8.011
81	C005A_Garnet3 Line 011	2.978	2.035	0.634	0.163	0.001	2.124	0.070	<LOD	8.004
82	C005A_Garnet3 Line 012	2.984	2.026	0.629	0.164	0.001	2.128	0.070	0.001	8.001
83	C005A_Garnet3 Line 013	2.976	2.029	0.628	0.141	0.001	2.161	0.073	<LOD	8.009
84	C005A_Garnet3 Line 014	2.979	2.031	0.636	0.134	<LOD	2.150	0.073	0.001	8.005
85	C005A_Garnet3 Line 015	2.977	2.040	0.607	0.136	0.002	2.163	0.075	0.001	8.001
86	C005A_Garnet3 Line 016	2.984	2.024	0.610	0.150	<LOD	2.158	0.077	0.001	8.004
87	C005A_Garnet3 Line 017	2.978	2.033	0.600	0.161	0.002	2.152	0.078	<LOD	8.004
88	C005A_Garnet3 Line 018	2.974	2.030	0.581	0.179	0.000	2.165	0.079	0.001	8.010

Comments:		Cations (Based on 12 Oxygens)								Sum
Point:	Sample ID:	Si	Al	Mg	Ca	Ti	Fe	Mn	Cr	All Cations
89	C005A_Garnet3 Line 019	2.971	2.027	0.549	0.193	<LOD	2.194	0.081	<LOD	8.015
90	C005A_Garnet3 Line 020	2.980	2.028	0.444	0.185	0.001	2.276	0.090	0.001	8.005
31	C005B_Garnet1 Line 001	2.981	2.031	0.564	0.164	<LOD	2.184	0.078	0.001	8.003
32	C005B_Garnet1 Line 002	2.972	2.036	0.553	0.181	<LOD	2.190	0.077	0.001	8.010
33	C005B_Garnet1 Line 003	2.968	2.036	0.554	0.180	0.000	2.199	0.077	0.000	8.014
34	C005B_Garnet1 Line 004	2.971	2.038	0.567	0.184	0.001	2.172	0.077	<LOD	8.009
35	C005B_Garnet1 Line 005	2.977	2.026	0.563	0.186	0.001	2.177	0.079	0.002	8.008
36	C005B_Garnet1 Line 006	2.969	2.041	0.552	0.211	0.000	2.160	0.075	0.000	8.010
37	C005B_Garnet1 Line 007	2.967	2.046	0.557	0.194	0.001	2.171	0.074	0.001	8.009
38	C005B_Garnet1 Line 008	2.976	2.040	0.563	0.185	0.000	2.164	0.076	0.000	8.004
39	C005B_Garnet1 Line 009	2.972	2.035	0.572	0.181	0.000	2.172	0.077	0.001	8.010
40	C005B_Garnet1 Line 010	2.978	2.029	0.576	0.162	0.000	2.183	0.078	0.000	8.007
41	C005B_Garnet2 Line 001	2.975	2.032	0.517	0.182	0.000	2.216	0.083	0.001	8.008
42	C005B_Garnet2 Line 002	2.982	2.031	0.520	0.247	0.000	2.142	0.079	0.000	8.002
43	C005B_Garnet2 Line 003	2.975	2.033	0.540	0.236	0.000	2.146	0.077	0.001	8.008
44	C005B_Garnet2 Line 004	2.969	2.035	0.556	0.234	0.002	2.138	0.079	<LOD	8.012
45	C005B_Garnet2 Line 005	2.993	2.006	0.578	0.235	0.001	2.115	0.076	0.000	8.004
46	C005B_Garnet2 Line 006	2.982	2.017	0.573	0.256	<LOD	2.102	0.076	0.001	8.008
47	C005B_Garnet2 Line 007	2.978	2.017	0.575	0.257	0.002	2.109	0.073	0.001	8.011
48	C005B_Garnet2 Line 008	2.981	2.022	0.549	0.270	0.001	2.108	0.075	0.000	8.007
49	C005B_Garnet2 Line 009	2.980	2.018	0.514	0.271	0.000	2.147	0.079	0.002	8.010
50	C005B_Garnet2 Line 010	2.970	2.032	0.451	0.179	0.002	2.288	0.089	0.002	8.012
61	C008_Garnet1 Line 001	2.979	2.034	0.233	0.973	0.003	0.545	1.236	0.000	8.001
62	C008_Garnet1 Line 002	2.990	2.025	0.348	0.806	0.002	0.616	1.208	0.001	7.995
63	C008_Garnet1 Line 003	2.986	2.015	0.469	0.704	0.005	0.674	1.148	<LOD	8.002
64	C008_Garnet1 Line 004	2.981	2.020	0.509	0.769	0.005	0.687	1.030	0.001	8.003
65	C008_Garnet1 Line 005	2.996	2.013	0.515	0.852	0.007	0.677	0.932	0.001	7.991
66	C008_Garnet1 Line 006	2.991	2.011	0.527	0.736	0.005	0.697	1.026	0.002	7.997
67	C008_Garnet1 Line 007	2.988	2.026	0.476	0.674	0.003	0.679	1.145	0.002	7.994
68	C008_Garnet1 Line 008	2.987	2.020	0.313	0.860	0.001	0.591	1.223	0.004	8.000
69	C008_Garnet1 Line 009	2.985	2.014	0.284	0.912	0.002	0.569	1.229	0.006	8.002
70	C008_Garnet1 Line 010	2.984	2.015	0.160	1.143	0.003	0.502	1.191	0.005	8.003

Comments:		Cations (Based on 12 Oxygens)								Sum
Point:	Sample ID:	Si	Al	Mg	Ca	Ti	Fe	Mn	Cr	All Cations
51	C010A_Garnet1 Line 001	2.970	2.035	0.710	0.163	<LOD	2.016	0.117	0.001	8.012
52	C010A_Garnet1 Line 002	2.977	2.029	0.704	0.222	0.001	1.965	0.106	0.002	8.006
53	C010A_Garnet1 Line 003	2.967	2.038	0.715	0.252	0.001	1.944	0.091	0.003	8.011
54	C010A_Garnet1 Line 004	2.969	2.031	0.718	0.289	0.001	1.925	0.075	0.004	8.012
55	C010A_Garnet1 Line 005	2.970	2.037	0.710	0.306	<LOD	1.914	0.070	0.004	8.010
56	C010A_Garnet1 Line 006	2.969	2.047	0.689	0.306	0.000	1.911	0.082	0.003	8.006
57	C010A_Garnet1 Line 007	2.974	2.026	0.653	0.312	0.003	1.927	0.112	0.003	8.010
58	C010A_Garnet1 Line 008	2.972	2.030	0.583	0.289	0.001	1.954	0.179	0.002	8.011
59	C010A_Garnet1 Line 009	2.966	2.034	0.540	0.273	0.001	1.961	0.239	0.001	8.015
60	C010A_Garnet1 Line 010	2.976	2.037	0.518	0.222	<LOD	1.972	0.278	0.002	8.005

Comments:		Structural Sites			Molar Fractions			
Point:	Sample ID:	X Site	Y Site	Z Site	X _{Grossular}	X _{Pyrope}	X _{Almandine}	X _{Spessartine}
91	BC18B_Garnet1_Line 001	2.729	2.013	2.996	29.758	7.094	54.511	8.586
92	BC18B_Garnet1_Line 002	2.827	2.024	2.989	24.255	13.898	56.489	5.355
93	BC18B_Garnet1_Line 003	2.878	2.018	2.991	22.492	18.453	55.272	3.739
94	BC18B_Garnet1_Line 004	2.889	2.017	2.995	23.139	20.940	52.785	3.066
95	BC18B_Garnet1_Line 005	2.894	2.016	2.993	23.193	20.583	52.980	3.152
96	BC18B_Garnet1_Line 006	2.895	2.020	2.994	23.020	21.651	52.390	2.911
97	BC18B_Garnet1_Line 007	2.903	2.020	2.988	23.473	21.529	52.098	2.774
98	BC18B_Garnet1_Line 008	2.887	2.025	2.992	22.924	21.627	52.492	2.886
99	BC18B_Garnet1_Line 009	2.897	2.022	2.992	23.048	21.937	52.205	2.752
100	BC18B_Garnet1_Line 010	2.884	2.033	2.990	22.716	22.042	52.330	2.845
101	BC18B_Garnet1_Line 011	2.896	2.019	2.992	22.730	21.518	52.696	3.041
102	BC18B_Garnet1_Line 012	2.896	2.028	2.985	22.630	21.029	53.266	3.069
103	BC18B_Garnet1_Line 013	2.904	2.013	2.989	22.925	20.689	53.203	3.098
104	BC18B_Garnet1_Line 014	2.889	2.019	2.988	22.559	19.573	54.323	3.510
105	BC18B_Garnet1_Line 015	2.878	2.030	2.984	22.525	18.853	54.954	3.645
106	BC18B_Garnet1_Line 016	2.872	2.031	2.992	23.136	19.610	54.017	3.175
107	BC18B_Garnet1_Line 017	2.899	2.029	2.983	23.347	20.584	53.068	2.932
108	BC18B_Garnet1_Line 018	2.875	2.022	2.996	23.296	19.165	54.207	3.286
109	BC18B_Garnet1_Line 019	2.866	2.023	2.990	23.216	16.519	56.244	3.979
110	BC18B_Garnet1_Line 020	2.726	2.021	2.985	30.531	6.956	53.398	9.060
111	BC18B_Garnet2_Line 001	2.664	2.024	2.982	30.856	5.434	52.519	11.143
112	BC18B_Garnet2_Line 002	2.821	2.025	2.987	24.178	11.824	58.380	5.617
113	BC18B_Garnet2_Line 003	2.811	2.027	2.985	27.298	10.311	56.378	5.974
114	BC18B_Garnet2_Line 004	2.821	2.029	2.985	24.321	12.356	57.786	5.525
115	BC18B_Garnet2_Line 005	2.855	2.025	2.977	23.403	13.221	58.302	5.051
116	BC18B_Garnet2_Line 006	2.850	2.011	2.995	22.923	14.016	58.250	4.799
117	BC18B_Garnet2_Line 007	2.847	2.027	2.987	23.249	14.677	57.459	4.599
118	BC18B_Garnet2_Line 008	2.851	2.027	2.986	22.235	15.170	58.055	4.511

Comments:		Structural Sites			Molar Fractions			
Point:	Sample ID:	X Site	Y Site	Z Site	X _{Grossular}	X _{Pyrope}	X _{Almandine}	X _{Spessartine}
119	BC18B_Garnet2_Line 009	2.847	2.010	2.996	22.970	14.138	58.043	4.849
120	BC18B_Garnet2_Line 010	2.849	2.021	2.987	22.811	14.040	58.276	4.873
121	BC18B_Garnet2_Line 011	2.857	2.026	2.985	22.527	15.365	57.639	4.428
122	BC18B_Garnet2_Line 012	2.872	2.027	2.984	21.450	16.592	57.975	3.956
123	BC18B_Garnet2_Line 013	2.860	2.021	2.997	21.259	16.959	57.924	3.842
124	BC18B_Garnet2_Line 014	2.864	2.024	2.984	21.539	15.648	58.396	4.401
125	BC18B_Garnet2_Line 015	2.781	2.017	2.985	27.893	8.858	55.775	7.450
126	BC18B_Garnet3_Line 001	2.734	2.020	2.987	24.194	7.989	59.137	8.627
127	BC18B_Garnet3_Line 002	2.828	2.011	2.991	23.573	12.036	58.640	5.683
128	BC18B_Garnet3_Line 003	2.855	2.014	2.990	22.675	14.229	58.293	4.754
129	BC18B_Garnet3_Line 004	2.854	2.023	2.989	24.244	13.869	57.439	4.428
130	BC18B_Garnet3_Line 005	2.832	2.018	2.988	24.037	12.093	58.390	5.473
131	BC18B_Garnet3_Line 006	2.774	2.025	2.979	26.819	8.275	57.217	7.663
132	BC18B_Garnet3_Line 007	2.788	2.010	2.988	29.168	7.915	55.528	7.363
133	BC18B_Garnet3_Line 008	2.841	2.019	2.984	26.115	11.006	57.436	5.422
134	BC18B_Garnet3_Line 009	2.819	2.028	2.985	25.832	10.728	57.816	5.582
135	BC18B_Garnet3_Line 010	2.844	2.021	2.983	24.827	11.810	58.101	5.261
136	BC18B_Garnet3_Line 011	2.849	2.033	2.981	25.651	12.622	57.087	4.616
137	BC18B_Garnet3_Line 012	2.859	2.020	2.988	22.652	14.401	58.473	4.427
138	BC18B_Garnet3_Line 013	2.868	2.008	2.991	22.887	14.270	58.272	4.554
139	BC18B_Garnet3_Line 014	2.851	2.017	2.985	21.913	13.617	59.331	5.127
140	BC18B_Garnet3_Line 015	2.767	2.015	2.987	25.849	8.718	57.574	7.859
1	BC20B_Garnet1_Line 001	2.644	2.013	2.984	31.276	7.810	48.692	12.193
2	BC20B_Garnet1_Line 002	2.746	2.013	2.988	27.598	11.055	52.769	8.566
3	BC20B_Garnet1_Line 003	2.682	2.007	2.981	31.082	8.285	49.253	11.380
4	BC20B_Garnet1_Line 004	2.743	2.020	2.977	29.873	8.792	52.250	9.076
5	BC20B_Garnet1_Line 005	2.841	2.015	2.980	22.915	15.839	55.375	5.838
6	BC20B_Garnet1_Line 006	2.869	2.010	2.984	23.712	16.638	54.800	4.776
7	BC20B_Garnet1_Line 007	2.850	2.024	2.976	23.394	14.167	57.104	5.301
8	BC20B_Garnet1_Line 008	2.887	2.007	2.983	23.403	19.308	52.829	4.355
9	BC20B_Garnet1_Line 009	2.874	2.007	2.988	23.351	18.532	53.565	4.469
10	BC20B_Garnet1_Line 010	2.886	2.012	2.976	23.516	18.209	53.580	4.628

Comments:		Structural Sites			Molar Fractions			
Point:	Sample ID:	X Site	Y Site	Z Site	X _{Grossular}	X _{Pyrope}	X _{Almandine}	X _{Spessartine}
11	BC20B_Garnet1_Line 011	2.824	2.022	2.981	24.028	15.644	54.239	6.052
12	BC20B_Garnet1_Line 012	2.839	2.016	2.984	24.056	15.032	55.298	5.569
13	BC20B_Garnet1_Line 013	2.859	2.010	2.985	23.126	17.408	54.259	5.207
14	BC20B_Garnet1_Line 014	2.814	2.019	2.985	24.074	15.329	54.374	6.219
15	BC20B_Garnet1_Line 015	2.631	2.020	2.978	33.877	6.712	46.692	12.645
16	BC20B_Garnet1_Line 016	2.553	2.014	2.982	33.458	5.642	45.581	15.295
17	BC20B_Garnet1_Line 017	2.533	2.019	2.987	34.069	5.603	44.829	15.458
18	BC20B_Garnet1_Line 018	2.715	2.027	2.967	27.844	9.788	52.113	10.222
19	BC20B_Garnet1_Line 019	2.737	2.023	2.977	27.590	10.624	52.682	9.100
20	BC20B_Garnet1_Line 020	2.627	2.016	2.984	32.991	7.207	47.109	12.681
21	BC20B_Garnet2_Line 001	2.574	2.010	2.996	30.422	7.980	47.591	13.954
22	BC20B_Garnet2_Line 002	2.832	2.014	2.985	22.786	16.811	54.516	5.877
23	BC20B_Garnet2_Line 003	2.828	2.017	2.991	22.980	17.415	54.098	5.504
24	BC20B_Garnet2_Line 004	2.830	2.011	2.988	22.894	16.777	54.480	5.823
25	BC20B_Garnet2_Line 005	2.821	2.008	2.991	23.209	16.263	54.416	6.085
26	BC20B_Garnet2_Line 006	2.688	2.023	2.986	26.072	12.124	51.583	10.181
27	BC20B_Garnet2_Line 007	2.654	2.020	2.989	29.279	10.591	48.809	11.246
28	BC20B_Garnet2_Line 008	2.652	2.020	2.989	28.524	10.722	49.424	11.291
29	BC20B_Garnet2_Line 009	2.651	2.023	2.985	29.368	10.353	48.785	11.493
30	BC20B_Garnet2_Line 010	2.523	2.019	2.983	32.526	7.587	43.805	16.064
31	BC20B_Garnet3_Line 001	2.529	2.013	2.984	32.659	5.842	45.429	16.048
32	BC20B_Garnet3_Line 002	2.748	2.009	2.984	26.574	11.624	52.836	8.947
33	BC20B_Garnet3_Line 003	2.741	2.023	2.987	26.926	11.974	52.678	8.374
34	BC20B_Garnet3_Line 004	2.769	2.016	2.995	25.941	13.392	53.448	7.219
35	BC20B_Garnet3_Line 005	2.810	2.020	2.983	25.443	14.202	53.883	6.468
36	BC20B_Garnet3_Line 006	2.814	2.017	2.985	23.379	15.380	54.939	6.278
37	BC20B_Garnet3_Line 007	2.829	2.023	2.984	23.399	16.125	54.814	5.654
38	BC20B_Garnet3_Line 008	2.809	2.025	2.984	23.744	15.586	54.530	6.078
39	BC20B_Garnet3_Line 009	2.675	2.014	2.987	28.453	10.317	50.267	10.939
40	BC20B_Garnet3_Line 010	2.522	2.026	2.989	33.672	5.852	45.040	15.393
81	BC28_Garnet1_Line 001	2.564	2.006	2.984	32.973	7.404	44.434	15.115
82	BC28_Garnet1_Line 002	2.836	2.019	2.995	25.197	18.263	51.729	4.737

Comments:		Structural Sites			Molar Fractions			
Point:	Sample ID:	X Site	Y Site	Z Site	X _{Grossular}	X _{Pyrope}	X _{Almandine}	X _{Spessartine}
83	BC28_Garnet1_Line 003	2.864	2.013	2.993	24.650	18.671	52.320	4.268
84	BC28_Garnet1_Line 004	2.866	2.024	2.989	25.561	18.564	51.876	3.957
85	BC28_Garnet1_Line 005	2.862	2.016	3.000	24.966	19.498	51.752	3.723
86	BC28_Garnet1_Line 006	2.874	2.023	2.988	25.064	19.478	51.689	3.705
87	BC28_Garnet1_Line 007	2.867	2.011	3.000	25.057	19.231	51.853	3.814
88	BC28_Garnet1_Line 008	2.839	2.026	2.998	25.110	18.777	51.893	4.169
89	BC28_Garnet1_Line 009	2.854	2.024	2.987	25.478	18.079	51.899	4.505
90	BC28_Garnet1_Line 010	2.836	2.016	2.997	25.048	17.908	52.208	4.750
91	BC28_Garnet1_Line 011	2.841	2.014	3.002	24.844	18.661	52.018	4.471
92	BC28_Garnet1_Line 012	2.809	2.019	2.994	24.360	17.058	52.814	5.645
93	BC28_Garnet1_Line 013	2.713	2.015	2.992	25.884	12.982	51.856	9.198
94	BC28_Garnet1_Line 014	2.804	2.012	2.997	25.627	15.562	52.695	6.073
95	BC28_Garnet1_Line 015	2.536	2.019	2.989	29.048	8.071	47.603	15.187
96	BC28_Garnet2_Line 001	2.505	2.006	2.994	32.433	6.777	44.220	16.500
97	BC28_Garnet2_Line 002	2.754	2.025	2.989	22.614	15.732	53.941	7.711
98	BC28_Garnet2_Line 003	2.811	2.024	2.991	22.930	18.922	52.482	5.610
99	BC28_Garnet2_Line 004	2.817	2.018	2.995	22.151	19.869	52.412	5.526
100	BC28_Garnet2_Line 005	2.823	2.025	2.989	22.006	20.165	52.406	5.414
101	BC28_Garnet2_Line 006	2.816	2.019	2.993	21.978	19.551	52.784	5.673
102	BC28_Garnet2_Line 007	2.794	2.021	2.997	22.110	18.566	53.229	6.091
103	BC28_Garnet2_Line 008	2.806	2.018	2.994	21.472	19.412	53.130	5.986
104	BC28_Garnet2_Line 009	2.800	2.024	2.988	21.851	18.219	53.663	6.267
105	BC28_Garnet2_Line 010	2.468	2.024	2.985	32.511	6.146	43.759	17.520
141	BC29B_Garnet1_Line 001	2.706	2.020	2.987	27.144	10.546	52.618	9.616
142	BC29B_Garnet1_Line 002	2.827	2.028	3.007	24.758	18.574	52.763	3.832
143	BC29B_Garnet1_Line 003	2.911	2.019	2.991	26.956	16.978	53.519	2.443
144	BC29B_Garnet1_Line 004	2.907	2.023	2.990	27.109	16.353	54.028	2.418
145	BC29B_Garnet1_Line 005	2.916	2.012	2.992	27.230	15.680	54.392	2.627
146	BC29B_Garnet1_Line 006	2.910	2.026	2.987	26.880	16.148	54.366	2.534
147	BC29B_Garnet1_Line 007	2.903	2.015	2.992	27.005	15.650	54.439	2.796
148	BC29B_Garnet1_Line 008	2.887	2.019	2.996	26.717	15.525	54.742	2.915
149	BC29B_Garnet1_Line 009	2.885	2.023	2.991	26.998	15.074	54.656	3.225

Comments:		Structural Sites			Molar Fractions			
Point:	Sample ID:	X Site	Y Site	Z Site	X _{Grossular}	X _{Pyrope}	X _{Almandine}	X _{Spessartine}
150	BC29B_Garnet1_Line 010	2.881	2.019	2.988	27.196	14.021	55.044	3.664
151	BC29B_Garnet1_Line 011	2.877	2.182	2.880	27.839	14.560	54.556	2.958
152	BC29B_Garnet1_Line 012	2.915	2.012	2.991	26.712	15.486	55.063	2.607
153	BC29B_Garnet1_Line 013	2.901	2.014	2.998	26.841	15.636	54.811	2.580
154	BC29B_Garnet1_Line 014	2.928	2.023	2.979	26.858	15.314	55.305	2.431
155	BC29B_Garnet1_Line 015	2.917	2.012	2.993	26.900	15.959	54.655	2.339
156	BC29B_Garnet1_Line 016	2.917	2.024	2.988	27.104	15.776	54.800	2.270
157	BC29B_Garnet1_Line 017	2.900	2.018	2.999	26.881	16.287	54.369	2.326
158	BC29B_Garnet1_Line 018	2.928	2.009	2.989	27.054	16.147	54.263	2.415
159	BC29B_Garnet1_Line 019	2.866	2.030	2.985	26.483	15.548	53.993	3.939
160	BC29B_Garnet1_Line 020	2.577	2.022	2.984	32.211	6.385	47.328	14.051
161	BC29B_Garnet2_Line 001	2.614	2.030	2.969	29.326	8.252	49.018	13.367
162	BC29B_Garnet2_Line 002	2.808	2.026	2.985	24.554	16.167	53.202	6.002
163	BC29B_Garnet2_Line 003	2.871	2.015	2.993	25.376	19.352	51.326	3.839
164	BC29B_Garnet2_Line 004	2.876	2.031	2.982	25.332	19.582	51.300	3.656
165	BC29B_Garnet2_Line 005	2.882	2.020	2.986	25.074	19.485	51.641	3.728
166	BC29B_Garnet2_Line 006	2.872	2.014	2.994	24.834	19.268	52.031	3.734
167	BC29B_Garnet2_Line 007	2.904	2.016	2.987	25.632	19.865	51.297	3.079
168	BC29B_Garnet2_Line 008	2.898	2.026	2.983	25.216	20.219	51.329	3.173
169	BC29B_Garnet2_Line 009	2.778	2.027	2.985	24.018	15.804	53.099	7.057
170	BC29B_Garnet2_Line 010	2.512	2.012	2.999	35.033	4.991	44.126	15.798
41	BC6_Garnet1_Line 001	2.904	2.039	2.991	5.536	20.197	72.374	1.891
42	BC6_Garnet1_Line 002	2.920	2.026	2.992	5.861	20.252	71.958	1.916
43	BC6_Garnet1_Line 003	2.931	2.041	2.975	5.863	20.835	71.407	1.857
44	BC6_Garnet1_Line 004	2.915	2.036	2.986	5.962	20.543	71.536	1.908
45	BC6_Garnet1_Line 005	2.925	2.034	2.982	5.886	20.866	71.314	1.858
46	BC6_Garnet1_Line 006	2.914	2.038	2.986	5.993	20.800	71.329	1.809
47	BC6_Garnet1_Line 007	2.925	2.037	2.981	5.815	20.964	71.317	1.819
48	BC6_Garnet1_Line 008	2.907	2.041	2.986	5.583	20.675	71.739	1.965
49	BC6_Garnet1_Line 009	2.924	2.031	2.985	5.401	20.356	72.267	1.897
50	BC6_Garnet1_Line 010	2.905	2.048	2.982	5.455	20.484	72.125	1.892
51	BC6_Garnet2_Line 001	2.912	2.041	2.983	5.293	18.067	74.550	2.042

Comments:		Structural Sites			Molar Fractions			
Point:	Sample ID:	X Site	Y Site	Z Site	X _{Grossular}	X _{Pyrope}	X _{Almandine}	X _{Spessartine}
52	BC6_Garnet2_Line 002	2.939	2.060	2.955	5.353	17.536	75.014	2.063
53	BC6_Garnet2_Line 003	2.917	2.035	2.985	5.599	18.604	73.722	2.024
54	BC6_Garnet2_Line 004	2.921	2.028	2.989	5.663	20.240	72.099	1.938
55	BC6_Garnet2_Line 005	2.923	2.034	2.984	5.824	20.754	71.530	1.850
56	BC6_Garnet2_Line 006	2.912	2.037	2.987	5.796	21.100	71.194	1.876
57	BC6_Garnet2_Line 007	2.925	2.032	2.986	5.741	21.801	70.658	1.764
58	BC6_Garnet2_Line 008	2.923	2.043	2.978	5.579	21.654	70.902	1.775
59	BC6_Garnet2_Line 009	2.916	2.030	2.992	5.526	21.767	70.875	1.792
60	BC6_Garnet2_Line 010	2.923	2.031	2.989	5.757	21.726	70.758	1.673
61	BC6_Garnet2_Line 011	2.902	2.044	2.988	5.703	21.070	71.321	1.874
62	BC6_Garnet2_Line 012	2.910	2.031	2.994	5.786	20.532	71.836	1.812
63	BC6_Garnet2_Line 013	2.924	2.035	2.981	5.681	20.176	72.119	1.926
64	BC6_Garnet2_Line 014	2.921	2.045	2.980	5.709	20.090	72.419	1.753
65	BC6_Garnet2_Line 015	2.917	2.030	2.989	5.592	20.308	72.124	1.976
66	BC6_Garnet2_Line 016	2.923	2.036	2.983	5.533	20.451	72.149	1.830
67	BC6_Garnet2_Line 017	2.926	2.030	2.987	5.385	20.518	72.216	1.839
68	BC6_Garnet2_Line 018	2.923	2.034	2.983	5.818	19.898	72.309	1.911
69	BC6_Garnet2_Line 019	2.901	2.040	2.989	5.878	19.198	72.894	1.977
70	BC6_Garnet2_Line 020	2.901	2.031	2.995	5.601	19.009	73.266	2.114
71	BC6_Garnet3_Line 001	2.904	2.040	2.990	5.508	20.003	72.583	1.864
72	BC6_Garnet3_Line 002	2.922	2.037	2.984	5.762	21.542	70.888	1.747
73	BC6_Garnet3_Line 003	2.916	2.042	2.985	6.076	22.148	70.067	1.666
74	BC6_Garnet3_Line 004	2.923	2.038	2.984	6.231	22.518	69.490	1.642
75	BC6_Garnet3_Line 005	2.917	2.045	2.983	6.458	22.462	69.471	1.518
76	BC6_Garnet3_Line 006	2.907	2.037	2.996	6.265	22.728	69.452	1.542
77	BC6_Garnet3_Line 007	2.920	2.039	2.986	6.255	22.920	69.185	1.571
78	BC6_Garnet3_Line 008	2.930	2.040	2.981	5.962	23.073	69.450	1.423
79	BC6_Garnet3_Line 009	2.912	2.044	2.987	5.808	23.450	69.157	1.529
80	BC6_Garnet3_Line 010	2.923	2.042	2.984	5.728	23.478	69.256	1.475
81	BC6_Garnet3_Line 011	2.914	2.036	2.993	5.739	23.168	69.504	1.520
82	BC6_Garnet3_Line 012	2.925	2.041	2.981	5.437	22.995	69.918	1.575
83	BC6_Garnet3_Line 013	2.935	2.036	2.980	5.731	22.962	69.610	1.559

Comments:		Structural Sites			Molar Fractions			
Point:	Sample ID:	X Site	Y Site	Z Site	X _{Grossular}	X _{Pyrope}	X _{Almandine}	X _{Spessartine}
84	BC6_Garnet3_Line 014	2.926	2.022	2.997	5.849	23.020	69.607	1.461
85	BC6_Garnet3_Line 015	2.913	2.041	2.989	5.753	22.886	69.746	1.601
86	BC6_Garnet3_Line 016	2.930	2.031	2.988	5.850	22.421	70.070	1.653
87	BC6_Garnet3_Line 017	2.930	2.030	2.987	5.863	22.319	70.155	1.632
88	BC6_Garnet3_Line 018	2.909	2.047	2.985	5.565	22.118	70.609	1.645
89	BC6_Garnet3_Line 019	2.917	2.038	2.989	5.507	21.883	70.900	1.655
90	BC6_Garnet3_Line 020	2.889	2.042	2.999	5.505	22.028	70.704	1.727
31	RO04_Garnet1_Line 001	2.826	2.022	3.003	9.824	26.317	59.264	4.595
32	RO04_Garnet1_Line 002	2.879	2.020	2.996	8.500	28.978	59.249	3.245
33	RO04_Garnet1_Line 003	2.867	2.022	2.997	8.369	27.920	60.119	3.585
34	RO04_Garnet1_Line 004	2.898	2.040	2.986	8.468	31.056	58.140	2.334
35	RO04_Garnet1_Line 005	2.901	2.024	2.994	8.455	30.725	58.325	2.477
36	RO04_Garnet1_Line 006	2.909	2.029	2.992	8.376	31.872	57.603	2.131
37	RO04_Garnet1_Line 007	2.907	2.027	2.997	8.345	33.493	56.213	1.949
38	RO04_Garnet1_Line 008	2.912	2.026	2.993	8.262	33.852	55.785	2.088
39	RO04_Garnet1_Line 009	2.897	2.030	2.997	8.123	33.664	56.064	2.130
40	RO04_Garnet1_Line 010	2.899	2.025	3.000	8.177	33.798	55.908	2.087
41	RO04_Garnet1_Line 011	2.905	2.024	2.996	8.104	33.999	55.650	2.226
42	RO04_Garnet1_Line 012	2.894	2.030	2.997	8.029	33.889	55.850	2.213
43	RO04_Garnet1_Line 013	2.889	2.027	3.002	8.127	33.805	55.789	2.271
44	RO04_Garnet1_Line 014	2.906	2.020	2.996	7.978	33.678	55.981	2.317
45	RO04_Garnet1_Line 015	2.896	2.027	2.997	8.070	33.593	55.994	2.312
46	RO04_Garnet1_Line 016	2.903	2.021	3.000	8.144	33.617	55.988	2.249
47	RO04_Garnet1_Line 017	2.900	2.032	2.991	8.139	33.713	55.840	2.283
48	RO04_Garnet1_Line 018	2.907	2.028	2.992	8.095	33.666	55.951	2.289
49	RO04_Garnet1_Line 019	2.900	2.027	2.995	8.072	33.457	56.148	2.295
50	RO04_Garnet1_Line 020	2.891	2.029	2.996	8.125	33.001	56.458	2.352
51	RO04_Garnet1_Line 021	2.905	2.033	2.985	8.006	32.195	57.313	2.410
52	RO04_Garnet1_Line 022	2.901	2.036	2.987	8.086	31.481	57.964	2.426
53	RO04_Garnet1_Line 023	2.863	2.023	3.002	8.077	29.507	59.151	3.222
54	RO04_Garnet1_Line 024	2.877	2.052	2.971	8.021	28.862	59.648	3.450
55	RO04_Garnet1_Line 025	2.814	2.032	2.987	9.631	21.992	62.832	5.491

Comments:		Structural Sites			Molar Fractions			
Point:	Sample ID:	X Site	Y Site	Z Site	X _{Grossular}	X _{Pyrope}	X _{Almandine}	X _{Spessartine}
56	RO04_Garnet2_Line 001	2.815	2.019	2.989	11.144	19.625	63.253	5.966
57	RO04_Garnet2_Line 002	2.904	2.024	2.996	8.462	32.879	56.396	2.247
58	RO04_Garnet2_Line 003	2.906	2.028	2.990	8.471	33.168	55.961	2.375
59	RO04_Garnet2_Line 004	2.879	2.023	3.001	8.296	32.571	56.261	2.782
60	RO04_Garnet2_Line 005	2.871	2.017	2.999	8.369	31.546	56.600	3.452
61	RO04_Garnet2_Line 006	2.844	2.022	2.999	8.329	30.956	56.538	4.144
62	RO04_Garnet2_Line 007	2.834	2.018	2.993	8.431	29.798	56.641	5.112
63	RO04_Garnet2_Line 008	2.802	2.007	3.000	9.622	27.639	56.509	6.229
64	RO04_Garnet2_Line 009	2.765	2.020	2.993	10.181	25.599	56.920	7.245
65	RO04_Garnet2_Line 010	2.761	2.016	2.996	10.028	25.641	56.903	7.394
66	RO04_Garnet2_Line 011	2.768	2.025	2.988	10.007	25.707	57.046	7.207
67	RO04_Garnet2_Line 012	2.769	2.013	2.998	9.549	25.625	57.573	7.200
68	RO04_Garnet2_Line 013	2.780	2.020	2.991	9.408	26.250	57.423	6.892
69	RO04_Garnet2_Line 014	2.782	2.017	2.996	9.660	26.991	56.646	6.644
70	RO04_Garnet2_Line 015	2.791	2.018	2.999	9.288	28.066	56.479	6.154
71	RO04_Garnet2_Line 016	2.821	2.024	2.989	8.967	29.377	56.167	5.474
72	RO04_Garnet2_Line 017	2.849	2.023	2.993	8.884	30.651	56.034	4.406
73	RO04_Garnet2_Line 018	2.884	2.019	2.995	8.551	31.774	56.439	3.193
74	RO04_Garnet2_Line 019	2.881	2.021	3.007	8.360	33.345	55.801	2.460
75	RO04_Garnet2_Line 020	2.913	2.026	2.990	8.473	33.696	55.533	2.298
76	RO04_Garnet2_Line 021	2.922	2.019	2.994	8.474	34.463	54.943	2.108
77	RO04_Garnet2_Line 022	2.906	2.025	2.999	8.735	34.459	54.790	1.934
78	RO04_Garnet2_Line 023	2.920	2.022	2.992	8.470	32.851	56.565	2.062
79	RO04_Garnet2_Line 024	2.873	2.029	2.999	8.600	29.309	59.211	2.856
80	RO04_Garnet2_Line 025	2.814	2.022	2.996	8.503	22.302	63.738	5.434
106	RO08A_Garnet1_Line 001	2.470	2.007	2.991	21.453	7.275	53.424	17.848
107	RO08A_Garnet1_Line 002	2.489	2.023	2.984	5.964	13.015	64.067	16.944
108	RO08A_Garnet1_Line 003	2.483	2.030	2.988	5.272	13.643	64.393	16.644
109	RO08A_Garnet1_Line 004	2.504	2.033	2.981	4.536	14.014	65.246	16.150
110	RO08A_Garnet1_Line 005	2.489	2.028	2.983	6.360	13.055	63.794	16.736
111	RO08A_Garnet1_Line 006	2.484	2.031	2.983	17.142	9.127	56.885	16.798
112	RO08A_Garnet1_Line 007	2.531	1.995	2.997	9.404	12.071	62.509	16.006

Comments:		Structural Sites			Molar Fractions			
Point:	Sample ID:	X Site	Y Site	Z Site	X _{Grossular}	X _{Pyrope}	X _{Almandine}	X _{Spessartine}
113	RO08A_Garnet1_Line 008	2.578	2.014	2.985	15.108	11.285	59.236	14.308
114	RO08A_Garnet1_Line 009	2.601	2.006	2.988	7.591	14.048	64.628	13.717
115	RO08A_Garnet1_Line 010	2.583	2.036	2.975	2.525	16.117	67.615	13.721
116	RO08A_Garnet1_Line 011	2.578	2.035	2.978	2.234	15.654	68.271	13.752
117	RO08A_Garnet1_Line 012	2.521	2.035	2.981	2.261	13.820	68.407	15.464
118	RO08A_Garnet1_Line 013	2.454	2.028	2.980	22.592	6.104	53.168	18.124
119	RO08A_Garnet1_Line 014	2.456	2.018	2.989	22.778	6.115	53.096	17.997
120	RO08A_Garnet1_Line 015	2.491	2.028	2.985	4.460	12.769	66.164	16.569
121	RO08A_Garnet1_Line 016	2.462	2.025	2.989	3.893	11.771	66.871	17.464
122	RO08A_Garnet1_Line 017	2.342	2.030	2.981	2.227	9.899	66.120	21.754
123	RO08A_Garnet1_Line 018	2.453	2.029	2.985	9.834	9.525	62.784	17.830
124	RO08A_Garnet1_Line 019	2.426	2.024	2.984	15.591	7.663	57.777	18.969
125	RO08A_Garnet1_Line 020	2.473	2.034	2.983	3.138	12.670	67.119	17.074
126	RO08A_Garnet1_Line 021	2.549	2.026	2.991	15.263	10.441	59.844	14.452
127	RO08A_Garnet1_Line 022	2.427	2.029	2.984	24.643	5.626	50.901	18.796
128	RO08A_Garnet1_Line 023	2.526	2.010	2.996	20.863	8.065	55.465	15.607
129	RO08A_Garnet1_Line 024	2.477	2.024	2.993	8.947	11.443	62.807	16.789
130	RO08A_Garnet1_Line 025	2.431	2.021	2.989	26.192	5.284	49.840	18.684
1	RO09B_Garnet1_Line 001	2.834	2.011	2.993	18.406	12.744	63.379	5.344
2	RO09B_Garnet1_Line 002	2.876	2.023	2.981	17.225	15.282	63.245	4.191
3	RO09B_Garnet1_Line 003	2.869	2.013	2.992	17.156	15.484	63.112	4.212
4	RO09B_Garnet1_Line 004	2.889	2.011	2.983	17.092	15.312	63.303	4.241
5	RO09B_Garnet1_Line 005	2.891	2.006	2.984	17.318	15.419	63.016	4.174
6	RO09B_Garnet1_Line 006	2.862	2.026	2.986	17.194	15.559	62.976	4.258
7	RO09B_Garnet1_Line 007	2.885	2.003	2.990	17.333	15.257	63.184	4.132
8	RO09B_Garnet1_Line 008	2.876	2.008	2.994	18.030	14.835	62.971	4.113
9	RO09B_Garnet1_Line 009	2.875	2.015	2.988	19.101	13.753	62.822	4.247
10	RO09B_Garnet1_Line 010	2.740	2.020	2.989	18.863	8.935	63.785	8.412
11	RO09B_Garnet2_Line 001	2.750	2.007	2.997	17.945	9.536	64.376	8.052
12	RO09B_Garnet2_Line 002	2.849	2.008	3.001	16.380	15.052	63.960	4.567
13	RO09B_Garnet2_Line 003	2.852	2.016	2.992	15.875	15.494	63.914	4.711
14	RO09B_Garnet2_Line 004	2.862	2.013	2.990	16.402	15.316	63.715	4.525

Comments:		Structural Sites			Molar Fractions			
Point:	Sample ID:	X Site	Y Site	Z Site	X _{Grossular}	X _{Pyrope}	X _{Almandine}	X _{Spessartine}
15	RO09B_Garnet2_Line 005	2.859	2.016	2.989	16.827	15.147	63.420	4.531
16	RO09B_Garnet2_Line 006	2.861	2.009	2.994	17.565	14.758	63.028	4.542
17	RO09B_Garnet2_Line 007	2.876	2.010	2.987	17.852	14.824	62.785	4.462
18	RO09B_Garnet2_Line 008	2.866	2.009	2.994	20.568	13.896	61.101	4.366
19	RO09B_Garnet2_Line 009	2.885	1.997	2.996	22.214	13.297	60.264	4.082
20	RO09B_Garnet2_Line 010	2.751	2.011	2.993	17.760	9.472	64.502	8.187
21	RO09B_Garnet3_Line 001	2.828	2.003	2.996	19.306	11.726	63.090	5.744
22	RO09B_Garnet3_Line 002	2.882	1.998	2.993	19.821	13.604	62.045	4.448
23	RO09B_Garnet3_Line 003	2.872	2.010	2.992	19.074	14.176	62.463	4.272
24	RO09B_Garnet3_Line 004	2.888	1.997	2.992	18.907	14.309	62.455	4.257
25	RO09B_Garnet3_Line 005	2.869	2.013	2.992	18.861	14.253	62.578	4.285
26	RO09B_Garnet3_Line 006	2.856	2.012	3.000	18.570	14.380	62.801	4.242
27	RO09B_Garnet3_Line 007	2.852	2.010	2.997	18.400	13.860	63.128	4.527
28	RO09B_Garnet3_Line 008	2.857	2.008	2.995	18.968	13.272	63.087	4.647
29	RO09B_Garnet3_Line 009	2.881	1.997	2.989	19.713	12.757	62.711	4.764
30	RO09B_Garnet3_Line 010	2.752	2.008	3.001	16.856	10.333	65.013	7.770
1	C005A_Garnet1 Line 001	2.922	2.039	2.968	5.510	18.952	72.812	2.686
2	C005A_Garnet1 Line 002	2.922	2.040	2.970	6.598	19.864	70.894	2.615
3	C005A_Garnet1 Line 003	2.923	2.043	2.968	6.276	20.436	70.683	2.576
4	C005A_Garnet1 Line 004	2.926	2.035	2.976	6.482	20.840	70.334	2.327
5	C005A_Garnet1 Line 005	2.935	2.035	2.969	6.358	21.198	70.049	2.299
7	C005A_Garnet1 Line 007	2.930	2.038	2.973	6.040	22.124	69.593	2.243
8	C005A_Garnet1 Line 008	2.916	2.041	2.979	5.994	22.124	69.745	2.101
9	C005A_Garnet1 Line 009	2.937	2.036	2.973	5.806	21.959	70.045	2.122
10	C005A_Garnet1 Line 010	2.930	2.038	2.974	5.746	22.068	69.968	2.178
11	C005A_Garnet1 Line 011	2.912	2.034	2.985	6.187	21.714	69.808	2.259
12	C005A_Garnet1 Line 012	2.946	2.044	2.960	6.241	21.481	69.947	2.287
13	C005A_Garnet1 Line 013	2.920	2.043	2.971	6.314	20.874	70.350	2.431
14	C005A_Garnet1 Line 014	2.916	2.034	2.977	6.597	19.808	70.982	2.568
15	C005A_Garnet1 Line 015	2.902	2.035	2.983	5.270	17.950	74.010	2.706
16	C005A_Garnet2 Line 001	2.902	2.037	2.979	5.305	17.233	74.614	2.848
17	C005A_Garnet2 Line 002	2.925	2.048	2.960	5.894	19.154	72.222	2.657

Comments:		Structural Sites			Molar Fractions			
Point:	Sample ID:	X Site	Y Site	Z Site	X _{Grossular}	X _{Pyrope}	X _{Almandine}	X _{Spessartine}
18	C005A_Garnet2 Line 003	2.920	2.042	2.969	6.367	20.383	70.641	2.604
19	C005A_Garnet2 Line 004	2.908	2.028	2.987	6.450	20.620	70.434	2.426
20	C005A_Garnet2 Line 005	2.922	2.037	2.973	6.262	20.615	70.627	2.457
6	C005A_Garnet2 Line 006	2.930	2.036	2.972	6.125	21.569	69.935	2.354
21	C005A_Garnet2 Line 006	2.935	2.036	2.967	5.612	20.949	70.964	2.421
22	C005A_Garnet2 Line 007	2.926	2.037	2.973	5.475	21.006	71.058	2.445
23	C005A_Garnet2 Line 008	2.941	2.033	2.966	5.172	20.999	71.253	2.549
24	C005A_Garnet2 Line 009	2.923	2.031	2.976	5.175	20.715	71.421	2.631
25	C005A_Garnet2 Line 010	2.915	2.037	2.976	5.215	20.658	71.536	2.572
26	C005A_Garnet2 Line 011	2.918	2.029	2.979	5.665	20.028	71.711	2.538
27	C005A_Garnet2 Line 012	2.911	2.042	2.973	5.315	19.667	72.332	2.647
28	C005A_Garnet2 Line 013	2.913	2.045	2.970	5.106	19.619	72.607	2.630
29	C005A_Garnet2 Line 014	2.957	2.023	2.962	5.191	19.107	72.928	2.755
30	C005A_Garnet2 Line 015	2.919	2.040	2.969	5.281	18.924	73.058	2.708
71	C005A_Garnet3 Line 001	2.903	2.035	2.980	5.718	17.237	74.209	2.797
72	C005A_Garnet3 Line 002	2.915	2.032	2.977	5.906	19.299	72.056	2.693
73	C005A_Garnet3 Line 003	2.905	2.029	2.988	5.993	19.925	71.565	2.492
74	C005A_Garnet3 Line 004	2.932	2.023	2.979	5.550	20.818	71.133	2.406
75	C005A_Garnet3 Line 005	2.925	2.023	2.984	4.877	21.734	70.951	2.328
76	C005A_Garnet3 Line 006	2.929	2.027	2.980	4.667	21.841	71.205	2.172
77	C005A_Garnet3 Line 007	2.942	2.026	2.975	4.784	21.948	70.961	2.225
78	C005A_Garnet3 Line 008	2.923	2.023	2.987	4.830	21.622	71.234	2.227
79	C005A_Garnet3 Line 009	2.926	2.020	2.987	5.172	21.710	70.771	2.241
80	C005A_Garnet3 Line 010	2.935	2.036	2.970	5.763	21.326	70.575	2.249
81	C005A_Garnet3 Line 011	2.921	2.035	2.978	5.435	21.201	70.996	2.338
82	C005A_Garnet3 Line 012	2.920	2.027	2.984	5.472	21.015	71.123	2.329
83	C005A_Garnet3 Line 013	2.930	2.029	2.976	4.707	20.906	71.927	2.442
84	C005A_Garnet3 Line 014	2.920	2.032	2.979	4.488	21.243	71.813	2.436
85	C005A_Garnet3 Line 015	2.906	2.041	2.977	4.562	20.338	72.485	2.527
86	C005A_Garnet3 Line 016	2.918	2.025	2.984	4.996	20.371	72.049	2.558
87	C005A_Garnet3 Line 017	2.913	2.033	2.978	5.375	20.061	71.900	2.611
88	C005A_Garnet3 Line 018	2.926	2.031	2.974	5.950	19.341	72.033	2.627

Comments:		Structural Sites			Molar Fractions			
Point:	Sample ID:	X Site	Y Site	Z Site	X _{Grossular}	X _{Pyrope}	X _{Almandine}	X _{Spessartine}
89	C005A_Garnet3 Line 019	2.936	2.027	2.971	6.408	18.189	72.723	2.681
90	C005A_Garnet3 Line 020	2.906	2.029	2.980	6.183	14.830	75.951	2.990
31	C005B_Garnet1 Line 001	2.912	2.032	2.981	5.482	18.867	73.027	2.596
32	C005B_Garnet1 Line 002	2.924	2.037	2.972	6.026	18.433	72.944	2.555
33	C005B_Garnet1 Line 003	2.933	2.036	2.968	5.965	18.415	73.031	2.571
34	C005B_Garnet1 Line 004	2.923	2.038	2.971	6.119	18.900	72.404	2.551
35	C005B_Garnet1 Line 005	2.925	2.027	2.977	6.172	18.720	72.420	2.613
36	C005B_Garnet1 Line 006	2.924	2.042	2.969	7.029	18.420	72.033	2.504
37	C005B_Garnet1 Line 007	2.921	2.047	2.967	6.464	18.572	72.456	2.458
38	C005B_Garnet1 Line 008	2.911	2.041	2.976	6.180	18.841	72.402	2.556
39	C005B_Garnet1 Line 009	2.926	2.035	2.972	6.040	19.053	72.320	2.555
40	C005B_Garnet1 Line 010	2.921	2.030	2.978	5.402	19.197	72.767	2.617
41	C005B_Garnet2 Line 001	2.916	2.033	2.975	6.081	17.237	73.871	2.759
42	C005B_Garnet2 Line 002	2.910	2.031	2.982	8.272	17.401	71.665	2.631
43	C005B_Garnet2 Line 003	2.922	2.034	2.975	7.851	18.017	71.530	2.554
44	C005B_Garnet2 Line 004	2.928	2.035	2.969	7.786	18.480	71.064	2.621
45	C005B_Garnet2 Line 005	2.929	2.006	2.993	7.825	19.242	70.383	2.516
46	C005B_Garnet2 Line 006	2.932	2.018	2.982	8.512	19.053	69.878	2.517
47	C005B_Garnet2 Line 007	2.941	2.018	2.978	8.522	19.049	69.939	2.418
48	C005B_Garnet2 Line 008	2.927	2.022	2.981	9.001	18.269	70.164	2.510
49	C005B_Garnet2 Line 009	2.932	2.019	2.980	9.000	17.068	71.260	2.606
50	C005B_Garnet2 Line 010	2.918	2.033	2.970	5.940	14.983	76.009	2.955
61	C008_Garnet1 Line 001	1.750	2.034	2.979	32.539	7.790	18.221	41.352
62	C008_Garnet1 Line 002	1.770	2.026	2.990	27.034	11.671	20.672	40.516
63	C008_Garnet1 Line 003	1.848	2.015	2.986	23.478	15.647	22.455	38.257
64	C008_Garnet1 Line 004	1.964	2.021	2.981	25.620	16.945	22.876	34.334
65	C008_Garnet1 Line 005	2.043	2.013	2.996	28.559	17.253	22.679	31.260
66	C008_Garnet1 Line 006	1.961	2.014	2.991	24.594	17.597	23.292	34.273
67	C008_Garnet1 Line 007	1.830	2.028	2.988	22.628	15.981	22.801	38.416
68	C008_Garnet1 Line 008	1.764	2.024	2.987	28.737	10.463	19.767	40.867
69	C008_Garnet1 Line 009	1.766	2.020	2.985	30.379	9.470	18.964	40.920
70	C008_Garnet1 Line 010	1.804	2.020	2.984	38.042	5.321	16.701	39.653

Comments:		Structural Sites			Molar Fractions			
Point:	Sample ID:	X Site	Y Site	Z Site	$X_{\text{Grossular}}$	X_{Pyrope}	$X_{\text{Almandine}}$	$X_{\text{Spessartine}}$
51	C010A_Garnet1 Line 001	2.889	2.036	2.970	5.435	23.602	67.056	3.887
52	C010A_Garnet1 Line 002	2.892	2.031	2.977	7.406	23.469	65.490	3.525
53	C010A_Garnet1 Line 003	2.911	2.041	2.967	8.392	23.768	64.648	3.038
54	C010A_Garnet1 Line 004	2.932	2.035	2.969	9.596	23.831	63.911	2.486
55	C010A_Garnet1 Line 005	2.929	2.041	2.970	10.174	23.636	63.727	2.329
56	C010A_Garnet1 Line 006	2.906	2.050	2.969	10.247	23.033	63.903	2.733
57	C010A_Garnet1 Line 007	2.893	2.029	2.974	10.366	21.710	64.036	3.716
58	C010A_Garnet1 Line 008	2.827	2.032	2.972	9.604	19.384	64.959	5.938
59	C010A_Garnet1 Line 009	2.774	2.035	2.966	9.054	17.919	65.034	7.911
60	C010A_Garnet1 Line 010	2.712	2.039	2.976	7.413	17.324	65.906	9.288

Appendix G:
Microprobe data
Part 4 – Biotite

Molar Mass	SiO ₂	Al ₂ O ₃	Na ₂ O	MgO	F	CaO	TiO ₂	FeO	MnO	K ₂ O	Cl
	60.08	101.96	61.98	40.30	19.00	56.08	79.87	71.85	70.94	94.20	35.45

Comments:		Mass (%)											
Point:	Sample ID:	SiO ₂	Al ₂ O ₃	Na ₂ O	MgO	F	CaO	TiO ₂	FeO	MnO	K ₂ O	Cl	Total
49	BC18B_Bt1_01	34.810	18.401	0.145	11.112	0.505	0.106	0.367	20.627	0.279	7.918	0.149	94.419
50	BC18B_Bt1_02	35.556	17.893	0.126	10.534	0.552	0.086	0.337	20.349	0.284	9.655	0.160	95.532
51	BC18B_Bt2_01	36.162	18.042	0.057	10.672	0.432	0.017	0.429	20.141	0.279	9.861	0.150	96.242
52	BC18B_Bt2_02	36.081	18.180	0.058	10.474	0.432	0.040	0.410	20.145	0.309	9.946	0.157	96.232
53	BC18B_Bt3_01	31.697	19.135	0.068	15.067	0.334	0.073	0.384	19.591	0.365	4.517	0.030	91.261
54	BC18B_Bt3_02	38.114	18.031	0.088	14.664	0.586	0.075	0.916	14.875	0.258	9.824	0.031	97.462
61	BC18B_Bt4_01	36.419	18.383	0.061	10.414	0.478	0.020	0.226	20.464	0.277	9.938	0.150	96.830
62	BC18B_Bt4_02	35.794	18.376	0.128	10.456	0.335	0.147	0.248	20.614	0.350	9.219	0.172	95.839
63	BC18B_Bt5_01	35.725	18.131	0.121	9.946	0.318	0.165	0.246	20.533	0.289	9.333	0.162	94.969
64	BC18B_Bt5_02	35.422	18.283	0.115	10.545	0.378	0.202	0.212	20.996	0.371	8.783	0.178	95.485
69	BC18B_Bt6_01	36.259	18.162	0.069	10.801	0.471	0.016	0.223	19.911	0.247	9.947	0.151	96.257
70	BC18B_Bt6_02	36.332	18.024	0.071	10.818	0.443	0.045	0.202	20.061	0.262	9.878	0.163	96.299
71	BC18B_Bt7_01	36.282	18.350	0.074	10.820	0.370	0.033	0.276	19.799	0.258	9.884	0.155	96.301
72	BC18B_Bt7_02	35.205	18.010	0.068	11.158	0.360	0.063	0.209	19.848	0.269	8.865	0.140	94.195
96	BC18B_Bt8_01	36.016	17.875	0.050	10.772	0.449	0.011	0.627	19.464	0.225	9.821	0.145	95.455
98	BC18B_Bt9_01	36.350	18.206	0.067	10.899	0.424	<LOD	0.610	19.763	0.265	10.076	0.136	96.785
101	BC18B_Bt10_01	36.032	18.509	0.097	10.837	0.414	0.040	0.235	19.497	0.232	9.724	0.155	95.772
1	BC20B_Bt1_01	38.261	16.365	0.045	15.599	1.105	0.002	0.964	13.818	0.215	8.921	0.013	95.308
2	BC20B_Bt1_02	29.383	21.015	0.003	18.763	0.129	0.025	0.279	17.452	0.258	2.392	0.009	89.708
5	BC20B_Bt2_01	36.267	17.572	0.064	11.002	0.625	0.036	0.673	19.267	0.435	9.910	0.120	95.971
6	BC20B_Bt2_02	29.617	19.657	0.034	12.626	0.225	0.076	0.282	23.096	0.722	3.857	0.051	90.243
11	BC20B_Bt3_01	36.538	17.097	0.091	11.377	0.471	0.070	1.894	18.205	0.361	9.756	0.108	95.968
12	BC20B_Bt3_02	37.171	18.019	0.093	10.921	0.539	0.078	1.847	18.222	0.448	9.538	0.100	96.976
13	BC20B_Bt4_01	36.528	17.460	0.069	11.452	0.562	0.000	1.504	17.867	0.378	10.032	0.114	95.966
14	BC20B_Bt4_02	36.510	17.605	0.065	11.474	0.559	0.010	1.438	17.867	0.391	10.045	0.109	96.073
15	BC20B_Bt5_01	37.178	18.087	0.068	12.359	0.734	0.016	0.178	17.495	0.421	10.030	0.110	96.676
16	BC20B_Bt5_02	37.014	18.002	0.078	12.234	0.645	0.048	0.202	17.348	0.455	9.841	0.113	95.980
21	BC20B_Bt6_01	37.475	18.231	0.063	13.135	0.634	0.026	0.406	16.060	0.397	9.983	0.101	96.511

Comments:		Mass (%)												
Point:	Sample ID:	SiO ₂	Al ₂ O ₃	Na ₂ O	MgO	F	CaO	TiO ₂	FeO	MnO	K ₂ O	Cl	Total	
22	BC20B_Bt6_02	37.291	18.459	0.048	12.588	0.637	0.044	0.310	16.715	0.490	10.005	0.093	96.680	
27	BC20B_Bt7_01	36.492	17.953	0.054	10.731	0.340	0.032	1.157	18.870	0.468	9.864	0.107	96.068	
28	BC20B_Bt7_02	36.049	18.124	0.068	11.861	0.370	0.129	1.141	19.100	0.535	8.367	0.116	95.860	
29	BC20B_Bt8_01	36.646	17.880	0.054	10.757	0.379	0.011	1.260	18.667	0.434	10.069	0.113	96.270	
30	BC20B_Bt8_02	35.708	17.917	0.038	11.563	0.257	0.072	1.243	19.151	0.495	8.463	0.099	95.006	
31	BC20B_Bt9_01	36.820	17.518	0.055	11.614	0.592	0.043	0.788	18.074	0.419	10.050	0.124	96.097	
91	BC20B_Bt9_01	37.594	18.133	0.113	12.177	0.484	0.091	1.191	18.328	0.385	9.604	0.120	98.220	
32	BC20B_Bt9_02	34.613	17.982	0.050	12.059	0.212	0.155	0.850	19.539	0.565	7.599	0.107	93.731	
93	BC20B_Bt10_01	36.679	17.204	0.075	11.382	0.392	0.040	2.044	18.091	0.293	9.907	0.107	96.214	
95	BC20B_Bt11_01	36.557	17.415	0.063	11.264	0.394	0.034	2.011	18.372	0.314	9.794	0.121	96.339	
41	BC28_Bt1_01	37.311	17.943	0.057	13.091	0.536	0.031	0.598	15.817	0.302	10.127	0.100	95.913	
42	BC28_Bt1_02	37.552	18.091	0.080	13.254	0.617	0.022	0.605	16.272	0.370	10.071	0.107	97.041	
43	BC28_Bt2_01	37.555	17.815	0.075	13.093	0.617	<LOD	0.743	16.236	0.339	10.145	0.095	96.710	
44	BC28_Bt2_02	37.343	18.162	0.073	12.910	0.617	0.018	0.701	16.113	0.374	10.230	0.095	96.636	
50	BC28_Bt3_01	36.968	17.754	0.088	12.642	0.637	0.032	0.767	16.664	0.346	9.912	0.128	95.938	
51	BC28_Bt3_02	36.255	17.845	0.080	12.747	0.363	0.057	0.640	17.436	0.430	8.796	0.116	94.765	
52	BC28_Bt4_01	38.081	16.880	0.119	17.351	0.813	0.026	1.296	11.274	0.169	9.895	0.050	95.954	
77	BC28_Bt4_01	37.231	17.090	0.068	12.428	0.488	0.018	2.098	16.595	0.408	10.114	0.099	96.637	
53	BC28_Bt4_02	38.020	16.957	0.117	17.294	0.817	0.024	1.281	11.010	0.112	10.156	0.060	95.848	
78	BC28_Bt5_01	37.468	17.418	0.087	12.465	0.559	0.031	1.985	16.375	0.369	9.987	0.090	96.834	
79	BC28_Bt6_01	37.172	17.829	0.071	12.252	0.462	0.009	0.999	17.118	0.337	10.092	0.116	96.457	
73	BC29B_Bt1_01	36.462	17.906	0.165	12.318	0.598	0.110	0.172	18.093	0.256	9.348	0.129	95.557	
74	BC29B_Bt1_02	36.256	17.894	0.125	12.532	0.555	0.162	0.179	18.241	0.317	9.107	0.151	95.519	
75	BC29B_Bt2_01	36.168	16.026	0.208	14.237	0.734	0.164	1.256	15.412	0.101	8.810	0.106	93.222	
76	BC29B_Bt2_02	36.445	16.070	0.163	14.674	0.935	0.148	1.273	15.309	0.141	9.028	0.087	94.273	
77	BC29B_Bt3_01	35.037	17.298	0.070	10.933	0.415	0.003	0.937	18.920	0.293	9.816	0.136	93.858	
78	BC29B_Bt3_02	34.632	17.402	0.048	11.267	0.433	0.021	1.000	19.228	0.339	9.701	0.130	94.201	
83	BC29B_Bt4_01	36.959	18.151	0.191	12.513	0.444	0.102	0.225	17.996	0.310	9.238	0.149	96.278	
84	BC29B_Bt4_02	37.042	18.176	0.078	12.419	0.553	0.027	0.249	17.886	0.348	9.878	0.115	96.771	
85	BC29B_Bt5_01	36.757	17.588	0.059	11.908	0.605	0.002	1.124	17.824	0.355	10.016	0.118	96.356	
86	BC29B_Bt5_02	36.811	17.602	0.069	11.733	0.419	0.040	1.124	17.752	0.374	10.036	0.121	96.081	
102	BC29B_Bt6_01	36.303	17.774	0.079	11.789	0.516	0.036	0.572	18.714	0.356	9.921	0.134	96.194	

Comments:		Mass (%)											
Point:	Sample ID:	SiO ₂	Al ₂ O ₃	Na ₂ O	MgO	F	CaO	TiO ₂	FeO	MnO	K ₂ O	Cl	Total
103	BC29B_Bt6_02	36.112	17.687	0.056	11.318	0.538	0.034	0.546	19.925	0.412	9.684	0.140	96.452
107	BC29B_Bt7_01	37.251	17.606	0.072	13.028	0.587	0.004	1.901	16.306	0.345	9.986	0.095	97.181
108	BC29B_Bt8_01	37.115	17.436	0.057	12.900	0.558	0.004	1.972	16.313	0.334	9.950	0.091	96.730
109	BC29B_Bt8_02	36.821	17.115	0.073	12.945	0.585	0.102	1.957	16.741	0.368	9.558	0.094	96.359
33	BC6_Bt1_01	35.896	19.005	0.088	12.155	0.519	0.007	3.501	14.428	0.017	10.073	0.093	95.782
34	BC6_Bt1_02	36.212	19.370	0.118	12.940	0.568	0.004	3.131	13.768	0.019	10.141	0.089	96.360
35	BC6_Bt2_01	35.862	18.892	0.085	11.070	0.480	0.001	3.917	15.482	0.021	10.050	0.091	95.951
36	BC6_Bt2_02	35.895	19.161	0.098	11.220	0.449	<LOD	3.920	15.666	0.034	10.076	0.093	96.609
37	BC6_Bt3_01	36.190	19.243	0.114	12.274	0.531	0.013	3.444	14.074	0.007	10.131	0.087	96.108
38	BC6_Bt3_02	36.354	19.116	0.122	12.444	0.565	0.002	3.444	14.126	0.019	10.031	0.086	96.309
39	BC6_Bt4_01	36.089	19.114	0.142	11.677	0.555	<LOD	3.604	15.234	0.008	10.107	0.097	96.618
40	BC6_Bt4_02	36.297	19.604	0.156	12.402	0.640	0.020	3.330	14.386	0.002	10.220	0.086	97.143
41	BC6_Bt5_01	36.260	19.399	0.136	12.174	0.458	0.011	3.534	14.300	<LOD	10.128	0.100	96.490
42	BC6_Bt5_02	36.254	19.254	0.095	12.156	0.272	0.000	3.564	14.503	<LOD	10.149	0.087	96.332
43	BC6_Bt6_01	36.299	19.237	0.094	12.630	0.586	0.015	3.138	14.560	0.012	10.157	0.093	96.821
44	BC6_Bt6_02	36.360	19.142	0.100	12.222	0.578	<LOD	3.263	14.516	0.019	9.954	0.092	96.239
45	BC6_Bt7_01	36.018	19.318	0.111	11.766	0.428	<LOD	3.536	14.926	0.023	9.972	0.096	96.193
46	BC6_Bt7_02	36.244	19.671	0.112	11.932	0.524	<LOD	3.600	14.969	0.016	10.020	0.089	97.176
47	BC6_Bt8_01	35.998	19.116	0.123	12.161	0.522	0.018	3.544	14.701	<LOD	10.097	0.099	96.376
48	BC6_Bt8_02	36.213	19.386	0.098	12.171	0.517	0.024	3.382	14.472	0.015	9.945	0.092	96.315
25	RO04_Bt1_01	36.602	19.752	0.602	14.812	0.165	0.019	1.035	13.786	0.065	8.871	0.117	95.826
26	RO04_Bt1_02	36.125	19.660	0.583	14.885	0.329	0.046	1.068	13.998	0.049	8.388	0.117	95.248
27	RO04_Bt2_01	36.728	19.767	0.651	14.829	0.259	0.020	1.285	13.820	0.048	8.817	0.110	96.334
28	RO04_Bt2_02	36.650	20.105	0.603	14.980	0.129	0.038	1.320	13.596	0.016	8.639	0.120	96.196
29	RO04_Bt3_01	37.171	20.390	0.591	16.562	0.369	0.163	0.624	12.435	0.030	8.084	0.101	96.520
30	RO04_Bt3_02	37.115	20.073	0.682	16.607	0.327	0.049	0.690	11.870	0.043	8.715	0.093	96.264
31	RO04_Bt4_01	36.066	19.424	0.610	14.941	0.333	0.137	1.045	14.455	0.058	8.249	0.123	95.441
32	RO04_Bt4_02	36.719	19.870	0.641	15.050	0.211	0.185	1.021	14.169	0.058	7.769	0.120	95.813
33	RO04_Bt5_01	35.970	19.550	0.590	14.828	0.189	0.069	0.972	14.450	0.069	8.534	0.110	95.331
34	RO04_Bt5_02	36.739	20.023	0.596	15.135	0.193	0.024	1.002	13.675	0.020	8.767	0.115	96.289
72	RO04_Bt6_01	37.153	19.093	0.614	15.605	0.302	0.004	0.999	13.578	0.043	8.765	0.115	96.271
73	RO04_Bt6_02	37.034	19.094	0.636	15.703	0.385	0.033	1.035	13.870	0.061	8.686	0.122	96.659

Comments:		Mass (%)											
Point:	Sample ID:	SiO ₂	Al ₂ O ₃	Na ₂ O	MgO	F	CaO	TiO ₂	FeO	MnO	K ₂ O	Cl	Total
75	RO04_Bt7_01	36.601	19.522	0.662	14.554	0.271	0.017	1.273	14.177	0.031	8.889	0.112	96.109
76	RO04_Bt8_01	36.412	19.614	0.633	14.662	0.302	<LOD	1.247	14.007	0.039	8.877	0.115	95.897
54	RO08A_Bt1_01	35.116	18.083	0.097	7.396	0.117	0.007	0.496	24.116	0.571	9.818	0.093	95.910
55	RO08A_Bt1_02	34.918	18.317	0.061	7.726	<LOD	0.025	0.508	23.709	0.567	9.492	0.088	95.390
56	RO08A_Bt2_01	35.183	18.533	0.067	7.426	0.182	0.012	0.171	24.394	0.505	9.808	0.086	96.367
57	RO08A_Bt2_02	30.000	18.320	0.047	8.950	0.003	0.104	0.072	28.794	0.757	3.676	0.047	90.770
58	RO08A_Bt3_01	34.699	17.932	0.170	6.648	0.042	0.160	0.219	25.523	0.670	8.930	0.079	95.072
59	RO08A_Bt3_02	31.343	18.450	0.117	7.930	0.098	0.205	0.293	28.193	0.853	4.869	0.065	92.416
64	RO08A_Bt4_01	35.368	17.002	0.086	8.135	0.067	0.008	1.963	23.194	0.336	9.775	0.096	96.030
65	RO08A_Bt4_02	35.499	16.991	0.084	8.117	0.059	0.014	2.041	22.882	0.332	9.841	0.102	95.962
68	RO08A_Bt5_01	35.400	16.827	0.089	8.229	0.073	0.027	1.953	23.143	0.367	9.759	0.108	95.975
69	RO08A_Bt5_02	35.387	16.777	0.082	8.126	0.147	0.014	1.914	23.077	0.336	9.767	0.107	95.734
1	RO09B_Bt1_01	35.195	16.730	0.198	9.774	0.172	0.035	3.073	20.809	0.078	9.114	0.049	95.227
2	RO09B_Bt1_02	35.601	17.055	0.215	9.776	0.158	0.061	3.261	20.869	0.088	9.086	0.065	96.235
3	RO09B_Bt2_01	36.061	16.830	0.169	10.223	0.173	0.009	3.216	20.334	0.089	9.457	0.054	96.615
4	RO09B_Bt2_02	34.532	16.678	0.153	9.989	0.191	0.045	3.040	20.843	0.113	8.932	0.053	94.569
5	RO09B_Bt3_01	35.783	17.040	0.177	9.806	0.159	0.043	2.967	21.071	0.079	9.339	0.047	96.511
6	RO09B_Bt3_02	35.901	17.190	0.154	9.680	0.248	0.039	3.051	21.003	0.137	9.393	0.054	96.850
7	RO09B_Bt4_01	36.338	16.634	0.326	12.055	0.128	0.035	3.720	17.885	0.038	9.069	0.032	96.260
8	RO09B_Bt4_02	36.500	16.709	0.366	12.034	0.093	0.137	3.633	17.980	0.058	8.370	0.042	95.922
9	RO09B_Bt5_01	35.459	16.683	0.159	10.101	0.084	0.030	3.054	21.204	0.108	9.088	0.055	96.025
10	RO09B_Bt5_02	35.462	16.997	0.168	9.953	0.191	0.055	2.992	20.842	0.104	9.314	0.052	96.130
15	RO09B_Bt6_01	35.688	17.220	0.173	9.810	0.169	0.014	3.114	20.477	0.085	9.335	0.049	96.134
16	RO09B_Bt6_02	35.665	17.396	0.182	9.892	0.135	0.050	3.047	20.471	0.108	9.303	0.049	96.298
17	RO09B_Bt7_01	35.849	17.384	0.148	10.139	0.078	0.022	3.020	19.765	0.097	9.489	0.057	96.048
18	RO09B_Bt7_02	35.700	17.265	0.153	10.379	0.227	0.022	3.109	19.517	0.109	9.534	0.047	96.062
80	RO09B_Bt8_01	35.522	17.265	0.179	9.828	0.198	0.029	3.211	20.234	0.100	9.262	0.062	95.890
82	RO09B_Bt9_01	35.840	17.184	0.170	9.993	0.250	0.012	3.075	20.331	0.071	9.521	0.053	96.500
1	C005A_Bt1_01	35.932	19.613	0.146	11.806	0.252	0.034	3.810	14.934	0.011	9.905	0.069	96.512
2	C005A_Bt1_02	35.874	19.441	0.140	11.488	0.472	0.012	3.776	15.489	0.033	9.741	0.065	96.531
3	C005A_Bt1_03	35.858	19.399	0.121	11.512	0.403	0.001	3.624	15.359	0.040	9.934	0.057	96.308
4	C005A_Bt1_04	35.728	19.528	0.126	11.458	0.396	0.020	3.694	15.410	0.028	9.816	0.056	96.260

Comments:		Mass (%)												
Point:	Sample ID:	SiO ₂	Al ₂ O ₃	Na ₂ O	MgO	F	CaO	TiO ₂	FeO	MnO	K ₂ O	Cl	Total	
5	C005A_Bt1_05	36.398	19.645	0.122	12.750	0.382	0.004	3.076	13.771	0.022	10.057	0.052	96.279	
6	C005A_Bt1_06	36.142	19.670	0.113	12.738	0.548	0.024	3.179	14.239	0.018	9.975	0.054	96.700	
7	C005A_Bt1_07	36.157	19.448	0.145	11.882	0.501	0.019	3.747	15.102	0.012	9.804	0.062	96.879	
8	C005A_Bt1_08	36.175	19.423	0.110	11.708	0.265	0.007	3.685	15.217	0.002	9.923	0.058	96.573	
9	C005A_Bt2_09	35.997	19.372	0.130	11.519	0.342	0.021	3.842	15.755	0.015	9.935	0.062	96.990	
10	C005A_Bt2_10	35.978	19.276	0.118	11.576	0.372	0.000	3.895	15.516	<LOD	9.952	0.062	96.745	
11	C005A_Bt2_11	36.187	18.952	0.125	12.618	0.369	0.020	4.136	14.553	0.035	9.875	0.065	96.935	
12	C005A_Bt2_12	36.227	19.185	0.114	12.089	0.234	0.005	4.184	14.575	0.017	9.960	0.055	96.645	
13	C005A_Bt2_13	36.123	19.133	0.122	11.593	0.453	0.009	3.635	15.544	<LOD	9.866	0.058	96.536	
14	C005A_Bt2_14	35.932	19.067	0.113	11.741	0.447	0.006	3.693	15.509	0.032	9.934	0.064	96.538	
15	C005A_Bt2_15	36.634	19.599	0.105	14.071	0.489	0.006	2.662	12.457	0.022	10.032	0.052	96.129	
16	C005A_Bt2_16	36.508	19.741	0.120	13.959	0.485	0.010	2.698	12.554	0.009	10.027	0.049	96.160	
43	C005A_Bt3_17	36.273	19.391	0.110	11.620	0.386	0.000	3.631	15.566	0.042	9.985	0.054	97.058	
44	C005A_Bt3_18	36.440	19.402	0.106	11.593	0.529	0.014	3.697	15.484	0.023	10.020	0.055	97.363	
45	C005A_Bt3_19	36.063	19.658	0.134	11.748	0.410	0.009	3.657	15.089	0.011	10.016	0.059	96.854	
46	C005A_Bt3_20	36.063	19.583	0.119	11.533	0.547	0.009	3.763	15.400	0.005	9.853	0.069	96.944	
47	C005A_Bt3_21	36.193	19.295	0.119	11.761	0.429	0.037	3.491	15.492	0.014	9.918	0.057	96.806	
48	C005A_Bt3_22	36.160	19.444	0.113	11.742	0.484	0.002	3.521	15.289	0.020	10.088	0.069	96.932	
49	C005A_Bt3_23	35.813	19.234	0.131	11.818	0.353	0.010	3.680	15.260	0.017	9.936	0.051	96.303	
50	C005A_Bt3_24	35.973	19.558	0.126	11.712	0.419	0.015	3.634	15.190	0.012	9.818	0.056	96.513	
17	C005B_Bt1_01	36.355	19.309	0.107	12.505	0.282	0.019	3.496	14.497	0.030	9.888	0.064	96.552	
18	C005B_Bt1_02	35.951	19.273	0.118	12.440	0.415	0.028	3.529	14.651	0.008	9.843	0.063	96.319	
19	C005B_Bt1_03	36.133	19.145	0.133	12.012	0.381	0.027	3.316	15.126	0.013	9.760	0.055	96.101	
20	C005B_Bt1_04	36.894	19.680	0.114	12.788	0.280	0.036	3.200	14.676	0.026	9.761	0.050	97.505	
21	C005B_Bt1_05	35.498	18.989	0.115	11.981	0.223	0.013	3.289	14.334	0.022	10.003	0.060	94.527	
22	C005B_Bt1_06	35.660	19.166	0.127	11.676	0.434	0.024	3.462	14.891	0.020	9.935	0.059	95.454	
23	C005B_Bt2_07	35.879	19.516	0.093	11.104	0.318	0.022	3.557	15.522	0.033	9.793	0.058	95.895	
24	C005B_Bt2_08	35.991	19.366	0.094	11.309	0.376	0.038	3.656	15.383	0.002	9.904	0.064	96.183	
25	C005B_Bt2_09	35.827	19.123	0.104	11.796	0.357	0.003	3.329	15.097	0.022	9.918	0.071	95.647	
26	C005B_Bt2_10	35.714	19.073	0.110	11.719	0.403	0.012	3.362	15.154	0.036	9.987	0.070	95.640	
27	C005B_Bt2_11	35.730	19.520	0.077	11.314	0.445	0.007	3.582	15.106	0.016	10.121	0.057	95.975	
28	C005B_Bt2_12	35.703	19.308	0.083	11.190	0.246	0.007	3.660	15.182	0.004	10.061	0.057	95.501	

Comments:		Mass (%)											
Point:	Sample ID:	SiO ₂	Al ₂ O ₃	Na ₂ O	MgO	F	CaO	TiO ₂	FeO	MnO	K ₂ O	Cl	Total
35	C008_Bt1_01	39.837	17.715	0.073	19.194	1.025	0.025	0.723	7.261	0.671	10.383	0.027	96.934
36	C008_Bt1_02	39.586	17.354	0.064	19.016	1.057	<LOD	0.814	7.216	0.585	10.432	0.033	96.157
37	C008_Bt1_03	39.664	17.412	0.055	19.316	0.926	0.053	0.903	7.458	0.671	10.320	0.026	96.804
38	C008_Bt1_04	39.802	17.253	0.067	19.354	1.015	0.016	0.871	7.376	0.677	10.388	0.027	96.846
39	C008_Bt1_05	39.183	17.313	0.104	18.918	1.082	0.074	0.994	7.435	0.734	9.978	0.028	95.843
40	C008_Bt1_06	39.333	17.460	0.046	18.967	0.955	0.034	0.917	7.602	0.607	10.275	0.028	96.224
41	C008_Bt1_07	39.305	17.303	0.051	19.402	1.155	0.050	0.706	7.279	0.745	10.360	0.025	96.381
42	C008_Bt1_08	39.573	17.540	0.058	19.108	1.093	0.017	0.699	7.423	0.617	10.296	0.024	96.448
29	C010A_Bt1_01	36.446	21.887	0.142	13.733	0.435	0.047	0.996	11.879	0.041	9.984	0.055	95.645
30	C010A_Bt1_02	36.415	21.807	0.148	14.067	0.433	0.062	0.978	11.835	0.044	9.805	0.049	95.643
31	C010A_Bt1_03	37.203	21.822	0.113	15.960	0.662	0.003	0.325	9.330	0.018	10.317	0.034	95.787
32	C010A_Bt1_04	37.597	22.415	0.105	15.696	0.678	0.006	0.326	9.210	0.020	10.027	0.035	96.115
33	C010A_Bt1_05	36.964	21.307	0.117	12.901	0.421	0.029	1.575	13.846	0.096	9.991	0.070	97.317
34	C010A_Bt1_06	36.239	20.967	0.100	12.532	0.488	0.042	1.523	13.599	0.120	9.966	0.059	95.635

Comments:		Moles Cation (Based on 11 Oxygens)										
Point:	Sample ID:	Si	Al	Na	Mg	F	Ca	Ti	Fe	Mn	K	Cl
49	BC18B_Bt1_01	2.696	1.679	0.022	1.283	0.124	0.009	0.021	1.336	0.018	0.782	0.020
50	BC18B_Bt1_02	2.743	1.627	0.019	1.212	0.135	0.007	0.020	1.313	0.019	0.950	0.021
51	BC18B_Bt2_01	2.758	1.622	0.008	1.214	0.104	0.001	0.025	1.285	0.018	0.959	0.019
52	BC18B_Bt2_02	2.755	1.636	0.009	1.192	0.104	0.003	0.024	1.286	0.020	0.969	0.020
53	BC18B_Bt3_01	2.491	1.772	0.010	1.765	0.083	0.006	0.023	1.287	0.024	0.453	0.004
54	BC18B_Bt3_02	2.787	1.554	0.012	1.599	0.135	0.006	0.050	0.910	0.016	0.916	0.004
61	BC18B_Bt4_01	2.763	1.644	0.009	1.178	0.115	0.002	0.013	1.298	0.018	0.962	0.019
62	BC18B_Bt4_02	2.739	1.657	0.019	1.193	0.081	0.012	0.014	1.319	0.023	0.900	0.022
63	BC18B_Bt5_01	2.760	1.651	0.018	1.146	0.078	0.014	0.014	1.327	0.019	0.920	0.021
64	BC18B_Bt5_02	2.725	1.657	0.017	1.209	0.092	0.017	0.012	1.350	0.024	0.862	0.023
69	BC18B_Bt6_01	2.763	1.631	0.010	1.227	0.113	0.001	0.013	1.269	0.016	0.967	0.020
70	BC18B_Bt6_02	2.768	1.618	0.010	1.229	0.107	0.004	0.012	1.278	0.017	0.960	0.021
71	BC18B_Bt7_01	2.757	1.644	0.011	1.226	0.089	0.003	0.016	1.258	0.017	0.958	0.020
72	BC18B_Bt7_02	2.731	1.646	0.010	1.290	0.088	0.005	0.012	1.287	0.018	0.877	0.018
96	BC18B_Bt8_01	2.762	1.616	0.007	1.232	0.109	0.001	0.036	1.248	0.015	0.961	0.019
98	BC18B_Bt9_01	2.752	1.624	0.010	1.230	0.102	<LOD	0.035	1.251	0.017	0.973	0.017
101	BC18B_Bt10_01	2.750	1.665	0.014	1.233	0.100	0.003	0.013	1.244	0.015	0.947	0.020
1	BC20B_Bt1_01	2.851	1.437	0.007	1.733	0.260	0.000	0.054	0.861	0.014	0.848	0.002
2	BC20B_Bt1_02	2.298	1.937	0.000	2.187	0.032	0.002	0.016	1.141	0.017	0.239	0.001
5	BC20B_Bt2_01	2.772	1.583	0.009	1.254	0.151	0.003	0.039	1.231	0.028	0.966	0.016
6	BC20B_Bt2_02	2.400	1.877	0.005	1.526	0.058	0.007	0.017	1.565	0.050	0.399	0.007
11	BC20B_Bt3_01	2.771	1.528	0.013	1.286	0.113	0.006	0.108	1.155	0.023	0.944	0.014
12	BC20B_Bt3_02	2.779	1.588	0.013	1.217	0.127	0.006	0.104	1.139	0.028	0.910	0.013
13	BC20B_Bt4_01	2.771	1.561	0.010	1.295	0.135	0.000	0.086	1.134	0.024	0.971	0.015
14	BC20B_Bt4_02	2.767	1.572	0.010	1.296	0.134	0.001	0.082	1.132	0.025	0.971	0.014
15	BC20B_Bt5_01	2.792	1.601	0.010	1.384	0.174	0.001	0.010	1.099	0.027	0.961	0.014
16	BC20B_Bt5_02	2.795	1.602	0.011	1.377	0.154	0.004	0.011	1.095	0.029	0.948	0.014
21	BC20B_Bt6_01	2.793	1.601	0.009	1.459	0.149	0.002	0.023	1.001	0.025	0.949	0.013

Comments:		Moles Cation (Based on 11 Oxygens)										
Point:	Sample ID:	Si	Al	Na	Mg	F	Ca	Ti	Fe	Mn	K	Cl
22	BC20B_Bt6_02	2.785	1.624	0.007	1.401	0.150	0.004	0.017	1.044	0.031	0.953	0.012
27	BC20B_Bt7_01	2.768	1.605	0.008	1.214	0.082	0.003	0.066	1.197	0.030	0.954	0.014
28	BC20B_Bt7_02	2.725	1.615	0.010	1.337	0.088	0.010	0.065	1.207	0.034	0.807	0.015
29	BC20B_Bt8_01	2.774	1.595	0.008	1.214	0.091	0.001	0.072	1.182	0.028	0.972	0.014
30	BC20B_Bt8_02	2.725	1.611	0.006	1.316	0.062	0.006	0.071	1.222	0.032	0.824	0.013
31	BC20B_Bt9_01	2.792	1.565	0.008	1.313	0.142	0.003	0.045	1.146	0.027	0.972	0.016
91	BC20B_Bt9_01	2.772	1.576	0.016	1.339	0.113	0.007	0.066	1.130	0.024	0.903	0.015
32	BC20B_Bt9_02	2.678	1.640	0.008	1.391	0.052	0.013	0.049	1.264	0.037	0.750	0.014
93	BC20B_Bt10_01	2.771	1.532	0.011	1.282	0.094	0.003	0.116	1.143	0.019	0.955	0.014
95	BC20B_Bt11_01	2.760	1.550	0.009	1.268	0.094	0.003	0.114	1.160	0.020	0.943	0.015
41	BC28_Bt1_01	2.796	1.585	0.008	1.463	0.127	0.002	0.034	0.991	0.019	0.968	0.013
42	BC28_Bt1_02	2.787	1.582	0.012	1.467	0.145	0.002	0.034	1.010	0.023	0.954	0.013
43	BC28_Bt2_01	2.798	1.564	0.011	1.454	0.145	<LOD	0.042	1.011	0.021	0.964	0.012
44	BC28_Bt2_02	2.785	1.596	0.011	1.435	0.146	0.001	0.039	1.005	0.024	0.973	0.012
50	BC28_Bt3_01	2.785	1.577	0.013	1.420	0.152	0.003	0.043	1.050	0.022	0.953	0.016
51	BC28_Bt3_02	2.756	1.599	0.012	1.444	0.087	0.005	0.037	1.108	0.028	0.853	0.015
52	BC28_Bt4_01	2.796	1.460	0.017	1.899	0.189	0.002	0.072	0.692	0.011	0.927	0.006
77	BC28_Bt4_01	2.784	1.506	0.010	1.385	0.115	0.001	0.118	1.038	0.026	0.965	0.013
53	BC28_Bt4_02	2.795	1.469	0.017	1.895	0.190	0.002	0.071	0.677	0.007	0.952	0.007
78	BC28_Bt5_01	2.789	1.528	0.013	1.383	0.132	0.002	0.111	1.019	0.023	0.948	0.011
79	BC28_Bt6_01	2.786	1.575	0.010	1.369	0.110	0.001	0.056	1.073	0.021	0.965	0.015
73	BC29B_Bt1_01	2.770	1.603	0.024	1.395	0.144	0.009	0.010	1.149	0.016	0.906	0.017
74	BC29B_Bt1_02	2.756	1.603	0.018	1.420	0.133	0.013	0.010	1.159	0.020	0.883	0.019
75	BC29B_Bt2_01	2.787	1.455	0.031	1.636	0.179	0.014	0.073	0.993	0.007	0.866	0.014
76	BC29B_Bt2_02	2.782	1.446	0.024	1.670	0.226	0.012	0.073	0.977	0.009	0.879	0.011
77	BC29B_Bt3_01	2.738	1.593	0.011	1.274	0.103	0.000	0.055	1.236	0.019	0.978	0.018
78	BC29B_Bt3_02	2.703	1.601	0.007	1.311	0.107	0.002	0.059	1.255	0.022	0.966	0.017
83	BC29B_Bt4_01	2.775	1.606	0.028	1.401	0.105	0.008	0.013	1.130	0.020	0.885	0.019
84	BC29B_Bt4_02	2.776	1.606	0.011	1.388	0.131	0.002	0.014	1.121	0.022	0.944	0.015
85	BC29B_Bt5_01	2.775	1.565	0.009	1.340	0.144	0.000	0.064	1.125	0.023	0.965	0.015
86	BC29B_Bt5_02	2.781	1.567	0.010	1.322	0.100	0.003	0.064	1.122	0.024	0.967	0.015
102	BC29B_Bt6_01	2.757	1.591	0.012	1.335	0.124	0.003	0.033	1.188	0.023	0.961	0.017

Comments:		Moles Cation (Based on 11 Oxygens)										
Point:	Sample ID:	Si	Al	Na	Mg	F	Ca	Ti	Fe	Mn	K	Cl
103	BC29B_Bt6_02	2.750	1.587	0.008	1.285	0.130	0.003	0.031	1.269	0.027	0.941	0.018
107	BC29B_Bt7_01	2.763	1.539	0.010	1.441	0.138	0.000	0.106	1.012	0.022	0.945	0.012
108	BC29B_Bt8_01	2.766	1.532	0.008	1.433	0.132	0.000	0.111	1.017	0.021	0.946	0.011
109	BC29B_Bt8_02	2.760	1.512	0.011	1.447	0.139	0.008	0.110	1.049	0.023	0.914	0.012
33	BC6_Bt1_01	2.679	1.672	0.013	1.353	0.122	0.001	0.197	0.901	0.001	0.959	0.012
34	BC6_Bt1_02	2.677	1.688	0.017	1.426	0.133	0.000	0.174	0.851	0.001	0.956	0.011
35	BC6_Bt2_01	2.684	1.666	0.012	1.235	0.114	0.000	0.221	0.969	0.001	0.959	0.012
36	BC6_Bt2_02	2.669	1.679	0.014	1.244	0.106	<LOD	0.219	0.974	0.002	0.956	0.012
37	BC6_Bt3_01	2.686	1.683	0.016	1.358	0.125	0.001	0.192	0.873	0.000	0.959	0.011
38	BC6_Bt3_02	2.691	1.668	0.018	1.373	0.132	0.000	0.192	0.874	0.001	0.947	0.011
39	BC6_Bt4_01	2.680	1.673	0.020	1.293	0.130	<LOD	0.201	0.946	0.001	0.957	0.012
40	BC6_Bt4_02	2.671	1.700	0.022	1.361	0.149	0.002	0.184	0.885	0.000	0.959	0.011
41	BC6_Bt5_01	2.680	1.690	0.019	1.341	0.107	0.001	0.196	0.884	<LOD	0.955	0.013
42	BC6_Bt5_02	2.681	1.678	0.014	1.340	0.064	0.000	0.198	0.897	<LOD	0.958	0.011
43	BC6_Bt6_01	2.681	1.675	0.013	1.391	0.137	0.001	0.174	0.899	0.001	0.957	0.012
44	BC6_Bt6_02	2.697	1.673	0.014	1.352	0.136	<LOD	0.182	0.900	0.001	0.942	0.012
45	BC6_Bt7_01	2.677	1.692	0.016	1.304	0.101	<LOD	0.198	0.928	0.001	0.945	0.012
46	BC6_Bt7_02	2.667	1.706	0.016	1.309	0.122	<LOD	0.199	0.921	0.001	0.940	0.011
47	BC6_Bt8_01	2.673	1.673	0.018	1.346	0.123	0.001	0.198	0.913	<LOD	0.956	0.012
48	BC6_Bt8_02	2.682	1.692	0.014	1.344	0.121	0.002	0.188	0.896	0.001	0.940	0.012
25	RO04_Bt1_01	2.691	1.712	0.086	1.624	0.038	0.001	0.057	0.848	0.004	0.832	0.015
26	RO04_Bt1_02	2.676	1.716	0.084	1.644	0.077	0.004	0.060	0.867	0.003	0.792	0.015
27	RO04_Bt2_01	2.688	1.705	0.092	1.618	0.060	0.002	0.071	0.846	0.003	0.823	0.014
28	RO04_Bt2_02	2.676	1.730	0.085	1.630	0.030	0.003	0.072	0.830	0.001	0.804	0.015
29	RO04_Bt3_01	2.684	1.735	0.083	1.783	0.084	0.013	0.034	0.751	0.002	0.745	0.012
30	RO04_Bt3_02	2.690	1.715	0.096	1.795	0.075	0.004	0.038	0.720	0.003	0.806	0.011
31	RO04_Bt4_01	2.672	1.696	0.088	1.650	0.078	0.011	0.058	0.896	0.004	0.780	0.015
32	RO04_Bt4_02	2.689	1.715	0.091	1.643	0.049	0.015	0.056	0.868	0.004	0.726	0.015
33	RO04_Bt5_01	2.668	1.709	0.085	1.640	0.044	0.005	0.054	0.896	0.004	0.807	0.014
34	RO04_Bt5_02	2.684	1.724	0.084	1.648	0.045	0.002	0.055	0.835	0.001	0.817	0.014
72	RO04_Bt6_01	2.717	1.646	0.087	1.701	0.070	0.000	0.055	0.830	0.003	0.818	0.014
73	RO04_Bt6_02	2.704	1.643	0.090	1.710	0.089	0.003	0.057	0.847	0.004	0.809	0.015

Comments:		Moles Cation (Based on 11 Oxygens)										
Point:	Sample ID:	Si	Al	Na	Mg	F	Ca	Ti	Fe	Mn	K	Cl
75	RO04_Bt7_01	2.692	1.692	0.094	1.596	0.063	0.001	0.070	0.872	0.002	0.834	0.014
76	RO04_Bt8_01	2.684	1.704	0.090	1.611	0.070	<LOD	0.069	0.863	0.002	0.835	0.014
54	RO08A_Bt1_01	2.740	1.663	0.015	0.860	0.029	0.001	0.029	1.573	0.038	0.977	0.012
55	RO08A_Bt1_02	2.725	1.685	0.009	0.899	<LOD	0.002	0.030	1.547	0.037	0.945	0.012
56	RO08A_Bt2_01	2.733	1.697	0.010	0.860	0.045	0.001	0.010	1.584	0.033	0.972	0.011
57	RO08A_Bt2_02	2.480	1.785	0.008	1.103	0.001	0.009	0.004	1.991	0.053	0.388	0.007
58	RO08A_Bt3_01	2.740	1.669	0.026	0.783	0.010	0.014	0.013	1.686	0.045	0.900	0.011
59	RO08A_Bt3_02	2.548	1.768	0.018	0.961	0.025	0.018	0.018	1.917	0.059	0.505	0.009
64	RO08A_Bt4_01	2.742	1.553	0.013	0.940	0.016	0.001	0.114	1.504	0.022	0.967	0.013
65	RO08A_Bt4_02	2.750	1.551	0.013	0.937	0.014	0.001	0.119	1.482	0.022	0.972	0.013
68	RO08A_Bt5_01	2.747	1.539	0.013	0.952	0.018	0.002	0.114	1.502	0.024	0.966	0.014
69	RO08A_Bt5_02	2.754	1.539	0.012	0.943	0.036	0.001	0.112	1.502	0.022	0.970	0.014
1	RO09B_Bt1_01	2.714	1.520	0.030	1.123	0.042	0.003	0.178	1.342	0.005	0.896	0.006
2	RO09B_Bt1_02	2.712	1.531	0.032	1.110	0.038	0.005	0.187	1.329	0.006	0.883	0.008
3	RO09B_Bt2_01	2.731	1.502	0.025	1.154	0.041	0.001	0.183	1.288	0.006	0.914	0.007
4	RO09B_Bt2_02	2.686	1.529	0.023	1.158	0.047	0.004	0.178	1.356	0.007	0.886	0.007
5	RO09B_Bt3_01	2.721	1.527	0.026	1.112	0.038	0.004	0.170	1.340	0.005	0.906	0.006
6	RO09B_Bt3_02	2.722	1.536	0.023	1.094	0.059	0.003	0.174	1.332	0.009	0.909	0.007
7	RO09B_Bt4_01	2.723	1.469	0.047	1.347	0.030	0.003	0.210	1.121	0.002	0.867	0.004
8	RO09B_Bt4_02	2.734	1.475	0.053	1.344	0.022	0.011	0.205	1.126	0.004	0.800	0.005
9	RO09B_Bt5_01	2.711	1.503	0.024	1.151	0.020	0.002	0.176	1.356	0.007	0.886	0.007
10	RO09B_Bt5_02	2.709	1.530	0.025	1.134	0.046	0.005	0.172	1.331	0.007	0.908	0.007
15	RO09B_Bt6_01	2.718	1.545	0.026	1.114	0.041	0.001	0.178	1.304	0.005	0.907	0.006
16	RO09B_Bt6_02	2.710	1.558	0.027	1.120	0.032	0.004	0.174	1.300	0.007	0.902	0.006
17	RO09B_Bt7_01	2.721	1.555	0.022	1.147	0.019	0.002	0.172	1.255	0.006	0.919	0.007
18	RO09B_Bt7_02	2.713	1.546	0.023	1.176	0.055	0.002	0.178	1.240	0.007	0.924	0.006
80	RO09B_Bt8_01	2.710	1.553	0.026	1.118	0.048	0.002	0.184	1.291	0.006	0.901	0.008
82	RO09B_Bt9_01	2.721	1.537	0.025	1.131	0.060	0.001	0.176	1.291	0.005	0.922	0.007
1	C005A_Bt1_01	2.655	1.708	0.021	1.301	0.059	0.003	0.212	0.923	0.001	0.934	0.009
2	C005A_Bt1_02	2.662	1.700	0.020	1.271	0.111	0.001	0.211	0.961	0.002	0.922	0.008
3	C005A_Bt1_03	2.666	1.700	0.017	1.276	0.095	0.000	0.203	0.955	0.003	0.942	0.007
4	C005A_Bt1_04	2.657	1.711	0.018	1.270	0.093	0.002	0.207	0.958	0.002	0.931	0.007

Comments:		Moles Cation (Based on 11 Oxygens)										
Point:	Sample ID:	Si	Al	Na	Mg	F	Ca	Ti	Fe	Mn	K	Cl
5	C005A_Bt1_05	2.683	1.707	0.017	1.401	0.089	0.000	0.171	0.849	0.001	0.946	0.006
6	C005A_Bt1_06	2.664	1.709	0.016	1.400	0.128	0.002	0.176	0.878	0.001	0.938	0.007
7	C005A_Bt1_07	2.668	1.691	0.021	1.307	0.117	0.002	0.208	0.932	0.001	0.923	0.008
8	C005A_Bt1_08	2.673	1.692	0.016	1.290	0.062	0.001	0.205	0.940	0.000	0.935	0.007
9	C005A_Bt2_09	2.660	1.687	0.019	1.269	0.080	0.002	0.214	0.973	0.001	0.936	0.008
10	C005A_Bt2_10	2.664	1.682	0.017	1.278	0.087	0.000	0.217	0.961	<LOD	0.940	0.008
11	C005A_Bt2_11	2.662	1.643	0.018	1.384	0.086	0.002	0.229	0.895	0.002	0.927	0.008
12	C005A_Bt2_12	2.668	1.665	0.016	1.327	0.054	0.000	0.232	0.898	0.001	0.936	0.007
13	C005A_Bt2_13	2.681	1.673	0.018	1.282	0.106	0.001	0.203	0.964	<LOD	0.934	0.007
14	C005A_Bt2_14	2.669	1.669	0.016	1.300	0.105	0.000	0.206	0.963	0.002	0.941	0.008
15	C005A_Bt2_15	2.689	1.696	0.015	1.540	0.114	0.000	0.147	0.765	0.001	0.939	0.006
16	C005A_Bt2_16	2.681	1.708	0.017	1.528	0.113	0.001	0.149	0.771	0.001	0.939	0.006
43	C005A_Bt3_17	2.675	1.686	0.016	1.278	0.090	0.000	0.201	0.960	0.003	0.939	0.007
44	C005A_Bt3_18	2.681	1.682	0.015	1.272	0.123	0.001	0.205	0.953	0.001	0.940	0.007
45	C005A_Bt3_19	2.662	1.710	0.019	1.293	0.096	0.001	0.203	0.931	0.001	0.943	0.007
46	C005A_Bt3_20	2.664	1.705	0.017	1.270	0.128	0.001	0.209	0.951	0.000	0.929	0.009
47	C005A_Bt3_21	2.677	1.682	0.017	1.297	0.100	0.003	0.194	0.958	0.001	0.936	0.007
48	C005A_Bt3_22	2.672	1.693	0.016	1.294	0.113	0.000	0.196	0.945	0.001	0.951	0.009
49	C005A_Bt3_23	2.661	1.684	0.019	1.309	0.083	0.001	0.206	0.948	0.001	0.942	0.006
50	C005A_Bt3_24	2.664	1.707	0.018	1.293	0.098	0.001	0.202	0.940	0.001	0.927	0.007
17	C005B_Bt1_01	2.678	1.676	0.015	1.373	0.066	0.001	0.194	0.893	0.002	0.929	0.008
18	C005B_Bt1_02	2.663	1.682	0.017	1.374	0.097	0.002	0.197	0.907	0.001	0.930	0.008
19	C005B_Bt1_03	2.685	1.676	0.019	1.331	0.090	0.002	0.185	0.940	0.001	0.925	0.007
20	C005B_Bt1_04	2.685	1.688	0.016	1.388	0.064	0.003	0.175	0.893	0.002	0.906	0.006
21	C005B_Bt1_05	2.677	1.687	0.017	1.347	0.053	0.001	0.187	0.904	0.001	0.962	0.008
22	C005B_Bt1_06	2.673	1.693	0.018	1.305	0.103	0.002	0.195	0.933	0.001	0.950	0.007
23	C005B_Bt2_07	2.675	1.715	0.013	1.234	0.075	0.002	0.200	0.968	0.002	0.931	0.007
24	C005B_Bt2_08	2.677	1.698	0.014	1.254	0.088	0.003	0.205	0.957	0.000	0.940	0.008
25	C005B_Bt2_09	2.679	1.685	0.015	1.315	0.084	0.000	0.187	0.944	0.001	0.946	0.009
26	C005B_Bt2_10	2.675	1.684	0.016	1.309	0.095	0.001	0.189	0.949	0.002	0.954	0.009
27	C005B_Bt2_11	2.666	1.717	0.011	1.259	0.105	0.001	0.201	0.943	0.001	0.963	0.007
28	C005B_Bt2_12	2.673	1.704	0.012	1.249	0.058	0.001	0.206	0.950	0.000	0.961	0.007

Comments:		Moles Cation (Based on 11 Oxygens)										
Point:	Sample ID:	Si	Al	Na	Mg	F	Ca	Ti	Fe	Mn	K	Cl
35	C008_Bt1_01	2.845	1.491	0.010	2.043	0.231	0.002	0.039	0.434	0.041	0.946	0.003
36	C008_Bt1_02	2.852	1.474	0.009	2.043	0.241	<LOD	0.044	0.435	0.036	0.959	0.004
37	C008_Bt1_03	2.838	1.468	0.008	2.060	0.209	0.004	0.049	0.446	0.041	0.942	0.003
38	C008_Bt1_04	2.848	1.455	0.009	2.065	0.230	0.001	0.047	0.441	0.041	0.948	0.003
39	C008_Bt1_05	2.835	1.476	0.015	2.040	0.248	0.006	0.054	0.450	0.045	0.921	0.003
40	C008_Bt1_06	2.834	1.482	0.006	2.037	0.218	0.003	0.050	0.458	0.037	0.944	0.003
41	C008_Bt1_07	2.833	1.470	0.007	2.085	0.263	0.004	0.038	0.439	0.045	0.953	0.003
42	C008_Bt1_08	2.844	1.486	0.008	2.047	0.248	0.001	0.038	0.446	0.038	0.944	0.003
29	C010A_Bt1_01	2.671	1.891	0.020	1.501	0.101	0.004	0.055	0.728	0.003	0.933	0.007
30	C010A_Bt1_02	2.667	1.882	0.021	1.536	0.100	0.005	0.054	0.725	0.003	0.916	0.006
31	C010A_Bt1_03	2.696	1.864	0.016	1.724	0.152	0.000	0.018	0.565	0.001	0.954	0.004
32	C010A_Bt1_04	2.704	1.900	0.015	1.683	0.154	0.000	0.018	0.554	0.001	0.920	0.004
33	C010A_Bt1_05	2.686	1.825	0.016	1.398	0.097	0.002	0.086	0.841	0.006	0.926	0.009
34	C010A_Bt1_06	2.685	1.830	0.014	1.384	0.114	0.003	0.085	0.842	0.008	0.942	0.007

Comments:					Sum	Sum	Structural Sites			
Point:	Sample ID:	OH	Al(IV)	Al(VI)	(Fe+Mg+Al(VI)+Ti)	All Cations	X	Y	Z	X _{Annite (Fe)}
49	BC18B_Bt1_01	0.857	1.304	0.375	3.014	7.845	0.813	3.033	4.000	0.443
50	BC18B_Bt1_02	0.844	1.257	0.370	2.914	7.908	0.976	2.932	4.000	0.451
51	BC18B_Bt2_01	0.876	1.242	0.380	2.903	7.890	0.969	2.921	4.000	0.443
52	BC18B_Bt2_02	0.875	1.245	0.390	2.892	7.893	0.980	2.912	4.000	0.445
53	BC18B_Bt3_01	0.913	1.509	0.263	3.338	7.832	0.469	3.363	4.000	0.386
54	BC18B_Bt3_02	0.861	1.213	0.341	2.899	7.850	0.935	2.915	4.000	0.314
61	BC18B_Bt4_01	0.866	1.237	0.407	2.897	7.887	0.973	2.915	4.000	0.448
62	BC18B_Bt4_02	0.897	1.261	0.397	2.923	7.877	0.931	2.946	4.000	0.451
63	BC18B_Bt5_01	0.901	1.240	0.411	2.898	7.869	0.952	2.917	4.000	0.458
64	BC18B_Bt5_02	0.885	1.275	0.382	2.954	7.874	0.896	2.978	4.000	0.457
69	BC18B_Bt6_01	0.867	1.237	0.394	2.903	7.897	0.978	2.919	4.000	0.437
70	BC18B_Bt6_02	0.872	1.232	0.387	2.905	7.896	0.974	2.922	4.000	0.440
71	BC18B_Bt7_01	0.891	1.243	0.401	2.901	7.889	0.972	2.918	4.000	0.434
72	BC18B_Bt7_02	0.893	1.269	0.377	2.967	7.877	0.893	2.985	4.000	0.434
96	BC18B_Bt8_01	0.872	1.238	0.378	2.894	7.878	0.969	2.909	4.000	0.431
98	BC18B_Bt9_01	0.881	1.248	0.376	2.893	7.892	0.983	2.910	4.000	0.433
101	BC18B_Bt10_01	0.880	1.250	0.415	2.905	7.885	0.964	2.920	4.000	0.428
1	BC20B_Bt1_01	0.738	1.149	0.288	2.936	7.804	0.855	2.949	4.000	0.293
2	BC20B_Bt1_02	0.967	1.702	0.234	3.579	7.837	0.241	3.596	4.000	0.319
5	BC20B_Bt2_01	0.833	1.228	0.355	2.879	7.886	0.979	2.907	4.000	0.428
6	BC20B_Bt2_02	0.935	1.600	0.278	3.386	7.846	0.411	3.435	4.000	0.462
11	BC20B_Bt3_01	0.873	1.229	0.300	2.849	7.835	0.963	2.872	4.000	0.405
12	BC20B_Bt3_02	0.860	1.221	0.367	2.827	7.785	0.929	2.855	4.000	0.403
13	BC20B_Bt4_01	0.851	1.229	0.333	2.847	7.853	0.981	2.872	4.000	0.398
14	BC20B_Bt4_02	0.852	1.233	0.339	2.849	7.856	0.981	2.874	4.000	0.397
15	BC20B_Bt5_01	0.812	1.208	0.392	2.885	7.883	0.972	2.911	4.000	0.381
16	BC20B_Bt5_02	0.832	1.205	0.397	2.880	7.873	0.963	2.909	4.000	0.380
21	BC20B_Bt6_01	0.838	1.207	0.394	2.877	7.863	0.960	2.902	4.000	0.348

Comments:					Sum	Sum	Structural Sites			
Point:	Sample ID:	OH	Al(IV)	Al(VI)	(Fe+Mg+Al(VI)+Ti)	All Cations	X	Y	Z	X _{Annite (Fe)}
22	BC20B_Bt6_02	0.838	1.215	0.409	2.871	7.866	0.963	2.902	4.000	0.363
27	BC20B_Bt7_01	0.905	1.232	0.373	2.850	7.845	0.965	2.880	4.000	0.420
28	BC20B_Bt7_02	0.897	1.275	0.340	2.949	7.811	0.827	2.984	4.000	0.409
29	BC20B_Bt8_01	0.895	1.226	0.370	2.837	7.846	0.981	2.865	4.000	0.416
30	BC20B_Bt8_02	0.925	1.275	0.336	2.945	7.813	0.835	2.977	4.000	0.415
31	BC20B_Bt9_01	0.842	1.208	0.357	2.860	7.871	0.984	2.887	4.000	0.401
91	BC20B_Bt9_01	0.872	1.228	0.348	2.883	7.834	0.927	2.907	4.000	0.392
32	BC20B_Bt9_02	0.934	1.322	0.318	3.023	7.831	0.770	3.060	4.000	0.418
93	BC20B_Bt10_01	0.893	1.229	0.302	2.843	7.830	0.969	2.861	4.000	0.402
95	BC20B_Bt11_01	0.890	1.240	0.310	2.852	7.827	0.955	2.872	4.000	0.407
41	BC28_Bt1_01	0.860	1.204	0.381	2.868	7.866	0.979	2.887	4.000	0.346
42	BC28_Bt1_02	0.842	1.213	0.370	2.880	7.870	0.967	2.903	4.000	0.351
43	BC28_Bt2_01	0.843	1.202	0.362	2.869	7.866	0.975	2.891	4.000	0.352
44	BC28_Bt2_02	0.842	1.215	0.381	2.861	7.869	0.985	2.884	4.000	0.351
50	BC28_Bt3_01	0.832	1.215	0.362	2.875	7.866	0.968	2.897	4.000	0.365
51	BC28_Bt3_02	0.898	1.244	0.354	2.944	7.841	0.869	2.971	4.000	0.376
52	BC28_Bt4_01	0.805	1.204	0.256	2.918	7.874	0.946	2.929	4.000	0.237
77	BC28_Bt4_01	0.872	1.216	0.290	2.831	7.832	0.976	2.857	4.000	0.367
53	BC28_Bt4_02	0.803	1.205	0.264	2.907	7.884	0.971	2.914	4.000	0.233
78	BC28_Bt5_01	0.857	1.211	0.317	2.830	7.817	0.963	2.853	4.000	0.360
79	BC28_Bt6_01	0.876	1.214	0.361	2.860	7.857	0.976	2.881	4.000	0.375
73	BC29B_Bt1_01	0.840	1.230	0.373	2.928	7.883	0.939	2.944	4.000	0.393
74	BC29B_Bt1_02	0.847	1.244	0.359	2.948	7.883	0.915	2.969	4.000	0.393
75	BC29B_Bt2_01	0.807	1.213	0.242	2.944	7.861	0.911	2.950	4.000	0.337
76	BC29B_Bt2_02	0.763	1.218	0.228	2.949	7.873	0.915	2.958	4.000	0.331
77	BC29B_Bt3_01	0.879	1.262	0.331	2.896	7.905	0.989	2.916	4.000	0.427
78	BC29B_Bt3_02	0.876	1.297	0.303	2.928	7.925	0.975	2.950	4.000	0.429
83	BC29B_Bt4_01	0.876	1.225	0.381	2.925	7.865	0.921	2.944	4.000	0.386
84	BC29B_Bt4_02	0.854	1.224	0.382	2.905	7.885	0.958	2.927	4.000	0.386
85	BC29B_Bt5_01	0.840	1.225	0.340	2.869	7.865	0.973	2.892	4.000	0.392
86	BC29B_Bt5_02	0.884	1.219	0.348	2.855	7.860	0.981	2.879	4.000	0.393
102	BC29B_Bt6_01	0.859	1.243	0.347	2.903	7.902	0.976	2.926	4.000	0.409

Comments:					Sum	Sum	Structural Sites			
Point:	Sample ID:	OH	Al(IV)	Al(VI)	(Fe+Mg+Al(VI)+Ti)	All Cations	X	Y	Z	X _{Annite (Fe)}
103	BC29B_Bt6_02	0.852	1.250	0.337	2.922	7.900	0.952	2.948	4.000	0.434
107	BC29B_Bt7_01	0.850	1.237	0.303	2.861	7.838	0.956	2.883	4.000	0.354
108	BC29B_Bt8_01	0.857	1.234	0.298	2.859	7.834	0.955	2.880	4.000	0.356
109	BC29B_Bt8_02	0.849	1.240	0.273	2.879	7.835	0.933	2.903	4.000	0.364
33	BC6_Bt1_01	0.866	1.321	0.351	2.801	7.774	0.972	2.802	4.000	0.322
34	BC6_Bt1_02	0.856	1.323	0.365	2.817	7.791	0.974	2.818	4.000	0.302
35	BC6_Bt2_01	0.875	1.316	0.350	2.775	7.748	0.972	2.776	4.000	0.349
36	BC6_Bt2_02	0.883	1.331	0.348	2.785	7.757	0.970	2.787	4.000	0.350
37	BC6_Bt3_01	0.864	1.314	0.368	2.792	7.769	0.976	2.792	4.000	0.313
38	BC6_Bt3_02	0.857	1.309	0.359	2.799	7.765	0.965	2.800	4.000	0.312
39	BC6_Bt4_01	0.857	1.320	0.353	2.793	7.771	0.978	2.793	4.000	0.339
40	BC6_Bt4_02	0.840	1.329	0.371	2.802	7.785	0.983	2.802	4.000	0.316
41	BC6_Bt5_01	0.880	1.320	0.369	2.791	7.766	0.975	2.791	4.000	0.317
42	BC6_Bt5_02	0.925	1.319	0.360	2.795	7.767	0.971	2.795	4.000	0.321
43	BC6_Bt6_01	0.851	1.319	0.356	2.820	7.792	0.972	2.821	4.000	0.319
44	BC6_Bt6_02	0.853	1.303	0.371	2.805	7.762	0.956	2.806	4.000	0.321
45	BC6_Bt7_01	0.887	1.323	0.369	2.798	7.760	0.961	2.799	4.000	0.332
46	BC6_Bt7_02	0.867	1.333	0.373	2.802	7.759	0.956	2.803	4.000	0.329
47	BC6_Bt8_01	0.865	1.327	0.346	2.804	7.779	0.976	2.804	4.000	0.326
48	BC6_Bt8_02	0.867	1.318	0.375	2.803	7.760	0.956	2.804	4.000	0.320
25	RO04_Bt1_01	0.947	1.309	0.403	2.931	7.855	0.919	2.935	4.000	0.289
26	RO04_Bt1_02	0.908	1.324	0.392	2.962	7.845	0.880	2.965	4.000	0.293
27	RO04_Bt2_01	0.926	1.312	0.393	2.927	7.847	0.917	2.930	4.000	0.289
28	RO04_Bt2_02	0.955	1.324	0.405	2.938	7.832	0.893	2.939	4.000	0.282
29	RO04_Bt3_01	0.903	1.316	0.419	2.987	7.828	0.840	2.988	4.000	0.251
30	RO04_Bt3_02	0.914	1.310	0.405	2.957	7.865	0.906	2.960	4.000	0.243
31	RO04_Bt4_01	0.907	1.328	0.369	2.973	7.855	0.878	2.977	4.000	0.301
32	RO04_Bt4_02	0.936	1.311	0.404	2.971	7.806	0.831	2.974	4.000	0.292
33	RO04_Bt5_01	0.942	1.332	0.377	2.967	7.869	0.898	2.972	4.000	0.302
34	RO04_Bt5_02	0.941	1.316	0.407	2.946	7.850	0.903	2.947	4.000	0.284
72	RO04_Bt6_01	0.916	1.283	0.363	2.950	7.857	0.905	2.952	4.000	0.282
73	RO04_Bt6_02	0.896	1.296	0.348	2.961	7.867	0.902	2.965	4.000	0.286

Comments:					Sum	Sum	Structural Sites			
Point:	Sample ID:	OH	Al(IV)	Al(VI)	(Fe+Mg+Al(VI)+Ti)	All Cations	X	Y	Z	X _{Annite (Fe)}
75	RO04_Bt7_01	0.923	1.308	0.385	2.923	7.855	0.930	2.925	4.000	0.298
76	RO04_Bt8_01	0.915	1.316	0.387	2.931	7.858	0.925	2.933	4.000	0.295
54	RO08A_Bt1_01	0.959	1.260	0.403	2.865	7.896	0.992	2.903	4.000	0.549
55	RO08A_Bt1_02	<LOD	1.275	0.410	2.886	7.880	0.956	2.923	4.000	0.536
56	RO08A_Bt2_01	0.944	1.267	0.429	2.884	7.900	0.983	2.917	4.000	0.549
57	RO08A_Bt2_02	0.993	1.520	0.265	3.363	7.821	0.404	3.416	4.000	0.592
58	RO08A_Bt3_01	0.979	1.260	0.410	2.891	7.875	0.939	2.936	4.000	0.583
59	RO08A_Bt3_02	0.966	1.452	0.316	3.212	7.812	0.541	3.270	4.000	0.597
64	RO08A_Bt4_01	0.971	1.258	0.296	2.854	7.856	0.980	2.876	4.000	0.527
65	RO08A_Bt4_02	0.972	1.250	0.301	2.840	7.848	0.986	2.862	4.000	0.522
68	RO08A_Bt5_01	0.968	1.253	0.286	2.854	7.859	0.982	2.878	4.000	0.526
69	RO08A_Bt5_02	0.950	1.246	0.293	2.850	7.855	0.983	2.872	4.000	0.527
1	RO09B_Bt1_01	0.952	1.286	0.234	2.877	7.811	0.929	2.882	4.000	0.466
2	RO09B_Bt1_02	0.954	1.288	0.242	2.868	7.793	0.919	2.874	4.000	0.463
3	RO09B_Bt2_01	0.952	1.269	0.233	2.859	7.804	0.939	2.864	4.000	0.450
4	RO09B_Bt2_02	0.946	1.314	0.215	2.906	7.827	0.913	2.914	4.000	0.466
5	RO09B_Bt3_01	0.956	1.279	0.249	2.870	7.811	0.936	2.876	4.000	0.467
6	RO09B_Bt3_02	0.934	1.278	0.258	2.858	7.801	0.934	2.867	4.000	0.466
7	RO09B_Bt4_01	0.966	1.277	0.193	2.870	7.790	0.917	2.872	4.000	0.391
8	RO09B_Bt4_02	0.973	1.266	0.209	2.883	7.751	0.864	2.887	4.000	0.391
9	RO09B_Bt5_01	0.973	1.289	0.214	2.897	7.817	0.912	2.904	4.000	0.468
10	RO09B_Bt5_02	0.947	1.291	0.239	2.876	7.820	0.937	2.883	4.000	0.463
15	RO09B_Bt6_01	0.953	1.282	0.263	2.859	7.798	0.933	2.864	4.000	0.456
16	RO09B_Bt6_02	0.961	1.290	0.267	2.862	7.802	0.932	2.869	4.000	0.454
17	RO09B_Bt7_01	0.974	1.279	0.276	2.851	7.799	0.942	2.857	4.000	0.440
18	RO09B_Bt7_02	0.939	1.287	0.260	2.854	7.809	0.949	2.861	4.000	0.435
80	RO09B_Bt8_01	0.944	1.290	0.263	2.856	7.793	0.930	2.863	4.000	0.452
82	RO09B_Bt9_01	0.933	1.279	0.258	2.856	7.808	0.948	2.860	4.000	0.452
1	C005A_Bt1_01	0.932	1.345	0.363	2.798	7.756	0.957	2.799	4.000	0.330
2	C005A_Bt1_02	0.881	1.338	0.361	2.804	7.749	0.943	2.806	4.000	0.343
3	C005A_Bt1_03	0.898	1.334	0.366	2.799	7.761	0.960	2.802	4.000	0.341
4	C005A_Bt1_04	0.900	1.343	0.368	2.803	7.756	0.951	2.805	4.000	0.342

Comments:					Sum	Sum	Structural Sites			
Point:	Sample ID:	OH	Al(IV)	Al(VI)	(Fe+Mg+Al(VI)+Ti)	All Cations	X	Y	Z	X _{Annite (Fe)}
5	C005A_Bt1_05	0.904	1.317	0.390	2.810	7.775	0.963	2.811	4.000	0.302
6	C005A_Bt1_06	0.866	1.336	0.372	2.826	7.783	0.956	2.827	4.000	0.311
7	C005A_Bt1_07	0.875	1.332	0.359	2.805	7.751	0.945	2.806	4.000	0.332
8	C005A_Bt1_08	0.931	1.327	0.365	2.800	7.752	0.952	2.800	4.000	0.336
9	C005A_Bt2_09	0.912	1.340	0.347	2.803	7.761	0.957	2.804	4.000	0.347
10	C005A_Bt2_10	0.905	1.336	0.345	2.800	7.757	0.957	2.800	4.000	0.343
11	C005A_Bt2_11	0.906	1.338	0.305	2.812	7.760	0.946	2.814	4.000	0.318
12	C005A_Bt2_12	0.939	1.332	0.333	2.790	7.743	0.952	2.791	4.000	0.322
13	C005A_Bt2_13	0.886	1.319	0.354	2.804	7.756	0.952	2.804	4.000	0.344
14	C005A_Bt2_14	0.887	1.331	0.338	2.808	7.769	0.958	2.811	4.000	0.343
15	C005A_Bt2_15	0.880	1.311	0.385	2.837	7.793	0.955	2.838	4.000	0.270
16	C005A_Bt2_16	0.881	1.319	0.389	2.837	7.794	0.957	2.837	4.000	0.272
43	C005A_Bt3_17	0.903	1.325	0.361	2.800	7.758	0.955	2.803	4.000	0.343
44	C005A_Bt3_18	0.870	1.319	0.364	2.793	7.751	0.957	2.794	4.000	0.341
45	C005A_Bt3_19	0.897	1.338	0.371	2.798	7.762	0.963	2.799	4.000	0.333
46	C005A_Bt3_20	0.864	1.336	0.369	2.800	7.747	0.946	2.800	4.000	0.340
47	C005A_Bt3_21	0.893	1.323	0.359	2.808	7.764	0.956	2.809	4.000	0.341
48	C005A_Bt3_22	0.878	1.328	0.366	2.800	7.769	0.967	2.801	4.000	0.337
49	C005A_Bt3_23	0.911	1.339	0.346	2.809	7.771	0.961	2.810	4.000	0.338
50	C005A_Bt3_24	0.895	1.336	0.370	2.806	7.753	0.947	2.807	4.000	0.335
17	C005B_Bt1_01	0.926	1.322	0.354	2.814	7.762	0.946	2.816	4.000	0.317
18	C005B_Bt1_02	0.895	1.337	0.345	2.823	7.773	0.949	2.824	4.000	0.321
19	C005B_Bt1_03	0.904	1.315	0.361	2.817	7.764	0.946	2.818	4.000	0.334
20	C005B_Bt1_04	0.929	1.315	0.374	2.830	7.756	0.925	2.831	4.000	0.316
21	C005B_Bt1_05	0.939	1.323	0.364	2.801	7.783	0.980	2.803	4.000	0.323
22	C005B_Bt1_06	0.890	1.327	0.365	2.798	7.770	0.970	2.800	4.000	0.333
23	C005B_Bt2_07	0.918	1.325	0.390	2.792	7.740	0.947	2.794	4.000	0.347
24	C005B_Bt2_08	0.903	1.323	0.375	2.790	7.746	0.956	2.790	4.000	0.343
25	C005B_Bt2_09	0.907	1.321	0.364	2.810	7.772	0.961	2.811	4.000	0.336
26	C005B_Bt2_10	0.896	1.325	0.358	2.806	7.779	0.971	2.808	4.000	0.338
27	C005B_Bt2_11	0.888	1.334	0.383	2.785	7.762	0.975	2.786	4.000	0.338
28	C005B_Bt2_12	0.935	1.327	0.376	2.782	7.756	0.973	2.782	4.000	0.342

Comments:					Sum	Sum	Structural Sites			
Point:	Sample ID:	OH	Al(IV)	Al(VI)	(Fe+Mg+Al(VI)+Ti)	All Cations	X	Y	Z	X _{Annite (Fe)}
35	C008_Bt1_01	0.765	1.155	0.335	2.851	7.849	0.958	2.891	4.000	0.152
36	C008_Bt1_02	0.755	1.148	0.326	2.847	7.851	0.968	2.883	4.000	0.153
37	C008_Bt1_03	0.787	1.162	0.306	2.860	7.855	0.953	2.901	4.000	0.156
38	C008_Bt1_04	0.767	1.152	0.303	2.856	7.856	0.959	2.897	4.000	0.155
39	C008_Bt1_05	0.749	1.165	0.311	2.855	7.841	0.941	2.900	4.000	0.158
40	C008_Bt1_06	0.779	1.166	0.316	2.861	7.851	0.953	2.898	4.000	0.160
41	C008_Bt1_07	0.734	1.167	0.303	2.865	7.874	0.964	2.910	4.000	0.153
42	C008_Bt1_08	0.749	1.156	0.330	2.861	7.851	0.953	2.898	4.000	0.156
29	C010A_Bt1_01	0.892	1.329	0.562	2.845	7.805	0.957	2.848	4.000	0.256
30	C010A_Bt1_02	0.894	1.333	0.548	2.863	7.807	0.942	2.865	4.000	0.253
31	C010A_Bt1_03	0.844	1.304	0.560	2.868	7.839	0.970	2.869	4.000	0.197
32	C010A_Bt1_04	0.842	1.296	0.604	2.859	7.795	0.935	2.860	4.000	0.194
33	C010A_Bt1_05	0.895	1.314	0.511	2.836	7.787	0.945	2.842	4.000	0.297
34	C010A_Bt1_06	0.878	1.315	0.515	2.826	7.793	0.959	2.834	4.000	0.298

Comments:		Molar Fractions		
Point:	Sample ID:	$X_{\text{Phlogopite(Mg)}}$	$X_{\text{Al(VI)}}$	X_{Ti}
49	BC18B_Bt1_01	0.426	0.124	0.007
50	BC18B_Bt1_02	0.416	0.127	0.007
51	BC18B_Bt2_01	0.418	0.131	0.008
52	BC18B_Bt2_02	0.412	0.135	0.008
53	BC18B_Bt3_01	0.529	0.079	0.007
54	BC18B_Bt3_02	0.551	0.118	0.017
61	BC18B_Bt4_01	0.407	0.141	0.004
62	BC18B_Bt4_02	0.408	0.136	0.005
63	BC18B_Bt5_01	0.395	0.142	0.005
64	BC18B_Bt5_02	0.409	0.129	0.004
69	BC18B_Bt6_01	0.423	0.136	0.004
70	BC18B_Bt6_02	0.423	0.133	0.004
71	BC18B_Bt7_01	0.423	0.138	0.005
72	BC18B_Bt7_02	0.435	0.127	0.004
96	BC18B_Bt8_01	0.426	0.131	0.012
98	BC18B_Bt9_01	0.425	0.130	0.012
101	BC18B_Bt10_01	0.424	0.143	0.005
1	BC20B_Bt1_01	0.590	0.098	0.018
2	BC20B_Bt1_02	0.611	0.065	0.005
5	BC20B_Bt2_01	0.435	0.123	0.013
6	BC20B_Bt2_02	0.451	0.082	0.005
11	BC20B_Bt3_01	0.452	0.105	0.038
12	BC20B_Bt3_02	0.431	0.130	0.037
13	BC20B_Bt4_01	0.455	0.117	0.030
14	BC20B_Bt4_02	0.455	0.119	0.029
15	BC20B_Bt5_01	0.480	0.136	0.003
16	BC20B_Bt5_02	0.478	0.138	0.004
21	BC20B_Bt6_01	0.507	0.137	0.008

Comments:		Molar Fractions		
Point:	Sample ID:	X _{Phlogopite(Mg)}	X _{Al(VI)}	X _{Ti}
22	BC20B_Bt6_02	0.488	0.142	0.006
27	BC20B_Bt7_01	0.426	0.131	0.023
28	BC20B_Bt7_02	0.453	0.115	0.022
29	BC20B_Bt8_01	0.428	0.130	0.025
30	BC20B_Bt8_02	0.447	0.114	0.024
31	BC20B_Bt9_01	0.459	0.125	0.016
91	BC20B_Bt9_01	0.464	0.121	0.023
32	BC20B_Bt9_02	0.460	0.105	0.016
93	BC20B_Bt10_01	0.451	0.106	0.041
95	BC20B_Bt11_01	0.445	0.109	0.040
41	BC28_Bt1_01	0.510	0.133	0.012
42	BC28_Bt1_02	0.509	0.128	0.012
43	BC28_Bt2_01	0.507	0.126	0.015
44	BC28_Bt2_02	0.502	0.133	0.014
50	BC28_Bt3_01	0.494	0.126	0.015
51	BC28_Bt3_02	0.491	0.120	0.012
52	BC28_Bt4_01	0.651	0.088	0.025
77	BC28_Bt4_01	0.489	0.102	0.042
53	BC28_Bt4_02	0.652	0.091	0.024
78	BC28_Bt5_01	0.489	0.112	0.039
79	BC28_Bt6_01	0.479	0.126	0.020
73	BC29B_Bt1_01	0.477	0.128	0.003
74	BC29B_Bt1_02	0.482	0.122	0.003
75	BC29B_Bt2_01	0.556	0.082	0.025
76	BC29B_Bt2_02	0.566	0.077	0.025
77	BC29B_Bt3_01	0.440	0.114	0.019
78	BC29B_Bt3_02	0.448	0.104	0.020
83	BC29B_Bt4_01	0.479	0.130	0.004
84	BC29B_Bt4_02	0.478	0.131	0.005
85	BC29B_Bt5_01	0.467	0.118	0.022
86	BC29B_Bt5_02	0.463	0.122	0.022
102	BC29B_Bt6_01	0.460	0.120	0.011

Comments:		Molar Fractions		
Point:	Sample ID:	X _{Phlogopite(Mg)}	X _{Al(VI)}	X _{Ti}
103	BC29B_Bt6_02	0.440	0.115	0.011
107	BC29B_Bt7_01	0.504	0.106	0.037
108	BC29B_Bt8_01	0.501	0.104	0.039
109	BC29B_Bt8_02	0.502	0.095	0.038
33	BC6_Bt1_01	0.483	0.125	0.070
34	BC6_Bt1_02	0.506	0.130	0.062
35	BC6_Bt2_01	0.445	0.126	0.079
36	BC6_Bt2_02	0.447	0.125	0.079
37	BC6_Bt3_01	0.486	0.132	0.069
38	BC6_Bt3_02	0.491	0.128	0.069
39	BC6_Bt4_01	0.463	0.126	0.072
40	BC6_Bt4_02	0.486	0.133	0.066
41	BC6_Bt5_01	0.481	0.132	0.070
42	BC6_Bt5_02	0.479	0.129	0.071
43	BC6_Bt6_01	0.493	0.126	0.062
44	BC6_Bt6_02	0.482	0.132	0.065
45	BC6_Bt7_01	0.466	0.132	0.071
46	BC6_Bt7_02	0.467	0.133	0.071
47	BC6_Bt8_01	0.480	0.124	0.071
48	BC6_Bt8_02	0.479	0.134	0.067
25	RO04_Bt1_01	0.554	0.137	0.020
26	RO04_Bt1_02	0.555	0.132	0.020
27	RO04_Bt2_01	0.553	0.134	0.024
28	RO04_Bt2_02	0.555	0.138	0.025
29	RO04_Bt3_01	0.597	0.140	0.011
30	RO04_Bt3_02	0.607	0.137	0.013
31	RO04_Bt4_01	0.555	0.124	0.020
32	RO04_Bt4_02	0.553	0.136	0.019
33	RO04_Bt5_01	0.553	0.127	0.018
34	RO04_Bt5_02	0.560	0.138	0.019
72	RO04_Bt6_01	0.577	0.123	0.019
73	RO04_Bt6_02	0.577	0.117	0.019

Comments:		Molar Fractions		
Point:	Sample ID:	X _{Phlogopite(Mg)}	X _{Al(VI)}	X _{Ti}
75	RO04_Bt7_01	0.546	0.132	0.024
76	RO04_Bt8_01	0.550	0.132	0.024
54	RO08A_Bt1_01	0.300	0.141	0.010
55	RO08A_Bt1_02	0.311	0.142	0.010
56	RO08A_Bt2_01	0.298	0.149	0.003
57	RO08A_Bt2_02	0.328	0.079	0.001
58	RO08A_Bt3_01	0.271	0.142	0.005
59	RO08A_Bt3_02	0.299	0.098	0.006
64	RO08A_Bt4_01	0.329	0.104	0.040
65	RO08A_Bt4_02	0.330	0.106	0.042
68	RO08A_Bt5_01	0.334	0.100	0.040
69	RO08A_Bt5_02	0.331	0.103	0.039
1	RO09B_Bt1_01	0.390	0.081	0.062
2	RO09B_Bt1_02	0.387	0.084	0.065
3	RO09B_Bt2_01	0.404	0.082	0.064
4	RO09B_Bt2_02	0.399	0.074	0.061
5	RO09B_Bt3_01	0.387	0.087	0.059
6	RO09B_Bt3_02	0.383	0.090	0.061
7	RO09B_Bt4_01	0.469	0.067	0.073
8	RO09B_Bt4_02	0.466	0.072	0.071
9	RO09B_Bt5_01	0.397	0.074	0.061
10	RO09B_Bt5_02	0.394	0.083	0.060
15	RO09B_Bt6_01	0.390	0.092	0.062
16	RO09B_Bt6_02	0.391	0.093	0.061
17	RO09B_Bt7_01	0.403	0.097	0.060
18	RO09B_Bt7_02	0.412	0.091	0.062
80	RO09B_Bt8_01	0.391	0.092	0.065
82	RO09B_Bt9_01	0.396	0.090	0.061
1	C005A_Bt1_01	0.465	0.130	0.076
2	C005A_Bt1_02	0.453	0.129	0.075
3	C005A_Bt1_03	0.456	0.131	0.072
4	C005A_Bt1_04	0.453	0.131	0.074

Comments:		Molar Fractions		
Point:	Sample ID:	X _{Phlogopite(Mg)}	X _{Al(VI)}	X _{Ti}
5	C005A_Bt1_05	0.499	0.139	0.061
6	C005A_Bt1_06	0.495	0.132	0.062
7	C005A_Bt1_07	0.466	0.128	0.074
8	C005A_Bt1_08	0.461	0.130	0.073
9	C005A_Bt2_09	0.453	0.124	0.076
10	C005A_Bt2_10	0.456	0.123	0.077
11	C005A_Bt2_11	0.492	0.108	0.081
12	C005A_Bt2_12	0.476	0.119	0.083
13	C005A_Bt2_13	0.457	0.126	0.072
14	C005A_Bt2_14	0.463	0.121	0.073
15	C005A_Bt2_15	0.543	0.136	0.052
16	C005A_Bt2_16	0.539	0.137	0.053
43	C005A_Bt3_17	0.456	0.129	0.072
44	C005A_Bt3_18	0.455	0.130	0.073
45	C005A_Bt3_19	0.462	0.133	0.073
46	C005A_Bt3_20	0.454	0.132	0.075
47	C005A_Bt3_21	0.462	0.128	0.069
48	C005A_Bt3_22	0.462	0.131	0.070
49	C005A_Bt3_23	0.466	0.123	0.073
50	C005A_Bt3_24	0.461	0.132	0.072
17	C005B_Bt1_01	0.488	0.126	0.069
18	C005B_Bt1_02	0.487	0.122	0.070
19	C005B_Bt1_03	0.472	0.128	0.066
20	C005B_Bt1_04	0.490	0.132	0.062
21	C005B_Bt1_05	0.481	0.130	0.067
22	C005B_Bt1_06	0.466	0.131	0.070
23	C005B_Bt2_07	0.442	0.140	0.071
24	C005B_Bt2_08	0.449	0.134	0.073
25	C005B_Bt2_09	0.468	0.129	0.067
26	C005B_Bt2_10	0.466	0.128	0.068
27	C005B_Bt2_11	0.452	0.138	0.072
28	C005B_Bt2_12	0.449	0.135	0.074

Comments:		Molar Fractions		
Point:	Sample ID:	X _{Phlogopite(Mg)}	X _{Al(VI)}	X _{Ti}
35	C008_Bt1_01	0.717	0.118	0.014
36	C008_Bt1_02	0.717	0.114	0.015
37	C008_Bt1_03	0.720	0.107	0.017
38	C008_Bt1_04	0.723	0.106	0.016
39	C008_Bt1_05	0.715	0.109	0.019
40	C008_Bt1_06	0.712	0.110	0.017
41	C008_Bt1_07	0.728	0.106	0.013
42	C008_Bt1_08	0.716	0.115	0.013
29	C010A_Bt1_01	0.527	0.197	0.019
30	C010A_Bt1_02	0.536	0.192	0.019
31	C010A_Bt1_03	0.601	0.195	0.006
32	C010A_Bt1_04	0.589	0.211	0.006
33	C010A_Bt1_05	0.493	0.180	0.030
34	C010A_Bt1_06	0.490	0.182	0.030

Appendix G:
Microprobe data
Part 5 – Amphiboles

Molar Mass	SiO ₂	Al ₂ O ₃	Na ₂ O	MgO	F	CaO	TiO ₂	FeO	MnO	K ₂ O	Cl
	60.08	101.96	61.98	40.30	19.00	56.08	79.87	71.85	70.94	94.20	35.45

Comments:		Mass (%)											
Point	Sample ID:	SiO ₂	Al ₂ O ₃	Na ₂ O	MgO	F	CaO	TiO ₂	FeO	MnO	K ₂ O	Cl	Total
55	BC18B_Amph1_01	42.203	14.883	1.054	7.600	0.244	11.837	0.023	18.759	0.362	1.532	0.090	98.587
56	BC18B_Amph1_02	41.769	15.385	1.095	7.444	0.149	11.729	0.049	18.866	0.354	1.617	0.101	98.558
57	BC18B_Amph2_01	42.208	14.819	1.118	7.803	0.227	11.847	0.034	18.690	0.369	1.551	0.078	98.744
58	BC18B_Amph2_02	41.619	15.183	1.082	7.472	0.219	11.827	0.020	18.451	0.341	1.592	0.098	97.904
59	BC18B_Amph3_01	42.588	13.871	1.188	8.168	0.223	11.694	0.052	18.694	0.330	1.510	0.049	98.367
60	BC18B_Amph3_02	41.683	15.257	1.144	7.580	0.160	11.815	0.034	18.815	0.364	1.610	0.128	98.590
65	BC18B_Amph4_01	43.068	13.208	1.066	8.539	0.122	11.801	0.054	18.214	0.349	1.408	0.057	97.886
66	BC18B_Amph4_02	41.554	15.577	1.071	7.300	0.154	11.703	0.065	18.578	0.388	1.613	0.149	98.152
67	BC18B_Amph5_01	42.483	14.323	1.109	8.055	0.181	11.774	0.071	18.575	0.368	1.516	0.076	98.531
68	BC18B_Amph5_02	41.466	15.590	1.106	7.361	0.220	11.802	0.060	18.741	0.401	1.646	0.154	98.547
97	BC18B_Amph6_01	42.774	13.324	1.186	8.682	0.252	11.578	0.170	17.918	0.360	1.501	0.051	97.796
99	BC18B_Amph7_01	43.504	12.789	1.045	8.911	0.263	11.780	0.128	18.132	0.322	1.360	0.051	98.285
100	BC18B_Amph8_01	42.597	13.543	1.138	8.522	0.307	11.504	0.045	18.384	0.338	1.483	0.057	97.918
3	BC20B_Amph1_01	41.842	18.131	2.228	9.252	0.262	10.890	0.274	14.503	0.323	0.324	0.025	98.054
4	BC20B_Amph1_02	42.011	18.023	1.941	9.118	0.108	11.474	0.227	14.468	0.356	0.380	0.055	98.161
7	BC20B_Amph2_01	43.327	13.248	1.208	9.544	0.288	11.652	0.259	16.500	0.486	1.504	0.094	98.110
8	BC20B_Amph2_02	43.197	13.494	1.171	9.534	0.183	11.801	0.246	16.446	0.515	1.516	0.109	98.212
9	BC20B_Amph3_01	44.620	12.341	1.000	10.065	0.276	12.126	0.164	15.986	0.441	1.151	0.082	98.252
10	BC20B_Amph3_02	42.836	14.153	1.155	9.134	0.178	11.863	0.173	16.551	0.471	1.551	0.109	98.174
17	BC20B_Amph4_01	43.396	13.688	1.173	10.061	0.250	11.757	0.084	15.445	0.561	1.467	0.107	97.989
18	BC20B_Amph4_02	43.585	13.633	1.119	10.011	0.194	12.038	0.089	15.357	0.505	1.402	0.124	98.057
19	BC20B_Amph5_01	43.911	13.216	1.181	10.391	0.204	11.746	0.080	15.161	0.517	1.461	0.098	97.966
20	BC20B_Amph5_02	52.557	4.052	0.373	15.249	0.257	12.460	0.023	11.737	0.474	0.251	0.012	97.445
23	BC20B_Amph6_01	43.147	13.566	1.107	9.376	0.308	11.938	0.329	16.412	0.485	1.476	0.107	98.251
24	BC20B_Amph6_02	43.349	13.953	1.098	9.354	0.148	12.048	0.263	16.227	0.545	1.383	0.127	98.495
25	BC20B_Amph7_01	43.257	13.569	1.093	9.310	0.218	11.867	0.286	16.334	0.479	1.469	0.115	97.997
26	BC20B_Amph7_02	51.425	4.360	0.325	12.819	0.074	12.440	0.048	15.271	0.745	0.264	0.057	97.828
92	BC20B_Amph8_01	43.670	12.789	1.142	9.921	0.230	11.811	0.374	16.327	0.473	1.439	0.100	98.276

Comments:		Mass (%)											
Point	Sample ID:	SiO ₂	Al ₂ O ₃	Na ₂ O	MgO	F	CaO	TiO ₂	FeO	MnO	K ₂ O	Cl	Total
94	BC20B_Amph9_01	44.027	12.507	1.122	10.354	0.160	11.897	0.096	15.610	0.505	1.353	0.085	97.716
45	BC28_Amph1_01	44.142	12.646	1.202	10.293	0.254	11.646	0.209	15.549	0.522	1.410	0.100	97.973
46	BC28_Amph1_02	43.536	12.932	1.144	10.045	0.371	11.673	0.225	15.586	0.526	1.446	0.098	97.582
47	BC28_Amph1_03	43.946	12.848	1.049	10.235	0.351	11.940	0.255	15.280	0.524	1.356	0.111	97.895
48	BC28_Amph1_04	44.507	12.547	1.068	10.510	0.221	11.927	0.210	14.996	0.530	1.350	0.104	97.970
49	BC28_Amph1_05	44.049	13.226	1.112	10.333	0.276	11.887	0.241	15.240	0.527	1.387	0.095	98.373
79	BC29B_Amph1_01	42.543	13.379	1.236	9.432	0.264	11.474	0.204	17.162	0.432	1.477	0.076	97.679
80	BC29B_Amph1_02	43.080	13.449	1.184	9.629	0.272	11.677	0.228	16.660	0.462	1.419	0.075	98.135
81	BC29B_Amph2_01	42.525	12.892	1.090	9.417	0.065	11.803	0.182	16.956	0.405	1.406	0.086	96.827
82	BC29B_Amph2_02	40.895	14.405	1.071	8.556	0.133	11.779	0.160	17.055	0.468	1.460	0.118	96.100
87	BC29B_Amph3_01	43.495	13.132	1.140	9.596	0.213	11.688	0.105	16.752	0.463	1.449	0.075	98.108
88	BC29B_Amph3_02	42.946	14.240	1.076	8.825	0.188	11.920	0.077	16.929	0.466	1.389	0.112	98.168
89	BC29B_Amph3_03	44.000	12.412	1.039	9.695	0.270	11.980	0.106	16.529	0.415	1.288	0.099	97.833
90	BC29B_Amph3_04	43.049	13.630	1.068	9.189	0.107	11.901	0.151	16.755	0.466	1.349	0.098	97.763
104	BC29B_Amph5_01	43.725	12.418	1.108	9.720	0.189	11.646	0.184	16.776	0.390	1.315	0.061	97.532
105	BC29B_Amph6_01	42.532	13.960	1.005	8.835	0.214	11.851	0.120	17.125	0.457	1.407	0.126	97.632
106	BC29B_Amph6_02	41.913	14.622	1.087	8.543	0.214	11.773	0.116	17.110	0.399	1.505	0.126	97.408
35	RO04_Amph1_01	39.779	18.751	2.063	9.006	0.071	10.704	0.305	15.702	0.212	0.505	0.231	97.329
36	RO04_Amph1_02	39.943	18.944	2.025	9.115	0.234	10.848	0.297	15.263	0.183	0.419	0.220	97.491
37	RO04_Amph2_01	40.680	17.694	2.046	9.985	0.122	10.687	0.385	15.411	0.214	0.480	0.191	97.895
38	RO04_Amph2_02	40.438	18.814	2.049	9.301	0.155	10.785	0.322	15.573	0.193	0.468	0.216	98.314
39	RO04_Amph3_01	40.173	18.476	2.039	9.505	0.090	10.713	0.342	15.484	0.222	0.519	0.206	97.769
40	RO04_Amph3_02	40.274	17.963	2.136	9.546	0.120	10.593	0.292	15.497	0.208	0.523	0.184	97.336
70	RO04_Amph4_01	40.897	17.236	2.078	10.402	0.275	10.572	0.366	15.140	0.265	0.557	0.174	97.962
71	RO04_Amph4_02	41.037	17.293	2.026	10.229	0.175	10.743	0.400	15.166	0.189	0.517	0.169	97.944
74	RO04_Amph5_01	40.885	17.112	2.035	10.132	0.150	10.702	0.441	15.246	0.213	0.591	0.178	97.685
60	RO08A_Amph1_01	39.701	13.528	1.309	6.304	0.056	11.452	1.171	21.772	0.455	1.896	0.187	97.831
61	RO08A_Amph2_01	39.776	13.317	1.299	6.267	<LOD	11.359	1.080	21.799	0.447	1.838	0.176	97.335
62	RO08A_Amph2_02	39.514	13.405	1.280	6.252	0.016	11.354	1.248	21.524	0.469	1.894	0.190	97.146
63	RO08A_Amph2_03	39.424	13.644	1.299	6.135	0.005	11.277	1.134	21.845	0.452	1.785	0.170	97.170
66	RO08A_Amph3_01	39.900	13.325	1.279	6.271	0.005	11.316	1.310	21.915	0.453	1.897	0.179	97.850
67	RO08A_Amph3_02	39.696	13.561	1.322	6.085	<LOD	11.268	0.969	22.265	0.477	1.827	0.201	97.619

Comments:		Mass (%)											
Point	Sample ID:	SiO ₂	Al ₂ O ₃	Na ₂ O	MgO	F	CaO	TiO ₂	FeO	MnO	K ₂ O	Cl	Total
11	RO09B_Amph1_01	42.538	13.064	1.296	8.542	0.101	11.085	0.964	18.739	0.226	0.827	0.045	97.427
12	RO09B_Amph1_02	41.485	14.812	1.233	7.530	0.031	11.161	0.682	19.333	0.212	0.730	0.061	97.270
13	RO09B_Amph2_01	41.851	13.835	1.393	8.095	0.065	11.304	0.958	18.851	0.219	0.836	0.047	97.454
14	RO09B_Amph2_02	41.375	14.351	1.312	7.979	0.215	11.268	0.868	18.866	0.216	0.841	0.055	97.346
19	RO09B_Amph3_01	41.628	14.464	1.286	8.014	0.076	11.260	0.801	19.104	0.198	0.776	0.040	97.647
20	RO09B_Amph3_02	41.465	14.972	1.289	7.575	<LOD	11.145	0.772	19.233	0.171	0.747	0.057	97.406
21	RO09B_Amph4_01	41.632	14.536	1.330	7.961	0.179	11.223	0.874	19.137	0.180	0.839	0.045	97.936
22	RO09B_Amph4_02	41.108	15.330	1.273	7.158	0.022	11.255	0.598	19.554	0.196	0.684	0.064	97.242
23	RO09B_Amph5_01	41.498	14.173	1.343	8.087	0.040	11.137	0.884	19.095	0.212	0.852	0.044	97.365
24	RO09B_Amph6_01	42.067	13.280	1.289	8.397	0.100	11.196	1.056	18.635	0.202	0.809	0.042	97.073
81	RO09B_Amph7_01	42.560	12.996	1.386	8.547	0.130	11.145	1.108	18.815	0.232	0.875	0.040	97.834

Comments:		Moles Cation (Based on 23 Oxygens)									Sum
Point	Sample ID:	Si	Al	Na	Mg	Ca	Ti	Fe	Mn	K	All Cations
55	BC18B_Amph1_01	6.355	2.641	0.308	1.706	1.909	0.003	2.362	0.046	0.294	15.623
56	BC18B_Amph1_02	6.294	2.732	0.320	1.672	1.893	0.006	2.377	0.045	0.311	15.650
57	BC18B_Amph2_01	6.345	2.625	0.326	1.749	1.908	0.004	2.349	0.047	0.297	15.650
58	BC18B_Amph2_02	6.310	2.713	0.318	1.689	1.921	0.002	2.339	0.044	0.308	15.644
59	BC18B_Amph3_01	6.423	2.465	0.347	1.836	1.889	0.006	2.357	0.042	0.290	15.657
60	BC18B_Amph3_02	6.286	2.711	0.334	1.704	1.909	0.004	2.372	0.046	0.310	15.677
65	BC18B_Amph4_01	6.500	2.349	0.312	1.921	1.908	0.006	2.299	0.045	0.271	15.611
66	BC18B_Amph4_02	6.284	2.776	0.314	1.646	1.896	0.007	2.349	0.050	0.311	15.633
67	BC18B_Amph5_01	6.390	2.539	0.323	1.806	1.897	0.008	2.336	0.047	0.291	15.639
68	BC18B_Amph5_02	6.261	2.774	0.324	1.657	1.909	0.007	2.366	0.051	0.317	15.666
97	BC18B_Amph6_01	6.468	2.374	0.348	1.957	1.876	0.019	2.266	0.046	0.290	15.644
99	BC18B_Amph7_01	6.539	2.265	0.304	1.997	1.897	0.014	2.279	0.041	0.261	15.597
100	BC18B_Amph8_01	6.448	2.416	0.334	1.923	1.866	0.005	2.327	0.043	0.286	15.649
3	BC20B_Amph1_01	6.154	3.143	0.635	2.029	1.716	0.030	1.784	0.040	0.061	15.592
4	BC20B_Amph1_02	6.169	3.119	0.553	1.996	1.805	0.025	1.776	0.044	0.071	15.558
7	BC20B_Amph2_01	6.491	2.339	0.351	2.132	1.870	0.029	2.067	0.062	0.287	15.629
8	BC20B_Amph2_02	6.461	2.379	0.340	2.126	1.891	0.028	2.057	0.065	0.289	15.636
9	BC20B_Amph3_01	6.632	2.162	0.288	2.230	1.931	0.018	1.987	0.056	0.218	15.522
10	BC20B_Amph3_02	6.413	2.497	0.335	2.039	1.903	0.019	2.072	0.060	0.296	15.634
17	BC20B_Amph4_01	6.474	2.407	0.339	2.238	1.879	0.009	1.927	0.071	0.279	15.623
18	BC20B_Amph4_02	6.490	2.392	0.323	2.222	1.920	0.010	1.912	0.064	0.266	15.599
19	BC20B_Amph5_01	6.534	2.318	0.341	2.305	1.872	0.009	1.886	0.065	0.277	15.607
20	BC20B_Amph5_02	7.596	0.690	0.105	3.286	1.929	0.003	1.419	0.058	0.046	15.131
23	BC20B_Amph6_01	6.457	2.393	0.321	2.092	1.914	0.037	2.054	0.061	0.282	15.611
24	BC20B_Amph6_02	6.450	2.447	0.317	2.075	1.920	0.029	2.019	0.069	0.262	15.587
25	BC20B_Amph7_01	6.478	2.395	0.317	2.079	1.904	0.032	2.045	0.061	0.281	15.591
26	BC20B_Amph7_02	7.536	0.753	0.092	2.801	1.953	0.005	1.871	0.092	0.049	15.153
92	BC20B_Amph8_01	6.521	2.251	0.331	2.208	1.889	0.042	2.039	0.060	0.274	15.614

Comments:		Moles Cation (Based on 23 Oxygens)									Sum
Point	Sample ID:	Si	Al	Na	Mg	Ca	Ti	Fe	Mn	K	All Cations
94	BC20B_Amph9_01	6.579	2.202	0.325	2.307	1.905	0.011	1.950	0.064	0.258	15.601
45	BC28_Amph1_01	6.581	2.222	0.347	2.288	1.860	0.023	1.938	0.066	0.268	15.593
46	BC28_Amph1_02	6.533	2.287	0.333	2.247	1.877	0.025	1.956	0.067	0.277	15.602
47	BC28_Amph1_03	6.557	2.259	0.303	2.277	1.909	0.029	1.907	0.066	0.258	15.565
48	BC28_Amph1_04	6.611	2.196	0.308	2.327	1.898	0.023	1.863	0.067	0.256	15.549
49	BC28_Amph1_05	6.531	2.311	0.320	2.284	1.888	0.027	1.889	0.066	0.262	15.578
79	BC29B_Amph1_01	6.427	2.382	0.362	2.124	1.857	0.023	2.168	0.055	0.285	15.683
80	BC29B_Amph1_02	6.454	2.375	0.344	2.151	1.874	0.026	2.087	0.059	0.271	15.640
81	BC29B_Amph2_01	6.466	2.310	0.321	2.135	1.923	0.021	2.156	0.052	0.273	15.655
82	BC29B_Amph2_02	6.292	2.612	0.319	1.962	1.941	0.019	2.194	0.061	0.287	15.687
87	BC29B_Amph3_01	6.512	2.317	0.331	2.142	1.875	0.012	2.097	0.059	0.277	15.621
88	BC29B_Amph3_02	6.431	2.513	0.312	1.970	1.912	0.009	2.120	0.059	0.265	15.592
89	BC29B_Amph3_03	6.598	2.193	0.302	2.167	1.924	0.012	2.072	0.053	0.246	15.568
90	BC29B_Amph3_04	6.464	2.412	0.311	2.057	1.915	0.017	2.104	0.059	0.258	15.597
104	BC29B_Amph5_01	6.577	2.201	0.323	2.180	1.877	0.021	2.110	0.050	0.252	15.590
105	BC29B_Amph6_01	6.420	2.483	0.294	1.988	1.917	0.014	2.162	0.058	0.271	15.607
106	BC29B_Amph6_02	6.348	2.610	0.319	1.929	1.910	0.013	2.167	0.051	0.291	15.639
35	RO04_Amph1_01	5.953	3.307	0.599	2.009	1.716	0.034	1.965	0.027	0.096	15.707
36	RO04_Amph1_02	5.959	3.330	0.586	2.027	1.734	0.033	1.904	0.023	0.080	15.676
37	RO04_Amph2_01	6.040	3.096	0.589	2.210	1.700	0.043	1.913	0.027	0.091	15.709
38	RO04_Amph2_02	5.981	3.279	0.588	2.051	1.709	0.036	1.926	0.024	0.088	15.682
39	RO04_Amph3_01	5.976	3.239	0.588	2.108	1.707	0.038	1.926	0.028	0.098	15.709
40	RO04_Amph3_02	6.020	3.165	0.619	2.127	1.696	0.033	1.937	0.026	0.100	15.724
70	RO04_Amph4_01	6.072	3.016	0.598	2.303	1.682	0.041	1.880	0.033	0.105	15.730
71	RO04_Amph4_02	6.084	3.021	0.582	2.261	1.706	0.045	1.880	0.024	0.098	15.701
74	RO04_Amph5_01	6.085	3.002	0.587	2.248	1.706	0.049	1.897	0.027	0.112	15.714
60	RO08A_Amph1_01	6.178	2.481	0.395	1.462	1.909	0.137	2.833	0.060	0.376	15.831
61	RO08A_Amph2_01	6.212	2.451	0.393	1.459	1.901	0.127	2.847	0.059	0.366	15.815
62	RO08A_Amph2_02	6.185	2.473	0.388	1.459	1.904	0.147	2.817	0.062	0.378	15.815
63	RO08A_Amph2_03	6.171	2.517	0.394	1.432	1.891	0.134	2.859	0.060	0.356	15.813
66	RO08A_Amph3_01	6.202	2.441	0.385	1.453	1.885	0.153	2.849	0.060	0.376	15.805
67	RO08A_Amph3_02	6.193	2.493	0.400	1.415	1.883	0.114	2.904	0.063	0.364	15.829

Comments:		Moles Cation (Based on 23 Oxygens)									Sum
Point	Sample ID:	Si	Al	Na	Mg	Ca	Ti	Fe	Mn	K	All Cations
11	RO09B_Amph1_01	6.442	2.332	0.381	1.929	1.798	0.110	2.373	0.029	0.160	15.553
12	RO09B_Amph1_02	6.303	2.652	0.363	1.706	1.817	0.078	2.456	0.027	0.141	15.545
13	RO09B_Amph2_01	6.349	2.473	0.410	1.831	1.837	0.109	2.391	0.028	0.162	15.591
14	RO09B_Amph2_02	6.296	2.573	0.387	1.810	1.837	0.099	2.400	0.028	0.163	15.594
19	RO09B_Amph3_01	6.302	2.581	0.377	1.809	1.826	0.091	2.418	0.025	0.150	15.580
20	RO09B_Amph3_02	6.285	2.674	0.379	1.712	1.810	0.088	2.438	0.022	0.144	15.551
21	RO09B_Amph4_01	6.294	2.590	0.390	1.794	1.818	0.099	2.419	0.023	0.162	15.588
22	RO09B_Amph4_02	6.256	2.749	0.376	1.624	1.835	0.068	2.488	0.025	0.133	15.555
23	RO09B_Amph5_01	6.306	2.538	0.396	1.832	1.813	0.101	2.426	0.027	0.165	15.604
24	RO09B_Amph6_01	6.398	2.380	0.380	1.904	1.824	0.121	2.370	0.026	0.157	15.560
81	RO09B_Amph7_01	6.428	2.313	0.406	1.925	1.803	0.126	2.376	0.030	0.169	15.576

Appendix G:
Microprobe data
Part 6 – Sulfides

Comments		Weight (%)							Likely mineral:
Point:	Comment:	As	S	Fe	Ni	Cu	Zn	Total	
1	BC20B_Sulf1_01	0.026	39.399	60.212	0.052	<LOD	0.008	99.694	Pyrrhotite
2	BC20B_Sulf1_02	0.019	53.018	46.780	0.038	0.043	<LOD	99.893	Pyrite
3	BC20B_Sulf1_03	0.044	39.459	59.767	0.049	<LOD	0.014	99.306	Pyrrhotite
4	BC20B_Sulf2_01	0.030	39.482	59.990	0.074	<LOD	<LOD	99.551	Pyrrhotite
5	BC20B_Sulf2_02	0.034	39.542	60.035	0.033	<LOD	<LOD	99.634	Pyrrhotite
8	BC18B_Sulf2_01	<LOD	39.415	59.585	0.041	<LOD	<LOD	98.995	Pyrrhotite
9	BC18B_Sulf2_02	<LOD	39.392	59.259	0.087	<LOD	0.004	98.721	Pyrrhotite
10	BC18B_Sulf3_01	0.032	39.304	59.814	0.055	0.018	0.035	99.258	Pyrrhotite
11	BC18B_Sulf3_02	0.018	39.376	59.560	0.047	<LOD	<LOD	98.967	Pyrrhotite
12	BC18B_Sulf4_01	0.042	39.455	59.574	0.055	<LOD	0.032	99.124	Pyrrhotite
13	BC18B_Sulf4_02	0.018	53.235	46.639	0.061	<LOD	<LOD	99.937	Pyrite
14	BC20B_Sulf3_01	0.020	39.575	60.087	0.030	0.007	0.015	99.734	Pyrrhotite
15	BC18B_Sulf5_01	0.039	39.500	60.188	0.056	0.008	0.000	99.791	Pyrrhotite
16	BC18B_Sulf5_02	0.028	39.290	59.913	0.078	<LOD	<LOD	99.280	Pyrrhotite
17	BC18B_Sulf6_01	0.011	53.019	46.774	0.039	<LOD	0.015	99.850	Pyrite
18	BC18B_Sulf6_02	0.021	39.148	60.009	0.043	<LOD	0.020	99.212	Pyrrhotite
19	BC18B_Sulf6_03	0.013	34.323	30.459	0.005	34.558	0.009	99.367	Chalcopyrite
20	BC29B_Sulf1_01	0.012	39.206	59.715	0.116	<LOD	<LOD	99.037	Pyrrhotite
21	BC29B_Sulf1_02	0.018	39.161	59.791	0.136	<LOD	<LOD	99.073	Pyrrhotite
22	BC29B_Sulf2_01	0.004	39.534	59.654	0.127	<LOD	0.013	99.313	Pyrrhotite
23	BC29B_Sulf3_01	0.024	39.357	59.835	0.095	<LOD	<LOD	99.265	Pyrrhotite
1	BC28_Sulf1_01	0.017	38.499	59.581	0.103	0.019	0.016	98.235	Pyrrhotite
2	BC28_Sulf1_02	0.013	38.717	59.633	0.098	0.018	<LOD	98.461	Pyrrhotite
3	BC28_Sulf1_03	0.035	38.689	59.711	0.093	0.005	0.002	98.535	Pyrrhotite
4	BC28_Sulf2_01	0.031	38.957	60.024	0.149	0.026	0.019	99.206	Pyrrhotite
5	BC28_Sulf2_02	0.004	38.862	59.781	0.157	<LOD	0.031	98.817	Pyrrhotite
6	BC28_Sulf3_01	0.031	38.681	59.443	0.177	<LOD	<LOD	98.320	Pyrrhotite
7	BC28_Sulf3_02	0.020	33.669	30.246	<LOD	34.130	0.017	98.080	Chalcopyrite
8	RO09B_Sulf1_01	<LOD	53.403	46.621	0.094	<LOD	<LOD	100.094	Pyrite
9	RO09B_Sulf2_01	0.010	52.964	44.899	0.012	0.024	<LOD	97.896	Pyrite
10	RO09B_Sulf2_02	0.007	53.609	44.877	1.567	0.000	0.021	100.081	Pyrite
11	RO09B_Sulf2_03	0.017	53.243	43.777	2.985	0.049	0.000	100.071	Pyrite